

BN Isosteres of Acenes for Potential Applications in Optoelectronic Devices

Author: Jacob Shotaro Afaga Ishibashi

Persistent link: <http://hdl.handle.net/2345/bc-ir:107613>

This work is posted on [eScholarship@BC](#),
Boston College University Libraries.

Boston College Electronic Thesis or Dissertation, 2017

Copyright is held by the author, with all rights reserved, unless otherwise noted.

Boston College
Morrissey Graduate School of Arts and Sciences
Department of Chemistry

BN ISOSTERES OF ACENES
FOR POTENTIAL APPLICATIONS IN OPTOELECTRONIC DEVICES

A dissertation
by
JACOB SHOTARO AFAGA ISHIBASHI

submitted in partial fulfillment of the requirements
for the degree of
Doctor of Philosophy

June 2017

© Copyright by JACOB SHOTARO AFAGA ISHIBASHI

2017

BN ISOSTERES OF ACENES
FOR POTENTIAL APPLICATION IN OPTOELECTRONIC DEVICES

by

JACOB SHOTARO AFAGA ISHIBASHI

Dissertation Adviser:

Professor Shih-Yuan Liu

ABSTRACT: This dissertation describes progress in the field of polycyclic boron-nitrogen-containing systems, especially for potential application in organic-based optoelectronic devices and hydrogen storage materials. The replacement of a BN unit for a CC unit organic compounds (BN/CC isosterism) can have a profound effect on the electronic structure and even function of a given molecular topology without changing its physical structure very much. Direct comparison between a BN-containing molecule and its direct all-carbon analogue is crucial to establishing the origin of these differences. The synthesis and optoelectronic characterization of boron- nitrogen-containing analogues of naphthalene, anthracene, and tetracene are disclosed. Also examined herein is the aromatic Claisen rearrangement applied to an azaboryl allyl ether. Finally, the chemistry of saturated BN heterocycles, including an iridium-catalyzed transfer dehydrogenation method for synthesizing BN-fused azaborines. Also disclosed is the actual application of these cyclic amine-boranes in supplying hydrogen for a proton exchange membrane (PEM) fuel cell.

Dedicated to the memory of my forebears who left their homes long ago so that their families might have a better life in Hawai'i.

ACKNOWLEDGEMENTS

I would like to begin by thanking Professor Shih-Yuan Liu for being an encouraging and thoughtful mentor. I would also like to thank the committee members, Professor Jeff Byers and Professor Marc Snapper, for reading this dissertation and for helpful discussions and feedback. The Liu research group has been extremely supportive, and no one could ask for better co-workers. I am indebted to Zhiqiang Liu and Jon Marshall for working closely with me on the synthesis of BN polyaromatic compounds. I am especially grateful to Zachary Giustra, with whom I have had the pleasure of writing a review article and who is always a great sounding board for ideas. Our materials subgroup, especially Andrew Baggett, Zhiqiang Liu, and Cameron McConnell, has been instrumental in shaping this research. Alec Brown never failed to give his honest and often helpful opinion, and Rich Burford inspired me with his critical reading of the literature and his regular five day, 60 hour work week. Lifeng Chen was an unusually inquisitive undergraduate who helped pave the way for some of this thesis, and I am confident one day he'll become a great physician and researcher. Professor Byers welcomed the Liu group to BC by inviting us to take part in his literature and mechanism meetings. Professor Larry Scott first introduced me to the world of novel aromatic compounds first in his organic chemistry course, and next in his research group. I also thank my mentors in the Scott lab, Natalie Smith and Eric Fort for taking a personal interest in my success. A big thank you also goes out to the staff who support our work. Thanks especially to Lynne Pflaumer and Dale Mahoney for helping me through graduate school. I am also grateful for my time at the University of Oregon. I thank my rotation advisers and former committee members Professors Mike Haley and Dave Tyler who provided a wider insight to the larger world of chemistry. I always think fondly of "brainstorming sessions" at Sixteen Tons in Eugene, Oregon with Gabe Rudebusch, Jon Marshall, and Alex Kendall. I strive to be like the wonderful, loving Dr. Breanna Zerfas, who has never failed to comfort me in trying times, to celebrate with me when fortune strikes, and to be there for me always. I couldn't have even begun learning anything without the steadfast support of my mother, who is the strongest person I know. Finally, I thank the LaMattina family for its funding of graduate researchers in this department.

List of Abbreviations

AB	Ammonia borane	KIE	Kinetic isotope effect
CBN	carbon-boron-nitrogen (containing heterocycle)	LUMO	Lowest unoccupied molecular orbital
Cp	Cyclopentadienyl	NICS	Nucleus-independent chemical shift
DART	Direct Analysis in Real Time	NMO	N-methylmorpholine- N-oxide
DDQ	2,3-dichloro-4,5- dicyanobenzoquinone	NMR	Nuclear magnetic resonance
DMSO	Dimethylsulfoxide	ODCB	ortho-dichlorobenzene
DPPA	Diphenyl(phosphoryl)azide	OFET	Organic field-effect transistor
e.u.	Entropy units	OLED	Organic light-emitting diode
ESP	Electrostatic potential	PAH	Polycyclic aromatic hydrocarbon
FMO	Frontier molecular orbital	PTFE	Polytetrafluoroethylene
G	Gibbs free energy	RCM	Ring-closing metathesis
h	Heptet (NMR)	RSE	Resonance stabilization energy
H	Enthalpy	S	Entropy
HMBC	Heteronuclear multiple-bond correlation	THF	Tetrahydrofuran
HOMO	Highest occupied molecular orbital	TIPS	Tri-isopropylsilyl
HRMS	High-resolution mass spectrometry	TOF	Turn-over frequency
HSQC	Heteronuclear single-quantum correlation	TON	Turn-over number
IR	Infrared	UV	Ultraviolet
KHMDS	Potassium hexamethyldisilazide		

TABLE OF CONTENTS

Chapter 1: BN Isosteres of Acenes

1.1 Introduction: Acenes as Materials for Organic Optoelectronics.....	1
1.2 Introduction: BN/CC Isosterism and BN Polyaromatic Compounds	10
1.3 Two BN Isosteres of Anthracene: Synthesis and Characterization	19
1.3.1 Synthesis of BN Anthracenes	20
1.3.2 Optoelectronic Properties of BN-1,2-Anthracenes	21
1.3.3 Reactivity Survey	25
1.3.4 Conclusions.....	28
1.3.5 Experimental Section	29
1.4 BN Tetracene	84
1.4.1 Synthesis of Substituted BN Tetracene.....	85
1.4.2 Synthesis of All-Carbon 2-Butyltetracene	88
1.4.3 Optoelectronic Properties of BN Tetracene	89
1.4.4 Conclusions.....	93
1.4.5 Experimental Section	94
1.5 Predictive Trends for the Optoelectronic Properties of BN Acenes	151
1.5.1 Introduction: Isomerism of BN Isosteres of PAHs	151
1.5.2 Synthesis of BN-9,1-Naph	154
1.5.3 Single-Crystal X-Ray analysis of BN-1,9-Naphthalenes.....	155
1.5.4 Optoelectronic Property Comparison of BN Naphthalenes.....	158
1.5.5 Conclusion and General Principles of BN Acene Orbital Energies	161
1.5.6 Experimental Section	167
1.6 Application of the General Principles of BN Acene Orbital Energetics	218

1.6.1 Background: Borenium-Intermediated Annulation Reactions.....	218
1.6.2 Synthesis of BN-9a,9-Anthracenes for Optical Application.....	220
1.6.3 Single-Crystal X-Ray Analysis.....	223
1.6.4 Optoelectronic Properties of BN-9a-9-Anthracenes.....	224
1.6.5 Periphery Modification Guided by Theory.....	228
1.6.6 Conclusion	233
1.6.7 Experimental Section.....	233

Chapter 2: The Aromatic Claisen Rearrangement of Azaborines

2.1 Introduction.....	273
2.2 Results: Synthesis of Substrates	282
2.3 Results: Regioselectivity of the Azaboryl Claisen Rearrangement.....	284
2.4 Results: Kinetic Comparison	286
2.5 Discussion.....	287
2.6 Summary.....	292
2.7 Experimental Section.....	293

Appendix

A.1 Purpose.....	330
A.2.1 Introduction: Azaborine Synthesis by Dehydrogenation	330
A.2.2 Introduction: Iridium-Catalyzed Transfer Dehydrogenation	332
A.2.3 Results: Screening.....	335
A.2.4 Results: Scope	338
A.2.5 Conclusion	339
A.2.6 Experimental Section	340

A.3 Introduction: Saturated BN Heterocycles for Hydrogen Storage	356
A.3.1 Synthesis of Compound D	357
A.3.2 Synthetic Process Optimization of Compound B and Fuel Cell Testing.....	358
A.3.3 Experimental Section	364

Chapter 1

BN Isosteres of Acenes

1.1 Introduction: Acenes as Materials for Organic Optoelectronics

Acenes (Figure 1.1) are linearly benzofused polycyclic aromatic hydrocarbons (PAHs) for which it is possible to draw only one complete Kekulé sextet.¹ In contrast, for PAHs containing non-linear fusion (such as phenanthrene, chrysene, and pyrene) it is possible to draw structures containing multiple Kekulé sextets. Since Kekulé sextets would serve to localize electrons, the fewer Kekulé sextets, the more electronic delocalization may be expected.

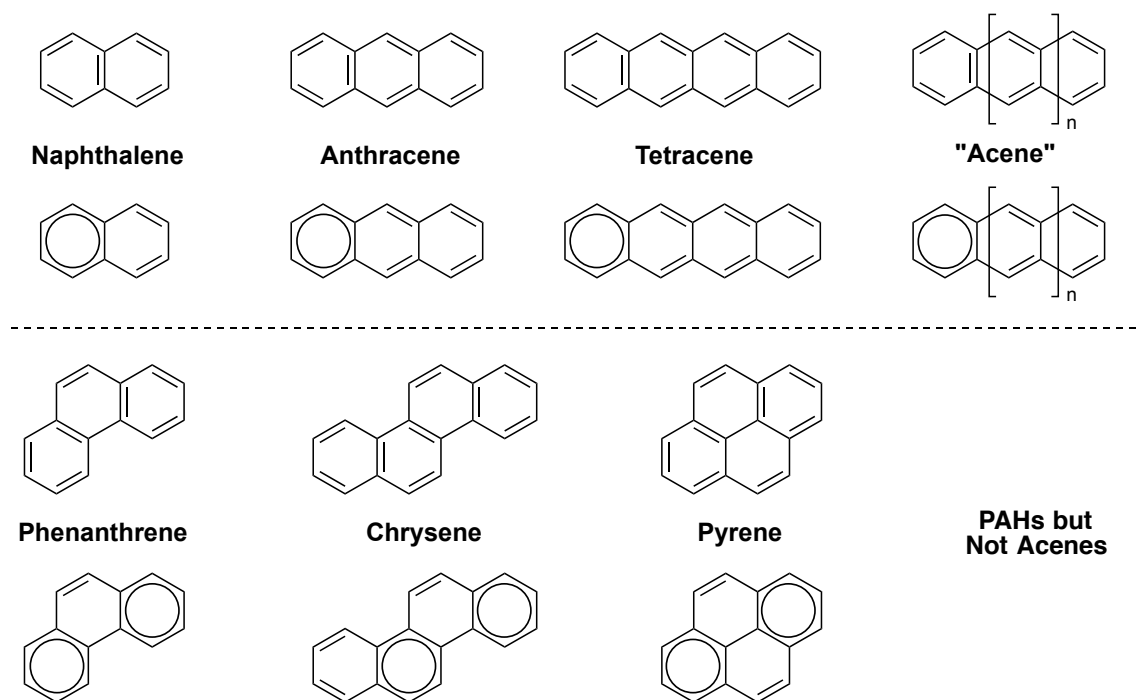


Figure 1.1: Kekulé structures of acenes (top) vs. other PAHs (bottom)

¹ Harvey, R. G. *Polycyclic Aromatic Hydrocarbons*; Wiley-VCH: Chicago, 1997.

The electronic delocalization in acenes can give rise to semiconducting or optical properties that place acenes at the forefront of organic-based optoelectronics research.² Organic-based optoelectronic materials are being explored because of their potential to be more cheaply processed using solution-based methods than traditional inorganic materials, which usually require high-energy methods for deposition.³ Acenes-based structures may be used as semiconducting material in organic-field effect transistors, where they may outperform of the benchmark inorganic semiconductor, amorphous silicon (hole mobility as high as $43 \text{ cm}^2 \text{ V}^{-1} \text{ s}^{-1}$ for rubrene versus $0.5 \text{ cm}^2 \text{ V}^{-1} \text{ s}^{-1}$ for amorphous silicon).⁴ Acenes may also be used as a component in the emissive layer of polymeric organic light-emitting diodes (OLEDs).⁵ Acenes are also known for their ability to perform singlet fission, and this is useful in creating multiple excitons for more efficient organic-based solar cells.⁶

Synthesis, reactivity, electronic structure, and applications of acenes are intimately intertwined. Classically, higher acenes were synthesized by assembling smaller, more oxidized building blocks and subsequently manipulating oxidation states. For example, Fieser's 1931 study of tetracene as a reduction product of tetracenequinone began with the double Friedel-Crafts acylation of tetralin with phthalic anhydride

² For reviews see: (a) Anthony, J. E. *Chem. Rev.* **2006**, *106*, 5028–5048. (b) Anthony, J. E. *Angew. Chem. Int. Ed.* **2008**, *47*, 452–483.

³ Yamashita, Y. *Sci. Technol. Adv. Mater.* **2009**, *10*, 024313.

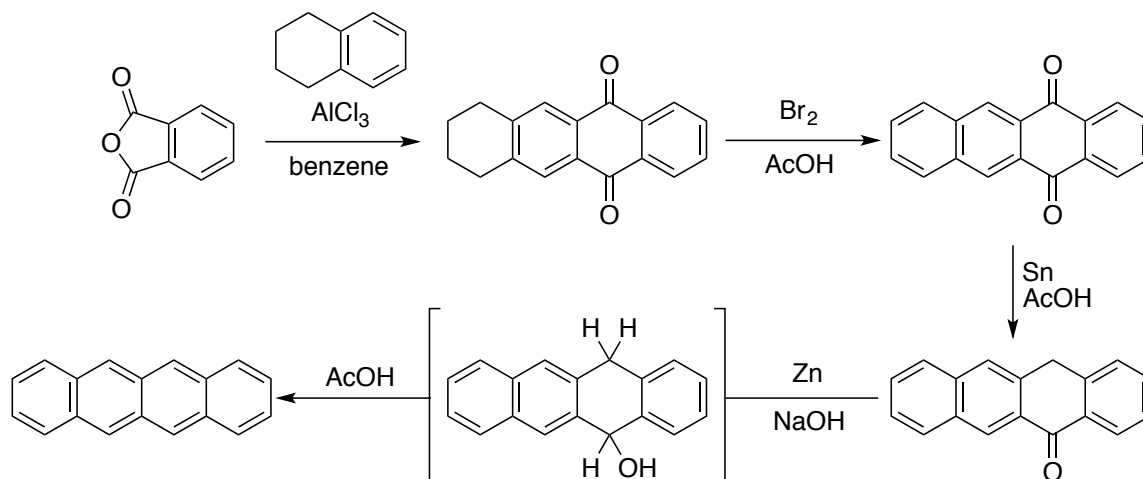
⁴ Yamagishi, M.; Takeya, J.; Tominari, Y.; Nakazawa, Y.; Kuroda, T.; Ikehata, S.; Uno, M.; Nishikawa, T.; Kawase, T. *Appl. Phys. Lett.* **2007**, *90*, 2005–2008.

⁵ Tokito, S.; Weifurtner, K.-H.; Fujikawa, H.; Tsutsui, T.; Taga, Y. *Proc. SPIE Organic Light-Emitting Materials and Devices IV*; **2001**, *4105*, 69–74.

⁶ For a review see: (a) Smith, M. B.; Michl, J. *Chem. Rev.* **2010**, *110*, 6891–6936. For recent studies on singlet fission see: (b) Zimmerman, P. M.; Bell, F.; Casanova, D.; Head-Gordon, M. *J. Am. Chem. Soc.* **2011**, *133*, 19944–19952. (c) Burdett, J. J.; Bardeen, C. J. *J. Am. Chem. Soc.* **2012**, *134*, 8597–8607. (d) Congreve, D. N.; Lee, J.; Thompson, N. J.; Hontz, E.; Yost, S. R.; Reuswig, P. D.; Bahlke, M. E.; Reineke, S.; Van Voorhis, T.; Baldo, M. A. *Science* **2013**, *340*, 334–337.

(Scheme 1.1).⁷ Fieser oxidized the remaining saturated ring with bromine. The oxygenated ring was reduced using tin in acetic acid, then with zinc in alkaline solution, followed by dehydration with acetic acid. As an alternative, Rickborn has shown that lithium aluminum hydride may be used as the final reducing agent in place of zinc.⁸

Scheme 1.1. Fieser's Synthesis of Tetracene



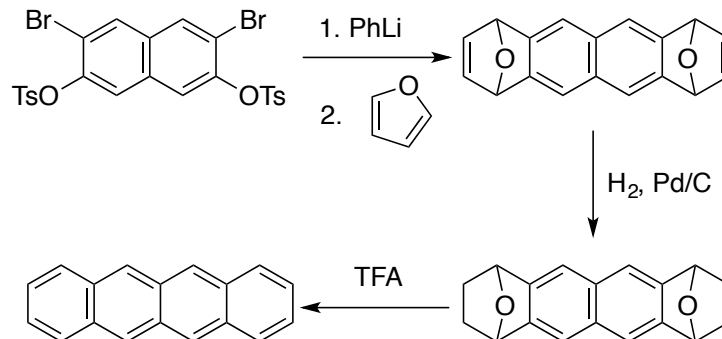
Gribble demonstrated another iconic acene synthesis in 1985 that involved the Diels-Alder reaction of arynes with furans.⁹ Arynes based on naphthalene can be generated using phenyllithium and 2,7-dibromo-3,6-ditosyl(oxy)naphthalene (Scheme 1.2). Treatment of this mixture with furan can generate oxabicyclic species that are hydrogenated to the correct oxidation state and dehydrated to obtain tetracene.

⁷ Fieser, L. F. *J. Am. Chem. Soc.* **1931**, 53, 2329–2341.

⁸ Netka, J.; Crump, S. L.; Rickborn, B. *J. Org. Chem.* **1986**, 51, 1189–1199.

⁹ Gribble, G. W.; Perni, R. B.; Onan, K. D. *J. Org. Chem.* **1985**, 50, 2934–2939.

Scheme 1.2. Gribble's Synthesis of Tetracene



The organic chemistry of acenes investigated in the early 20th century hints at their potential in 21st century optoelectronic applications. It is obvious from these synthetic examples that redox states of the acene topology can be manipulated quite easily. From what we now know to be a first approximation, Clar hypothesized that the large level of electronic delocalization present in longer (poly)acenes results from the absence of many Kekulé sextets (which would serve to localize six electrons in a single ring).¹⁰ Energetically, this delocalization can be observed as HOMO energies rise and LUMO energies fall with acene length (Figure 1.2)¹¹; these orbital energetics are commensurate with the increased reactivity of higher acenes.

¹⁰ Bendikov, M.; Wudl, F.; Perepichka, D. F. *Chem. Rev.* **2004**, *104*, 4891–946.

¹¹ For reviews on acene structure and electronics see: (a) Zade, S. S.; Bendikov, M. *J. Phys. Org. Chem.* **2012**, *25*, 452–461. (b) Bettinger, H. F. *Pure Appl. Chem.* **2010**, *82*, 905–915.

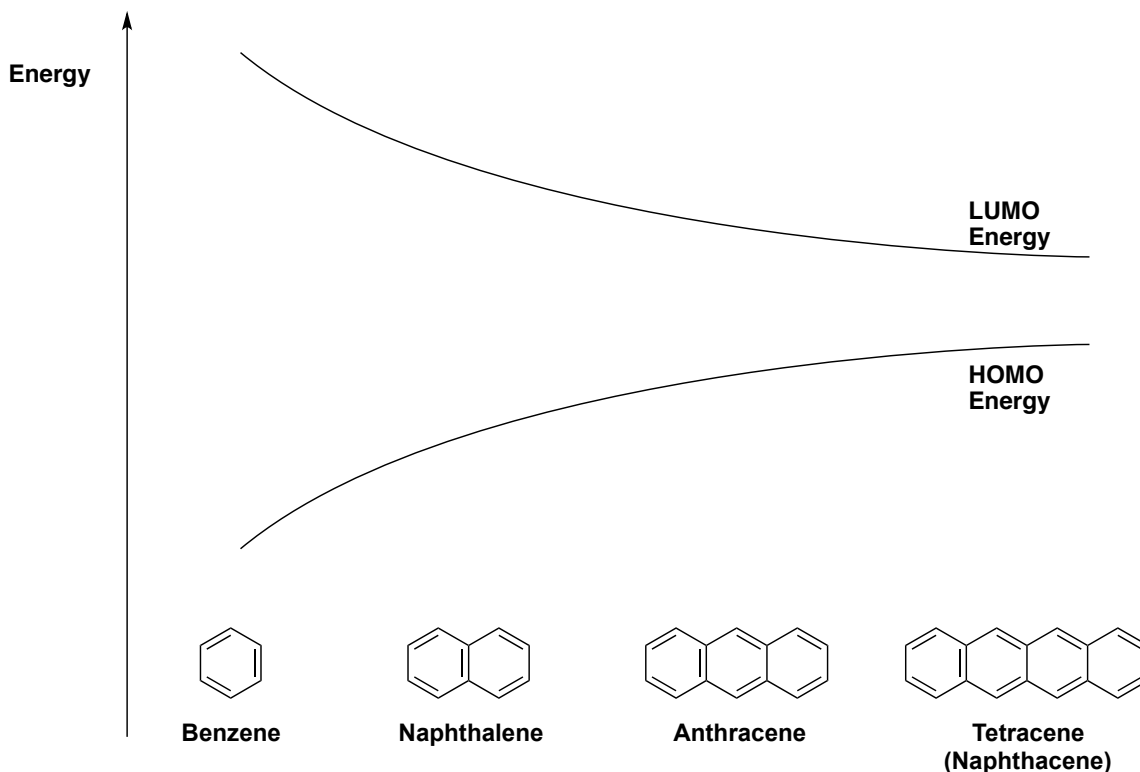


Figure 1.2. Acenes and a schematic of their HOMO and LUMO energies.

While naphthalene and anthracene are available on large commercial scale as a result of being readily isolable from natural sources or resulting from facile synthesis using cheap feedstock chemicals, the instability—and more complex synthesis—of higher acenes tetracene and pentacene are concomitant with their lower availability. Unsubstituted, or “parent” hexacene has only recently been isolated by Chow¹², while parent heptacene and higher parent acenes have only been observed using gas matrices, most notably by Bettinger.¹³ Miller and Anthony showed that nonacene (nine fused rings) must be synthesized with substitution on the apical positions for added stability.¹⁴

¹² Watanabe, M.; Chang, Y. J.; Liu, S.-W.; Chao, T.-H.; Goto, K.; Islam, M. M.; Yuan, C.-H.; Tao, Y.-T.; Shinmyozu, T.; Chow, T. J. *Nat. Chem.* **2012**, *4*, 574–578.

¹³ Mondal, R.; Tönshoff, C.; Khon, D.; Neckers, D. C.; Bettinger, H. F. *J. Am. Chem. Soc.* **2009**, *131*, 14281–14289. (b) Tönshoff, C.; Bettinger, H. F. *Angew. Chem. Int. Ed.* **2010**, *49*, 4125–4128.

¹⁴ (a) Kaur, I.; Jazdyk, M.; Stein, N. N.; Prusevich, P.; Miller, G. P. *J. Am. Chem. Soc.* **2010**, *132*, 1261–1263. (b) Purushothaman, B.; Bruzek, M.; Parkin, S. R.; Miller, A. F.; Anthony, J. E. *Angew. Chem. Int. Ed.* **2011**, *50*, 7013–7017.

It is the smaller HOMO-LUMO gaps of higher acenes that ultimately give rise to their applications in organic optoelectronic devices. In analogy to the band theory of solids, conjugated organic molecules such as acenes can display semiconducting properties; the LUMO is a simile for the conduction band, while the HOMO is a simile for the valence band.¹⁵ When an acene becomes of appropriate length (the fourth fused ring, or tetracene), the HOMO-LUMO gap has an energy (about 2–3 eV) that is useful for semiconducting or optical applications involving visible light.² Many factors govern device performance, such as device architecture, substrate and conducting contact smoothness, and fabrication method.¹⁶ While these factors are unlikely to be influenced by molecular design and thus cannot be changed by the synthetic organic chemist, other performance contributors can be controlled by the physical and electronic structure of the constituent molecules and thus may be tailored through synthesis.

Intermolecular packing orientation is important to charge transport efficiency through the solid system.¹⁷ Charge-carrying capability is maximized by face-to-face interactions at a close distance with minimal displacement in either the short or long axis of the acene. Charge-carrying ability decreases with increasing distance between the crystal's constituent acene molecules, but is sinusoidal with respect to displacement along the acene's long axis, as orbital overlap between constituent molecules is actually the key driver behind high charge mobility. This behavior is similar with short-axis displacement, but charge-carrying ability drops off as parallel acenes begin to make an angle to one

¹⁵ Haddon, R. C.; Chi, X.; Itkis, M. E.; Anthony, J. E.; Eaton, D. L.; Siegrist, T.; Mattheus, C. C.; Palstra, T. T. M. *J. Phys. Chem. B* **2002**, *106*, 8288–8292.

¹⁶ (a) Klauk, H.; Zschieschang, U.; Weitz, R. T. T.; Meng, H.; Sun, F.; Nunes, G.; Keys, D. E. E.; Fincher, C. R. R.; Xiang, Z. *Adv. Mater.* **2007**, *19*, 3882–3887. (b) Allard, S.; Forster, M.; Souharce, B.; Thiem, H.; Scherf, U. *Angew. Chem. Int. Ed.* **2008**, *47*, 4070–4098. (c) Jurchescu, O. D.; Baas, J.; Palstra, T. T. M. *Appl. Phys. Lett.* **2004**, *84*, 3061–3063.

¹⁷ Wang, C.; Dong, H.; Hu, W.; Liu, Y.; Zhu, D. *Chem. Rev.* **2012**, *112*, 2208–2267.

another.¹⁸ A two-dimensional “brickwork” motif (Figure 1.3) thus maximizes face-to-face π -stacking and charge mobility.^{18b} However, the brickwork motif is not observed in parent acenes; instead, the “herringbone” motif, which features edge-to-face packing, is observed.^{2a} Consistent with these observations, Sherill’s computational study of benzene dimers predicted edge-to-face interactions are favored by about 1 kcal/mol with respect to the “sandwich” face-to-face dimer.¹⁹

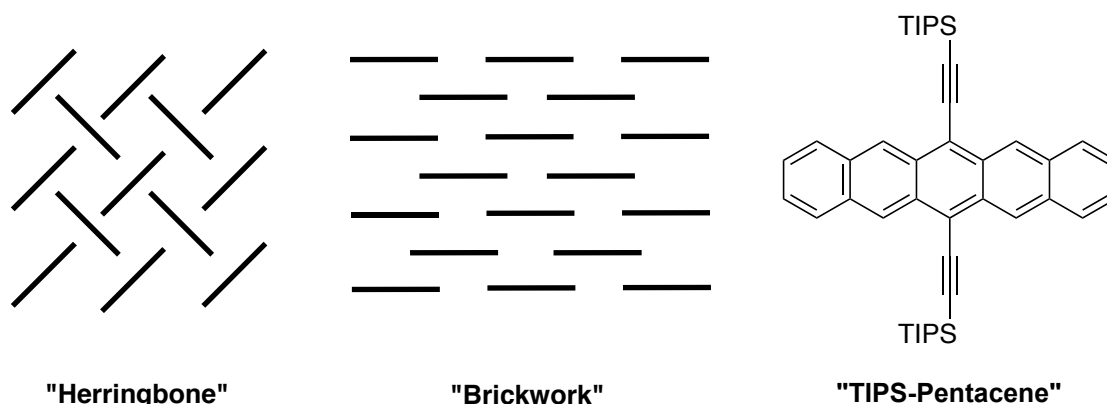


Figure 1.3. Typical packing motifs and the “benchmark” TIPS-Pentacene

Although the herringbone motif exhibits some π -orbital overlap among the constituent molecules and can give rise to working organic semiconductors, molecular engineering can be applied to enforce a brickwork crystal structure for better charge transport. Substituting apical positions can enforce a brickwork motif by sterically blocking the edge-to-face interactions. For example, Anthony showed that TIPS-ethynyl modified pentacene (“TIPS-Pentacene”) packs in a brickwork motif resulting from the

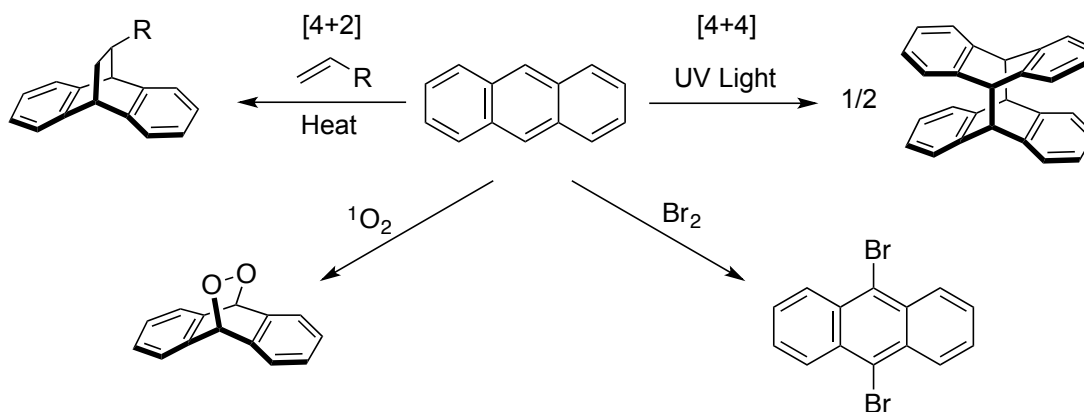
¹⁸ (a) Curtis, M. D.; Cao, J.; Kampf, J. W. *J. Am. Chem. Soc.* **2004**, *126*, 4318–4328. (b) Dong, H.; Fu, X.; Liu, J.; Wang, Z.; Hu, W. *Adv. Mater.* **2013**, *25*, 6158–6183.

¹⁹ Sinnokrot, M. O.; Valeev, E. F.; Sherrill, C. D. *J. Am. Chem. Soc.* **2002**, *124*, 10887–10893.

large blocking groups.²⁰ As a result, high hole mobility can be realized in organic field-effect transistors (OFETs) utilizing TIPS-pentacene as the organic semiconductor.²¹

One other factor in materials design over which the synthetic organic chemist has control is electronic structure. Judicious use of substituents can tune the electronic structure. Acenes are prone to cycloaddition,²² electrophilic substitution reactions,²³ and oxidation²⁴ at apical positions (Scheme 1.3), so modifying these sites also creates greater chemical stability and thus create a stable device. In the example of the TIPS-pentacene, the electron-withdrawing alkynes thermodynamically disfavor the most reactive site from deleterious cycloaddition and oxidation reactions; additionally, the large pendant silyl groups sterically block reaction at the apical sites.²⁵

Scheme 1.3. Typical reactivity of acenes



Replacing skeletal acene carbons with heteroatoms is an emerging strategy to modify the electronics of a given framework without changing its physical footprint. For

²⁰ (a) Anthony, J. E.; Brooks, J. S.; Eaton, D. L.; Parkin, S. R. *J. Am. Chem. Soc.* **2001**, *123*, 9482–9483. (b) Anthony, J. E.; Eaton, D. L.; Parkin, S. R. *Org. Lett.* **2002**, *4*, 15–18.

²¹ Giri, G.; Verploegen, E.; Mannsfeld, S. C. B.; Atahan-Evrenk, S.; Kim, D. H.; Lee, S. Y.; Becerril, H. a.; Aspuru-Guzik, A.; Toney, M. F.; Bao, Z. *Nature* **2011**, *480*, 504–508.

²² Diels-Alder reactions: Yates, P.; Eaton, P. *J. Am. Chem. Soc.* **1960**, *82*, 4436–4437.

²³ For example, bromination: Heilbron, I. M.; Heaton, J. S. *Org. Synth.* **1923**, *3*, 41.

²⁴ Bender, P.; Farber, J. *J. Am. Chem. Soc.* **1952**, *74*, 1450–1452.

²⁵ Kaur, I.; Jia, W.; Kopreski, R. P.; Selvarasah, S.; Dokmeci, M. R.; Pramanik, C.; McGruer, N. E.; Miller, G. P. *J. Am. Chem. Soc.* **2008**, *130*, 16274–16286.

example, Bunz synthesized a series of TIPS-ethynylated aza-pentacene in analogy to Anthony's work and found that both HOMO and LUMO levels were lowered in comparison to the carbonaceous analogues (Figure 1.4).²⁶ Additionally, nitrogenous compounds showed similar brickwork packing to Anthony's TIPS-Pentacene. Higher azaacenes can also be synthesized, with the presence of heteroaromatic rings and the TIPS-ethynyl groups preventing cycloaddition and oxidation reactions.²⁷ Thiophene-fused acenes generally have lower HOMO-LUMO gaps as estimated by UV-visible absorption with respect to all-carbon analogues; the source of this difference was the fact that the thiophene-fused species had lower LUMO energies.²⁸ Boron-doped acenes may also be synthesized, leading to more diversity among heteroacene structures.²⁹ In a similar vein of creating electronic and structural diversity using an atom-replacement strategy, we chose to enter the field of organic optoelectronic materials by replacing carbon-carbon units with isoelectronic and isostructural boron-nitrogen units.

²⁶ Tverskoy, O.; Rominger, F.; Peters, A.; Himmel, H.-J.; Bunz, U. H. F. *Angew. Chem. Int. Ed.* **2011**, *50*, 3557–3560.

²⁷ (a) Lindner, B. D.; Engelhart, J. U.; Tverskoy, O.; Appleton, A. L.; Rominger, F.; Peters, A.; Himmel, H.-J.; Bunz, U. H. F. *Angew. Chem. Int. Ed.* **2011**, *50*, 8588–8591. (b) Bunz, U. H. F.; Engelhart, J. U.; Lindner, B. D.; Schaffroth, M. *Angew. Chem. Int. Ed.* **2013**, *52*, 3810–3821. (c) Engelhart, J. U.; Lindner, B. D.; Tverskoy, O.; Rominger, F.; Bunz, U. H. F. *Chem. Eur. J.* **2013**, *19*, 15089–15092.

²⁸ (a) Lehnher, D.; Waterloo, A. R.; Goetz, K. P.; Payne, M. M.; Hampel, F.; Anthony, J. E.; Jurchescu, O. D.; Tykwinski, R. R. *Org. Lett.* **2012**, *14*, 3660–3663. (b) Zhang, J.; Smith, Z. C.; Thomas, S. W., III *J. Org. Chem.* **2014**, *79*, 10081–10093.

²⁹ (a) Chen, J.; Kampf, J. W.; Ashe, A. J., III *Organometallics* **2008**, *27*, 3639–3641. (b) Hoffend, C.; Schödel, F.; Bolte, M.; Lerner, H. W.; Wagner, M. *Chem. Eur. J.* **2012**, *18*, 15394–15405. (c) John, A.; Bolte, M.; Lerner, H.; Wagner, M. *Angew. Chem. Int. Ed.* **2017**, *56*, 5588–5592.

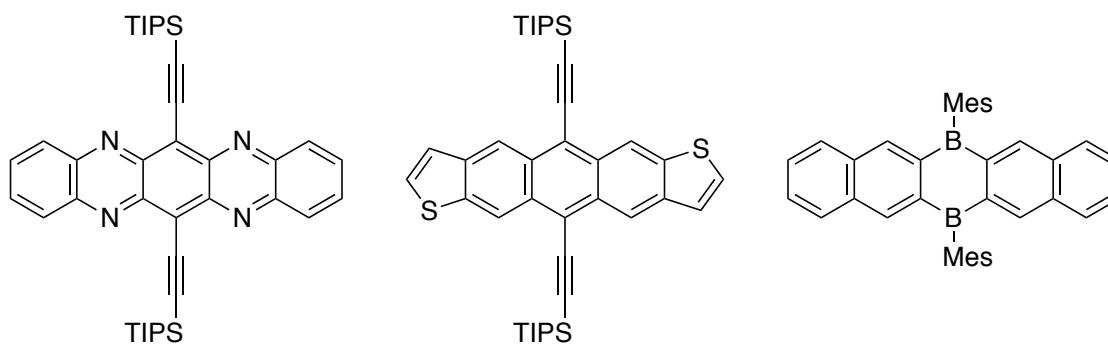


Figure 1.4. Examples of heteroatom-doped acenes

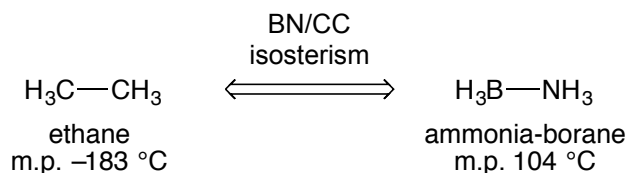
1.2 Introduction: BN/CC Isosterism and BN Polyaromatic Compounds

Replacement of a CC unit with a BN unit in an organic compound can lead to dramatically different properties of the BN-containing compound relative to the all-carbon analogue.³⁰ An instructive example of the potential differences between an organic molecule and its BN isostere is also the simplest: the isosteric pair of ethane and ammonia borane (Figure 1.5a). While ethane is a gas at room temperature, ammonia borane, with its polarized boron-nitrogen dative bond, is a high-melting (m. p. = 104 °C) solid. Furthermore, ethane has an endothermic heat of dehydrogenation, while ammonia borane, with its exothermic heat of dehydrogenation, has been widely investigated for its potential as a chemical hydrogen store.³¹

³⁰ Liu, Z.; Marder, T. B. *Angew. Chem. Int. Ed.* **2008**, *47*, 242–244.

³¹ Staubitz, A.; Robertson, A. P. M.; Manners, I. *Chem. Rev.* **2010**, *110*, 4079–4124.

a.



b.

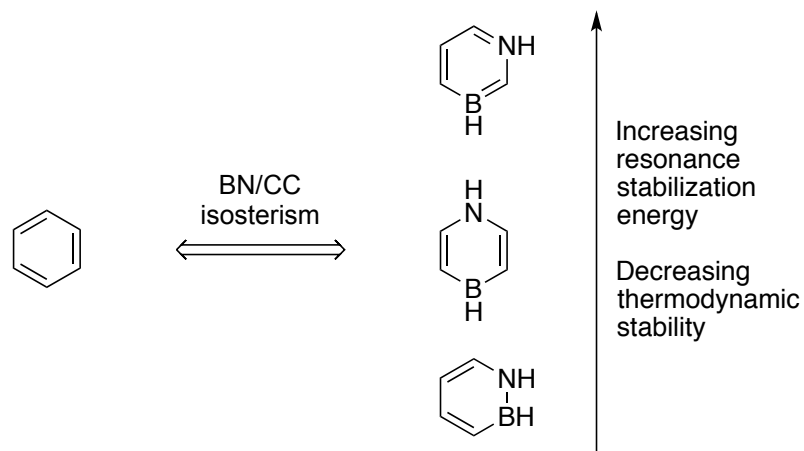


Figure 1.5. BN/CC isosterism in a) ethane/ammonia-borane; b) benzene/azaborines

In aromatic compounds, BN/CC isosterism can similarly produce properties divergent of the all-carbon analogue without significantly perturbing the spatial imprint of the molecule.³² There are three isomers of a 6-membered arene containing a single BN unit (Figure 1.5b), and derivatives of all three of these “azaborines” have been rationally synthesized and experimentally characterized.³³ While the first azaborine was synthesized by Dewar in 1958,³⁴ the modern interest in azaborines can be traced to the work of Ashe

³² Bosdet, M. J. ; Piers, W. E. *Can. J. Chem.* **2009**, *87*, 8–29.

³³ Monocyclic examples: 1,2-azaborine: (a) Marwitz, A. J. V; Matus, M. H.; Zakharov, L. N.; Dixon, D. A.; Liu, S.-Y. *Angew. Chem. Int. Ed.* **2009**, *48*, 973–977. 1,3-azaborine: (b) Xu, S.; Zakharov, L. N.; Liu, S.-Y. *J. Am. Chem. Soc.* **2011**, *133*, 20152–20155. (c) Xu, S.; Mikulas, T. C.; Zakharov, L. N.; Dixon, D. A.; Liu, S.-Y. *Angew. Chem. Int. Ed.* **2013**, *52*, 7527–7531. 1,4-azaborine: (d) Braunschweig, H.; Damme, A.; Jimenez-Halla, J. O. C.; Pfaffinger, B.; Radacki, K.; Wolf, J. *Angew. Chem. Int. Ed.* **2012**, *51*, 10034–10037. (e) Liu, X.; Zhang, Y.; Li, B.; Zakharov, L. N.; Vasiliu, M.; Dixon, D. A.; Liu, S.-Y. *Angew. Chem. Int. Ed.* **2016**, *55*, 8333–8337.

³⁴ Dewar, M. J. S.; Kubba, V. P.; Pettit, R. *J. Chem. Soc.* **1958**, 3073–3076.

who used ring-closing olefin metathesis to modernize the synthesis of azaborines.³⁵ For the sake of brevity and to focus the discussion, this introduction will encompass only azaborines where the boron and nitrogen atoms are directly bound (1,2-azaborines).³⁶

In the past decade, our group and others have developed the chemistry of 1,2-azaborines.³⁷ From a fundamental standpoint, our group and the group of Ashe have experimentally characterized the aromaticity of azaborine using structural, energetic, and reactivity-based metrics.³⁸ The increased polarity of the parent 1,2-azaborine vs. benzene was observed using Reichardt's betaine dye.^{36b} The polarization of the N–H and B–H bonds in the 1,2-azaborine parent leads to very organized behavior on copper surfaces.³⁹ In biomedical applications, we have demonstrated structurally similar binding in an engineered T4-lysozyme with respect to the all-carbon analogues⁴⁰; we have furthermore quantified binding of azaborines in these T4-lysozymes to be energetically favored by hydrogen bonding interactions to the protein.⁴¹ The ability to engage in hydrogen bonding and the increased polarity of azaborine vs. benzene may lead to increased solubility and efficacy of some azaborine-based druglike molecules vs. the all-carbon

³⁵ Ashe, A. J., III; Fang, X. *Org. Lett.* **2000**, *14*, 2089–2091.

³⁶ Isolation of the parent: (a) Marwitz, A. J. V; Matus, M. H.; Zakharov, L. N.; Dixon, D. A.; Liu, S.-Y. *Angew. Chem. Int. Ed.* **2009**, *48*, 973–977. Further characterization: (b) Abbey, E. R.; Lamm, A. N.; Baggett, A. W.; Zakharov, L. N.; Liu, S.-Y. *J. Am. Chem. Soc.* **2013**, *135*, 12908–12913.

³⁷ For an overview see: Campbell, P. G.; Marwitz, A. J. V; Liu, S.-Y. *Angew. Chem. Int. Ed.* **2012**, *51*, 6074–6092.

³⁸ Planarization and bond homogenization: (a) Abbey, E. R.; Zakharov, L. N.; Liu, S.-Y. *J. Am. Chem. Soc.* **2008**, *130*, 7250–7252. Resonance stabilization energy: (b) Campbell, P. G.; Abbey, E. R.; Neiner, D.; Grant, D. J.; Dixon, D. A.; Liu, S.-Y. *J. Am. Chem. Soc.* **2010**, *132*, 18048–18050. Electrophilic aromatic substitution: (c) Pan, J.; Kampf, J. W.; Ashe, A. J., III *Org. Lett.* **2007**, *9*, 679–681.

³⁹ (a) Murphy, C. J.; Baggett, A. W.; Miller, D. P.; Simpson, S.; Marcinkowski, M. D.; Mattera, M. F. G.; Pronschinske, A.; Therrien, A.; Liriano, M. L.; Zurek, E.; Liu, S.-Y.; Sykes, E. C. H. *J. Phys. Chem. C* **2015**, *119*, 14624–14631. (b) Murphy, C. J.; Miller, D. P.; Simpson, S.; Baggett, A.; Pronschinske, A.; Liriano, M. L.; Therrien, A. J.; Enders, A.; Liu, S.-Y.; Zurek, E.; Sykes, E. C. H. *J. Phys. Chem. C* **2016**, *120*, 6020–6030.

⁴⁰ Liu, L.; Marwitz, A. J. V; Matthews, B. W.; Liu, S.-Y. *Angew. Chem. Int. Ed.* **2009**, *48*, 6817–6819.

⁴¹ Lee, H.; Fischer, M.; Shoichet, B. K.; Liu, S.-Y. *J. Am. Chem. Soc.* **2016**, *138*, 12021–12024.

analogues.⁴² We have also observed divergent activity (inhibition for BN-ethylbenzenes as opposed to turnover) in ethylbenzene dehydrogenase.⁴³

Ring-fused azaborines can also be synthesized. While there are numerous examples of materials containing a tetracoordinate boron atom with a boron-nitrogen dative bond, these materials are beyond the scope of this introduction.⁴⁴ Instead, this introduction will summarize the state of the art in BN-containing polycyclic aromatic compounds. Due to the relative ease of access and the potential utility of BN-containing polycyclic aromatic compounds in optoelectronic devices, there are many more examples of these compounds than there are of the unfused azaborines previously discussed.⁴⁵ In fact, the first 1,2-azaborine ever synthesized by Dewar was an isostere of phenanthrene.³⁴ The BN isostere had a hypsochromically shifted absorption onset with respect to the all-carbon analogue. Dewar quickly followed this result with the syntheses of BN-1,2-naphthalene (1959)⁴⁶, BN-9,10-naphthalene (1968)⁴⁷, and a slew of various other BN-containing polyaromatic systems (Figure 1.6).⁴⁸

⁴² Zhao, P.; Nettleton, D. O.; Karki, R. G.; Zécari, F. J.; Liu, S.-Y. *ChemMedChem* **2017**, *12*, 358–361.

⁴³ Knack, D. H.; Marshall, J. L.; Harlow, G. P.; Dudzik, A.; Szaleniec, M.; Liu, S.-Y.; Heider, J. *Angew. Chem. Int. Ed.* **2013**, *52*, 2599–2601.

⁴⁴ These systems use boron largely as a bridging, 4-coordinate element, and conjugation necessarily cannot extend through boron. Recent examples: (a) Zhu, C.; Guo, Z.-H.; Mu, A. U.; Liu, Y.; Wheeler, S. E.; Fang, L. *J. Org. Chem.* **2016**, *81*, 4347–4352. (b) Grandl, M.; Kaese, T.; Krautsieder, A.; Sun, Y.; Pammer, F. *Chem. Eur. J.* **2016**, *22*, 14373–14382.

⁴⁵ Reviews of BN-containing extended π -systems: (a) Wang, X.-Y.; Wang, J.-Y.; Pei, J. *Chem. Eur. J.* **2015**, *21*, 3528–3539. (b) Morgan, M. M.; Piers, W. E. *Dalton Trans.* **2016**, *45*, 5920–5924. (c) Helten, H. *Chem. Eur. J.* **2016**, *22*, 12972–12982.

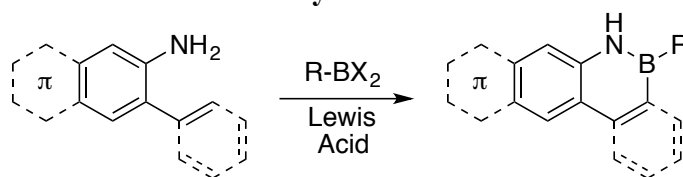
⁴⁶ (a) Dewar, M. J. S.; Dietz, R. *J. Chem. Soc.* **1959**, 2728–2730. (b) Dewar, M. J. S.; Dietz, R. *J. Org. Chem.* **1961**, *26*, 3253–3256.

⁴⁷ Dewar, M. J. S.; Jones, R. *J. Am. Chem. Soc.* **1968**, *90*, 2137–2144.

⁴⁸ Notable examples: (a) Dewar, M. J. S.; Kaneko, C.; Bhattacharjee, M. K. *J. Am. Chem. Soc.* **1962**, *84*, 4884–4887. (b) Dewar, M. J. S.; Poesche, W. H. *J. Am. Chem. Soc.* **1963**, *85*, 2253–2256. (c) Dewar, M. J. S.; Poesche, W. H. *J. Org. Chem.* **1964**, *29*, 1757–1762. (d) Culling, G. C.; Dewar, M. J. S.; Marr, P. A. *J. Am. Chem. Soc.* **1964**, *86*, 1125–1127.

The easiest (from an operational standpoint) synthetic strategy was introduced by Dewar for the synthesis of 9,10-BN-phenanthrene and 1,2-BN-naphthalene and involves electrophilic borylation (Scheme 1.4).

Scheme 1.4: Electrophilic Aromatic Borylation for BN-containing extended π -systems



This general strategy continues on to the modern era with syntheses of BN-1,2-naphthalenes by Molander (Figure 1.6), whose innovation—itsself an extension of Paetzold’s⁴⁹ strategy of using pre-formed organodihaloboranes as boron sources—was using organotrifluoroborates as a convenient boron source for efficiently generating the BN naphthalene core.⁵⁰ Even larger π -systems may be constructed using this type of reactivity. Nakamura and Hatakeyama synthesized and characterized a dibenzochrysene analogue⁵¹, along with some BN-containing helicenes.⁵² Lukoyanova and Perepichka were able to synthesize multiple-thiophene-fused azaborines as precursors for polymeric materials.⁵³ More recently, the Pei group has undertaken efforts toward “BN-heterosuperbenzenes” for which application in organic-based electronics is promising.⁵⁴

⁴⁹ Paetzold, P.; Stanesco, C.; Stubenrauch, J. R.; Bienmüller, M.; Englert, U. *Z. Anorg. Allg. Chem.* **2004**, 630, 2632–2640.

⁵⁰ (a) Wisniewski, S. R.; Guenther, C. L.; Argintaru, O. A.; Molander, G. A. *J. Org. Chem.* **2014**, 79, 365–378. (b) Molander, G. A.; Wisniewski, S. R.; Amani, J. *Org. Lett.* **2014**, 16, 5636–5639. (c) Molander, G. A.; Wisniewski, S. R.; Etemadi-Davan, E. *J. Org. Chem.* **2014**, 79, 11199–11204. (d) Molander, G. A.; Wisniewski, S. R. *J. Org. Chem.* **2014**, 79, 6663–6678.

⁵¹ (a) Hatakeyama, T.; Hashimoto, S.; Seki, S.; Nakamura, M. *J. Am. Chem. Soc.* **2011**, 133, 18614–18617. (b) Hashimoto, S.; Ikuta, T.; Shiren, K.; Nakatsuka, S.; Ni, J.; Nakamura, M.; Hatakeyama, T. *Chem. Mater.* **2014**, 26, 6265–6271.

⁵² Hatakeyama, T.; Hashimoto, S.; Oba, T.; Nakamura, M. *J. Am. Chem. Soc.* **2012**, 134, 19600–19603.

⁵³ Lukoyanova, O.; Lepeltier, M.; Laferrière, M.; Perepichka, D. F. *Macromolecules* **2011**, 44, 4729–4734.

⁵⁴ (a) Wang, X.-Y.; Zhuang, F.-D.; Wang, R.-B.; Wang, X.-C.; Cao, X.-Y.; Wang, J.-Y.; Pei, J. *J. Am. Chem. Soc.* **2014**, 136, 3764–3767. (b) Guo, Z.-H.; Jin, Z.-X.; Wang, J.-Y.; Pei, J. *Chem. Commun.* **2014**, 50, 6088–6090. (c) Wang, X.-Y.; Zhuang, F.-D.; Wang, J.-Y.; Pei, J. *Chem. Commun.* **2015**, 51, 17532–

Cui⁵⁵ and Pei⁵⁶ have constructed heavily substituted BN naphthalene analogues in addition to some tetracyclic BN-containing polycyclic compounds.⁵⁷ Sun and Zhang have shown the promise of an azaborine-fused perylene-bisimide in an OLED emissive layer.⁵⁸ Bettinger has synthesized cyclic (BN)₃ oligomers of Dewar's BN phenanthrene through electrophilic borylation of a borazine precursor.⁵⁹

17535. (d) Wang, X. Y.; Yang, D. C.; Zhuang, F. D.; Liu, J. J.; Wang, J. Y.; Pei, J. *Chem. Eur. J.* **2015**, *21*, 8867–8873.

⁵⁵ Liu, X.; Wu, P.; Li, J.; Cui, C. *J. Org. Chem.* **2015**, *80*, 3737–3744.

⁵⁶ Zhuang, F.-D.; Han, J.-M.; Tang, S.; Yang, J.-H.; Chen, Q.-R.; Wang, J.-Y.; Pei, J. *Organometallics* In Press, DOI: acs.organomet.6b00811.

⁵⁷ (a) Ma, C.; Zhang, J.; Li, J.; Cui, C. *Chem. Commun.* **2015**, *51*, 5732–5734. (b) Huang, H.; Pan, Z.; Cui, C. *Chem. Commun.* **2016**, *52*, 4227–4230.

⁵⁸ Li, G.; Zhao, Y.; Li, J.; Cao, J.; Zhu, J.; Sun, X. W.; Zhang, Q. *J. Org. Chem.* **2015**, *80*, 196–203.

⁵⁹ (a) Biswas, S.; Müller, M.; Tönshoff, C.; Eichele, K.; Maichle-Mössmer, C.; Ruff, A.; Speiser, B.; Bettinger, H. F. *Eur. J. Org. Chem.* **2012**, *2012*, 4634–4639. (b) Müller, M.; Behnle, S.; Maichle-Mössmer, C.; Bettinger, H. F. *Chem. Commun.* **2014**, *50*, 7821–7823. (c) Krieg, M.; Reicherter, F.; Haiss, P.; Ströbele, M.; Eichele, K.; Treanor, M.-J.; Schaub, R.; Bettinger, H. F. *Angew. Chem. Int. Ed.* **2015**, *54*, 8284–8286. (d) Sánchez-Sánchez, C.; Brüller, S.; Sachdev, H.; Müllen, K.; Krieg, M.; Bettinger, H. F.; Nicolai, A.; Meunier, V.; Talirz, L.; Fasel, R.; Ruffieux, P. *ACS Nano* **2015**, *9*, 9228–9235. Further characterization: (e) Dosso, J.; Tasseroul, J.; Fasano, F.; Marinelli, D.; Biot, N.; Fermi, A.; Bonifazi, D. *Angew. Chem. Int. Ed.* **2017**, 4483–4487.

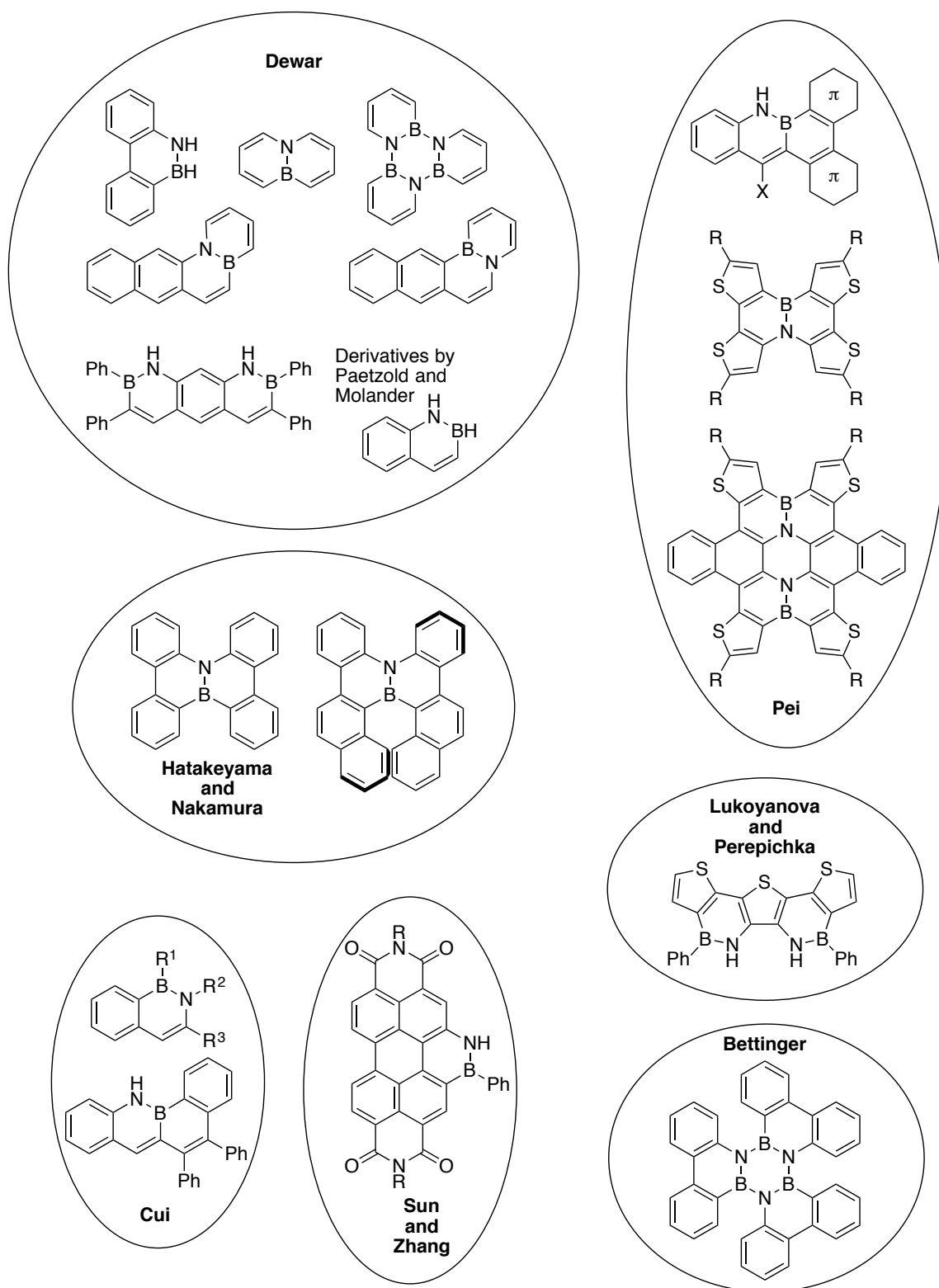
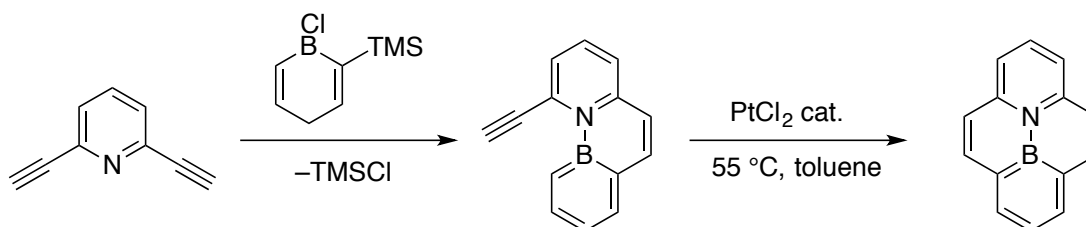


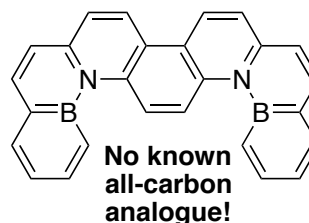
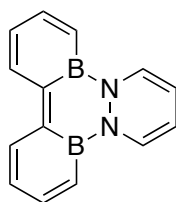
Figure 1.6. Selected examples of BN-containing extended π -systems.

A second strategy involves the separate construction of a boron heterocycle *via* transmetallation of a precursor stannacycle⁶⁰ and linking it to an initially separate nitrogen-containing heterocycle (Scheme 1.5). Piers has synthesized and characterized a number of conjugated systems with internalized BN units using this method.⁶¹ An interesting BN dibenzopicene Piers synthesized has no known all-carbon analogue.⁶²

Scheme 1.5. Piers's Synthetic Strategy



Other Examples:



Miscellaneous other strategies have been used to construct BN-containing extended π -systems. Most notably, Wang initially synthesized a partially saturated BN-heterocycle containing a boron-nitrogen dative bond, and then performed a photoelimination reaction to yield the fully aromatic system (Scheme 1.6).⁶³ Wang has

⁶⁰ (a) Ashe, A. J. III; Shu, P. *J. Am. Chem. Soc.* **1971**, *93*, 1804–1805. (b) Boese, R.; Finke, N.; Henkelmann, J.; Maier, G.; Paetzold, P.; Reisenauer, H. P.; Schmid, G. *Chem. Ber.* **1985**, *118*, 1644–1654. (c) Hoic, D. A.; Wolf, J. R.; Davis, W. M.; Fu, G. C. *Organometallics* **1996**, *15*, 1315–1318.

⁶¹ (a) Examples: Jaska, C. A.; Emslie, D. J. H.; Bosdet, M. J. D.; Piers, W. E.; Sorensen, T. S.; Parvez, M. *J. Am. Chem. Soc.* **2006**, *128*, 10885–10896. (b) Bosdet, M. J. D.; Piers, W. E.; Sorensen, T. S.; Parvez, M. *Angew. Chem. Int. Ed.* **2007**, *46*, 4940–4943. (c) Bosdet, M. J. D.; Jaska, C. A.; Piers, W. E.; Sorensen, T. S.; Parvez, M. *Org. Lett.* **2007**, *9*, 1395–1398 (d) Jaska, C. A.; Piers, W. E.; McDonald, R.; Parvez, M.; Bosdet, M. J. D.; Jaska, C. A.; Piers, W. E.; Sorensen, T. S. *J. Org. Chem.* **2007**, *72*, 5234–5243.

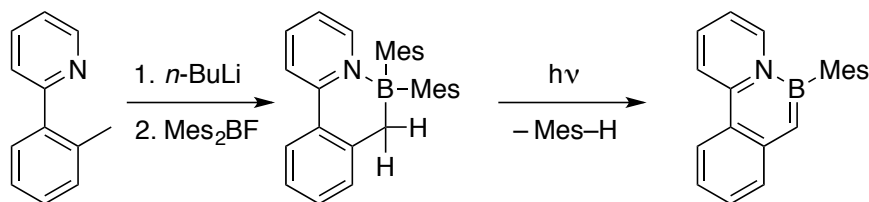
⁶² Neue, B.; Araneda, J. F.; Piers, W. E.; Parvez, M. *Angew. Chem. Int. Ed.* **2013**, *52*, 9966–9969.

⁶³ Examples: (a) Lu, J.-S.; Ko, S.-B.; Walters, N. R.; Kang, Y.; Sauriol, F.; Wang, S. *Angew. Chem. Int. Ed.* **2013**, *52*, 4544–4548. (b) Ko, S.-B.; Lu, J.-S.; Wang, S. *Org. Lett.* **2014**, *16*, 616–619. (c) Wang, S.; Yang,

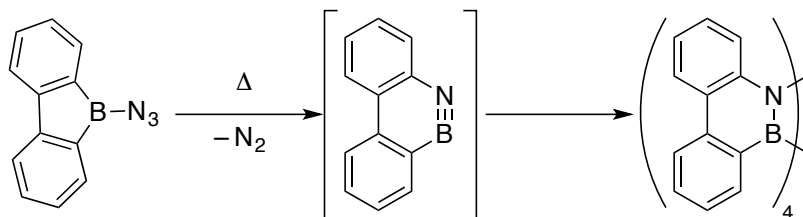
also utilized a unique 1,1-hydroboration reaction to give BN-containing extended π -systems.⁶⁴ Bettinger has utilized a ring expansion reaction of *B*-azidodibenzoborole to form BN phenanthryne, which can cyclotetramerize *in situ* to form extremely distorted (BN)₄ systems.⁶⁵

Scheme 1.6. Miscellaneous Syntheses of BN Extended π -Systems

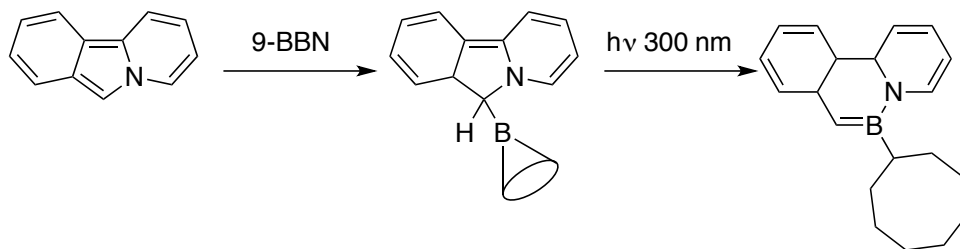
Wang 2013: Lithiation/borylation/elimination



Bettinger 2014: Azide insertion into a borole



Wang 2015: 1,1-hydroboration/elimination



D.-T.; Lu, J.; Shimogawa, H.; Gong, S.; Wang, X.; Mellerup, S. K.; Wakamiya, A.; Chang, Y.-L.; Yang, C.; Lu, Z.-H. *Angew. Chem. Int. Ed.* **2015**, *54*, 15074–15078.

⁶⁴ Shi, Y.; Yang, D.-T.; Mellerup, S. K.; Wang, N.; Peng, T.; Wang, S. *Org. Lett.* **2016**, *18*, 1626–1629.

⁶⁵ (a) Müller, M.; Maichle-Mössmer, C.; Bettinger, H. F. *Angew. Chem. Int. Ed.* **2014**, *53*, 9380–9383. It is hypothesized that the tetramers are formed through the dimerization of (BN)₂ intermediates. Borole ring expansion for monocyclic azaborine synthesis has been explored elsewhere: (b) Braunschweig, H.; Hörl, C.; Mailänder, L.; Radacki, K.; Wahler, J. *Chem. Eur. J.* **2014**, *20*, 9858–9861. (c) Braunschweig, H.; Celik, M. A.; Hupp, F.; Krummenacher, I.; Mailänder, L. *Angew. Chem. Int. Ed.* **2015**, *54*, 6347–6351. (d) Couchman, S. A.; Thompson, T. K.; Wilson, D. J. D.; Dutton, J. L.; Martin, C. D. *Chem. Commun.* **2014**, *50*, 11724–11726.

With the exception of some of Piers's work, experimental efforts describing the fundamental differences between π -conjugated azaborines and all-carbon analogues are lacking in the literature, and this type of research specifically regarding BN acenes is completely nonexistent, as BN isosteres of acenes have not been synthesized. This chapter will focus on our efforts to fill this gap in the literature with comparisons between BN acenes and their direct all-carbon analogues.

1.3 Two BN Isosteres of Anthracene: Synthesis and Characterization

The best way to make a comparison between a BN-containing compound and an all-carbon compound is to compare directly; the only difference between the two is the presence of the BN unit where a CC unit once stood. The best way to make a direct comparison is between parent molecules (e.g., benzene with the 1,2-dihydro-1,2-azaborine parent) because the all-carbon parent molecules have been most thoroughly studied. Secondly, and perhaps, more importantly, we can be certain that the differences observed are a direct consequence of BN/CC isosterism, and not a consequence of any steric or electronic effects resulting from substitution. At the outset of this research, no synthesis of a parental BN anthracene or any BN isosteres of higher acenes had been executed. We decided to target BN-1,2-anthracene using electrophilic aromatic borylation in analogy to Dewar's BN-1,2-naphthalene synthesis (see Scheme 1.4 above).

One synthetic challenge in constructing a BN acene is the lack of syntheses for 2,3-unsymmetrically substituted acene precursors with no other substitution. Electrophilic aromatic substitution, an obvious method of derivatizing aromatic compounds, generally

occurs preferentially at the 1-position of 2-substituted naphthalene and at apical positions of higher acenes, giving us the undesired regiochemistry.⁶⁶

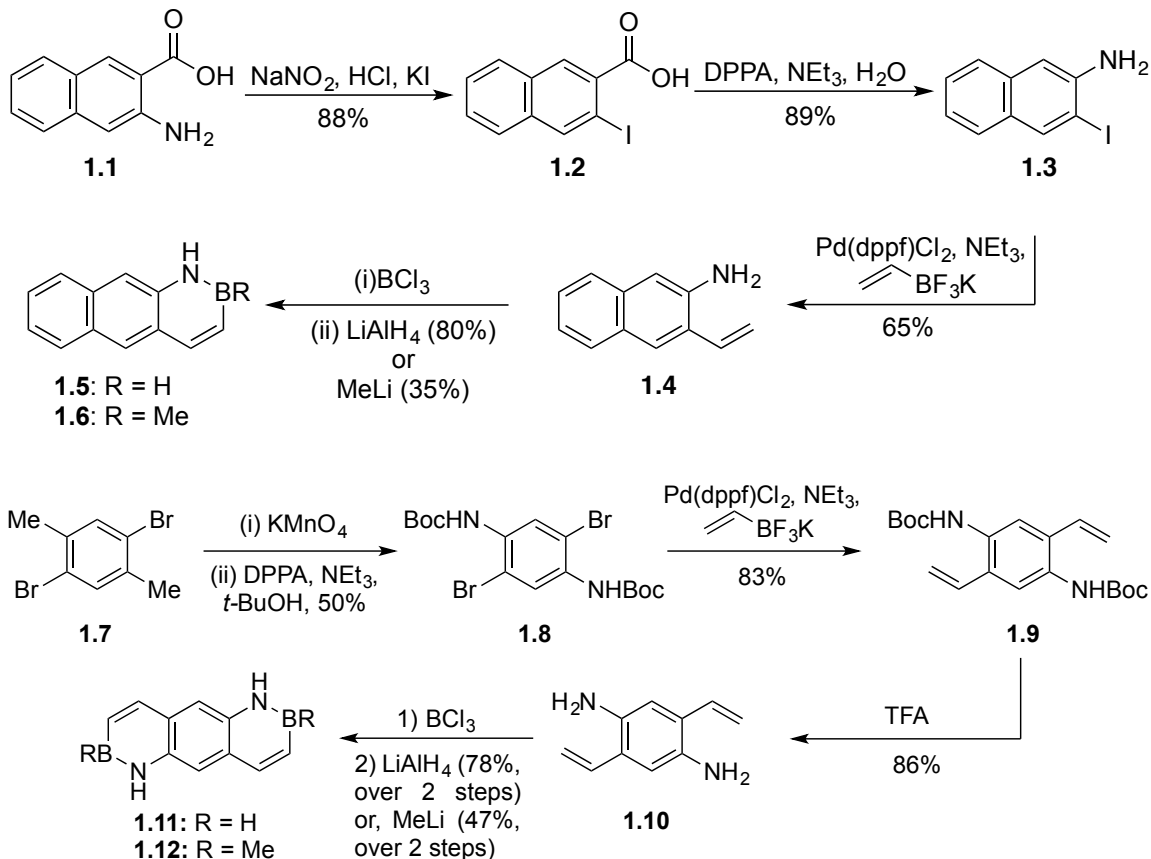
1.3.1 Synthesis of BN Anthracenes⁶⁷

Beginning with the commercially available **1.1**, a Sandmeyer reaction afforded **1.2** (Scheme 1.7). The resulting iodinated compound **1.2** was treated with diphenylphosphoryl azide (DPPA) to affect the Curtius rearrangement, giving **1.3**. This compound underwent Suzuki coupling with potassium vinyltrifluoroborate to give the key cyclization precursor **1.4**. To our delight, **1.4** easily cyclized upon heating with boron trichloride to give the corresponding *B*-chloro-BN-anthracene. This intermediate was not isolated and instead was further reacted with nucleophiles such as lithium aluminum hydride or methyllithium to give products **1.5** and **1.6**. A similar scheme was employed for the syntheses of so-called “bis-BN-anthracenes” **1.11** and **1.12**.

⁶⁶ Wasilewska, A.; Woźniak, B. A.; Doridot, G.; Piotrowska, K.; Witkowska, N.; Retailleau, P.; Six, Y. *Chem. Eur. J.* **2013**, *19*, 11759–11767.

⁶⁷ The following section details the following published article: Ishibashi, J. S. A.; Marshall, J. L.; Mazière, A.; Lovinger, G. J.; Li, B.; Zakharov, L. N.; Dargelos, A.; Graciaa, A.; Chrostowska, A.; Liu, S. *J. Am. Chem. Soc.* **2014**, *136*, 15414–15421.

Scheme 1.7. Syntheses of BN-1,2-anthracenes



1.3.2 Optoelectronic Properties of BN-1,2-Anthracenes

The parent compounds **1.5** and **1.11** were subjected to UV-photoelectron spectroscopy (UV-PES) to investigate the energy levels of their occupied orbitals. This work was done by Prof. Anna Chrostowska (Univ. Pau et des Pays de l'Adour) whose group has investigated other BN-heterocycles with UV-PES.⁶⁸ The UV-PES technique expels electrons from occupied orbitals and measures the energy of these resulting photoelectrons. The inverse of the measured photoelectron ionization energy is taken as

⁶⁸ (a) Lemierre, V.; Chrostowska, A.; Dargelos, A.; Chermette, H. *J. Phys. Chem. A* **2005**, *109*, 8348–8355. (b) Chrostowska, A.; Maciejczyk, M.; Dargelos, A.; Baylère, P.; Weber, L.; Werner, V.; Eickhoff, D.; Stammler, H.-G.; Neumann, B. *Organometallics* **2010**, *29*, 5192–5198. (c) Chrostowska, A.; Xu, S.; Lamm, A. N.; Mazière, A.; Weber, C. D.; Dargelos, A.; Baylère, P.; Graciaa, A.; Liu, S.-Y. *J. Am. Chem. Soc.* **2012**, *134*, 10279–10285. (d) Chrostowska, A.; Xu, S.; Mazière, A.; Boknevit, K.; Li, B.; Abbey, E. R.; Dargelos, A.; Graciaa, A.; Liu, S.-Y. *J. Am. Chem. Soc.* **2014**, *136*, 11813–11820.

the energy of the orbitals from which they are expelled. Among the occupied orbitals, we are most interested in the HOMO energies (Figure 1.7).

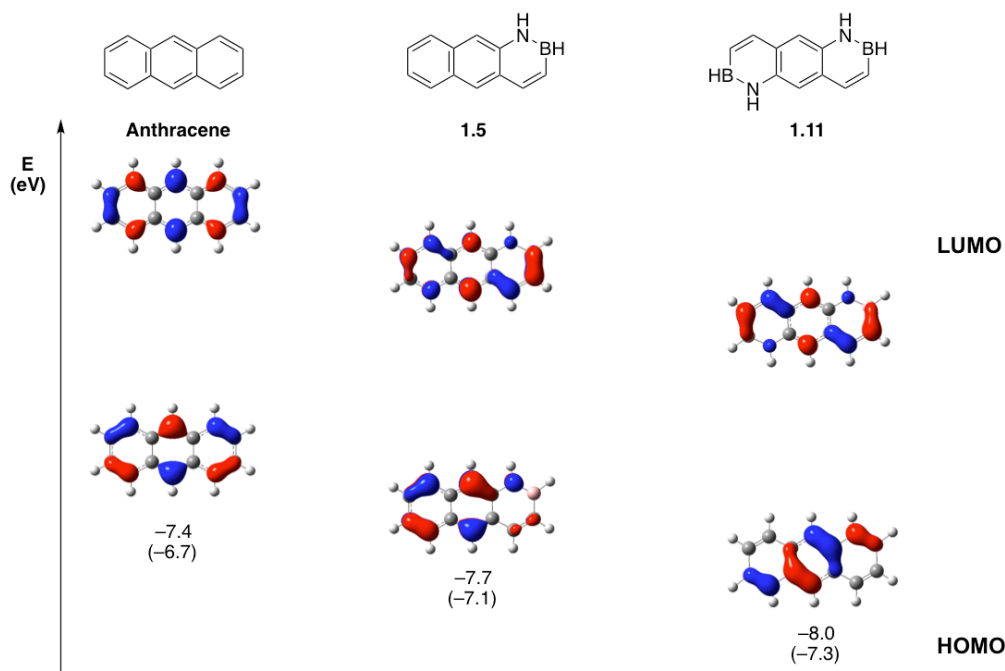


Figure 1.7. Frontier orbital maps (CAM-B3LYP/6-311G(d,p), HOMO energies as measured by UV-PES, and calculated HOMO energies in parenthesis

Anthracene's first ionization occurs at 7.4 eV and corresponds to ejection of an electron from the HOMO (b_{2g} symmetry). The first band of the UV-PE spectrum of BN anthracene **1.5** (point group C_s) can be found at 7.7 eV and also corresponds to its HOMO (A'' symmetry). For bis-BN anthracene **1.11** (point group C_{2h}), the first ionization band was found at 8.0 eV (corresponding to the HOMO, b_g). It is worth noting that the four highest occupied MOs for each anthracene molecule are π -type orbitals. A diagram showing the orbital energies (measured and calculated, CAM-B3LYP/6-311G(d,p)) is shown in Figure 1.7 above. BN/CC isosterism lowers HOMO energies with respect to the all-carbon analogue, and the more BN units present, the lower the HOMO energy.

Figure 1.8 shows the electronic absorption spectra for anthracene, **1.5**, and **1.11**. The lowest-energy absorption band for each of the compounds is centered around 360 nm, and the absorption onset for each compound indicates a similar HOMO-LUMO gap for each as estimated by the tangent drawn at the onset of absorption (3.26 eV for anthracene, 3.22 eV for **1.5**, and 3.23 eV for **1.11**).⁶⁹ Each spectrum exhibits vibronic fine structure common with polyaromatic systems. Interestingly, and in contrast to the absorption spectrum of anthracene, both **1.5** and **1.11** have higher-energy absorption bands that appear in the window between 400 and 250 nm. These additional absorption bands warrant further investigation.

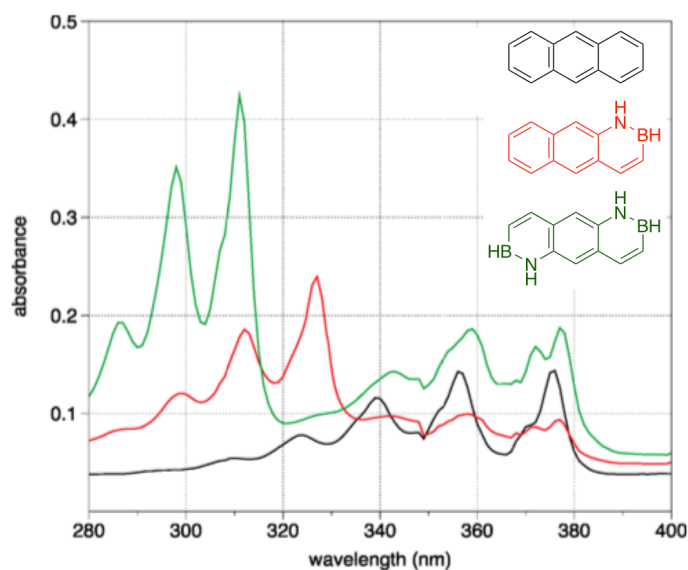


Figure 1.8. Absorption spectra of anthracene and the BN isosteres **1.5** and **1.11** taken in cyclohexane at 5.5×10^{-6} M.

The absorption bands do not change location and moreover follow the Beer-Lambert law through a wide range of concentrations (see Experimental Section); these

⁶⁹ This method is standard for the estimation of HOMO-LUMO gaps. See: (a) Chase, D. T.; Rose, B. D.; McClintock, S. P.; Zakharov, L. N.; Haley, M. M. *Angew. Chem. Int. Ed.* **2011**, *50*, 1127–1130. (b) Popere, B. C.; Della Pelle, A. M.; Poe, A.; Balaji, G.; Thayumanavan, S. *Chem. Sci.* **2012**, *3*, 3093–3102.

observations rule out aggregation phenomena as the origin of the additional absorption bands. According to TD-DFT calculations (B3LYP/6-311++G(d,p)), the low-energy bands should correspond to the HOMO to LUMO transition, while the higher-energy bands for the BN isosteres (327 nm for **1.5** and 311 nm for **1.11**) correspond to excitation from lower-lying orbitals. In anthracene, the HOMO-1 is much lower-lying (−8.6 eV) than those of the BN isosteres **1.5** and **1.11** (−8.3 and −8.2 eV, respectively). The origin of the higher-energy bands in the BN isosteres, therefore, might be that excitation from these orbitals to the respective LUMOs is lower in energy in the BN anthracenes than the corresponding excitation event in anthracene. Alternatively, these absorption modes may have become allowed as a result of the decreased symmetry in the BN anthracenes relative to the all-carbon analogue.

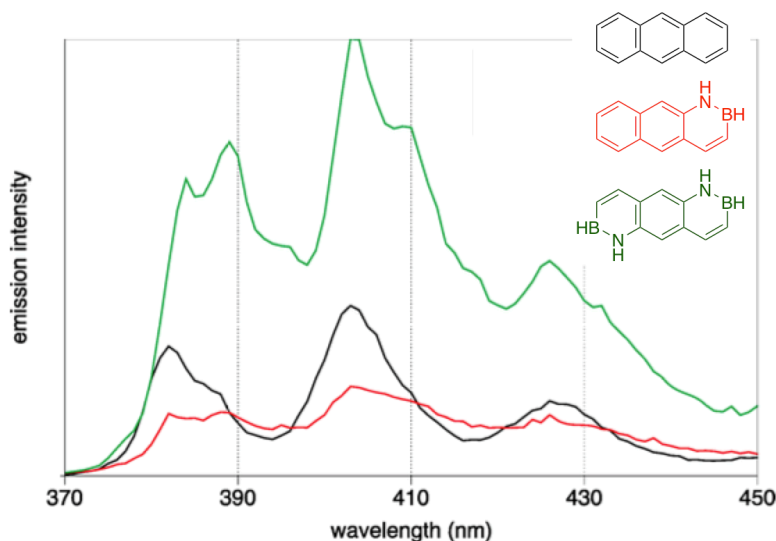
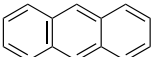
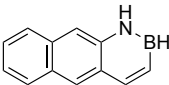
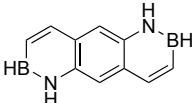


Figure 1.9. Emission spectra of anthracene and the BN isosteres **1.5** and **1.11** taken in cyclohexane at 5.5×10^{-6} M (excitation wavelength: 360 nm).

The emission spectra of the BN anthracenes **1.5** and **1.11** are also similar to that of anthracene (Figure 1.9). Vibronic fine structure is similarly preserved, and the highest-intensity emission peak is found at almost exactly at 403 nm in all cases. Excitation

spectra correlate well with the absorption spectra (see Experimental Section), and the same emission spectrum is obtained when **1.5** and **1.11** respectively are excited both at the high- and low-energy absorption bands, further supporting our hypothesis of higher-energy HOMO–1 orbitals for **1.5** and **1.11** than for anthracene. Key optoelectronic data are summarized in Table 1.1.

Table 1.1: Key optoelectronic data for anthracene, **1.5**, and **1.11**

	$E_{\text{HOMO}}^{\text{a}}$	$E_{\text{gap}}^{\text{b}}$	λ_{max1}	ϵ_1^{c}	λ_{max2}	ϵ_2^{d}	$\lambda_{\text{max(em)}}^{\text{e}}$	$\Phi_{\text{F}}^{\text{f}}$
	–7.4 eV	3.26 eV	-	-	356 nm	9700	403 nm	0.36
	–7.7 eV	3.22 eV	327 nm	14000	359 nm	4900	403 nm	0.38
	–8.0 eV	3.23 eV	311 nm	27000	357 nm	10000	403 nm	0.68

^a Determined by UV-PES. ^b Determined by UV-Vis spectroscopy in cyclohexane solution (the intersection of the "wavelength" axis and the tangent passing through the inflection point of the lowest energy absorption peak). ^c Molar absorptivity constant at high-energy band in $\text{M}^{-1} \text{cm}^{-1}$. ^d Molar absorptivity constant at low-energy band in $\text{M}^{-1} \text{cm}^{-1}$. ^e Wavelength of highest emission intensity. ^f Determined by the comparative method using anthracene ($\Phi_{\text{F}} = 0.36$) and phenylanthracene ($\Phi_{\text{F}} = 0.49$) in cyclohexane as the standards

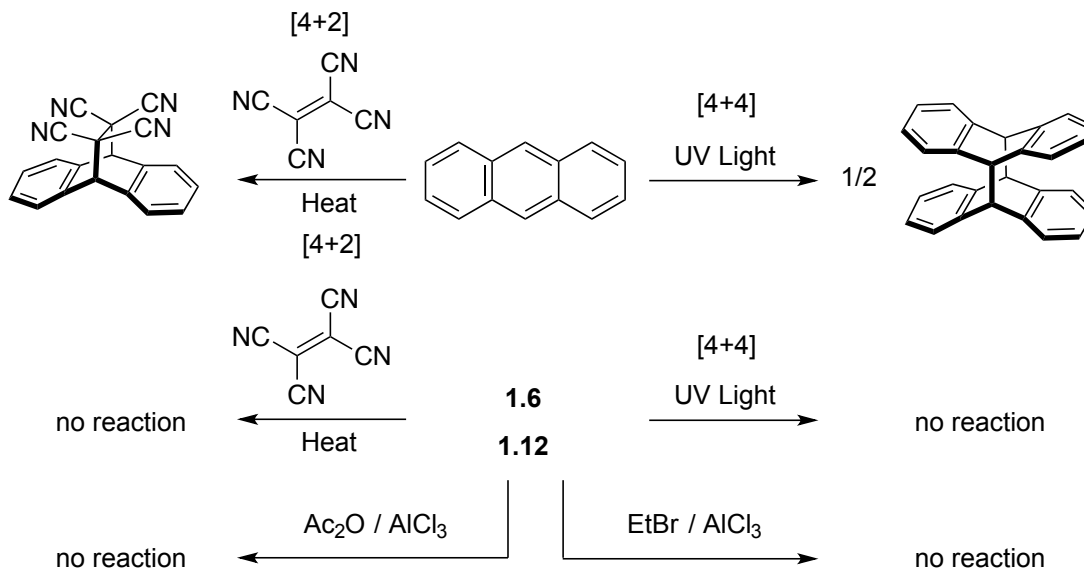
1.3.3 Reactivity Survey

Consistent with the lowered HOMO levels of the BN isosteres with respect to the all-carbon analogue anthracene, we observe an overall decrease in reactivity in some classic acene reactivity modes. Anthracene is known to undergo both thermally allowed [4+2] and photochemically allowed [4+4] cyclizations (Scheme 1.8).⁷⁰ However, using a range of activated dienophiles we were not able to observe a Diels-Alder reaction. For example, methylated derivatives **1.6** and **1.12** both did not react with tetracyanoethylene (an active normal-demand Diels-Alder dienophile) or with methyl vinyl ether (an active inverse-demand Diels-Alder dienophile), when heated in C_6D_6 to 130 °C. By contrast,

⁷⁰ Atherton, J. C. C.; Jones, S. *Tetrahedron* **2003**, 59, 9039–9057.

anthracene, under the same conditions, converts to the Diels-Alder product within hours.⁷¹ Friedel-Crafts acylation using acetic anhydride and aluminum chloride (even in excess) was also attempted but to no avail.⁷² Friedel-Crafts alkylation with ethyl bromide and Lewis acids also was ineffective.

Scheme 1.8. Survey of Ineffective Reactivity. [4+2] and [4+4] Cycloadditions and Friedel-Crafts Reactions



Bromination, however, does occur regioselectively at the 9-position of **1.6** (Figure 1.10). This reactivity contrasts with that observed in most other azaborines; monocyclic azaborines,^{38c} BN-1,2-naphthalene,^{46b,73} and BN-9,10-naphthalene^{47,74} all are brominated at the position adjacent to boron. In these cases, bromination occurs at the position with the most negative charge according to the calculated electrostatic potential maps. This position adjacent to boron also contains a large HOMO coefficient. In the present case of compound **1.6**, the position adjacent to boron is also very electron rich according to the ESP map. However, at that site, the HOMO coefficient is very small in comparison to the

⁷¹ Lotfi, M.; Roberts, R. M. G. *Tetrahedron* **1979**, 35, 2131–2136.

⁷² Ball, J. C.; Brennan, P.; Elsunaki, T. M.; Jaunet, A.; Jones, S. *Tetrahedron: Asymmetry* **2011**, 22, 253–255.

⁷³ Dewar, M. J. S.; Dietz, R. J. *Org. Chem.* **1961**, 26, 3253–3256.

⁷⁴ Sun, F.; Lv, L.; Huang, M.; Zhou, Z.; Fang, X. *Org. Lett.* **2014**, 16, 5024–5027.

coefficient at the 9-position. It appears in this case that the reaction is orbitally-controlled instead of charge-controlled. The regiochemistry of the bromination was confirmed by HSQC and HMBC NMR experiments.

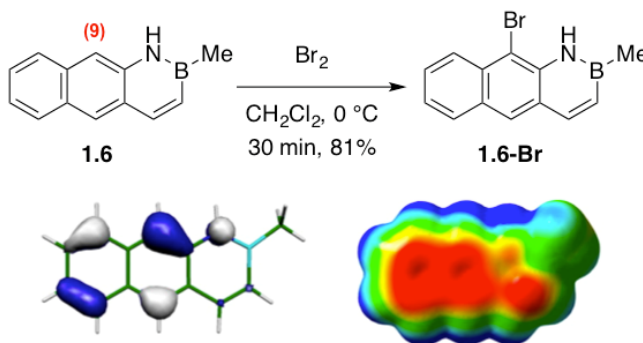
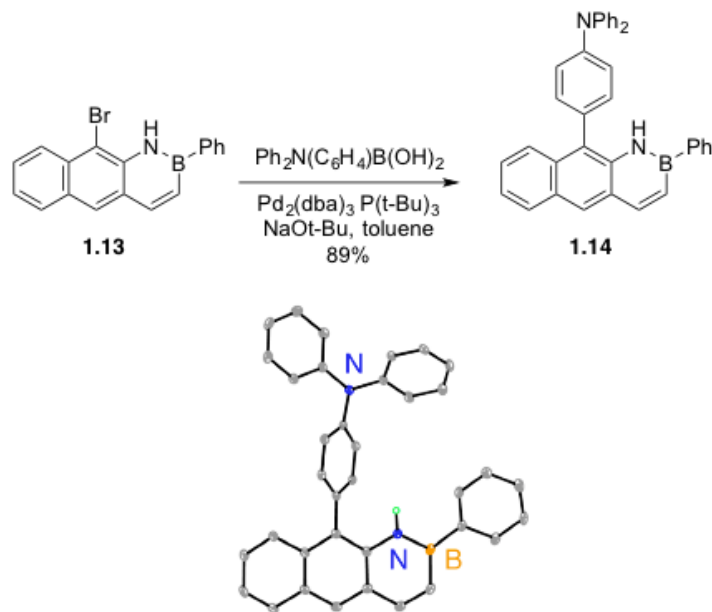


Figure 1.10. Bromination of 1,2-BN-anthracenes at the 9-position and calculated HOMO and ESP maps (CAM-B3LYP/6-311G(d,p))

These 9-brominated BN anthracenes can be further functionalized *via* Suzuki coupling. Compound **1.13** can be arylated to produce compound **1.14** (Scheme 1.9). We were able to perform single-crystal x-ray diffraction on compound **1.14**, further confirming the regiochemistry of the initial bromination.

Scheme 1.9. Suzuki coupling of brominated BN anthracene derivative and crystal structure of the product



Finally, we used a bracketing study to estimate the pK_a of the acidic $N\text{--H}$ proton. Deprotonation of **1.6** cleanly proceeded using KHMDS as the base. We treated the resulting potassium salt **1.6-K** with proton sources to determine if these proton sources would be deprotonated by the **1.6-K**. Triphenylmethane (DMSO $pK_a = 30.6$) was not deprotonated, but diphenylamine (DMSO $pK_a = 25.0$) was completely deprotonated. Treating **1.6-K** with pentamethylcyclopentadiene (Cp^*H) produced peaks corresponding both to deprotonated Cp^* anion and the starting Cp^*H , indicating the pK_a of both of these are similar (26.1).

1.3.4 Conclusions

In conclusion, we synthesized two BN isosteres of anthracene and compared their optoelectronic properties with the all-carbon analogue, anthracene. The BN anthracenes **1.5** and **1.11** have HOMO energies lower than that of anthracene. The HOMO-LUMO gaps, however, remain approximately the same as estimated by UV-visible absorption

spectroscopy. The lower HOMO energies for the BN isosteres are further evidenced by the total lack of cycloaddition chemistry and Friedel-Crafts chemistry, both of which are easily accomplished with the all-carbon analogue. Bromination, however, proceeds exclusively at the 9-position of BN anthracene **1.6**. We have demonstrated here that BN/CC isosterism can stabilize the HOMO energy of the acene topology whilst maintaining the optical bandgap. This relationship should extend to higher acene isosteres more useful for optoelectronic device application.

1.3.5 Experimental Section

All oxygen- and moisture-sensitive manipulations were carried out under an inert atmosphere using either standard Schlenk technique or a nitrogen-filled drybox. Tetrahydrofuran, diethyl ether, methylene chloride, pentane, and toluene were purified by passing through a neutral alumina column under argon. All UV-grade solvents were dried over calcium hydride or 3 Å mol sieves, distilled under nitrogen and degassed *via* freeze-pump-thaw method.

Solutions of *tert*-butyllithium, *n*-butyllithium, boron trichloride, and ethereal hydrogen chloride were purchased from Sigma-Aldrich and used as received. Ferrocene was purchased from Sigma-Aldrich and sublimed before use. All other chemicals were purchased from TCI, Sigma-Aldrich, or Strem and used as received.

For all chromatography involving air- and moisture-sensitive compounds, silica gel (240-300 mesh) was heated under vacuum in a 150 °C oil bath for 12 hours. Chromatography was performed under an inert atmosphere using dry, degassed solvents. ¹¹B NMR spectra were recorded on a Varian Unity/Inova 300 spectrometer or a Bruker Avance III HD 600 spectrometer with a Prodigy BBO cryoprobe at ambient temperature. ¹H NMR spectra were recorded on a Varian Unity/Inova 300 spectrometer, a Varian Unity/Inova 500 spectrometer or a Bruker Avance III HD 600 spectrometer with a Prodigy BBO cryoprobe at ambient temperature. ¹³C spectra were recorded on a Varian Unity/Inova 500 spectrometer or a Bruker Avance III HD 600 spectrometer with a

Prodigy BBO cryoprobe at ambient temperature. ^{11}B spectra were externally referenced to $\text{BF}_3 \cdot \text{Et}_2\text{O}$. (δ 0)

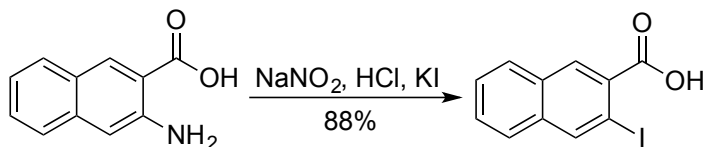
UV-visible absorption spectra were acquired on a Cary 100 spectrometer equipped with a Quantum Northwest TLC-42 dual cuvette temperature controller at $25.00\text{ }^\circ\text{C} \pm 0.05\text{ }^\circ\text{C}$. Emission spectra were acquired on a Quanta Master 40 spectrofluorimeter (Photon Technology International) equipped with a Quantum Northwest TLC-50 temperature controller set at $25.00\text{ }^\circ\text{C} \pm 0.05\text{ }^\circ\text{C}$. Fluorescence quantum yields were determined using the comparative method,⁷⁵ referenced to anthracene ($\Phi_{\text{F}} = 0.36$).² Emission spectra for the determination of quantum yields were collected using excitation and emission slit widths of 2 nm, and all samples were excited at 360 nm. Values reported are the average of two runs at four different concentrations in cyclohexane as the solvent.

Electron impact (EI) high-resolution mass spectrometry was performed at the Mass Spectrometry Facilities and Services Core of the Environmental Health Sciences Center at Oregon State University. Financial support for this facility has been furnished in part by the National Institute of Environmental Health Sciences, NIH (P30 ES00210). Direct Analysis in Real Time (DART) HRMS data were obtained at the Boston College Center for Mass Spectrometry.

⁷⁵ Rhys Williams, A. T.; Winfield, S. A.; Miller, J. N. *Analyst* **1983**, *108*, 1067–1071.

Synthetic Details

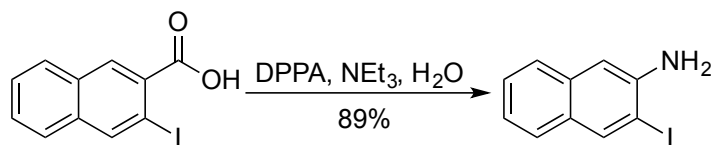
3-iodo-2-naphthoic acid (**1.2**) [63212-42-0]:



To an ice-cold suspension of 3-amino-2-naphthoic acid **1.1** (10 g, 53 mmol, 1 equiv.) in water (100 mL), crushed ice (50 g), and concentrated hydrochloric acid (12 M, 76.0 mL, 910 mmol, 17 equiv.) were added. Sodium nitrite (4.4 g, 64 mmol, 1.2 equiv.) in 20 mL water was added slowly to the reaction. This solution was stirred at 0 °C for 30 minutes. Then, potassium iodide (17.7 g, 107 mmol, 2.0 equiv.) in 40 mL water was carefully added. The reaction was stirred at 0 °C for 5 minutes, then heated to 90 °C for one hour. If heating is maintained for four hours, there is no deleterious effect on yield. The reaction mixture was then cooled to room temperature and extracted 4 times with ethyl acetate. The organic extract was washed three times with saturated sodium bisulfite solution, three times with brine, dried over magnesium sulfate, and concentrated. The product was obtained as a light red powder (14.8 g, 88%). ^1H NMR (300 MHz, DMSO-d_6) δ 13.30 (s, 1H), 8.64 (s, 1H), 8.39 (s, 1H), 8.05 (d, $J = 7.7$ Hz, 1H), 7.94 (d, $J = 7.6$ Hz, 1H), 7.70 – 7.53 (m, 2H). The spectrum agrees with previous report.⁷⁶

⁷⁶ Uyanik, M.; Akakura, M.; Ishihara, K. *J. Am. Chem. Soc.* **2009**, *131*, 251–262.

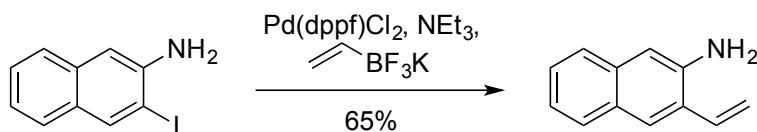
3-iodonaphthalen-2-amine (1.3) [116632-14-5]:



Diphenyl phosphoryl azide (15.2 mL, 70.5 mmol, 1.5 equiv.), 3-iodo-2-naphthoic acid **1.2** (14.0 g, 47.0 mmol 1.0 equiv.), and triethylamine (9.83 mL, 70.5 mmol, 1.5 equiv.) were combined in anhydrous N,N-dimethylformamide (375 mL), and stirred under nitrogen. Nitrogen evolution may be observed if the reaction is executed at this scale, and the reaction may become warm. (Take care to keep the reaction under anaerobic and anhydrous conditions but DO NOT seal the reaction vessel, as it may build pressure.) After 3 hours of stirring, degassed water (47 mL) was added, and the solution was heated to 90 °C for 1 hour. The reaction mixture was then cooled to room temperature and diluted with 500 mL of water. The reaction mixture was washed five times with Et₂O, and each Et₂O extract was washed liberally with water to remove DMF. The organic layers were combined, washed twice with a saturated solution of sodium bicarbonate, twice with brine, then dried over magnesium sulfate. The ether was removed via rotary evaporator and the off-white solid remaining was taken on to the next step without further purification (11.18 g, 89%). ¹H NMR (300 MHz, CD₂Cl₂) δ 8.29 (s, 1H), 7.62 (t, *J* = 8.5 Hz, 2H), 7.41 (ddd, *J* = 8.2, 6.8, 1.4 Hz, 1H), 7.25 (ddd, *J* = 8.2, 6.8, 1.3 Hz, 1H), 7.13 (s, 1H), 4.32 (s, 2H). The spectrum agrees with previous report.⁷⁷

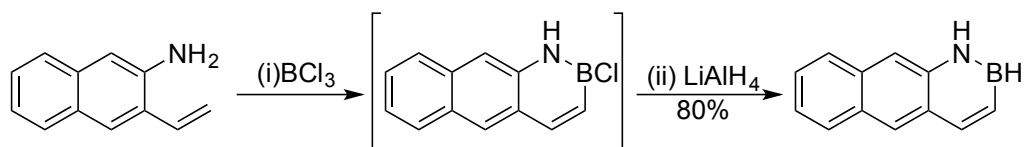
⁷⁷ Ma, C.; Liu, X.; Li, X.; Flippen-Anderson, J.; Yu, S.; Cook, J. M. *J. Org. Chem.* **2001**, *66*, 4525–4542.

3-vinyl-naphthylene-2-amine (1.4) [1330067-40-7]:



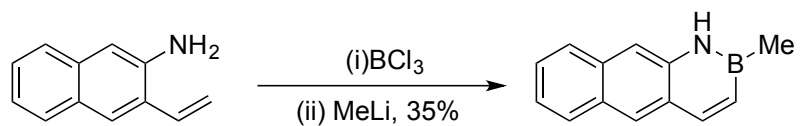
In a glove box, an oven-dried, three-necked round-bottomed flask was charged with compound **1.3** (11.2 g, 41.6 mmol, 1.0 equiv.), Pd(dppf)Cl₂·CH₂Cl₂ (1.7 g, 2.1 mmol, 0.05 equiv.), potassium vinyltrifluoroborate (6.68 g, 49.9 mmol, 1.2 equiv.), triethylamine (7.0 mL, 50 mmol, 1.2 equiv.), and toluene (300 mL). A reflux condenser was fitted to the flask, and the flask was brought outside of the glovebox. Normal propyl alcohol (300 mL), which had been purged with nitrogen for 2 hours beforehand, was transferred via cannula to the reaction flask and this mixture was heated under nitrogen to 120 °C for 18 hours. The reaction was then cooled to room temperature, and 600 mL of cold H₂O was added. The resulting mixture was extracted three times with Et₂O. The combined organic fraction was washed with brine, concentrated and purified via a silica gel plug, using methylene chloride as the eluent. The product was obtained as an off-white powder (4.55 g, 65%). ¹H NMR (300 MHz, CD₂Cl₂) δ 7.80 (s, 1H), 7.73 (d, *J* = 8.1 Hz, 1H), 7.60 (d, *J* = 8.2 Hz, 1H), 7.44 – 7.31 (m, 1H), 7.25 (dd, *J* = 8.2, 6.7 Hz, 1H), 7.03 (s, 1H), 6.96 (dd, *J* = 17.3, 10.9 Hz, 1H), 5.85 (dd, *J* = 17.4, 1.5 Hz, 1H), 5.48 (dd, *J* = 11.0, 1.5 Hz, 1H), 4.01 (s, 2H). This compound has been previously reported without spectral characterization by Baudoin and co-workers as the product of a tert-butylcarbamate deprotection.⁷⁸ In their hands, **1.4** was taken on to more synthetic steps, the products of which were spectrally characterized.

⁷⁸ Baudoin, O.; Claveau, F.; Thoret, S.; Herrbach, A.; Guénard, D.; Guéritte, F. *Bioorg. Med. Chem.* **2002**, *10*, 3395–3400.

1,2-azaboroanthracene (1.5):

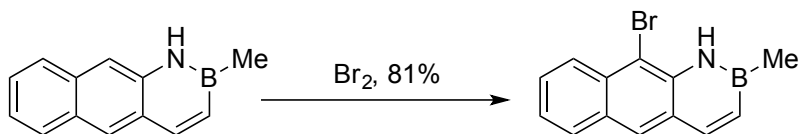
Under an inert atmosphere, a 1 L oven-dried, round-bottomed flask was charged with 3-vinylnaphthalen-2-amine **1.4** (4.05 g, 23.9 mmol, 1.0 equiv.) and 500 mL of toluene. The flask was then fitted with a condenser, and the reaction mixture was cooled to -30°C . Cold boron trichloride solution (1.0 M in hexanes, 47.9 mL, 47.9 mmol, 2.0 equiv.) was added dropwise via syringe to the vigorously stirring cold solution of amine in toluene. At the conclusion of the addition, the reaction mixture was allowed to warm to room temperature over one hour, and then it was heated at reflux for 18 hours. At the conclusion of the reaction, the mixture was concentrated under reduced pressure. In a glove box, the residue was redissolved in Et₂O and cooled to -30°C . In a separate flask, lithium aluminum hydride (LAH) (1.82 g, 47.9 mmol, 2.0 equiv.) was dissolved in Et₂O and cooled to -30°C . Then, the LAH solution was slowly added to the solution containing the crude residue, and the combined mixture was allowed to warm to room temperature and stirred for 18 hours. Then, a hydrogen chloride solution (2 M in ether, 26.3 mL, 52.6 mmol, 2.2 equiv.) was added, and the resulting mixture was passed through a silica gel plug. The resulting crude material was purified via recrystallization from hot chlorobenzene (3.4 g, 80% over 2 steps). ¹¹B NMR (96 MHz, CD₂Cl₂) δ 32.3 (d, $J_{\text{BH}} = 133.1$ Hz). ¹H NMR (600 MHz, CD₂Cl₂) δ 8.36 (s, 1H), 8.25 (d, $J = 11.5$ Hz, 1H), 8.23 (s, 1H), 8.00 (d, $J = 8.3$ Hz, 1H), 7.92 (d, $J = 8.4$ Hz, 1H), 7.77 (s, 1H), 7.54 (ddd, $J = 8.2, 6.7, 1.2$ Hz, 1H), 7.45 (ddd, $J = 8.0, 6.7, 1.2$ Hz, 1H), 7.02 (dt, $J = 11.5, 2.0$ Hz, 1H), 5.48 – 4.73 (m, 1H). ¹³C NMR (151 MHz, CD₂Cl₂) δ 145.3, 138.4, 133.6, 130.3(br), 129.2, 129.1, 128.5, 126.9, 126.9, 126.9, 124.3, 113.8. HRMS (EI+) calcd. for C₁₂H₁₀NB [M⁺] 179.09063, found 179.09044.

B-methyl-1,2azaboroanthracene (1.6):



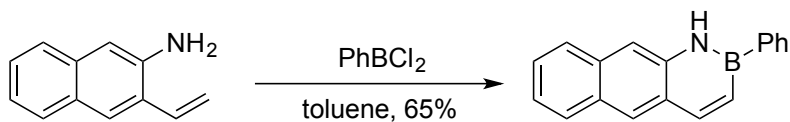
Under an inert atmosphere, a 1 L oven-dried, round-bottomed flask was charged with 3-vinylnaphthylene-2-amine **6** (2.56 g, 15.1 mmol, 1.0 equiv.) and 50 mL of toluene. The flask was then fitted with a condenser, and the reaction mixture was cooled to $-30\text{ }^{\circ}\text{C}$. Cold boron trichloride solution (1.0 M in hexanes, 30.2 mL, 30.2 mmol, 2.0 equiv.) was added dropwise via syringe to the vigorously stirring cold solution of amine in toluene. At the conclusion of the addition, the reaction mixture was allowed to warm to room temperature over one hour, and then it was heated at reflux for 18 hours. At the conclusion of the reaction, the mixture was concentrated under reduced pressure. In a glove box, the residue was redissolved in THF (100 mL) and cooled to $-78\text{ }^{\circ}\text{C}$. Methyllithium (1.6 M in ether, 18.9 mL, 30.2 mmol, 2.0 equiv.) was added dropwise to the solution containing the crude residue at $-78\text{ }^{\circ}\text{C}$, and the combined mixture was allowed to warm to room temperature and stirred for 18 hours. Then, ammonium chloride (807 mg, 15.1 mmol, 1.0 equiv.) was added, and the mixture was allowed to stir for one hour at room temperature. The reaction mixture was concentrated under reduced pressure, and the resulting residue was passed through a silica gel plug. This crude material was purified via recrystallization from a concentrated CH_2Cl_2 / hexane solution (1.03 g, 35% over 2 steps). ^{11}B NMR (160 MHz, CD_2Cl_2) δ 34.5 (s). ^1H NMR (500 MHz, CD_2Cl_2) δ 8.10 (s, 1H), 8.05 (d, $J = 11.5\text{ Hz}$, 1H), 7.92 (d, $J = 8.3\text{ Hz}$, 1H), 7.84 (d, $J = 8.3\text{ Hz}$, 1H), 7.75 (s, 1H), 7.59 (s, br, 1H), 7.47 (t, $J = 7.5\text{ Hz}$, 1H), 7.38 (t, $J = 7.5\text{ Hz}$, 1H), 6.81 (d, $J = 11.6\text{ Hz}$, 1H) 0.78 (s, 3H). ^{13}C NMR (126 MHz, CD_2Cl_2) δ 144.4, 139.1, 133.9, 132.0 (br), 129.1, 128.9, 128.6, 126.9, 126.8, 126.7, 124.1, 113.0, 2.8 (br). HRMS (DART+) calcd. for $\text{C}_{13}\text{H}_{13}\text{BN}$ $[\text{M}+\text{H}]^+$ 194.11410, found 194.11341.

***B*-methyl-9-bromo-1,2-BN-anthracene (1.6-Br):**



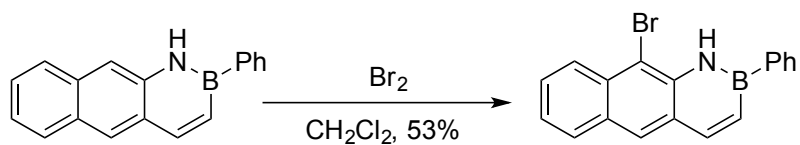
Under an inert atmosphere, a vial was charged with **1.6** (33.5 mg, 0.174 mmol, 1 equiv.) and methylene chloride (4 mL), and the reaction was cooled using an ice bath. A solution of bromine (27.7 mg, 0.174 mmol, 1.0 equiv) in methylene chloride (1 mL) was added slowly. The cooling bath was maintained for 30 minutes, and then it was removed. The reaction was stirred for an hour following the removal of the ice bath. The crude reaction mixture was passed through a plug of silica in the air, and the solvent was removed under reduced pressure to yield an off-white powder. (38.2 mg, 81%). ^{11}B NMR (160 MHz, CD_2Cl_2) δ 39.14. ^1H NMR (500 MHz, CD_2Cl_2) δ 8.35 (s, br, 1H), 8.25 (d, J = 8.6 Hz, 1H), 8.09 (s, 1H), 7.92 (dd, J = 8.2, 0.5 Hz, 1H), 7.64 – 7.57 (m, 1H), 7.44 (ddd, J = 8.0, 6.7, 1.0 Hz, 1H), 6.83 (dd, J = 11.5, 1.7 Hz, 1H) 0.86 (s, 3H). ^{13}C NMR (126 MHz, CD_2Cl_2) δ 144.36, 136.57, 131.93, 131.65, 129.55, 129.09, 129.07, 128.40, 127.10, 126.32, 124.58, 109.55, 3.64. Regiochemical assignment was obtained by HSQC and HMBC NMR studies. HRMS (DART+) $[\text{M}+\text{H}]^+$ calcd. for $\text{C}_{13}\text{H}_{12}\text{BBrN}$ 272.02462, found 272.02343.

***B*-Phenyl-1,2-BN-anthracene:**

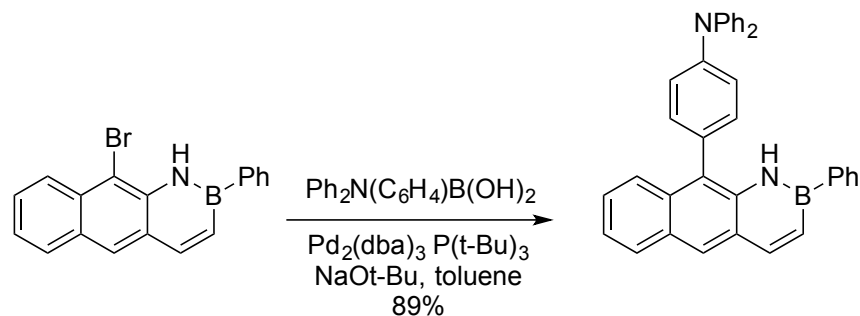


Under an inert atmosphere, compound **1.4** (474 mg, 2.80 mmol, 1.0 equiv) was combined with 70 mL toluene in an oven-dried, round-bottomed flask. Phenylboron dichloride (880 mg, 5.6 mmol, 2.0 equiv.) was added slowly to the stirring reaction at room temperature. Then, the reaction mixture was heated to reflux for 18 hours. At the conclusion of the reaction the mixture was allowed to cool to room temperature. The solvent was removed under reduced pressure, and the residue was taken up in methylene chloride and passed through a short plug of silica gel. This crude material was purified by recrystallization from hot chlorobenzene to furnish a flaky, off-white, crystalline solid (465 mg, 65%). ¹¹B NMR (160 MHz, CD₂Cl₂) δ 34.0. ¹H NMR (500 MHz, CD₂Cl₂) δ 8.28 (d, *J* = 11.6 Hz, 2H, overlaps with N–H peak), 8.20 (s, 1H), 8.02 – 7.98 (m, 2H), 7.96 (d, *J* = 7.9 Hz, 1H), 7.89 (d, *J* = 8.3 Hz, 1H), 7.79 (s, 1H), 7.53 – 7.47 (m, 4H), 7.41 (ddd, *J* = 8.0, 6.7, 1.2 Hz, 1H), 7.30 (dd, *J* = 11.6, 1.9 Hz, 1H). ¹³C NMR (126 MHz, CD₂Cl₂) δ 146.0, 138.8, 133.9, 133.3, 130.4, 129.2, 129.0, 128.7, 128.5, 127.0, 126.9, 126.86, 124.2, 113.7. The carbons adjacent to boron were not observed. HRMS (DART+) [*M*+*H*]⁺ for C₁₈H₁₅BN calcd. 256.13029, found 256.12975.

***B*-phenyl-9-bromo-1,2-BN-anthracene (1.13):**

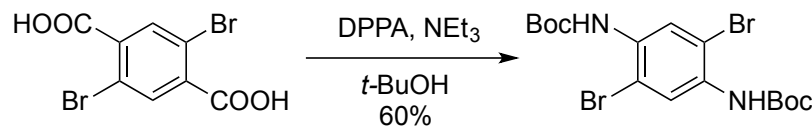


Compound **1.8** (28 mg, 0.11 mmol, 1.0 equiv) was dissolved in 5.0 mL dry methylene chloride. Bromine (19 mg, 0.12 mmol, 1.1 equiv) was dissolved in 1.0 mL methylene chloride. Both solutions were cooled in an ice bath, then the bromine solution was added slowly to the solution of the starting material. The reaction was allowed to stir 30 minutes at 0 °C. Then, the reaction was allowed to warm to room temperature and stir for 2 hours. The entire mixture was passed through a plug of silica under ambient conditions, and volatiles were removed to reveal an off-white solid. Crude yield: 34 mg, 93%. This material can be used in the subsequent Suzuki coupling reaction. Analytically pure product was obtained by rinsing the crude material with methanol (15 mg, 53%). ¹¹B NMR (160 MHz, CD₂Cl₂) δ 34.6 (s). ¹H NMR (500 MHz, CD₂Cl₂) δ 8.94 (s, 1H), 8.30 (dd, *J* = 8.6, 0.8 Hz, 1H), 8.25 (d, *J* = 11.6 Hz, 1H), 8.21 (s, 1H), 8.08 – 8.03 (m, 2H), 7.98 (dd, *J* = 8.3, 0.5 Hz, 1H), 7.69 – 7.62 (m, 1H), 7.58 – 7.44 (m, 4H), 7.35 (dd, *J* = 11.6, 1.9 Hz, 1H). ¹³C NMR (126 MHz, CD₂Cl₂) δ 146.0, 136.3, 133.5, 132.1, 130.9, 129.8, 129.2, 129.1, 128.8, 128.5, 127.3, 126.3, 124.7, 110.3. The carbons adjacent to boron were not observed. HRMS (DART+) [*M*+*H*]⁺ calcd. for C₁₈H₁₄BrBN: 344.03027, found 344.04129.

Compound 1.14:

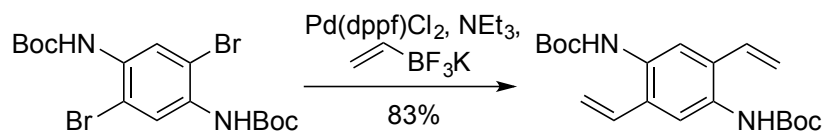
In a glove box, a 15-ml pressure vessel with a re-sealable screw cap was charged with compound **1.8** (39 mg, 0.12 mmol, 1.0 equiv), 4-(diphenylamino)phenylboronic acid (66.8 mg, 0.231 mmol, 2.0 equiv), $\text{Pd}_2(\text{dba})_3$ (5.0 mg, 0.0060 mmol, 0.05 equiv.), tri-tertbutylphosphine (5.0 mg, 0.020 mmol, 0.2 equiv), sodium tert-butoxide (22 mg, 0.23 mmol, 2.0 equiv), and 7.0 mL of Toluene. The reaction mixture was stirred at 110 °C for 18 hours. After cooling to room temperature, the solvent was removed under reduced pressure. The crude material was purified by silica gel chromatography using 95:5 pentane:ether solution as the eluent to afford the desired product as a lemon-lime-colored solid (49 mg, 89% yield). ^{11}B NMR (160 MHz, CD_2Cl_2) δ 32.8 (s). ^1H NMR (500 MHz, CD_2Cl_2) δ 8.33 (d, J = 11.6 Hz, 1H), 8.29 (s, 1H), 8.25 (s, 1H), 8.01 (d, J = 8.0 Hz, 1H), 7.80 – 7.75 (m, 2H), 7.73 (d, J = 8.6 Hz, 1H), 7.55 – 7.20 (m, 18H), 7.11 (td, J = 7.4, 1.0 Hz, 2H). ^{13}C NMR (126 MHz, CD_2Cl_2) δ 148.4, 148.1, 146.3, 136.1, 133.2, 132.8, 132.6, 130.4, 129.8, 129.6, 129.1, 128.8, 128.7, 128.6, 126.8, 126.6, 125.7, 125.09, 125.07, 124.6, 124.0, 123.7. The carbons adjacent to boron were not observed. HRMS (DART+) $[\text{M}+\text{H}]^+$ calcd. for $\text{C}_{36}\text{H}_{28}\text{BN}$: 499.23455, found 499.23261. X-ray quality crystals were grown from an ether/pentane solution at –30 °C.

Tert-butyl 2,5-dibromo-1,4-phenylene dicarbamate (1.8):



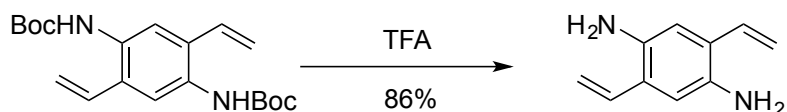
2,5-dibromoterephthalic acid (4.9 g, 15.1 mmol), triethylamine (6.33 mL, 45.4 mmol, 3.0 equiv.), and diphenyl phosphoryl azide (9.8 mL, 45.4 mmol, 3.0 equiv.), were combined in *tert*-butyl alcohol (175 mL), and refluxed for 12 hours under nitrogen. The reaction mixture was then cooled to room temperature and diluted with 175 mL of water. The reaction mixture was then extracted three times with ether. The ether extractions were combined and washed three times brine, dried over magnesium sulfate, and concentrated using a rotary evaporator. The crude reaction mixture was purified via flash chromatography eluting with methylene chloride. After removing the solvent, the product was obtained as an off-white solid (4.16 g, 60%). ¹H NMR (300 MHz, CDCl₃) δ 8.41 (s, 2H), 6.91 (s, 2H), 1.56 (s, 18H). ¹³C NMR (126 MHz, CD₂Cl₂) δ 152.3, 132.3, 123.0, 111.7, 81.4, 28.1. HRMS (DART+) [M]⁺ calcd. for C₁₆H₂₂Br₂N₂O₄ 463.99463, found 463.99415.

Tert-butyl 2,5-divinyl-1,4-phenylene dicarbamate (1.9):

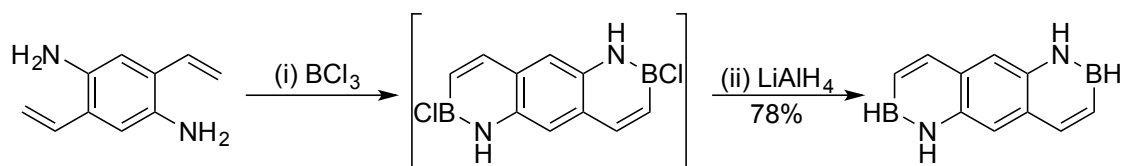


Under an inert atmosphere, an oven dried 3 necked round-bottomed flask was charged with **1.8** (4.068 g, 8.73 mmol), Pd(dppf)Cl₂·CH₂Cl₂ (0.713 g, 0.873 mmol 0.1 equiv.), potassium vinyltrifluoroborate (3.51 g, 26.2 mmol, 3.0 equiv.), triethylamine (2.9 mL, 21 mmol, 2.4 equiv.), and toluene (200 mL). A condenser was fitted to the flask and the flask was brought outside of the glovebox. Normal propyl alcohol (200 mL), which had been purged beforehand with nitrogen for 2 hours, was transferred *via* cannula to the reaction flask and this mixture was refluxed overnight under nitrogen. The reaction was cooled to room temperature, and cold water (600 mL) was added. The resulting mixture was extracted three times with ether, washed with brine, concentrated and purified *via* a silica gel plug eluting with methylene chloride. After removing the solvent, the product was obtained as an off-white solid (2.6 g, 82.8%). ¹H NMR (300 MHz, CDCl₃) δ 7.86 (s, 2H), 6.80 (dd, *J* = 17.5, 11.2 Hz, 2H), 6.37 (s, 2H), 5.76 (d, *J* = 18.2 Hz, 2H), 5.44 (d, *J* = 10.9 Hz, 2H), 1.64 – 1.49 (m, 18H). ¹³C NMR (126 MHz, CD₂Cl₂) δ 153.5, 132.0, 131.89, 130.4, 120.8, 117.9, 80.7, 28.5. HRMS (DART+) [M+NH₄]⁺ calcd. for C₂₀H₃₂N₃O₄ 378.24004, found 378.23928.

2,5-divinylbenzene-1,4-diamine (1.10):

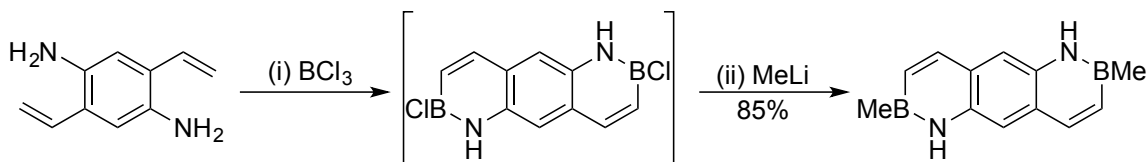


Compound **1.9** (2.60 g, 7.23 mmol) was dissolved in methylene chloride (27 mL) and trifluoroacetic acid (13.5 mL, 176 mmol, 24 equiv.) was added with stirring. The solution was stirred at room temperature for 2 hours and then the solvent was removed under reduced pressure. The resulting material was redissolved in ethyl acetate, washed three times with saturated sodium bicarbonate solution, three times with brine, dried over magnesium sulfate, and concentrated using a rotary evaporator. The crude material was purified *via* flash chromatography eluting with CH₂Cl₂:EtOAc (4:1) (837.7 mg, 72.3%). ¹H NMR (500 MHz, CDCl₃) δ 6.78 (dd, *J* = 17.5, 11.1 Hz, 2H), 6.74 (s, 2H), 5.66 – 5.59 (m, 2H), 5.31 (dd, *J* = 11.0, 1.5 Hz, 2H), 3.47 (s, 4H). ¹³C NMR (126 MHz, CD₂Cl₂) δ 137.0, 132.7, 125.6, 115.0, 115.0. HRMS (DART+) [M+H]⁺ calcd. for C₁₀H₁₃N₂ 161.10758 found 161.10787.

1,5-aza-2,6-boraanthracene (1.11):

Under an inert atmosphere, a 250 mL oven-dried, two-necked round-bottomed flask was charged with **1.10** (491.6 mg, 3.07 mmol), 100 mL of toluene, fitted with a condenser, and cooled to $-30\text{ }^{\circ}\text{C}$. Cold ($-30\text{ }^{\circ}\text{C}$) boron trichloride solution (1 M in hexanes, 12.3 mL, 12.3 mmol, 4 equiv.) was added to the vigorously stirring cold solution of **11** in toluene and warmed to room temperature and then heated to reflux overnight. The reaction was cooled to room temperature, and then the toluene was removed *in vacuo*. In a glove box, the unpurified product was re-dissolved in ether and cooled to $-30\text{ }^{\circ}\text{C}$. In a separate flask, lithium aluminum hydride (466.0 mg, 12.28 mmol, 4 equiv.) was dissolved in ether and cooled to $-30\text{ }^{\circ}\text{C}$. The LiAlH₄ solution was added slowly to the stirring starting material solution in the glove box, and the reaction was warmed to room temperature overnight. Hydrogen chloride (2 M in ether, 6.75 mL, 13.5 mmol, 4.4 equiv.) was then added and the resulting mixture was filtered through a silica gel plug. The product was purified via recrystallization from hot chlorobenzene. (430.7 mg, 78%). ¹¹B NMR (96 MHz, CD₂Cl₂) δ 31.9 (d, $J_{\text{BH}} = 125\text{ Hz}$). ¹H NMR (300 MHz, CD₂Cl₂) δ 8.38 (s, 2H), 8.18 (d, $J = 11.4\text{ Hz}$, 2H), 7.64 (s, 2H), 7.12 – 7.03 (m, 2H), 5.75 – 4.44 (m, 2H). ¹³C NMR (151 MHz, CD₂Cl₂) δ 143.9, 134.8, 126.6, 116.8. The C(3) carbon was not observed. HRMS (DART+) $[\text{M}+\text{H}]^{+}$ for C₁₀H₁₁B₂N₂ calcd. 181.11095, found 181.11083.

bis-B-methyl-1,5-aza-2,6-boraanthracene (1.12):

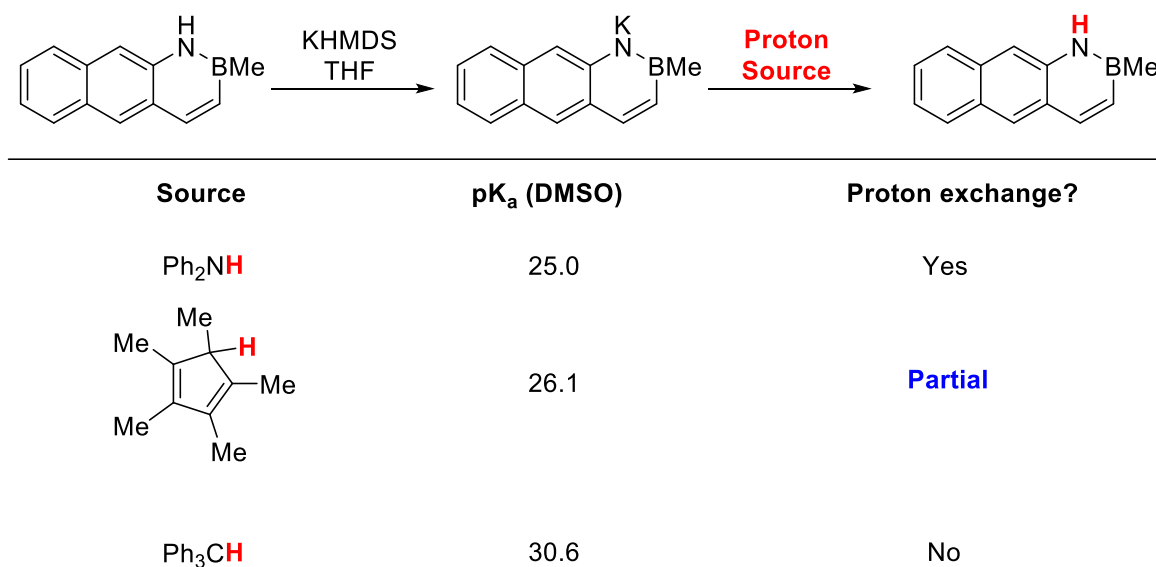


Under an inert atmosphere, a 250 mL oven-dried, round-bottomed flask was charged with **1.10** (376 mg, 2.35 mmol, 1.0 equiv.) and 100 mL of toluene. Boron trichloride (1.0 M in hexanes, 9.4 mL, 9.4 mmol, 4.0 equiv.) was added dropwise via syringe to the vigorously stirring solution of amine in toluene at room temperature followed by heating at reflux for 18 hours. At the conclusion of the reaction, the mixture was concentrated under reduced pressure. In a glove box, the residue was suspended in ether (100 mL) and cooled to -78°C . Methyllithium (1.6 M in ether, 5.9 mL, 9.4 mmol, 4.0 equiv.) was added dropwise to the solution containing the crude residue at -78°C , and the combined mixture was allowed to warm to room temperature and stirred for 18 hours. Then, aqueous ammonium chloride was added. The mixture was washed with ether and the combined organic layer was dried over sodium sulfate and concentrated under reduced pressure. This crude material was purified via recrystallization from a concentrated CH₂Cl₂/hexane solution to furnish the desired product as a brown solid (231 mg, 47%). ¹¹B NMR (160 MHz, THF-*d*₈) δ 37.2. ¹H NMR (500 MHz, THF-*d*₈) δ 9.04 (s, 2H), 7.90 (d, *J* = 11.5 Hz, 2H), 7.45 (s, 2H), 6.71 (dd, *J* = 11.5, 1.6 Hz, 2H), 0.69 (s, 6H). ¹³C NMR (126 MHz, THF-*d*₈) δ 143.8, 136.1, 132.0 (br), 126.8, 116.5, 2.0 (br). (HRMS (DART+) [M+H]⁺ for C₁₂H₁₅B₂N₂ calcd. 209.14213, found 209.14176.

General Procedure for pK_a Bracketing Studies

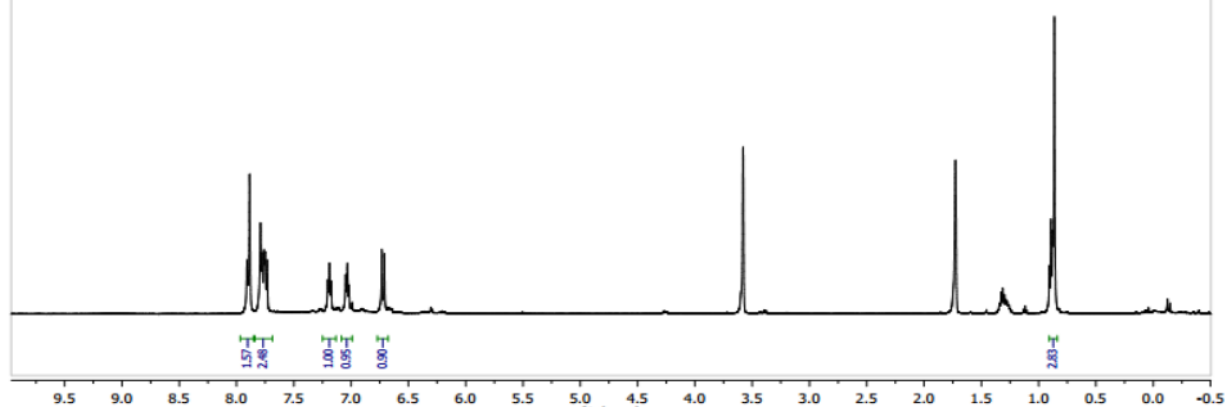
In a glovebox, compound **1.6** (52 mg, 0.269 mmol) was taken into tetrahydrofuran. It was cooled to $-30\text{ }^{\circ}\text{C}$, and potassium hexamethyldisilazane solution (0.53 mL, 0.5 M in toluene, 0.269 mmol, 1 equiv.) was added dropwise to the cold solution of **1.6**. The solution was left to stir and warm to room temperature over four hours. The deep green solution was taken out of the box, and volatiles were removed *via* hi-vacuum through a Schlenk line. The residue was rinsed three times with pentane. Following the rinse, vacuum was applied to remove excess volatiles, and a known amount of THF- d_8 was added. The bulk solution was split into portions, and an appropriate amount of the proton source to quench the potassium salt was introduced to each portion. The state of protonation/deprotonation was characterized by ^1H NMR. Acidity values in DMSO are taken from Bordwell's pK_a table.

Scheme 1.10. pK_a bracketing experiment results



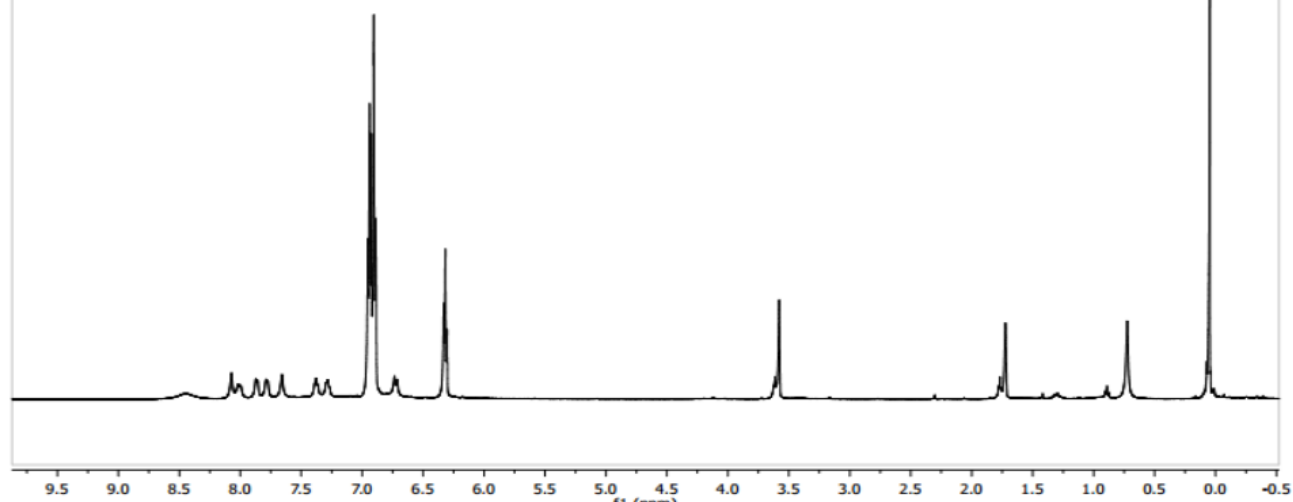
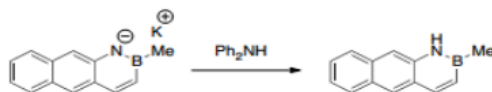
ji-III-H235_B

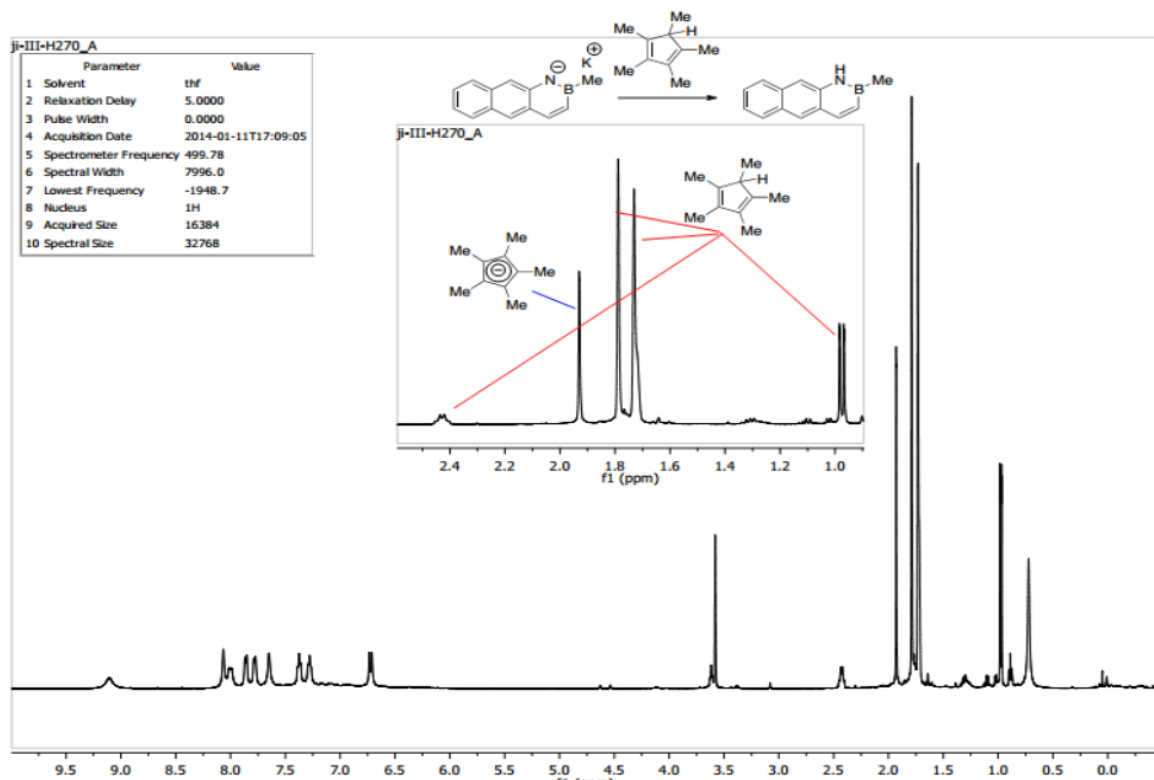
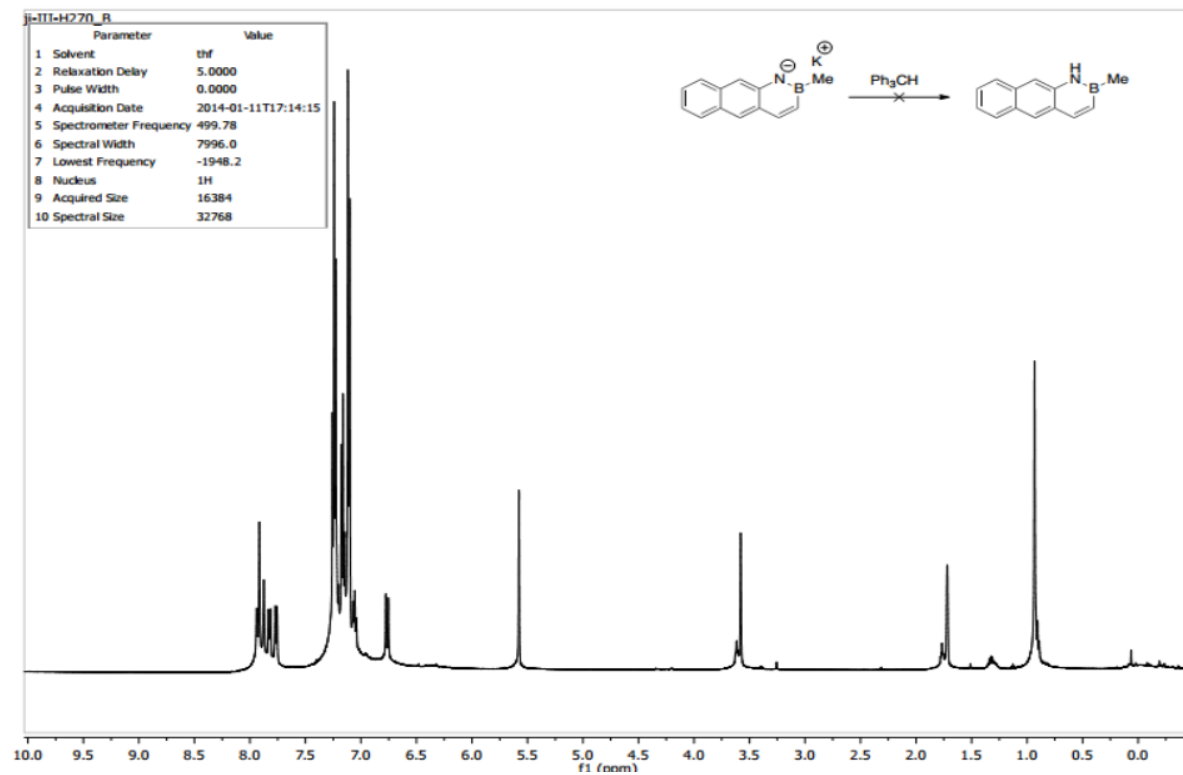
Parameter	Value
1 Solvent	cd2cl2
2 Relaxation Delay	1.0000
3 Pulse Width	0.0000
4 Acquisition Date	2013-11-22T17:36:07
5 Spectrometer Frequency	499.88
6 Spectral Width	8012.8
7 Lowest Frequency	-1879.9
8 Nucleus	1H
9 Acquired Size	16384
10 Spectral Size	32768

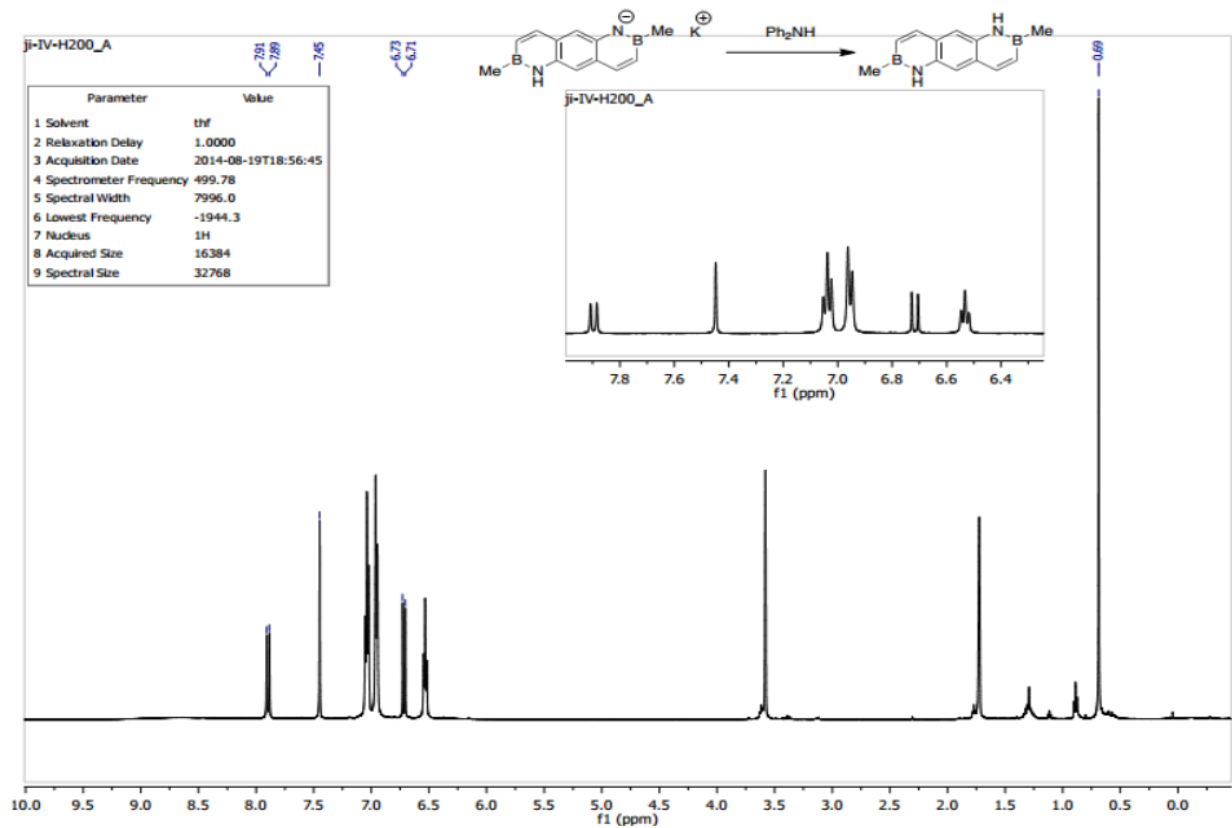
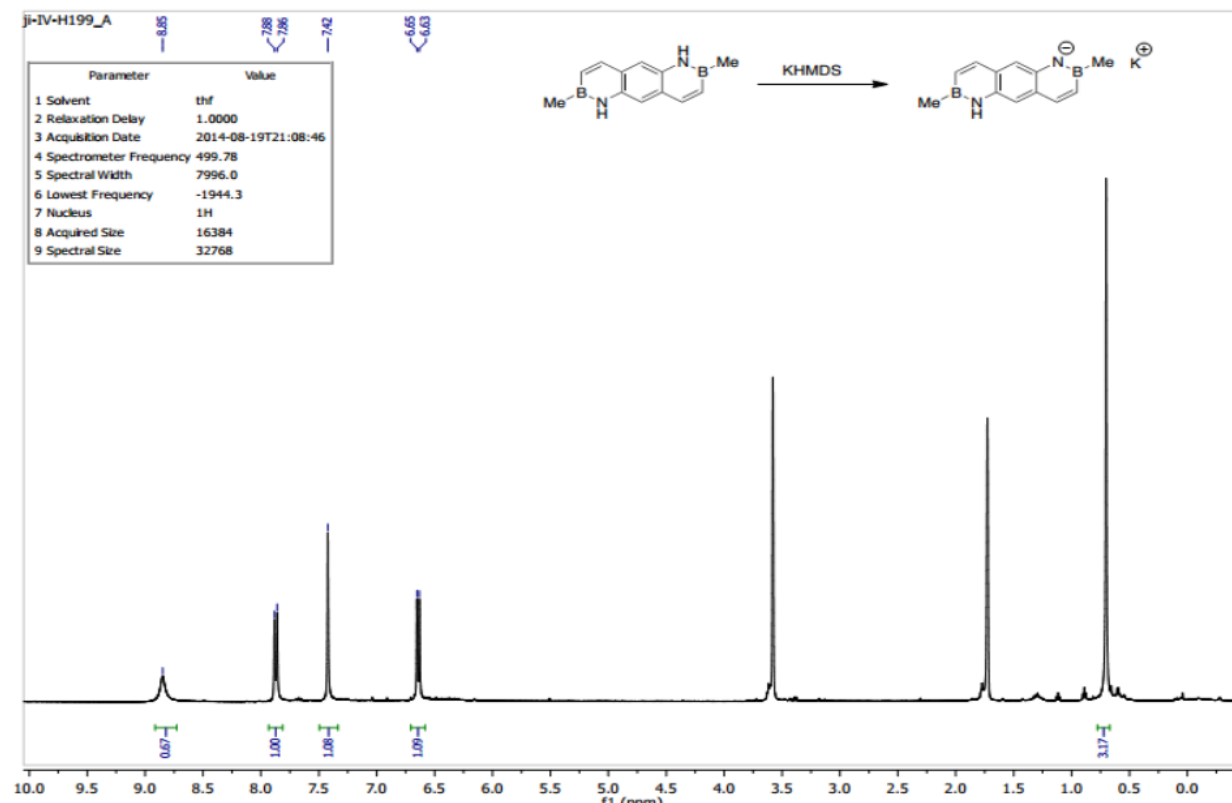


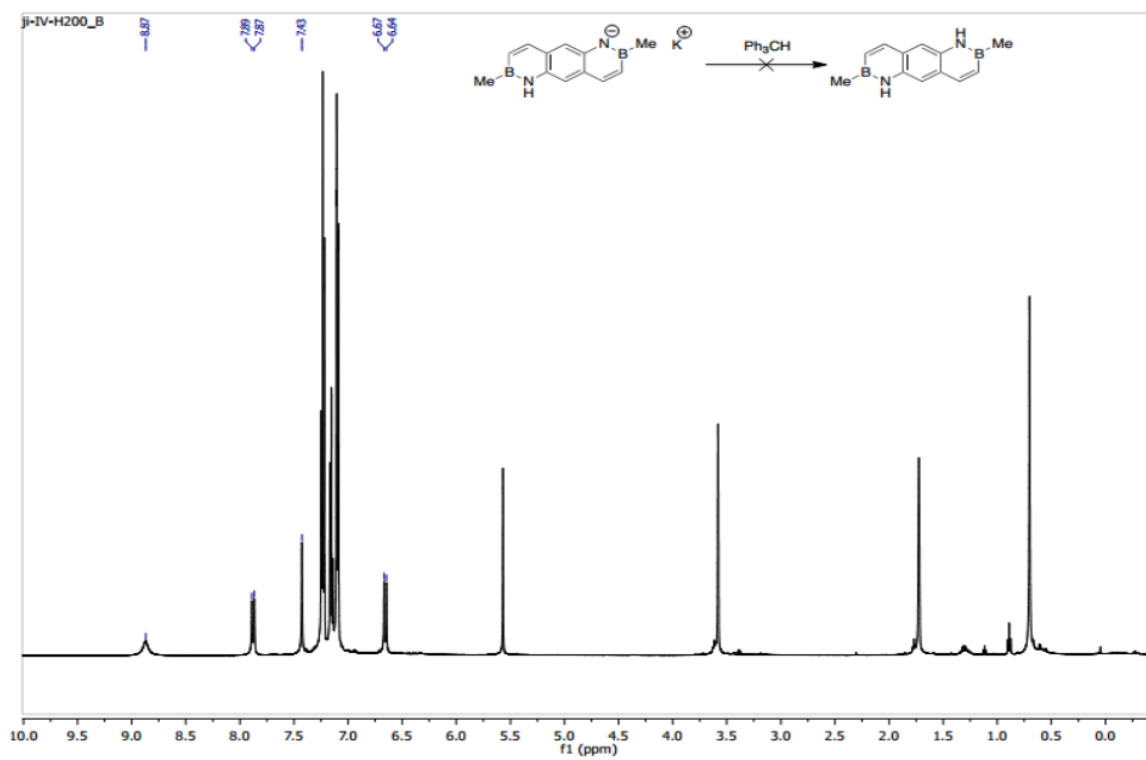
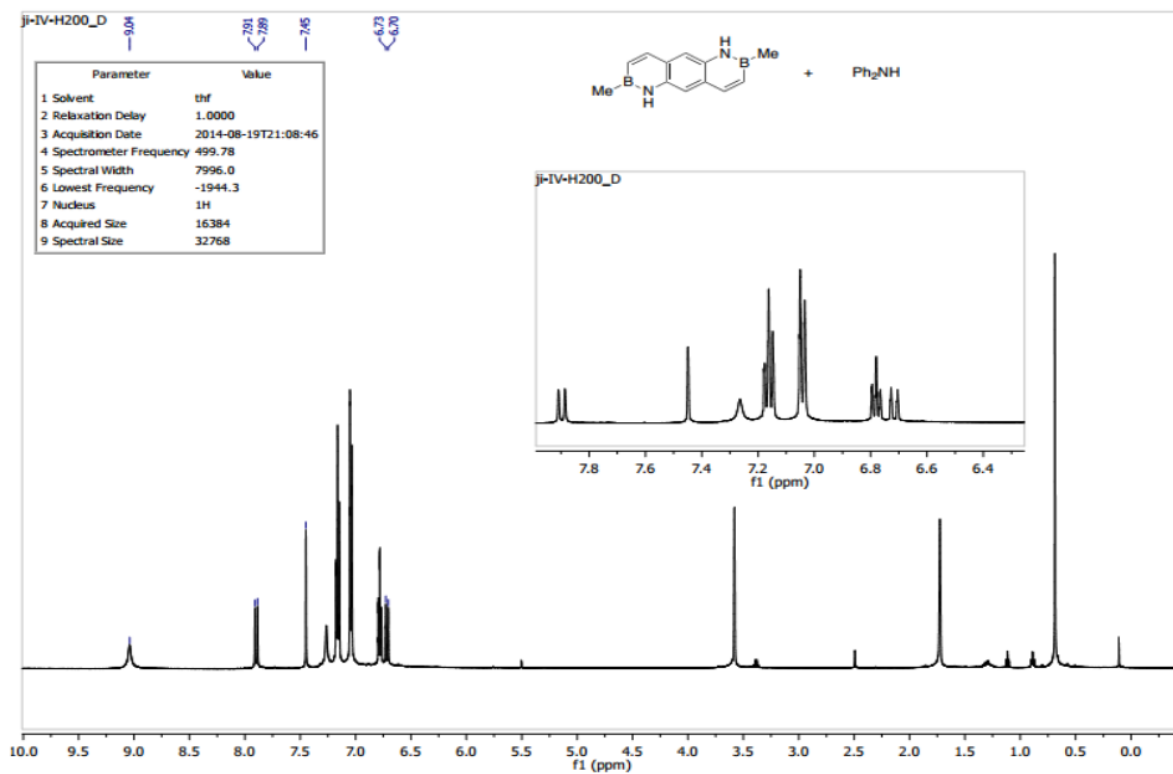
ji-III-H263_C

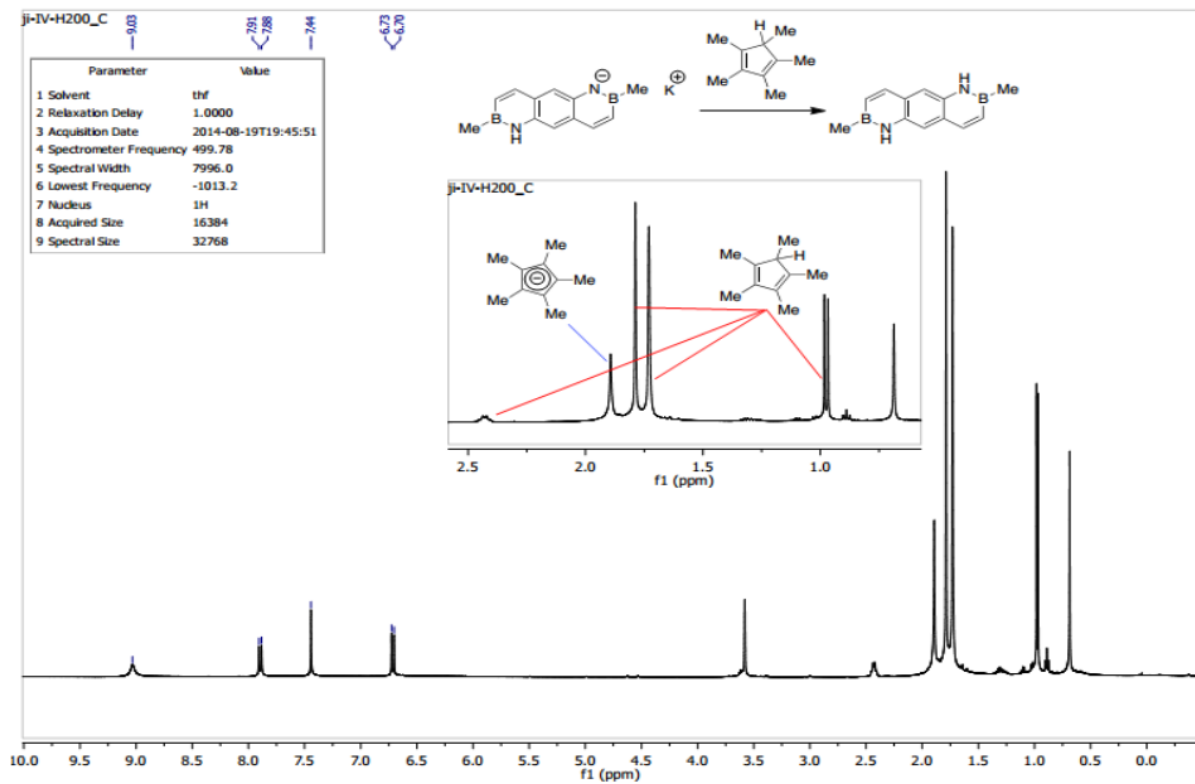
Parameter	Value
1 Solvent	thf
2 Relaxation Delay	5.0000
3 Pulse Width	0.0000
4 Acquisition Date	2013-12-18T17:45:51
5 Spectrometer Frequency	499.78
6 Spectral Width	7996.0
7 Lowest Frequency	-1016.0
8 Nucleus	1H
9 Acquired Size	16384
10 Spectral Size	32768











Ultraviolet Photoelectron Spectroscopy and Associated Calculations

Coupled UV-Photoelectron Spectroscopy – Mass Spectrometry Measurements. The UV-PES spectra were recorded on a home-built (IPREM/ECP), three-part spectrometer equipped with a main body device, He-I radiation source (21.21 eV and/or 48 eV) and a 127° cylindrical analyzer. The spectrometer works at constant analyzer energy under 5×10^{-6} hPa working pressure and $\leq 10^{-7}$ hPa for channeltron (X914L) pressure. The monitoring is done by a microcomputer supplemented by a digital–analogue converter (AEI spectrum). The spectra resulting from a single scan are built from 2048 points and are accurate within 0.05 eV. Spectra are calibrated with lines of xenon (12.13 and 13.44 eV) and of argon (15.76 and 15.94 eV). The accuracy of the ionization energies is ± 0.03 eV for sharp peaks and ± 0.05 eV for broad and overlapping signals. Mass spectra were recorded on a modified quadrupole mass spectrometer (PFEIFFER Prisma QMS200) with an electron-impact at 50 eV (mass range: 200 amu; detection limit: $\leq 10^{-14}$ hPa; working pressure: 2×10^{-7} hPa; operating temperature: 200 °C; electronic amplifier in working conditions: 10^{-10} A, QUAD STAR422 software for recording and treatment of MS data). The samples were slowly vaporized under low pressure (10^{-6} Torr) inside a handmade three-valve injector (3/4 inch diameter; 10 cm length; working temperature: $-190\text{ °C} \leq T \leq +300\text{ °C}$), and the gaseous flow was then continuously and simultaneously analyzed by both UV-photoelectron and mass spectrometers.

Anthracene's first ionization occurs at 7.4 eV and corresponds to ejection of an electron from the HOMO (b_{2g} symmetry). The second, third, and fourth ionizations occur at 8.6, 9.2, and 10.2 eV and correspond to HOMO–1 (b_{1g}), HOMO–2 (a_u), and HOMO–3 (b_{2g}), respectively. The first band of the PE spectrum of BN anthracene **1.5** (point group C_s) can be found at 7.7 eV and corresponds to its HOMO. This orbital has A'' symmetry and can be compared with the HOMO of anthracene. The second (8.3 eV), third (9.6 eV), and fourth ionizations (10.2 eV) correspond to HOMO–1 (A''), HOMO–2 (A''), and HOMO–3 (A), respectively. For bis- BN anthracene **2** (point group C_{2h}), the first ionization band was found at 8.0 eV (corresponding to the HOMO, b_g), followed by bands at 8.2 eV (b_g), 9.7 eV (a_u), and 10.4 eV (a_u). It is worth noting that the four highest occupied MOs for each anthracene molecule are π -type orbitals. A diagram showing the orbital energies (measured and calculated, CAM-B3LYP/6-311G(d,p)) is shown in Figure 1.4. BN/CC isosterism, lowers HOMO energies with respect to the all-carbon analogue.

Computational Methods. All calculations were performed using the Gaussian 09⁷⁹ program package with the 6-311G(d,p)⁸⁰ basis set. Extra diffuse functions (6-311++G(d,p)) are included in the basis set to improve the description of the Electron affinities (EA). DFT has been shown to predict various molecular properties of similar compounds successfully.⁸¹ All geometry optimizations were carried out with the CAM-

⁷⁹ Frisch, M. J.; et al. Gaussian 09, revision B.01; Gaussian, Inc.: Wallingford, CT, 2009.

⁸⁰ Raghavachari, K.; Binkley, J. S.; Seeger, R.; Pople, J. A. J. Chem. Phys. 1980, 72, 650–654.

⁸¹ (a) Parr, R. G.; Yang, W. Functional Theory of Atoms and Molecules; Oxford University Press: New York, 1989. (b) Frisch, M. J.; Trucks, G. W.; Cheeseman, J. R. in *Recent Development and Applications of Modern Density Functional Theory, Theoretical and Computational Chemistry*; Seminario, J. M., Ed.;

B3LYP⁸² functionals and were followed by frequency calculations in order to verify that the stationary points obtained were true energy minima. Ionization energies (IE) were calculated with Δ SCF-DFT, which means that separate SCF calculations were performed to optimize the orbitals of the ground state and the appropriate ionic state ($IE = E_{\text{cation}} - E_{\text{neutral}}$). The advantages of the most frequently employed Δ SCF-DFT method of calculations of the first ionization energies have been demonstrated previously.⁸³ The TD-DFT^{84,85} approach provides a first-principal method for the calculation of excitation energies within a density functional context taking into account the low-lying ion calculated by the Δ SCF method (the excitation energies of the radical cation obtained from a TD-DFT treatment were added to the ionization energy that was computed with the Δ SCF-DFT method). The vertical ionization energies were also calculated at the ab initio level according to OVGF⁸⁶ (in this case the effects of electron correlation and reorganization are included beyond the Hartree-Fock approximation and the self-energy part was expanded up to third order) and SAC-CI⁸⁷ (Symmetry Adapted Cluster / Configuration Interaction methods of Nakatsuji and coworkers which describes accurately and efficiently the electronic structures of the excited, ionized and electron-attached states of molecules) methods. MOLEKEL⁸⁸ was used as a visualization tool for all MOs.

Gaussian 09 Full reference:

Gaussian 09, Revision **E.01**, Frisch, M. J.; Trucks, G. W.; Schlegel, H. B.; Scuseria, G. E.; Robb, M. A.; Cheeseman, J. R.; Scalmani, G.; Barone, V.; Mennucci, B.; Petersson, G. A.; Nakatsuji, H.; Caricato, M.; Li, X.; Hratchian, H. P.; Izmaylov, A. F.; Bloino, J.; Zheng, G.; Sonnenberg, J. L.; Hada, M.; Ehara, M.; Toyota, K.; Fukuda, R.; Hasegawa, J.; Ishida, M.; Nakajima, T.; Honda, Y.; Kitao, O.; Nakai, H.; Vreven, T.; Montgomery, J. A., Jr.; Peralta, J. E.; Ogliaro, F.; Bearpark, M.; Heyd, J. J.; Brothers, E.; Kudin, K. N.;

Elsevier: Amsterdam, 1996; Vol. 4; pp 679–707. (c) Limacher, P. A.; Mikkelsen, K. V.; Lüthi, H. P. *J. Chem. Phys.* **2009**, *130*, 194114. (d) Kobayashi, R.; Amos, R. D. *Chem. Phys. Lett.* **2006**, *420*, 106–109. (e) Jacquemin, D.; Perpete, E. A.; Scalmani, G.; Frisch, M. J.; Kobayashi, R.; Adamo, C. *J. Chem. Phys.* **2007**, *126*, 144105.

⁸² (a) Becke, A. D. *Phys. Rev.* **1988**, *38*, 3098–3100. (b) Becke, A. D. *J. Chem. Phys.* **1993**, *98*, 5648–5652. (c) Lee, C.; Yang, W.; Parr, R. G. *Phys. Rev. B* **1988**, *37*, 785–789. (d) Yanai, T.; Tew, D.; Handy, N. *Chem. Phys. Lett.* **2004**, *393*, 51–57.

⁸³ (a) Bartnik, R.; Bayle, P.; Chrostowska, A.; Galindo, A.; Lesniak, S.; Pfister-Guillouzo, G. *Eur. J. Org. Chem.* **2003**, 2475–2479. (b) Chrostowska, A.; Matrane, A.; Maki, D.; Khayar, S.; Ushiki, H.; Gracia, A.; Belachemi, L.; Guillemin, J.-C. *ChemPhysChem* **2012**, *13*, 226–236. (c) Chrostowska, A.; Dargelos, A.; Khayar, S.; Wentrup, C. *J. Phys. Chem. A* **2012**, *116*, 9315–9320. (d) Vu, T. Y.; Chrostowska, A.; Huynh, T. K. X.; Khayar, S.; Dargelos, A.; Justyna, K.; Pasternak, B.; Lesniak, S.; Wentrup, C. *Chem. Eur. J.* **2013**, *19*, 14983–14988.

⁸⁴ Lemierre, V.; Chrostowska, A.; Dargelos, A.; Chermette, H. *J. Phys. Chem. A* **2005**, *109*, 8348–8355.

⁸⁵ (a) Stratmann, R. E.; Scuseria, G. E.; Frisch, M. J. *J. Chem. Phys.* **1998**, *109*, 8218–8224. (b) Casida, M. E.; Jamorski, C.; Casida, K. C.; Salahub, D. R. *J. Chem. Phys.* **1998**, *108*, 4439–4449.

⁸⁶ (a) von Niessen, W.; Schirmer, J.; Cederbaum, L. S. *Comput. Phys. Rep.* **1984**, *1*, 57–125. (b) Ortiz, J. V. *J. Chem. Phys.* **1988**, *89*, 6348–6352.

⁸⁷ Nakatsuji, H.; Hirao, K. *J. Chem. Phys.* **1978**, *68*, 2053–2065. See also: <http://www.qcri.or.jp/sacaci/> (accessed August 2014).

⁸⁸ (a) Portmann, S.; Lüthi, H. P. MOLEKEL 4.3; Swiss National Supercomputing Center: Lugano, Switzerland. (b) Portmann, S.; Lüthi, H. P. CHIMIA 2000, *54*, 766–770.

Staroverov, V. N.; Kobayashi, R.; Normand, J.; Raghavachari, K.; Rendell, A.; Burant, J. C.; Iyengar, S. S.; Tomasi, J.; Cossi, M.; Rega, N.; Millam, J. M.; Klene, M.; Knox, J. E.; Cross, J. B.; Bakken, V.; Adamo, C.; Jaramillo, J.; Gomperts, R.; Stratmann, R. E.; Yazyev, O.; Austin, A. J.; Cammi, R.; Pomelli, C.; Ochterski, J. W.; Martin, R. L.; Morokuma, K.; Zakrzewski, V. G.; Voth, G. A.; Salvador, P.; Dannenberg, J. J.; Dapprich, S.; Daniels, A. D.; Farkas, Ö.; Foresman, J. B.; Ortiz, J. V.; Cioslowski, J.; Fox, D. J. Gaussian, Inc., Wallingford CT, 2009.

Table 1.2. Calculated Kohn-Sham energies of MO ($-\epsilon^{K-S}$), Δ SCF/TD-DFT (CAM-B3LYP), OVGF, SAC-CI and “corrected” ionization energies with the MOLEKEL MOs visualization of anthracene in comparison with experimental values (in eV). For all calculations 6-311G(d,p) basis set was applied.

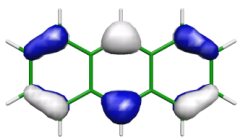
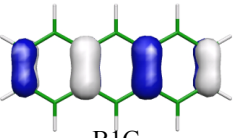
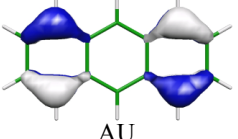
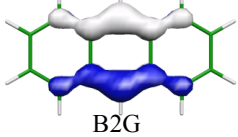
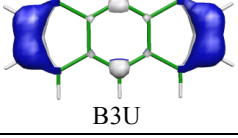
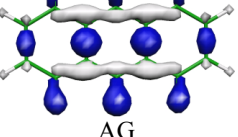
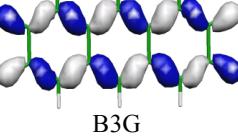
Nature of MO	$-\epsilon^{K-S}$	Δ SCF/TD-DFT	OVGF	P3	SAC-CI	Corrected $x_{exp} = 0.711$	Exp. ^{ref}
 B2G	6.73	7.27	7.15	7.35	6.779	7.44	7.4
 B1G	8.00	8.64	8.31	8.55	8.039	8.72	8.6
 AU	8.67	9.15	8.97	9.163	8.88	9.38	9.2
 B2G	9.95	10.36	10.16	10.309	9.99	10.67	10.2
 B3U	10.12	10.58	10.29	10.389	10.21	10.83	10.5
 AG	10.66	11.20	11.18	11.384	11.24	11.37	11.0
 B3G	10.95	11.53	11.38	11.675	11.52	11.66	11.5
B2U	11.23	11.86	11.84	11.954	11.85	11.94	11.9

Table 1.3 Calculated Kohn-Sham energies of MO ($-\epsilon^{K-S}$), Δ SCF/TD-DFT (CAM-B3LYP), OVGf, SAC-CI and “corrected” ionization energies with the MOLEKEL MOs visualization of NH-BH-anthracene **1.5** in comparison with experimental values (in eV). For all calculations 6-311G(d,p) basis set was applied.

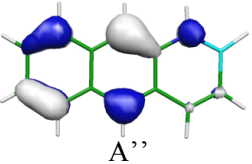
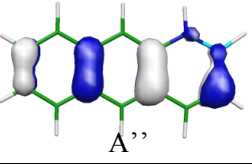
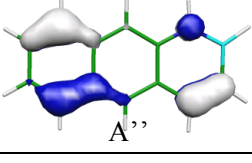
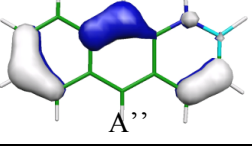
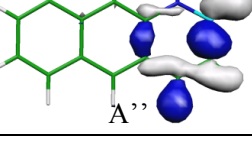
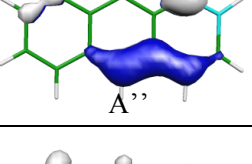
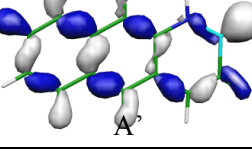
Nature of MO	$-\epsilon^{K-S}$	Δ SCF/TD-DFT	OVGF	P3	SAC-CI	Corrected $x_{exp}=0.629$	Exp.
 A''	7.07	7.60	7.47	7.66	6.97	7.7	7.7
 A''	7.70	8.36	9.03	8.24	7.56	8.33	8.3
 A''	9.13	9.59	9.44	8.59	9.12	9.76	9.6
 A''	9.88	10.30	10.14	10.22	9.83	10.51	10.2
 A''	10.36	10.95	10.73	10.80	10.48	10.99	10.7
 A''	10.49	11.12	11.01	11.02	10.60	11.12	11.3
 A'	10.92	11.53	11.53	11.66	11.17	11.55	
	11.05	11.66	11.62	11.76	11.23	11.68	

Table 1.4. Calculated Kohn-Sham energies of MO ($-\epsilon^{K-S}$), Δ SCF/TD-DFT (CAM-B3LYP), OVGF, SAC-CI and “corrected” ionization energies with the MOLEKEL MOs visualization of *anti*-NH-BH-anthracene **1.11** in comparison with experimental values (in eV). For all calculations 6-311G(d,p) basis set was applied.

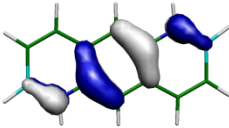
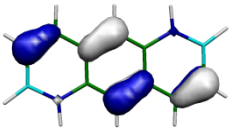
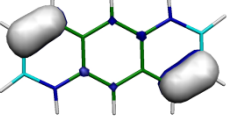
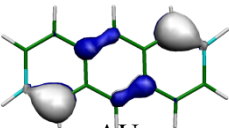
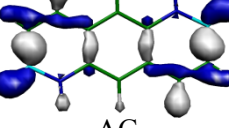
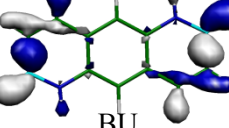
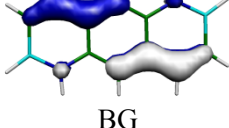
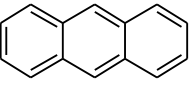
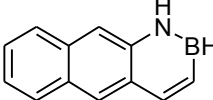
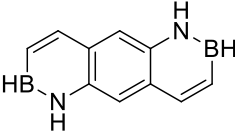
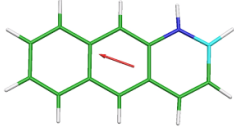
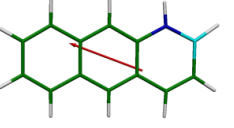
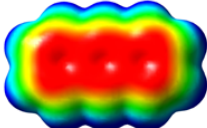
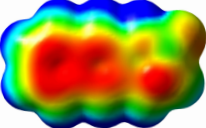
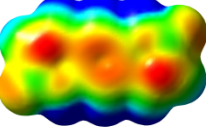
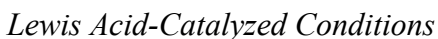
Nature of MO	$-\epsilon^{K-S}$	Δ SCF/TD-DFT	OVGF	P3	SAC-CI	Corrected $x_{exp}=0.634$	Exp.
 BG	7.32	7.82	7.66	7.83	7.27	7.95	7.95
 BG	7.61	8.14	7.87	8.10	7.68	8.25	8.2
 AU	9.40	9.74	9.76	9.88	9.58	10.04	9.7
 AU	10.16	10.44	10.47	10.42	10.28	10.79	10.4
 AG	10.39	11.07	11.03	11.04	10.79	11.02	11.0
 BU	10.44	11.15	11.12	11.09	10.88	11.07	11.0
 BG	10.54	10.98	10.83	10.91	10.66	11.18	11.0
AG	10.98	11.61	11.70	11.75	11.53	11.61	11.6

Table 1.5. CAM-B3LYP/6-311G(d,p) Ground and First Excited State Dipole Moments (Debye) and Electrostatic Potential Surface Map at the 0.001 electron a.u.⁻³ density iso-contour level (from +12.55 to -12.55 kcal mole⁻¹), Δ SCF Ionization Energy (IE), HOMO, LUMO energies and HOMO-LUMO gap, Electron Affinity (EA, calculated with 6-311++G(d,p)), Δ (EA-IE), first HOMO \rightarrow LUMO UV transition (calculated with 6-311++G(d,p)) for anthracene, **1.5**, and **1.11**.

	 Anthracene	 1.5	 1.11
Ground state dipole moment (Debye)	0.000	 1.258	0.000
First excited state dipole moment (Debye)	0.000	 3.065	0.000
Electrostatic potential surface Map			
Δ SCF (Ionization Energy IE (eV))	7.273	7.596	7.818
HOMO (eV)	-6.729	-7.071	-7.316
LUMO (eV)	-0.742	-0.677	-0.745
HOMO-LUMO Gap (eV)	5.987	6.394	6.571
Electron affinity (eV)	0.369	0.323	0.393
Δ (IE+EA) (eV)	7.642	7.919	8.211
First HOMO \rightarrow LUMO UV transition (eV)	3.6245	3.9246	3.9556

Uncatalyzed Conditions

Scheme 1.11. Attempted Diels-Alder Reactions



58

[CAM-B3LYP/6-311G(d,p)] Atomic Coordinates of Optimized Geometry

Atomic coordinates for [CAM-B3LYP/6-311G(d,p)] optimized geometry, value of total energy of anthracene

C	3.63934500	-0.71188300	0.00000000
C	2.46925100	-1.39974700	0.00000100
C	1.21562200	-0.71594300	0.00000000
C	1.21562200	0.71594300	0.00000000
C	2.46925100	1.39974700	0.00000000
C	3.63934500	0.71188300	0.00000000
C	0.00000000	-1.39455100	0.00000000
C	0.00000000	1.39455100	0.00000000
C	-1.21562200	0.71594300	0.00000000
C	-1.21562200	-0.71594300	0.00000000
C	-2.46925100	-1.39974700	0.00000000
H	-2.46653100	-2.48402900	0.00000000
C	-3.63934500	-0.71188300	-0.00000100
C	-3.63934500	0.71188300	0.00000000
C	-2.46925100	1.39974700	0.00000000
H	0.00000000	-2.47970700	0.00000100
H	4.58363500	-1.24298800	0.00000000
H	2.46653100	-2.48402900	0.00000100
H	2.46653100	2.48402900	0.00000000
H	4.58363500	1.24298800	-0.00000100
H	0.00000000	2.47970700	0.00000000
H	-4.58363500	-1.24298800	-0.00000100
H	-4.58363500	1.24298800	-0.00000100
H	-2.46653100	2.48402900	0.00000000

E_{tot}= -539.65518037 au

Atomic coordinates for [CAM-B3LYP/6-311G(d,p)] optimized geometry, value of total energy of Mono-BN-anthracene **1.5**

C	-3.62783200	0.72290300	-0.00000100
C	-2.44924700	1.40506200	-0.00000100
C	-1.20721600	0.71469800	0.00000000
C	-1.20862600	-0.70983100	0.00000000
C	-2.45740500	-1.38816600	-0.00000100
C	-3.62945200	-0.69368200	-0.00000100
C	0.02376700	1.38553100	0.00000000
C	0.01651800	-1.39467400	0.00000000
C	1.21589800	-0.71605800	0.00000100
C	1.22915000	0.71138300	0.00000000
C	2.49251100	1.41500500	0.00000000
H	2.43534100	2.50100400	0.00000000
C	3.67974600	0.77614700	0.00000100
H	0.03113000	2.47066700	0.00000000
H	-4.56900300	1.25904300	-0.00000200
H	-2.44077100	2.48937600	-0.00000100
H	-2.46184900	-2.47239500	-0.00000100
H	-4.57360300	-1.22526600	-0.00000200
H	0.01498800	-2.48012200	0.00000000
H	4.58668400	1.37111800	0.00000100
B	3.69398800	-0.75317800	0.00000200
H	4.66495300	-1.44224200	0.00000100
N	2.43075200	-1.38353200	0.00000100
H	2.36006300	-2.39046000	0.00000100

E_{tot}= -542.78167034

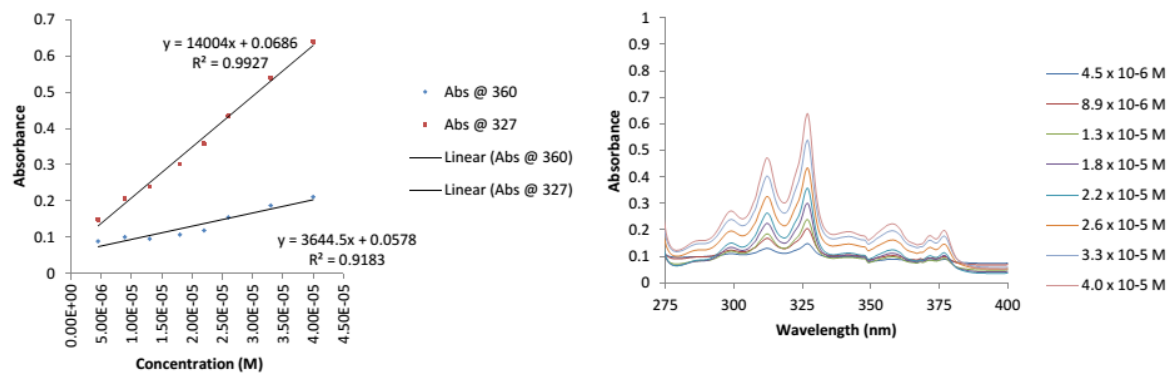
Atomic coordinates for [CAM-B3LYP/6-311G(d,p)] optimized geometry, value of total energy of Bis-BN-anthracene **1.11**

C	-1.20771900	0.71208700	-0.00000100
C	-1.22012000	-0.70337200	-0.00000100
C	0.00476900	1.38429500	0.00000000
C	-0.00476900	-1.38429500	0.00000000
C	1.20771900	-0.71208700	0.00000100
C	1.22012000	0.70337200	0.00000100
C	2.48093200	1.40484100	0.00000100
H	2.42871900	2.49112600	0.00000100
C	3.66814100	0.76166600	0.00000200
H	0.01390400	2.46978200	0.00000000
H	-0.01390400	-2.46978200	0.00000000
H	4.57533500	1.35641100	0.00000300
B	3.68264200	-0.76602400	0.00000300
H	4.65183200	-1.45734600	0.00000300
N	2.41664700	-1.38945700	0.00000200
H	2.33963100	-2.39593700	0.00000100
B	-3.68264200	0.76602400	-0.00000300
H	-4.65183200	1.45734600	-0.00000400
N	-2.41664700	1.38945700	-0.00000200
C	-2.48093200	-1.40484100	-0.00000200
H	-2.42871900	-2.49112600	-0.00000200
C	-3.66814100	-0.76166600	-0.00000300
H	-4.57533500	-1.35641100	-0.00000400
H	-2.33963100	2.39593700	-0.00000300

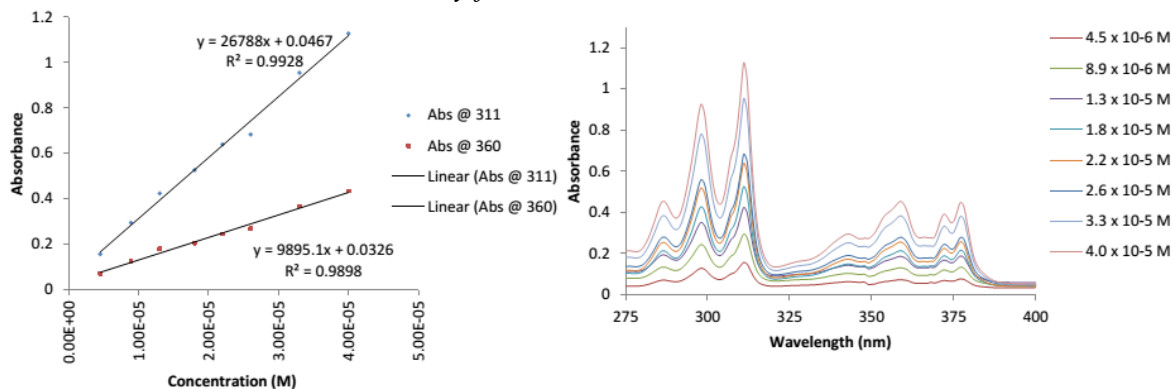
E_{tot}= -546.22619426

Supplemental Photophysical Studies

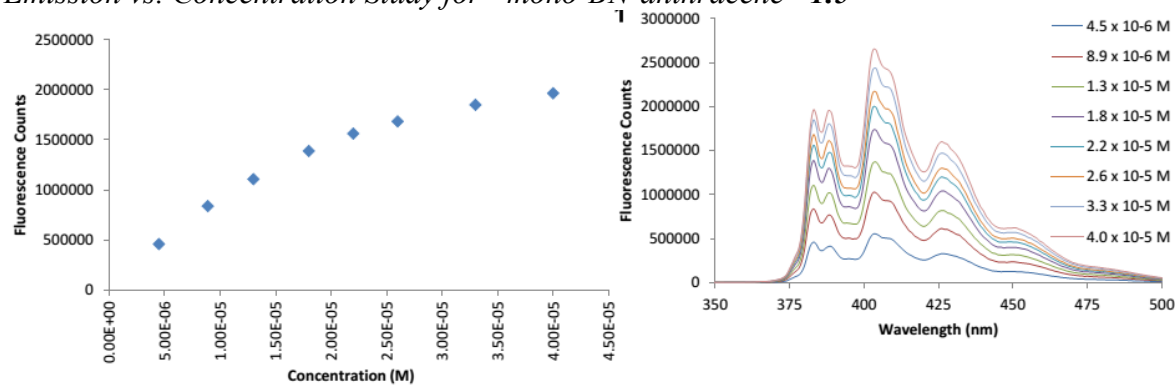
Absorbance vs. Concentration Study for "mono-BN-anthracene" 1.5



Absorbance vs. Concentration Study for "bis-BN-anthracene" 1.11

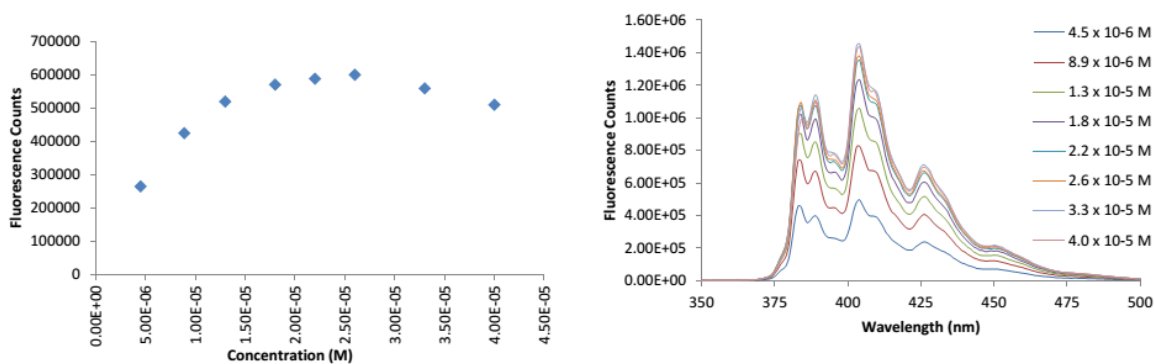


Emission vs. Concentration Study for "mono-BN-anthracene" 1.5



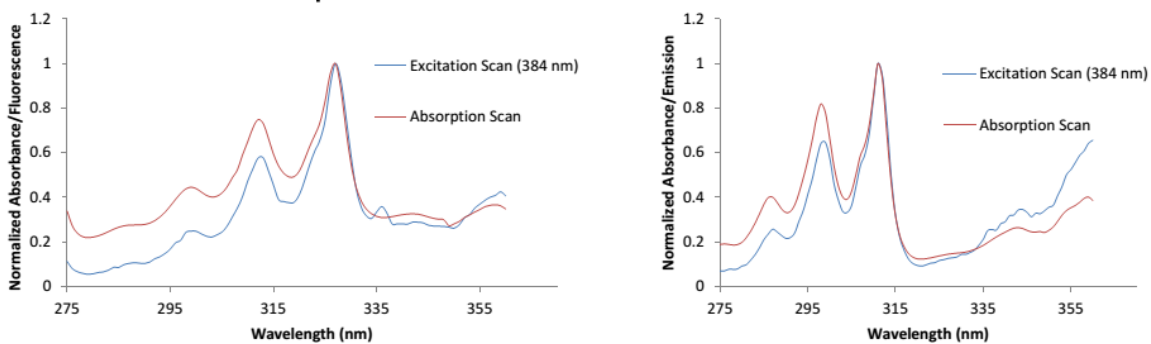
Left graph is emission at 384 nm vs. concentration

Emission vs. Concentration Study for “bis-BN-anthracene” 1.11

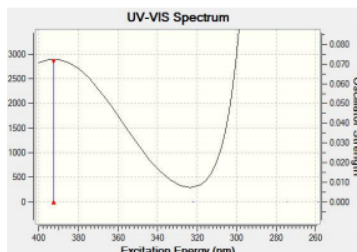
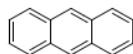


Left graph is emission at 384 nm vs. concentration.

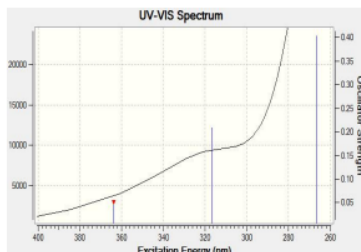
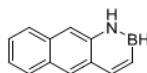
Excitation Scan (Detection at 384 nm) Overlay with Absorbance (1.5 Left, 1.11 Right)



TD-DFT Results

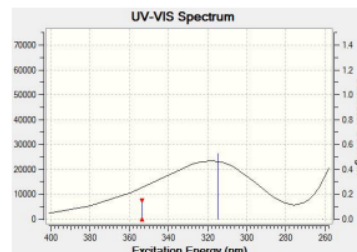
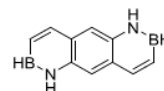


Excited State 1: Singlet-B1U 3.1597 eV
392.39 nm f=0.0714 HOMO→LUMO



Excited State 1: Singlet-A 3.4095 eV
363.64 nm f=0.0501 HOMO→LUMO

Excited State 2: Singlet-A 3.9157 eV
316.64 nm f=0.2081
HOMO-1→LUMO 75%
HOMO-1→LUMO+1 18%



Excited State 1: Singlet 3.5084 eV
353.39 nm f=0.1479
HOMO→LUMO 96%
HOMO-1→LUMO+2 4%

Excited State 2: Singlet 3.9388 eV
314.77 nm f=0.5260
HOMO-1→LUMO 93%
HOMO-1→LUMO+2 4%

Full Reference for Gaussian 09

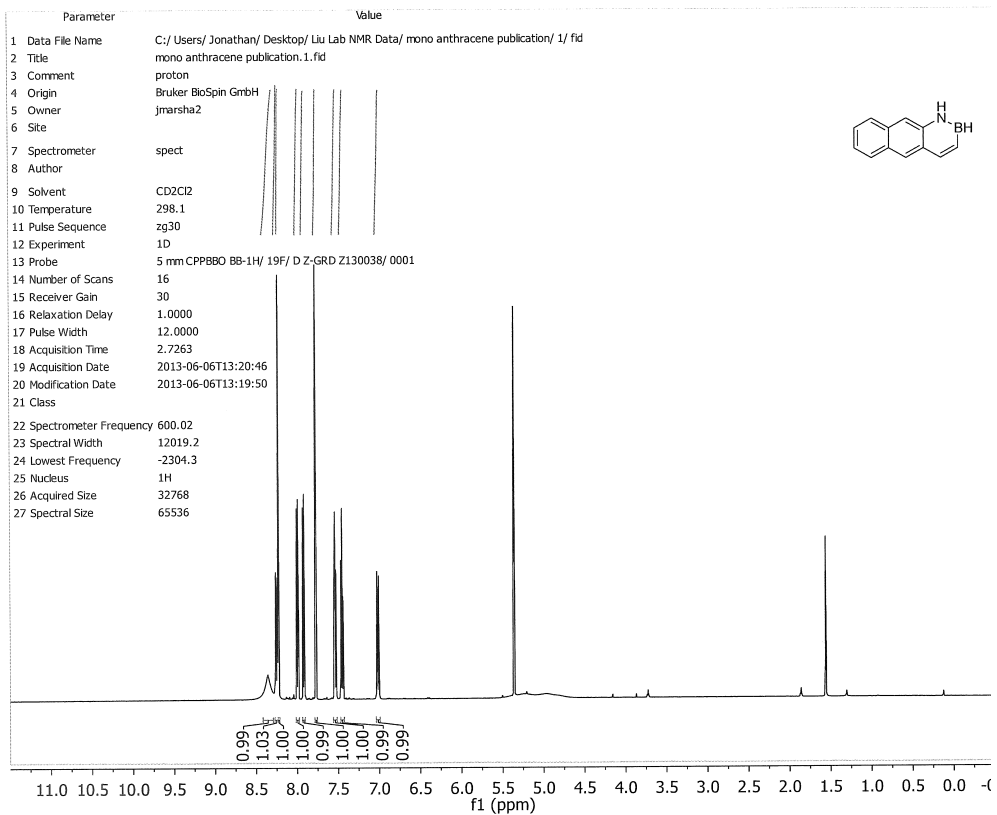
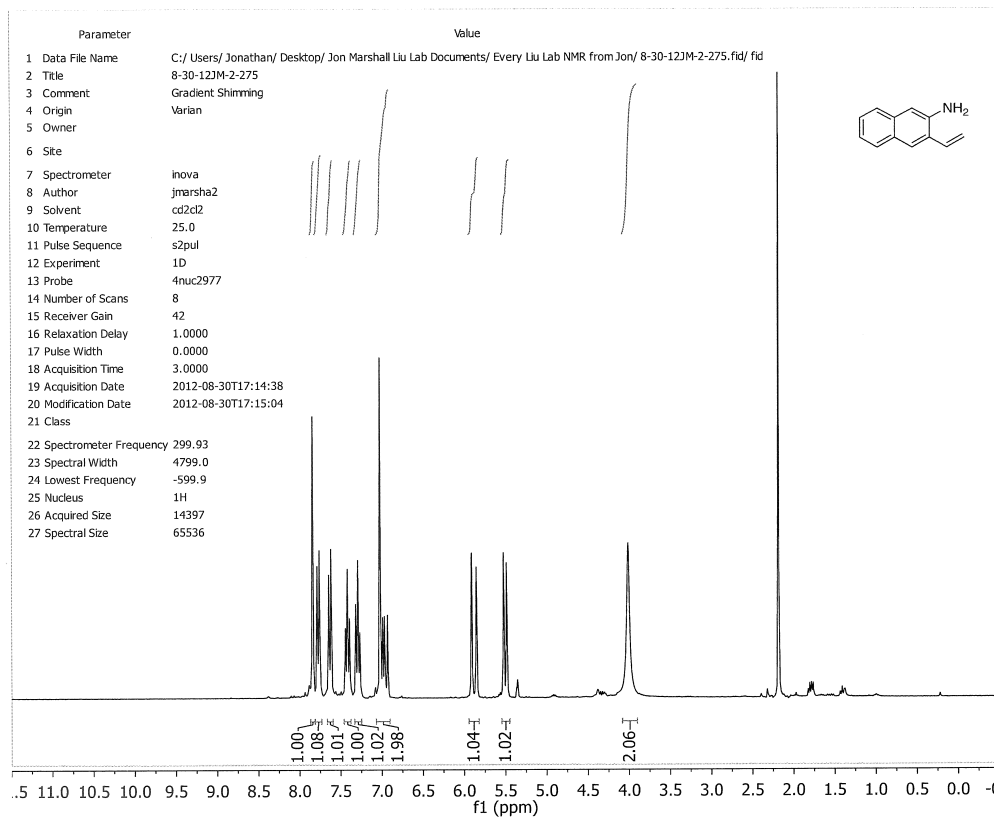
Frisch, M. J.; Trucks, G. W.; Schlegel, H. B.; Scuseria, G. E.; Robb, M. A.; Cheeseman, J. R.; Scalmani, G.; Barone, V.; Mennucci, B.; Petersson, G. A.; Nakatsuji, H.; Caricato, M.; Li, X.; Hratchian, H. P.; Izmaylov, A. F.; Bloino, J.; Zheng, G.; Sonnenberg, J. L.; Hada, M.; Ehara, M.; Toyota, K.; Fukuda, R.; Hasegawa, J.; Ishida, M.; Nakajima, T.; Honda, Y.; Kitao, O.; Nakai, H.; Vreven, T.; Montgomery, J. A., Jr.; Peralta, J. E.; Ogliaro, F.; Bearpark, M.; Heyd, J. J.; Brothers, E.; Kudin, K. N.; Staroverov, V. N.; Kobayashi, R.; Normand, J.; Raghavachari, K.; Rendell, A.; Burant, J. C.; Iyengar, S. S.; Tomasi, J.; Cossi, M.; Rega, N.; Millam, J. M.; Klene, M.; Knox, J. E.; Cross, J. B.; Bakken, V.; Adamo, C.; Jaramillo, J.; Gomperts, R.; Stratmann, R. E.; Yazyev, O.; Austin, A. J.; Cammi, R.; Pomelli, C.; Ochterski, J. W.; Martin, R. L.; Morokuma, K.; Zakrzewski, V. G.; Voth, G. A.; Salvador, P.; Dannenberg, J. J.; Dapprich, S.; Daniels, A. D.; Farkas, O.; Foresman, J. B.; Ortiz, J. V.; Cioslowski, J.; Fox, D. J. *Gaussian 09, Revision C.01*; Gaussian Inc., Wallingford, CT, 2010.

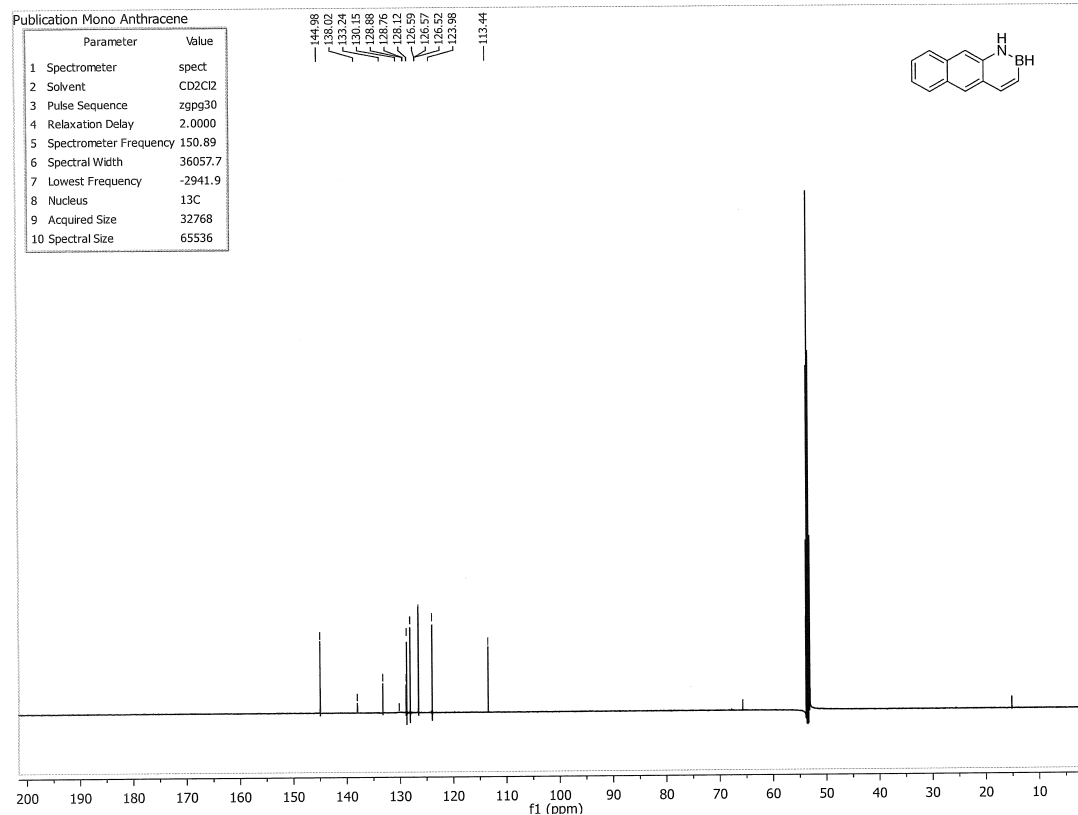
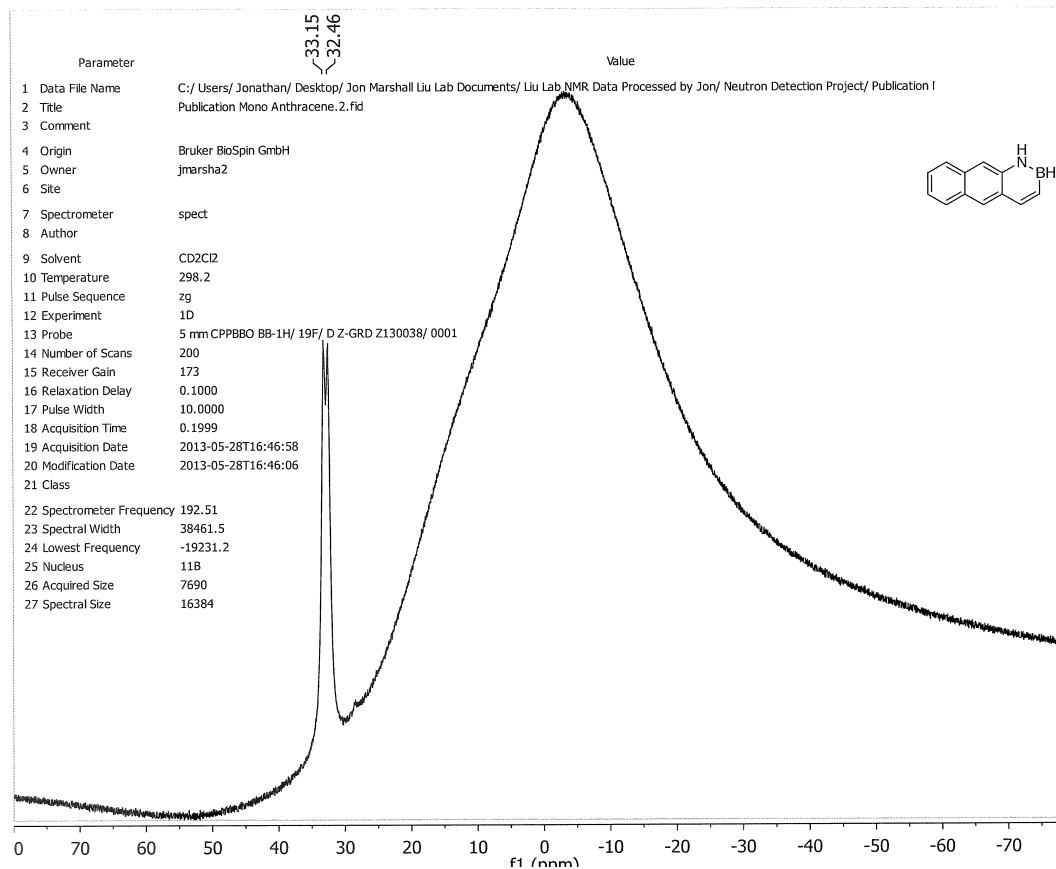
Crystal data and structure refinement for B-Ph BN anthracene

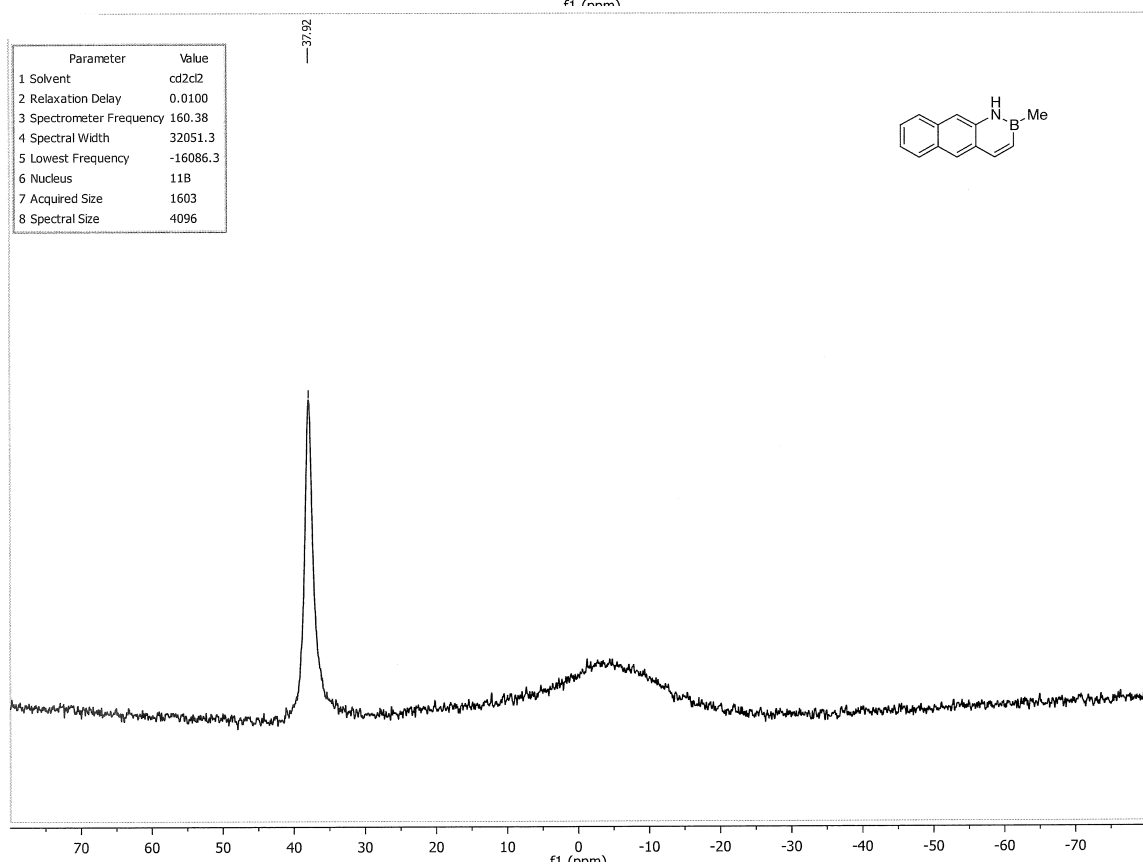
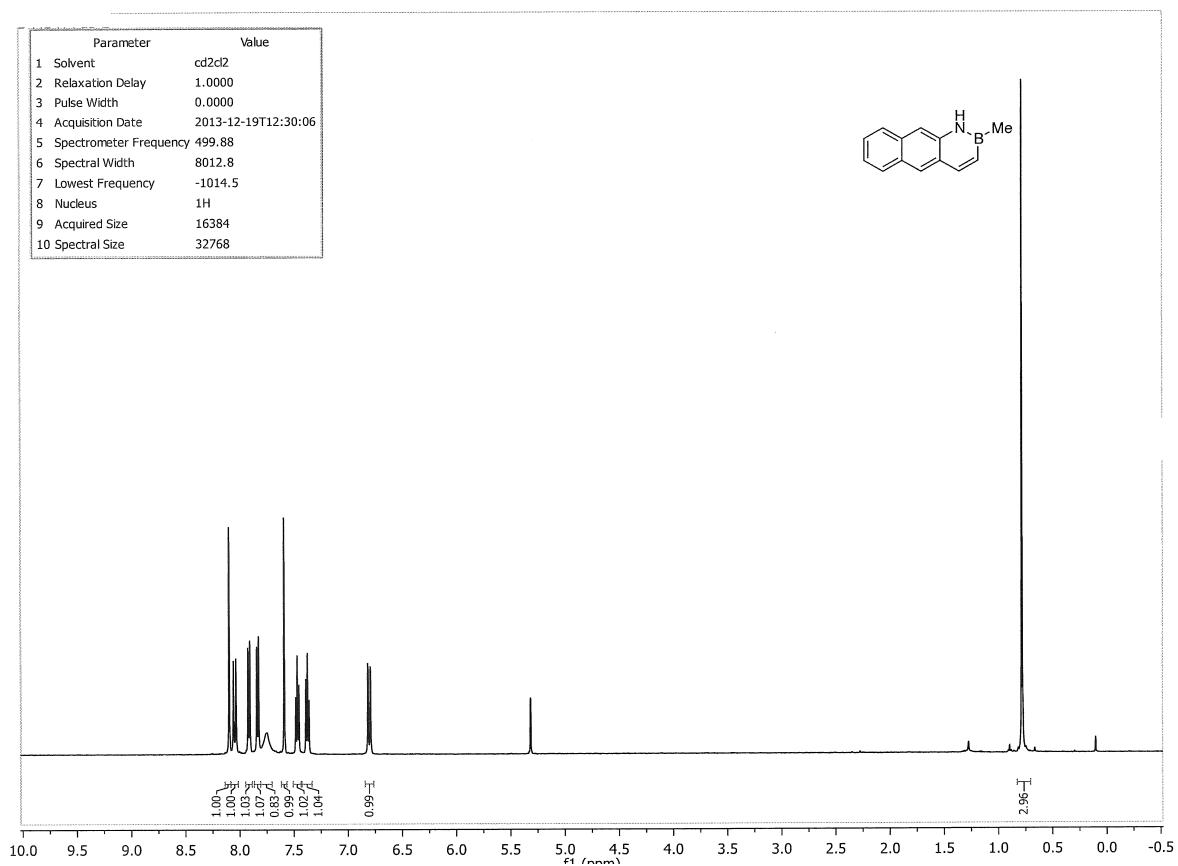
Identification code	liu245	
Empirical formula	C ₁₈ H ₁₄ B N	
Formula weight	255.11	
Temperature	173(2) K	
Wavelength	1.54178 Å	
Crystal system	Monoclinic	
Space group	P1 21/n1	
Unit cell dimensions	a = 7.6082(4) Å	$\alpha = 90^\circ$
	b = 5.8948 (3) Å	$\beta = 93.583(3)^\circ$
	c = 28.699(15) Å	$\gamma = 90^\circ$
Volume	1284.60(12) Å ³	
Z	4	
Density (calculated)	1.319 g/cm ³	
Absorption coefficient	0.574 mm ⁻¹	
F(000)	536	
Crystal size	0.250 x 0.230 x 0.040 mm ³	
Theta range for data collection	3.09 to 66.78°	
Index ranges	-8<= <i>h</i> <=9, -7<= <i>k</i> <=6, -34<= <i>l</i> <=32	
Reflections collected	8807	
Independent reflections	2260 [R(int) = 0.0385]	
Completeness to theta = 28.00°	99.6 %	
Absorption correction	multi-scan	
Refinement method	Full-matrix least-squares on F ²	
Data / restraints / parameters	2260 / 0 / 237	
Goodness-of-fit on F ²	1.103	
Final R indices [I>2sigma(I)]	R1 = 0.0616, wR2 = 0.1449	
R indices (all data)	R1 = 0.0666, wR2 = 0.1485	
Largest diff. peak and hole	0.375 and -0.250 e.Å ⁻³	

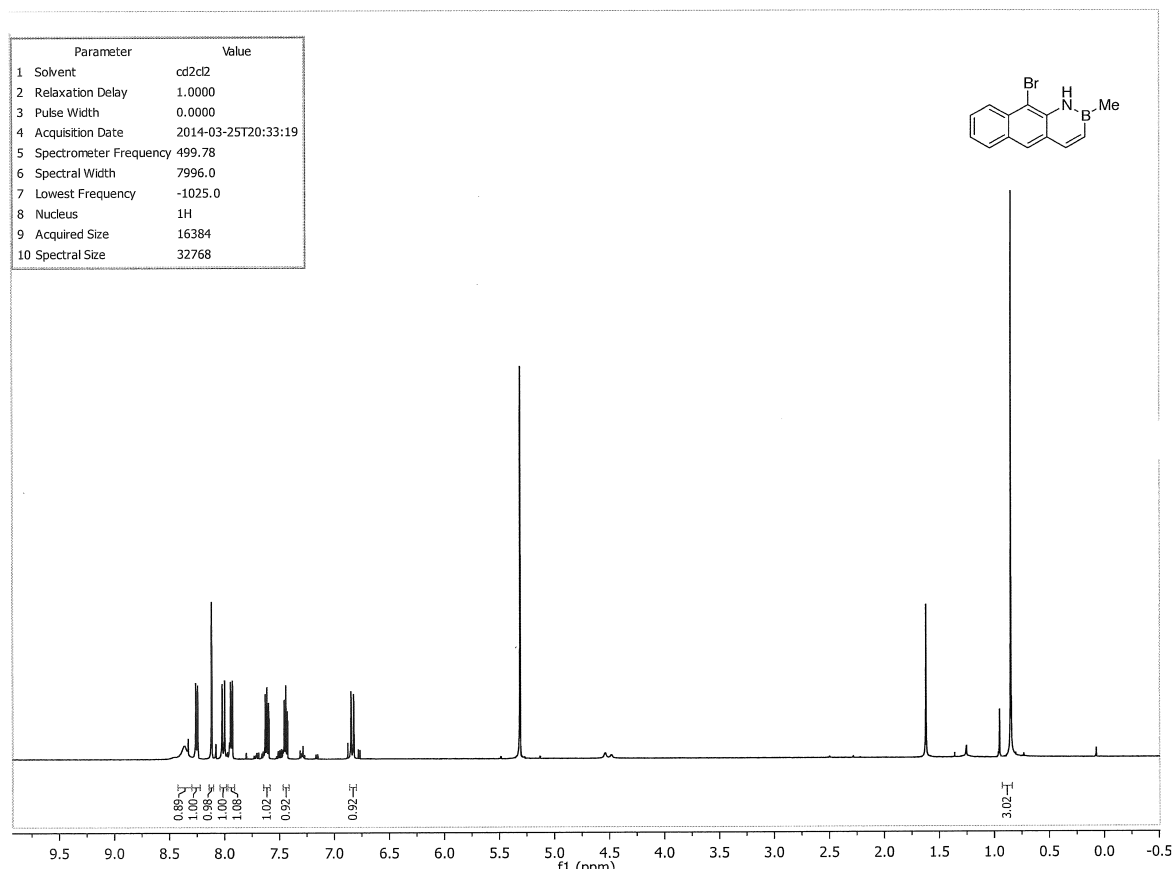
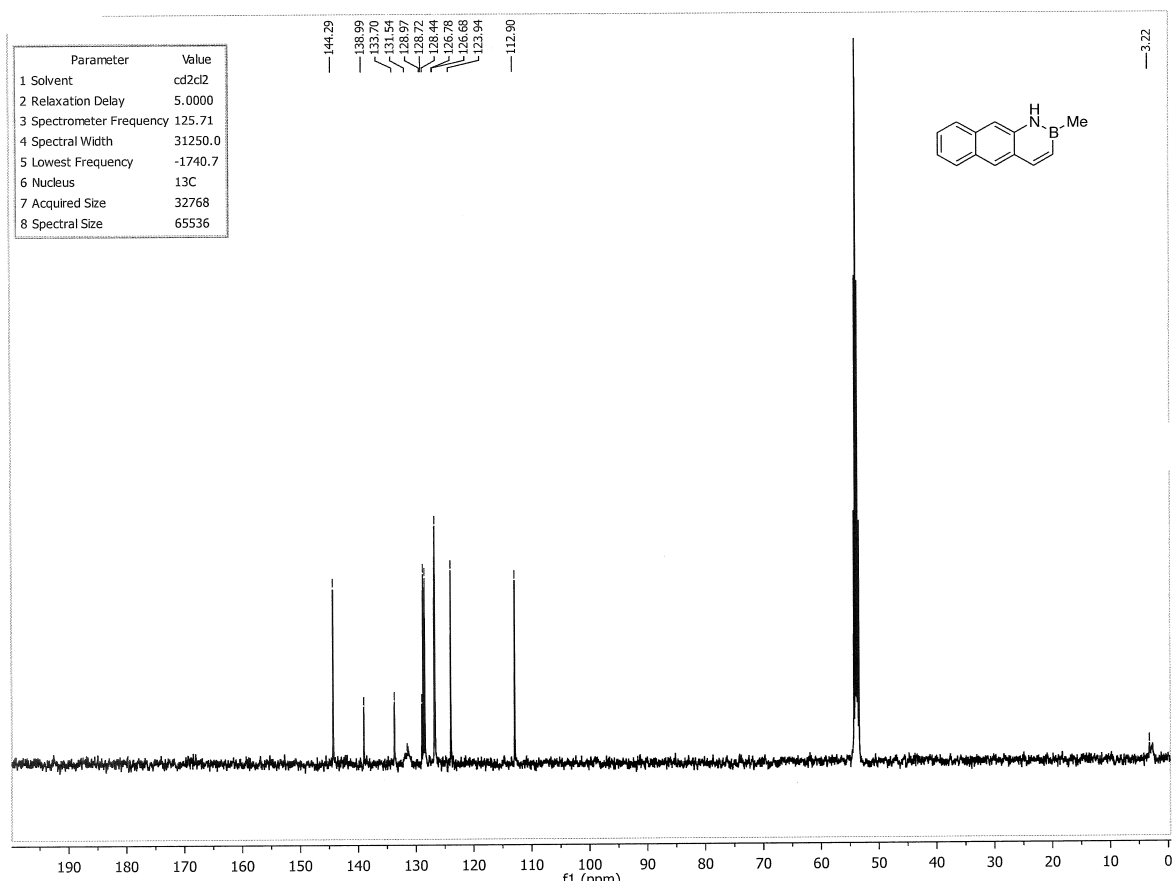
Crystal data and structure refinement for **1.14**

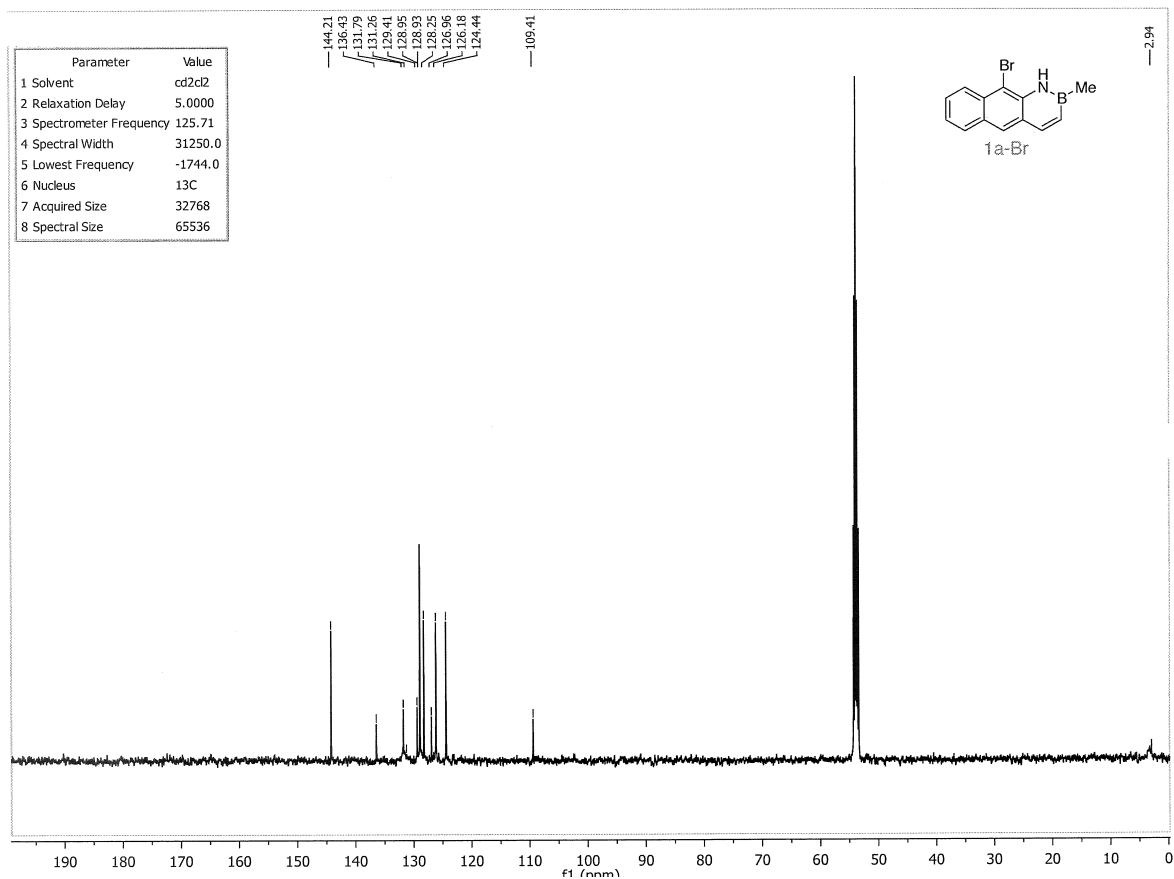
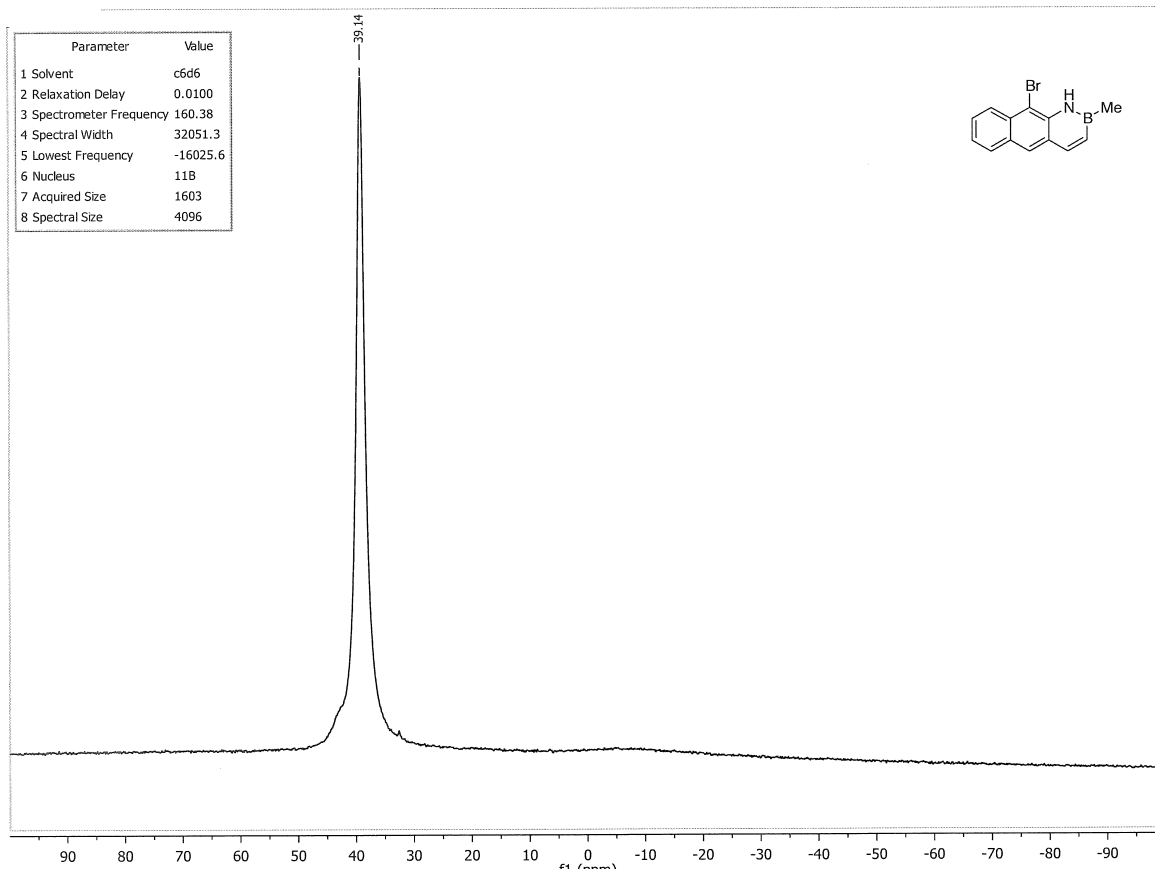
Identification code	C36H27BN2	
Empirical formula	C36 H27 B N2	
Formula weight	498.40	
Temperature	100(2) K	
Wavelength	0.71073 Å	
Crystal system	Monoclinic	
Space group	Cc	
Unit cell dimensions	a = 10.982(3) Å	$\alpha = 90^\circ$
	b = 40.431(10) Å	$\beta = 132.593(4)^\circ$
	c = 8.0776(18) Å	$\gamma = 90^\circ$
Volume	2640.4(11) Å ³	
Z	4	
Density (calculated)	1.254 Mg/m ³	
Absorption coefficient	0.072 mm ⁻¹	
F(000)	1048	
Crystal size	0.620 x 0.480 x 0.120 mm ³	
Theta range for data collection	2.015 to 30.173°	
Index ranges	-15 ≤ h ≤ 14, -53 ≤ k ≤ 53, -10 ≤ l ≤ 11	
Reflections collected	19259	
Independent reflections	6317 [R(int) = 0.0385]	
Completeness to theta = 28.00°	99.8 %	
Absorption correction	Semi-empirical from equivalents	
Max. and min. transmission	0.7460 and 0.6177	
Refinement method	Full-matrix least-squares on F ²	
Data / restraints / parameters	6317 / 3 / 356	
Goodness-of-fit on F ²	1.017	
Final R indices [I > 2sigma(I)]	R1 = 0.0418, wR2 = 0.0924	
R indices (all data)	R1 = 0.0507, wR2 = 0.0974	
Largest diff. peak and hole	0.277 and -0.241 e.Å ⁻³	



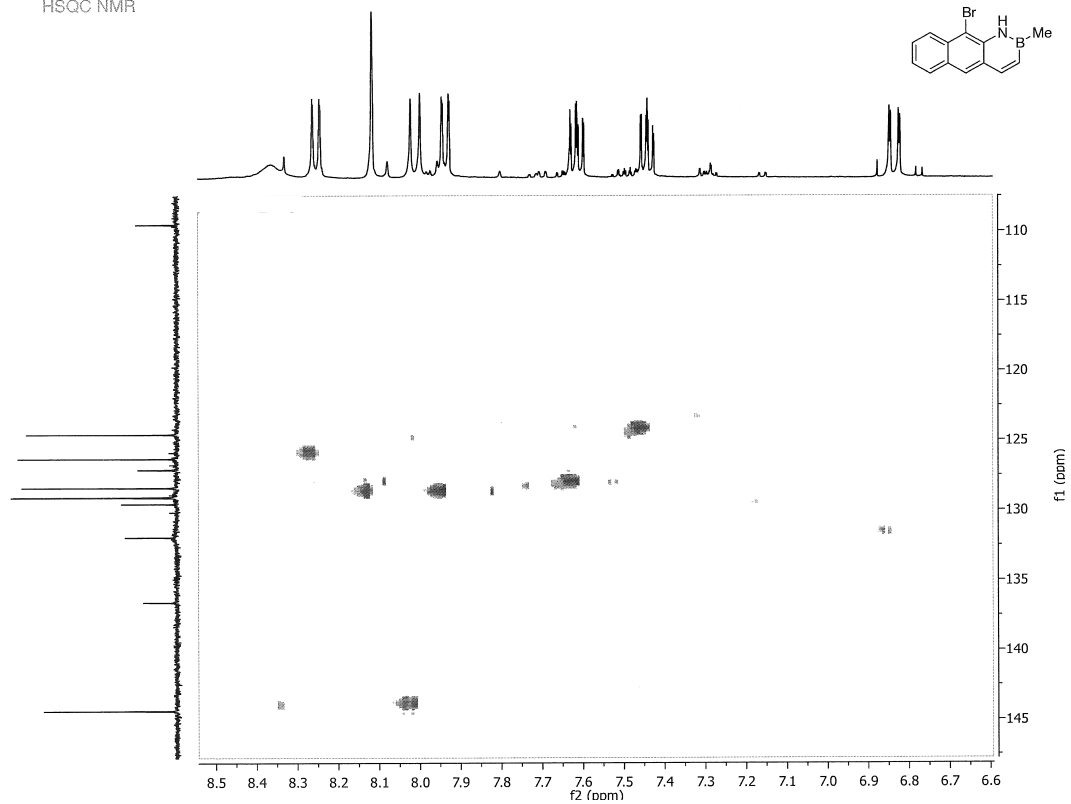




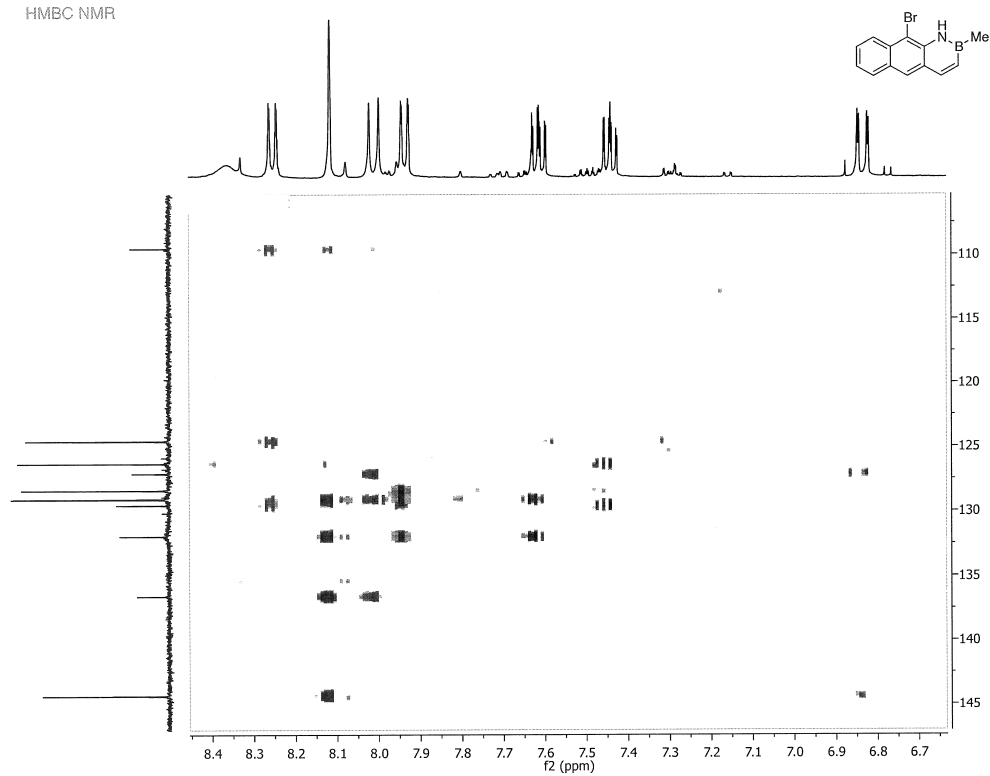


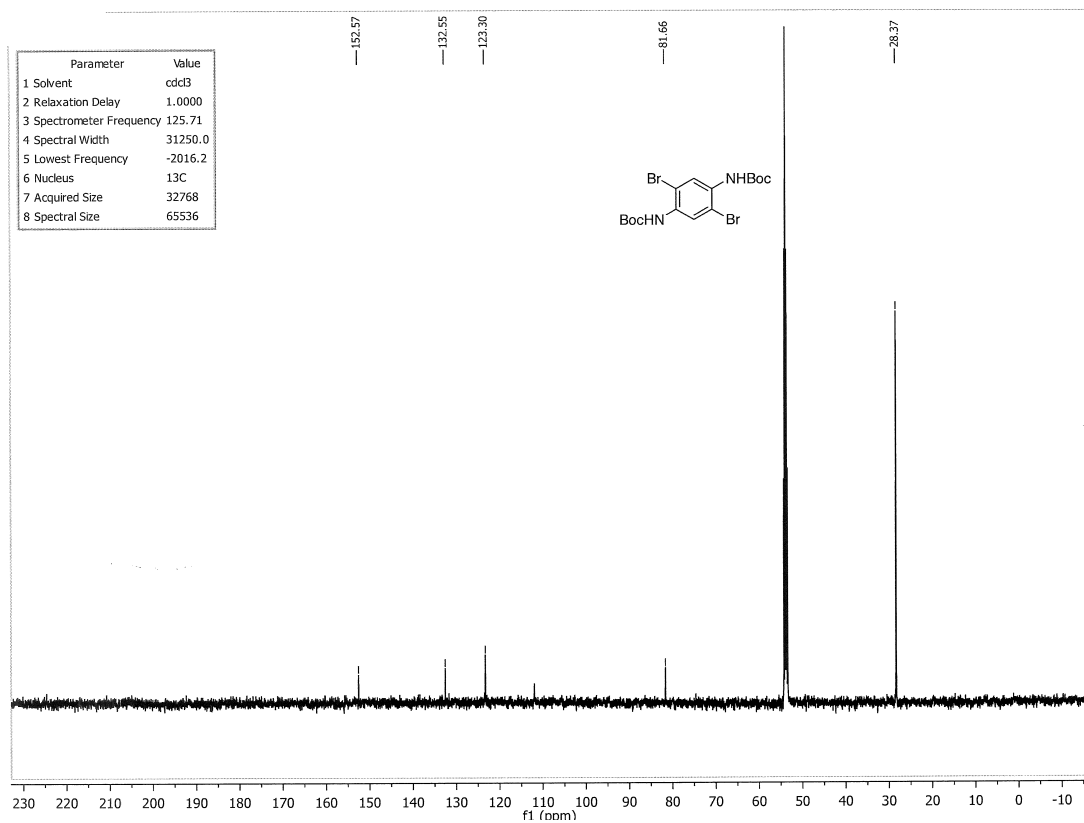
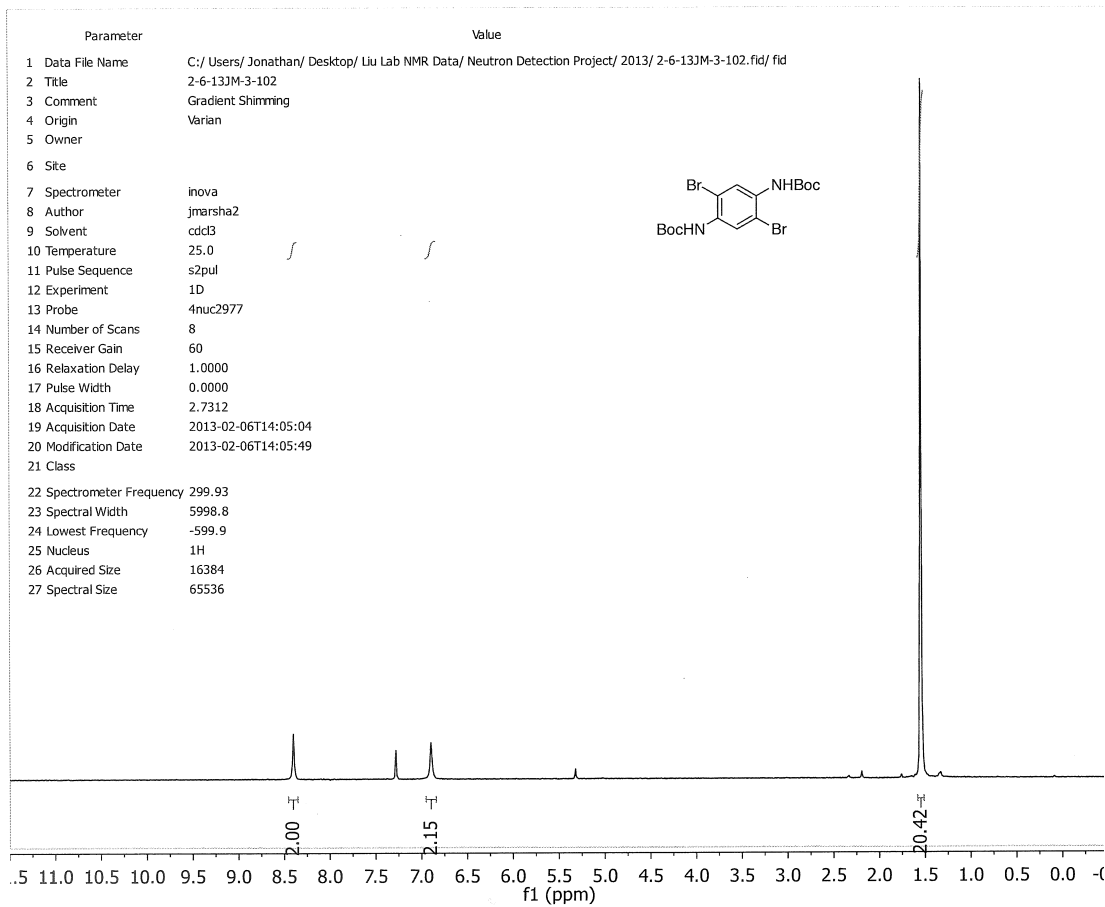


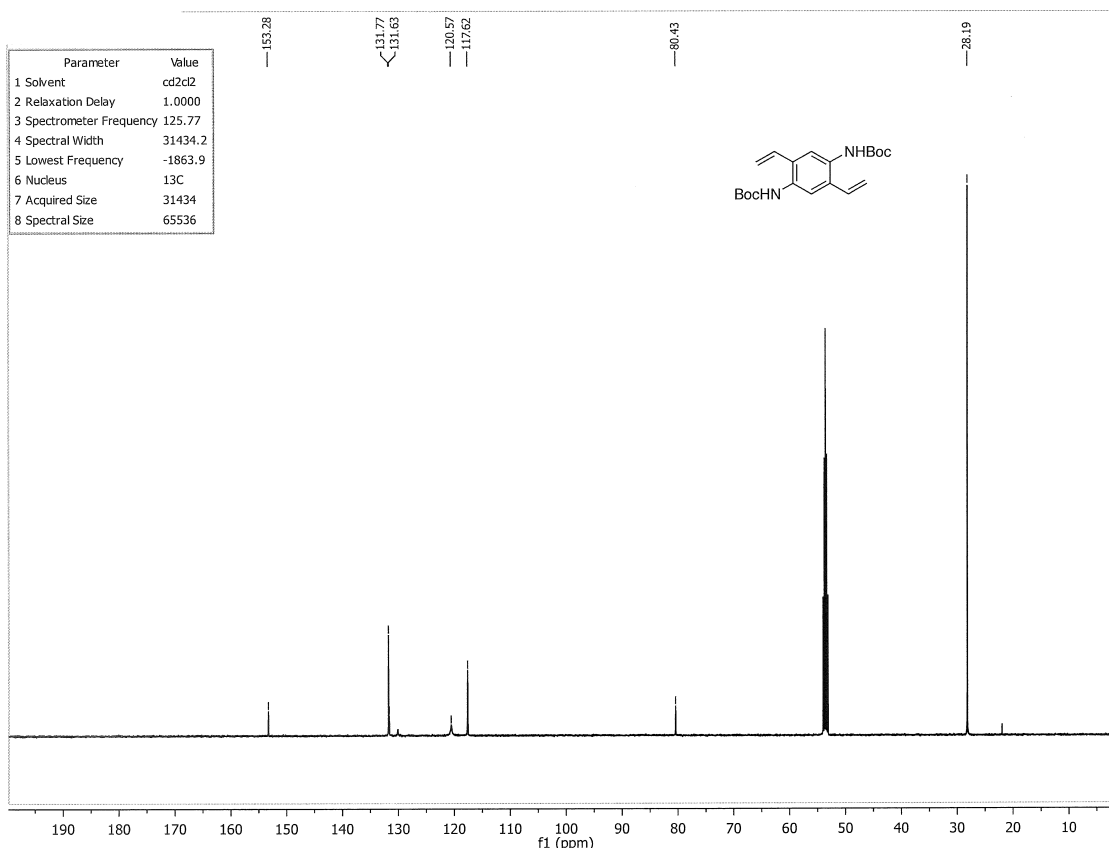
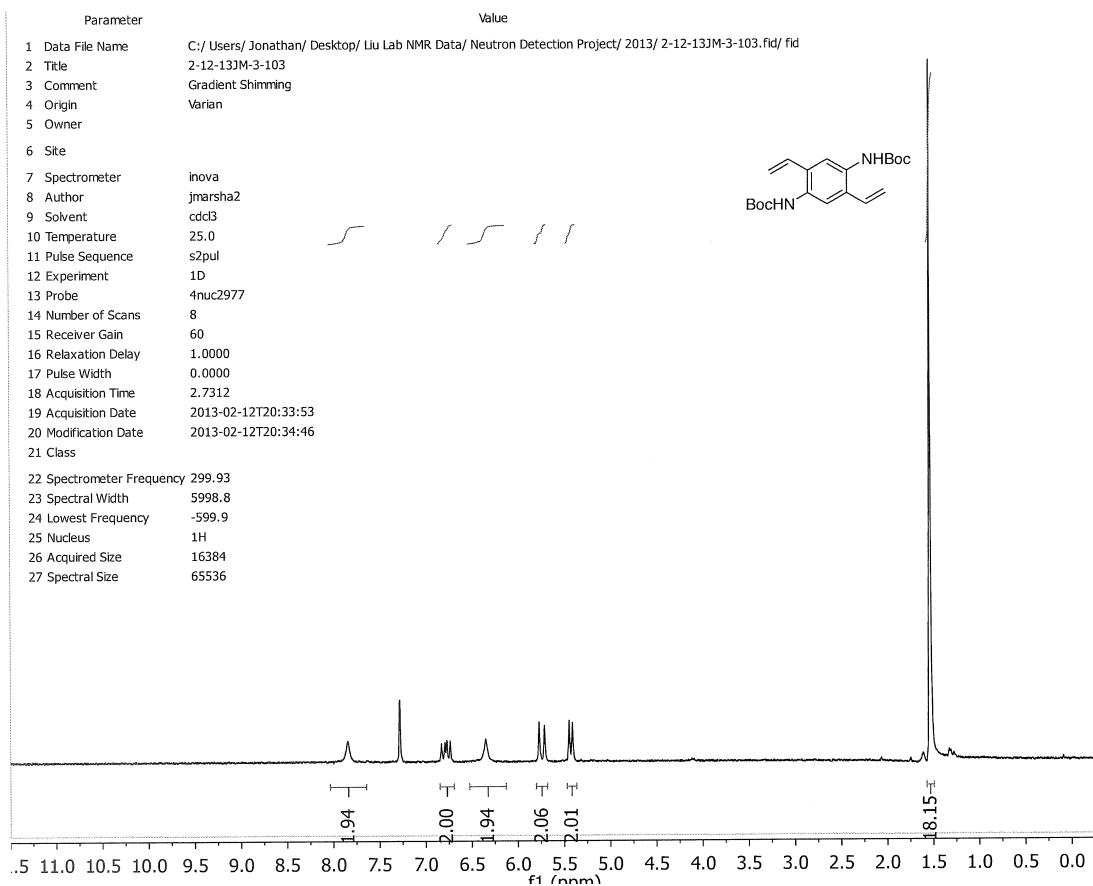
HSQC NMR

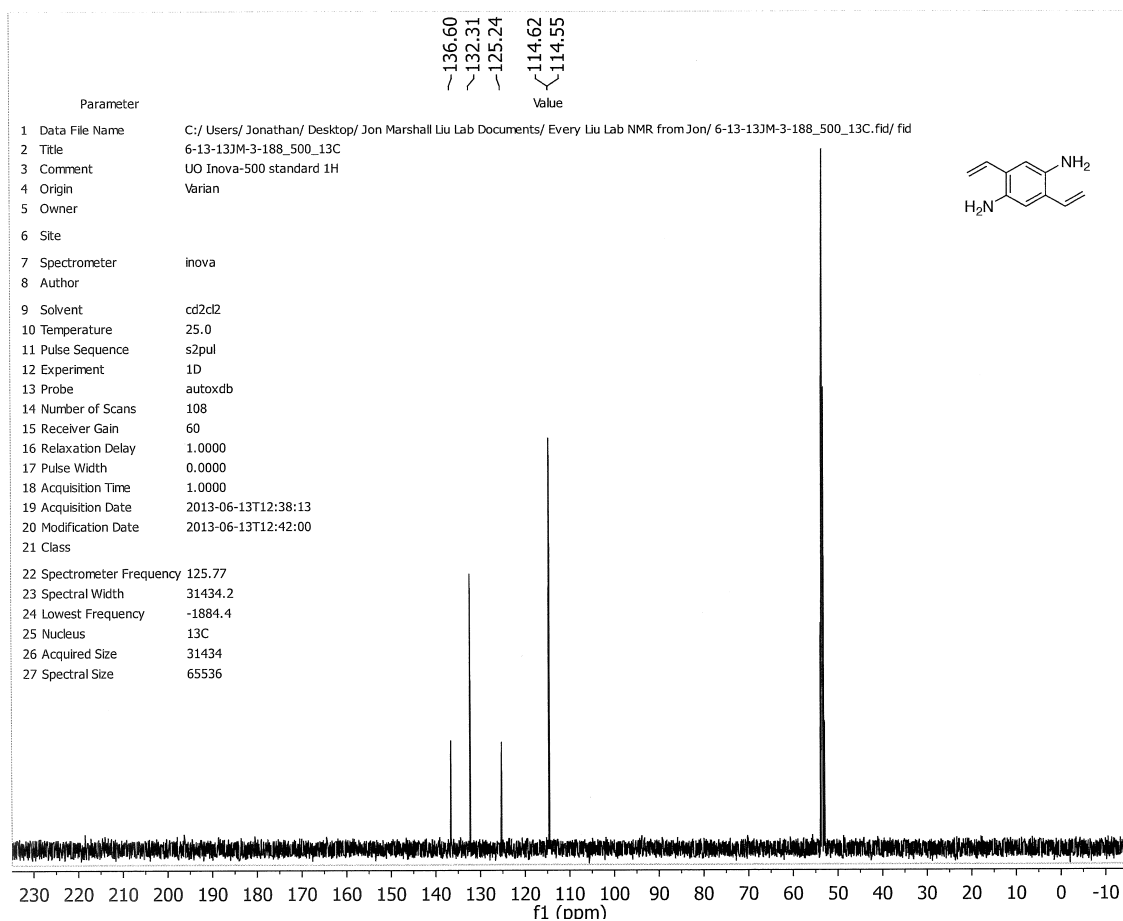
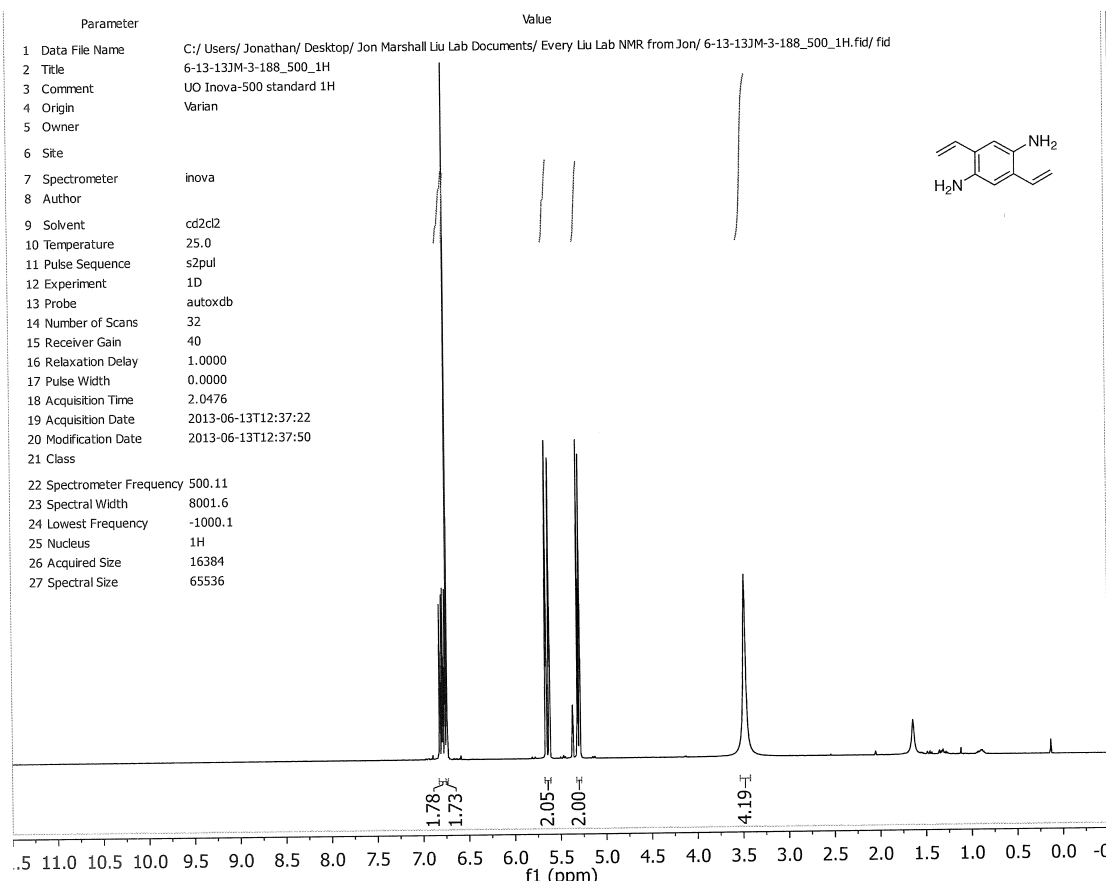


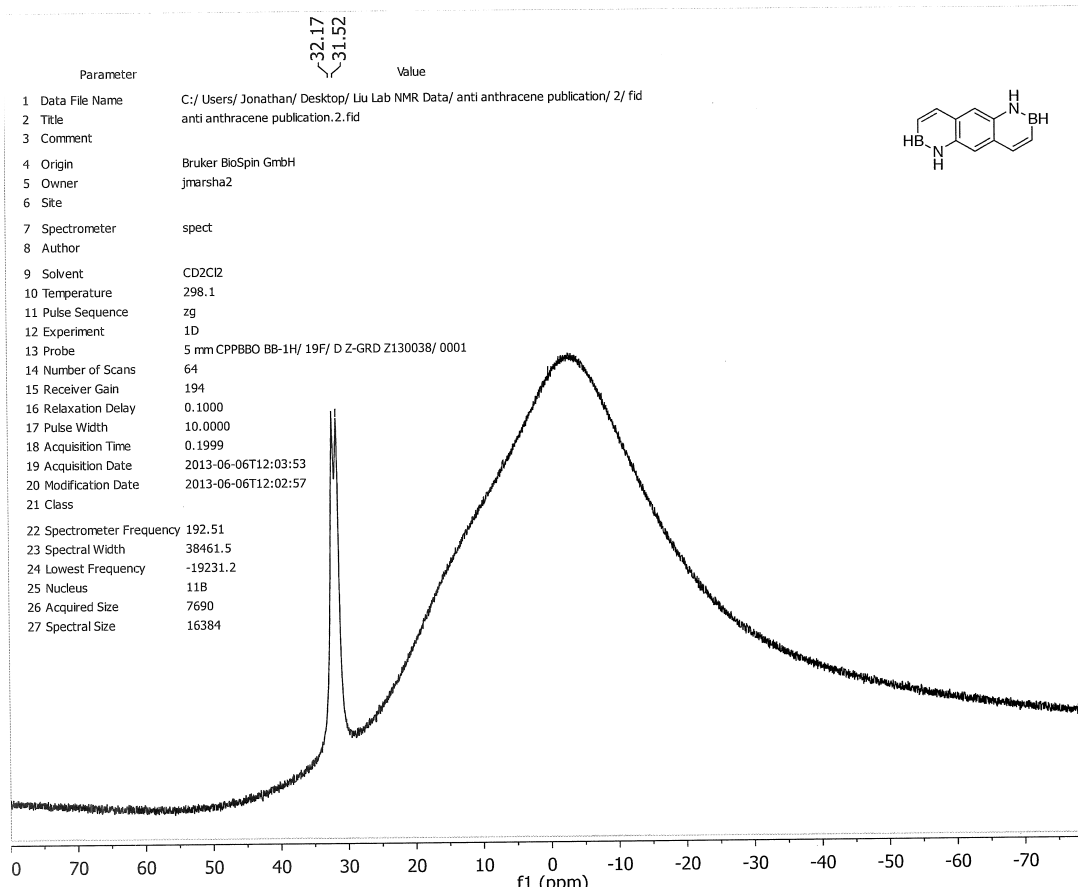
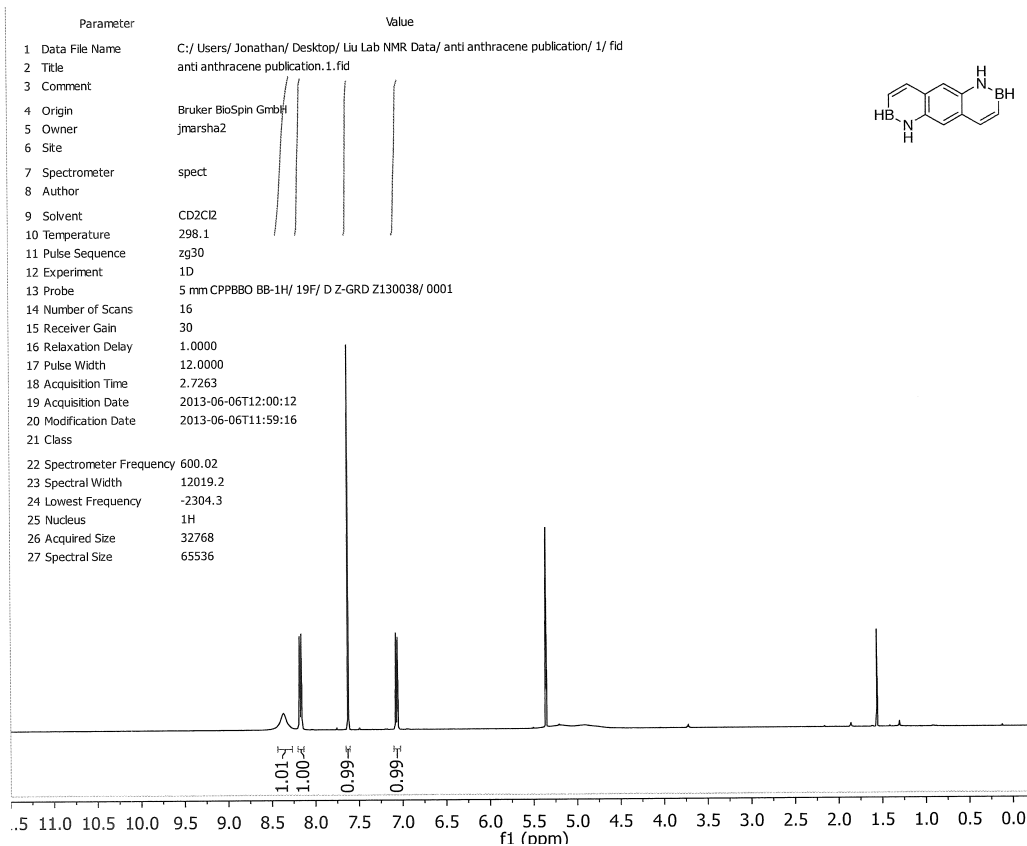
HMBC NMR

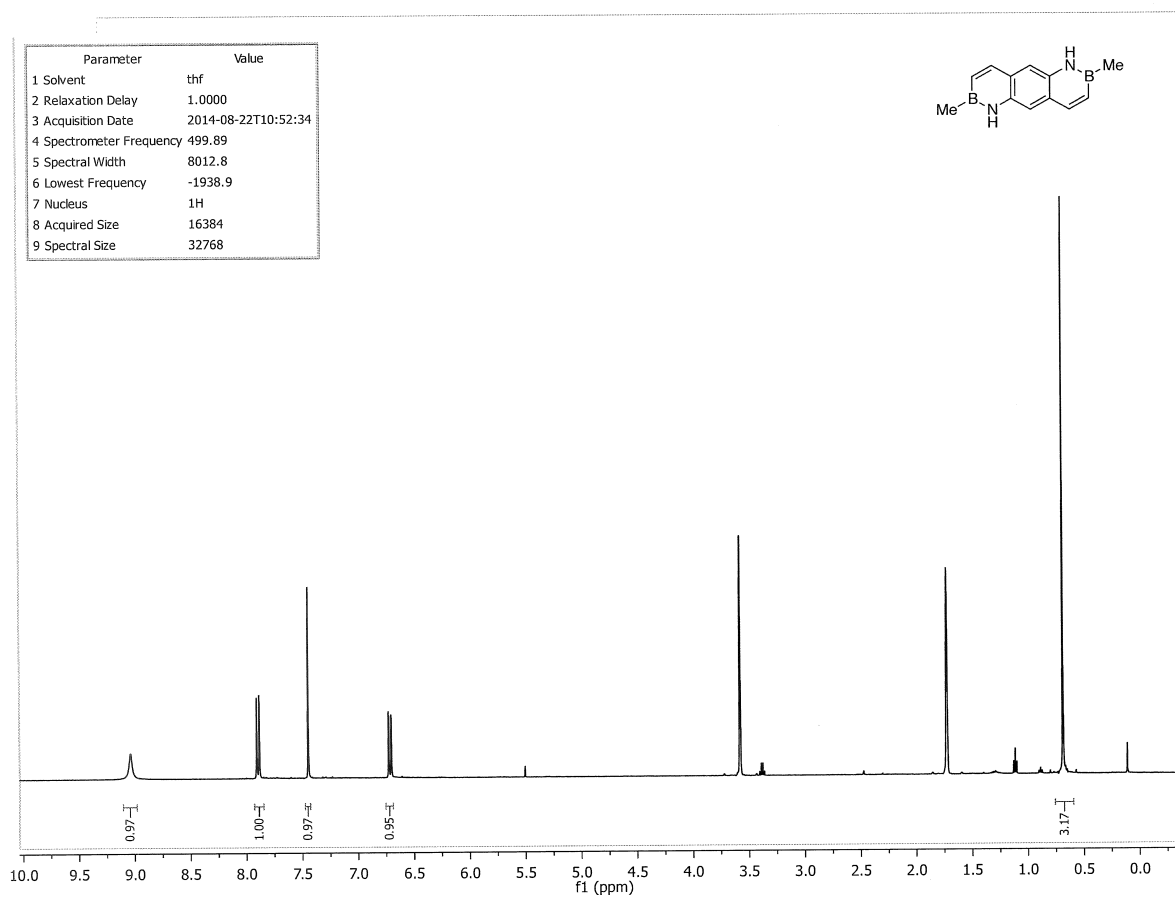
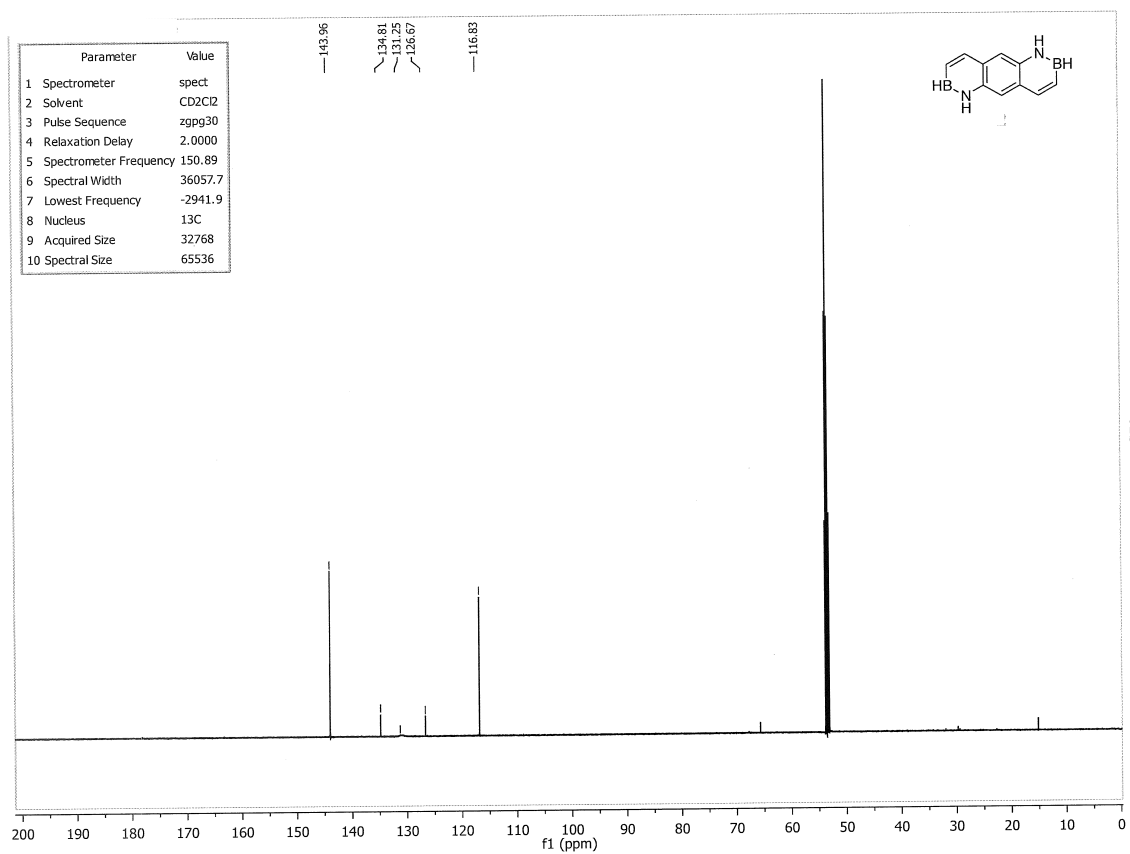


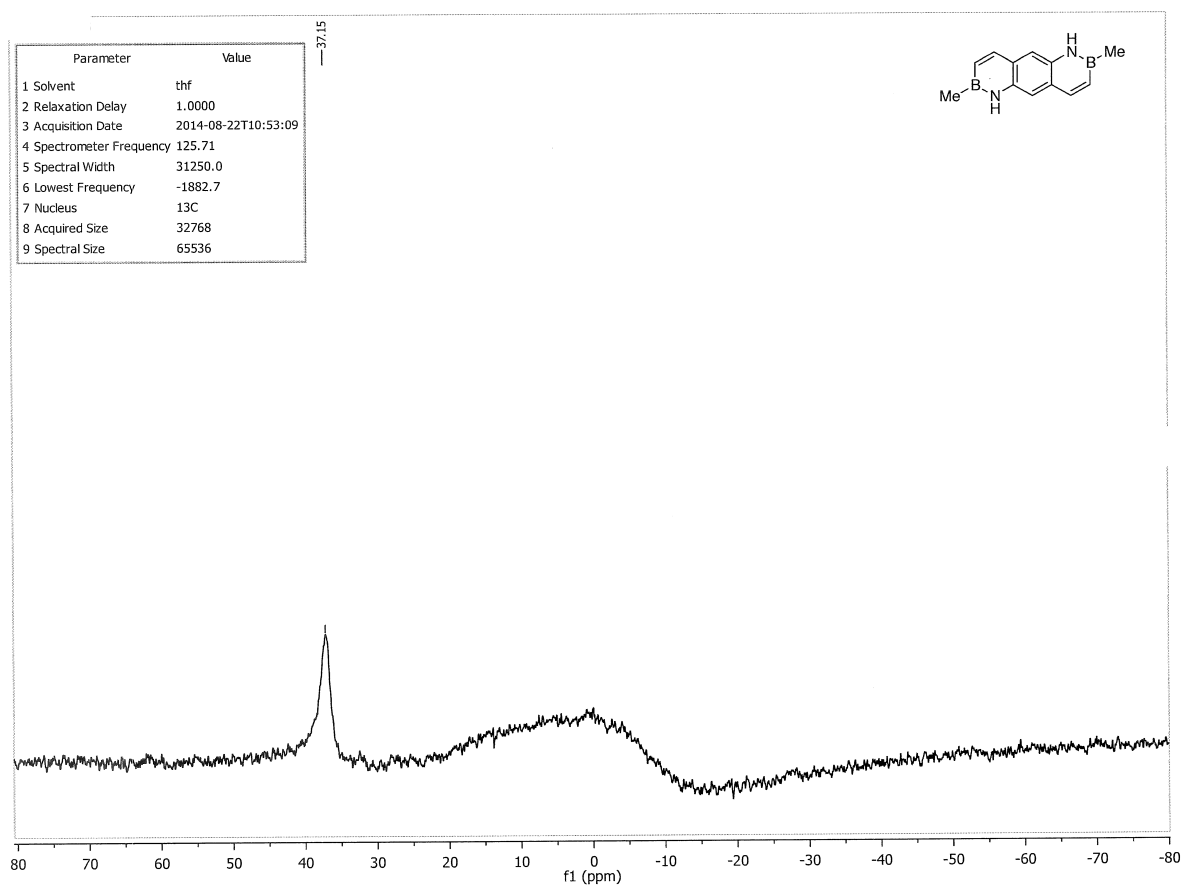
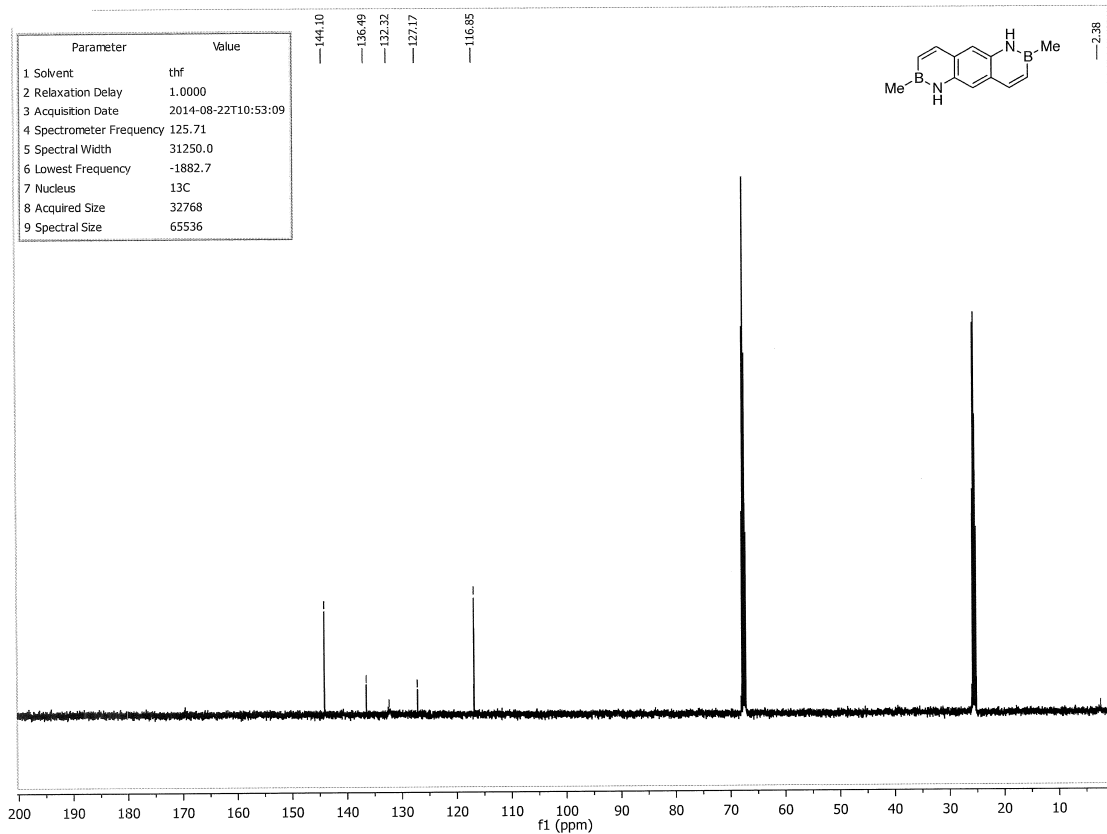


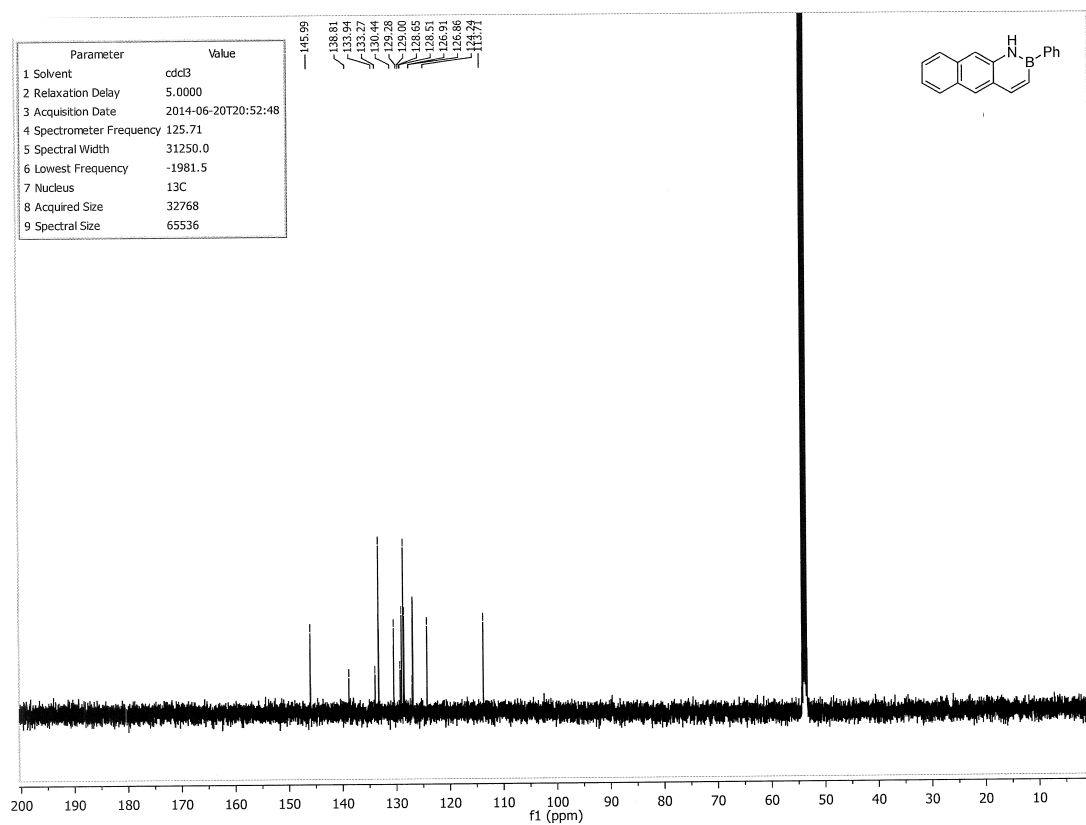
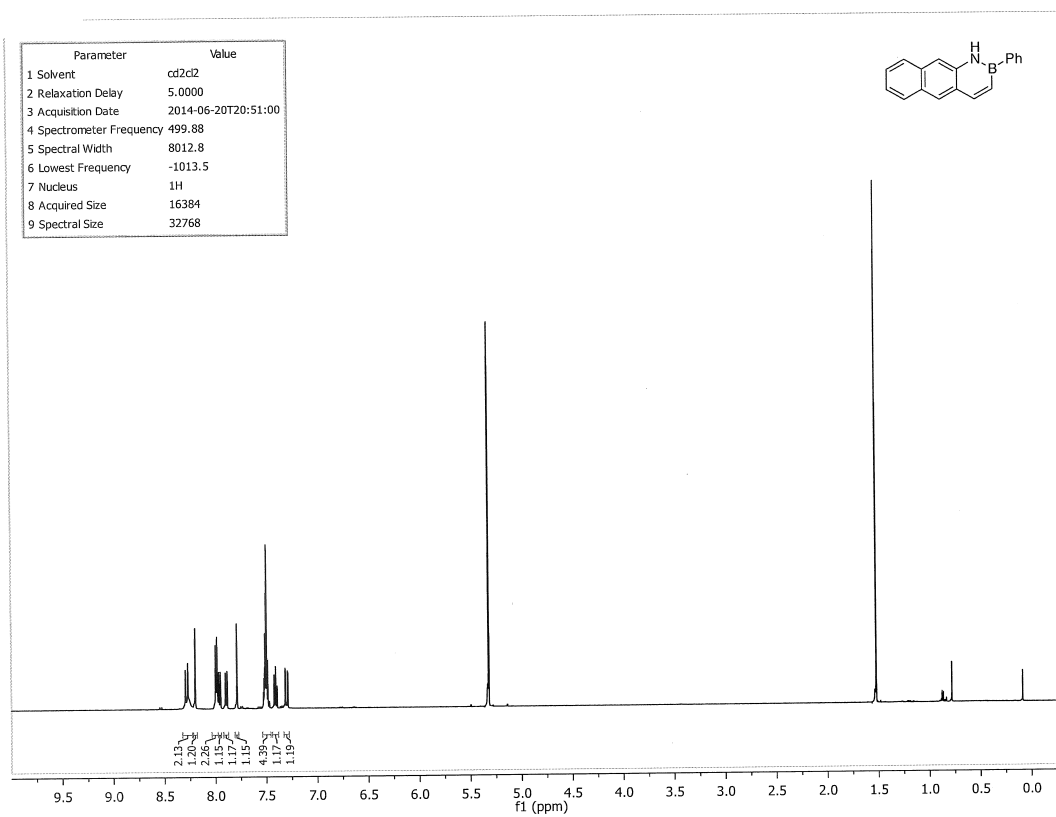


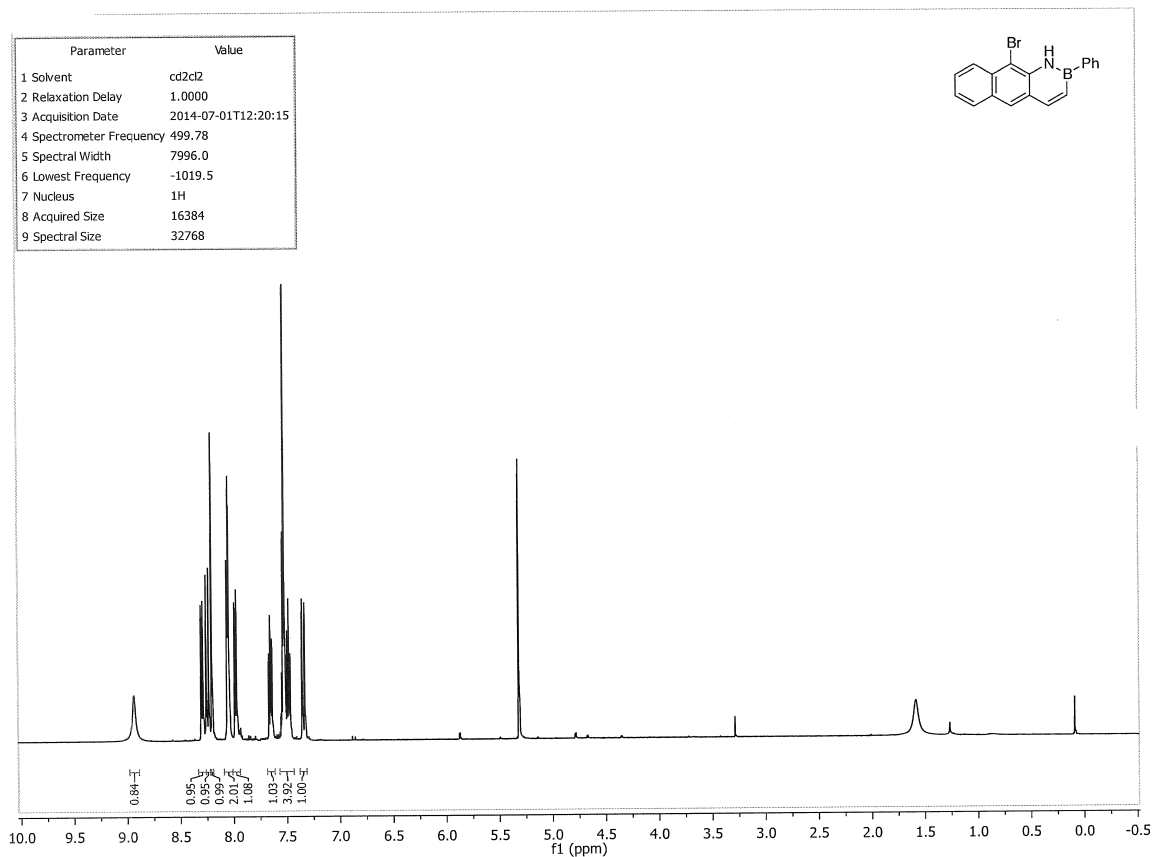
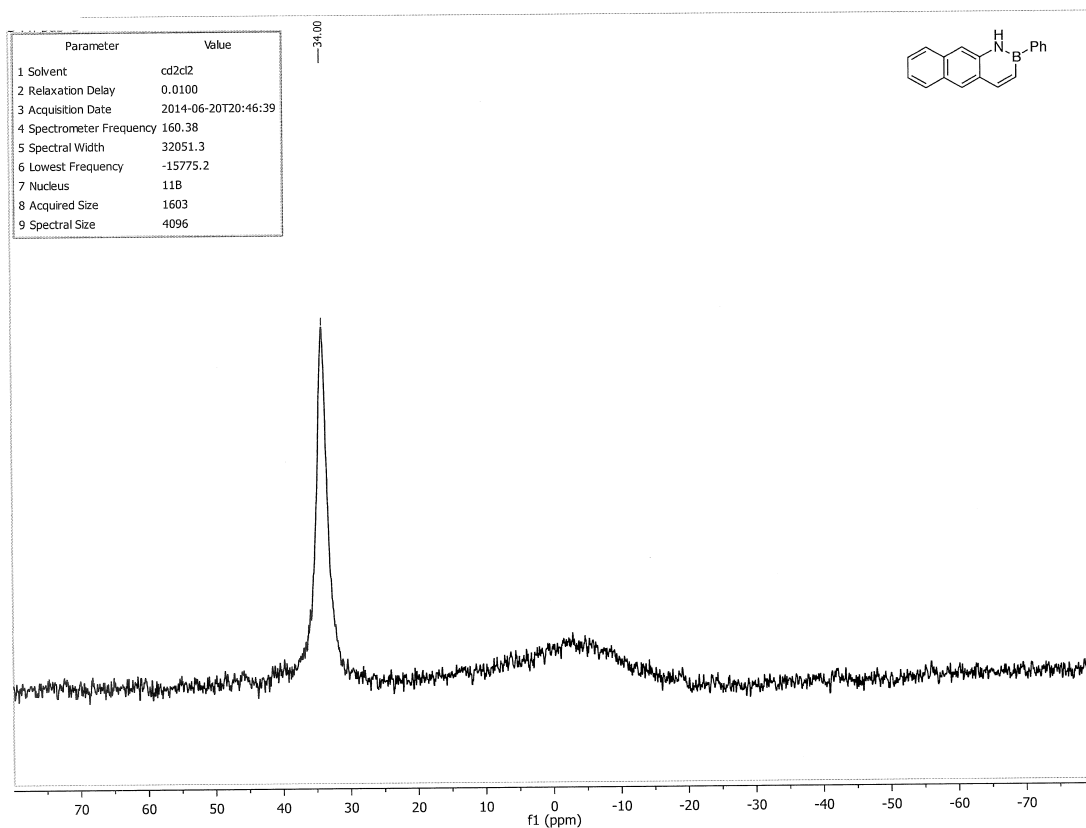


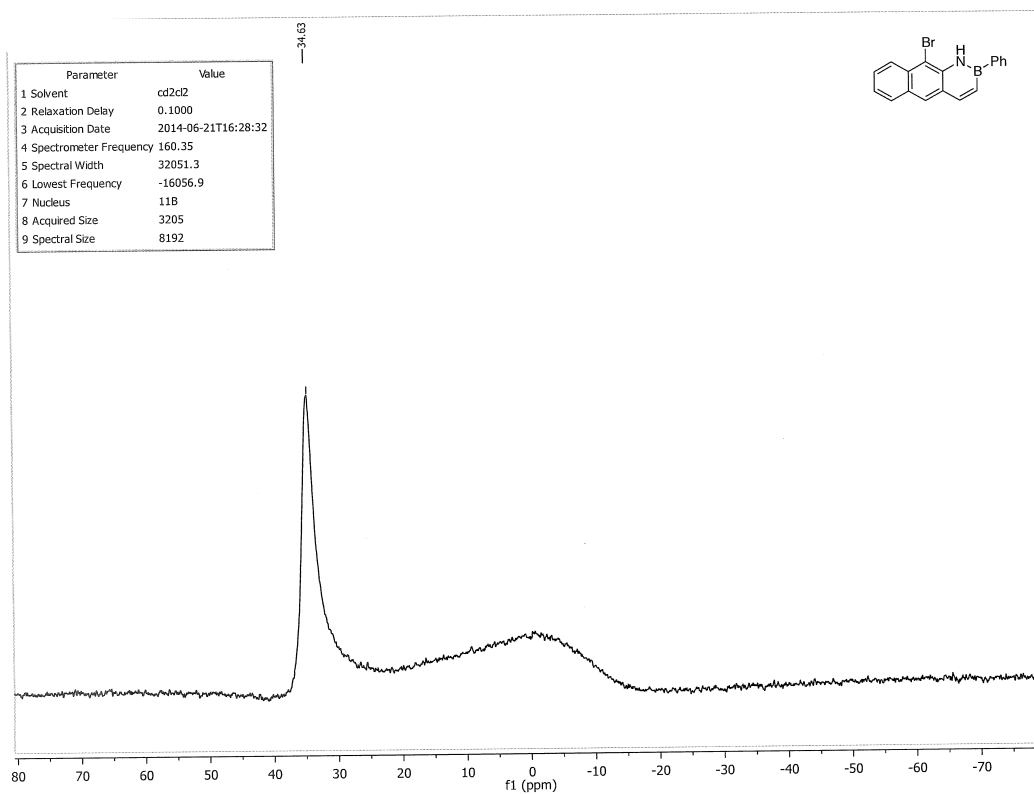
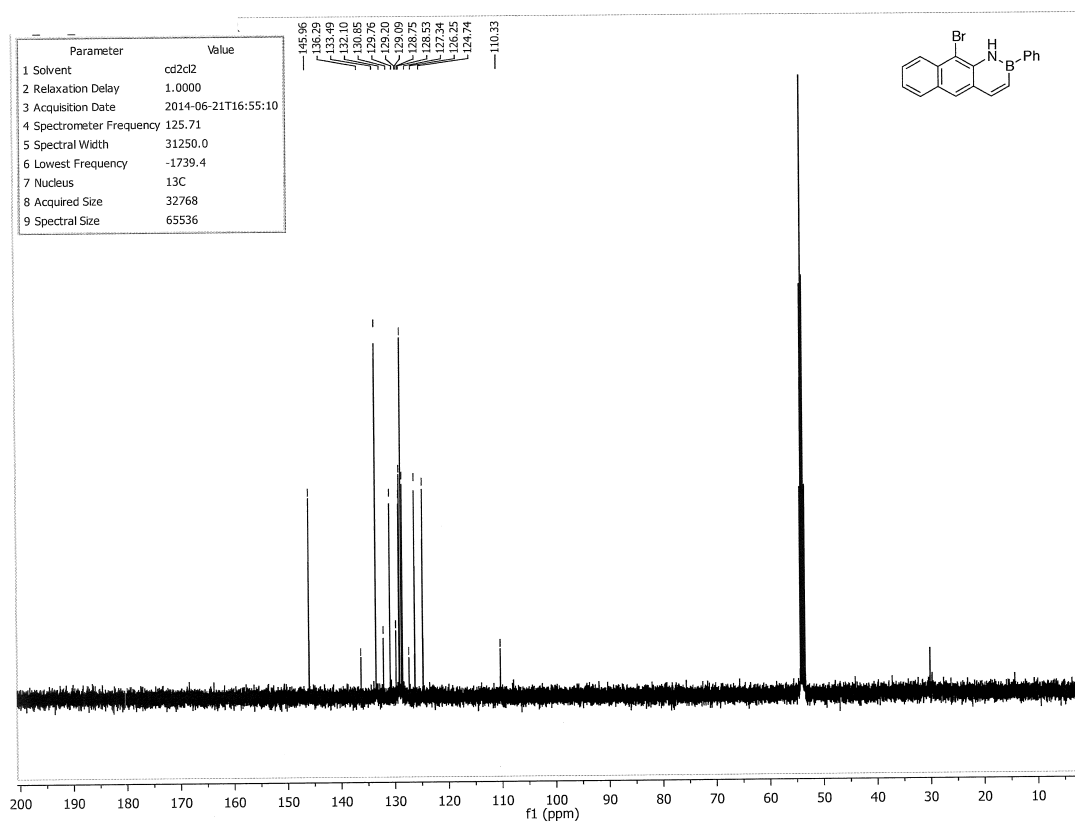


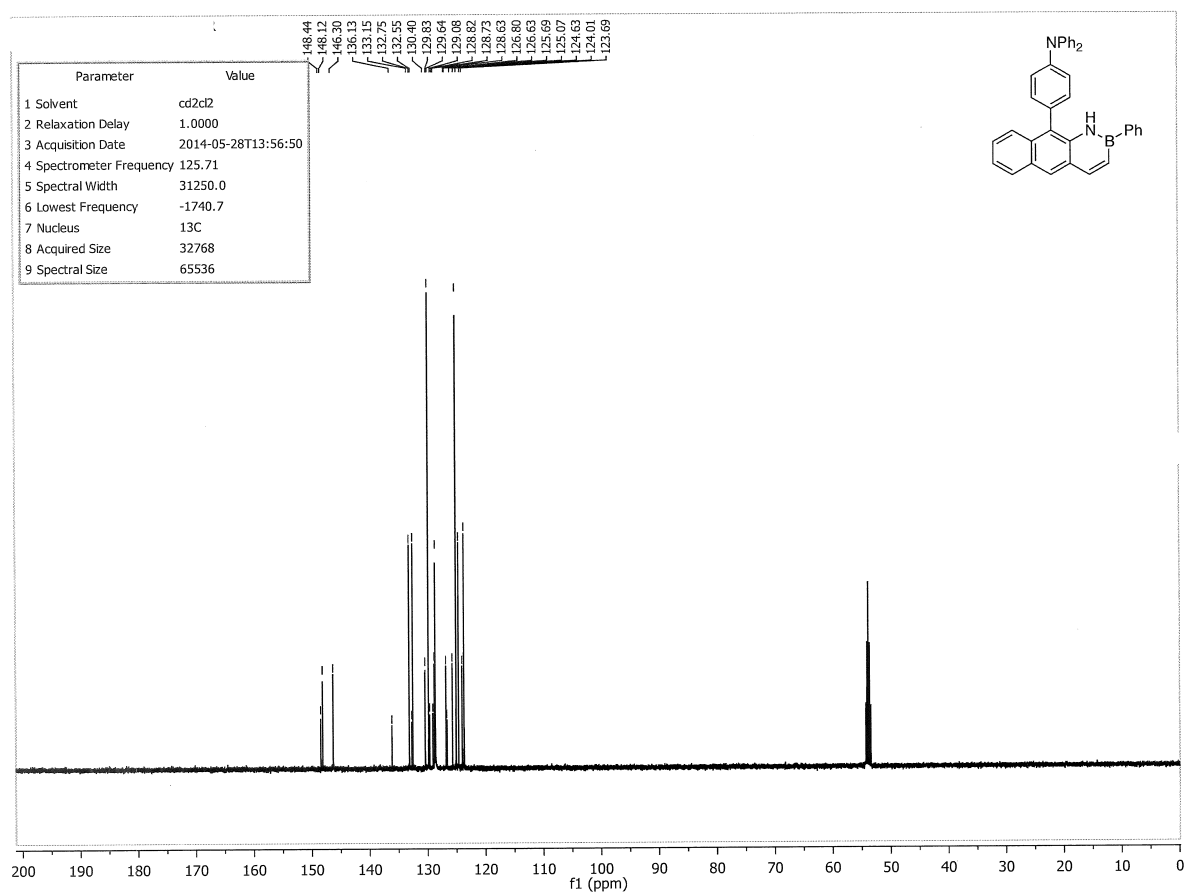
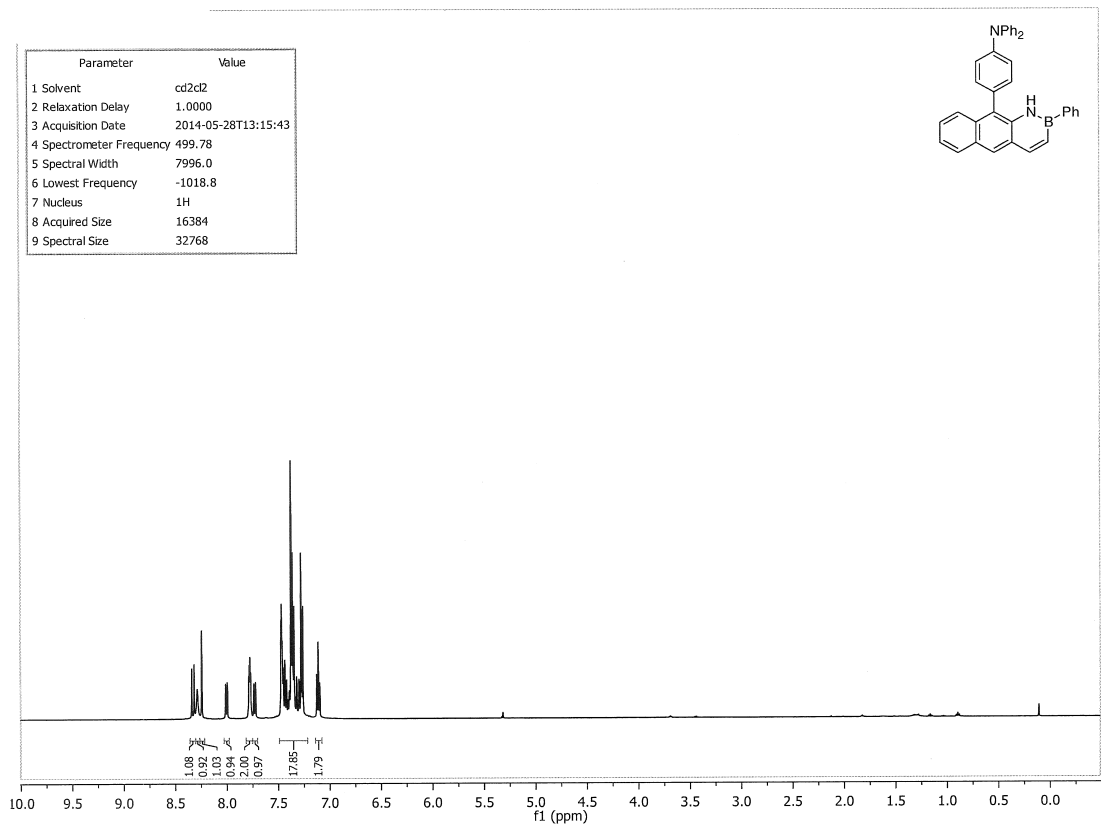


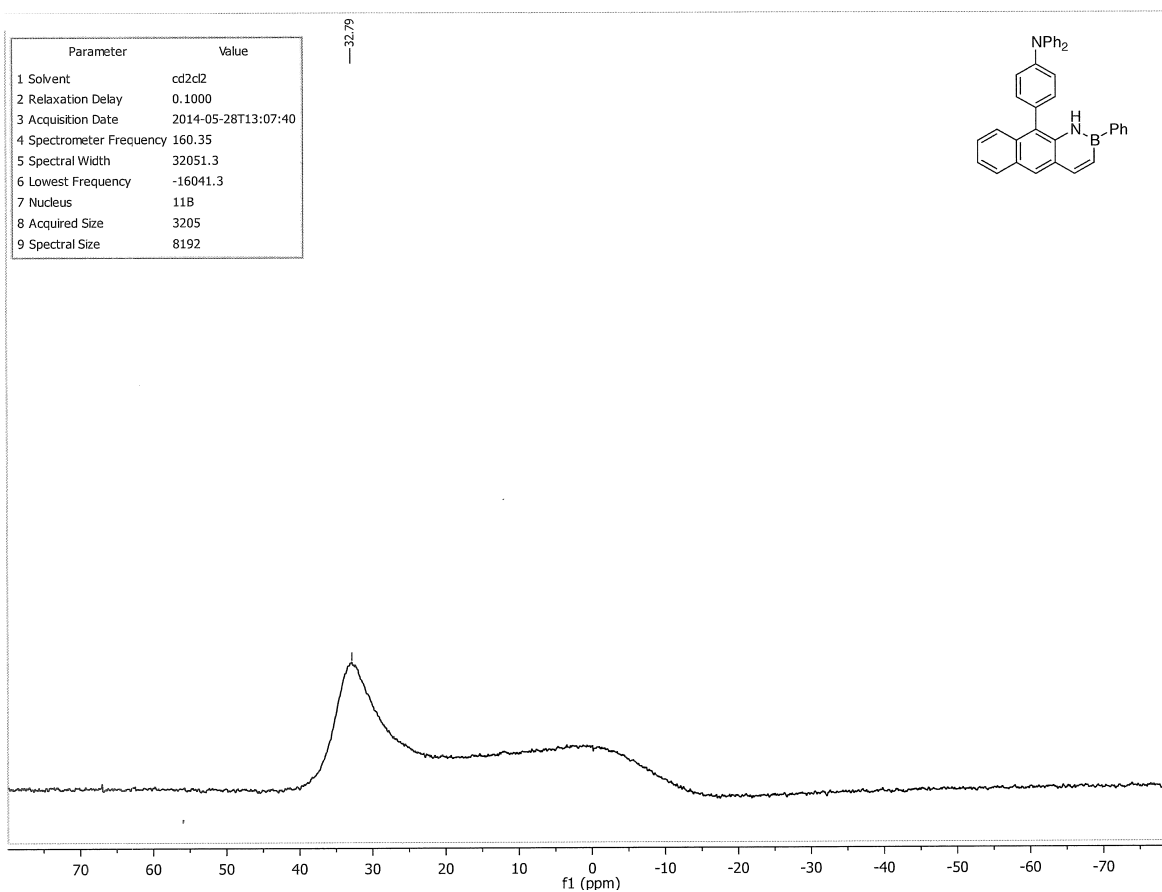












1.4 BN Tetracene

If BN/CC isosterism is to be utilized for generating new materials for organic-based optoelectronic devices, smaller HOMO-LUMO gaps are required so more useful charge-carrying and emissive properties can be obtained,⁸⁹ and singlet fission might also be possible.^{6c} One way to lower HOMO-LUMO gaps in acenes is to lengthen the acene. We targeted BN-1,2-tetracene for these reasons. BN tetracene should also have a lower HOMO energy than all-carbon tetracene, similar to what we observed for BN-1,2-anthracene (Figure 1.11).

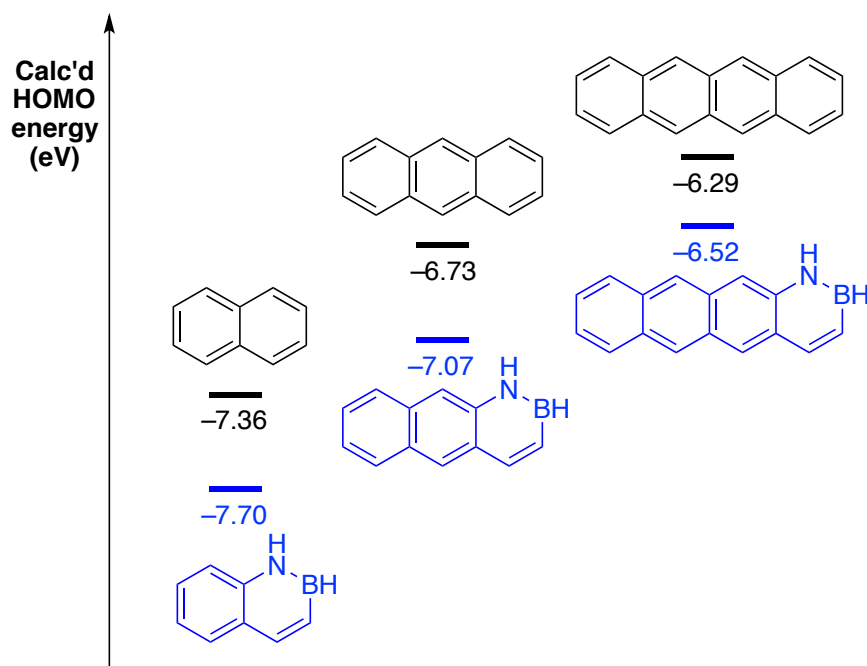


Figure 1.11. Calculated (CAM-B3LYP/6-311G(d,p)) HOMO energies of acenes and their 2,1-BN-isosteres.

⁸⁹ Organic semiconductors commonly have bandgaps of 2–3 eV which also happens to span most of the energy of the visible spectrum. See: Zaumseil, J.; Sirringhaus, H. *Chem. Rev.* **2007**, *107*, 1296–1323.

1.4.1 Synthesis of Substituted BN Tetracene⁹⁰

The primary synthetic challenge, as with the previously synthesized BN anthracene **1.5** is to overcome the natural tendency of acenes to undergo electrophilic substitution at the apical positions. We designed a synthesis revolving around the functional group manipulation of the fully aromatic anthracene core (Scheme 1.12), since reduction of the potential precursor BN tetraquinones completely deboronated the product. The synthesis began with a reduction of commercially available 2-amino-3-hydroxyanthraquinone to the corresponding anthracene.⁹¹ With this anthracene in hand, Boc-protection of the amine,⁹² triflation of the hydroxyl group, and Suzuki cross-coupling afforded a protected 2-amino-3-vinyanthracene **1.19**. Treatment of **1.19** with trifluoroacetic acid revealed the key cyclization precursor **1.20**.

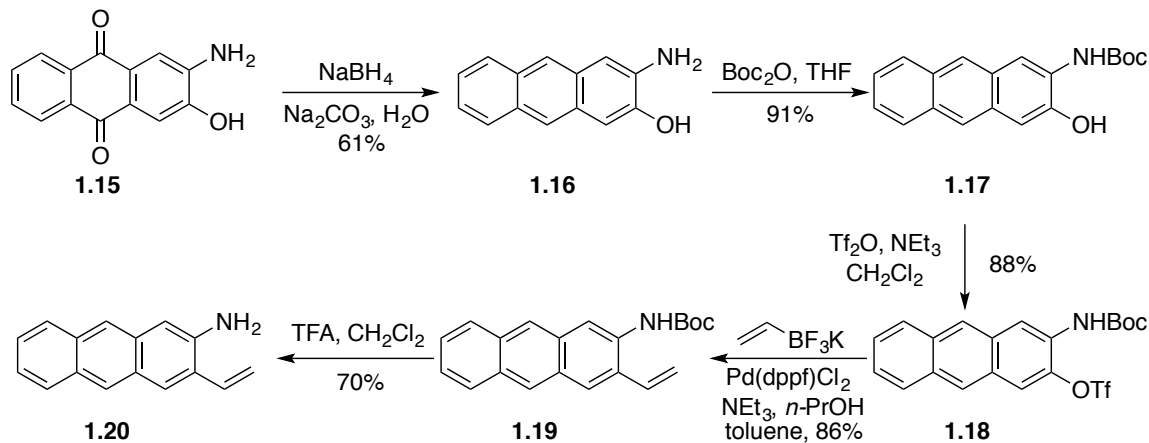
Many of the intermediates cannot be purified using chromatography because they are largely insoluble in non-polar organic solvents. For example, compound **1.16** must be purified by Soxhlet extraction using ethyl acetate as the solvent. An intractable mixture of products was obtained when crude **1.16** was treated with Boc₂O.

⁹⁰ Ishibashi, J. S. A.; Dargelos, A.; Darrigan, C.; Chrostowska, A.; Liu, S.-Y. *Organometallics* In Press. DOI: 10/1021/acs.organomet.7b00296.

⁹¹ Dadvand, A.; Moiseev, A. G.; Sawabe, K.; Sun, W.-H.; Djukic, B.; Chung, I.; Takenobu, T.; Rosei, F.; Perepichka, D. F. *Angew. Chem. Int. Ed.* **2012**, *51*, 3837–3841.

⁹² Li, G.-Q.; Gao, H.; Keene, C.; Devonas, M.; Ess, D. H.; Kürti, L. *J. Am. Chem. Soc.* **2013**, *135*, 7414–7417.

Scheme 1.12. Synthesis of the BN Tetracene Cyclization Precursor



Interestingly, heating the cyclization precursor **1.20** with boron trichloride or phenylboron dichloride, conditions identical to the syntheses of BN anthracene and naphthalene, returned starting material. We also attempted Molander's halogen exchange reactions of potassium alkyl and aryltrifluoroborates to no avail.^{50a}

We hypothesize that the more extensive electronic delocalization in **1.20** versus BN anthracene precursor **1.4** renders the nitrogen of **1.20** less nucleophilic toward boron. Figure 1.12 shows the HOMO maps for 2-amino-3-vinylnaphthalene **1.4** and benzo-fused homologue **1.20**. The HOMO coefficient on nitrogen is slightly diminished in the latter case, as the HOMO has become more delocalized, and may be less available for bonding to boron.

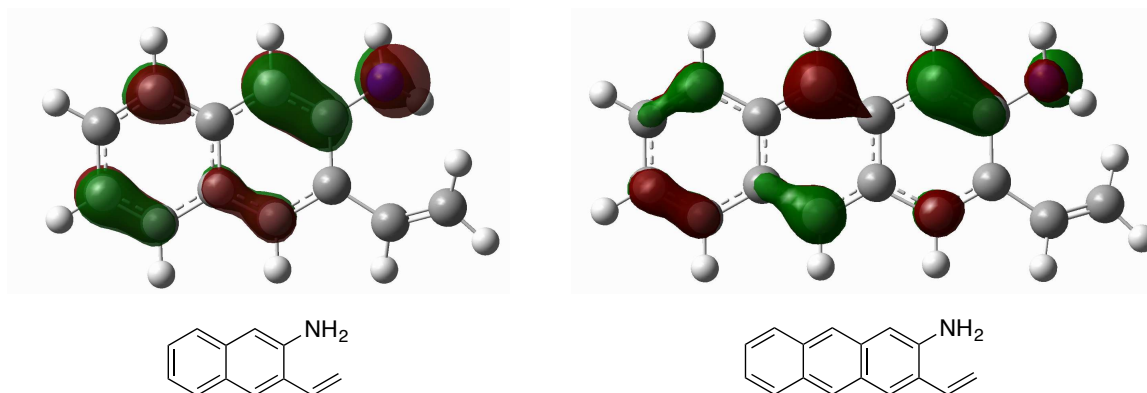
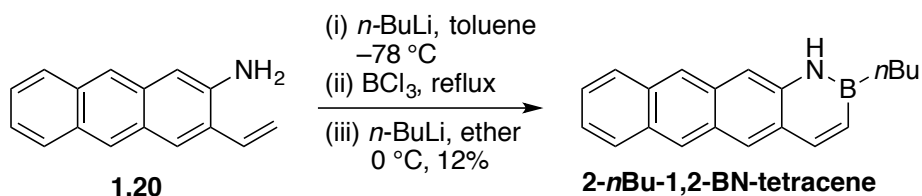


Figure 1.12. HOMO coefficients (CAM-B3LYP/6-311G(d,p)) of **1.4** and **1.20**. Lower HOMO density on nitrogen in **1.20** leads to lower nucleophilicity toward BCl_3 .

To overcome this challenge, the cyclization precursor **1.20** was treated first with *n*-butyllithium then with boron trichloride in order to form a *bona fide* covalent bond between nitrogen and boron. Heating the mixture produced the B–Cl BN tetracene as the only observable species by ^1H NMR in hot *ortho*-dichlorobenzene- d_4 . In an attempt to synthesize the parent BN tetracene, treatment of this crude material with lithium aluminum hydride yielded an intractable mixture of products. Thankfully, treatment of the boron-chloride with *n*-butyllithium gave **2-*n*Bu-1,2-BN-tetracene** (Scheme 1.13). We attempted to synthesize *B*-arylated products, but treatment of the *B*–Cl intermediate with aryl Grignard or aryllithium reagents only produced only complex mixtures.

Scheme 1.13. Final Synthesis of BN Tetracene 1.20



1.4.2 Synthesis of All-Carbon 2-Butyltetracene

Having not synthesized the parent BN tetracene, the direct, all-carbon analogue of **2-*n*Bu-1,2-BN-tetracene**, **2-*n*Bu-tetracene**, had to be synthesized in order for a meaningful comparison to be made (Scheme 1.14). Again faced with the problem of the inherent reactivity of acenes, we chose to build 2-butyltetracene from simpler precursors. Beginning with diester **1.21**, Suzuki coupling was executed using tributylborane as the nucleophile, producing butylated **1.22**.⁹³ The esters were reduced using DIBAL-H, and the resulting diol **1.23** was treated with hydrobromic acid to yield dibromide **1.24**.⁹⁴ This dibromide was heated with potassium iodide, producing a quinoidal intermediate *in situ*, and naphthoquinone acted as a Diels-Alder dienophile to produce tetraquinone **1.25** after autoxidation.⁹⁵ This quinone was reduced to the fully aromatic **2-*n*Bu-tetracene** in a two-step process beginning with sodium borohydride and finishing with stannous chloride dihydrate.⁹⁶

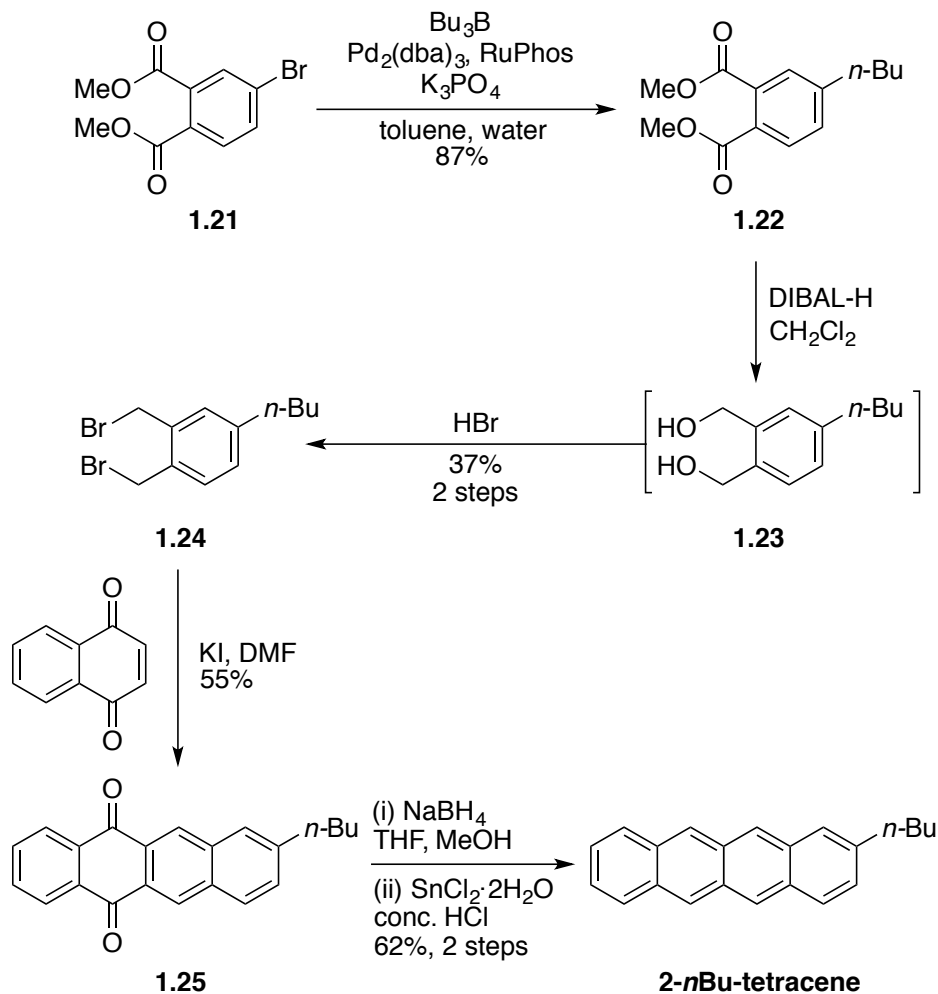
⁹³ Li, H.; Zhong, Y. L.; Chen, C. Y.; Ferraro, A. E.; Wang, D. *Org. Lett.* **2015**, *17*, 3616–3619.

⁹⁴ Shu, Y.; Lim, Y.-F.; Li, Z.; Purushothaman, B.; Hallani, R.; Kim, J. E.; Parkin, S. R.; Malliaras, G. G.; Anthony, J. E. *Chem. Sci.* **2011**, *2*, 363–368.

⁹⁵ (a) Cava, M. P.; Napier, D. R. *J. Am. Chem. Soc.* **1957**, *79*, 1701–1705. (b) Cava, M. P.; Deana, A. A.; Muth, K. *J. Am. Chem. Soc.* **1959**, *81*, 6458–6460. (c) Parakka, J. P.; Sadanandan, E. V.; Cava, M. P. *J. Org. Chem.* **1994**, *59*, 4308.

⁹⁶ Kitamura, C.; Ohe, G.; Kawase, T.; Saeki, A.; Seki, S. *Bull. Chem. Soc. Jpn.* **2014**, *87*, 915–921.

Scheme 1.14. Synthesis of 2-*n*Bu-tetracene



1.4.3 Optoelectronic Properties of BN Tetracene

2-*n*Bu-1,2-BN-tetracene displays optical properties consistent with expectations based on our experience with the BN anthracene series. The HOMO-LUMO gap of **2-*n*Bu-1,2-BN-tetracene** (2.61 eV, Figure 1.13) as estimated by the onset of absorption is similar, though slightly larger than that of the direct all-carbon analogue **2-*n*Bu-tetracene** (2.53 eV). Much like the BN anthracene series, **2-*n*Bu-1,2-BN-tetracene** displays two low-energy absorption bands. TD-DFT calculations (single-point CAM-B3LYP/6-311G(d,p), with PCM solvent model for CH₂Cl₂) indicate that the lowest energy

excitation involves the HOMO-LUMO transition for both **2-*n*Bu-1,2-BN-tetracene** and the all-carbon analogue and that the lowest energy excitation for **2-*n*Bu-1,2-BN-tetracene** should occur at a higher energy than that of the all-carbon analogue.

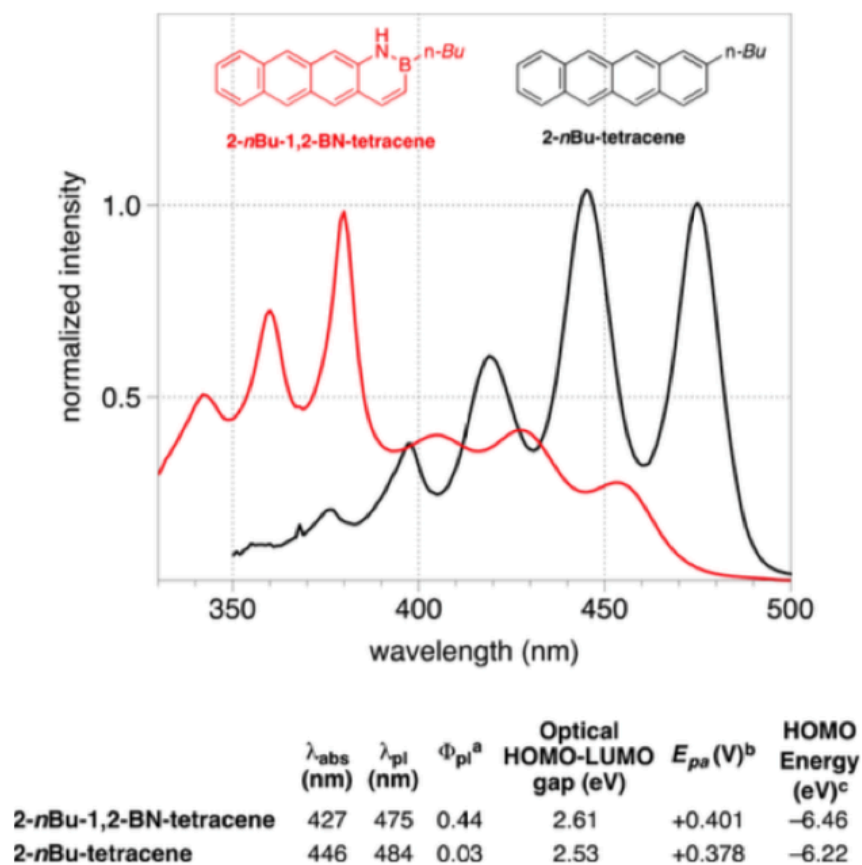


Figure 1.13. Normalized absorption spectra taken in methylene chloride solvent. ^a Quantum yield measured using an integrating sphere. ^b Optical gap estimated by the onset of UV-Visible absorption. ^c Measured by cyclic voltammetry (0.1 M Bu₄NBF₄/DMF, V vs. the ferrocene/ferrocenium redox couple. ^d Calculated at the CAM-B3LYP/6-311G(d,p) level.

We collected the fluorescence spectra for both the BN tetracene and its all-carbon analogue in methylene chloride (Figure 1.14). Though similar in appearance, the fluorescence spectrum for **2-*n*Bu-tetracene** is bathochromically shifted from that of **2-*n*Bu-1,2-BN-tetracene**, owing to the former's lower-energy absorption onset. The

photoluminescence quantum yield for **2-*n*Bu-1,2-BN-tetracene** is much higher ($\Phi_{\text{pl}} = 0.44$) than that of the all-carbon analogue ($\Phi_{\text{pl}} = 0.03$).⁹⁷

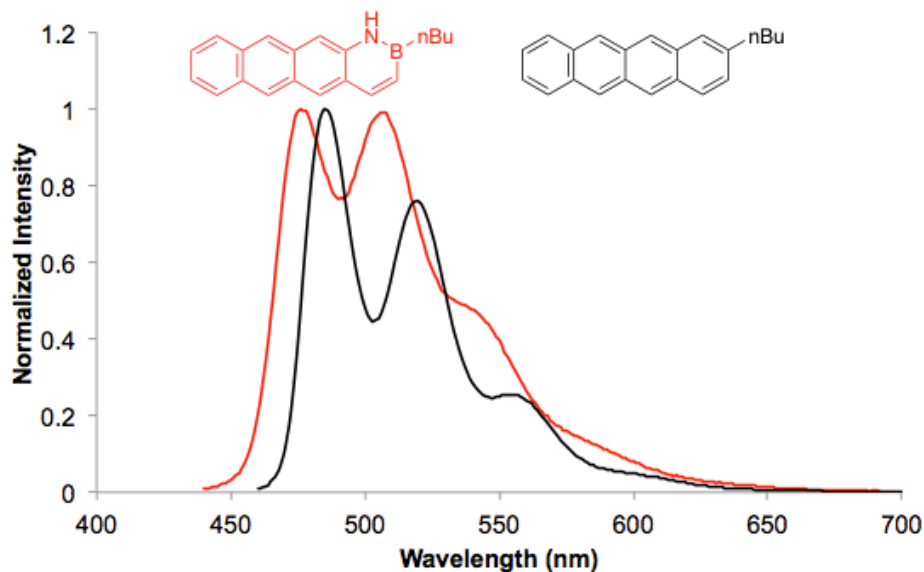


Figure 1.14. Normalized fluorescence spectra of **2-*n*Bu-1,2-BN-tetracene** and the all-carbon analogue **2-*n*Bu-tetracene**

Based on these differences in photoluminescence efficiency, it would be unsurprising to discover that all-carbon **2-*n*Bu-tetracene** engaged in non-radiative photochemical decomposition pathways more readily than its BN isostere. We performed a simple photobleaching experiment with the two compounds in degassed methylene chloride (Figure 1.15). More than 50% of **2-*n*Bu-tetracene** (*ca.* 3.3×10^{-5} M) degraded over 4 hours under ambient light from a fluorescent lamp as measured by the disappearance of the λ_{max} absorption band at 446 nm; this degradation likely corresponds to tetracene dimer formation.⁹⁸ In contrast, **2-*n*Bu-1,2-BN-tetracene** (5.64×10^{-4} M) does not degrade in solution over four hours under the same light, despite being nearly 10 times more concentrated than in the all-carbon experiment.

⁹⁷ Low photoluminescence quantum yields are typical for alkylated tetracene in solution. See: Kitamura, C.; Ohe, G.; Kawase, T.; Saeki, A.; Seki, S. *Bull. Chem. Soc. Jpn.* **2014**, 87, 915–921.

⁹⁸ Lapouyade, R.; Nourmamode, A.; Bouaslaurent, H. *Tetrahedron* **1980**, 36, 2311–2316.

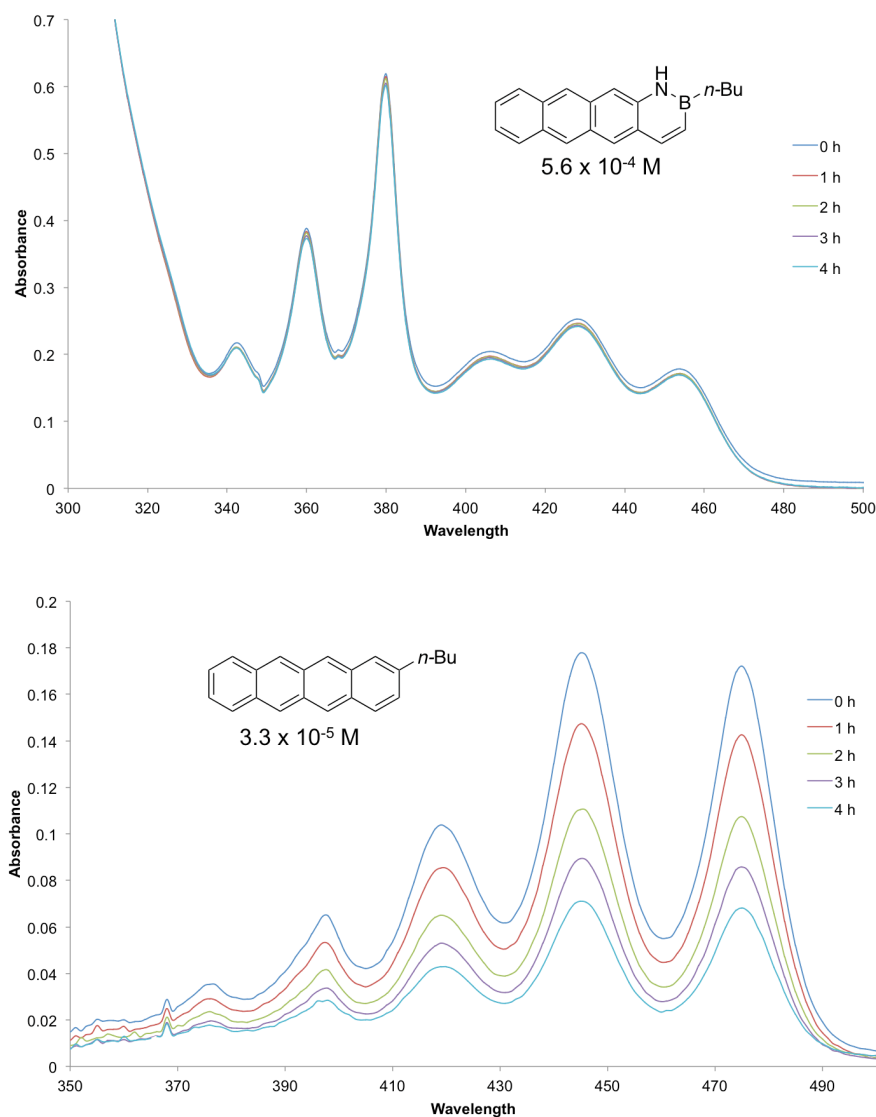


Figure 1.15. Photobleaching experiment. UV-Vis absorption spectra over time for samples of BN tetracene and the direct all-carbon analogue left under ambient laboratory light over 4 hours.

To investigate the relative HOMO energies of **2-*n*Bu-1,2-BN-tetracene** and its all-carbon analogue, we performed cyclic voltammetry (CV). **2-*n*Bu-1,2-BN-tetracene** does not exhibit reversible oxidation ($E_{pa} = +0.401$ V vs. the ferrocene/ferrocenium couple in *N,N*-dimethylformamide/0.1 M Bu₄NBF₄) in its cyclic voltammogram (Figure 1.16). Similarly, all-carbon **2-*n*Bu-tetracene** irreversibly oxidizes in its respective CV ($E_{pa} = +0.378$ V). Since it is thus more difficult to oxidize **2-*n*Bu-1,2-BN-tetracene** than

the all-carbon **2-*n*Bu-tetracene**, this suggests that the 1,2-BN-acene has a lower-lying HOMO than its all-carbon analogue.

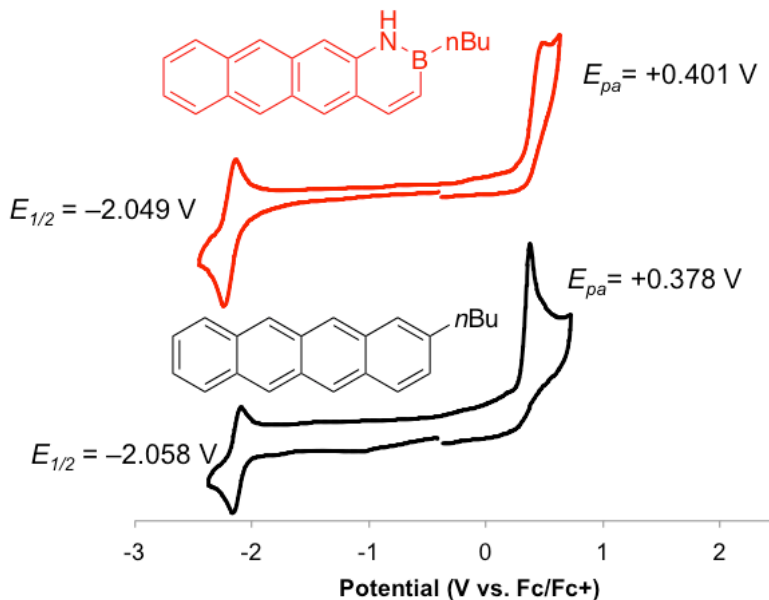


Figure 1.16. CV of **2-*n*Bu-1,2-BN-tetracene** and **2-*n*Bu-tetracene** in DMF (0.1 M Bu₄NBF₄, 50 mV/s scan rate)

The reduction of each of the compounds is quasi-reversible. The BN-containing compound has a less negative reduction potential (-2.049 V) than the all-carbon compound (-2.058 V). That these reduction potentials are roughly similar to one another, and comparing the oxidation potentials, we can estimate that the HOMO-LUMO gap is higher in energy for **2-*n*Bu-1,2-BN-tetracene** than for the all-carbon analogue. This CV-derived result supports the UV-vis absorption data.

1.4.4 Conclusions

In conclusion, we synthesized the first example of a BN tetracene as a step toward practical application of BN acenes in optoelectronic devices. We characterized the electronic structure of **2-*n*Bu-1,2-BN-tetracene** and that of its all-carbon analogue **2-*n*Bu-tetracene** using UV-vis absorption and emission spectroscopy and cyclic

voltammetry. The BN species exhibits an absorption spectrum reminiscent of the lower BN homologue, 1,2-BN-anthracene **1.5**, but in contrast to the anthracene case, the optical HOMO-LUMO gap is slightly larger than that of its all-carbon analogue instead of nearly identical as with the anthracenes. In analogy to **1,2-BN-anthracene**, however, the HOMO energy of **2-nBu-1,2-BN-tetracene** is lower than that of its all-carbon analogue as predicted by DFT calculations and experimentally suggested by its higher oxidation potential.

1.4.5 Experimental Section

All oxygen- and moisture-sensitive manipulations were carried out under an inert atmosphere using either standard Schlenk technique or a nitrogen-filled glovebox. For air- and moisture-sensitive techniques, tetrahydrofuran, diethyl ether, methylene chloride, pentane, and toluene were purified by passing through a neutral alumina column under argon. All other solvents for air- and moisture-sensitive work were distilled after drying over calcium hydride.

^{11}B NMR spectra were recorded on a Varian 500 spectrometer and externally referenced to neat $\text{BF}_3 \cdot \text{Et}_2\text{O}$. (δ 0). ^1H and ^{13}C NMR spectra were recorded on a Varian 500 spectrometer, or a Varian 600 spectrometer.

High-resolution mass spectrometry (HRMS) data were collected at the Boston College Center for Mass Spectrometry using the Direct Analysis in Real Time (DART) technique or the Atmospheric Pressure Photoionization (APPI) technique.

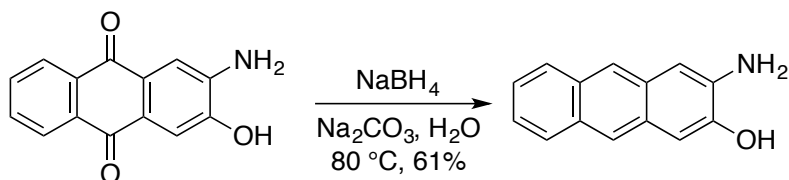
UV-visible absorption spectra were acquired on a Cary 100 spectrometer. Emission spectra were acquired on a Quanta Master 40 spectrofluorimeter (Photon Technology International) in dry, degassed methylene chloride as solvent. Fluorescence quantum yield (F_F) was determined using a PTI K-Sphere “Petite” integrating sphere.

Cyclic voltammetry was executed using a Bio-Logic SP-200 potentiostat controlled by the ECLab software package. Glassy carbon was the working electrode, platinum wire was the counter electrode, and silver wire was used as a pseudoreference. Reported potentials are referenced to the ferrocene/ferrocenium redox couple as an

internal standard. Scans were performed at 100 mV/s using a 0.1 M Bu₄NBF₄ solution in *N,N*-dimethylformamide (DMF) as the solvent.

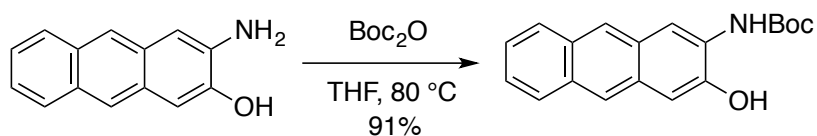
Synthetic Details

2-Amino-3-hydroxyanthracene (**1.16**) [167307-60-0]¹



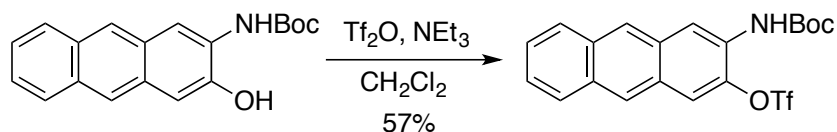
Sodium borohydride (22.7 g, 601 mmol, 12 equiv) was added to 400 mL of a 1.0 M aqueous Na₂CO₃ solution in a **5 L 3-necked round-bottomed flask**, and the solution was stirred using an overhead mechanical stirrer. Compound **1.15** (12.0 g, 50.2 mmol, 1 equiv) was added slowly to the mixture. When gas evolution ceased or slowed considerably (about 20-30 minutes) the reaction mixture was heated to 80 °C for 3 hours using a rotary evaporator bath to supply the heat. Note: at this point, the reaction *must* be monitored since the foaming will fill the entire flask. Vigorous stirring and manipulation of the foam with a rod will keep the foam down and prevent messy overflow. At the conclusion of the reaction, the reaction was cooled to room temperature and acidified to pH 1.5 with concentrated hydrochloric acid. The slurry was passed through a filter paper, and the solids washed with water and then methanol. The solids were continuously extracted with ethyl acetate over 48 hours using a Soxhlet apparatus. The solid obtained from the extraction was washed with hexane and collected to yield **1.16** as a brown powder (5.84 g, 61%). ¹H NMR (400 MHz, DMSO-*d*₆) δ 8.05 (s, 1H), 7.96 (s, 1H), 7.86 – 7.78 (m, 2H), 7.30 – 7.22 (m 2H), 7.13 (s, 1H), 6.95 (s, 1H). ¹³C NMR (126 MHz, DMSO-*d*₆) δ 147.44, 139.6, 1230.0, 129.7, 128.8, 127.9, 127.3, 127.0, 123.6, 122.9, 122.3, 120.6, 106.0, 103.8. FTIR (ATR thin film): 3374, 3288, 3046, 2618, 1452, 1352, 952, 788, 471. HRMS (DART+) [M+H]⁺ calcd. for C₁₄H₁₂NO, 210.09189, found 210.09105.

2-Amino-N-Boc-3-hydroxyanthracene (1.17)



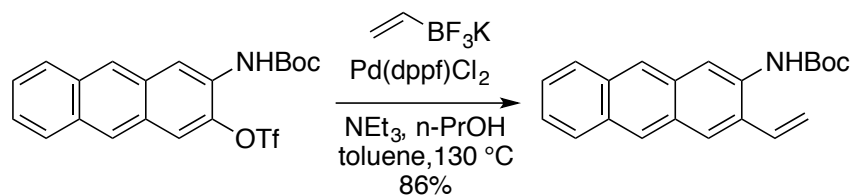
2-Amino-3-hydroxyanthracene **1.16** (2.70 g, 12.9 mmol, 1 equiv) was combined with di-*tert*-butyldicarbamate “ Boc_2O ” (2.73 g, 12.5 mmol, 0.97 equiv) and anhydrous THF under inert atmosphere. The reaction was heated to reflux at $90\text{ }^\circ\text{C}$ for 72 hours. At the conclusion of the reaction, the reaction mixture was cooled to room temperature, and the volatiles were removed using a rotary evaporator. The residue was triturated with hexane and the solids were collected to yield **1.17** as a brown powder (3.65 g, 91%). ^1H NMR (500 MHz, CD_2Cl_2) δ 8.27 (s, 1H), 8.25 (s, 1H), 8.16 (s, 1H), 7.93 – 7.87 (m, 2H), 7.43 – 7.35 (m, 2H), 7.33 (s, 1H), 7.27 (s, 1H), 1.54 (s, 9H). ^{13}C NMR (126 MHz, $\text{DMSO}-d_6$) δ 152.4, 146.7, 130.6, 129.9, 129.1, 129.1, 127.7, 127.3, 124.6, 124.56, 124.54, 124.1, 122.6, 113.7, 106.5, 79.9, 28.0. FTIR (ATR thin film): 3321, 1667, 1542, 1250, 905, 783, 472. HRMS (DART+) $[\text{M}+\text{H}]^+$ calcd. for $\text{C}_{19}\text{H}_{20}\text{NO}_3$ 310.14432, found 310.14316.

2-Amino-N-Boc-anthracene-3-triflate (1.18)



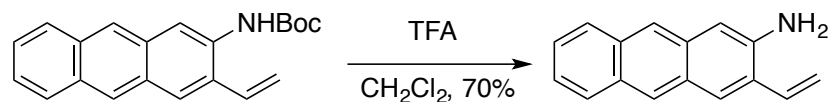
Under an inert atmosphere, a mixture of compound **1.17** (3.65 g, 11.7 mmol, 1 equiv) and triethylamine (8.2 mL, 59 mmol, 5 equiv) in 100 mL dry methylene chloride was cooled in an ice bath to 0 °C. Triflic anhydride (8.18 g, 29.0 mmol, 2.46 equiv) was mixed with 10 mL methylene chloride in a glovebox and then added dropwise to the reaction at 0 °C. The reaction was allowed to warm to room temperature over 2 hours. At the conclusion of the reaction, the reaction mixture was quenched with saturated sodium bicarbonate solution then washed with brine. The combined organic layers were dried over sodium sulfate, and the volatiles were removed via rotary evaporator. The crude brown powder was run through a plug of silica gel using methylene chloride as the mobile phase to yield **1.18** as a brown powder (2.97 g, 57%). ^1H NMR (400 MHz, CD_2Cl_2) δ 8.60 (s, 1H), 8.39 (2 overlapping singlets, 2H), 8.06 – 7.92 (overlapping s and m, 3H), 7.56–7.44 (m, 2H), 1.57 (s, 9H). ^{13}C NMR (126 MHz, CD_2Cl_2) δ 152.8, 150.7, 140.0, 133.1, 132.0, 130.8, 128.4, 128.4, 128.1, 127.6, 127.1, 126.8, 126.3, 126.3, 120.0, 81.9, 28.4. Trifluoromethyl carbon not observed. ^{19}F NMR (376 MHz, CD_2Cl_2) δ -74.92 (s). FTIR (ATR thin film): 3051, 2980, 1698, 1536, 1241, 1159, 1029, 739. HRMS (DART+) $[\text{M}+\text{H}]^+$ calcd. for $\text{C}_{20}\text{H}_{17}\text{F}_3\text{NO}_5\text{S}$ 441.08568, found 441.08480.

2-Amino-N-Boc-3-vinylanthracene (1.19)



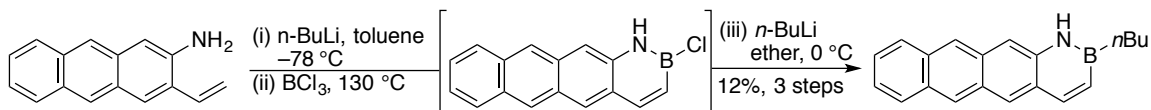
Compound **1.18** (2.20 g, 4.99 mmol, 1 equiv), potassium vinyltrifluoroborate (1.00 g, 7.48 mmol, 1.5 equiv), triethylamine (1.04 mL, 7.48 mmol, 1.5 equiv), and palladium diphenylphosphinoferrocene dichloride (204 mg, 0.260 mmol, 0.05 equiv) were all combined under inert atmosphere in 100 mL of a 1:1 mixture of toluene/normal propyl alcohol. The reaction was heated to reflux for 18 hours at $130\text{ }^\circ\text{C}$ then cooled to room temperature. Volatiles were then removed using a rotary evaporator, and the residue was extracted into ethyl acetate and washed with brine. The organic layer was dried over sodium sulfate, and the solvent was removed using a rotary evaporator to yield **1.19** as a brown solid (1.37 g, 86%). ^1H NMR (400 MHz, CD_2Cl_2) δ 8.46 (s, 1H), 8.36 (s, 1H), 8.33 (s, 1H) 8.00 (s 1H), 7.99 – 7.93 (m, 2H). 7.47-7.37 (m, 2H) 7.14 – 6.86 (m, 1H), 6.71 (s, 1H), 5.86 (d, $J = 17.2\text{ Hz}$, 1H), 5.56 (d, $J = 11.0\text{ Hz}$, 1H), 1.56 (s, 9H). ^{13}C NMR (126 MHz, CD_2Cl_2) δ 153.3, 133.5, 133.1, 132.6, 132.1, 131.6, 130.8, 129.3, 128.5, 128.3, 126.9, 126.4, 125.9, 125.5, 125.4, 119.6, 116.4, 81.0, 28.5. FTIR (ATR thin film): 3309, 2977, 16715, 1536, 1160, 738. HRMS (DART+) $[\text{M}+\text{H}]^+$ calcd. for $\text{C}_{21}\text{H}_{22}\text{NO}_2$ 320.16505, found 320.16372.

2-Amino-3-vinylanthracene (1.20)



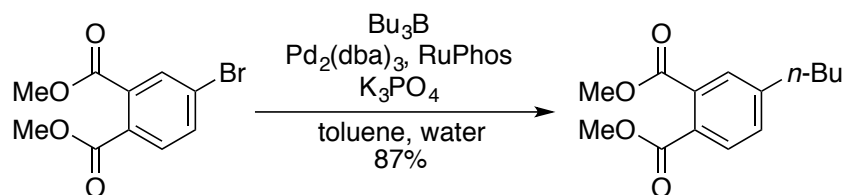
2-Amino-*N*-Boc-3-vinylanthracene **1.19** (1.37 g, 4.28 mmol, 1 equiv) was dissolved in 50 mL methylene chloride under ambient conditions, and trifluoroacetic acid (7.90 mL, 100 mmol, 24 equiv) was added carefully at room temperature. The reaction was stirred and monitored by TLC. At the conclusion of the reaction, the reaction mixture was quenched with saturated sodium bicarbonate solution, washed with brine, and the organic layer was dried over sodium sulfate. Volatiles were removed with a rotary evaporator, and the residue was precipitated from cold CH₂Cl₂/hexane to yield **1.20** as a yellow-orange powder (653 mg, 70%). ¹H NMR (500 MHz, CD₂Cl₂) δ 8.27 (s, 1H), 8.06 (s, 1H), 7.94 (s, 1H), 7.92 – 7.84 (m, 2H), 7.42 – 7.29 (m, 2H), 7.09 (s, 1H), 6.95 (dd, *J* = 17.3, 11.0 Hz, 1H), 5.87 (dd, *J* = 17.3, 1.4 Hz, 1H), 5.48 (dd, *J* = 10.9, 1.4 Hz, 1H), 4.05 (s, 2H). ¹³C NMR (126 MHz, CD₂Cl₂) δ 142.7, 133.4, 132.8, 130.3, 129.7, 128.58, 128.56, 128.2, 127.8, 127.0, 126.6, 125.7, 124.3, 122.4, 118.1, 107.2. FTIR (ATR thin film): 3359, 3050, 2929, 1635, 1479, 906, 740. HRMS (DART+) [M+H]⁺ calcd. for C₁₆H₁₄N 220.11262, found 220.11354.

2-*n*Bu-1,2-BN-tetracene



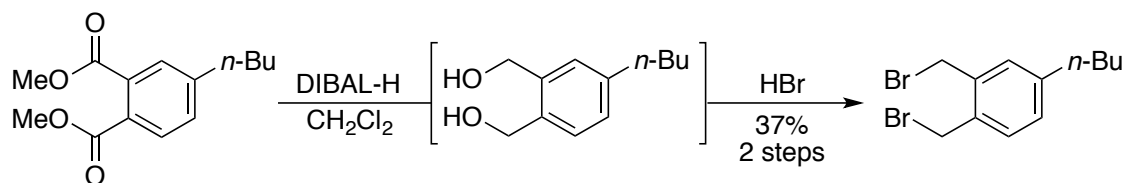
2-Amino-3-vinylanthracene **1.20** (100 mg, 0.456 mmol, 1 equiv) was mixed with 10 mL toluene and cooled to $-78\text{ }^{\circ}\text{C}$. *n*-Butyllithium solution was added dropwise (0.29 mL, 1.6 M, 0.46 mmol, 1 equiv). This mixture was warmed to $0\text{ }^{\circ}\text{C}$ over 1 hour, then boron trichloride solution (0.46 mL, 1.0 M in hexanes, 0.46 mmol, 1 equiv) was added at $0\text{ }^{\circ}\text{C}$. The reaction mixture was warmed to room temperature over 4 hours then heated to reflux at $130\text{ }^{\circ}\text{C}$ for 18 hours. After cooling to room temperature (*B*-Cl intermediate **7**: ^{11}B NMR (160 MHz, toluene) δ 33.1 (s) was observed), the volatiles were removed under reduced pressure. The residue was suspended in 15 mL ether, cooled in an ice bath, and *n*-butyllithium (0.58 mL, 1.6 M, 0.92 mmol, 2 equiv) was added dropwise at $0\text{ }^{\circ}\text{C}$. The reaction mixture was then warmed to room temperature over 18 hours. In the air, silica gel (~2 g) was added to the mixture, and volatiles were removed using a rotary evaporator. This residue was passed through a short silica plug using methylene chloride as the eluent, and **2-*n*Bu-1,2-BN-tetracene** was obtained by precipitation from a cold mixture of CH_2Cl_2 /pentane as a yellow solid (16 mg, 12%). ^1H NMR (500 MHz, $\text{THF-}d_8$) δ 8.97 (s, 1H), 8.54 (s, 1H), 8.40 (s, 1H), 8.31 (s, 1H), 8.05 (d, $J = 11.7\text{ Hz}$, 1H), 8.00 – 7.90 (dd, $J = 15.8, 8.3\text{ Hz}$, 2H), 7.84 (s, 1H), 7.41 – 7.28 (m, 2H), 6.76 (dd, $J = 11.6, 1.6\text{ Hz}$, 1H), 1.63 (dd, $J = 15.5, 7.8\text{ Hz}$, 2H), 1.47 – 1.39 (m, 2H), 1.31 – 1.25 (m, 2H), 0.97 (t, $J = 7.3\text{ Hz}$, 3H). ^1H NMR (500 MHz, CD_2Cl_2) δ 8.55 (s, 1H), 8.42 (s, 1H), 8.30 (s, 1H), 8.06 (d, $J = 11.8\text{ Hz}$, 1H), 8.02 – 7.94 (m, 2H), 7.76 (s, 1H), 7.68 (s, 1H), 7.47 – 7.35 (m, 2H), 6.80 (d, $J = 11.5\text{ Hz}$, 1H), 1.62 (q, $J = 7.5\text{ Hz}$, 2H), 1.44 (q, $J = 7.3\text{ Hz}$, 2H), 1.33 – 1.29 (m, 2H), 0.97 (t, $J = 7.3\text{ Hz}$, 3H). ^{13}C NMR (126 MHz, $\text{THF-}d_8$) δ 145.2, 140.1, 133.4, 133.0, 131.5, 129.5, 129.3, 129.1, 129.0, 128.6, 127.5, 126.2, 125.0, 124.7, 112.3, 29.1, 27.0, 14.6. Carbons adjacent to boron were not observed. ^{11}B NMR (160 MHz, CD_2Cl_2) δ 39.0 (s, broad). FTIR (ATR thin film): 2924, 1563, 1457, 1260, 1019, 801, 743. HRMS (DART+) $[\text{M}+\text{H}]^+$ calcd. for $\text{C}_{20}\text{H}_{21}\text{NB}$ 286.17670, found 286.17596.

4-Butylphthalic acid dimethyl ester (1.21)



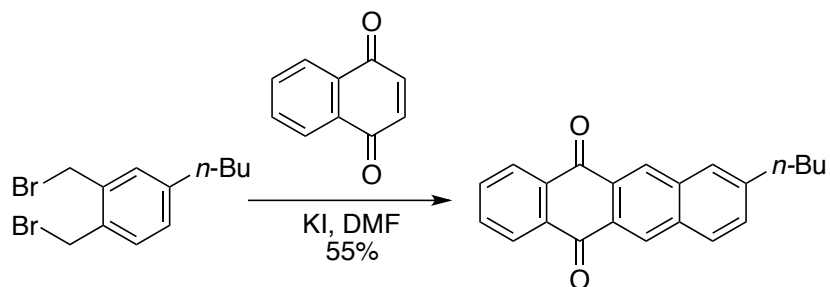
4-Bromophthalic acid dimethyl ester **1.21** (1.35 g, 4.94 mmol, 1 equiv) was dissolved in 5.0 mL toluene along with tributylborane (360. mg, 1.98 mmol, 0.4 equiv), potassium phosphate (2.10 g, 9.88 mmol, 2 equiv), $\text{Pd}_2(\text{dba})_3$ (68 mg, 0.074 mmol, 1.5 mol%) and RuPhos (115 mg, 0.247 mmol, 5 mol%). Water (0.5 mL) that had been purged with nitrogen for 40 minutes was injected, and the pressure vessel was sealed. The mixture was heated to 120 °C for 13 hours. The toluene was decanted off, and the solvent removed using a rotary evaporator, and the residue was extracted with ethyl acetate and washed with brine. The combined organic layers were dried over sodium sulfate, and the solvent was removed using a rotary evaporator. The residue was passed through a silica gel plug using hexane:ethyl acetate (3:1) as the mobile phase to yield **1.22** as a pale yellow oil (1.08 g, 87%). ^1H NMR (500 MHz, CDCl_3): δ 7.68 (d, J = 8.2 Hz, 1H), 7.48 (s, 1H), 7.33 (d, J = 8.1 Hz, 1H), 3.91 (s, 3H), 3.89 (s, 3H), 2.67 (t, J = 7.8 Hz, 2 H), 1.66 – 1.58 (m, 2H), 1.35 (h, J = 7.2 Hz, 2H), 0.93 (td, J = 7.4, 1.5 Hz, 3H). ^{13}C NMR (151 MHz, CDCl_3) δ 171.3, 170.5, 149.6, 135.3, 133.5, 131.8, 131.3 (2x), 55.3, 55.1, 38.0, 35.7, 24.9, 16.5. FTIR (ATR thin film): 2953, 1728, 1288, 1200, 1127. HRMS (DART+) $[\text{M}+\text{H}]^+$ calcd for $\text{C}_{14}\text{H}_{19}\text{O}_4$ 251.1283, found 251.1275.

1,2-bis(bromomethyl)-4-butylbenzene (1.24)



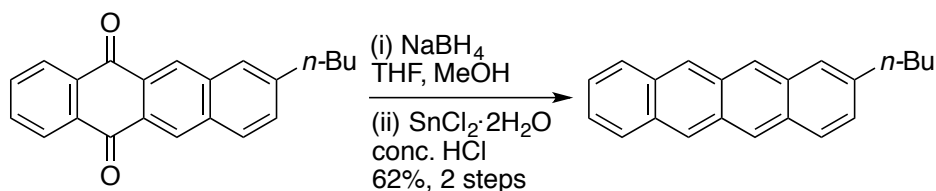
The diester **1.22** (4.62 g, 18.5 mmol, 1 equiv) was dissolved in 50 mL dry CH₂Cl₂ and cooled to 0 °C. DIBAL-H solution (1 M in hexanes) (77 mL, 77 mmol, 4.2 equiv) was added dropwise *via* cannula. The mixture was warmed to room temperature and stirred for 18 hours. The reactive aluminum residue was quenched using an aqueous workup: 3 mL water then 3 mL 15% NaOH solution then 8 mL water. Magnesium sulfate was added to dry the product, and the mixture was stirred for 15 minutes. The mixture was passed through a glass frit, and the solids were washed with hot ethyl acetate.⁵ Volatiles were removed using a rotary evaporator to yield a yellow viscous liquid **1.23** (Crude yield: 1.37 g, 38%) which was carried forward without further purification. Hydrogen bromide solution (48% in water) (17.5 mL, 155 mmol, 22 equiv) was added to the neat organic crude diol **1.23**, and the mixture was heated to 110 °C for 18 hours with a reflux condenser attached. After cooling to room temperature, the organics were extracted with hexane and dried over sodium sulfate. The volatiles were removed using a rotary evaporator to yield **1.24** as a red oil (1.88 g, 32%). ¹H NMR (500 MHz, CDCl₃) δ 7.27 (d, *J* = 7.7 Hz, 1H overlaps with CHCl₃ residual), 7.18 (d, *J* = 1.8 Hz, 1H), 7.12 (dd, *J* = 7.8, 1.8 Hz, 1H), 4.66 (s, 2H), 4.65 (s, 2H), 2.62 – 2.56 (m, 2H), 1.64 – 1.55 (m, 2H), 1.36 (dt, *J* = 14.9, 7.4 Hz, 2H), 0.93 (t, *J* = 7.4 Hz, 3H). ¹³C NMR (151 MHz, CDCl₃) δ 147.2, 139.0, 136.4, 133.8, 133.7, 132.1, 37.9, 35.9, 33.0, 32.9, 25.0, 16.6. FTIR (ATR thin film): 2927, 1502, 1440, 1160, 831, 607.

8-butyltetracene-5,12-dione (1.25)



The dibromide **1.24** (384 mg, 1.20 mmol, 1 equiv) was combined with 1,4-naphthoquinone (247 mg, 1.56 mmol, 1.3 equiv) and 5.0 mL degassed DMF under nitrogen. The mixture was heated to 90 °C, and potassium iodide (617 mg, 3.72 mmol, 3.1 equiv) was added. The mixture was then heated to 130 °C for 48 hours. After cooling to room temperature, a precipitate was collected on filter paper and washed with water and copious amounts of acetone to yield **1.25** as a light green powder (210 mg, 55%). ¹H NMR (500 MHz, CDCl₃) δ 8.82 (s, 1H), 8.79 (s, 1H), 8.40 (d, *J* = 9.0 Hz, two overlapping signals, 2H), 8.02 (d, *J* = 8.4 Hz, 1H), 7.87 (s, 1H), 7.83 (d, *J* = 5.8 Hz, 1H), 7.82 (d, *J* = 5.8 Hz, 1H), 7.55 (dd, *J* = 8.4, 1.7 Hz, 1H), 2.88 – 2.82 (m, 2H), 1.79 – 1.69 (m, 2H), 1.43 (h, *J* = 7.4 Hz, 2H), 0.97 (t, *J* = 7.3 Hz, 3H). ¹³C NMR (101 MHz, CDCl₃) δ 183.6, 183.5, 145.4 135.9 135.04, 135.00, 134.5, 134.5, 134.1, 131.7, 130.4, 130.3, 129.8, 129.6, 129.5, 129.0, 127.9, 110.0, 36.4, 33.6, 22.8, 14.4. FTIR (ATR thin film): 2919, 1672, 1320, 712. HRMS (APPI+) [*M*+*H*]⁺ calcd for C₂₂H₁₉O₂ 315.13850, found 315.13751.

2-Butyltetracene



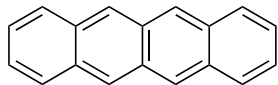
The dione **S-5** (61 mg, 0.19 mmol, 1 equiv) was dissolved in 1.0 mL THF and 1.0 mL methanol. Sodium borohydride (76 mg, 2.0 mmol, 10.4 equiv) was added in portions. The mixture was stirred at room temperature for 1 hour. Tin(II) chloride dihydrate (963 mg, 4.29 mmol, 22 equiv) was dissolved separately in 1.0 mL concentrated hydrochloric acid, and this solution was added all at once to the reaction mixture, which was stirred for 10 minutes in the dark. The suspension was filtered, and the solids were washed with 1.0 M hydrochloric acid (10 mL) and water (100 mL). The solids were subsequently dried using an air current generated by the vacuum filtration apparatus to yield **2-*n*Bu-tetracene** as a yellow-brown powder (34 mg, 61%). ^1H NMR (500 MHz, CDCl_3) δ 8.64 (s, 1H), 8.63 (s, 1H), 8.62 (s, 1H), 8.57 (s, 1H), 8.00 – 7.96 (m, 2H), 7.93 (d, $J = 8.8$ Hz, 1H), 7.73 (s, 1H), 7.41 – 7.35 (m, 2H), 7.26 (dd, $J = 2.1, 1.2$ Hz, 1H, overlaps with solvent residual), 2.80 (t, $J = 7.8$ Hz, 2H), 1.74 (td, $J = 7.5, 1.7$ Hz, 2H), 1.48 – 1.40 (m, 2H), 0.98 (td, $J = 7.4, 1.7$ Hz, 3H). ^{13}C NMR (151 MHz, CDCl_3) δ 142.2, 134.5, 134.1, 133.9, 133.2, 133.1, 132.6, 130.9, 130.9, 130.8, 130.2, 128.9, 128.7, 128.6, 128.2, 127.9, 127.7, 127.5, 38.7, 35.6, 25.1, 16.7. FTIR (ATR thin film): 2918, 1457, 1295, 904, 736, 467. HRMS (DART+) $[\text{M}+\text{H}]^+$ calcd for $\text{C}_{22}\text{H}_{21}$ 285.16433, found 285.16504.

Calculation Details

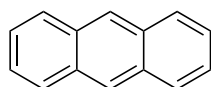
Calculations were carried out using the Gaussian 09 program.

Optimizations and TD-DFT calculations were carried out using the CAM-B3LYP method and the 6-311G(d,p) basis set. Single-point TD-DFT calculations were performed using the PCM solvent model for methylene chloride. These DFT coordinates were used to begin G3MP2 calculations for theoretical determination of ΔH_f values.

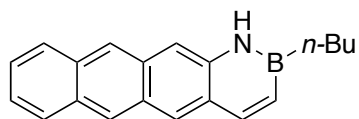
Optimized CAM-B3LYP/6-311G(d,p) Coordinates



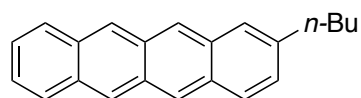
C	-3.522102	1.084239	0.000000
C	-4.712947	0.441042	0.000000
C	-2.288256	0.354557	0.000000
C	-2.342591	-1.084909	0.000000
C	-3.628109	-1.719202	0.000000
C	-4.766917	-0.987807	0.000000
C	-1.059318	0.985854	0.000000
C	0.144334	0.261285	0.000000
C	0.090085	-1.175923	0.000000
C	-1.164944	-1.807356	0.000000
C	1.399363	0.892719	0.000000
C	2.577010	0.170272	0.000000
C	2.522675	-1.269194	0.000000
C	1.293737	-1.900491	0.000000
C	3.862527	0.804564	0.000000
C	5.001336	0.073169	0.000000
C	4.947366	-1.355679	0.000000
C	3.756521	-1.998877	0.000000
H	3.901173	1.888127	0.000000
H	5.966089	0.566031	0.000000
H	5.872140	-1.920008	0.000000
H	3.713054	-3.082257	0.000000
H	1.252703	-2.984754	0.000000
H	1.440563	1.976974	0.000000
H	-1.018284	2.070117	0.000000
H	-1.206145	-2.891611	0.000000
H	-3.478635	2.167619	0.000000
H	-5.637721	1.005371	0.000000
H	-3.666754	-2.802764	0.000000



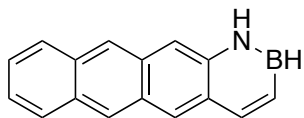
C	3.639345	-0.711883	0.000000
C	2.469251	-1.399747	0.000001
C	1.215622	-0.715943	0.000000
C	1.215622	0.715943	0.000000
C	2.469251	1.399747	0.000000
C	3.639345	0.711883	0.000000
C	0.000000	-1.394551	0.000000
C	0.000000	1.394551	0.000000
C	-1.215622	0.715943	0.000000
C	-1.215622	-0.715943	0.000000
C	-2.469251	-1.399747	0.000000
H	-2.466531	-2.484029	0.000000
C	-3.639345	-0.711883	-0.000001
C	-3.639345	0.711883	0.000000
C	-2.469251	1.399747	0.000000
H	0.000000	-2.479707	0.000001
H	4.583635	-1.242988	0.000000
H	2.466531	-2.484029	0.000001
H	2.466531	2.484029	0.000000
H	4.583635	1.242988	-0.000001
H	0.000000	2.479707	0.000000
H	-4.583635	-1.242988	-0.000001
H	-4.583635	1.242988	-0.000001
H	-2.466531	2.484029	0.000000



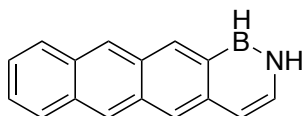
C	6.421328	-1.235501	0.235390
C	5.177399	-1.747530	0.063543
C	4.027903	-0.897232	0.038200
C	4.220382	0.515602	0.199282
C	5.549707	1.010905	0.377642
C	6.611960	0.168469	0.395438
C	2.743198	-1.395140	-0.136082
C	1.626969	-0.555311	-0.159478
C	1.820967	0.855928	0.001449
C	3.114414	1.353666	0.176734
C	0.310048	-1.046433	-0.336685
C	-0.769765	-0.205862	-0.357170
C	-0.584707	1.211720	-0.196219
C	0.684621	1.699099	-0.023986
C	-1.739008	2.089200	-0.221297
C	-2.992677	1.632913	-0.388147
N	-2.063997	-0.677740	-0.530388
B	-3.233394	0.120417	-0.565715
H	7.282733	-1.892475	0.252465
H	5.032111	-2.815129	-0.058030
H	5.690079	2.079286	0.498719
H	7.614385	0.556034	0.531453
H	2.602572	-2.464178	-0.257167
H	3.255939	2.422704	0.297830
H	0.826856	2.768001	0.096788
H	0.162431	-2.114799	-0.458481
H	-1.532726	3.149917	-0.098202
H	-3.803931	2.354533	-0.398487
H	-2.133845	-1.679828	-0.638234
C	-4.646469	-0.547661	-0.772690
H	-5.073628	-0.166497	-1.710249
H	-4.559534	-1.633291	-0.907459
C	-5.643106	-0.261071	0.360297
H	-5.246899	-0.648993	1.306051
H	-5.740490	0.821268	0.500402
C	-7.027792	-0.857365	0.120577
H	-7.427072	-0.464217	-0.820848
H	-6.932614	-1.939749	-0.019407
C	-8.008389	-0.572026	1.252848
H	-8.989055	-1.009951	1.054535
H	-8.147268	0.503473	1.392067
H	-7.646992	-0.982239	2.199669



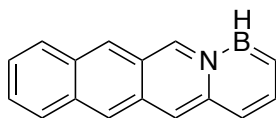
C	6.372969	-1.268101	0.222908
C	5.132742	-1.762847	0.000427
C	3.983750	-0.906012	0.004168
C	4.177634	0.499295	0.250720
C	5.509954	0.974682	0.481058
C	6.565322	0.127078	0.468064
C	2.706764	-1.384976	-0.220111
C	1.587167	-0.536869	-0.215203
C	1.781261	0.866423	0.030551
C	3.082691	1.342708	0.257852
C	0.284163	-1.013223	-0.442990
C	-0.810013	-0.170347	-0.436430
C	-0.613973	1.234235	-0.190805
C	0.660420	1.715006	0.034085
C	-1.766623	2.086501	-0.194757
C	-3.002419	1.586566	-0.418193
C	-2.142739	-0.645303	-0.668482
C	-3.214184	0.185995	-0.661836
H	7.232479	-1.927623	0.217016
H	4.984745	-2.820711	-0.185705
H	5.653460	2.033262	0.666730
H	7.567103	0.500213	0.643896
H	2.561181	-2.444053	-0.405768
H	3.228563	2.401778	0.443466
H	0.805471	2.774433	0.218356
H	0.139077	-2.072381	-0.628557
H	-1.624183	3.146880	-0.018238
H	-3.860825	2.249756	-0.423351
H	-2.279848	-1.705520	-0.856120
C	-4.616925	-0.315362	-0.878927
H	-5.117432	0.318608	-1.619665
H	-4.581659	-1.322257	-1.304022
C	-5.454282	-0.337690	0.404310
H	-4.962501	-0.984924	1.138278
H	-5.472070	0.664139	0.847247
C	-6.884952	-0.815669	0.175299
H	-7.368457	-0.166059	-0.562508
H	-6.863811	-1.816709	-0.269115
C	-7.714904	-0.842590	1.454154
H	-8.732408	-1.190138	1.263638
H	-7.781908	0.152753	1.901106
H	-7.269916	-1.508447	2.198132



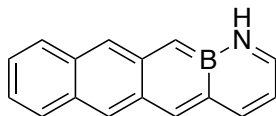
C	-6.794678	2.391749	0.090741
C	-5.442706	2.403841	0.193098
C	-4.685620	1.194615	0.091694
C	-5.391484	-0.036999	-0.121714
C	-6.817524	-0.001677	-0.223377
C	-7.495469	1.167824	-0.121221
C	-3.301204	1.178655	0.192973
C	-2.571164	-0.008835	0.092400
C	-3.277492	-1.238329	-0.120956
C	-4.671360	-1.218329	-0.222314
C	-1.159426	-0.042749	0.193505
C	-0.464371	-1.217643	0.091837
C	-1.163494	-2.456331	-0.122449
C	-2.531396	-2.435381	-0.221820
C	-0.414703	-3.692773	-0.228363
C	0.927364	-3.739377	-0.134226
N	0.920504	-1.261208	0.189782
B	1.697700	-2.433660	0.094257
H	-7.354526	3.315980	0.169752
H	-4.909869	3.334276	0.354268
H	-7.346343	-0.934481	-0.384507
H	-8.575827	1.181356	-0.199781
H	-2.772076	2.112038	0.354366
H	-5.201341	-2.151362	-0.383709
H	-3.061892	-3.367997	-0.383390
H	-0.623673	0.887177	0.355113
H	-1.003348	-4.592820	-0.390021
H	1.420050	-4.701532	-0.223405
H	1.360436	-0.365263	0.340037
H	2.879870	-2.334278	0.195747



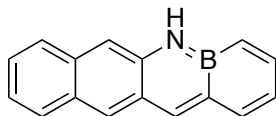
C	-5.053097	2.727701	0.000000
C	-6.304423	2.205883	0.000000
C	-3.901902	1.879662	0.000000
C	-4.095219	0.456853	0.000000
C	-5.433556	-0.048091	0.000000
C	-6.497118	0.792780	0.000000
C	-2.609644	2.385033	0.000000
C	-1.493212	1.545226	0.000000
C	-1.684450	0.123244	0.000000
C	-2.988815	-0.380908	0.000000
C	-0.168629	2.049043	0.000000
C	0.928231	1.224658	0.000000
C	0.726635	-0.205839	0.000000
C	-0.546562	-0.719057	0.000000
B	2.366991	1.763244	0.000000
N	3.392968	0.797262	0.000000
C	3.139683	-0.568853	0.000000
C	1.893842	-1.064212	0.000000
H	-7.505057	0.395353	0.000000
H	-7.168348	2.859522	0.000000
H	-4.902379	3.801503	0.000000
H	-5.579247	-1.122520	0.000000
H	-2.459697	3.459848	0.000000
H	-3.138553	-1.455619	0.000000
H	-0.028334	3.125586	0.000000
H	-0.696909	-1.793889	0.000000
H	4.007504	-1.216504	0.000000
H	1.755099	-2.137897	0.000000
H	2.652470	2.919618	0.000000
H	4.364758	1.063461	0.000000



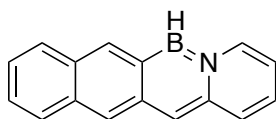
C	-5.012379	2.745612	0.000000
C	-6.263603	2.240638	0.000000
C	-3.862762	1.880234	0.000000
C	-4.077520	0.444613	0.000000
C	-5.433714	-0.036137	0.000000
C	-6.476979	0.820450	0.000000
C	-2.582671	2.370426	0.000000
C	-1.465524	1.498989	0.000000
C	-1.673150	0.073427	0.000000
C	-3.003409	-0.410966	0.000000
C	-0.171872	1.969468	0.000000
C	0.748259	-0.229741	0.000000
C	-0.555803	-0.741354	0.000000
B	2.268460	1.772526	0.000000
C	3.162467	-0.524041	0.000000
C	1.883175	-1.048675	0.000000
H	-7.491968	0.441750	0.000000
H	-7.120987	2.902428	0.000000
H	-4.846280	3.816879	0.000000
H	-5.596550	-1.107758	0.000000
H	-2.414644	3.442015	0.000000
H	-3.170372	-1.482430	0.000000
H	0.041925	3.029546	0.000000
H	-0.671246	-1.818038	0.000000
H	3.991948	-1.226571	0.000000
H	1.721620	-2.118408	0.000000
H	2.282226	2.963479	0.000000
H	4.439082	1.181632	0.000000
C	3.408256	0.846845	0.000000
N	0.917044	1.165252	0.000000



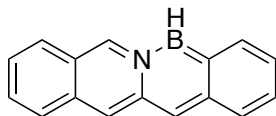
C	-5.017521	2.753817	0.000000
C	-6.274620	2.260788	0.000000
C	-3.876483	1.879066	0.000000
C	-4.102275	0.449038	0.000000
C	-5.462695	-0.021544	0.000001
C	-6.500256	0.842494	0.000001
C	-2.588305	2.349670	-0.000001
C	-1.460532	1.490078	-0.000001
C	-1.679997	0.044611	0.000000
C	-3.030270	-0.405976	0.000000
C	3.208976	-0.502778	0.000000
H	-7.518476	0.471720	0.000001
H	-7.126038	2.930707	0.000000
H	-4.842263	3.824060	0.000000
H	-5.633702	-1.092303	0.000001
H	-2.415569	3.421332	-0.000001
H	-3.207612	-1.476590	0.000000
H	-0.073393	3.111570	-0.000001
H	-0.866859	-1.908856	0.000000
H	4.071457	-1.159459	0.000001
H	1.981171	-2.082125	-0.000001
H	2.434834	2.794874	0.000005
H	4.373980	1.274986	0.000002
C	3.369228	0.874905	0.000000
C	2.266625	1.719743	-0.000002
C	-0.176195	2.028420	-0.000001
B	0.768443	-0.300869	-0.000001
C	0.962216	1.213165	-0.000001
C	-0.613430	-0.850902	0.000000
N	2.002591	-1.071553	-0.000001



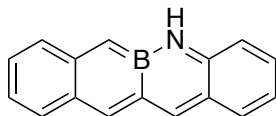
C	-5.029639	2.738172	0.000000
C	-6.292879	2.234450	0.000000
C	-3.898520	1.873740	0.000000
C	-4.106162	0.462383	0.000000
C	-5.442859	-0.026981	0.000000
C	-6.499812	0.830130	0.000000
C	-2.587742	2.357666	0.000000
C	-1.486239	1.515402	0.000000
C	-1.705702	0.099007	0.000000
C	-2.997577	-0.392578	0.000000
C	3.181592	-0.564574	0.000000
C	1.978342	-1.181699	0.000000
H	-7.511583	0.442360	0.000000
H	-7.147382	2.900007	0.000000
H	-4.862622	3.809620	0.000000
H	-5.603995	-1.099174	0.000000
H	-2.422953	3.430236	0.000000
H	-3.158943	-1.465991	0.000000
H	-0.047514	3.122574	0.000000
H	-0.832223	-1.726808	0.000000
H	4.097751	-1.149904	0.000000
H	1.959478	-2.268582	0.000000
H	2.472856	2.804789	0.000000
H	4.355572	1.268620	0.000000
C	3.343843	0.878067	0.000000
C	2.299340	1.732049	0.000000
C	-0.149268	2.038242	0.000000
B	0.734924	-0.290874	0.000000
C	0.945849	1.232509	0.000000
N	-0.612904	-0.740769	0.000000



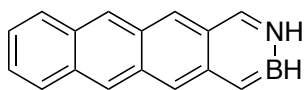
C	-5.069786	2.721460	0.000000
C	-6.321943	2.190684	0.000000
C	-3.919560	1.883118	0.000000
C	-4.095300	0.465137	0.000000
C	-5.423651	-0.052205	0.000000
C	-6.498238	0.781328	0.000000
C	-2.618340	2.398028	0.000000
C	-1.501423	1.576111	0.000000
C	-1.685067	0.154811	0.000000
C	-2.972096	-0.367357	0.000000
C	0.746950	-0.207489	0.000000
C	-0.527895	-0.684690	0.000000
C	3.150530	-0.606966	0.000000
C	1.894053	-1.082917	0.000000
H	-7.501623	0.371983	0.000000
H	-7.190907	2.837419	0.000000
H	-4.925965	3.796364	0.000000
H	-5.561119	-1.127723	0.000000
H	-2.484159	3.475389	0.000000
H	-3.115468	-1.443076	0.000000
H	0.187377	3.280015	0.000000
H	-0.660974	-1.759358	0.000000
H	3.996271	-1.283024	0.000000
H	1.696244	-2.147216	0.000000
H	2.409234	2.713873	0.000000
H	4.371497	1.222581	0.000000
C	3.370904	0.813892	0.000000
N	0.997070	1.182537	0.000000
C	2.314479	1.637418	0.000000
B	-0.088066	2.121962	0.000000



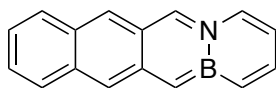
C	-5.040312	2.762544	0.000000
C	-6.280001	2.231596	0.000000
C	-3.876886	1.913232	0.000000
C	-4.084249	0.480203	0.000000
C	-5.428788	-0.035341	0.000000
C	-6.482089	0.804936	0.000000
C	-2.597915	2.385974	0.000000
C	-1.463798	1.526029	0.000000
C	-2.994755	-0.331061	0.000000
C	3.206813	-0.533677	0.000000
H	-7.493111	0.417197	0.000000
H	-7.147341	2.880910	0.000000
H	-4.894490	3.836454	0.000000
H	-5.571728	-1.109928	0.000000
H	-2.410008	3.452586	0.000000
H	-3.085539	-1.408514	0.000000
H	-0.039042	3.075413	0.000000
H	-0.881130	-1.961636	0.000000
H	4.080870	-1.173536	0.000000
H	1.817788	-2.148047	0.000000
H	2.406625	2.772151	0.000001
H	4.361189	1.291766	0.000001
C	3.363492	0.867339	0.000000
C	2.275310	1.695656	-0.000001
C	-0.174445	2.001244	0.000000
C	0.962794	1.160115	0.000000
C	1.947408	-1.071089	0.000000
C	0.795453	-0.250796	0.000000
B	-0.597655	-0.805155	0.000000
N	-1.701429	0.135524	0.000000



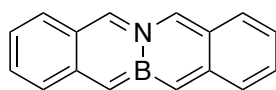
C	-5.096700	2.739443	0.000000
C	-6.325952	2.187877	0.000000
C	-3.891835	1.936785	0.000000
C	-4.068058	0.479297	0.000000
C	-5.411919	-0.046360	0.000000
C	-6.491683	0.759483	0.000000
C	-2.647490	2.518857	0.000000
C	-2.994337	-0.374115	0.000000
C	3.165875	-0.585893	0.000000
H	-7.490898	0.341189	0.000000
H	-7.206386	2.820045	0.000000
H	-4.977752	3.817242	0.000000
H	-5.529768	-1.124541	0.000000
H	-2.614164	3.606356	0.000000
H	-3.179724	-1.445977	0.000000
H	0.172736	3.032049	0.000000
H	-0.676533	-1.797782	0.000000
H	4.010669	-1.262766	0.000000
H	1.707483	-2.140432	0.000000
H	2.490650	2.746118	-0.000001
H	4.390349	1.192895	0.000000
C	3.378945	0.804533	0.000000
C	2.321094	1.674659	0.000000
C	0.996622	1.193434	0.000000
C	1.887155	-1.071104	0.000000
C	0.767417	-0.207718	0.000000
C	-0.558704	-0.714996	0.000000
B	-1.432173	1.624608	0.000000
C	-1.657006	0.109188	0.000000
N	-0.064881	2.049717	0.000000



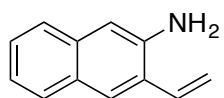
C	-5.021116	2.753096	-0.000001
C	-6.270795	2.242654	0.000001
C	-3.867740	1.893781	-0.000001
C	-4.076026	0.459319	0.000001
C	-5.429743	-0.028720	0.000003
C	-6.478122	0.821898	0.000003
C	-2.587575	2.386453	-0.000003
C	-1.458666	1.530598	-0.000003
C	-1.662140	0.096935	-0.000002
C	-2.995349	-0.386764	0.000000
C	-0.162558	2.017764	-0.000005
C	0.943838	1.156130	-0.000005
C	0.759724	-0.283023	-0.000003
C	-0.566692	-0.753696	-0.000002
N	3.303272	0.887401	-0.000002
C	1.880819	-1.129323	-0.000002
H	-7.491267	0.437991	0.000004
H	-7.130907	2.901208	0.000001
H	-4.860700	3.825463	-0.000003
H	-5.586850	-1.101392	0.000004
H	-2.426980	3.459669	-0.000005
H	-3.157013	-1.459380	0.000002
H	0.001825	3.090688	-0.000007
H	-0.732421	-1.825411	0.000000
H	4.285996	-1.147569	0.000003
H	1.682094	-2.196404	-0.000001
H	2.396965	2.751482	0.000032
H	4.199375	1.354863	0.000001
C	2.237788	1.678653	-0.000008
B	3.243992	-0.572277	0.000000



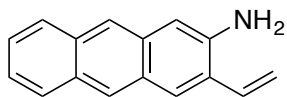
C	-4.982572	2.778379	0.000000
C	-6.247783	2.308563	0.000000
C	-3.857689	1.881715	0.000000
C	-4.110605	0.454257	0.000000
C	-5.480111	0.010671	0.000000
C	-6.500208	0.894716	0.000000
C	-2.563071	2.331420	0.000000
C	-1.464162	1.435236	0.000000
C	-1.704086	0.005386	0.000000
C	-3.058228	-0.425826	0.000000
C	-0.624176	-0.866600	0.000000
C	3.264524	-0.477250	0.000000
C	2.081829	-1.135727	0.000000
H	-7.525197	0.543562	0.000000
H	-7.086417	2.994207	0.000000
H	-4.787571	3.845052	0.000000
H	-5.671663	-1.056354	0.000000
H	-2.368342	3.399119	0.000000
H	-3.254789	-1.492588	0.000000
H	0.010297	2.992270	0.000000
H	-0.845968	-1.930022	0.000000
H	4.212998	-1.005367	0.000000
H	2.091690	-2.221449	0.000000
H	2.201230	2.782035	0.000000
H	4.251539	1.471593	0.000000
C	3.299564	0.955922	0.000000
N	0.913753	1.120886	0.000000
C	2.176954	1.699400	0.000000
C	-0.172089	1.923237	0.000000
B	0.773379	-0.354354	0.000000



C	-5.164969	2.710534	0.000000
C	-6.366827	2.095476	0.000000
C	-3.933718	1.961244	0.000000
C	-4.036347	0.515307	0.000000
C	-5.340165	-0.092874	0.000000
C	-6.457904	0.663380	0.000000
C	-2.692492	2.552847	0.000000
C	-2.912352	-0.265681	0.000000
C	3.084745	-0.687326	0.000000
H	-7.434568	0.194987	0.000000
H	-7.278923	2.680428	0.000000
H	-5.096800	3.792432	0.000000
H	-5.405397	-1.175372	0.000000
H	-2.655054	3.638753	0.000000
H	-2.988522	-1.347055	0.000000
H	0.256883	3.226766	0.000000
H	-0.806183	-1.655938	0.000000
H	3.893147	-1.408282	0.000000
H	1.563411	-2.161722	0.000000
H	2.645606	2.696743	0.000000
H	4.433306	1.022804	0.000000
C	3.394710	0.713976	0.000000
C	2.410931	1.638433	0.000000
C	-0.008178	2.173044	0.000000
C	1.019945	1.260354	0.000000
C	1.801116	-1.103648	0.000000
C	0.717132	-0.157536	0.000000
N	-1.648956	0.254522	0.000000
C	-0.579281	-0.595930	0.000000
B	-1.441266	1.721422	0.000000

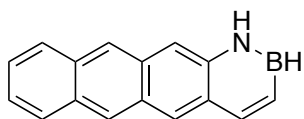


C	-6.173958	1.614694	0.123208
C	-7.380315	0.956644	0.128026
C	-4.953452	0.894885	0.029416
C	-5.006460	-0.530806	-0.059475
C	-6.268234	-1.179631	-0.053359
C	-7.431572	-0.454823	0.038810
C	-3.691888	1.530033	-0.001575
C	-2.508133	0.820757	-0.086608
C	-2.548560	-0.618936	-0.130301
C	-3.786466	-1.237110	-0.148139
C	-1.357775	-1.482728	-0.165053
C	-0.118618	-1.243530	0.283539
H	-1.553813	-2.471585	-0.575237
H	0.165442	-0.318113	0.767231
H	0.639986	-2.014727	0.217535
H	-8.391019	-0.959270	0.044452
H	-8.303556	1.520951	0.200940
H	-6.140345	2.697253	0.190807
H	-6.299187	-2.262511	-0.120142
H	-3.822965	-2.320761	-0.209278
N	-1.284764	1.492308	-0.101548
H	-3.654817	2.615332	0.031623
H	-1.358974	2.472800	-0.333406
H	-0.558318	1.033762	-0.634545

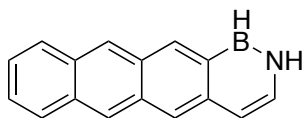


C	-6.262026	1.614704	-0.187344
C	-7.502171	0.972206	-0.275125
C	-5.065381	0.896700	-0.093305
C	-5.119166	-0.543114	-0.088764
C	-6.356183	-1.187781	-0.175445
C	-7.553050	-0.470237	-0.269087
C	-3.794970	1.523843	0.023816
C	-2.622614	0.809257	0.108340
C	-2.662430	-0.640824	0.058203
C	-3.892358	-1.256018	-0.000351
C	-1.470269	-1.503320	0.070361
C	-0.221543	-1.234428	-0.332493
H	-1.674400	-2.516343	0.411565
H	0.071016	-0.278590	-0.746847
H	0.537254	-2.007438	-0.297301
H	-6.229998	2.700067	-0.191036
H	-6.388601	-2.273322	-0.172675
H	-3.931446	-2.341132	-0.007671
N	-1.395608	1.464517	0.214333
H	-3.756472	2.608730	0.062832
H	-1.470106	2.432916	0.492304
H	-0.697052	0.970261	0.752223
C	-8.731156	1.693915	-0.371300
C	-8.824981	-1.112740	-0.359165
C	-9.977865	-0.383566	-0.449503
C	-9.928691	1.039476	-0.455723
H	-10.852122	1.603233	-0.528661
H	-8.695956	2.778475	-0.376499
H	-8.858702	-2.197462	-0.354388
H	-10.936943	-0.884496	-0.517403

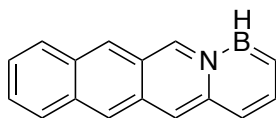
G3MP2 Coordinantes



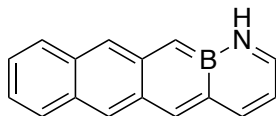
C	-6.808491	2.403588	0.091440
C	-5.440504	2.410823	0.194502
C	-4.692553	1.201629	0.092294
C	-5.402207	-0.037375	-0.122619
C	-6.824295	-0.002540	-0.224220
C	-7.506777	1.182912	-0.120228
C	-3.299294	1.183384	0.193912
C	-2.569291	-0.010326	0.092388
C	-3.281090	-1.250013	-0.122773
C	-4.681328	-1.229154	-0.224572
C	-1.160340	-0.039860	0.193702
C	-0.459299	-1.227127	0.090857
C	-1.154013	-2.464943	-0.122783
C	-2.538340	-2.446025	-0.223648
C	-0.411482	-3.698751	-0.228613
C	0.946059	-3.740478	-0.132735
N	0.928327	-1.264573	0.189545
B	1.717968	-2.434424	0.095591
H	-7.365587	3.333966	0.171454
H	-4.904316	3.344824	0.356601
H	-7.359887	-0.936688	-0.386294
H	-8.591244	1.193325	-0.199819
H	-2.765682	2.120901	0.356278
H	-5.215854	-2.166018	-0.386920
H	-3.068862	-3.384987	-0.385971
H	-0.621582	0.894666	0.356061
H	-0.998799	-4.604709	-0.390864
H	1.435206	-4.708179	-0.222699
H	1.364187	-0.358901	0.340455
H	2.904307	-2.328459	0.197994



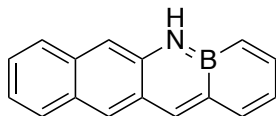
C	-5.057276	2.733040	0.000000
C	-6.322184	2.202220	0.000000
C	-3.909992	1.885962	0.000000
C	-4.105160	0.454811	0.000000
C	-5.436947	-0.054812	0.000000
C	-6.515260	0.792989	0.000000
C	-2.610627	2.398281	0.000000
C	-1.489025	1.554292	0.000000
C	-1.682138	0.120795	0.000000
C	-2.991375	-0.387563	0.000000
C	-0.167332	2.058272	0.000000
C	0.941251	1.223290	0.000000
C	0.738587	-0.204401	0.000000
C	-0.550137	-0.722937	0.000000
B	2.379049	1.767370	0.000000
N	3.404075	0.792955	0.000000
C	3.155437	-0.576426	0.000000
C	1.892917	-1.068045	0.000000
H	-7.525084	0.389647	0.000000
H	-7.187276	2.861138	0.000000
H	-4.910199	3.811996	0.000000
H	-5.583232	-1.134021	0.000000
H	-2.461085	3.478844	0.000000
H	-3.141020	-1.468206	0.000000
H	-0.022484	3.139620	0.000000
H	-0.699703	-1.803723	0.000000
H	4.025523	-1.226913	0.000000
H	1.750711	-2.145775	0.000000
H	2.671273	2.927657	0.000000
H	4.381742	1.061730	0.000000



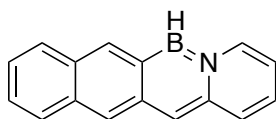
C	-3.702368	1.350890	0.000000
C	-4.870158	0.636538	0.000000
C	-2.436788	0.683167	0.000000
C	-2.423806	-0.766361	0.000000
C	-3.669175	-1.468059	0.000000
C	-4.858313	-0.790693	0.000000
C	-1.237718	1.388606	0.000000
C	0.000000	0.708798	0.000000
C	0.016687	-0.737185	0.000000
C	-1.206262	-1.438152	0.000000
C	1.212877	1.386600	0.000000
C	2.467901	-0.659797	0.000000
C	1.259352	-1.368178	0.000000
B	3.663928	1.556746	0.000000
C	4.906478	-0.607429	0.000000
C	3.716355	-1.309743	0.000000
H	-5.798729	-1.335882	0.000000
H	-5.822825	1.160786	0.000000
H	-3.718572	2.439286	0.000000
H	-3.653670	-2.556952	0.000000
H	-1.251735	2.478694	0.000000
H	-1.193991	-2.528780	0.000000
H	1.261486	2.471285	0.000000
H	1.312662	-2.455951	0.000000
H	5.836606	-1.176728	0.000000
H	3.706294	-2.396496	0.000000
H	3.512499	2.743010	0.000000
H	5.901258	1.283613	0.000000
C	4.928977	0.795571	0.000000
N	2.423547	0.751848	0.000000



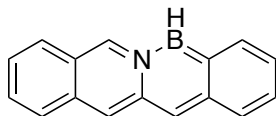
C	-5.022882	2.751097	0.000000
C	-6.295503	2.244247	0.000000
C	-3.888712	1.880165	0.000000
C	-4.118264	0.453389	0.000000
C	-5.462555	-0.030759	0.000000
C	-6.522982	0.835817	0.000000
C	-2.584123	2.363827	0.000000
C	-1.459986	1.507619	0.000000
C	-1.685698	0.058680	0.000000
C	-3.023644	-0.403679	0.000000
C	3.220591	-0.523384	0.000000
H	-7.541554	0.455416	0.000000
H	-7.146681	2.921372	0.000000
H	-4.855397	3.827061	0.000000
H	-5.628802	-1.107374	0.000000
H	-2.418684	3.442218	0.000000
H	-3.197051	-1.481214	0.000000
H	-0.056969	3.140344	0.000000
H	-0.869000	-1.909309	0.000000
H	4.076695	-1.193371	0.000000
H	1.959219	-2.090118	0.000000
H	2.469205	2.802712	0.000000
H	4.391332	1.259150	0.000000
C	3.379266	0.865473	0.000000
C	2.290150	1.724839	0.000000
C	-0.161801	2.051948	0.000000
B	0.774204	-0.290451	0.000000
C	0.968717	1.226538	0.000000
C	-0.610760	-0.847619	0.000000
N	1.994701	-1.072546	0.000000



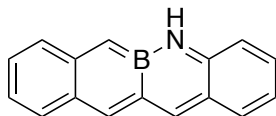
C	-5.035479	2.747431	0.000000
C	-6.308066	2.231915	0.000000
C	-3.902330	1.884292	0.000000
C	-4.112007	0.460426	0.000000
C	-5.446208	-0.033817	0.000000
C	-6.516552	0.827486	0.000000
C	-2.591950	2.373498	0.000000
C	-1.479284	1.522290	0.000000
C	-1.701467	0.103161	0.000000
C	-3.001945	-0.395128	0.000000
C	3.200964	-0.569966	0.000000
C	1.982211	-1.192292	0.000000
H	-7.530442	0.434554	0.000000
H	-7.165130	2.900969	0.000000
H	-4.873504	3.824141	0.000000
H	-5.606854	-1.110943	0.000000
H	-2.424898	3.451195	0.000000
H	-3.162172	-1.474234	0.000000
H	-0.042463	3.135111	0.000000
H	-0.835535	-1.732178	0.000000
H	4.119489	-1.158287	0.000000
H	1.966430	-2.282629	0.000000
H	2.474641	2.810543	0.000000
H	4.368606	1.267258	0.000000
C	3.356465	0.867209	0.000000
C	2.299560	1.733596	0.000000
C	-0.151318	2.046101	0.000000
B	0.744063	-0.296262	0.000000
C	0.956757	1.226790	0.000000
N	-0.608553	-0.740137	0.000000



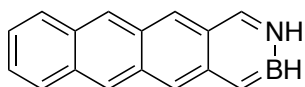
C	-5.073535	2.728565	0.000000
C	-6.336122	2.187698	0.000000
C	-3.923637	1.890037	0.000000
C	-4.102743	0.460267	0.000000
C	-5.428664	-0.060138	0.000000
C	-6.515827	0.779087	0.000000
C	-2.619899	2.408417	0.000000
C	-1.494729	1.579200	0.000000
C	-1.680252	0.153431	0.000000
C	-2.978234	-0.373954	0.000000
C	0.756855	-0.207874	0.000000
C	-0.534460	-0.686185	0.000000
C	3.169098	-0.611975	0.000000
C	1.893936	-1.084380	0.000000
H	-7.521944	0.366187	0.000000
H	-7.206919	2.839061	0.000000
H	-4.933194	3.808472	0.000000
H	-5.567008	-1.140448	0.000000
H	-2.483899	3.490834	0.000000
H	-3.120025	-1.455779	0.000000
H	0.193912	3.297451	0.000000
H	-0.666852	-1.766620	0.000000
H	4.013384	-1.295641	0.000000
H	1.693790	-2.153121	0.000000
H	2.422046	2.723215	0.000000
H	4.389205	1.217846	0.000000
C	3.386331	0.804307	0.000000
N	1.001671	1.187143	0.000000
C	2.323660	1.643508	0.000000
B	-0.082914	2.133480	0.000000



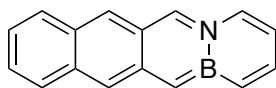
C	-5.038141	2.767618	0.000000
C	-6.298866	2.241170	0.000000
C	-3.891527	1.910452	0.000000
C	-4.096546	0.479210	0.000000
C	-5.434430	-0.036134	0.000000
C	-6.496908	0.821476	0.000000
C	-2.593000	2.379186	0.000000
C	-1.468297	1.519132	0.000000
C	-2.999748	-0.349696	0.000000
C	3.217651	-0.528101	0.000000
H	-7.510214	0.427477	0.000000
H	-7.164354	2.899297	0.000000
H	-4.886345	3.845926	0.000000
H	-5.585555	-1.114214	0.000000
H	-2.402517	3.451687	0.000000
H	-3.093810	-1.431683	0.000000
H	-0.036734	3.082330	0.000000
H	-0.874453	-1.987480	0.000000
H	4.095495	-1.170103	0.000000
H	1.827664	-2.157579	0.000000
H	2.410408	2.789349	0.000000
H	4.380878	1.304216	0.000000
C	3.379645	0.878026	0.000000
C	2.281559	1.707573	0.000000
C	-0.165461	2.001381	0.000000
C	0.966013	1.166034	0.000000
C	1.952849	-1.075838	0.000000
C	0.794424	-0.255378	0.000000
B	-0.595852	-0.823762	0.000000
N	-1.700803	0.120519	0.000000



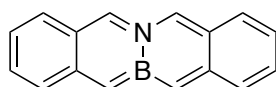
C	-5.097736	2.744975	0.000000
C	-6.347639	2.194630	0.000000
C	-3.906755	1.937418	0.000000
C	-4.077915	0.484019	0.000000
C	-5.411918	-0.044596	0.000000
C	-6.505717	0.774099	0.000000
C	-2.644402	2.523632	0.000000
C	-2.990159	-0.386083	0.000000
C	3.177992	-0.584143	0.000000
H	-7.505321	0.345791	0.000000
H	-7.227516	2.833831	0.000000
H	-4.976788	3.827530	0.000000
H	-5.535276	-1.126684	0.000000
H	-2.611104	3.615671	0.000000
H	-3.180556	-1.462608	0.000000
H	0.170114	3.035428	0.000000
H	-0.670336	-1.818888	0.000000
H	4.027894	-1.261341	0.000000
H	1.722487	-2.157314	0.000000
H	2.491482	2.758845	0.000000
H	4.408234	1.204876	0.000000
C	3.394095	0.813016	0.000000
C	2.325479	1.682220	0.000000
C	0.999346	1.192250	0.000000
C	1.896930	-1.082818	0.000000
C	0.766516	-0.218852	0.000000
C	-0.549172	-0.730970	0.000000
B	-1.436574	1.620130	0.000000
C	-1.664448	0.102787	0.000000
N	-0.068208	2.045239	0.000000



C	-5.029412	2.749263	0.000000
C	-6.295052	2.224577	0.000000
C	-3.883282	1.894890	0.000000
C	-4.093192	0.463835	0.000000
C	-5.430161	-0.038624	0.000000
C	-6.502256	0.813852	0.000000
C	-2.586024	2.403102	0.000000
C	-1.461196	1.552067	0.000000
C	-1.670097	0.114019	0.000000
C	-2.988749	-0.384068	0.000000
C	-0.150441	2.043990	0.000000
C	0.951848	1.174033	0.000000
C	0.762444	-0.267759	0.000000
C	-0.561741	-0.742569	0.000000
N	3.315161	0.860736	0.000000
C	1.878422	-1.133504	0.000000
H	-7.515174	0.418978	0.000000
H	-7.155360	2.889857	0.000000
H	-4.877509	3.827401	0.000000
H	-5.581956	-1.117159	0.000000
H	-2.434347	3.483242	0.000000
H	-3.144860	-1.463883	0.000000
H	0.015518	3.122298	0.000000
H	-0.729229	-1.820434	0.000000
H	4.298835	-1.183425	0.000000
H	1.658374	-2.201091	0.000000
H	2.442786	2.759756	0.000000
H	4.221665	1.324715	0.000000
C	2.257881	1.687348	0.000000
B	3.260136	-0.593354	0.000000



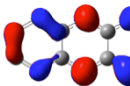
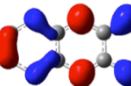
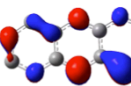
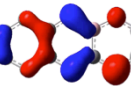
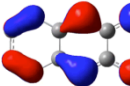
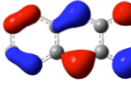
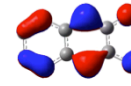
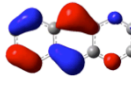
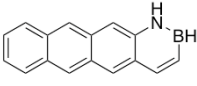
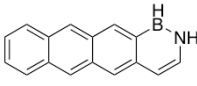
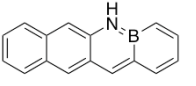
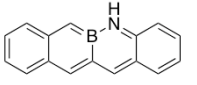
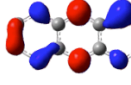
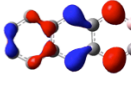
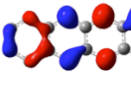
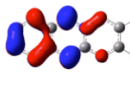
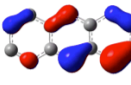
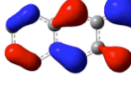
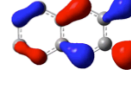
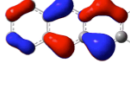
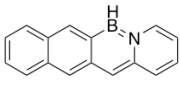
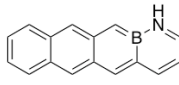
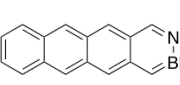
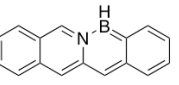
C	-4.988625	2.776787	0.000000
C	-6.271561	2.295098	0.000000
C	-3.873732	1.883249	0.000000
C	-4.128689	0.461303	0.000000
C	-5.481474	0.004338	0.000000
C	-6.524704	0.892577	0.000000
C	-2.559011	2.344862	0.000000
C	-1.469193	1.450300	0.000000
C	-1.712296	0.017840	0.000000
C	-3.052364	-0.423793	0.000000
C	-0.618744	-0.863196	0.000000
C	3.284475	-0.487770	0.000000
C	2.078196	-1.143906	0.000000
H	-7.550192	0.531255	0.000000
H	-7.109223	2.988727	0.000000
H	-4.800223	3.849303	0.000000
H	-5.669432	-1.068505	0.000000
H	-2.370065	3.419340	0.000000
H	-3.246869	-1.497264	0.000000
H	0.027181	3.019520	0.000000
H	-0.846352	-1.930417	0.000000
H	4.232344	-1.024156	0.000000
H	2.083092	-2.233451	0.000000
H	2.219906	2.786455	0.000000
H	4.271688	1.457932	0.000000
C	3.318690	0.935404	0.000000
N	0.923296	1.127844	0.000000
C	2.186382	1.699720	0.000000
C	-0.162625	1.946737	0.000000
B	0.783157	-0.354043	0.000000

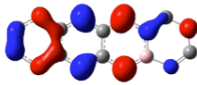
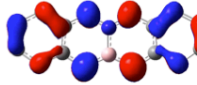
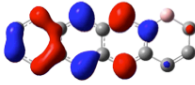
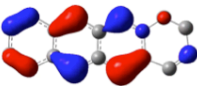
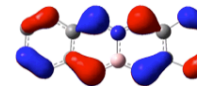
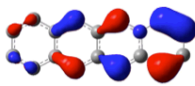
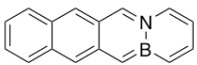
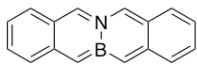
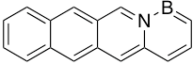


C	-5.164851	2.716257	0.000000
C	-6.389595	2.101026	0.000000
C	-3.950573	1.960877	0.000000
C	-4.051235	0.519332	0.000000
C	-5.343414	-0.090225	0.000000
C	-6.477020	0.679695	0.000000
C	-2.685577	2.552136	0.000000
C	-2.915772	-0.283420	0.000000
C	3.107711	-0.676834	0.000000
H	-7.454008	0.202334	0.000000
H	-7.300090	2.695342	0.000000
H	-5.094271	3.802925	0.000000
H	-5.414859	-1.176872	0.000000
H	-2.645734	3.642748	0.000000
H	-2.997982	-1.369560	0.000000
H	0.249151	3.233034	0.000000
H	-0.803360	-1.680165	0.000000
H	3.913859	-1.406562	0.000000
H	1.572066	-2.165733	0.000000
H	2.645971	2.707447	0.000000
H	4.457800	1.031245	0.000000
C	3.418142	0.712934	0.000000
C	2.412227	1.643872	0.000000
C	-0.015218	2.174200	0.000000
C	1.036020	1.255124	0.000000
C	1.804973	-1.101937	0.000000
C	0.732698	-0.157739	0.000000
N	-1.651396	0.236421	0.000000
C	-0.580935	-0.613869	0.000000
B	-1.441699	1.718059	0.000000

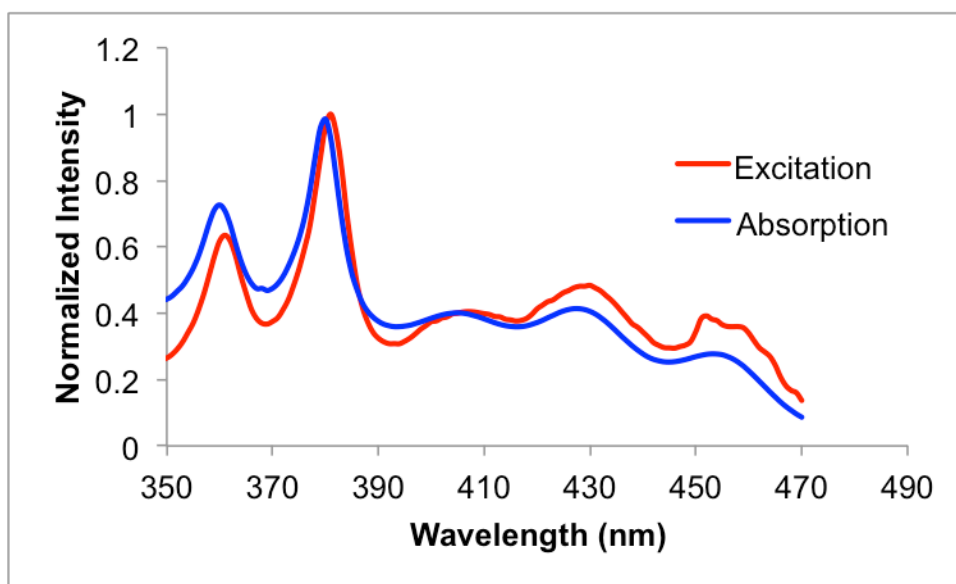
BN Tetracene Frontier Orbital Energies

Orbital energies calculated at the CAM-B3LYP/6-311G(d,p) level. ΔH_f values calculated at the G3MP2 level.

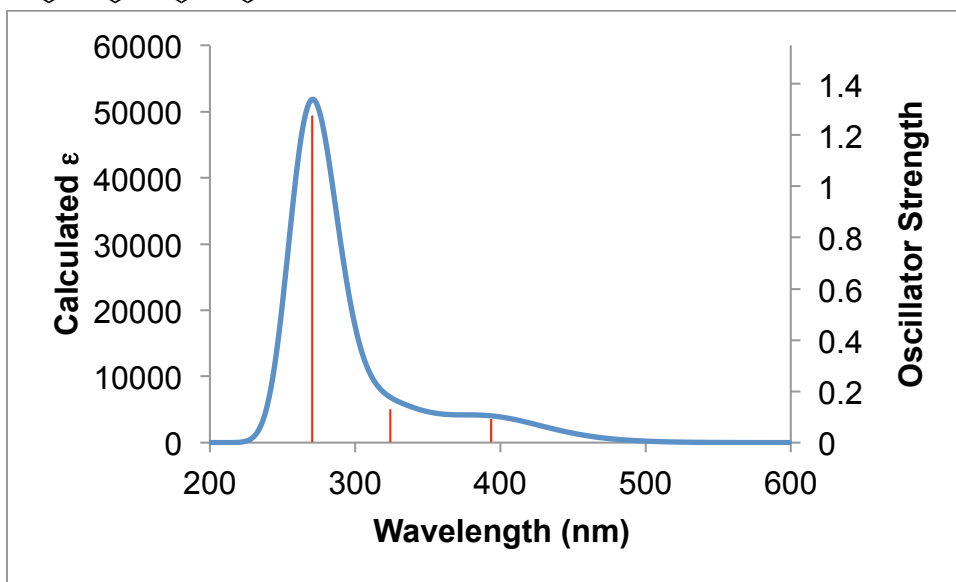
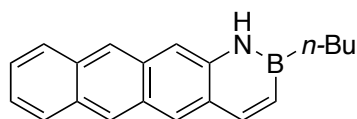
LUMO (eV)	 -1.15	 -1.00	 -1.26	 -1.50
HOMO (eV)	 -6.52	 -6.39	 -6.78	 -6.35
ΔH_f (kcal/mol)	 46.1	 46.4	 48.2	 53.6
LUMO (eV)	 -0.78	 -1.52	 -1.58	 -1.12
HOMO (eV)	 -6.14	 -5.81	 -5.88	 -5.92
ΔH_f (kcal/mol)	 58.7	 61.9	 64.1	 64.7

LUMO (eV)	 -1.15	 -1.15	 -1.67
HOMO (eV)	 -6.15	 -6.43	 -5.93
ΔH_f (kcal/mol)	 66.6	 67.1	 72.2

Absorbance and Excitation



TD-DFT Results

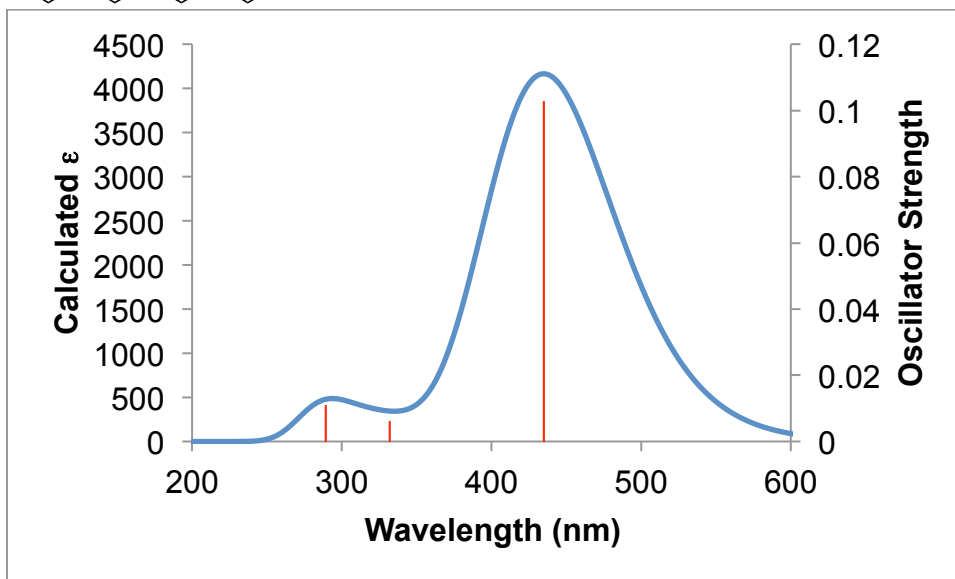
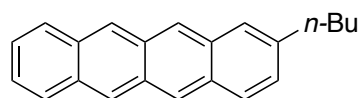


Excited state energies and oscillator strengths

Excited State 1: Singlet-A 3.15 eV 393.70 nm f=0.0923 $\langle S^2 \rangle$ =0.000
76 -> 77 0.69766

Excited State 2: Singlet-A 3.82 eV 324.39 nm f=0.1284 $\langle S^2 \rangle$ =0.000
75 -> 77 0.56121
76 -> 78 -0.35326
76 -> 79 -0.19223

Excited State 3: Singlet-A 4.58 eV 270.65 nm f=1.2766 $\langle S^2 \rangle$ =0.000
74 -> 77 0.27434
75 -> 77 0.28287
76 -> 78 0.54257
76 -> 79 -0.18576

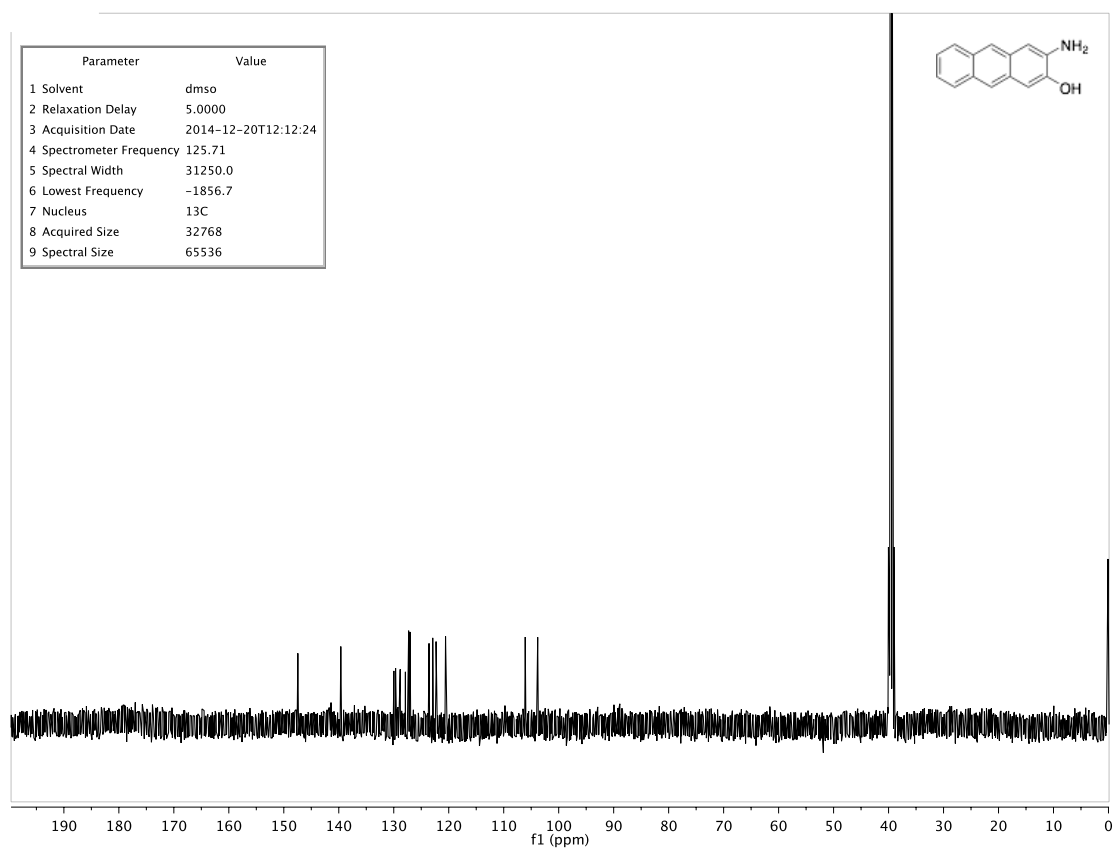
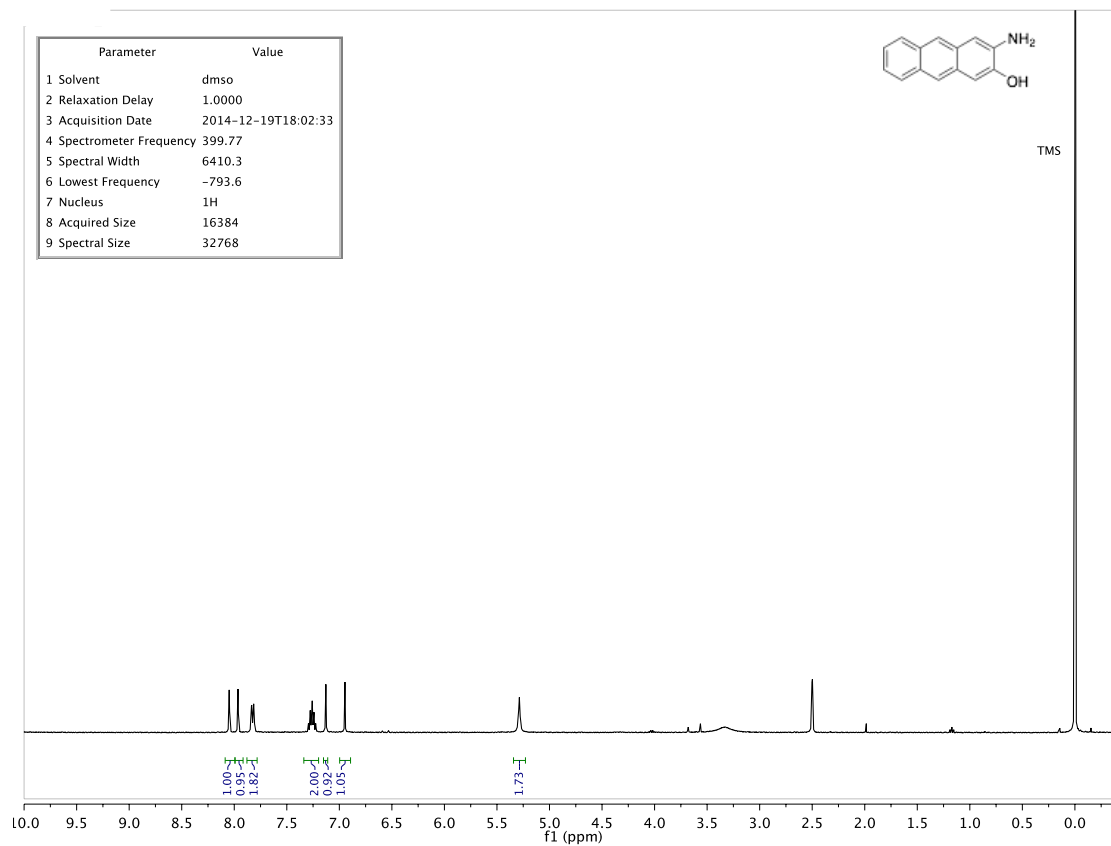


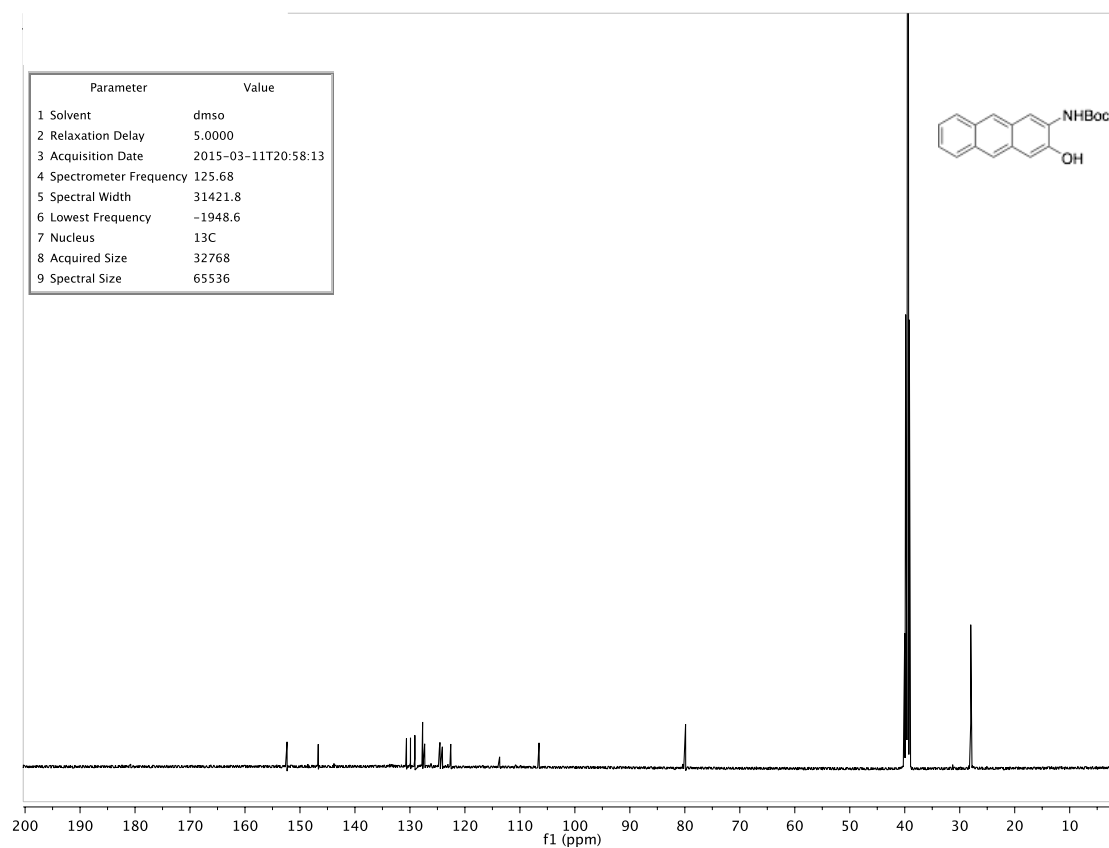
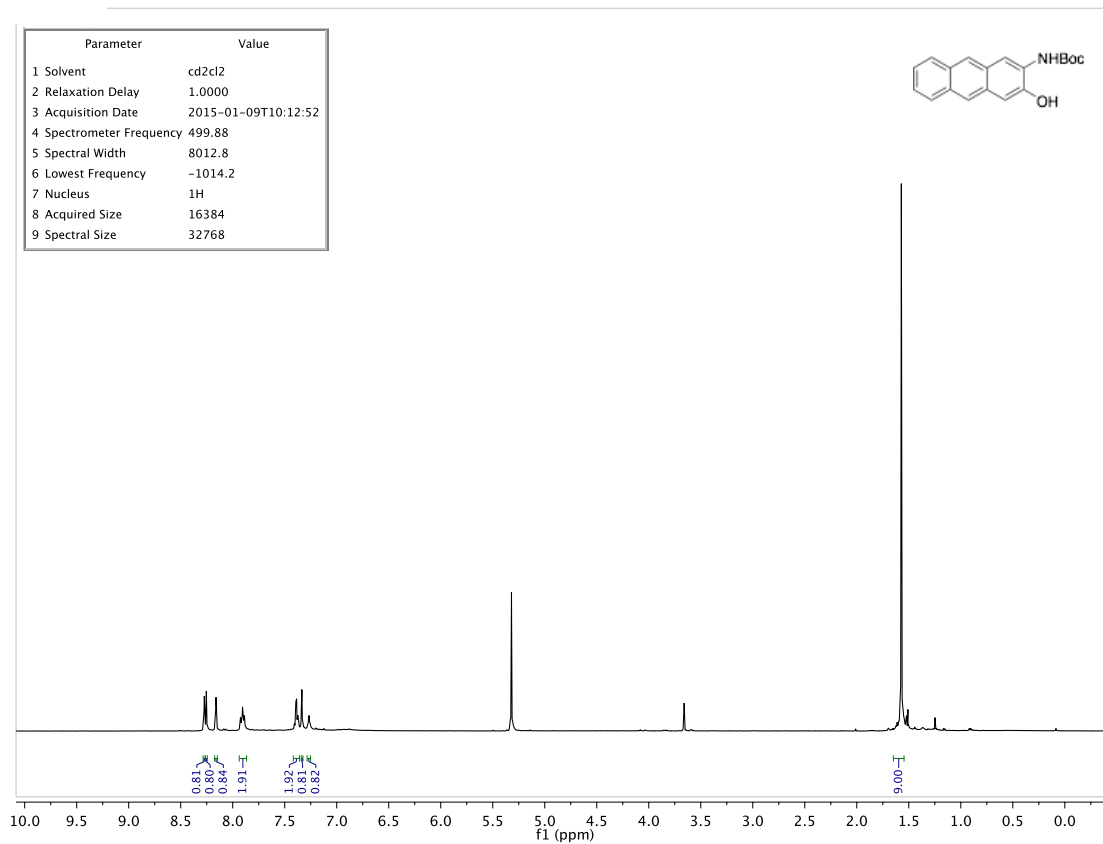
Excited state energies and oscillator strengths:

Excited State 1: Singlet-A 2.85 eV 434.98 nm $f=0.1028$ $\langle S^2 \rangle=0.000$
 76 -> 77 0.70302

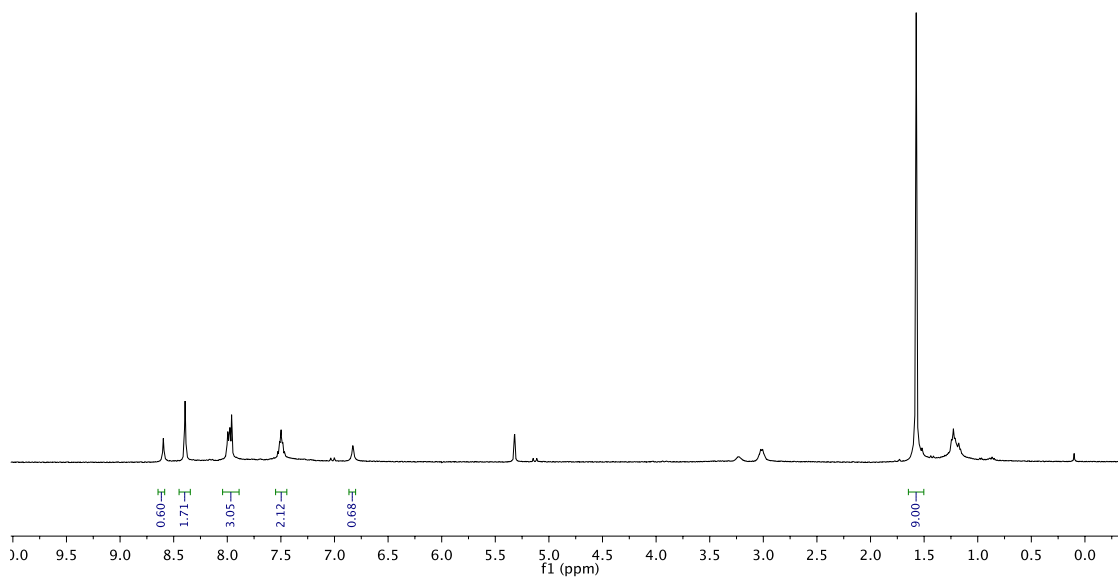
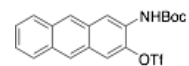
Excited State 2: Singlet-A 3.73 eV 332.01 nm $f=0.0061$ $\langle S^2 \rangle=0.000$
 74 -> 77 0.16924
 75 -> 77 0.48178
 76 -> 78 -0.46763

Excited State 3: Singlet-A 4.29 eV 289.32 nm $f=0.0109$ $\langle S^2 \rangle=0.000$
 74 -> 77 0.55118
 75 -> 77 -0.22940
 76 -> 79 0.36985

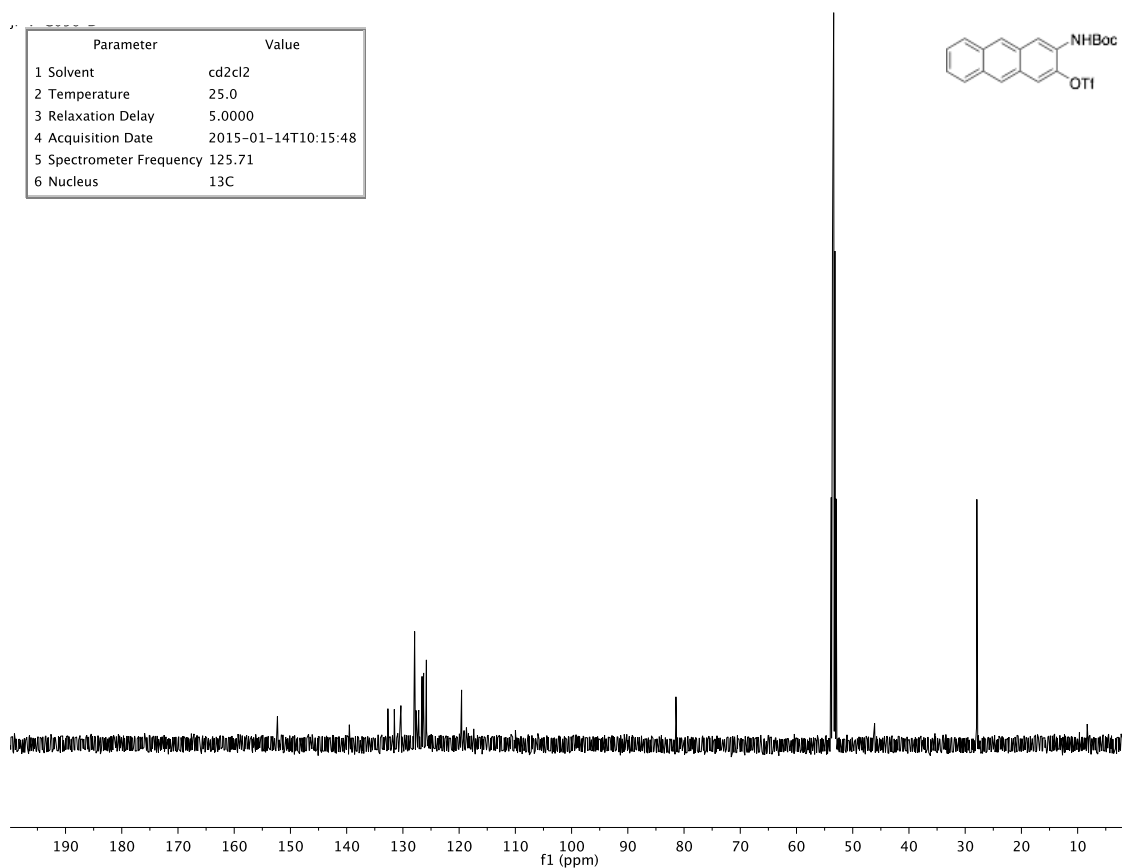
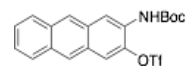


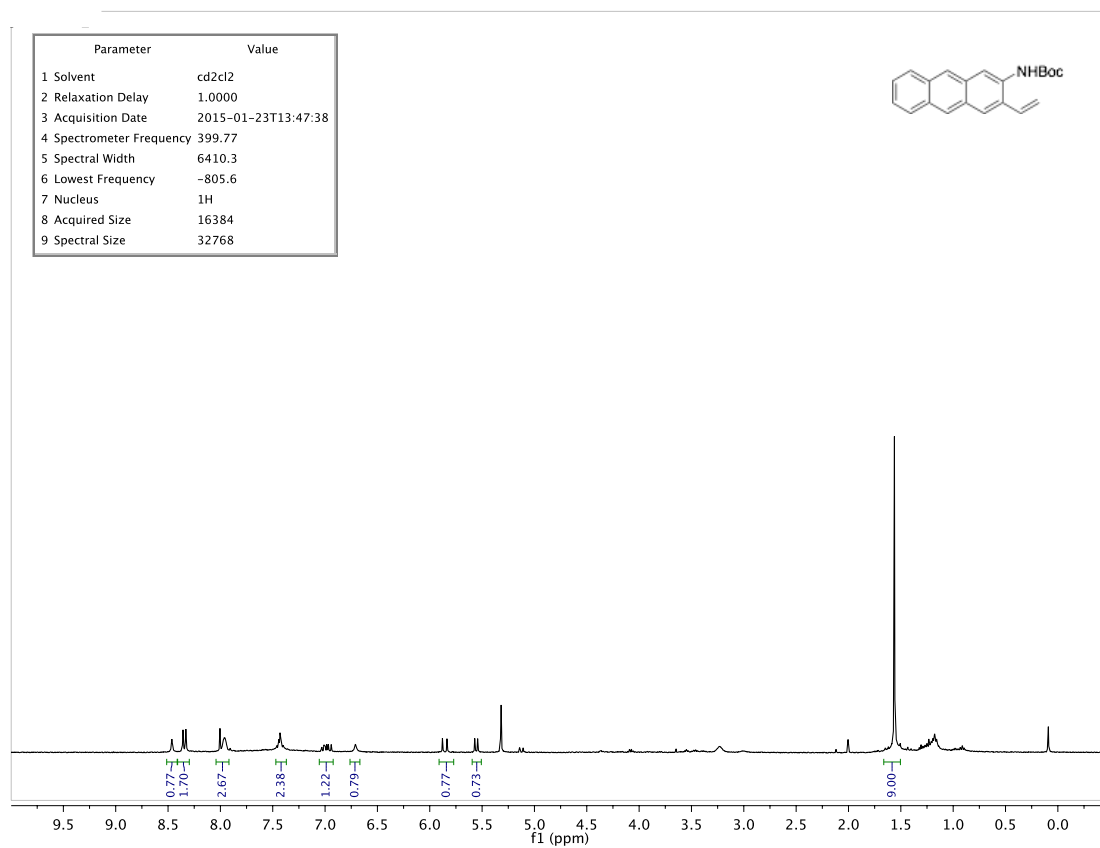
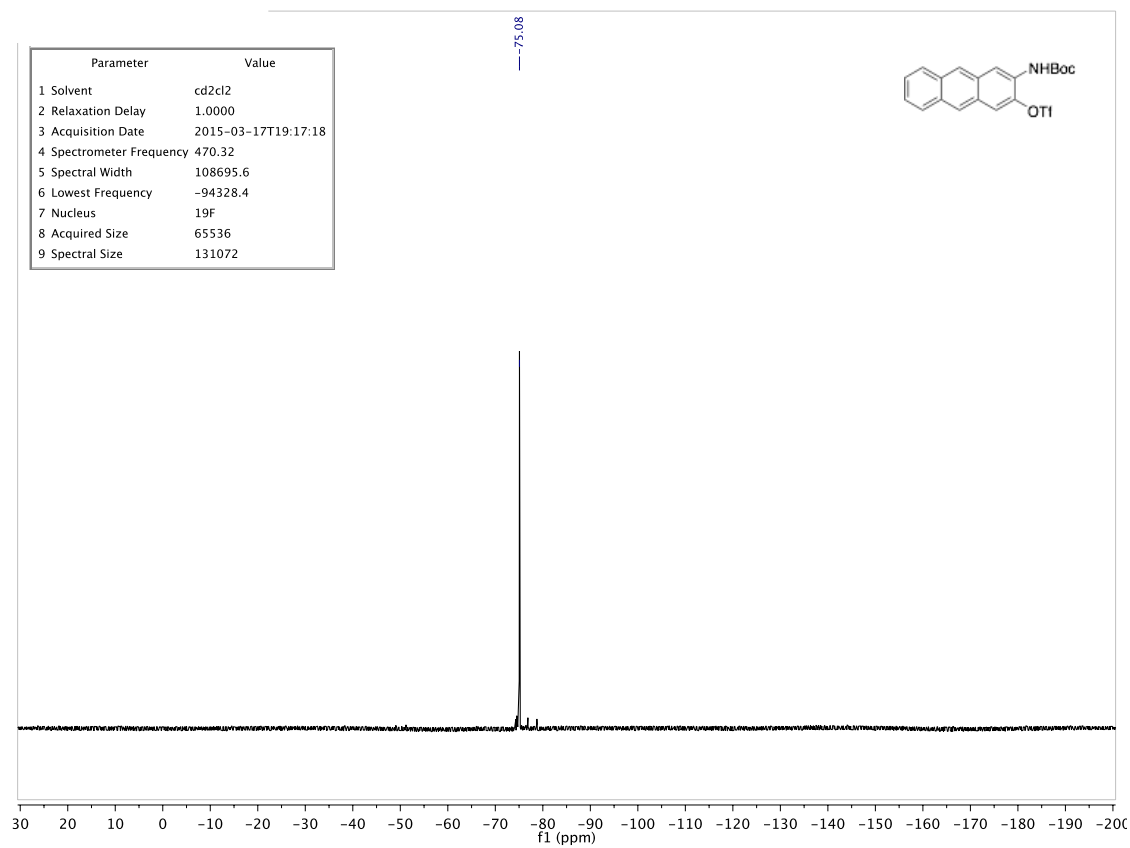


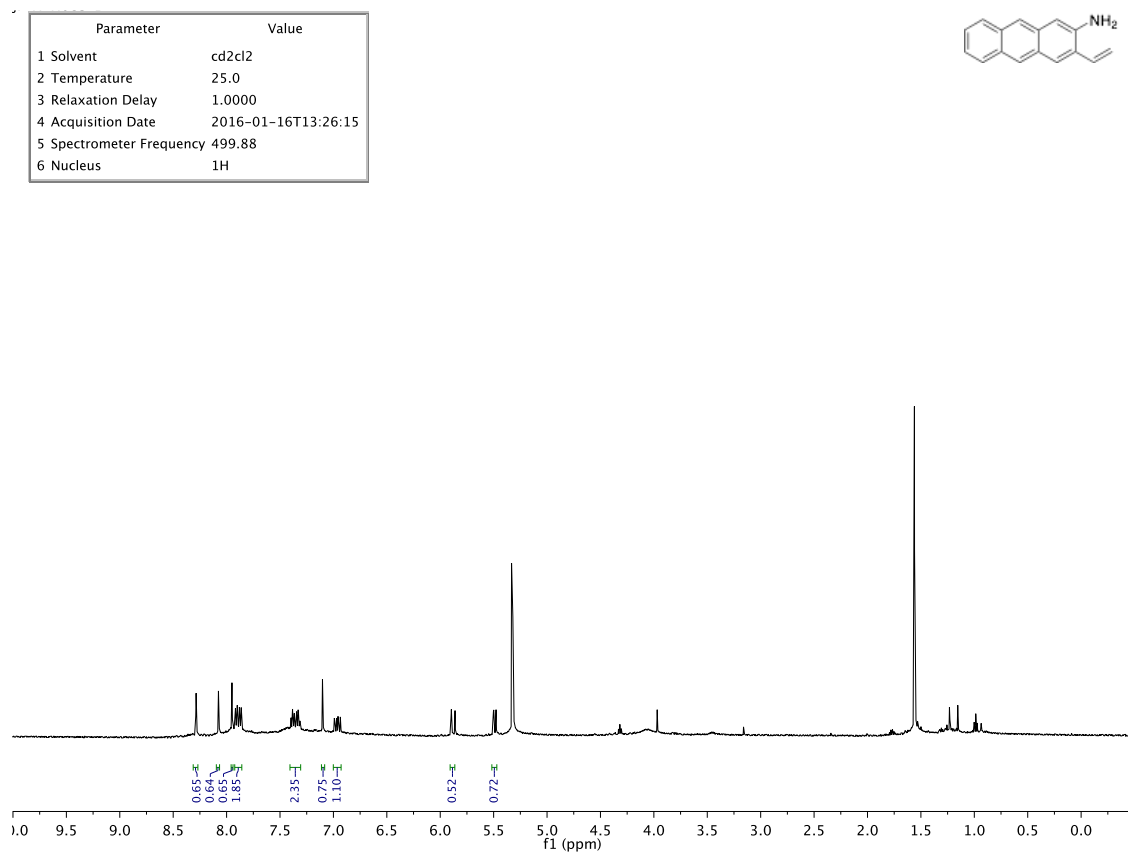
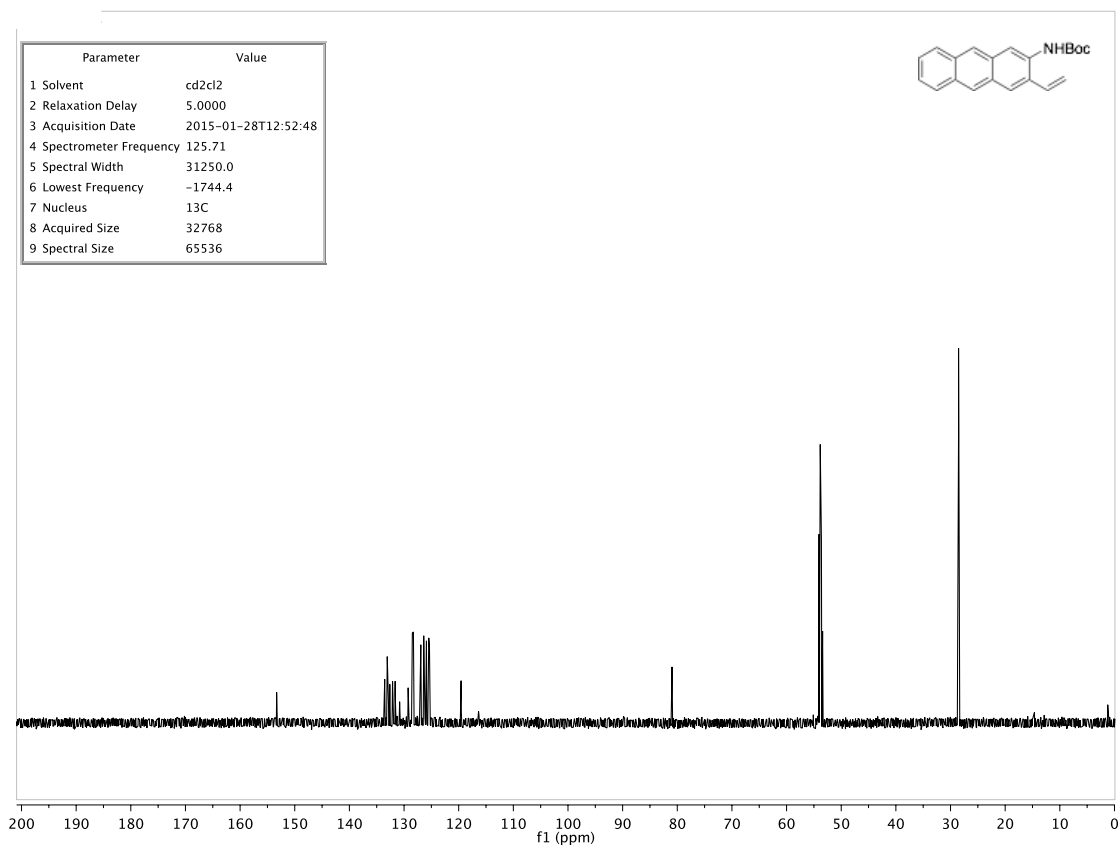
Parameter	Value
1 Solvent	cd2cl2
2 Temperature	25.0
3 Relaxation Delay	1.0000
4 Acquisition Date	2015-01-14T10:08:57
5 Spectrometer Frequency	399.77
6 Nucleus	¹ H

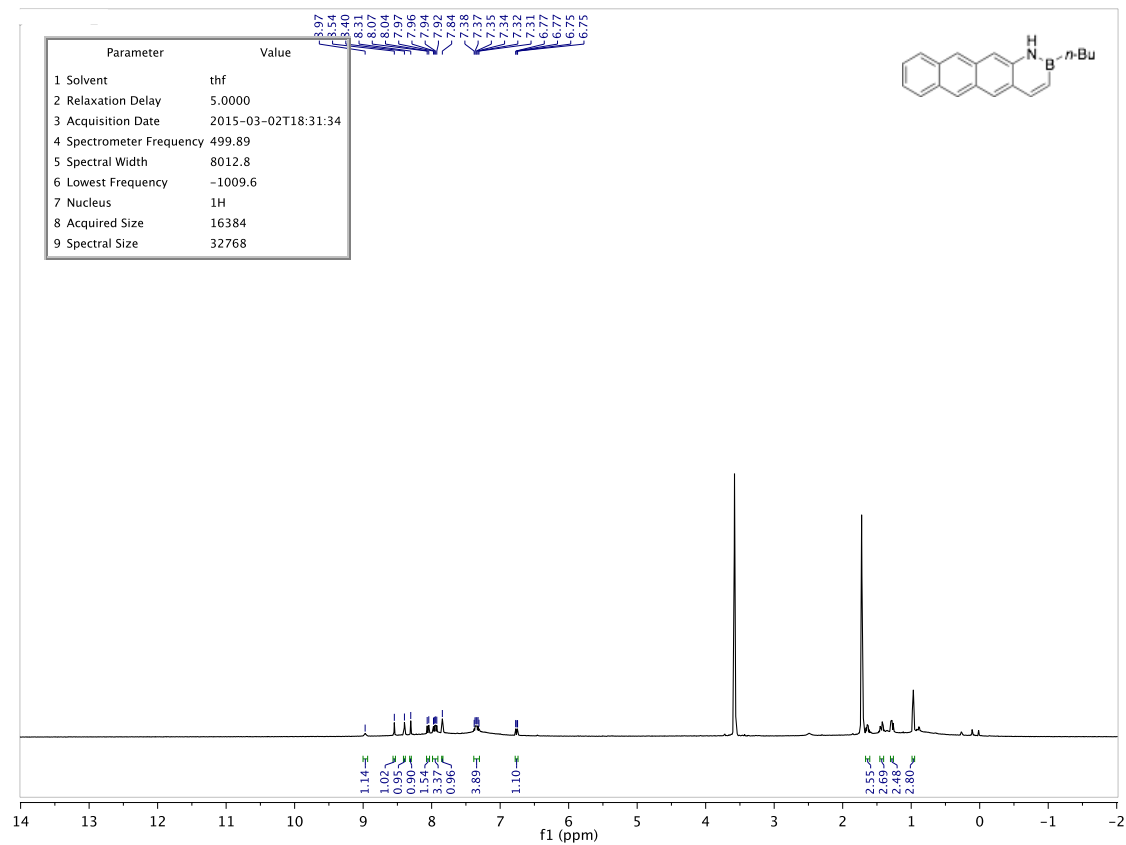
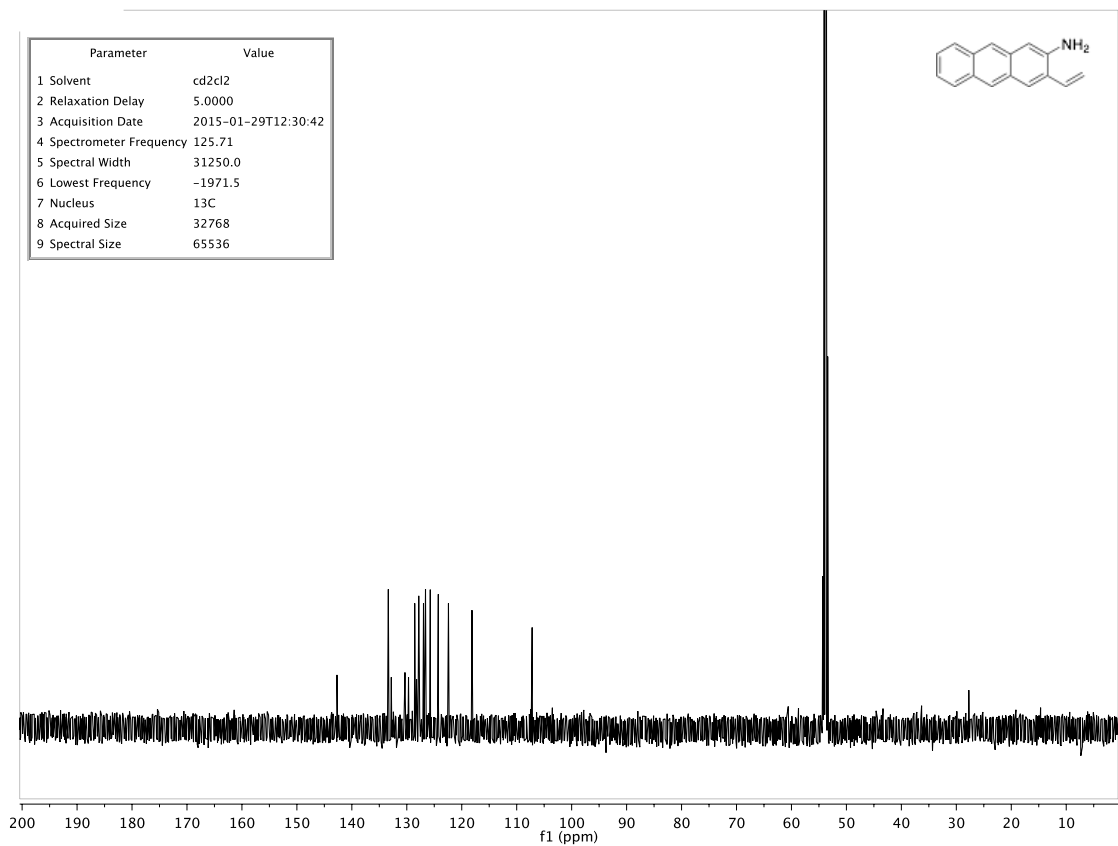


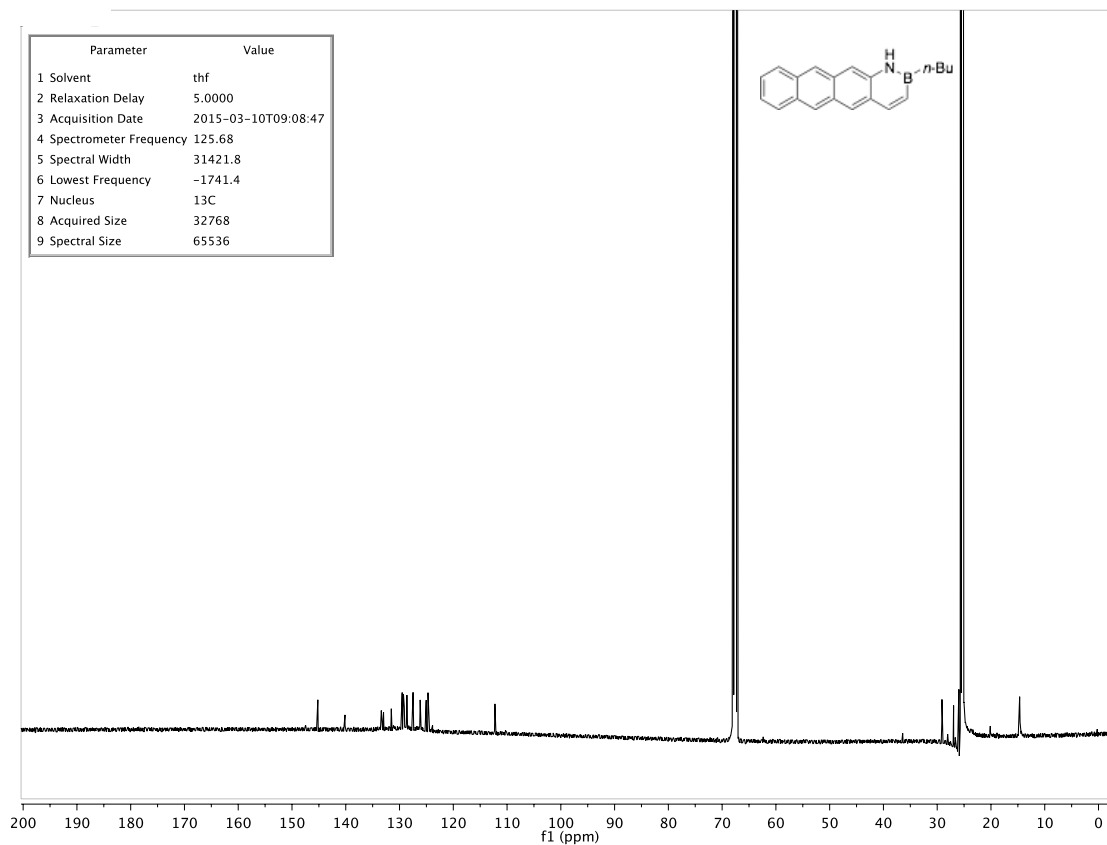
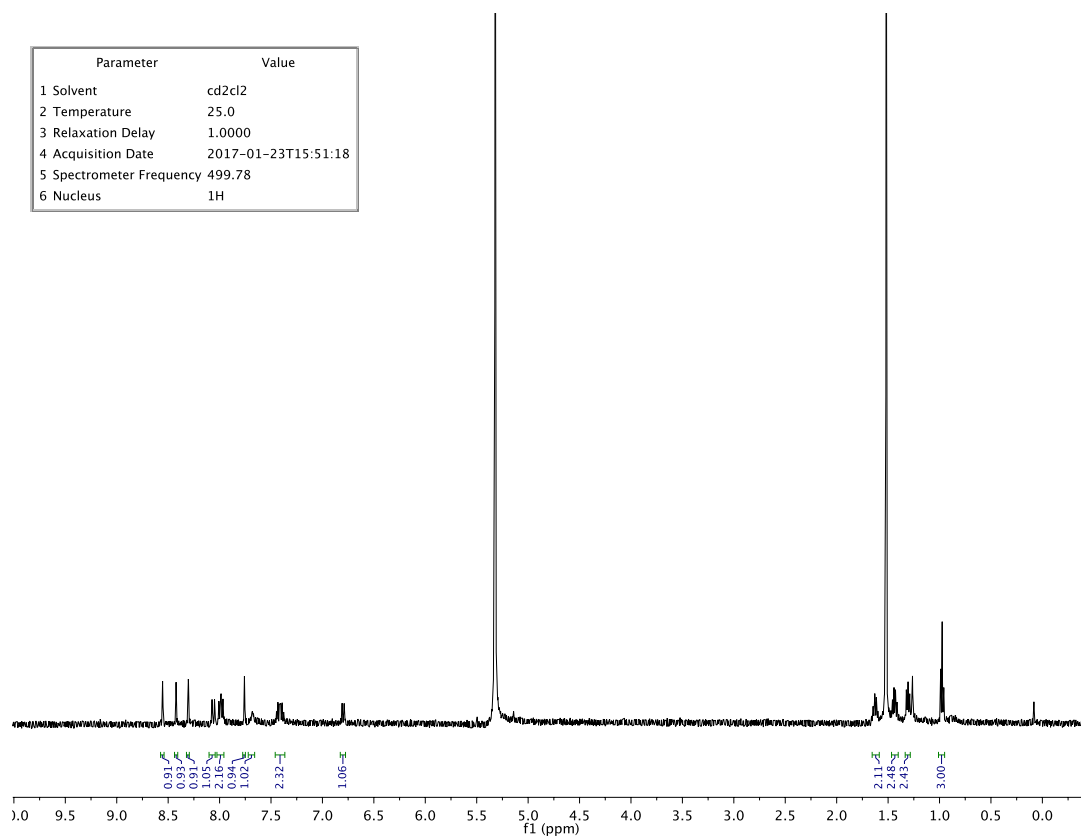
Parameter	Value
1 Solvent	cd2cl2
2 Temperature	25.0
3 Relaxation Delay	5.0000
4 Acquisition Date	2015-01-14T10:15:48
5 Spectrometer Frequency	125.71
6 Nucleus	¹³ C

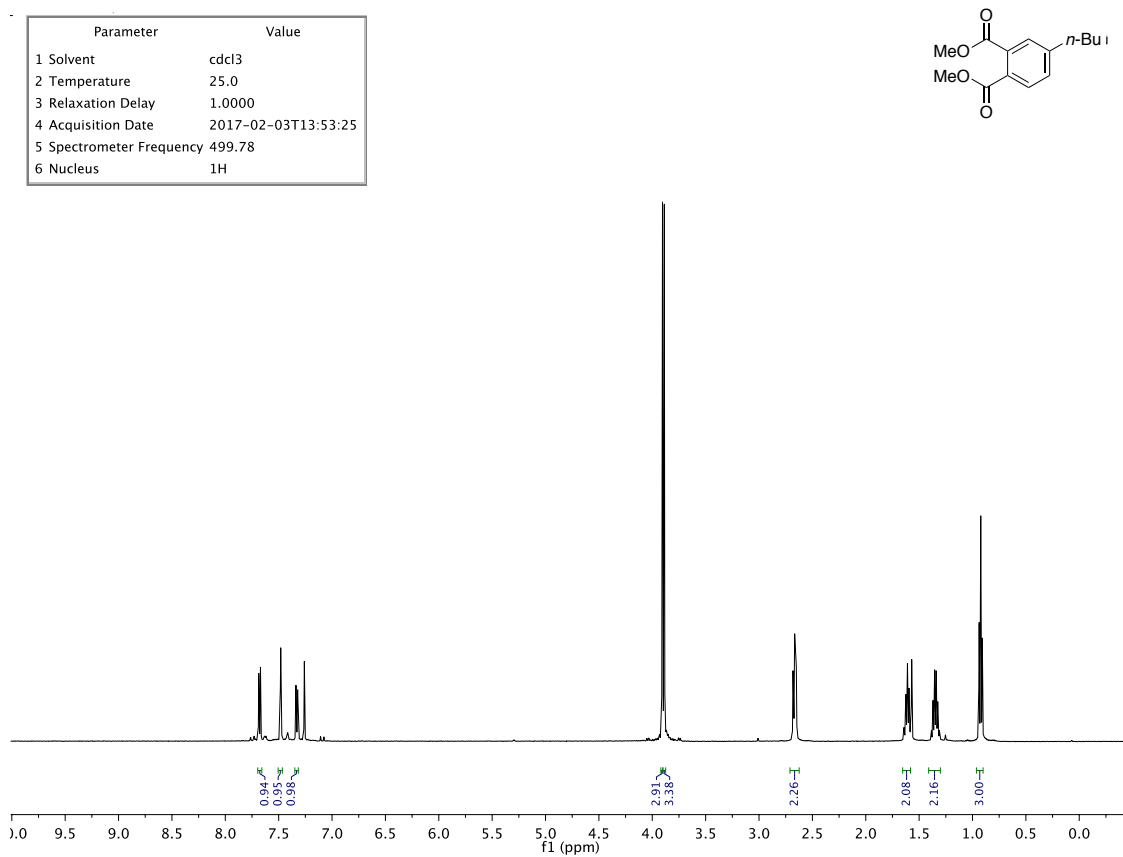
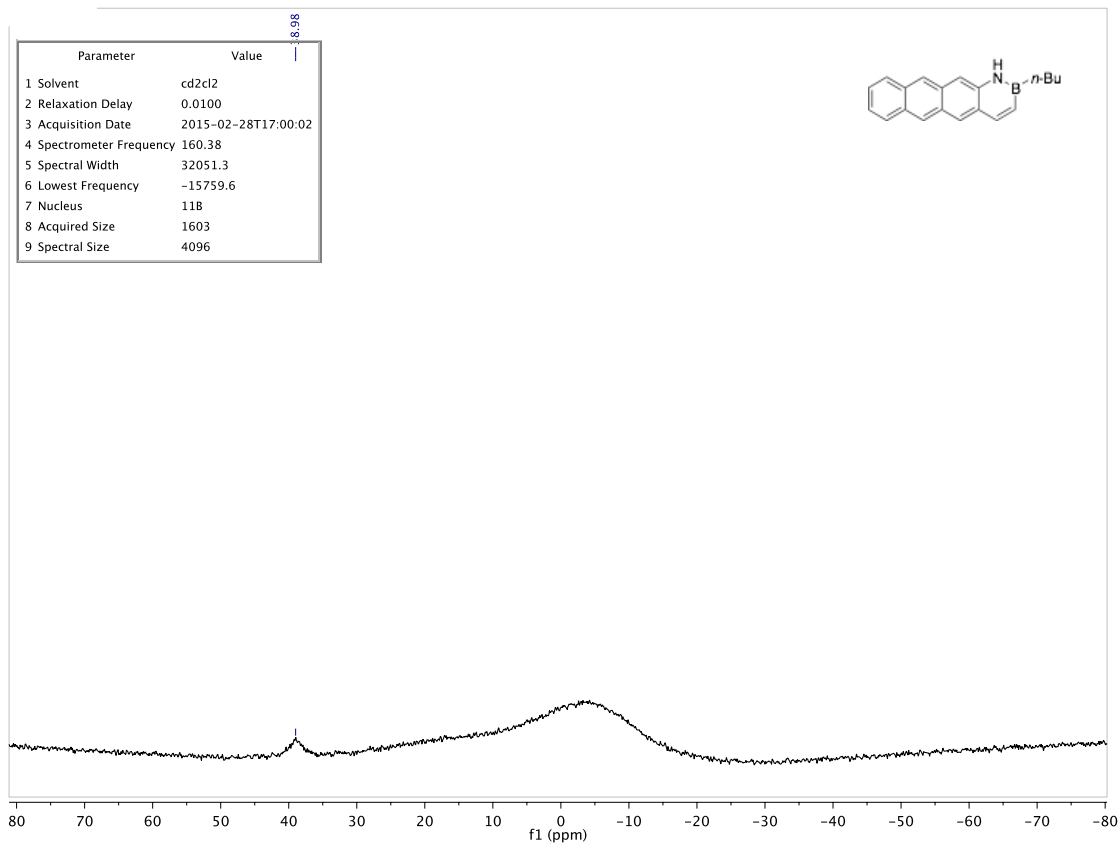




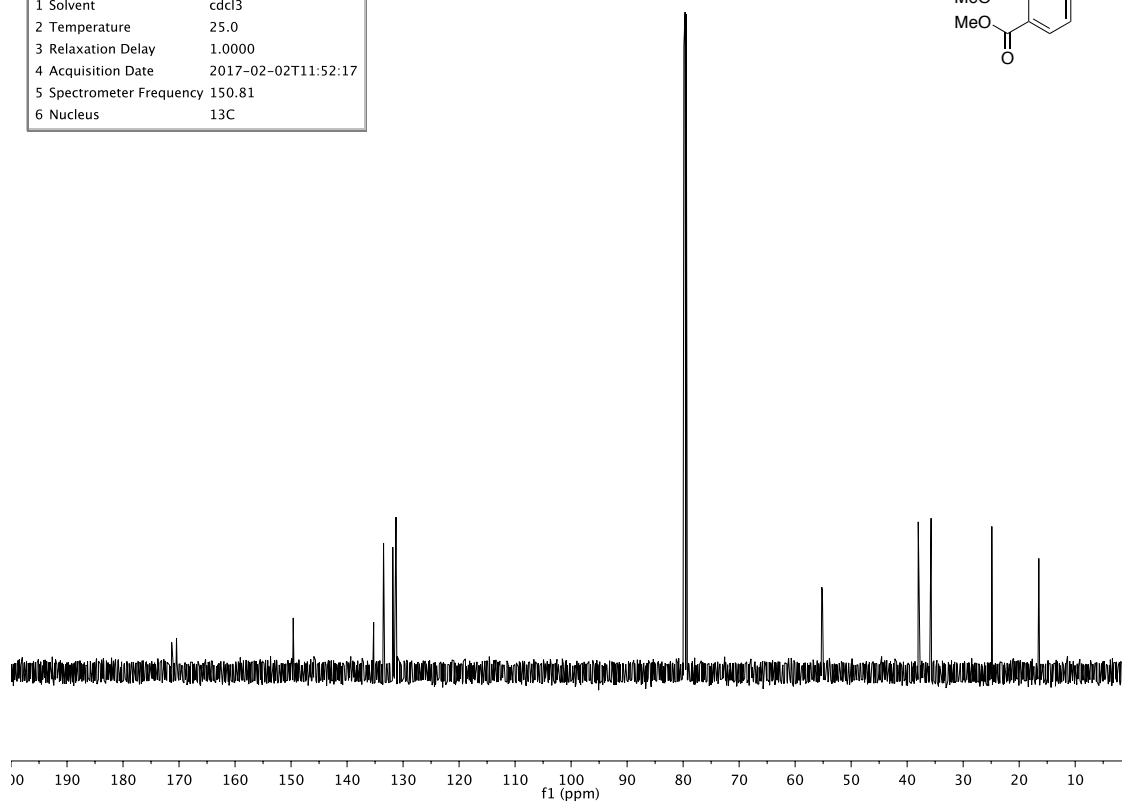
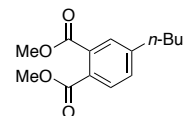




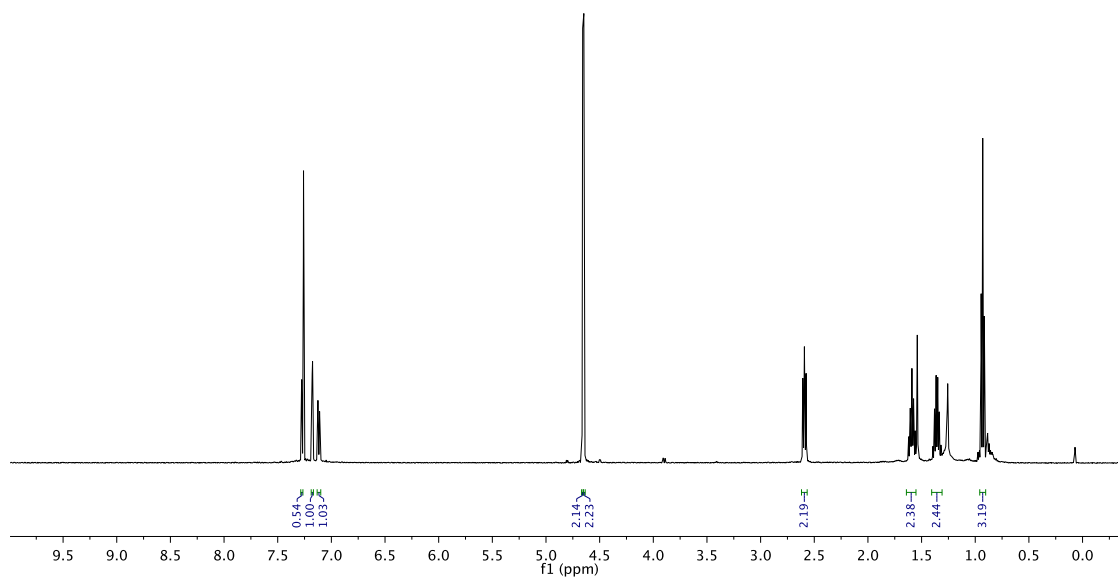
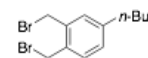


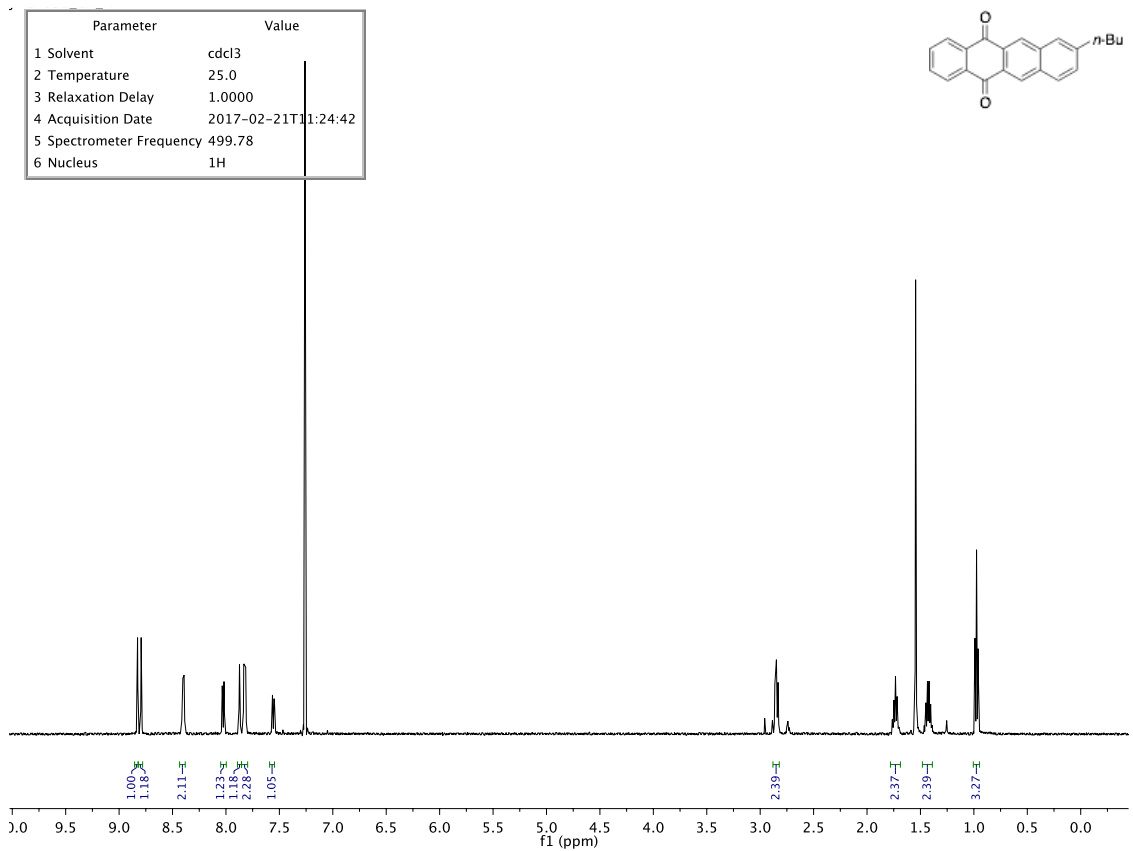
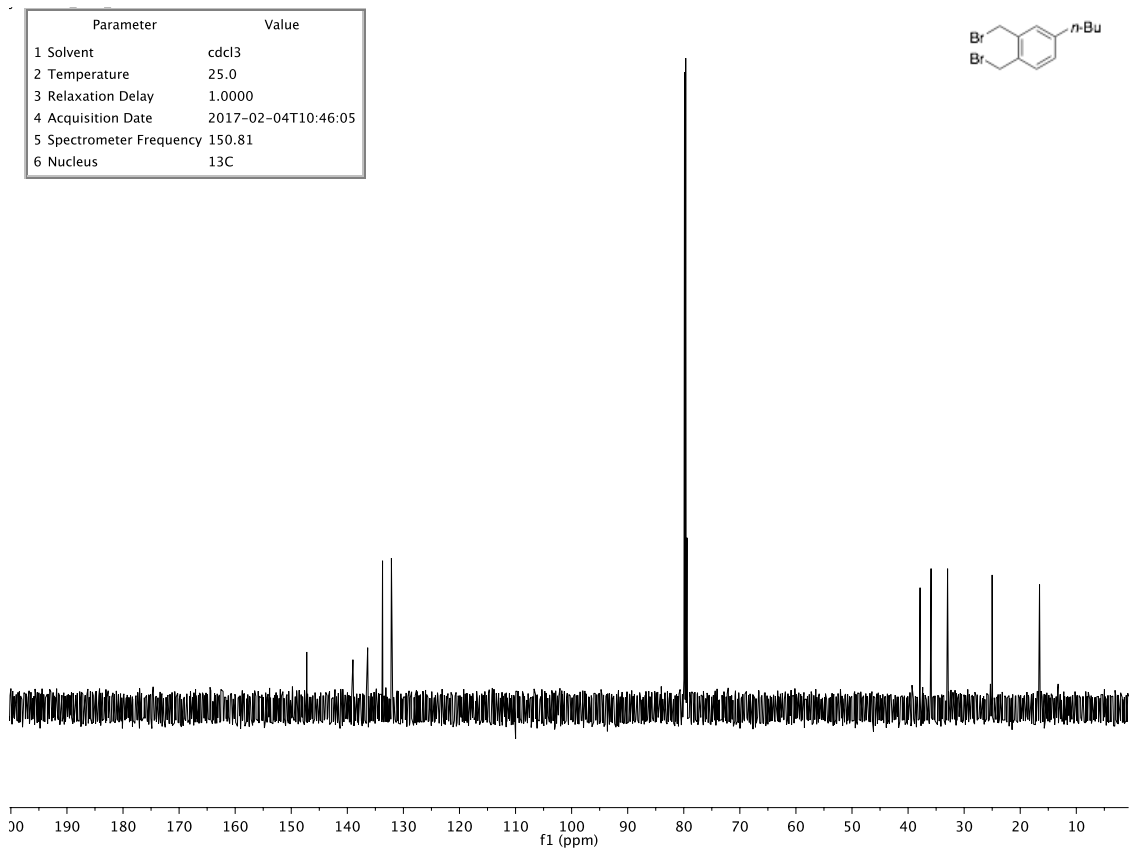


Parameter	Value
1 Solvent	cdcl3
2 Temperature	25.0
3 Relaxation Delay	1.0000
4 Acquisition Date	2017-02-02T11:52:17
5 Spectrometer Frequency	150.81
6 Nucleus	¹³ C

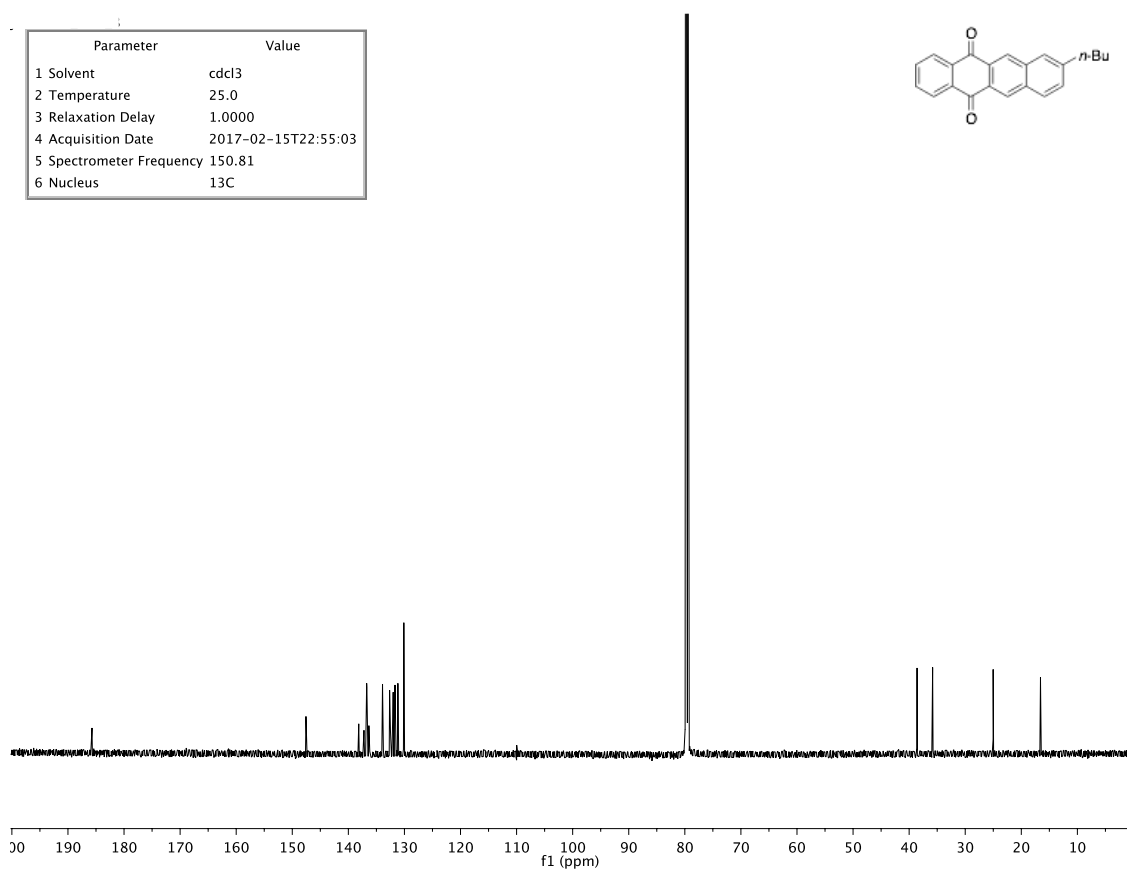
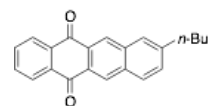


Parameter	Value
1 Solvent	cdcl3
2 Temperature	25.0
3 Relaxation Delay	1.0000
4 Acquisition Date	2017-02-03T18:57:25
5 Spectrometer Frequency	499.78
6 Nucleus	¹ H

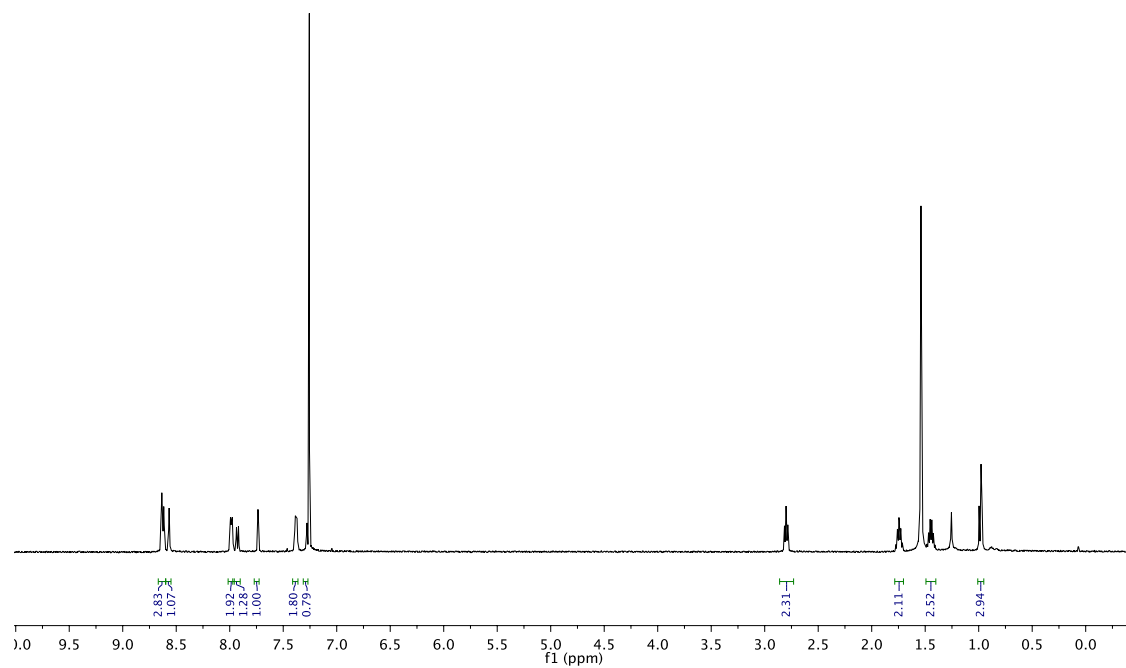
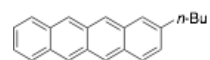


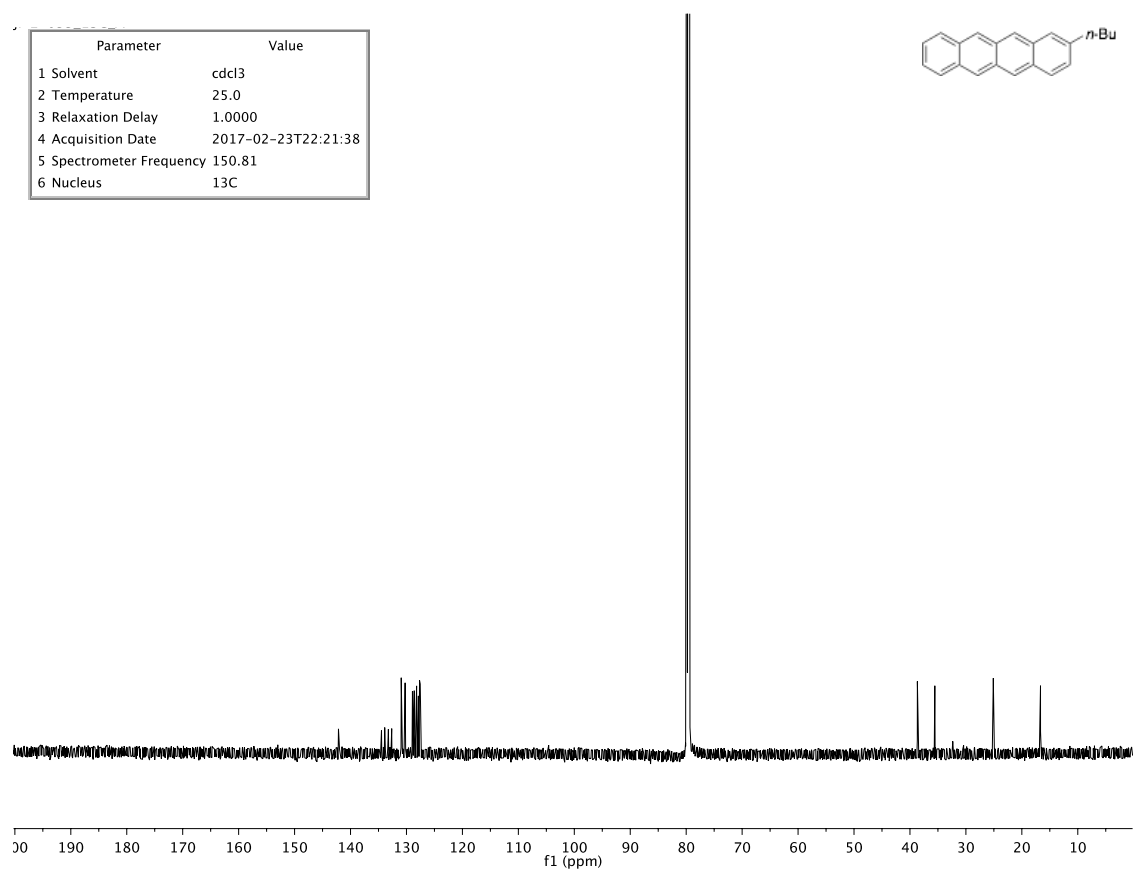


Parameter	Value
1 Solvent	cdcl3
2 Temperature	25.0
3 Relaxation Delay	1.0000
4 Acquisition Date	2017-02-15T22:55:03
5 Spectrometer Frequency	150.81
6 Nucleus	¹³ C



Parameter	Value
1 Solvent	cdcl3
2 Temperature	25.0
3 Relaxation Delay	1.0000
4 Acquisition Date	2017-02-21T16:29:45
5 Spectrometer Frequency	499.88
6 Nucleus	¹ H





1.5 Predictive Trends for the Optoelectronic Properties of BN Acenes

We have so far only explored BN/CC isosterism in acenes with one of the possible arrangements of the BN unit within the topologies of the acenes. These BN-1,2-acenes have lowered frontier orbital energies with respect to their all-carbon analogues. In theory, each isomer should have unique orbital energetics. In aromatic chemistry, a classic case of isomerism changing electronic structure is that of colorless naphthalene versus the aptly named azulene.⁹⁹

It might be possible to discern energetic trends with respect to position and orientation of the BN unit within the acene topology. We decided to study the BN naphthalene series (Figure 1.17) to begin to elucidate trends to inform further targeted synthesis of BN acenes since naphthalene represents the simplest polycyclic aromatic hydrocarbon.

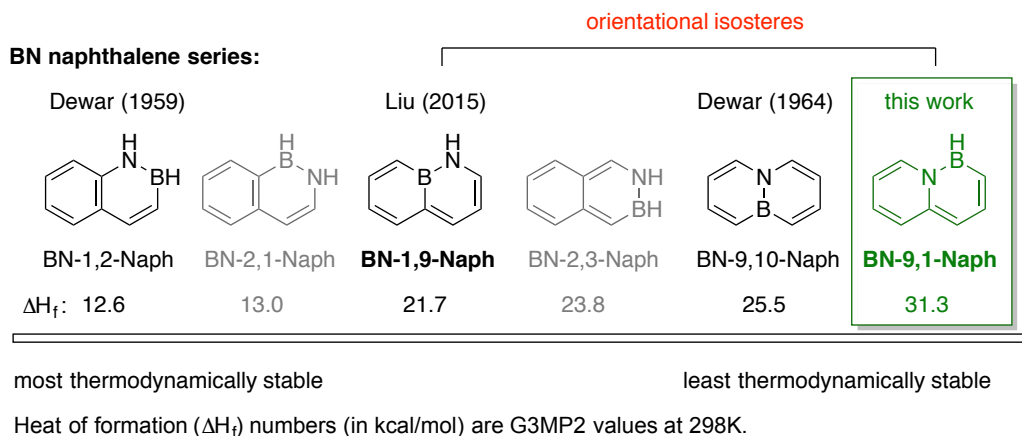


Figure 1.17. The six possible isomers of BN naphthalene and their calculated ΔH_f values

1.5.1 Introduction: Isomerism of BN Isosteres of PAHs

There have been only a few studies of isomerism of BN polyaromatic compounds, and none of the previous studies concern acene topologies. Isomerism within the

⁹⁹ (a) Mann, D. E.; Platt, J. R.; Kleven, H. B. *J. Chem. Phys.* **1949**, *17*, 481–484. (b) Michl, J.; Thulstrup, E. W. *Tetrahedron* **1976**, *32*, 205–209.

framework of BN/CC isosterism has been investigated by Dewar, who synthesized two isomers of BN benz[a]anthracene and found that the UV-vis absorption spectrum for each isomer of BN benz[a]anthracene resembled that of the all-carbon analogue, albeit hypsochromically shifted.^{48b} Wang and Lu computationally evaluated isomers of BN pyrene (Figure 1.18) and concluded that location of the BN unit does indeed affect properties.^{63a} They did not, however, comment on underlying causes or apparent trends.

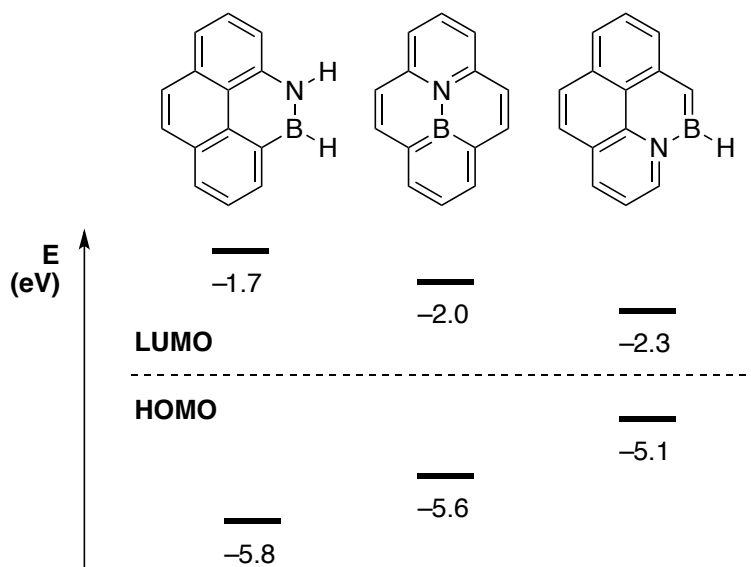


Figure 1.18. Wang and Lu’s computational results regarding BN pyrene isomers

Piers compared the properties of all-carbon phenanthrene to Dewar’s “original” BN phenanthrene **1.26** and a newly synthesized BN phenanthrene **1.27** (Table 1.6).^{61c} Varying the *location* of the B–N bond resulted in a large bathochromic shift in both the absorption and emission spectra. In this case, Piers could not investigate the effect caused by the polarization of the B–N bond since inversion of the B–N bond in both **1.26** and **1.27** produces the same compound.

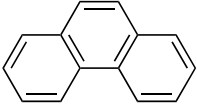
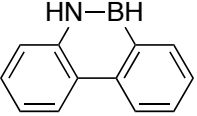
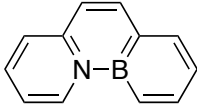
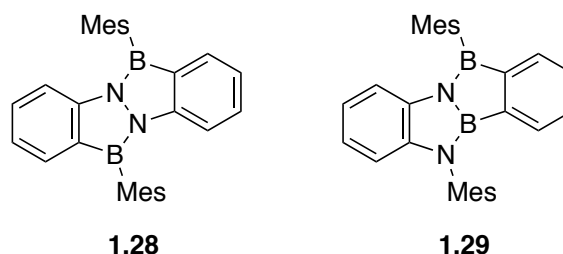
			
	Phenanthrene	1.26	1.27
λ_{abs}	293 nm	326 nm	446 nm
λ_{em}	347 nm	327 nm	450 nm
Φ_{F}	0.09	0.61	0.58

Table 1.6. Piers's analysis of BN phenanthrene isomers

Recently, Feng and Müllen addressed the question of B–N bond polarization in B_2N_2 dibenzopentalenes.¹⁰⁰ Nucleus independent chemical shift (NICS) values showed that while the inner, heterocyclic rings of **1.28** remain nonaromatic, the B–N–B ring of **1.28** is strongly antiaromatic (The N–B–N ring shows NICS values consistent with a non-aromatic compound.). Bond polarity thus modulates *antiaromaticity* in these cases.



Three isomers of BN naphthalene have already been synthesized, but a study of the optoelectronic properties as a function of BN bond location and orientation has not been executed. To provide an experimental foundation upon which to elucidate any trends regarding electronic structures of BN naphthalenes, we targeted the synthesis of the least stable isomer of BN naphthalene (Figure 1.16, *vide supra*). Importantly, the issue of BN unit *orientation* can be addressed with the synthesis of this least stable isomer, **BN-9,1-Naph**, since the BN unit occupies the same space within the naphthalene

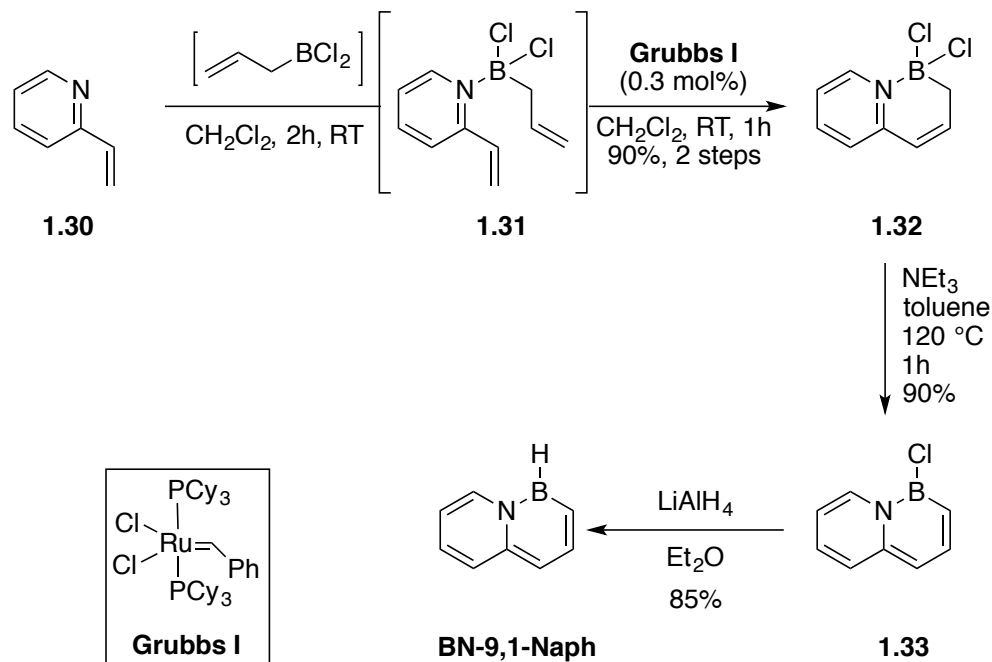
¹⁰⁰ Wang, X.-Y.; Narita, A.; Feng, X.; Müllen, K. *J. Am. Chem. Soc.* **2015**, *137*, 7668–7671.

topology as our previously synthesized **BN-1,9-Naph**¹⁰¹, but the orientation of the bond is inverted.

1.5.2 Synthesis of BN-9,1-Naph¹⁰²

The synthesis of **BN-9,1-Naph** begins with the commercially available 2-vinylpyridine, which is condensed with *in situ*-generated allylboron dichloride (Scheme 1.15) to give adduct **1.31**.¹⁰³ Crude **1.31** is treated with Grubbs' 1st generation metathesis catalyst to yield ring-closed **1.32**. Elimination of HCl using triethylamine as the base furnished the aromatic boron-chloride **1.33**, and this compound was reduced with lithium aluminum hydride to yield the parent **BN-9,1-Naph**.

Scheme 1.15. Synthesis of BN naphthalene parent BN-9,1-Naph



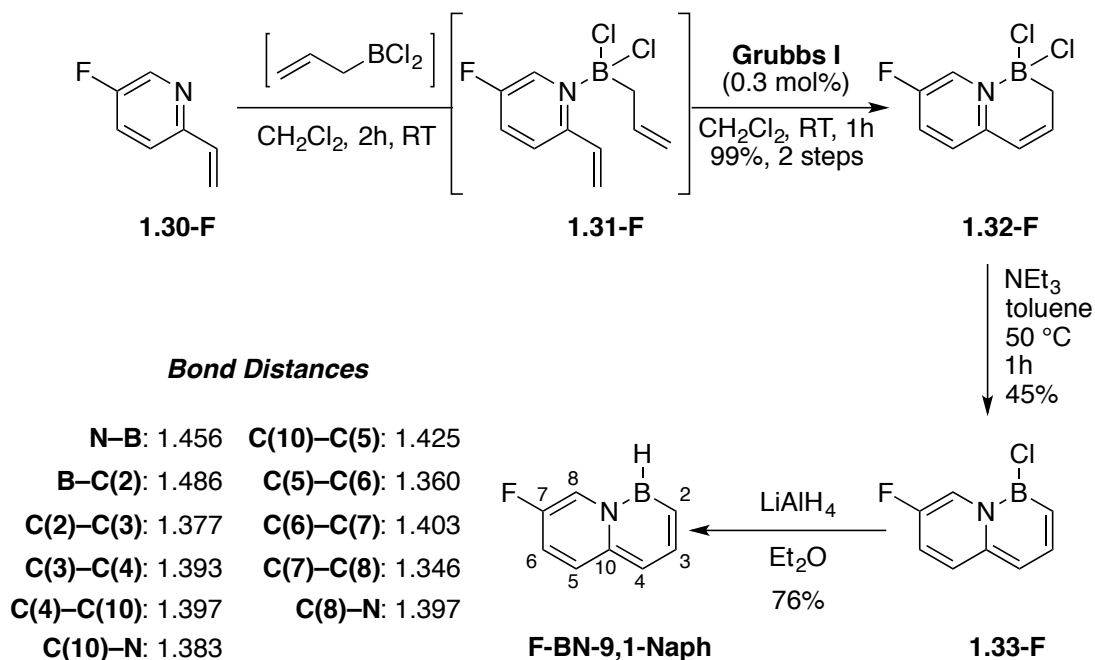
¹⁰¹ Brown, A. N.; Li, B.; Liu, S.-Y. *J. Am. Chem. Soc.* **2015**, *137*, 8932–8935.

¹⁰² Liu, Z.; Ishibashi, J. S. A.; Darrigan, C.; Dargelos, A.; Chrostowska, A.; Li, B.; Vasiliu, M.; Dixon, D. A.; Liu, S.-Y. *J. Am. Chem. Soc.* **2017**, *139*, 6082–6085.

¹⁰³ Bubnov, Y. N.; Kuznetsov, N. Y.; Pastukhov, F. V.; Kublitsky, V. V. *Eur. J. Org. Chem.* **2005**, 4633–4639.

Unfortunately, the parent **BN-9,1-Naph** is disordered in the solid state, and thus the crystal structure cannot reveal unambiguous structural information. A similar synthesis can be executed starting with fluorinated vinylpyridine **1.30-F** (Scheme 1.16), and the final product, **F-BN-9,1-Naph**, gives an unambiguous X-ray crystal structure (bond distances listed below).

Scheme 1.16. Synthesis of fluorinated derivative F-BN-9,1-Naph



1.5.3 Single-Crystal X-Ray Analysis of BN-9,1-Naphthalenes

X-ray quality crystals indeed reveal the unambiguous connectivity shown in Scheme 1.15. The azaboryl ring of **F-BN-9,1-Naph** features an unusually short (1.486 Å) C–B bond, a relatively long N–B distance (1.456 Å) that suggests aromatic delocalization, and relative bond homogenization with respect to known non-aromatic N–B systems.¹⁰⁴

¹⁰⁴ Abbey, E. R.; Zakharov, L. N.; Liu, S.-Y. *J. Am. Chem. Soc.* **2008**, *130*, 7250–7252.

Though the crystal structure of parent **BN-9,1-Naph** is disordered, its packing is readily identifiable; the molecule adopts a herringbone-like packing motif (Figure 1.19a) that features edge-to-face π -stacking. This packing motif is typical of all-carbon acenes, and is also displayed in crystal structures of **BN-1,2-Naph**¹⁰⁵ and **BN-9,10-Naph**.¹⁰⁶ In contrast, the fluorinated compound **F-BN-9,1-Naph** displays a more stratified packing motif featuring face-to-face π -stacking (Figure 1.19c) The stacking layers are 3.36 Å apart. In a single layer, the individual molecules arrange in an asymmetric, dimeric, and coplanar fashion through H-F interaction (Figure 1.19b).¹⁰⁷ The crystal packing of 2-fluoronaphthalene shows no such organization.¹⁰⁸ Therefore, the observed packing motif in this polymorph of **F-BN-9,1-Naph** is a result of BN/CC isosterism.

¹⁰⁵ Pan, J.; Kampf, J. W.; Ashe, A. J. III *Organometallics* **2009**, *28*, 506–511.

¹⁰⁶ Fang, X.; Yang, H.; Kampf, J. W.; Banaszak Holl, M. M.; Ashe, A. J., III *Organometallics* **2006**, *25*, 513–518.

¹⁰⁷ Anthony and Brammer have demonstrated H-F interactions can be energy-minimizing (nearly 6 kcal/mol) in the solid state and can contribute to coplanar organization in the crystals of extended π -systems. See: (a) Loader, J. R.; Libri, S.; Meijer, A. J. H. M.; Perutz, R. N.; Brammer, L. *CrystEngComm* **2014**, *16*, 9711–9720. (b) Hallani, R. K.; Thorley, K. J.; Mei, Y.; Parkin, S. R.; Jurchescu, O. D.; Anthony, J. E. *Adv. Funct. Mater.* **2016**, *26*, 2341–2348.

¹⁰⁸ Crystal structures of 2-halonaphthalenes are disordered, and this disorder may be caused by molecular rotation in the crystal lattice. See: (a) Chanh, N. B.; Haget-Bouillaud, Y. *Acta Crystallogr. B* **1972**, *28*, 3400–3404. (b) Aihara, A. *Chem. Lett.* **1987**, No. 6, 1201–1204.

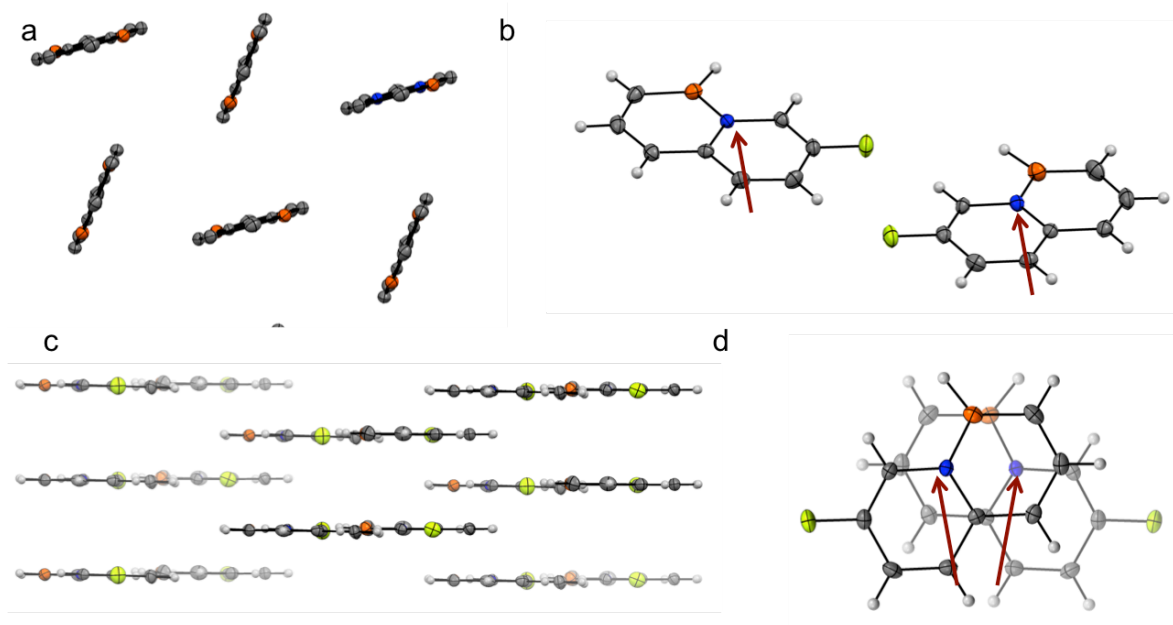


Figure 1.19. Crystal packing of a) **BN-9,1-Naph**, representative of the packing of naphthalene, 2-fluoronaphthalene, **BN-1,2-Naph**, **BN-9,10-Naph**, and **BN-1,9-Naph**; b) Fluorinated molecule **F-BN-9,1-Naph** viewed as an H-F interacting dimer with dipole vectors drawn (2.2235 D; CAM-B3LYP/6-311G(d,p)); c) **F-BN-9,1-Naph** viewed along the crystallographic *b*-axis; d) **F-BN-9,1-Naph** viewed along the crystallographic *c*-axis with dipole vectors drawn. Thermal ellipsoids drawn at the 50% probability level.

Curiously, the arrangement of the molecules in the dimer does not minimize the overall dipole moment; rather, the dipole is reinforced in one dimension, as all B–N vectors have a component in that dimension (Figure 1.19b). The dipole is also not minimized when looking down the third dimension (Figure 1.19d). This stands in contrast with the findings of Klausen,¹⁰⁹ Piers,^{61b} and our own group,⁶⁷ which show that the solid-state arrangement of BN-containing polyaromatics can minimize the overall dipole moment by alternating the orientation of the molecules.

¹⁰⁹ Though Klausen shows that crystal packing of *B*-aryl BN anthracenes may or may not minimize molecular dipole moments in 1-D stacks, dipoles are always minimized within the crystallographic unit cell. See: van de Wouw, H. L.; Lee, J. Y.; Siegler, M. A.; Klausen, R. S. *Org. Biomol. Chem.* **2016**, *14*, 3256–3263.

For a possible explanation of the unusual crystal packing, we turned to the calculated electrostatic potential map (ESP) for **F-BN-9,1-Naph** (Figure 1.20). These calculations show an electron-deficient fluorine-substituted pyridyl ring and regions of electron richness at fluorine and the azaboryl ring. While the parent compound **BN-9,1-Naph** exhibits an electron-rich azaboryl ring, the fused pyridyl ring is more electron-rich than in **F-BN-9,1-Naph**. Edge-to-face stacking in aromatic systems can be interpreted as the consequence of the electron-rich π -cloud interacting with the electron-deficient proton periphery.^{19,110} When this preferred mode of stacking is eliminated by steric or electronic effects, face-to-face interactions can be observed.^{20a}

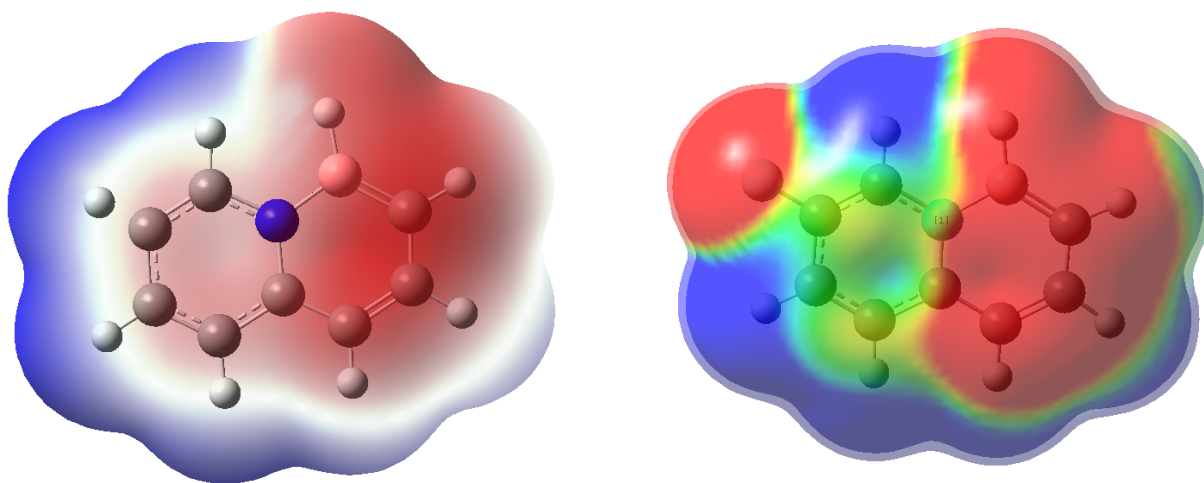


Figure 1.20. Electrostatic potential maps (CAM-B3LYP/6-311G(d,p), gas phase) for parent compound **BN-9,1-Naph** (left) and the fluorinated compound **F-BN-9,1-Naph** (right) at a 0.0002 electron au isocontour level (+3.14 to −3.14 kcal/mol). Red is the most negative, and blue is the most positive.

1.5.4 Optoelectronic Property Comparison of BN Naphthalenes

We began our electronic structure characterization of the BN naphthalenes using UV-PES (performed by the group of Prof. Anna Chrostowska, Figure 1.21). The experimentally-determined first ionization energies of the BN naphthalenes followed the

¹¹⁰ Martinez, C. R.; Iverson, B. L. *Chem. Sci.* **2012**, 3, 2191–2201.

trend established by calculations (**BN-1,2-Naph** > **BN-9,10-Naph** > **BN-1,9-Naph** > **BN-9,1-Naph**).

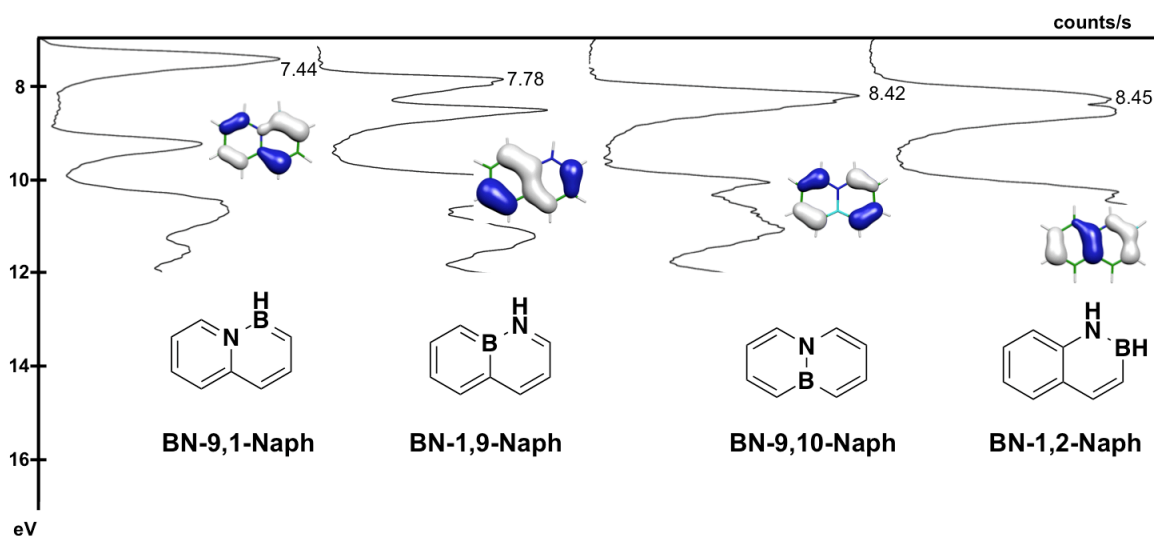


Figure 1.21. UV-PE spectra for parent BN naphthalenes investigated

To evaluate the relative LUMO energies of the BN naphthalenes, we measured reduction potentials (E_{pc} , as all reductions were irreversible) using cyclic voltammetry (Figure 1.22). The LUMO energy trend established by calculations is supported by experiment: (**BN-1,9-Naph** > **BN-9,1-Naph** > **BN-1,2-Naph** > **BN-9,10-Naph**) **BN-1,9-Naph** is most easily reduced, and thus has the lowest-lying LUMO.

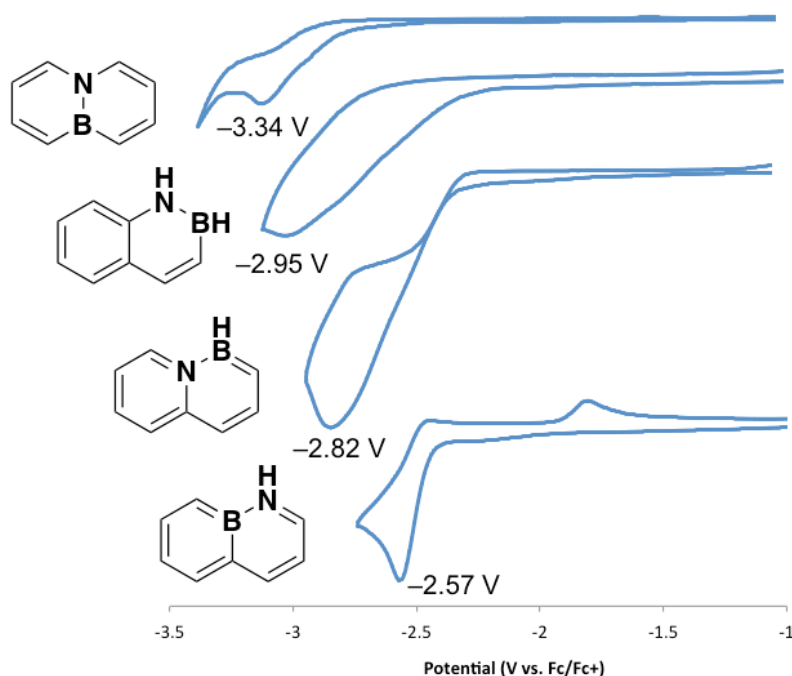


Figure 1.22. Cyclic voltammetry of BN naphthalenes in 0.1 M Bu₄NPF₆/acetonitrile solution. Scans taken at 150 mV/s, and potentials reported are cathodic peak potentials versus the ferrocene/ferrocenium couple.

We used UV-vis absorption spectroscopy to estimate optical HOMO-LUMO gaps. Figure 1.23 shows the UV-vis spectra in addition to key optoelectronic data for each of the compounds. The trend for the HOMO-LUMO excitation energies established by TD-DFT calculations (CAM-B3LYP/6-311G(d,p), PCM solvent model for cyclohexane) (Largest HOMO-LUMO excitation energy: **BN-9,10-Naph** > **BN-1,2-Naph** > **BN-1,9-Naph** > **BN-9,1-Naph**) is borne out in the experimental UV-vis spectra.

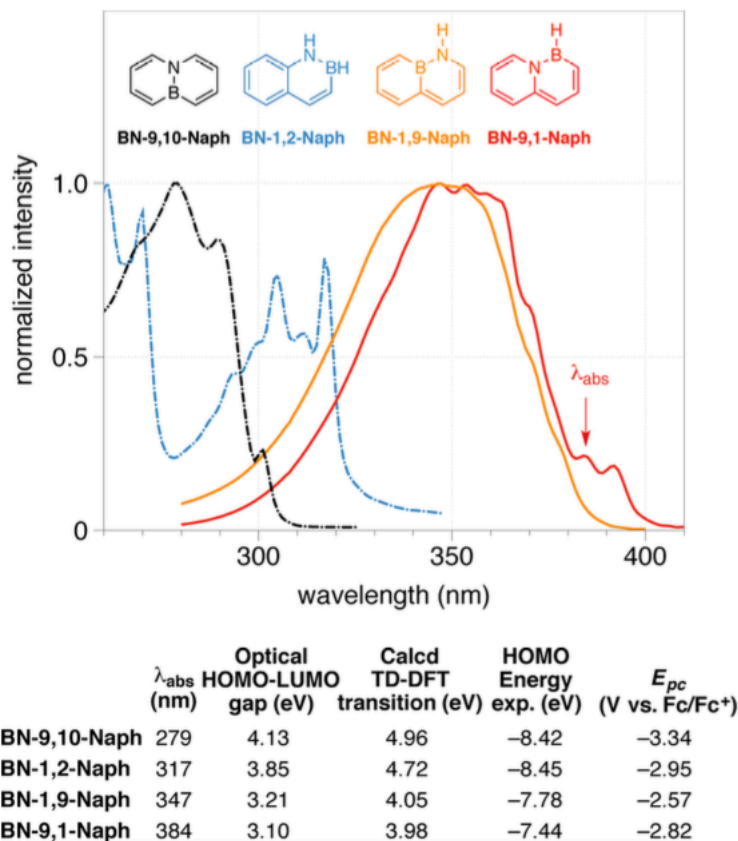


Figure 1.23. Normalized absorption spectra of BN naphthalenes obtained in cyclohexane and key optoelectronic data. Calculated transition energies were obtained using TD-DFT at the CAM-B3LYP/6-311G(d,p) level. E_{pc} values were collected in 0.1 M Bu₄NPF₆/MeCN at a scan rate of 150 mV/s.

1.5.5 Conclusion and General Principles of BN Acene Orbital Energies

The HOMO-LUMO gaps of the BN naphthalenes, estimated by UV-visible absorption spectroscopy and validated by UV-PES and CV data show that BN naphthalenes that share a BN unit location, but with opposite polarity, with respect to the rest of the topology have approximately the same bandgap. Figure 1.24 shows the TD-DFT calculated HOMO-LUMO-associated transition for the BN naphthalenes, and Figure 1.25 shows the Kohn-Sham gaps for the BN anthracene series for validation. Between the two orientational isomers, the higher HOMO always belongs to the molecule that is less thermodynamically stable. This trend may be general in the BN

acene series; indeed, the BN tetracene series retains the HOMO-LUMO gap similarities to a reasonable extent between the sets of orientational isomers (Figure 1.26).

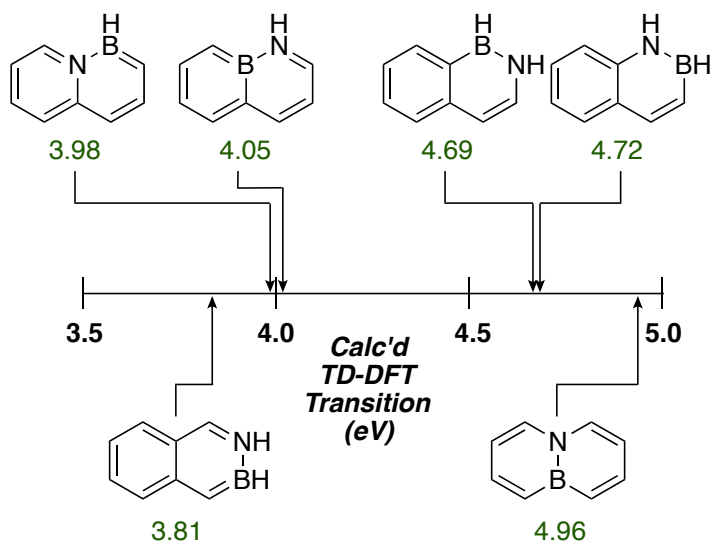


Figure 1.24. Calculated TD-DFT transitions associated with the HOMO-LUMO gap for the BN naphthalene series

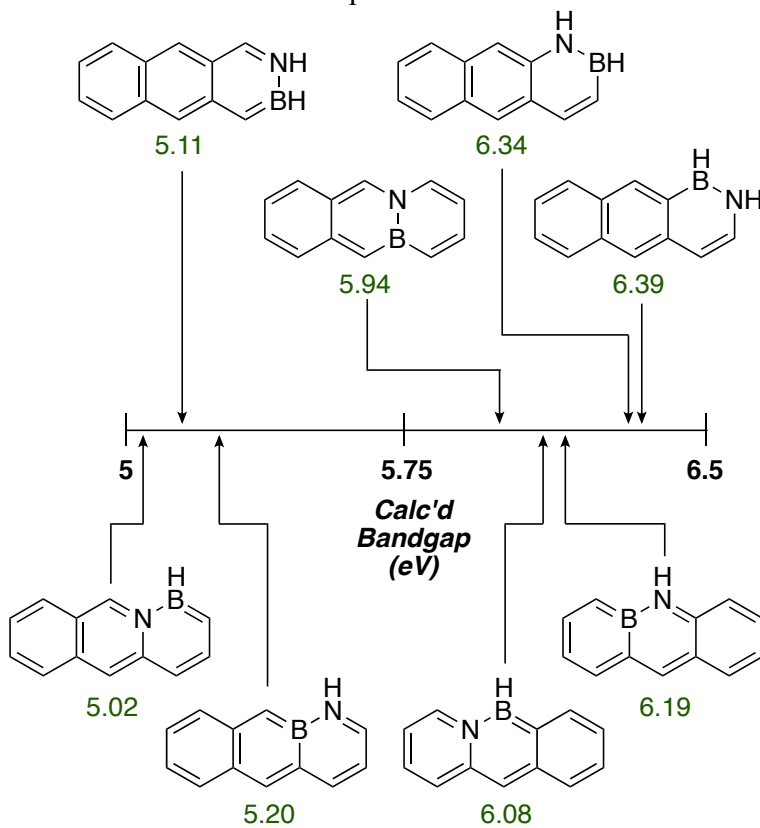


Figure 1.25. Calculated Kohn-Sham HOMO-LUMO gaps for the BN anthracene series

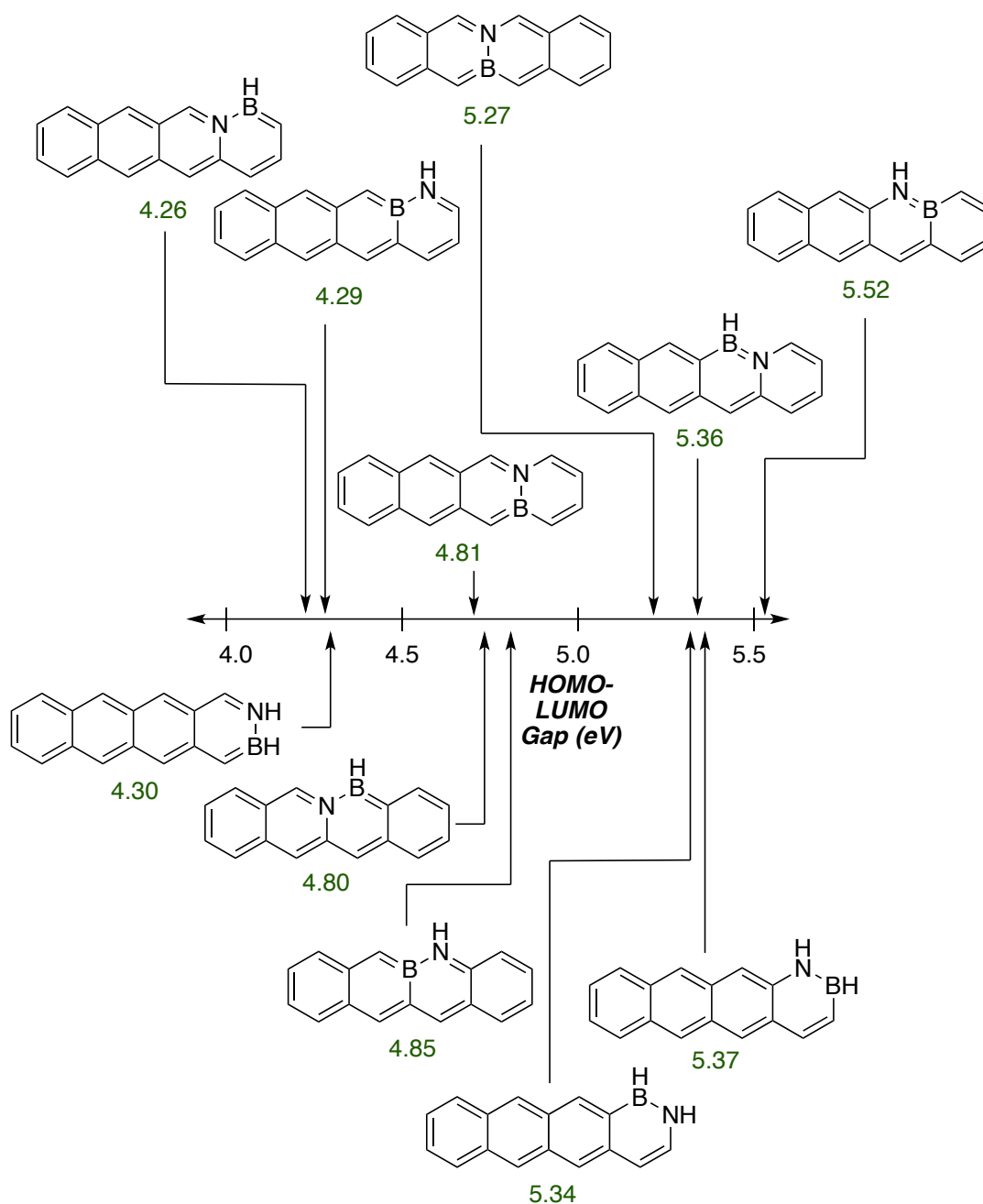
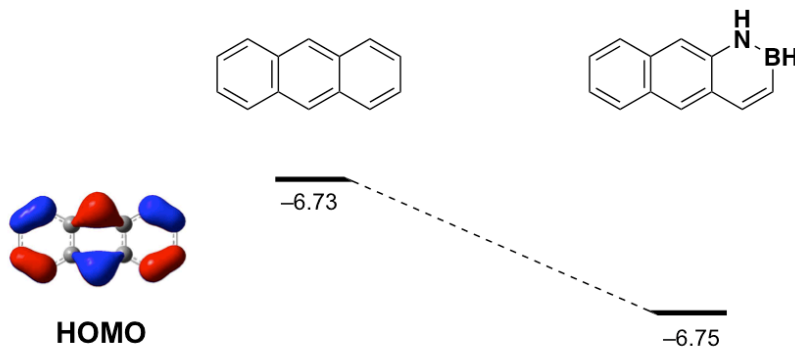


Figure 1.26. Calculated Kohn-Sham HOMO-LUMO gaps for the BN tetracene series

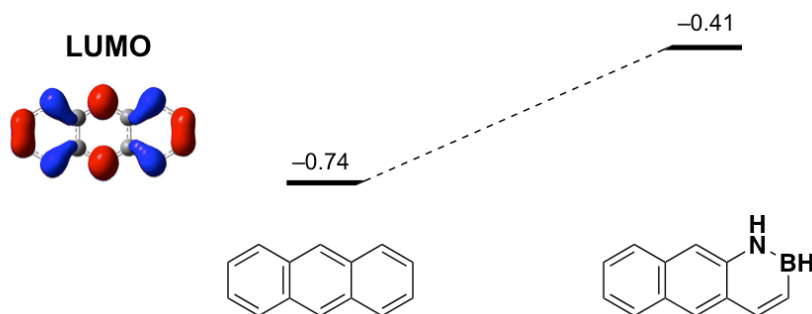
We have also analyzed the positioning of the BN bond within the acene frameworks and have discerned empirical and practical guiding principles for the BN compounds' frontier molecular orbital (FMO) energies with respect to BN unit position

within the particular acene topology. We list these principles and illustrate an example below the statement of each principle. These principles apply to both types of FMO.

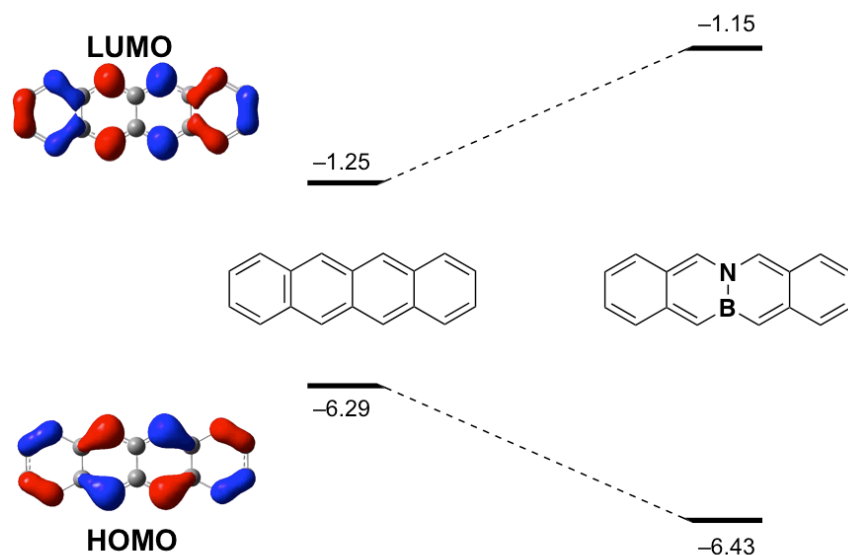
1) If the BN bond is placed in the acene topology where the all-carbon analogue's FMO contains a bonding interaction (same phase), the orbital will be lower in energy than that of the all-carbon analogue.



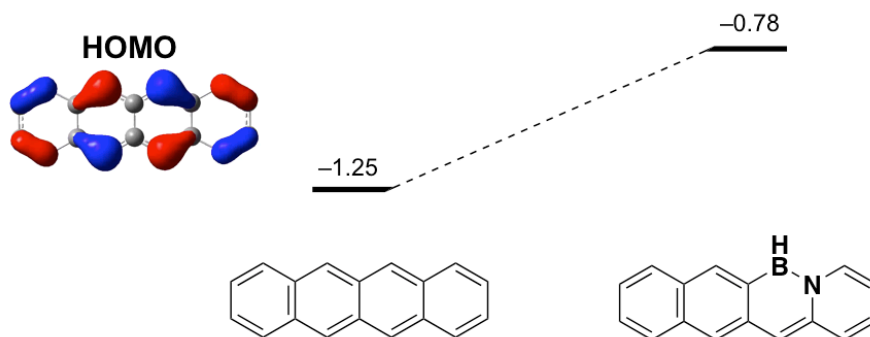
2) If the BN bond is placed where the all-carbon analogue's FMO contains an antibonding (opposite phase) or non-bonding interaction, then the FMO will be higher in energy than that of the all-carbon analogue.



3) If the BN bond is placed at a node, the HOMO energy of the BN isostere will be lower than that of the all-carbon analogue, while the LUMO will be higher in energy than that of the all-carbon analogue.



4) If the BN bond occupies a bonding region with respect to the all-carbon analogue's HOMO but the more electronegative element, nitrogen, occupies a positions with a relatively smaller orbital coefficient, the HOMO energy of the BN isostere will actually be higher than that of the all-carbon analogue.



Of the 50 FMOs for all the BN naphthalenes, anthracenes, and tetracenes, the guidelines can be successfully applied to 44. Of the six exceptions, five are associated with virtual orbitals. The cases color-coded green (Figures 1.27–29) below are successful applications of the principles, while those color-coded red are the outliers.

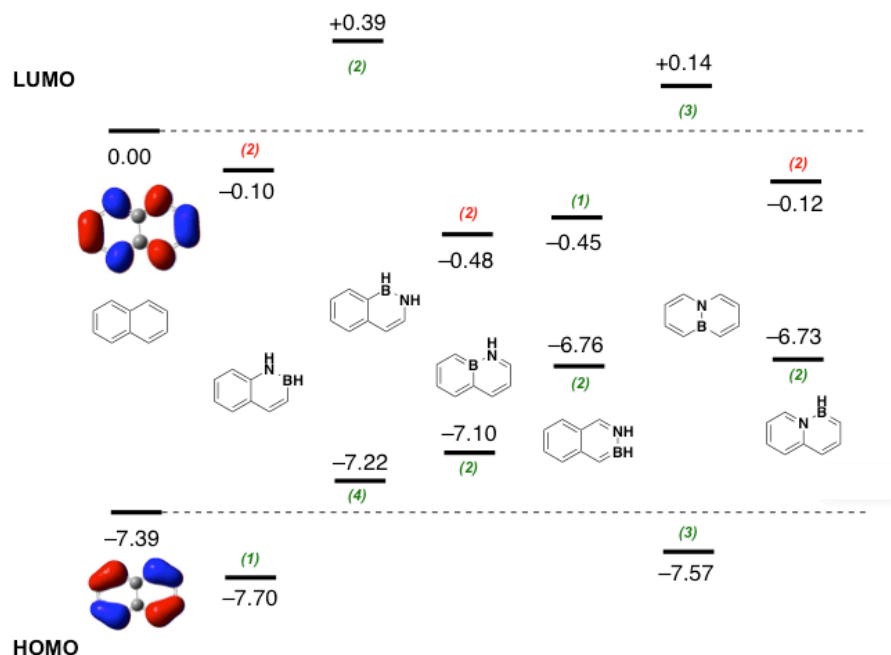


Figure 1.27. Visualization of the general empirical guidelines encompassing BN bond location within the naphthalene topology.

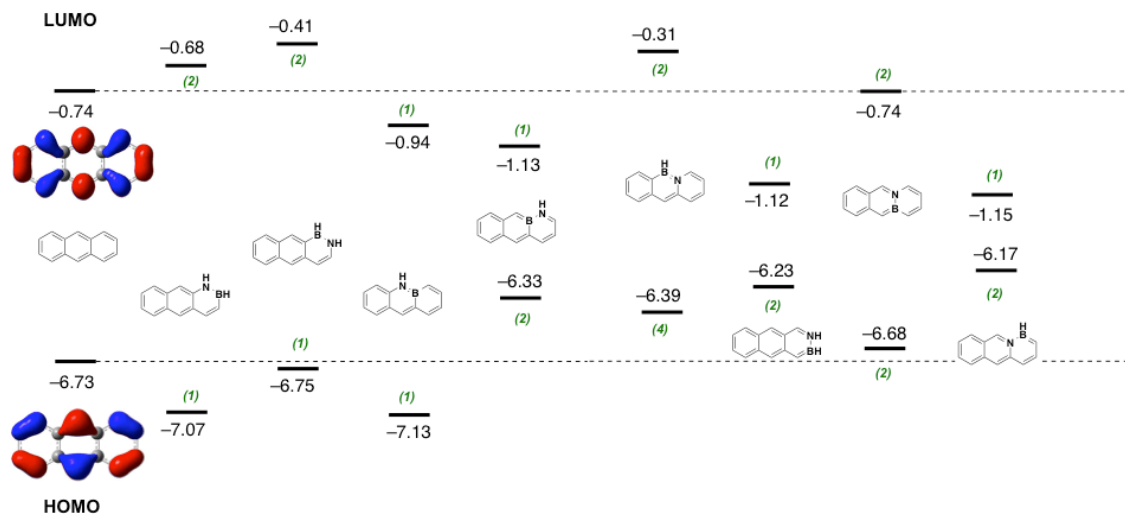


Figure 1.28. Visualization of the general empirical guidelines encompassing BN bond location within the anthracene topology.

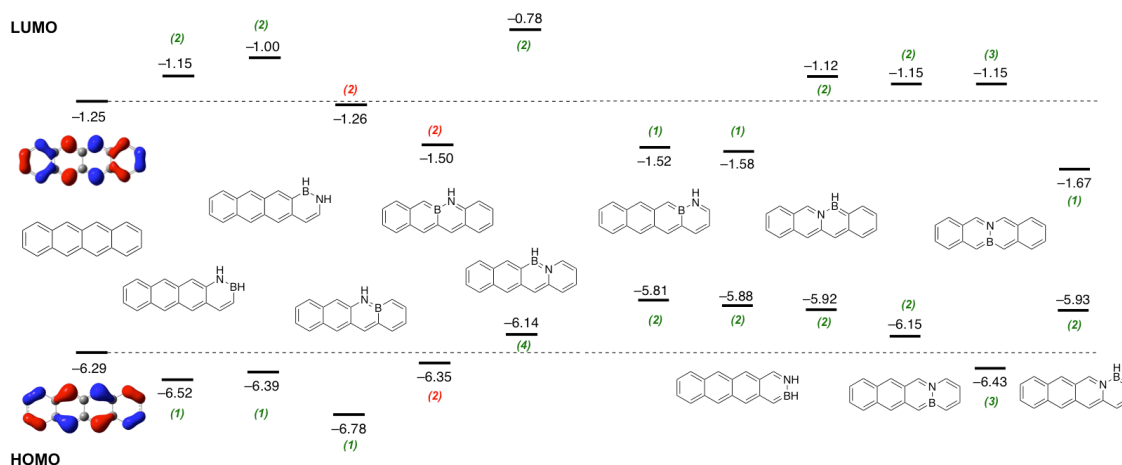


Figure 1.29. Visualization of the general empirical guidelines encompassing BN bond location within the tetracene topology.

1.5.6 Experimental Section

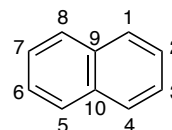
All oxygen- and moisture-sensitive manipulations were carried out under N₂ using either standard Schlenk techniques or a nitrogen-filled glovebox. THF, Et₂O, CH₂Cl₂, toluene, and pentane were dried with a solvent purification system consisting of columns of molecular sieves under argon. Cyclohexane and acetonitrile for photophysical characterizations and cyclic voltammetry, respectively, were dried over calcium hydride, distilled, and degassed via the freeze-pump-thaw method prior to use. All other chemicals were purchased (Acros, Sigma-Aldrich or TCI) and used as received.

NMR spectra were recorded on a Varian VNMRS 600 MHz, VNMRS 500 MHz, INOVA 500 MHz, or VNMRS 400 MHz spectrometer. ¹¹B NMR spectra were externally referenced to BF₃•Et₂O (δ 0.0 ppm).

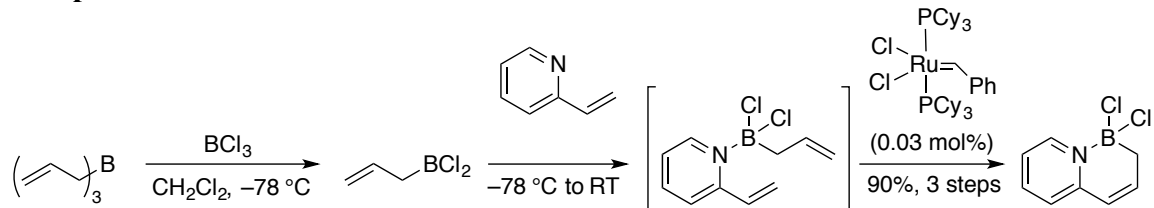
UV-vis absorption spectra were collected on an Agilent Cary 100 UV-Vis spectrometer. Emission spectra were collected on Photon Technology International spectrometer. Cyclic Voltammograms were collected using a BioLogic SP-200 potentiostat and the EC-Lab software package. Cathodic peak potentials are reported against an internally referenced ferrocene/ferrocenium couple. The CV were collected using a glassy carbon working electrode, a platinum wire counter electrode, and a silver wire pseudoreference electrode in acetonitrile with 0.1 M tetrabutylammonium hexafluorophosphate as the supporting electrolyte.

High-resolution mass spectra were collected by Marek Domin on a JEOL AccuTOF instrument (JEOL USA, Peabody, MA), equipped with a DART ion source (IonSense, Inc., Danvers, MA) in positive ion mode at the Boston College Center for Mass Spectrometry.

A note on nomenclature: Numbering refers to the positions on the naphthalene framework that are exchanged with heteroatoms. M. J. S. Dewar introduced non-standard numbering¹ of the bridging positions as 9 and 10 instead of 4a and 8a; we follow the former, non-standard system. Nitrogen is given priority over boron, so the number listed first corresponds to the position of the nitrogen and the second number corresponds to the position of the boron.

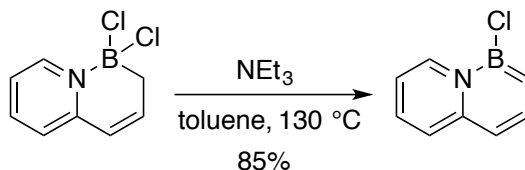


Synthetic Procedures
Compound 1.32

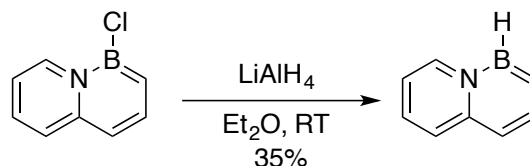


Triallylborane (0.40 g, 3.0 mmol, 0.33 equiv) was dissolved in dry methylene chloride (20 mL). This solution was cooled to $-78\text{ }^\circ\text{C}$ and then a solution of boron trichloride (1.0 M in hexane, 6.0 mL, 6.0 mmol, 0.67 equiv) was added dropwise to the triallylborane solution *via* syringe over 5 minutes. The mixture was stirred at $-78\text{ }^\circ\text{C}$ for 30 minutes (the formation of allylboron dichloride may be monitored by ^{11}B NMR δ 61 ppm (s)). Then a solution of 2-vinylpyridine **1.30** (0.95 g, 9.0 mmol, 1.0 equiv) in methylene chloride (5 mL) was added dropwise to the in-situ generated allylborondichloride solution over 5 minutes at $-78\text{ }^\circ\text{C}$, and the cooling bath was removed so the mixture could be allowed to warm to room temperature over 30 min. Once complete conversion to the pyridine-borane adduct **1.31** was judged complete by ^{11}B NMR (δ 9.2 (s)), Grubbs' 1st generation metathesis catalyst (20 mg, 0.02 mmol, 0.03 mol%) was added to the crude mixture as a solid, and the mixture was stirred at room temperature for 16 hours. Volatiles were removed under reduced pressure to afford **1.32** as a pale grey solid, which was carried forward without further purification. Yield: 1.62 g, 90%. ^1H NMR (500 MHz, C_6D_6) δ 9.04 (d, J = 6.1 Hz, 1H), 6.59 (td, J = 7.7, 1.4 Hz, 1H), 6.35 (brs, 1H), 6.18 (t, J = 6.8 Hz, 1H), 6.03 (d, J = 7.9 Hz, 1H), 5.70 (d, J = 9.7 Hz, 1H), 2.32 (d, J = 5.1 Hz, 2H). ^{13}C NMR (151 MHz, CD_2Cl_2) δ 150.5, 145.2, 144.0, 143.1, 125.6, 123.5, 121.7. Carbon adjacent to boron not observed. ^{11}B NMR (160 MHz, CD_2Cl_2) δ 7.2 (s). FTIR (ATR thin film): 2932, 1638, 1486, 1152, 584. HRMS (DART+) calcd for $\text{C}_8\text{H}_8\text{BClN}$ $[\text{M}+\text{H}-\text{Cl}]^+$: 164.04383; found: 164.04402.

Compound 1.33

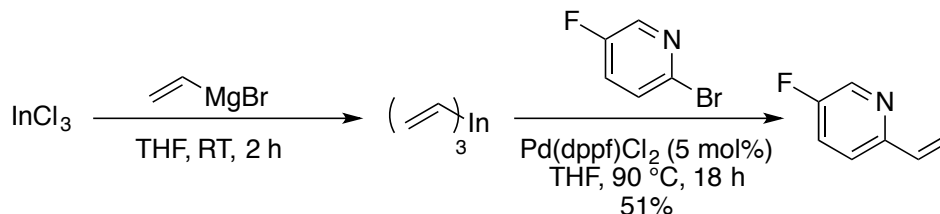


Compound **1.32** (1.62 g, 8.11 mmol, 1.0 equiv) was dissolved in dry toluene (20 mL) and triethylamine (2.0 mL, 1.5 g, 14 mmol, 1.8 equiv) was added. The mixture was heated to reflux in a 130 °C oil bath until the reaction was judged to be complete by ¹¹B NMR (32.2 ppm (s)) (about 40 minutes). The reaction mixture was allowed to cool to room temperature, and subsequently passed through an acrodisc. The filtrate was concentrated to dryness, and the product **1.33**, a dark red oil, was carried forward without further purification. Yield: 1.13 g, 85%. ¹H NMR (500 MHz, C₆D₆) δ 8.18 (d, *J* = 7.3 Hz, 1H), 7.51 (app. t, 1H), 6.78 (d, *J* = 10.8 Hz, 1H), 6.54 (dd, *J* = 9.0, 1.4 Hz, 1H), 6.22 (d, *J* = 6.0 Hz, 1H), 6.14 (dd, *J* = 9.1, 6.4 Hz, 1H), 5.77 (dd, *J* = 7.5, 6.3 Hz, 1H). ¹³C NMR (126 MHz, C₆D₆) δ 143.7, 142.2, 131.8, 125.9, 125.8, 121.2 (br), 113.0, 108.8. ¹¹B NMR (160 MHz, toluene) δ 32.2 (s). FTIR (ATR thin film): 3035, 1638, 1560, 1489, 1362, 1043, 800, 694.

BN-9,1-Naph

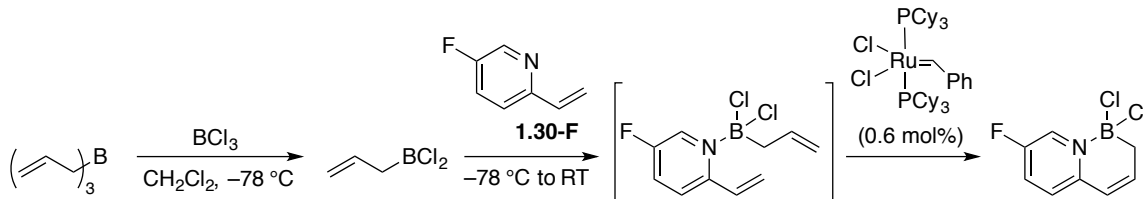
Compound **1.33** (0.81 g, 5.0 mmol, 1.0 equiv) was dissolved in dry ether (20 mL), and a solution of lithium aluminum hydride (1.0 M in ether, 1.5 mL, 1.5 mmol, 0.3 equiv) was added at room temperature. The mixture was stirred until the reaction was judged complete by ^{11}B NMR. Then, the reaction mixture was passed through an acrodisc, and the filtrate was concentrated to afford a pale yellow viscous liquid as the crude product (85% crude yield). The pure product **BN-9,1-Naph** was obtained as a pale yellow crystalline solid by sublimation. Yield: 226 mg (35%). ^1H NMR (500 MHz, CD_2Cl_2) δ 8.18 (d, $J = 7.1$ Hz, 1H), 7.94 (app. t, 1H), 7.38 (d, $J = 9.0$ Hz, 1H), 7.12 (ddd, $J = 8.9, 6.5, 1.4$ Hz, 1H), 6.84 (m, 2H), 6.66 (t, $J = 6.8$ Hz, 1H). The B–H proton is observed as a broad 1:1:1:1 quartet (6.0–4.9 ppm). ^{13}C NMR (126 MHz, C_6D_6) δ 143.1, 142.3, 138.4, 125.9, 125.6, 112.2, 109.6. Carbon adjacent to boron not observed. ^{11}B NMR (160 MHz, C_6D_6) δ 34.0 (d, $J = 134$ Hz). FTIR (ATR thin film): 2940, 2517, 1635, 1560, 1362, 763, 452. HRMS (DART+) calcd for $\text{C}_{12}\text{H}_9\text{BN}$ $[\text{M}+\text{H}]^+$: 130.08280; found: 130.08299.

Compound 1.30-F



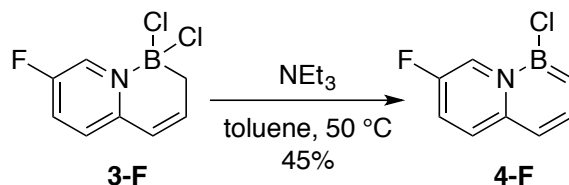
To a solution of indium trichloride (1.06 g, 4.77 mmol, 0.42 equiv) in 50 mL THF, a solution of vinylmagnesium bromide (14.5 mL, 14.5 mmol, 1.0 M, 1.27 equiv) was added dropwise over 10 minutes at room temperature. The mixture was stirred for 2 hours. This freshly prepared trivinylindium solution was brought into the glovebox, where 2-bromo-5-fluoropyridine (2.00 g, 11.4 mmol, 1 equiv) was added along with Pd(dppf)Cl_2 (470 mg, 0.57 mmol, 5 mol%). The reaction mixture was subsequently removed from the glovebox and heated to reflux with the heating bath at $90\text{ }^\circ\text{C}$ for 18 hours. At the conclusion of the reaction, the reaction mixture was allowed to cool to room temperature, and the excess vinylindium species was quenched with 0.5 mL of ethanol. The solvent was removed using a rotary evaporator. The resulting residue was re-dissolved in ether with 5 mL dichloromethane and passed through a short plug of silica gel using ether as the mobile phase. Volatiles were removed using a rotary evaporator. Residual volatiles were carefully removed *in vacuo* to provide **1.30-F** as a colorless liquid. Yield: 717 mg (51%). ^1H NMR (600 MHz, CD_2Cl_2) δ 8.42 (d, $J = 2.7$ Hz, 1H), 7.44 – 7.30 (m, 2H), 6.80 (dd, $J = 17.5, 10.8$ Hz, 1H), 6.13 (dd, $J = 17.5, 1.4$ Hz, 1H), 5.45 (d, $J = 10.8$ Hz, 1H). ^{13}C NMR (151 MHz, CD_2Cl_2) δ 158.7 (d, $J = 255.9$ Hz), 152.1, 137.5 (d, $J = 23.6$ Hz), 135.7, 122.9 (d, $J = 18.7$ Hz), 122.0 (d, $J = 4.4$ Hz), 117.5 (d, $J = 2.6$ Hz). ^{19}F NMR (376 MHz, CD_2Cl_2) δ -129.0 (t, $J = 6.0$ Hz). FTIR (ATR thin film): 1578, 1477, 1220, 913, 837, 416. HRMS (DART+) $[\text{M}+\text{H}]^+$ Calcd. for $\text{C}_7\text{H}_7\text{NF}$ 124.05625, found 124.05610.

Compound 1.32-F



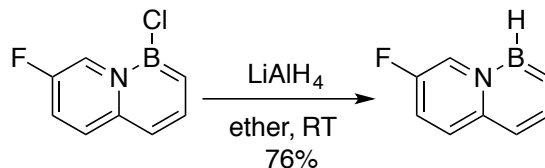
Allylboron dichloride was prepared *in situ* (5.82 mmol) as described above for compound **1.32**. Compound **1.30-F** (717 mg, 5.82 mmol, 1.0 equiv) was dissolved in 5.0 mL CH_2Cl_2 , and the solution was added to the cold ($-78\text{ }^\circ\text{C}$) solution of allylboron dichloride over 5 minutes. The cooling bath was subsequently removed, and the reaction mixture was allowed to warm up to room temperature. When pyridine-borane adduct **1.31-F** was formed completely (judged by ^{11}B NMR δ 9.7 (s), 75 min.), Grubbs' 1st generation catalyst (30. mg, 0.040 mmol, 0.6 mol%) was added carefully to the crude mixture as a solution in 8 mL CH_2Cl_2 . The mixture was stirred at room temperature for 16 hours, and the reaction was judged to be complete by ^{11}B NMR (δ 7.6 (s)). Subsequently, the crude mixture was passed through an acrodisc, and the filtrate was concentrated *in vacuo* to furnish **1.32** as a red solid that was carried forward without further purification. Yield: 1.15 g (quantitative). ^1H NMR (500 MHz, CD_2Cl_2) δ 9.17 (d, J = 3.3 Hz, 1H), 7.88 (ddd, J = 9.2, 6.6, 2.8 Hz, 1H), 7.43 (dd, J = 8.9, 5.3 Hz, 1H), 6.89 – 6.78 (m, 1H), 6.50 (dd, J = 9.7, 1.9 Hz, 1H), 2.11 (s, 2H). Minor signals consistent with isomerized *B*-vinyl product visible at δ 6.04 (d, 17.2 Hz) and 5.86 (d, 11.3 Hz). ^{19}F NMR (470 MHz, CD_2Cl_2) δ -122.5 (m). ^{13}C NMR (151 MHz, CD_2Cl_2) δ 158.2 (d, J = 252.7 Hz), 147.9, 144.8, 132.7 (d, J = 35.3 Hz), 131.1 (d, J = 18.9 Hz), 127.1 (d, J = 6.3 Hz), 120.7, 25.8 (br). FTIR (ATR thin film): 2925, 1499, 1346, 1251, 847, 648. HRMS (DART+) $[\text{M}-\text{Cl}+\text{H}]^+$ Calcd. for $\text{C}_8\text{H}_7\text{NBFCl}$ 182.03441, found 182.03375.

Compound 1.33-F



Compound **1.32** (1.15 g, 5.82 mmol, 1.0 equiv) was dissolved in toluene, and triethylamine (1.30 mL, 9.31 mmol, 1.6 equiv) was added. The reaction mixture was stirred at 50 °C until the reaction was judged complete by ^{11}B NMR (δ 32.2 (s), 1 hour). Subsequently, the mixture was passed through an acrodisc, and the filtrate was concentrated to dryness *in vacuo* then recrystallized from pentane at -30 °C. Yielded a crop of pale yellow crystals (479 mg, 45%). ^1H NMR (400 MHz, CD_2Cl_2) δ 8.48 (d, J = 4.2 Hz, 1H), 7.89 (m, 1H), 7.44 (dd, J = 9.8, 6.0 Hz, 1H), 7.08 (ddd, J = 9.6, 6.9, 2.4 Hz, 1H), 6.88 (d, J = 7.4 Hz, 1H), 6.76 (d, J = 10.8 Hz, 1H). ^{13}C NMR (151 MHz, CD_2Cl_2) δ 153.3 (d, J = 239.9 Hz), 143.2, 140.3, 128.5 (d, J = 8.0 Hz), 127.7 (br), 119.7 (d, J = 26.3 Hz), 117.0 (d, J = 38.9 Hz), 109.8. ^{19}F NMR (376 MHz, CD_2Cl_2) δ -140.07 (q, J = 6.2 Hz). ^{11}B NMR (160 MHz, toluene) δ 32.2 (s). FTIR (ATR thin film): 2921, 1642, 1502, 1299, 779, 693. HRMS (DART+) $[\text{M}+\text{H}]^+$ Calcd. for $\text{C}_8\text{H}_7\text{NBFCl}$ 182.03441, found 182.03423.

Compound F-BN-9,1-Naph



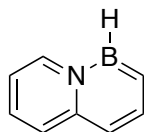
Compound **1.33-F** (479 mg, 2.64 mmol, 1.0 equiv) was dissolved in ether (50 mL), and lithium aluminum hydride was added at room temperature as a solid (100. mg, 2.64 mmol, 1.0 equiv). The reaction mixture was then stirred at room temperature for 5 hours. The mixture was then passed through a glass frit, and the filtrate was concentrated *in vacuo*. The residue was extracted into pentane, and the pentane mixture was passed through an acrodisc. The product **F-BN-9,1-Naph** was isolated by placing a concentrated pentane solution of **F-BN-9,1-Naph** in the glovebox freezer (−30 °C) and collecting the crystals that formed (pale yellow rods that were suitable for single-crystal X-ray diffraction analysis). Yield: 301 mg (76%). ¹H NMR (600 MHz, CD₂Cl₂) δ 8.12 – 7.99 (m, 1H), 7.93 (t, *J* = 9.0 Hz, 1H), 7.40 (dd, *J* = 9.8, 5.8 Hz, 1H), 7.06 (ddd, *J* = 9.7, 7.2, 2.5 Hz, 1H), 6.95 – 6.86 (m, 2H). The B–H proton is observed as a broad 1:1:1:1 quartet (6.0–5.0 ppm). ¹³C NMR (151 MHz, CD₂Cl₂-*d*₂) δ 153.2 (d, 239 Hz), 143.1, 141.0, 128.5 (d, *J* = 7.9 Hz), 125.3 (br), 123.6 (d, *J* = 36.3 Hz), 120.4 (d, *J* = 25.9 Hz), 110.9. ¹⁹F NMR (CD₂Cl₂, 376 MHz,) δ −139.04 (q, *J* = 6.0 Hz). ¹¹B NMR (128 MHz, CD₂Cl₂) δ 35.48 (d, *J* = 134.1 Hz). FTIR (ATR thin film): 3100, 2517, 1659, 1566, 1386, 1239, 829, 447. HRMS (DART+) calcd for C₈H₈BFN [M+H]⁺ 148.07338; found: 148.07379.

Computational Details

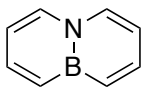
All calculations were performed using the Gaussian 09 program.

The coordinates for the BN tetracenes optimized at the CAM-B3LYP/6-311G(d,p) level were the same as used in § 1.4. The coordinates for the G3MP2 calculations (Prof. David A. Dixon, The University of Alabama) for BN naphthalenes and the BN anthracenes (J. S. A. Ishibashi) are given below. Single-point TD-DFT calculations (CAM-B3LYP/6-311G(d,p)) were executed using the ground-state geometries listed below.

Naphthalenes: CAM-B3LYP/6-311G(d,p)

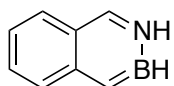


C	-2.39786	-0.71202	0.00000
C	-1.21696	-1.35757	0.00000
C	0.01836	0.69292	0.00000
C	-1.23622	1.38222	0.00000
C	-2.40947	0.71378	0.00000
H	-3.31825	-1.27900	0.00000
H	-1.13806	-2.43487	0.00000
C	1.22759	1.36242	0.00000
H	-1.20489	2.46411	0.00000
H	-3.35074	1.24886	0.00000
C	2.44601	0.67731	0.00000
H	1.20371	2.44414	0.00000
H	3.35638	1.27108	0.00000
B	1.24068	-1.47119	0.00000
H	1.11526	-2.65514	0.00000
N	0.00148	-0.69832	0.00000
C	2.50829	-0.69964	0.00000
H	3.48439	-1.17159	0.00000

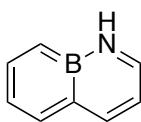


C	0.00000	2.38559	-0.71841
C	0.00000	1.18721	-1.33971
C	0.00000	1.36931	1.48233
C	0.00000	2.48326	0.70679
H	0.00000	-1.10021	-2.41970
H	0.00000	3.28169	-1.32516
H	0.00000	1.10021	-2.41970
C	0.00000	-1.18721	-1.33971
C	0.00000	-1.36931	1.48233
H	0.00000	1.48891	2.56142

H	0.00000	3.47735	1.14440
C	0.00000	-2.48326	0.70679
C	0.00000	-2.38559	-0.71841
H	0.00000	-1.48891	2.56142
H	0.00000	-3.47735	1.14440
H	0.00000	-3.28169	-1.32516
N	0.00000	0.00000	-0.63668
B	0.00000	0.00000	0.82642

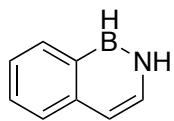


C	-1.241557	-1.437059	0.000000
C	-2.407433	-0.748842	0.000000
C	0.029226	-0.764829	0.000000
C	0.000000	0.677076	0.000000
C	-1.255422	1.365922	0.000000
C	-2.421605	0.680488	0.000000
C	1.239877	-1.444538	0.000000
B	2.521368	-0.690282	0.000000
N	2.372972	0.746020	0.000000
C	1.188274	1.376751	0.000000
H	3.188441	1.341687	0.000000
H	1.194502	-2.529251	0.000000
H	3.629529	-1.125371	0.000000
H	-1.241478	-2.521016	0.000000
H	-3.350449	-1.283313	0.000000
H	-1.251400	2.450695	0.000000
H	-3.368966	1.205031	0.000000
H	1.194008	2.461003	0.000000

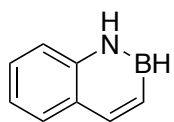


N	-1.293379	-1.372446	0.000004
C	-2.434897	-0.653584	0.000007
B	0.010075	-0.758998	-0.000005
C	0.009716	0.761489	-0.000012
C	-1.204108	1.421996	-0.000006
C	-2.419906	0.717864	0.000002
C	1.342783	-1.486864	-0.000007
C	2.462283	-0.716099	0.000005
C	2.431347	0.723195	0.000003
C	1.274685	1.432872	-0.000030
H	3.380117	1.248765	0.000031
H	1.465470	-2.567293	-0.000004
H	3.445808	-1.179536	0.000020

H	-1.397733	-2.377080	0.000010
H	-3.367927	-1.204636	0.000015
H	-1.237968	2.509836	-0.000011
H	-3.363145	1.247209	0.000005
H	1.307236	2.519632	0.000155



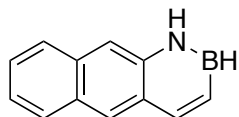
C	1.179269	1.444258	0.000000
C	2.409735	0.830430	0.000000
C	0.000000	0.677736	0.000000
C	0.086386	-0.734436	0.000000
C	1.360883	-1.328477	0.000000
C	2.506883	-0.566451	0.000000
C	-1.295597	1.308611	0.000000
C	-2.430062	0.585647	0.000000
N	-2.407739	-0.793549	0.000000
B	-1.208637	-1.543789	0.000000
H	-3.307154	-1.248782	0.000000
H	-1.271773	-2.733446	0.000000
H	-1.358032	2.389383	0.000000
H	-3.405955	1.055062	0.000000
H	1.109792	2.526659	0.000000
H	3.311807	1.431637	0.000000
H	1.432162	-2.410831	0.000000
H	3.481525	-1.039803	0.000000



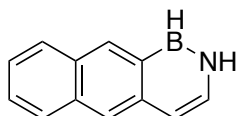
C	-2.40207	-0.83316	0.00000
C	-1.17857	-1.46032	0.00000
C	0.01994	-0.72818	0.00000
C	-0.05283	0.67813	0.00000
C	-1.30380	1.31018	0.00000
C	-2.45995	0.56471	0.00000
H	1.29949	-2.46230	0.00000
H	-3.31538	-1.41471	0.00000
H	-1.12012	-2.54339	0.00000
C	1.30716	-1.37444	0.00000
H	-1.34945	2.39432	0.00000
H	-3.42039	1.06625	0.00000
C	2.46875	-0.68182	0.00000
H	3.40109	-1.23652	0.00000
N	1.11906	1.40725	0.00000

H	0.99647	2.40957	0.00000
B	2.41579	0.84068	0.00000
H	3.35166	1.57704	0.00000

Anthracenes: CAM-B3LYP/6-311G(d,p)

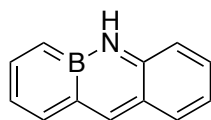


C	-3.627832	0.722903	-0.000001
C	-2.449247	1.405062	-0.000001
C	-1.207216	0.714698	0.000000
C	-1.208626	-0.709831	0.000000
C	-2.457405	-1.388166	-0.000001
C	-3.629452	-0.693682	-0.000001
C	0.023767	1.385531	0.000000
C	0.016518	-1.394674	0.000000
C	1.215898	-0.716058	0.000001
C	1.229150	0.711383	0.000000
C	2.492511	1.415005	0.000000
H	2.435341	2.501004	0.000000
C	3.679746	0.776147	0.000001
H	0.031130	2.470667	0.000000
H	-4.569003	1.259043	-0.000002
H	-2.440771	2.489376	-0.000001
H	-2.461849	-2.472395	-0.000001
H	-4.573603	-1.225266	-0.000002
H	0.014988	-2.480122	0.000000
H	4.586684	1.371118	0.000001
B	3.693988	-0.753178	0.000002
H	4.664953	-1.442242	0.000001
N	2.430752	-1.383532	0.000001
H	2.360063	-2.390460	0.000001

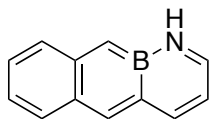


C	-4.512524	2.692840	0.471682
C	-5.465405	1.911534	-0.107603
C	-3.213742	2.179453	0.743258
C	-2.929467	0.826926	0.396102
C	-3.949476	0.041873	-0.206957
C	-5.181857	0.565928	-0.452854
H	-4.730091	3.721781	0.735664
H	-6.450314	2.316207	-0.308692
H	-3.725487	-0.986489	-0.468395

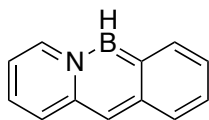
H	-5.952109	-0.041098	-0.913033
C	-2.210584	2.959393	1.338599
C	-0.954167	2.443046	1.594427
C	1.304055	2.750445	2.458501
C	0.082070	3.245090	2.207524
H	-2.433408	3.988819	1.600848
H	2.077850	3.353138	2.917498
H	-0.134511	4.272516	2.471015
H	1.105934	-0.568727	1.303852
H	2.587750	1.168943	2.374358
H	-1.434743	-0.713859	0.396926
C	-1.648402	0.316908	0.662650
C	-0.659018	1.083153	1.248666
B	0.744065	0.540247	1.545042
N	1.645590	1.443939	2.145931



C	-4.500472	2.670879	0.468411
C	-5.469264	1.895986	-0.114108
C	-3.212557	2.163845	0.738499
C	-2.932676	0.819753	0.392694
C	-3.936771	0.036903	-0.204198
C	-5.178585	0.565137	-0.451974
H	-4.711179	3.700699	0.734957
H	-6.452080	2.303706	-0.313548
H	-3.715659	-0.992213	-0.466757
H	-5.940501	-0.052200	-0.912662
C	-2.204517	2.972733	1.345060
C	1.302204	2.757872	2.460372
C	0.082843	3.289737	2.222570
H	-2.475015	3.999014	1.590087
H	2.071579	3.367929	2.920347
H	-0.121312	4.322701	2.492168
H	1.120343	-0.482984	1.336690
H	2.652728	1.072308	2.364385
H	-1.558930	-0.660757	0.372408
B	-0.629813	1.045094	1.246027
C	0.772802	0.524879	1.549661
C	1.640536	1.389951	2.126415
C	-0.953298	2.497361	1.612575
N	-1.688394	0.303675	0.644933

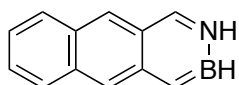


C	-4.493182	2.683039	0.475052
C	-5.455479	1.928889	-0.098808
C	-3.181148	2.161131	0.748468
C	-2.897645	0.774834	0.389994
C	-3.969357	0.024551	-0.219290
C	-5.183403	0.567595	-0.453055
H	-4.692567	3.714292	0.746027
H	-6.436365	2.344742	-0.295068
H	-3.768470	-1.006427	-0.489243
H	-5.965574	-0.025481	-0.912831
C	-2.224486	2.964782	1.335912
C	1.333411	2.751496	2.468687
C	0.063557	3.267246	2.208597
H	-2.490486	3.990667	1.582331
H	2.096200	3.365745	2.927702
H	-0.141226	4.301438	2.478285
H	1.066570	-0.311442	1.374717
H	2.631569	1.043435	2.347636
H	-1.538783	-0.836278	0.321897
B	-0.598947	1.045074	1.256634
C	1.645500	1.445651	2.146247
C	-0.927505	2.487022	1.618023
C	-1.661497	0.202760	0.621111
N	0.751326	0.627245	1.575984

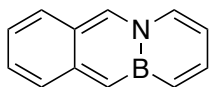


C	-4.491222	2.685881	0.4765020
C	-5.463057	1.914833	-0.1053210
C	-3.209499	2.148481	0.7340920
C	-2.940731	0.801824	0.3837330
C	-3.967641	0.039907	-0.2136120
C	-5.205962	0.577383	-0.4567090
N	-0.602619	1.123644	1.2802380
B	-1.567804	0.248131	0.6666890
H	-4.697449	3.716219	0.7446660
H	-6.442234	2.338596	-0.2979060
H	-3.762470	-0.990834	-0.4820370
H	-5.985460	-0.018460	-0.9158960
C	-2.186763	2.931611	1.3367630
C	-0.936239	2.450992	1.6023220
C	0.678959	0.658589	1.5615130
C	1.623429	1.421218	2.1314620
C	1.313330	2.779846	2.4719590
C	0.084267	3.262262	2.2137740

H	-2.396942	3.959969	1.6030320
H	2.066905	3.406154	2.9325480
H	-0.182150	4.282542	2.4581420
H	0.846541	-0.371037	1.2804680
H	2.602335	1.006717	2.3270120
H	-1.215513	-0.862466	0.4215760

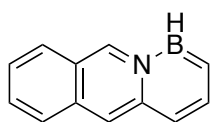


C	-4.503035	2.702541	0.478014
C	-5.446716	1.925358	-0.096673
C	-3.189918	2.190353	0.754732
C	-2.890415	0.819166	0.406555
C	-3.932195	0.037073	-0.202691
C	-5.152408	0.565255	-0.442972
H	-4.718600	3.731840	0.742765
H	-6.433850	2.321572	-0.301190
H	-3.713026	-0.991496	-0.465730
H	-5.925131	-0.039281	-0.902965
C	-2.209302	2.955834	1.337766
C	-0.924099	2.433329	1.601314
C	0.050584	3.228503	2.191510
H	-2.422450	3.986506	1.603782
H	1.912203	3.407891	2.879406
H	-0.163758	4.258003	2.456405
H	0.843905	-0.482016	1.243710
H	2.821119	1.116268	2.436231
H	-1.429734	-0.728767	0.393347
C	-1.641245	0.301196	0.659637
C	-0.607909	1.063497	1.259269
B	1.701051	1.400363	2.150610
C	0.666829	0.551940	1.522898
N	1.270107	2.757077	2.449281



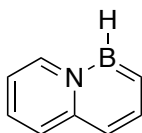
C	-4.457716	2.704963	0.494598
C	-5.440217	1.976779	-0.077878
C	-3.164376	2.131061	0.744605
C	-2.916360	0.753799	0.376774
C	-4.004680	0.030770	-0.229620
C	-5.205150	0.611529	-0.446354
H	-4.628288	3.738363	0.776180
H	-6.412100	2.417350	-0.262970
H	-3.831761	-1.001990	-0.509922
H	-6.007466	0.045041	-0.904473

C	-2.174650	2.881094	1.325720
C	1.253138	2.799943	2.456917
C	0.005172	3.222123	2.173840
H	-2.355232	3.913808	1.603285
H	1.938102	3.500251	2.917421
H	-0.325590	4.230219	2.392262
H	1.199091	-0.425004	1.383136
H	2.702971	1.195923	2.421512
H	-1.535301	-0.841265	0.321510
C	-1.678765	0.195517	0.613095
N	-0.933972	2.390473	1.584441
B	-0.584884	0.998126	1.246412
C	0.837158	0.577653	1.589215
C	1.682883	1.465483	2.165307

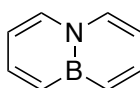


C	-4.528229	2.712582	0.472840
C	-5.448238	1.907109	-0.102725
C	-3.208549	2.224863	0.759352
C	-2.899282	0.861318	0.416984
C	-3.909209	0.042904	-0.193195
C	-5.136291	0.547538	-0.443103
N	-0.667182	1.147306	1.266011
H	-4.767924	3.738099	0.728254
H	-6.441332	2.284571	-0.315023
H	-3.664985	-0.982252	-0.446820
H	-5.898624	-0.068618	-0.903240
C	-2.226225	2.985312	1.341043
C	-0.938004	2.476020	1.609910
C	1.667773	1.418285	2.145013
C	1.325778	2.725747	2.458050
C	0.063786	3.243429	2.200503
H	-2.422264	4.015212	1.612600
H	2.054068	3.386465	2.921229
H	-0.177256	4.267043	2.454604
H	0.771537	-0.587922	1.183554
H	2.672245	1.081424	2.374553
C	-1.645163	0.392092	0.687504
H	-1.355453	-0.622785	0.452591
B	0.656022	0.549259	1.517509

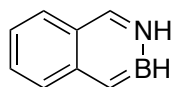
Naphthalenes: G3MP2



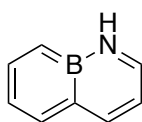
C	2.524083	0.646986	0.000000
C	0.000000	-0.694392	0.000000
C	1.206011	-1.394855	0.000000
C	2.437861	-0.742593	0.000000
H	-1.088654	2.471379	0.000000
H	3.515361	1.094933	0.000000
H	1.179607	2.648654	0.000000
C	-1.187496	1.392168	0.000000
C	-1.262541	-1.356561	0.000000
H	1.152028	-2.480035	0.000000
H	3.339346	-1.356058	0.000000
C	-2.439194	-0.662367	0.000000
C	-2.391396	0.758160	0.000000
H	-1.255067	-2.443596	0.000000
H	-3.392429	-1.183142	0.000000
H	-3.300092	1.351042	0.000000
N	0.020370	0.704677	0.000000
B	1.276668	1.456962	0.000000



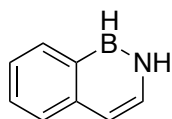
C	0.000000	2.396219	0.730052
C	0.000000	1.187213	1.364256
C	0.000000	1.367252	-1.468416
C	0.000000	2.497954	-0.688275
H	0.000000	-1.100267	2.448109
H	0.000000	3.291494	1.344917
H	0.000000	1.100267	2.448109
C	0.000000	-1.187213	1.364256
C	0.000000	-1.367252	-1.468416
H	0.000000	1.489845	-2.550647
H	0.000000	3.494393	-1.129075
C	0.000000	-2.497954	-0.688275
C	0.000000	-2.396219	0.730052
H	0.000000	-1.489845	-2.550647
H	0.000000	-3.494393	-1.129075
H	0.000000	-3.291494	1.344917
N	0.000000	0.000000	0.656161
B	0.000000	0.000000	-0.814228



C	-2.426839	0.692077	0.000000
C	-1.242744	1.380578	0.000000
C	0.000000	0.679344	0.000000
C	0.017688	-0.762442	0.000000
C	-1.248645	-1.429354	0.000000
C	-2.428314	-0.730667	0.000000
H	1.224721	2.467500	0.000000
H	-3.370599	1.231379	0.000000
H	-1.234572	2.469630	0.000000
C	1.203046	1.379532	0.000000
C	1.236076	-1.456606	0.000000
H	-1.256366	-2.518046	0.000000
H	-3.375716	-1.264782	0.000000
H	1.175202	-2.544750	0.000000
H	3.640584	-1.158424	0.000000
H	3.208351	1.317120	0.000000
N	2.382168	0.723968	0.000000
B	2.530320	-0.716435	0.000000

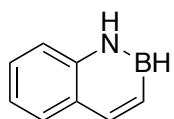


C	-2.455635	-0.614962	0.000000
C	0.027458	0.760932	0.000000
C	-1.187100	1.453826	0.000000
C	-2.407903	0.770079	0.000000
H	1.420345	-2.604063	0.000000
H	-3.399859	-1.153343	0.000000
H	-1.439755	-2.358676	0.000000
C	1.314001	-1.518447	0.000000
C	1.294763	1.414251	0.000000
H	-1.198013	2.546352	0.000000
H	-3.346710	1.315147	0.000000
C	2.450656	0.671634	0.000000
C	2.462598	-0.761484	0.000000
H	1.349267	2.504317	0.000000
H	3.408379	1.188985	0.000000
H	3.440410	-1.244960	0.000000
B	0.000000	-0.761404	0.000000
N	-1.318156	-1.348816	0.000000



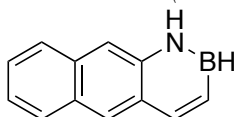
C	2.421948	0.828370	0.000000
C	1.186014	1.448729	0.000000

C	0.000000	0.681326	0.000000
C	0.079373	-0.740028	0.000000
C	1.357701	-1.340017	0.000000
C	2.511698	-0.575512	0.000000
H	-1.348151	2.402089	0.000000
H	3.329452	1.428183	0.000000
H	1.119435	2.535776	0.000000
C	-1.286888	1.316998	0.000000
H	1.427604	-2.426493	0.000000
H	3.488158	-1.054133	0.000000
C	-2.438207	0.595503	0.000000
H	-1.288707	-2.744109	0.000000
H	-3.320251	-1.242852	0.000000
H	-3.416272	1.068231	0.000000
N	-2.413934	-0.787184	0.000000
B	-1.216713	-1.549724	0.000000



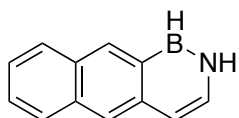
C	-2.410376	-0.725453	0.000000
C	-1.207111	-1.406437	0.000000
C	0.023745	-0.716326	0.000000
C	0.000000	0.698813	0.000000
C	-1.227910	1.383973	0.000000
C	-2.419243	0.679754	0.000000
H	1.235806	-2.502449	0.000000
H	-3.348453	-1.274023	0.000000
H	-1.192722	-2.495017	0.000000
C	1.280630	-1.411610	0.000000
H	-1.232178	2.473193	0.000000
H	-3.363482	1.218496	0.000000
C	2.477519	-0.752001	0.000000
H	1.115278	2.395904	0.000000
H	3.448894	1.480314	0.000000
H	3.387186	-1.348933	0.000000
B	2.484976	0.773205	0.000000
N	1.203039	1.383174	0.000000

Anthracenes (G3MP2)



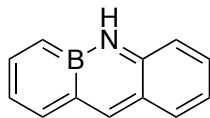
C	-4.501907	2.687774	0.473449
C	-5.457243	1.890391	-0.111302
C	-3.202549	2.180261	0.746824

C	-2.900829	0.818900	0.402641
C	-3.913275	0.025334	-0.200196
C	-5.160871	0.547077	-0.451391
H	-4.727549	3.720260	0.735572
H	-6.447614	2.290059	-0.315461
H	-3.686062	-1.007122	-0.461779
H	-5.925864	-0.072397	-0.913395
C	-2.202070	2.965575	1.342904
C	-0.930060	2.463304	1.608745
C	1.337624	2.805328	2.488385
C	0.088327	3.280097	2.221207
H	-2.425351	3.999963	1.606450
H	2.052286	3.482126	2.952152
H	-0.193235	4.306981	2.462571
H	0.771585	-0.354744	1.260794
H	2.726768	0.812588	2.305233
H	-1.386281	-0.720531	0.410541
C	-1.616778	0.313278	0.671440
C	-0.642606	1.106677	1.261281
N	0.628768	0.614840	1.530329
B	1.676794	1.355985	2.128018

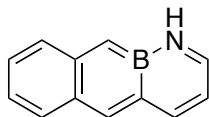


C	-4.515897	2.699887	0.472684
C	-5.479330	1.911997	-0.111696
C	-3.218413	2.184530	0.742845
C	-2.930622	0.820522	0.393111
C	-3.949970	0.034439	-0.209630
C	-5.193520	0.566762	-0.455983
H	-4.735516	3.733272	0.737134
H	-6.467296	2.319794	-0.312375
H	-3.727891	-0.998536	-0.473117
H	-5.965269	-0.044624	-0.917628
C	-2.214544	2.966276	1.338921
C	-0.947497	2.444547	1.596690
C	1.315740	2.754807	2.464418
C	0.079267	3.248428	2.207763
H	-2.437084	4.001197	1.602886
H	2.092360	3.358685	2.925253
H	-0.138513	4.280019	2.472263
H	1.119063	-0.579640	1.304652
H	2.600370	1.167158	2.378688
H	-1.430604	-0.726650	0.393543
C	-1.647192	0.308834	0.659667
C	-0.650270	1.082202	1.250668

B	0.752214	0.533533	1.545448
N	1.652422	1.444566	2.148805

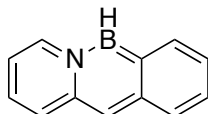


C	-4.507912	2.680750	0.469117
C	-5.477517	1.895980	-0.116335
C	-3.212256	2.172526	0.741005
C	-2.933886	0.819125	0.391531
C	-3.938580	0.030307	-0.207137
C	-5.188990	0.558613	-0.457131
H	-4.722501	3.714346	0.735346
H	-6.464410	2.304680	-0.316356
H	-3.715297	-1.002935	-0.470305
H	-5.953427	-0.061321	-0.919104
C	-2.211535	2.980494	1.344589
C	1.313010	2.751680	2.462464
C	0.079383	3.292361	2.222201
H	-2.478510	4.012496	1.592565
H	2.080011	3.370233	2.924845
H	-0.125097	4.329473	2.493004
H	1.127267	-0.493413	1.335714
H	2.671457	1.071980	2.371551
H	-1.557812	-0.667160	0.369994
B	-0.622780	1.043462	1.247265
C	0.776565	0.517148	1.548324
C	1.655963	1.390517	2.132287
C	-0.945203	2.496161	1.614399
N	-1.685933	0.304503	0.645179

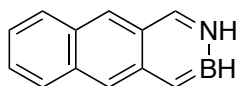


C	-4.491219	2.683909	0.475797
C	-5.464799	1.917042	-0.105125
C	-3.186323	2.160314	0.745783
C	-2.908173	0.775429	0.385897
C	-3.967518	0.020897	-0.220008
C	-5.200991	0.562667	-0.459863
H	-4.696049	3.719025	0.745829
H	-6.447310	2.341568	-0.298479
H	-3.764185	-1.014653	-0.490689
H	-5.982692	-0.036708	-0.920932
C	-2.219989	2.978423	1.341052
C	1.336880	2.755848	2.471909
C	0.074494	3.280382	2.216618
H	-2.490243	4.008899	1.587420

H	2.106149	3.367970	2.932950
H	-0.129548	4.318972	2.488056
H	1.060396	-0.319720	1.370027
H	2.645384	1.028817	2.348577
H	-1.533960	-0.844730	0.319842
B	-0.599851	1.048741	1.256755
C	1.658228	1.438067	2.148643
C	-0.929948	2.494712	1.619086
C	-1.655987	0.198653	0.620608
N	0.749264	0.627482	1.575258

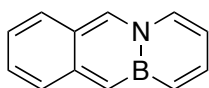


C	-4.497517	2.694723	0.477210
C	-5.476334	1.920467	-0.107900
C	-3.211008	2.153725	0.735267
C	-2.936928	0.797703	0.383468
C	-3.968488	0.033434	-0.216219
C	-5.213362	0.577776	-0.459091
N	-0.600722	1.117858	1.279106
B	-1.565226	0.235600	0.663418
H	-4.703985	3.729676	0.746634
H	-6.459216	2.345016	-0.301374
H	-3.764907	-1.001436	-0.486599
H	-5.995432	-0.020912	-0.920051
C	-2.195099	2.933851	1.334868
C	-0.929828	2.450636	1.604677
C	0.684828	0.651151	1.561198
C	1.634332	1.428662	2.137469
C	1.328266	2.782985	2.477896
C	0.081904	3.262683	2.213327
H	-2.402694	3.967880	1.603613
H	2.080180	3.416374	2.940039
H	-0.186613	4.287379	2.458395
H	0.856044	-0.381839	1.280476
H	2.615784	1.009341	2.332175
H	-1.211967	-0.880731	0.417007

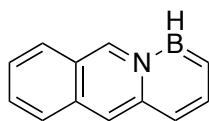


C	-4.505159	2.704197	0.477704
C	-5.458631	1.911719	-0.104795
C	-3.199479	2.191697	0.751643
C	-2.904226	0.821527	0.402312
C	-3.930170	0.032971	-0.203379
C	-5.170454	0.559246	-0.450646

H	-4.728039	3.737052	0.740884
H	-6.447930	2.315251	-0.307353
H	-3.706450	-0.999949	-0.466292
H	-5.941364	-0.052996	-0.912255
C	-2.208291	2.970584	1.342437
C	-0.927829	2.443655	1.603102
C	0.056101	3.242996	2.198169
H	-2.426052	4.006072	1.608231
H	1.928239	3.400880	2.883540
H	-0.145076	4.277638	2.469302
H	0.837548	-0.489153	1.239015
H	2.842203	1.105001	2.440131
H	-1.422743	-0.731408	0.394592
C	-1.636829	0.304188	0.661749
C	-0.612349	1.070431	1.259607
B	1.718444	1.393005	2.154226
C	0.671277	0.549872	1.523397
N	1.279265	2.747529	2.449690



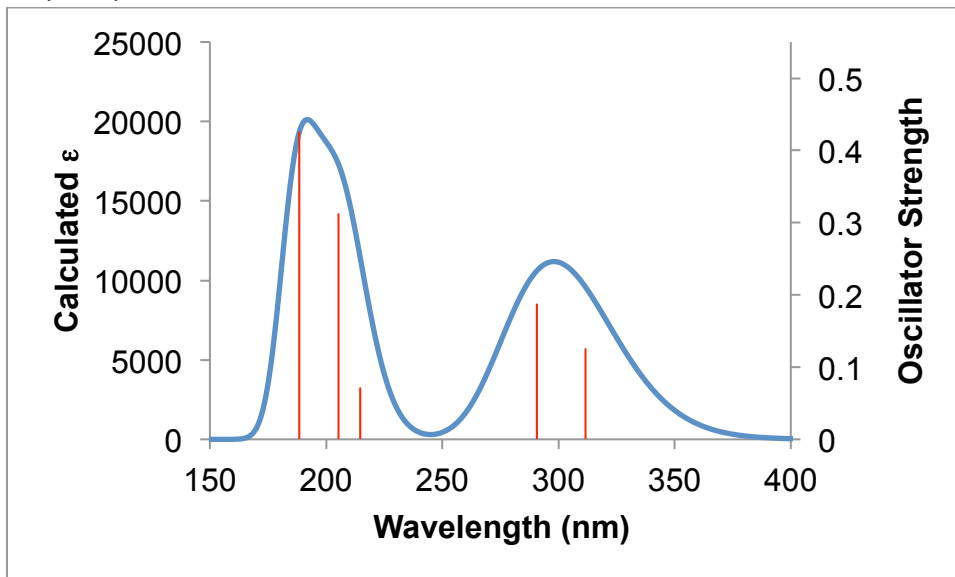
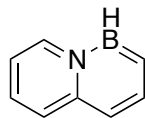
C	-4.457915	2.707000	0.494650
C	-5.453051	1.966136	-0.085046
C	-3.173598	2.129956	0.740143
C	-2.928544	0.755047	0.372317
C	-4.003996	0.027747	-0.230116
C	-5.224566	0.608968	-0.452664
H	-4.632877	3.744504	0.775580
H	-6.426419	2.414895	-0.267356
H	-3.829220	-1.009638	-0.511070
H	-6.026282	0.035601	-0.911983
C	-2.175655	2.895732	1.328955
C	1.268738	2.792117	2.460739
C	0.006775	3.228576	2.176721
H	-2.355987	3.933087	1.608021
H	1.951020	3.499778	2.923664
H	-0.321579	4.241215	2.397584
H	1.199562	-0.433435	1.379829
H	2.722715	1.193007	2.428569
H	-1.530119	-0.846393	0.320581
C	-1.672738	0.194856	0.613685
N	-0.932205	2.397009	1.586294
B	-0.579312	0.997217	1.246809
C	0.837256	0.572772	1.587091
C	1.700005	1.466252	2.172016



C	-4.527334	2.717420	0.474600
C	-5.466530	1.909770	-0.108141
C	-3.218427	2.219736	0.754298
C	-2.905807	0.856574	0.413088
C	-3.910001	0.039608	-0.194712
C	-5.151528	0.557474	-0.445032
N	-0.657209	1.135307	1.265495
H	-4.764301	3.748268	0.732479
H	-6.461236	2.294541	-0.318567
H	-3.671608	-0.990673	-0.451924
H	-5.913156	-0.065590	-0.907136
C	-2.220393	2.981759	1.342034
C	-0.936374	2.472444	1.609554
C	1.670559	1.422470	2.147498
C	1.331745	2.742704	2.465828
C	0.069063	3.250205	2.204922
H	-2.417657	4.017376	1.614910
H	2.062216	3.405871	2.930551
H	-0.183788	4.276841	2.456058
H	0.793659	-0.605329	1.185656
H	2.679842	1.089604	2.379917
C	-1.639626	0.374629	0.683493
H	-1.350300	-0.644808	0.447089
B	0.667016	0.536629	1.517323

TD-DFT Calculations CAM-B3LYP/6-311G(d,p):

The transition from orbital 34 -> 35 is the HOMO-LUMO transition in all cases.



Excitation energies and oscillator strengths:

Excited State 1: Singlet-A' 3.98 eV 311.65 nm f=0.1245 <S**2>=0.000

33 -> 36 0.10297

34 -> 35 0.68395

44 -> 36 0.10562

Excited State 2: Singlet-A' 4.26 eV 290.71 nm f=0.1874 <S**2>=0.000

33 -> 35 -0.16424

34 -> 36 0.67467

Excited State 3: Singlet-A' 5.77 eV 214.79 nm f=0.0720 <S**2>=0.000

33 -> 36 0.15821 34 -> 37 0.67357

Excited State 4: Singlet-A' 6.04 eV 205.34 nm f=0.3125 <S**2>=0.000

32 -> 36 -0.12640

33 -> 35 0.65043

34 -> 36 0.14655

Excited State 5: Singlet-A'' 6.26 eV 198.08 nm f=0.0000 <S**2>=0.000

34 -> 38 0.66011

34 -> 39 0.19838

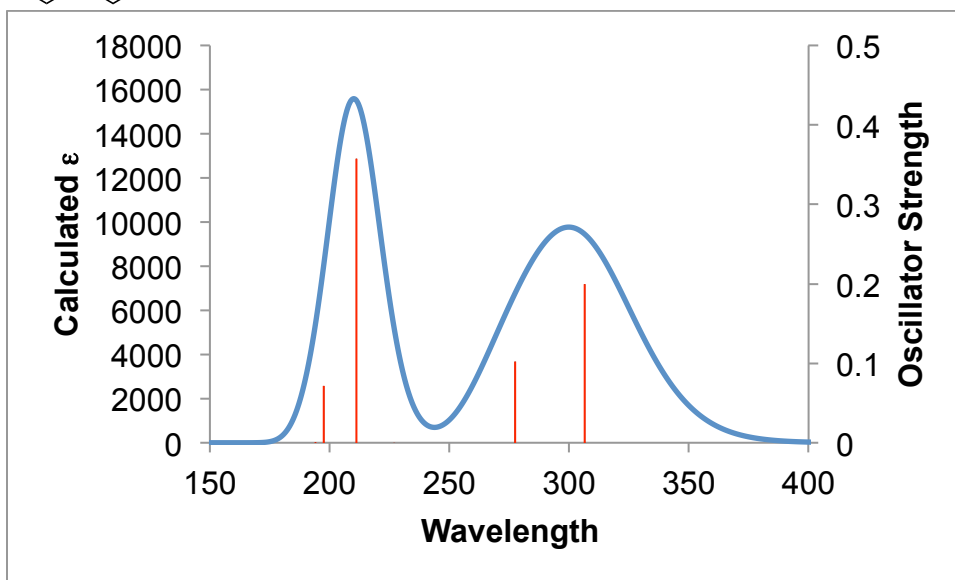
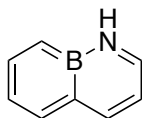
Excited State 6: Singlet-A' 6.58 eV 188.48 nm f=0.4260 <S**2>=0.000

32 -> 35 0.14423

33 -> 36 0.65667

34 -> 35 -0.11952

34 -> 37 -0.13527



Excitation energies and oscillator strengths:

Excited State 1: Singlet-A 4.05 eV 306.50 nm $f=0.1998$ $\langle S^2 \rangle=0.000$
 33 -> 36 -0.13576
 34 -> 35 0.68767

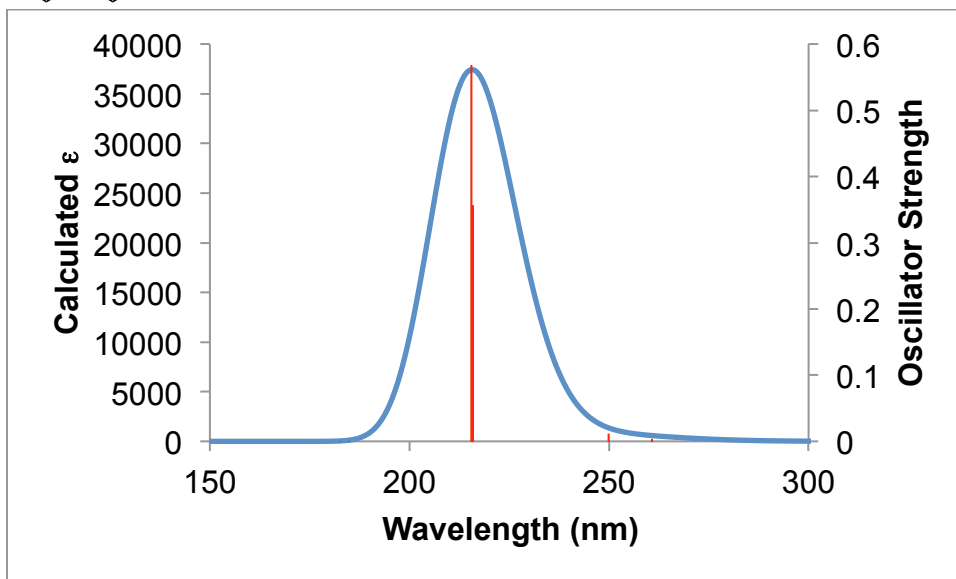
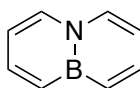
Excited State 2: Singlet-A 4.47 eV 277.55 nm $f=0.1022$ $\langle S^2 \rangle=0.000$
 33 -> 35 0.66647
 34 -> 36 0.21793

Excited State 3: Singlet-A 5.46 eV 226.96 nm $f=0.0000$ $\langle S^2 \rangle=0.000$
 32 -> 35 0.69643

Excited State 4: Singlet-A 5.87 eV 211.20 nm $f=0.3575$ $\langle S^2 \rangle=0.000$
 33 -> 35 -0.20388
 33 -> 38 -0.10946
 34 -> 36 0.64616

Excited State 5: Singlet-A 6.28 eV 197.54 nm $f=0.0712$ $\langle S^2 \rangle=0.000$
 31 -> 35 0.41535
 33 -> 36 0.46358
 34 -> 38 0.29151

Excited State 6: Singlet-A 6.39 eV 194.17 nm $f=0.0001$ $\langle S^2 \rangle=0.000$
 33 -> 37 0.28770
 34 -> 37 0.63198



Excitation energies and oscillator strengths:

Excited State 1: Singlet-B2 4.75 eV 260.77 nm $f=0.0036$ $\langle S^2 \rangle=0.000$
 33 -> 35 0.52107
 34 -> 36 0.46503

Excited State 2: Singlet-A1 4.96 eV 249.91 nm $f=0.0116$ $\langle S^2 \rangle=0.000$
 33 -> 36 -0.39761
 34 -> 35 0.58005

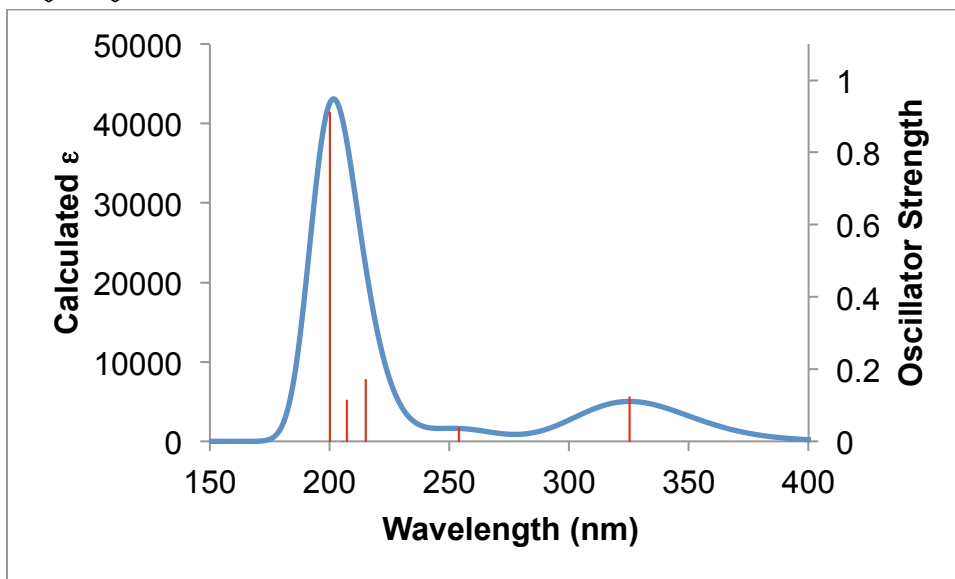
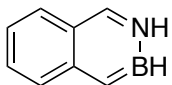
Excited State 3: Singlet-A1 5.74 eV 215.92 nm $f=0.3562$ $\langle S^2 \rangle=0.000$
 33 -> 36 0.56803
 34 -> 35 0.39854

Excited State 4: Singlet-B2 5.75 eV 215.52 nm $f=0.5679$ $\langle S^2 \rangle=0.000$
 33 -> 35 -0.46236
 34 -> 36 0.51827

Excited State 5: Singlet-B1 6.70 eV 184.95 nm $f=0.0000$ $\langle S^2 \rangle=0.000$
 30 -> 36 -0.19307
 31 -> 35 0.66280

Excited State 6: Singlet-A2 6.79 eV 182.59 nm $f=0.0000$ $\langle S^2 \rangle=0.000$
 30 -> 35 -0.39375
 31 -> 36 0.57202

As in naphthalene, the lowest energy transition does not correspond to the HOMO-LUMO gap. We have assigned, the 2nd-lowest energy transition (experimental optical gap: 4.13 eV) as the HOMO-LUMO transition.



Excitation energies and oscillator strengths:

Excited State 1: Singlet-A' 3.81 eV 325.25 nm $f=0.1241$ $\langle S^2 \rangle=0.000$
34 -> 35 0.69768

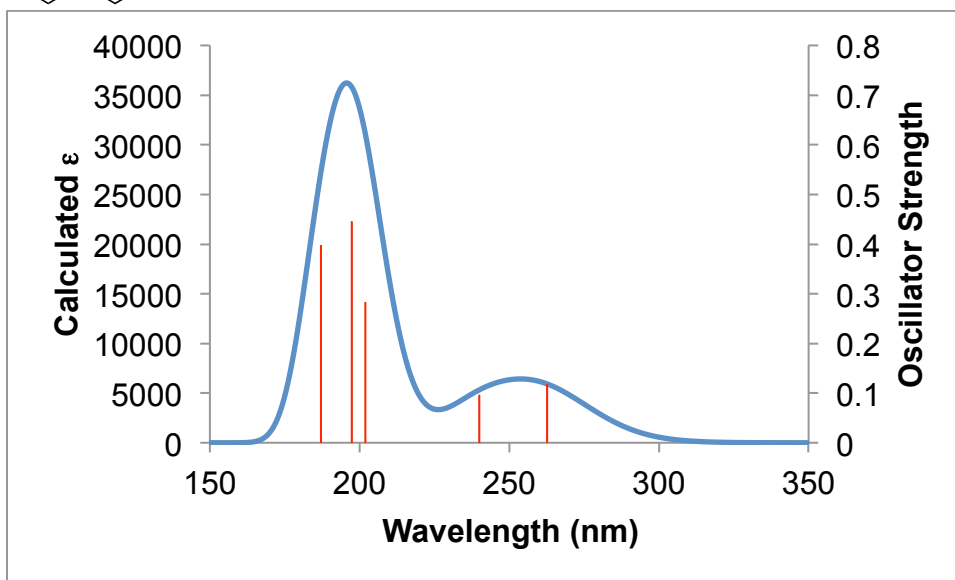
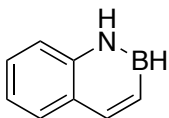
Excited State 2: Singlet-A' 4.88 eV 253.97 nm $f=0.0386$ $\langle S^2 \rangle=0.000$
33 -> 35 -0.40825
34 -> 36 0.56482

Excited State 3: Singlet-A' 5.76 eV 215.09 nm $f=0.1717$ $\langle S^2 \rangle=0.000$
32 -> 35 0.14574
33 -> 35 -0.32002
34 -> 36 -0.22934
34 -> 38 0.56153

Excited State 4: Singlet-A' 5.98 eV 207.19 nm $f=0.1145$ $\langle S^2 \rangle=0.000$
32 -> 35 0.53335
33 -> 35 -0.26617
34 -> 36 -0.12533
34 -> 38 -0.32723

Excited State 5: Singlet-A'' 6.03 eV 205.64 nm $f=0.0001$ $\langle S^2 \rangle=0.000$
33 -> 37 -0.10437
34 -> 37 0.69158

Excited State 6: Singlet-A' 6.20 eV 200.11 nm $f=0.9120$ $\langle S^2 \rangle=0.000$
32 -> 35 0.39725
33 -> 35 0.38084
33 -> 36 -0.10800
34 -> 36 0.31975
34 -> 38 0.26265



Excitation energies and oscillator strengths:

Excited State 1: Singlet-A' 4.72 eV 262.72 nm $f=0.1183$ $\langle S^2 \rangle=0.000$

33 -> 35 -0.12885

33 -> 36 0.27062

34 -> 35 0.62951

Excited State 2: Singlet-A' 5.17 eV 240.01 nm $f=0.0966$ $\langle S^2 \rangle=0.000$

33 -> 35 0.62099

34 -> 35 0.13368

34 -> 36 -0.28925

Excited State 3: Singlet-A' 6.14 eV 201.98 nm $f=0.2834$ $\langle S^2 \rangle=0.000$

29 -> 35 0.10008 32 -> 36 0.11860

33 -> 36 -0.42392 34 -> 35 0.21714

34 -> 37 0.48297

Excited State 4: Singlet-A' 6.28 eV 197.39 nm $f=0.4456$ $\langle S^2 \rangle=0.000$

33 -> 35 0.29134

33 -> 37 0.17274

34 -> 36 0.61147

Excited State 5: Singlet-A'' 6.50 eV 190.65 nm $f=0.0004$ $\langle S^2 \rangle=0.000$

31 -> 35 0.66779

31 -> 37 0.19733

Excited State 6: Singlet-A' 6.63 eV 187.10 nm $f=0.3981$ $\langle S^2 \rangle=0.000$

32 -> 35 -0.13292

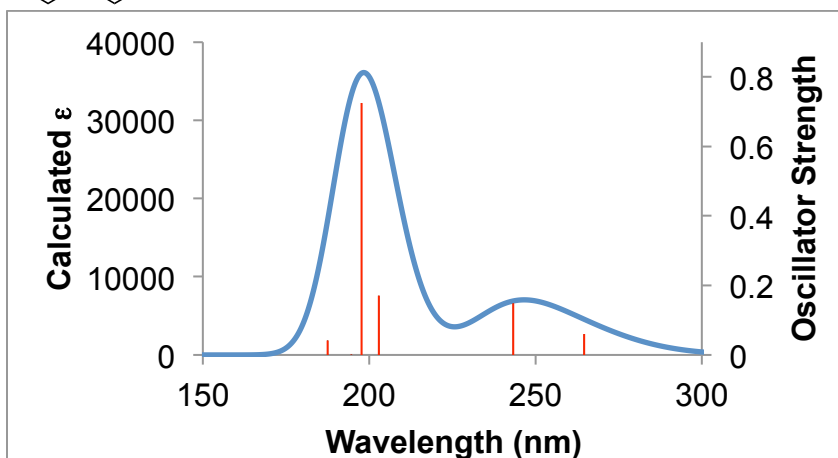
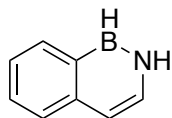
32 -> 36 0.10142

33 -> 36 0.46859

33 -> 37 -0.10541

34 -> 35 -0.15554

34 -> 37 0.45284



Excitation energies and oscillator strengths:

Excited State 1: Singlet-A' 4.69 eV 264.63 nm $f=0.0605$ $\langle S^2 \rangle=0.000$

33 -> 36 0.25569

34 -> 35 0.63495

34 -> 36 0.12051

Excited State 2: Singlet-A' 5.09 eV 243.35 nm $f=0.1489$ $\langle S^2 \rangle=0.000$

33 -> 35 -0.27872

34 -> 35 -0.14496

34 -> 36 0.62357

Excited State 3: Singlet-A' 6.11 eV 202.95 nm $f=0.1702$ $\langle S^2 \rangle=0.000$

32 -> 35 0.30401

32 -> 36 0.11993

33 -> 36 0.50827

33 -> 38 0.10528

34 -> 35 -0.24129

34 -> 38 -0.22598

Excited State 4: Singlet-A' 6.27 eV 197.73 nm $f=0.7248$ $\langle S^2 \rangle=0.000$

32 -> 35 0.11085

32 -> 36 -0.12743

33 -> 35 0.62312

34 -> 36 0.26868

Excited State 5: Singlet-A'' 6.37 eV 194.63 nm $f=0.0003$ $\langle S^2 \rangle=0.000$

32 -> 37 -0.18024

34 -> 37 0.67529

Excited State 6: Singlet-A' 6.61 eV 187.59 nm $f=0.0408$ $\langle S^2 \rangle=0.000$

32 -> 35 -0.12338

32 -> 36 -0.11331

33 -> 36 0.31379

34 -> 35 -0.10327

34 -> 38 0.59006

Photoelectron Spectroscopy

These spectra were taken in much the same manner as those of the BN anthracenes.

Figure 1.30. Full UV-PE spectra for the investigated compounds

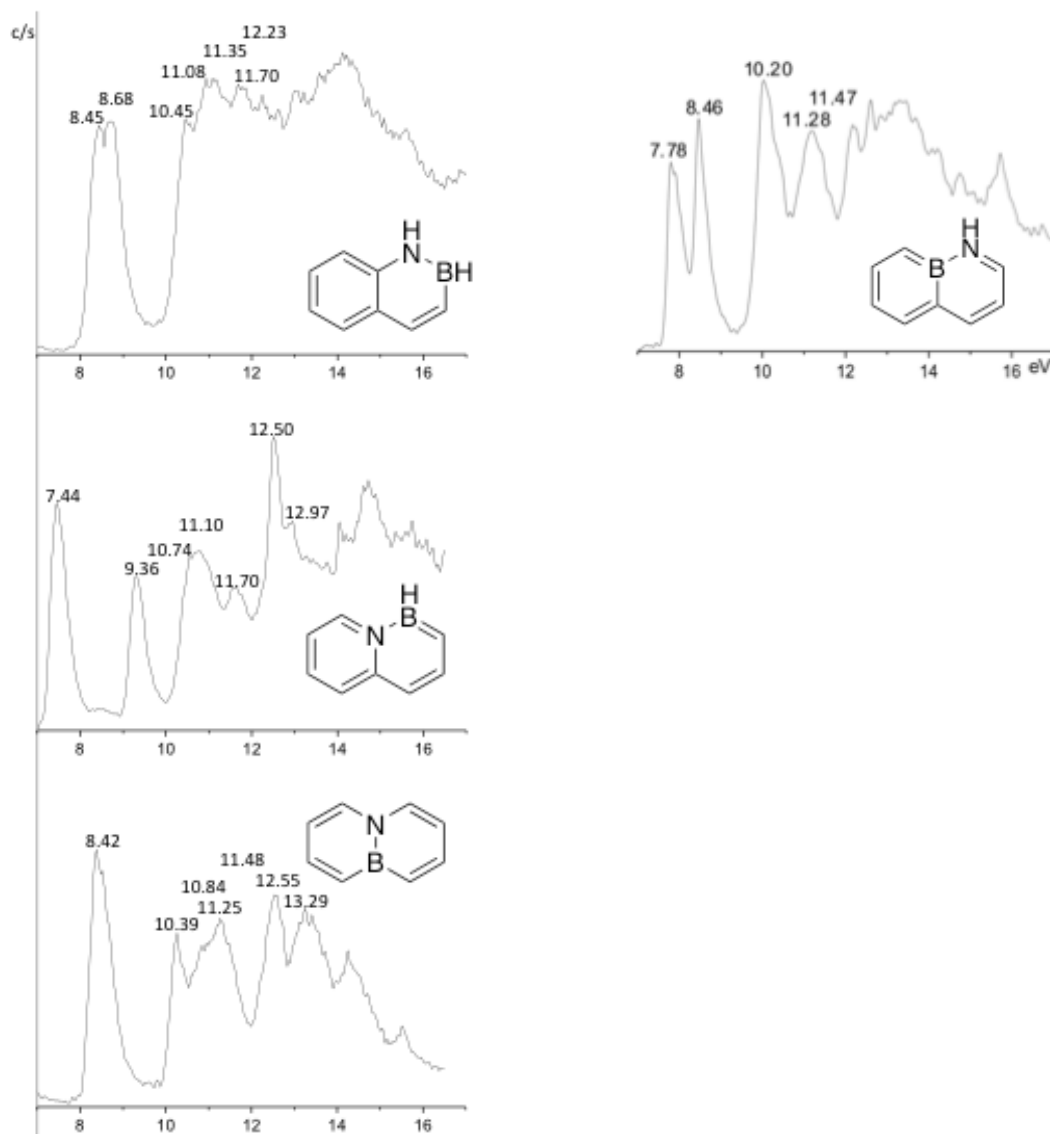


Table 1.7. Calculated Kohn-Sham energies of MO ($-\epsilon^{K-S}$), Δ SCF+TD-DFT (CAM-B3LYP), OVGF, P3, SAC-CI and “corrected” ionization energies with the Molekel MOs visualization of **BN-9,1-Naph** in comparison with experimental values (in eV). For all calculations 6-311G(d,p) basis set was applied.

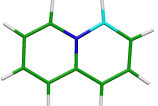
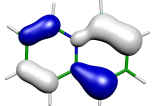
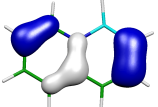
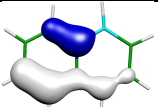
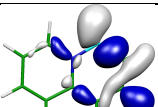
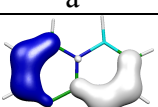
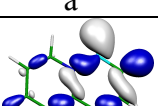
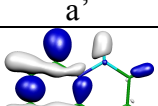
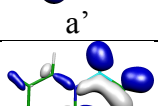
 Nature of MO	$-\epsilon^{K-S}$	Δ SCF+ TD- DFT	OVGF	P3	SAC-CI	Corrected $x_{exp.}=0.71$ 0	Exp.
 a''	6.73	7.34	7.18	7.31	6.78	7.44	7.44
 a''	8.81	9.45	9.16	9.34	8.92	9.52	9.36
 a''	10.30	10.70	10.62	10.75	10.45	11.01	10.74
 a'	10.32	10.96	11.06	11.04	10.73	11.03	11.10
 a''	10.82	11.06	11.11	11.13	10.94	11.53	11.10
 a'	10.96	11.61	11.77	11.78	11.44	11.67	11.70
 a'	12.02	12.72	12.78	12.85	12.58	12.73	12.50
 a'	12.37	12.96	13.20	13.15	12.90	13.08	12.97

Table 1.8. Calculated Kohn-Sham energies of MO ($-\epsilon^{K-S}$), Δ SCF+TD-DFT (CAM-B3LYP), OVGf, P3, SAC-CI and “corrected” ionization energies with the Molekel MOs visualization of **BN-9,10-Naph** in comparison with experimental values (in eV). For all calculations 6-311G(d,p) basis set was applied.

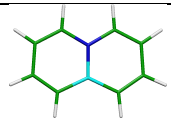
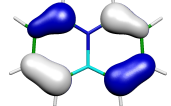
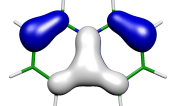
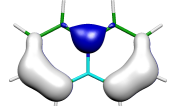
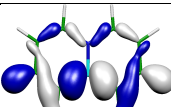
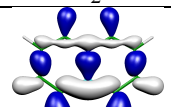
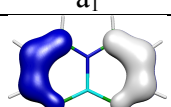
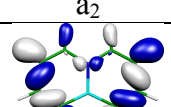
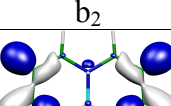
 Nature of MO	$-\epsilon^{K-S}$	Δ SCF+ TD-DFT	OVGF	P3	SAC-CI	Corrected $x_{exp.}=0.847$	Exp.
 a ₂	7.57	8.26	8.17	8.26	7.94	8.42	8.42
 b ₁	7.75	8.33	8.25	8.34	7.97	8.42	8.42
 b ₁	9.72	10.40	10.13	10.23	10.03	10.57	10.39
 b ₂	10.23	10.88	10.81	10.90	10.82	11.08	10.84
 a ₁	10.55	11.23	11.28	11.31	11.11	11.40	11.25
 a ₂	10.88	11.38	11.29	11.30	11.22	11.72	11.48
 b ₂	11.80	12.55	12.59	12.60	12.59	12.64	12.55
 a ₁	12.61	13.36	13.50	13.48	13.48	13.46	13.29

Table 1.9. Calculated Kohn-Sham energies of MO ($-\epsilon^{K-S}$), Δ SCF+TD-DFT (CAM-B3LYP), OVGf, P3, SAC-CI and “corrected” ionization energies with the Molekel MOs visualization of **BN-1,9-Naph** in comparison with experimental values (in eV). For all calculations 6-311G(d,p) basis set was applied.

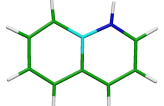
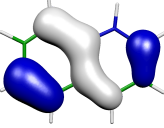
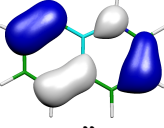
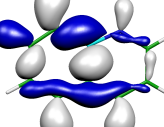
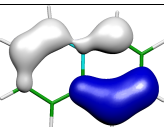
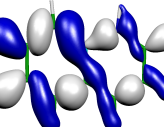
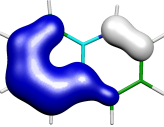
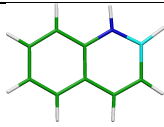
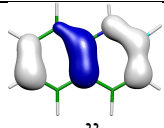
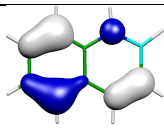
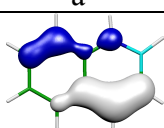
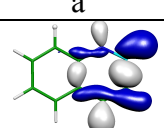
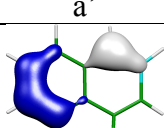
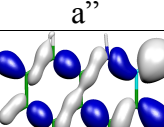
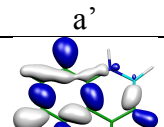
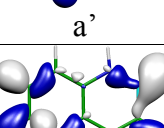
 Nature of MO	$-\epsilon^{K-S}$	Δ SCF+TD-DFT	OVGF	P3	SAC-CI	Corrected $x_{exp}=0.679$	Exp.
 a''	7.10	7.71	7.60	7.74	7.22	7.78	7.78
 a''	7.73	8.45	8.11	8.31	7.89	8.41	8.46
 a'	9.58	10.21	10.16	10.23	9.88	10.26	10.20
 a''	9.72	10.21	10.05	10.14	9.87	10.40	10.20
 a'	10.63	11.26	11.26	11.36	11.00	11.31	11.28
 a''	10.91	11.50	11.23	11.22	11.01	11.59	11.47

Table 1.10. Calculated Kohn-Sham energies of MO ($-\epsilon^{K-S}$), Δ SCF+TD-DFT (CAM-B3LYP), OVGF, P3, SAC-CI and “corrected” ionization energies with the Molekel MOs visualization of **BN-1,2-Naph** in comparison with experimental values (in eV). For all calculations 6-311G(d,p) basis set was applied.

 Nature of MO	$-\epsilon^{K-S}$	Δ SCF+ TD-DFT	OVGF	P3	SAC-CI	Corrected $x_{exp}=0.749$	Exp.
 a''	7.70	8.32	8.16	8.04	7.79	8.45	8.45
 a''	7.96	8.67	8.47	8.57	8.164	8.71	8.68
 a''	10.05	10.65	10.46	10.57	10.28	10.74	10.45
 a'	10.32	11.04	11.06	11.07	10.84	11.07	11.08
 a''	10.97	11.35	11.31	11.27	11.14	11.72	11.35
 a'	10.97	11.69	11.78	11.84	11.54	11.72	11.70
 a'	11.55	12.28	12.28	12.36	12.07	12.30	12.23
 a'	12.35	13.08	13.33	13.27	13.11	13.10	13.00

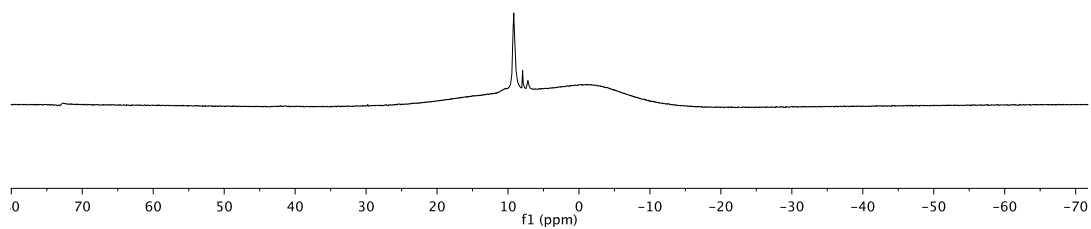
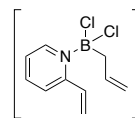
Crystal data and structure refinement for BN-9,1-Naph.

Identification code	C8H8BN	
Empirical formula	C8 H8 B N	
Formula weight	128.96	
Temperature	100(2) K	
Wavelength	0.71073 Å	
Crystal system	Monoclinic	
Space group	P2 ₁ /c	
Unit cell dimensions	a = 7.850(2) Å	$\alpha = 90^\circ$
	b = 6.0119(16) Å	$\beta = 112.370(4)^\circ$
	c = 7.995(2) Å	$\gamma = 90^\circ$
Volume	348.89(16) Å ³	
Z	2	
Density (calculated)	1.228 Mg/m ³	
Absorption coefficient	0.071 mm ⁻¹	
F(000)	136	
Crystal size	0.510 x 0.320 x 0.260 mm ³	
Theta range for data collection	2.806 to 28.674°	
Index ranges	-10 ≤ h ≤ 10, -8 ≤ k ≤ 7, -10 ≤ l ≤ 9	
Reflections collected	5412	
Independent reflections	902 [R(int) = 0.0179]	
Completeness to theta = 25.242°	100.0 %	
Absorption correction	Semi-empirical from equivalents	
Max. and min. transmission	0.7457 and 0.7082	
Refinement method	Full-matrix least-squares on F ²	
Data / restraints / parameters	902 / 0 / 62	
Goodness-of-fit on F ²	1.062	
Final R indices [I > 2σ(I)]	R1 = 0.0380, wR2 = 0.1058	
R indices (all data)	R1 = 0.0395, wR2 = 0.1079	
Extinction coefficient	na	
Largest diff. peak and hole	0.335 and -0.211 e.Å ⁻³	

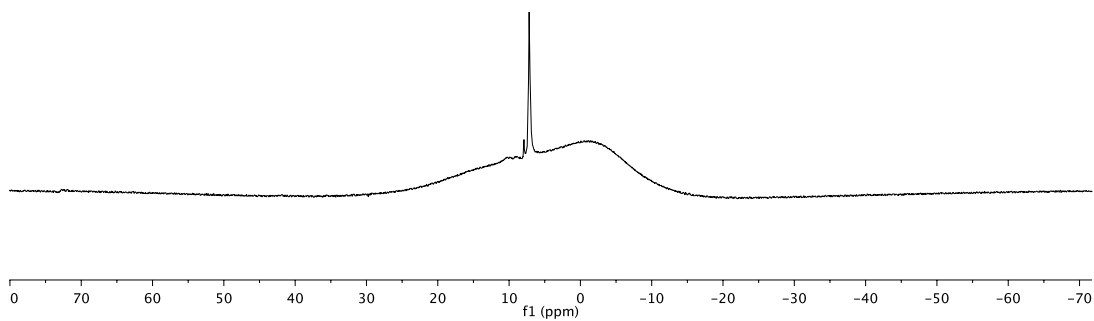
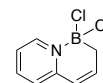
Crystal data and structure refinement for 7F-BN-9,1-Naph.

Identification code	C8H7BFN	
Empirical formula	C8 H7 B F N	
Formula weight	146.96	
Temperature	100(2) K	
Wavelength	0.71073 Å	
Crystal system	Monoclinic	
Space group	Pc	
Unit cell dimensions	a = 7.465(3) Å	$\alpha = 90^\circ$
	b = 14.687(6) Å	$\beta = 103.790(7)^\circ$
	c = 6.709(3) Å	$\gamma = 90^\circ$
Volume	714.4(5) Å ³	
Z	4	
Density (calculated)	1.366 Mg/m ³	
Absorption coefficient	0.097 mm ⁻¹	
F(000)	304	
Crystal size	0.600 x 0.380 x 0.320 mm ³	
Theta range for data collection	2.774 to 28.431°	
Index ranges	-10 ≤ h ≤ 8, -19 ≤ k ≤ 14, -8 ≤ l ≤ 6	
Reflections collected	3916	
Independent reflections	2294 [R(int) = 0.0217]	
Completeness to theta = 25.242°	98.5 %	
Absorption correction	Semi-empirical from equivalents	
Max. and min. transmission	0.7457 and 0.6999	
Refinement method	Full-matrix least-squares on F ²	
Data / restraints / parameters	2294 / 2 / 205	
Goodness-of-fit on F ²	1.066	
Final R indices [I > 2sigma(I)]	R1 = 0.0403, wR2 = 0.1094	
R indices (all data)	R1 = 0.0468, wR2 = 0.1176	
Extinction coefficient	na	
Largest diff. peak and hole	0.246 and -0.218 e.Å ⁻³	

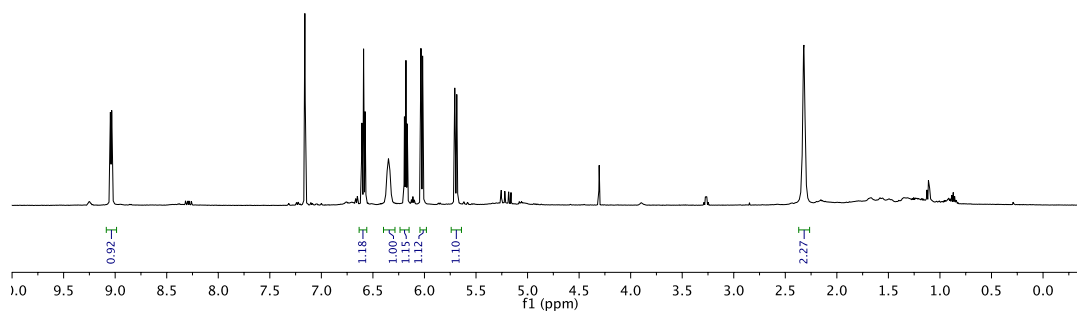
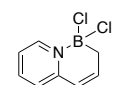
Parameter	Value
1 Solvent	cd2cl2
2 Temperature	25.0
3 Relaxation Delay	0.1000
4 Acquisition Date	2015-07-22T15:48:25
5 Spectrometer Frequency	192.41
6 Nucleus	11B



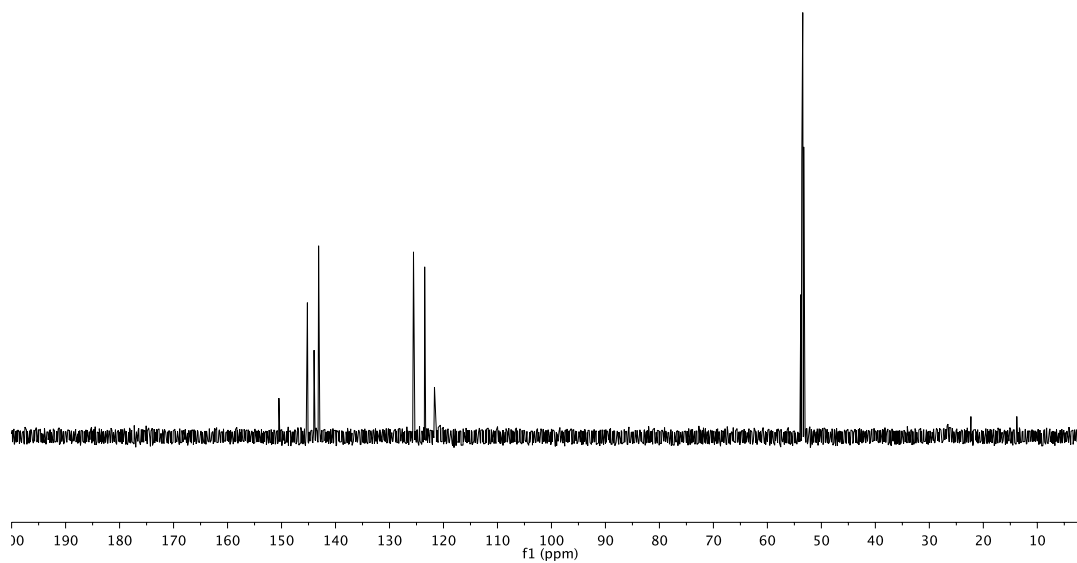
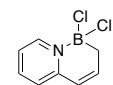
Parameter	Value
1 Solvent	cd2cl2
2 Temperature	25.0
3 Relaxation Delay	0.1000
4 Acquisition Date	2015-07-22T15:50:58
5 Spectrometer Frequency	192.41
6 Nucleus	11B



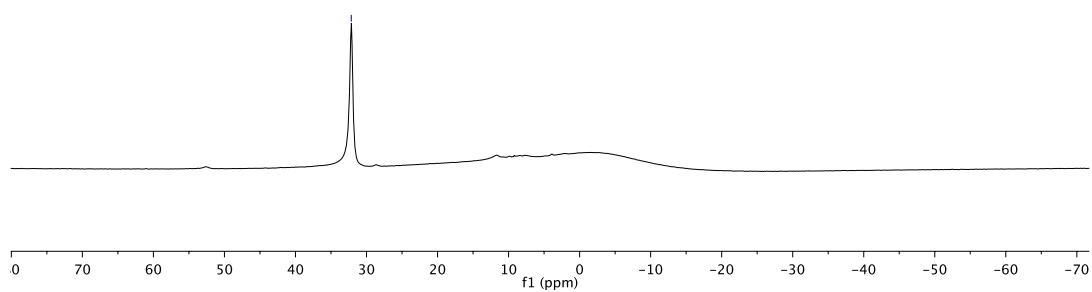
Parameter	Value
1 Solvent	c6d6
2 Temperature	25.0
3 Relaxation Delay	1.0000
4 Acquisition Date	2015-03-27T16:53:52
5 Spectrometer Frequency	499.88
6 Nucleus	¹ H



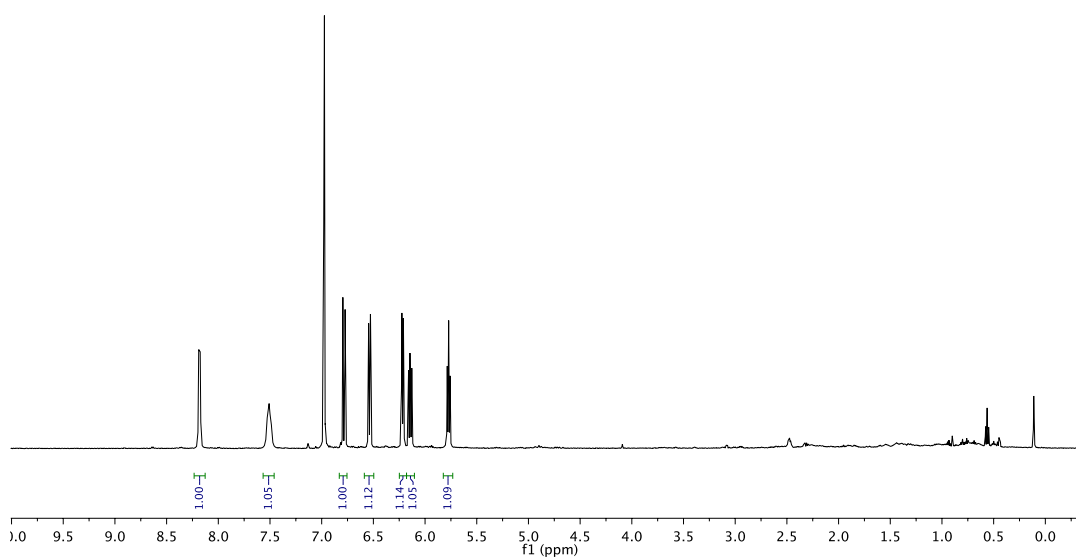
Parameter	Value
1 Solvent	cd2cl2
2 Temperature	25.0
3 Relaxation Delay	1.0000
4 Acquisition Date	2015-11-02T14:37:06
5 Spectrometer Frequency	150.81
6 Nucleus	¹³ C

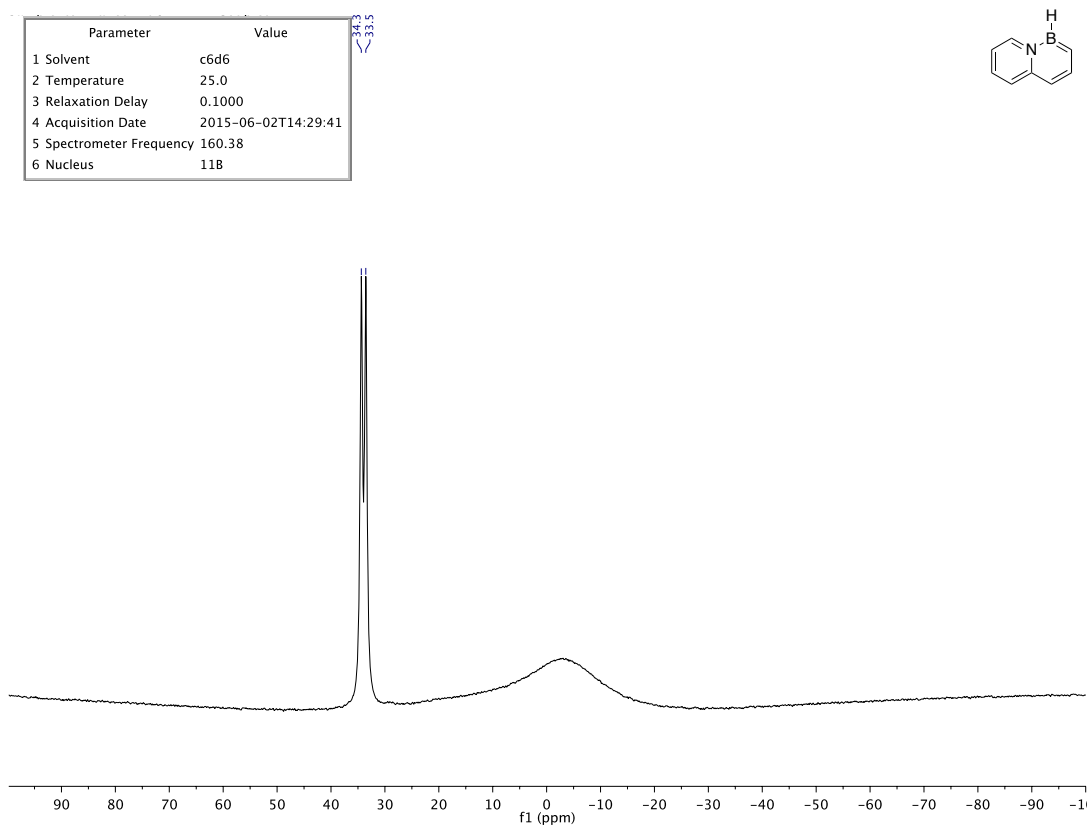
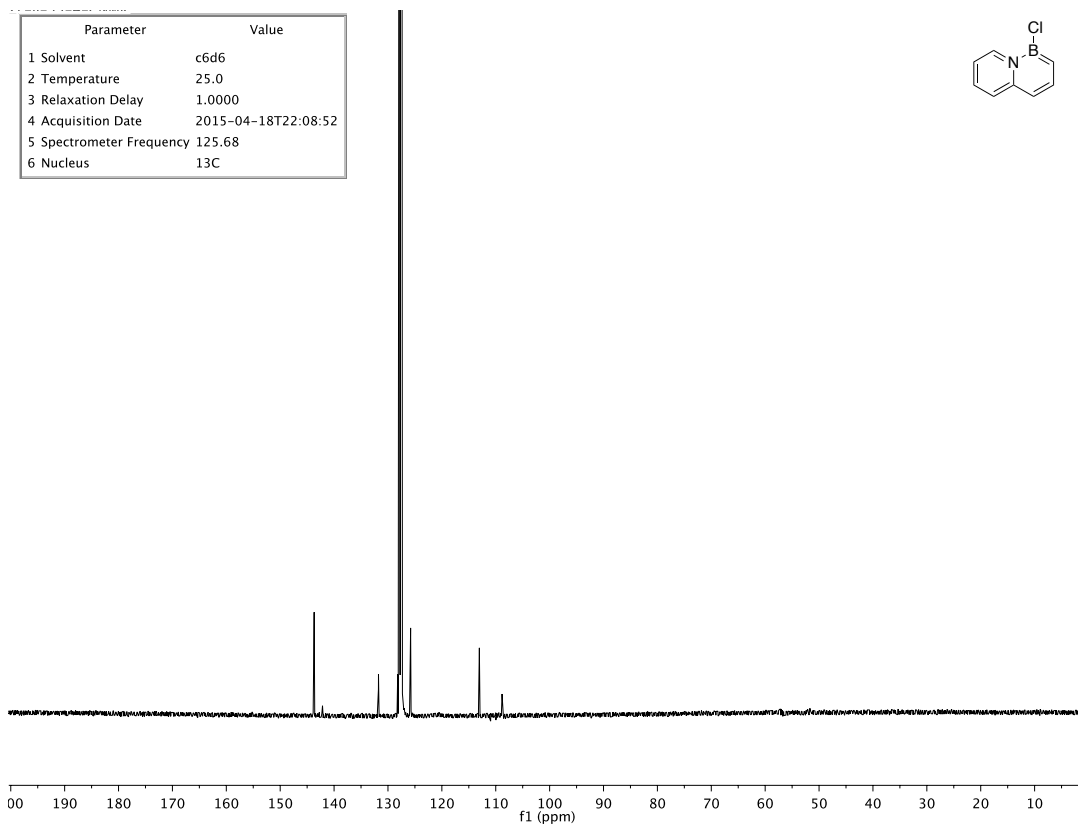


Parameter	Value
1 Solvent	cd2cl2
2 Temperature	25.0
3 Relaxation Delay	0.1000
4 Acquisition Date	2015-07-23T11:38:11
5 Spectrometer Frequency	160.38
6 Nucleus	11B

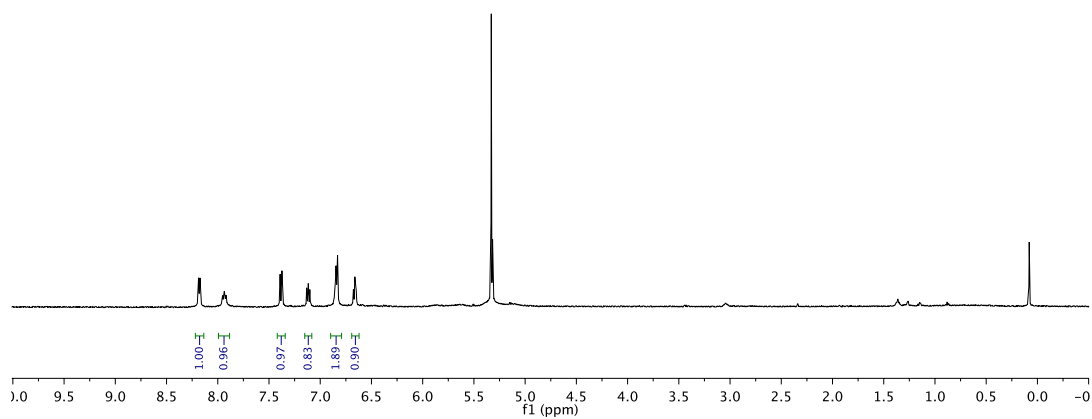


Parameter	Value
1 Solvent	c6d6
2 Temperature	25.0
3 Relaxation Delay	1.0000
4 Acquisition Date	2015-04-18T19:42:16
5 Spectrometer Frequency	499.88
6 Nucleus	1H

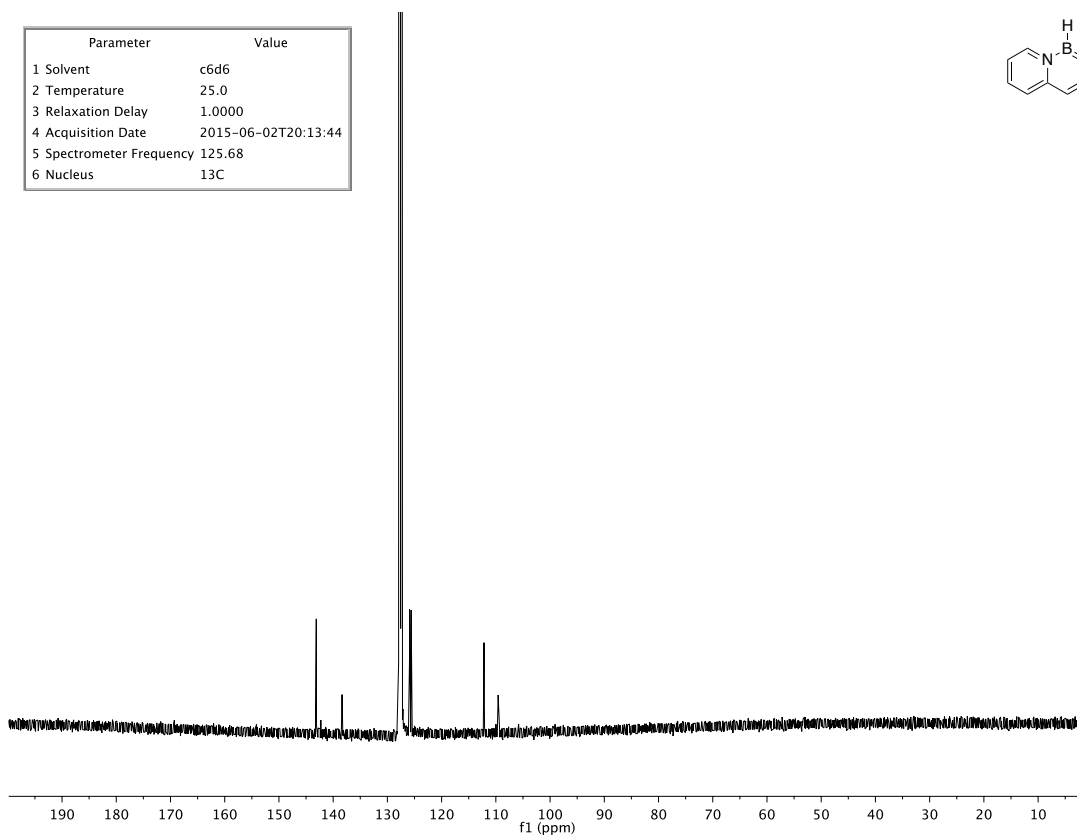




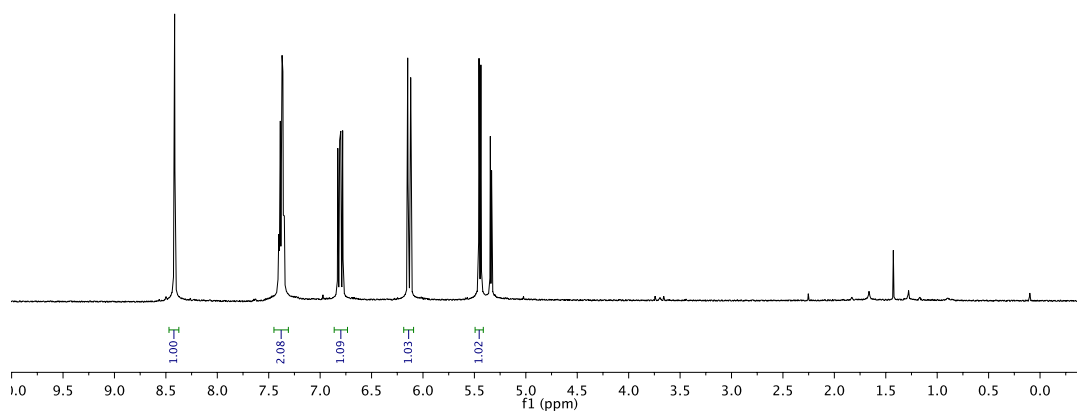
Parameter	Value
1 Solvent	cd2cl2
2 Temperature	25.0
3 Relaxation Delay	1.0000
4 Acquisition Date	2016-01-13T14:06:07
5 Spectrometer Frequency	499.88
6 Nucleus	¹ H



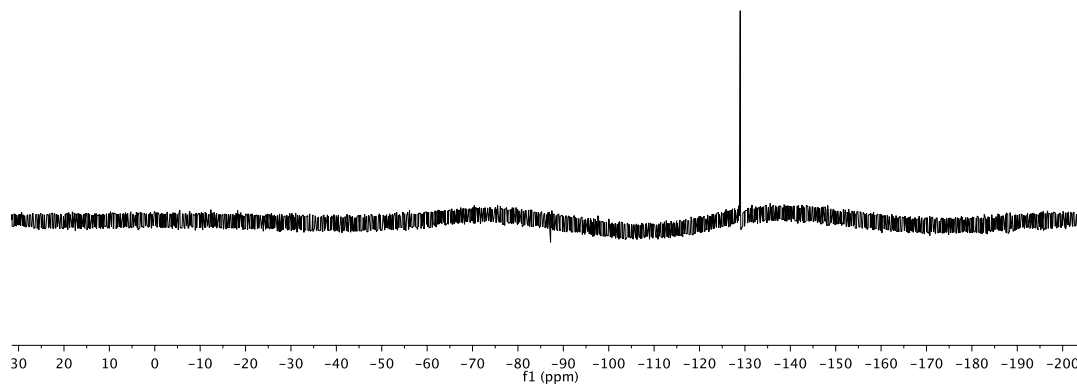
Parameter	Value
1 Solvent	c6d6
2 Temperature	25.0
3 Relaxation Delay	1.0000
4 Acquisition Date	2015-06-02T20:13:44
5 Spectrometer Frequency	125.68
6 Nucleus	¹³ C



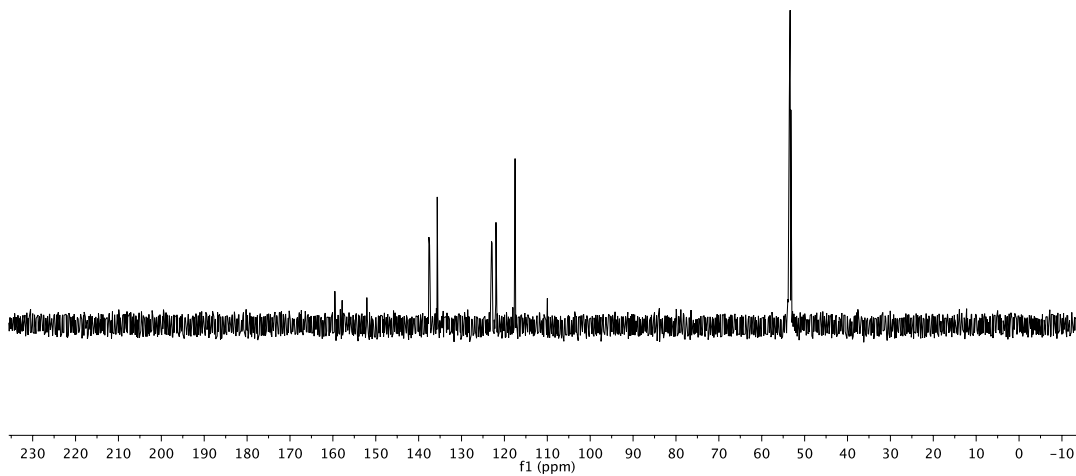
Parameter	Value
1 Solvent	cd2cl2
2 Temperature	25.0
3 Relaxation Delay	1.0000
4 Acquisition Date	2016-02-19T14:04:04
5 Spectrometer Frequency	599.69
6 Nucleus	¹ H



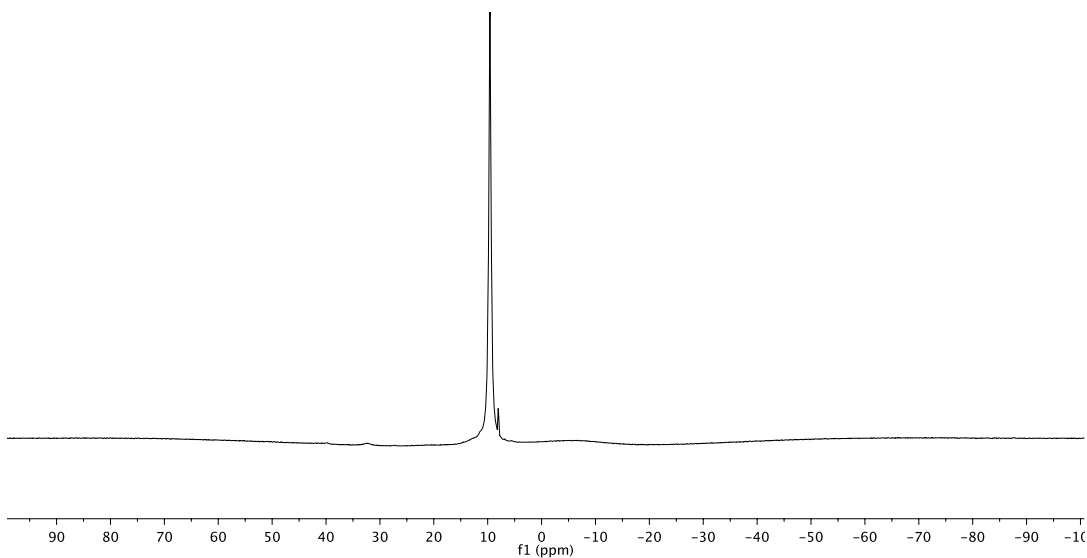
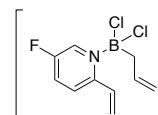
Parameter	Value
1 Solvent	cd2cl2
2 Temperature	25.0
3 Relaxation Delay	1.0000
4 Acquisition Date	2016-02-18T11:56:53
5 Spectrometer Frequency	376.12
6 Nucleus	¹⁹ F



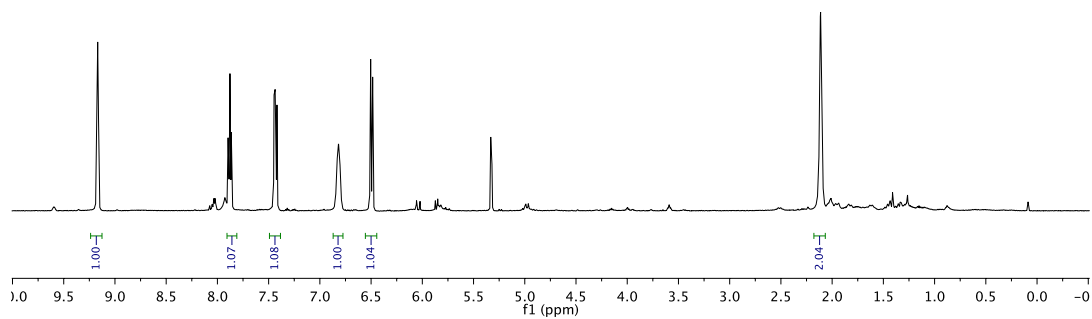
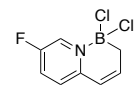
Parameter	Value
1 Solvent	cd2cl2
2 Temperature	25.0
3 Relaxation Delay	1.0000
4 Acquisition Date	2016-02-19T14:06:09
5 Spectrometer Frequency	150.81
6 Nucleus	¹³ C



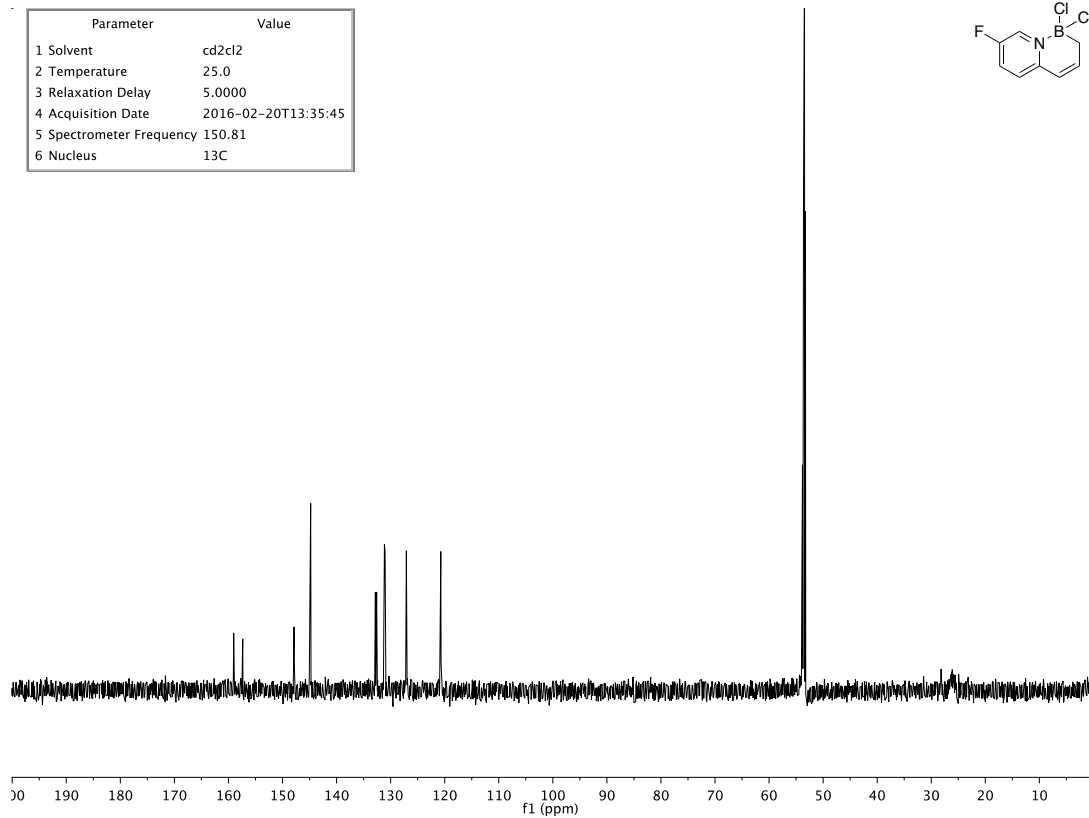
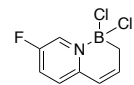
Parameter	Value
1 Solvent	cd2cl2
2 Temperature	25.0
3 Relaxation Delay	0.0100
4 Acquisition Date	2016-02-19T17:01:05
5 Spectrometer Frequency	160.35
6 Nucleus	¹¹ B



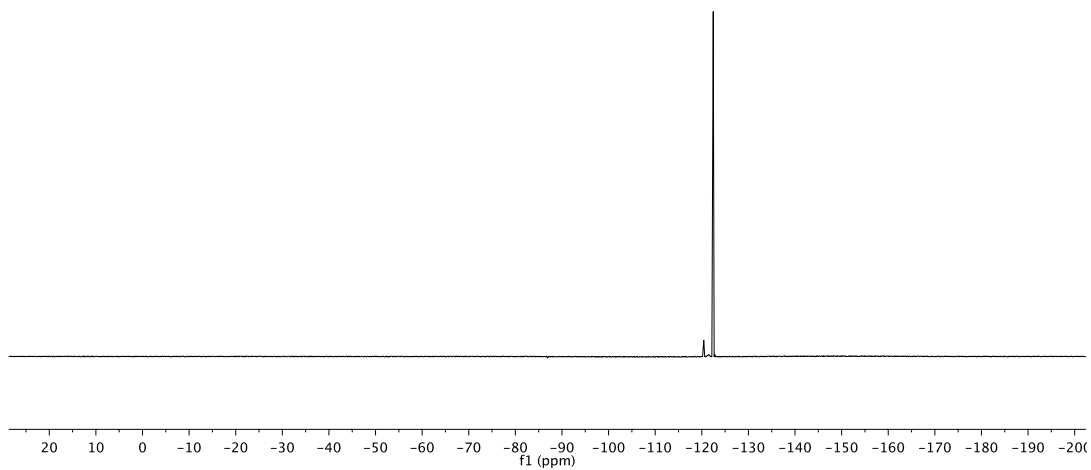
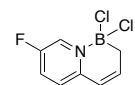
Parameter	Value
1 Solvent	cd2cl2
2 Temperature	25.0
3 Relaxation Delay	1.0000
4 Acquisition Date	2016-02-20T12:49:45
5 Spectrometer Frequency	499.89
6 Nucleus	¹ H



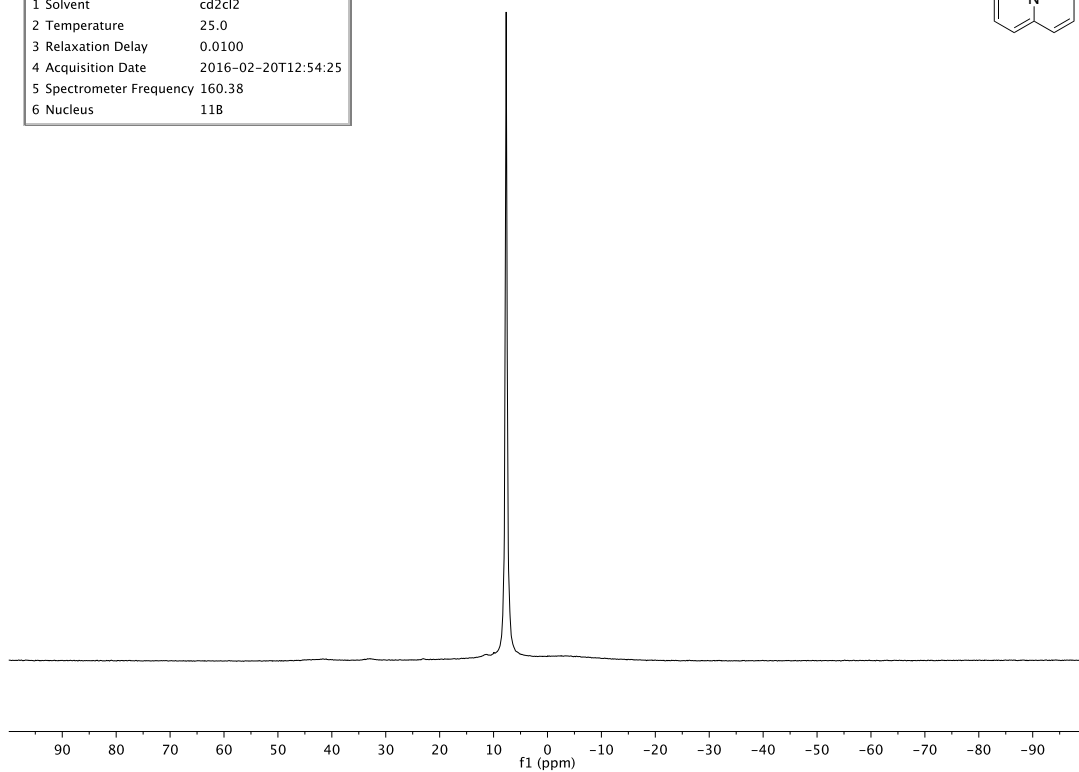
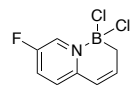
Parameter	Value
1 Solvent	cd2cl2
2 Temperature	25.0
3 Relaxation Delay	5.0000
4 Acquisition Date	2016-02-20T13:35:45
5 Spectrometer Frequency	150.81
6 Nucleus	¹³ C



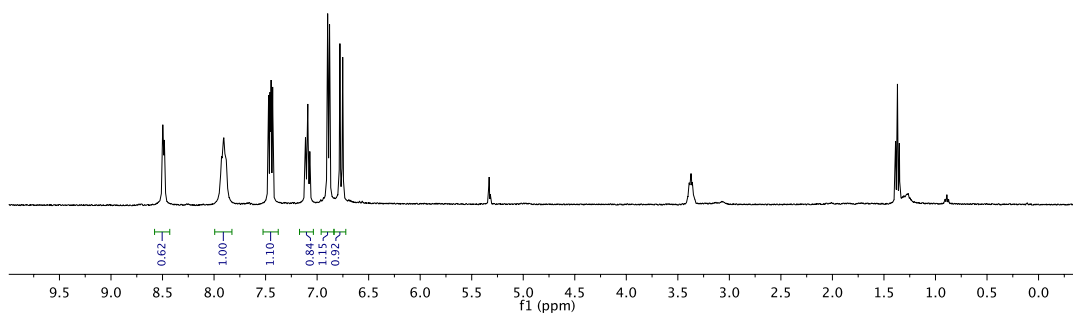
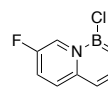
Parameter	Value
1 Solvent	cd2cl2
2 Temperature	25.0
3 Relaxation Delay	1.0000
4 Acquisition Date	2016-02-20T12:52:08
5 Spectrometer Frequency	470.32
6 Nucleus	¹⁹ F



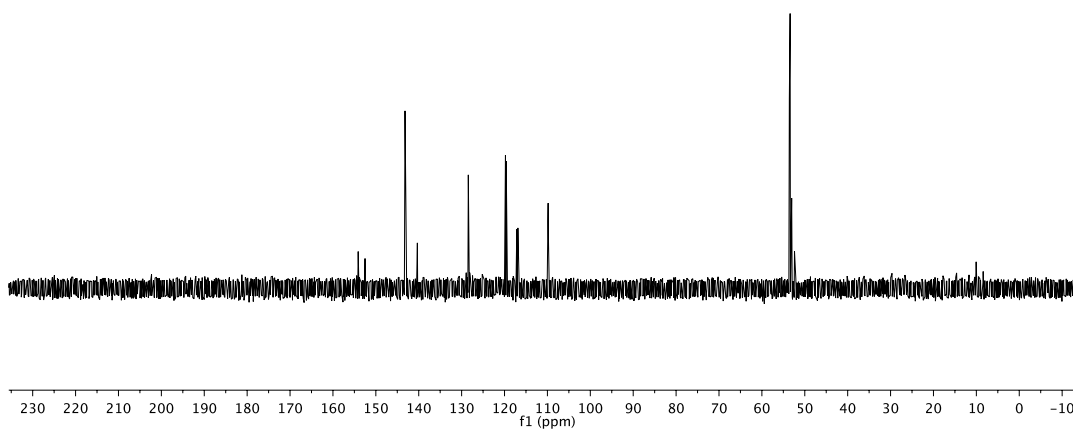
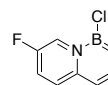
Parameter	Value
1 Solvent	cd2cl2
2 Temperature	25.0
3 Relaxation Delay	0.0100
4 Acquisition Date	2016-02-20T12:54:25
5 Spectrometer Frequency	160.38
6 Nucleus	¹¹ B



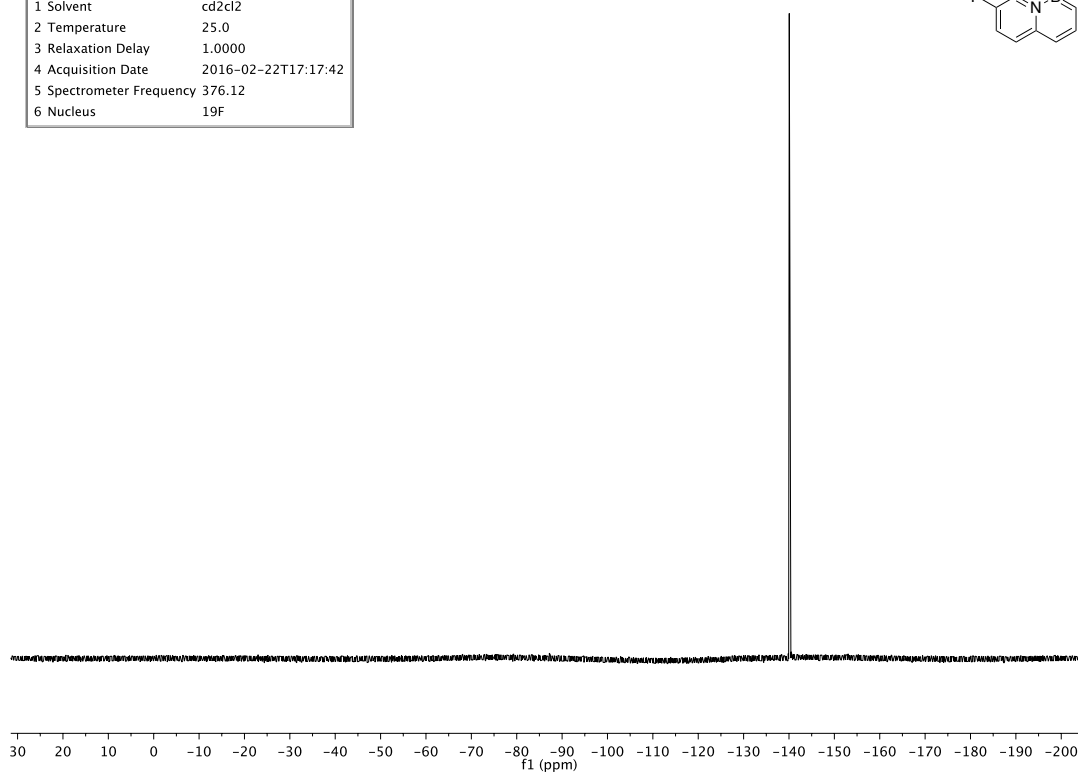
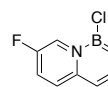
Parameter	Value
1 Solvent	cd2cl2
2 Temperature	25.0
3 Relaxation Delay	1.0000
4 Acquisition Date	2016-02-23T10:10:48
5 Spectrometer Frequency	399.77
6 Nucleus	¹ H



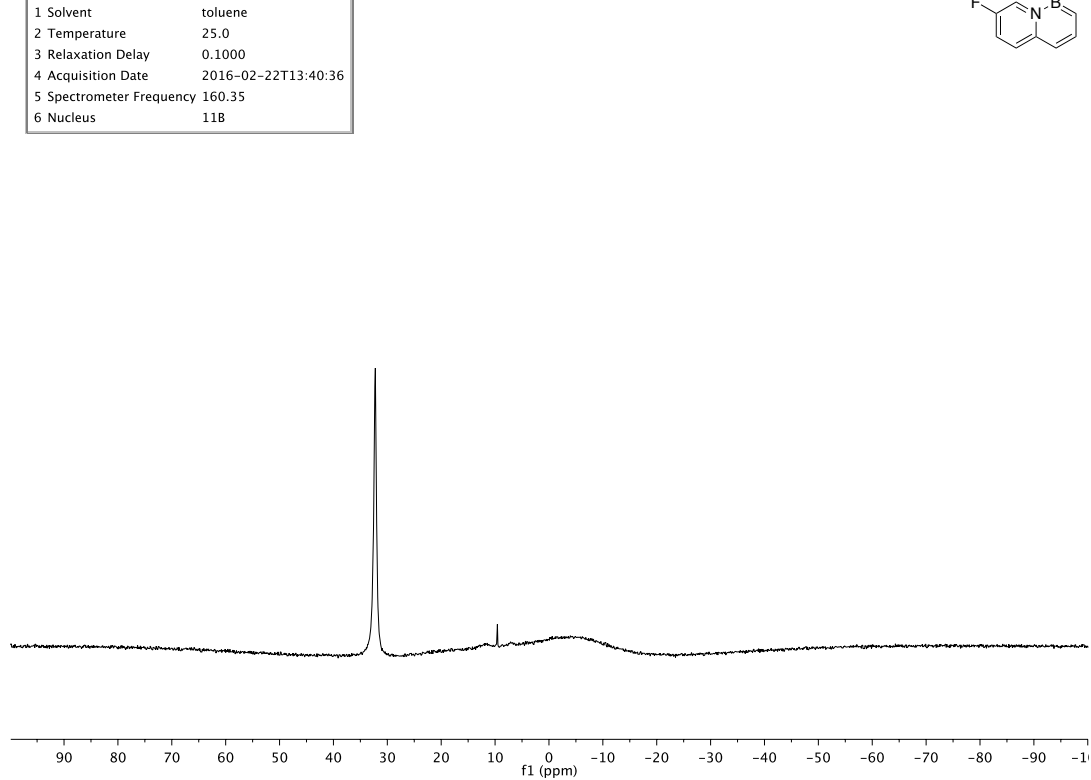
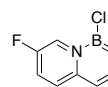
Parameter	Value
1 Solvent	cd2cl2
2 Temperature	25.0
3 Relaxation Delay	1.0000
4 Acquisition Date	2016-02-22T17:25:58
5 Spectrometer Frequency	150.81
6 Nucleus	¹³ C



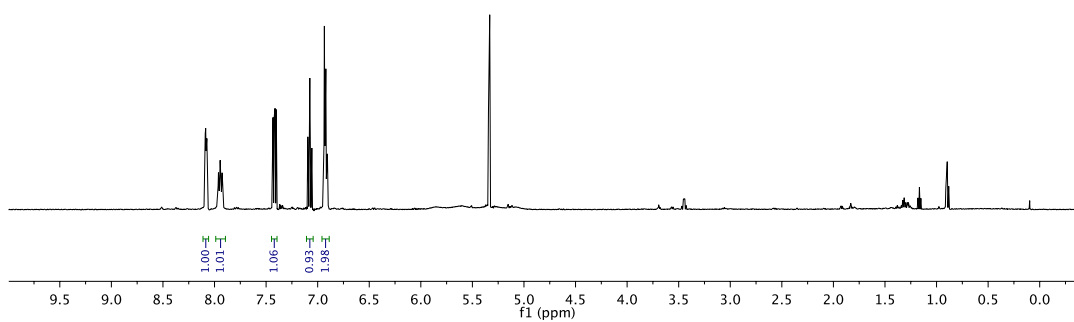
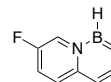
Parameter	Value
1 Solvent	cd2cl2
2 Temperature	25.0
3 Relaxation Delay	1.0000
4 Acquisition Date	2016-02-22T17:17:42
5 Spectrometer Frequency	376.12
6 Nucleus	19F



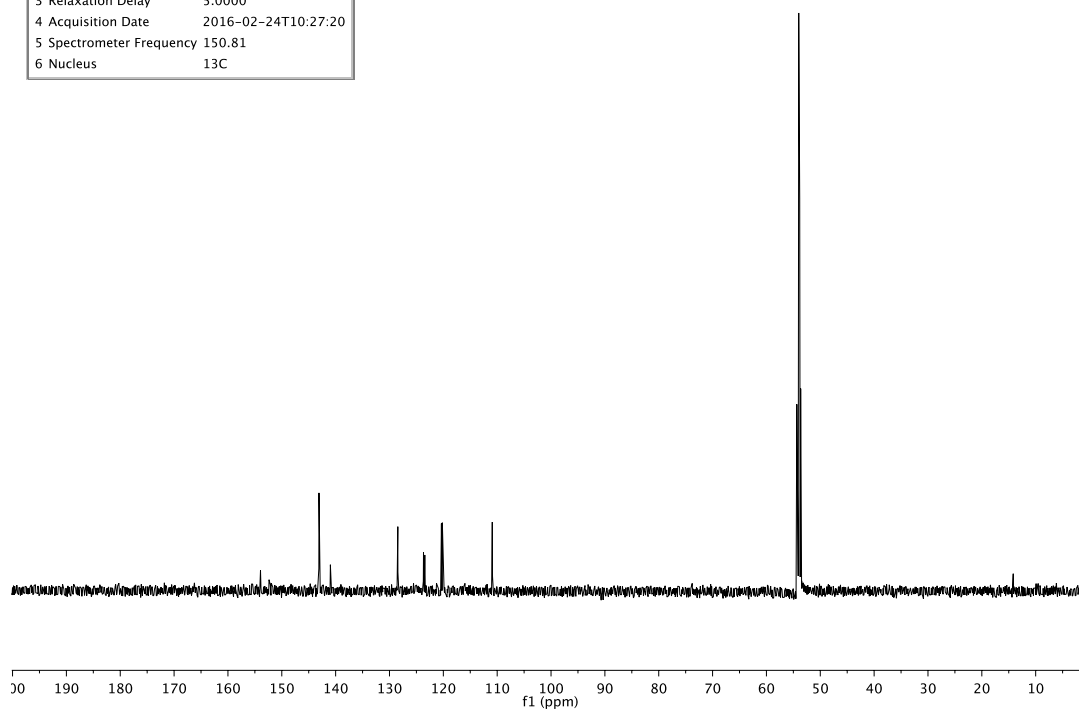
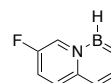
Parameter	Value
1 Solvent	toluene
2 Temperature	25.0
3 Relaxation Delay	0.1000
4 Acquisition Date	2016-02-22T13:40:36
5 Spectrometer Frequency	160.35
6 Nucleus	11B



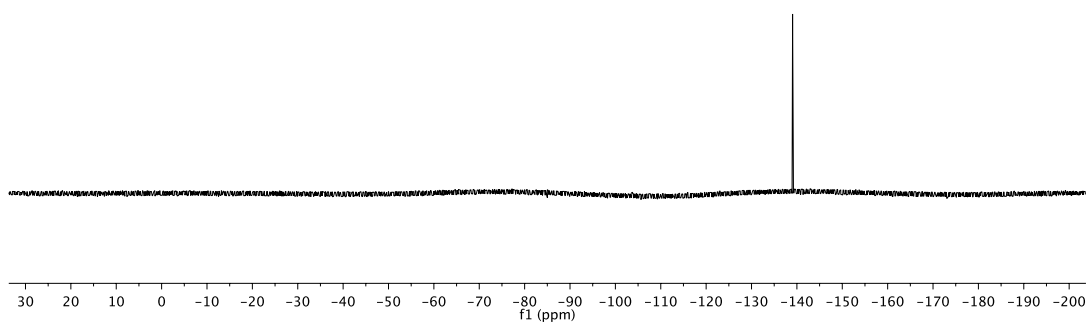
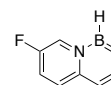
Parameter	Value
1 Solvent	cd2cl2
2 Temperature	25.0
3 Relaxation Delay	10.0000
4 Acquisition Date	2015-10-06T11:17:51
5 Spectrometer Frequency	499.88
6 Nucleus	¹ H



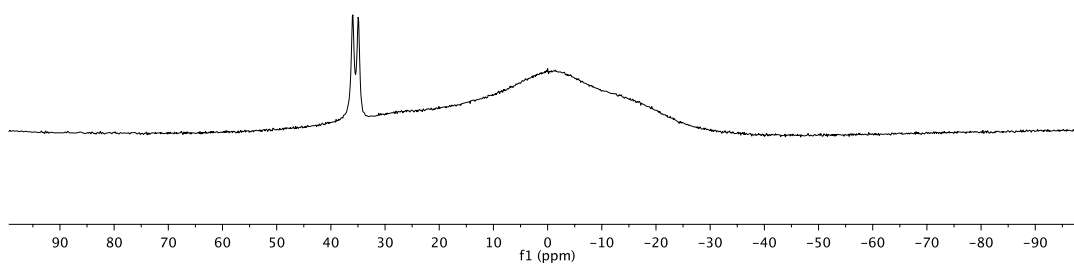
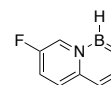
Parameter	Value
1 Solvent	cd2cl2
2 Temperature	25.0
3 Relaxation Delay	5.0000
4 Acquisition Date	2016-02-24T10:27:20
5 Spectrometer Frequency	150.81
6 Nucleus	¹³ C



Parameter	Value
1 Solvent	"cd2cl2"
2 Temperature	25.0
3 Relaxation Delay	1.0000
4 Acquisition Date	2016-02-24T10:07:50
5 Spectrometer Frequency	376.12
6 Nucleus	¹⁹ F



Parameter	Value
1 Solvent	cd2cl2"
2 Temperature	25.0
3 Relaxation Delay	0.0100
4 Acquisition Date	2016-02-24T10:11:23
5 Spectrometer Frequency	128.26
6 Nucleus	¹¹ B



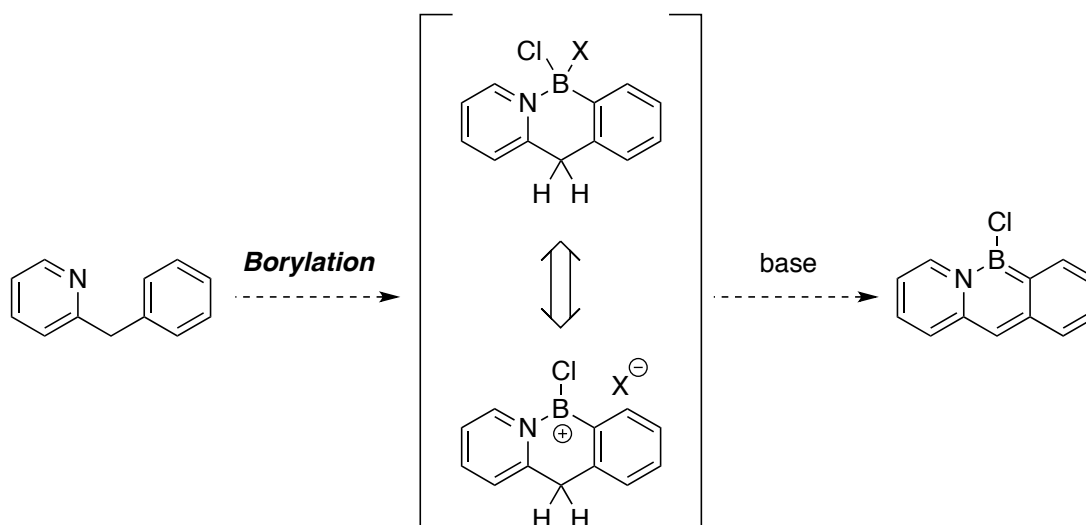
1.6 Application of the General Principles of BN Acene Orbital Energetics

To validate the general principles outlined in section 1.5, we wanted to synthesize a hitherto unknown isomer of BN anthracene. This isomer should be easily synthesized from readily available, modular precursors and also have the potential to for more device-relevant HOMO-LUMO gaps. As will become evident, these requirements are potentially fulfilled by BN-9a,9-anthracenes.

1.6.1 Background: Borenium-Intermediated Annulation Reactions

We thought to use synthetic lessons learned from the synthesis of **BN-9,1-Naph** toward the synthesis of our new target: BN-9a,9-anthracenes. Previously we showed elimination of HCl from across a B–C bond could furnish the fully aromatic BN naphthalene (§ 1.5.2). A borenium ion $[N\rightarrow B(Cl)R]^+$ could act as a synthetic equivalent of the $N\rightarrow BCl_2R$ boron chelate from which HCl elimination could take place (Scheme 1.17).

Scheme 1.17. Potential synthetic equivalence of a boron chelate and a borenium ion



Even before this proposed HCl elimination can take place, a B–C bond must be forged. We envisioned a synthesis involving the directed borylation of 2-benzylpyridine.

Though a number of transition metal-catalyzed directed C–H borylation protocols exist for the regioselective formation of a carbon-boron bond,¹¹¹ we wanted to take a simpler, more cost-effective route. Electrophilic borylation directed by nitrogen-based functionality has been a mainstay of the BN heterocycle synthesis since Dewar synthesized 9,10-BN-phenanthrene in 1958.³⁴ Since then, a host of BN polyaromatics has been synthesized by strongly heating a neutral boron source in the presence of electron rich arenes or olefins.¹¹²

On the other hand, highly electrophilic borocations¹¹³ can be generated using halide or hydride abstractors such as salts of silver,¹¹⁴ trityl cation,¹¹⁵ and thallium.¹¹⁶ Ingleson and Murakami, among others, showed borenium cations could be generated at room temperature to furnish BN annulated polycyclic molecules (Scheme 1.18, top).¹¹⁷ Many BN heterocyclic systems constructed using electrophilic borylation chemistry, however, use boron as a tetracoordinate bridging element to enforce co-planarity through an extended π -system; therefore, the boron atom exerts only an inductive electronic

¹¹¹ Recent examples: (a) Kawamorita, S.; Miyazaki, T.; Ohmiya, H.; Iwai, T.; Sawamura, M. *J. Am. Chem. Soc.* **2011**, *133*, 19310–19313. (b) Fernández-Salas, J. A.; Manzini, S.; Piola, L.; Slawin, A. M. Z.; Nolan, S. P. *Chem. Commun.* **2014**, *2*, 6782–6784. (c) Wang, G.; Liu, L.; Wang, H.; Ding, Y.-S.; Zhou, J.; Mao, S.; Li, P. *J. Am. Chem. Soc.* **2017**, *139*, 91–94.

¹¹² Notable recent examples: (a) Wang, X.-Y.; Lin, H.-R.; Lei, T.; Yang, D.-C.; Zhuang, F.-D.; Wang, J.-Y.; Yuan, S.-C.; Pei, J. *Angew. Chem. Int. Ed.* **2013**, *52*, 3117–3120. (b) Wang, X.; Zhang, F.; Liu, J.; Tang, R.; Fu, Y.; Wu, D.; Xu, Q.; Zhuang, X.; He, G.; Feng, X. *Org. Lett.* **2013**, *15*, 5714–5717. (c) Zhang, W.; Zhang, F.; Tang, R.; Fu, Y.; Wang, X.; Zhuang, X.; He, G.; Feng, X. *Org. Lett.* **2016**, *18*, 3618–3621. (d) Tasior, M.; Gryko, D. T. *J. Org. Chem.* **2016**, *81*, 6580–6586.

¹¹³ For reviews on borocations see: (a) Piers, W. E.; Bourke, S. C.; Conroy, K. D. *Angew. Chem. Int. Ed.* **2005**, *44*, 5016–5036. (b) De Vries, T. S.; Prokofjevs, A.; Vedejs, E. *Chem. Rev.* **2012**, *112*, 4246–4282.

¹¹⁴ (a) Narula, C. K.; Nöth, H. *Inorg. Chem.* **1984**, *23*, 4147–4152. (b) Marwitz, A. J. V.; Jenkins, J. T.; Zakharov, L. N.; Liu, S.-Y. *Angew. Chem. Int. Ed.* **2010**, *49*, 7444–7447. (c) Marwitz, A. J. V.; McClintock, S. P.; Zakharov, L. N.; Liu, S.-Y. *Chem. Commun.* **2010**, *46*, 779–781. (d) Marwitz, A. J. V.; Jenkins, J. T.; Zakharov, L. N.; Liu, S.-Y. *Organometallics* **2011**, *30*, 52–54.

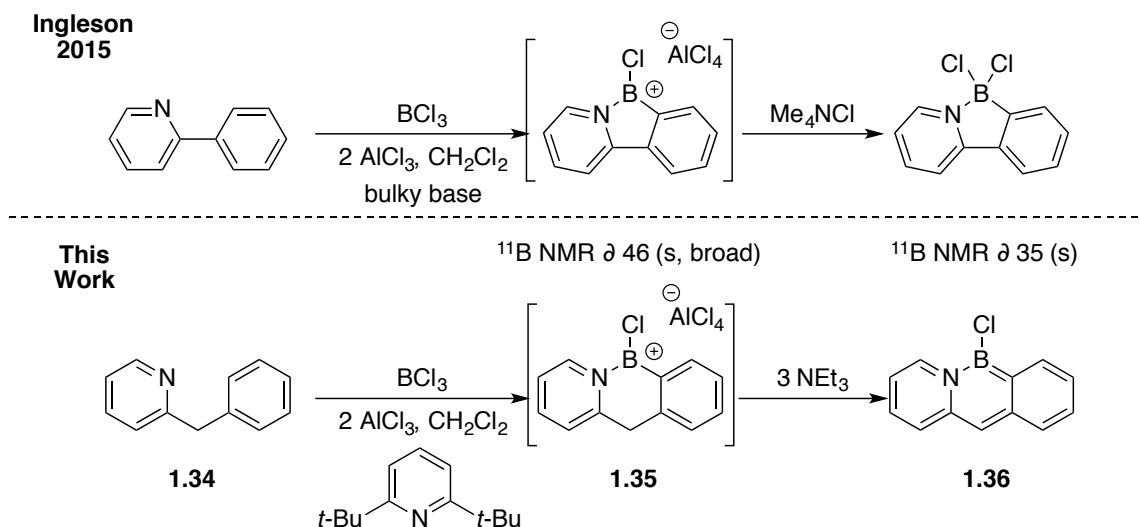
¹¹⁵ De Vries, T. S.; Prokofjevs, A.; Harvey, J. N.; Vedejs, E. *J. Am. Chem. Soc.* **2009**, *131*, 14679–14687.

¹¹⁶ Ghesner, I.; Piers, W. E.; Parvez, M.; McDonald, R. *Chem. Commun.* **2005**, No. 19, 2480–2482.

¹¹⁷ (a) Ishida, N.; Moriya, T.; Goya, T.; Murakami, M. *J. Org. Chem.* **2010**, *75*, 8709–8712. (b) Crossley, D. L.; Cid, J.; Curless, L. D.; Turner, M. L.; Ingleson, M. J. *Organometallics* **2015**, *34*, 5767–5774.

influence on the rest of the conjugated system.¹¹⁸ In contrast, our target, BN-9a,9-anthracene, features co-planar geometry through both the boron atom and the rest of the conjugated system, necessitating conjugation through the B–N bond.¹¹⁹

Scheme 1.18. Synthetic inspiration for this work and initial results



1.6.2 Synthesis of BN-9a,9-Anthracenes for Optical Application

It should be noted that Dewar tried to make the same B–C bond connection and affect cyclization with 2-benzylpyridine and BCl₃ or phenylboron dichloride, but even under “drastic conditions” (i.e., vigorous heating), cyclization was not observed.^{48a} To invoke borenium as intermediates to accomplish the required B–C bond formation and

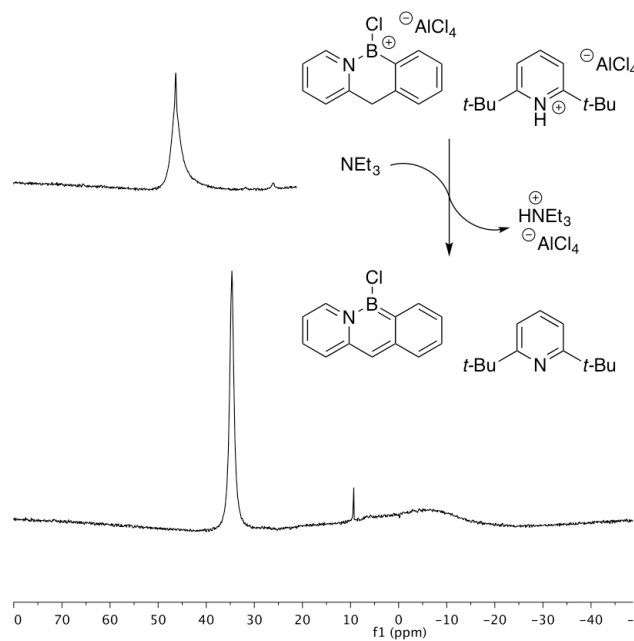
¹¹⁸ There are several examples of boron being used as a non-participant, bridging atom where the BN heterocycle was not constructed using borenium-intermediated electrophilic borylation. See: (a) Grandl, M.; Kaese, T.; Krautsieder, A.; Sun, Y.; Pammer, F. *Chem. Eur. J.* **2016**, *22*, 14373–14382. (b) Grandl, M.; Rudolf, B.; Sun, Y.; Bechtel, D. F.; Pierik, A. J.; Pammer, F. *Organometallics* **2017**, In Press. DOI: 10.1021/acs.organomet.6b00916. (c) Crossley, D. L.; Cade, I. A.; Clark, E. R.; Escande, A.; Humphries, M. J.; King, S. M.; Vitorica-Yrezabal, I.; Ingleson, M. J.; Turner, M. L. *Chem. Sci.* **2015**, *6*, 5144–5151. (d) Crossley, D. L.; Vitorica-Yrezabal, I.; Humphries, M. J.; Turner, M. L.; Ingleson, M. J. *Chem. Eur. J.* **2016**, *22*, 12439–12448. (e) Yusuf, M.; Liu, K.; Guo, F.; Lalancette, R. A.; Jäkle, F. *Dalton Trans.* **2016**, *45*, 4580–4587. Wang initially synthesized heterocycles with tetracoordinate boron but proceeded to photoelimination of Ar–H from across a B–C bond, yielding the fully conjugated BN-containing species. See refs. 55a, 55c, and 56.

¹¹⁹ Effects of conjugation may be decreased through the BN unit versus CC units. See: Lorenz, T.; Crumbach, M.; Eckert, T.; Lik, A.; Helten, H. *Angew. Chem. Int. Ed.* **2017**, *56*, 2780–2784.

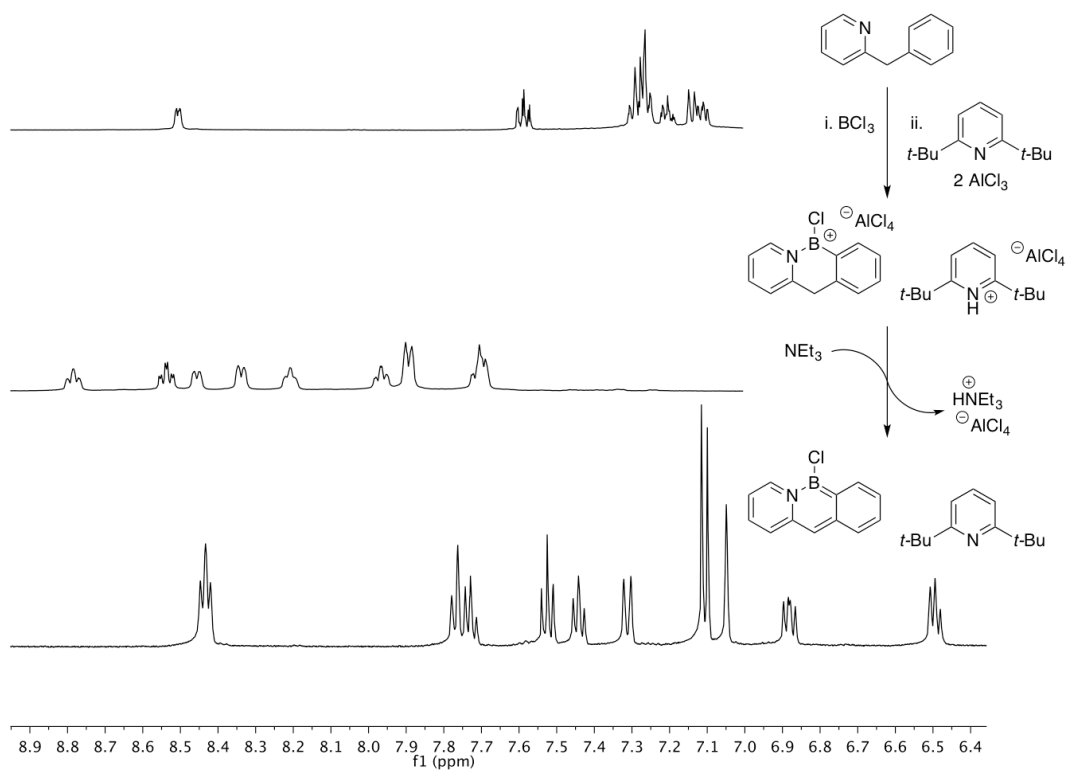
then to provide an entry to fully aromatic BN-9a,9-anthracenes, we studied the reaction among 2-benzylpyridine **1.34**, BCl₃, AlCl₃, and the bulky base 2,6-di-*tert*-butylpyridine using ¹¹B and ¹H NMR. At room temperature, treatment of 2-benzylpyridine with boron trichloride then the bulky base 2,6-di-*tert*-butylpyridine and finally with aluminum chloride resulted in a low-field and broad ¹¹B NMR signal (δ 46 (s)) (Scheme 1.19).¹²⁰ This ¹¹B NMR signal, together with the shift of the ¹H NMR signals to positions downfield relative to 2-benzylpyridine suggests the existence of borenium ion **1.35** (Scheme 1.20). Treatment of the purported borenium with triethylamine quantitatively shifts the ¹¹B NMR signal to a more upfield chemical shift (δ 35 (s)), and the ¹H NMR signals also shift to upfield positions. The *B*-Cl BN anthracene **1.36** can also be observed by high-resolution mass spectrometry. In the present case, the six-membered boron chelate could not be isolated, since the aqueous workup used for Ingleson's and Murakami's five-membered chelates was not tolerated.

¹²⁰ The ¹¹B NMR signal corresponding to boron trichloride also appears at δ 46 but as a sharp singlet rather than a broad one.

Scheme 1.19. ^{11}B NMR of BN anthracene formation from the borenium

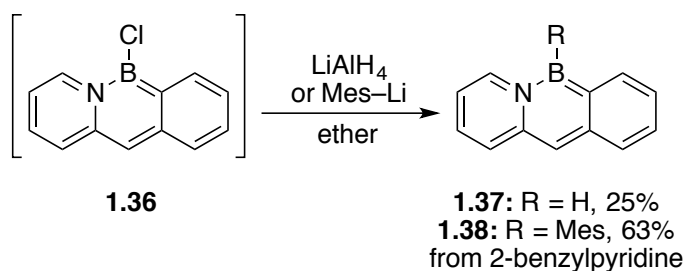


Scheme 1.20: ^1H NMR of BN anthracene formation



We chose not to isolate the *B*-Cl BN anthracene **1.36**, owing to its sensitive nature. Instead, we added nucleophiles to obtain isolable compounds (Scheme 1.21). While the parent BN anthracene **1.37** is not stable to silica gel chromatography and must be isolated by recrystallization from cold diethyl ether, mesityl-substituted **1.38** may be purified using a silica gel plug. The synthesis of **1.38** may be executed easily on gram scale; with this synthetic method, we have realized a simple, scalable, and cheap method for BN-containing extended π -systems.

Scheme 1.21. Synthesis of BN-9a,9-anthracenes



1.6.3 Single-Crystal X-Ray Analysis

Single crystals of **1.37** and **1.38** were grown from cold ($-30\text{ }^{\circ}\text{C}$) ether. The crystal structure of parent BN anthracene **1.37** is disordered (Figure 1.31, left), but it is observed that the constituent molecules pack in the herringbone motif with average $3.6\text{ }\text{\AA}$ intermolecular spacing; this is consistent with the fact that all isolated parent BN naphthalenes pack with the same herringbone motif. The crystal structure of mesitylated **1.38** (Figure 1.29, right), however, unambiguously confirms the connectivity of atoms within the BN anthracene framework. Compound **1.38** packs in asymmetric face-to-face dimers featuring $3.8\text{ }\text{\AA}$ average spacing.

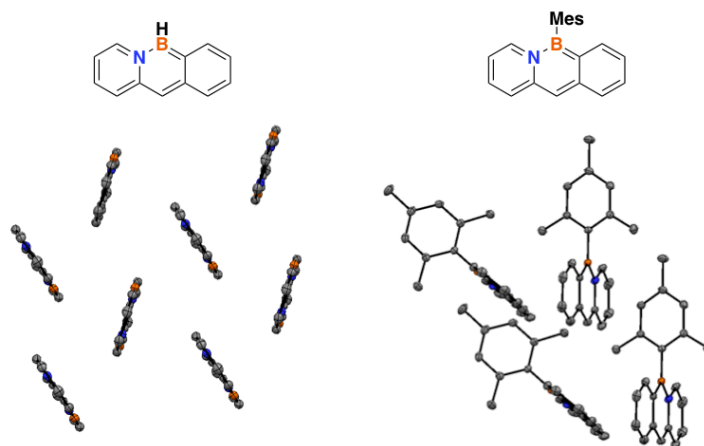


Figure 1.31. Crystal packing of **1.37** (left) and **1.38** (right). Hydrogen atoms omitted for clarity

1.6.4 Optoelectronic Properties of BN-9a,9-Anthracenes

Prof. Anna Chrostowska's group collected the UV-PES of **1.37** (Figure 1.32) to begin its electronic structure characterization. Compound **1.37** has a higher-lying HOMO (-7.04 eV) with respect to either BN-1,2-anthracene (-7.7 eV) or anthracene itself (-7.4 eV). This first ionization energy of **1.37** is in fact the same as that measured for tetracene by Clar and Schmidt using photoelectron spectroscopy.¹²¹ With these data, we have validated general principle 4 from § 1.5.5 ("If the BN bond occupies a bonding region with respect to the all-carbon analogue's HOMO but the more electronegative element, nitrogen, occupies a position with a relatively smaller orbital coefficient, the HOMO energy of the BN isostere will actually be higher than that of the all-carbon analogue.").

¹²¹ Clar, E.; Schmidt, W. *Tetrahedron* **1975**, *31*, 2263–2271.

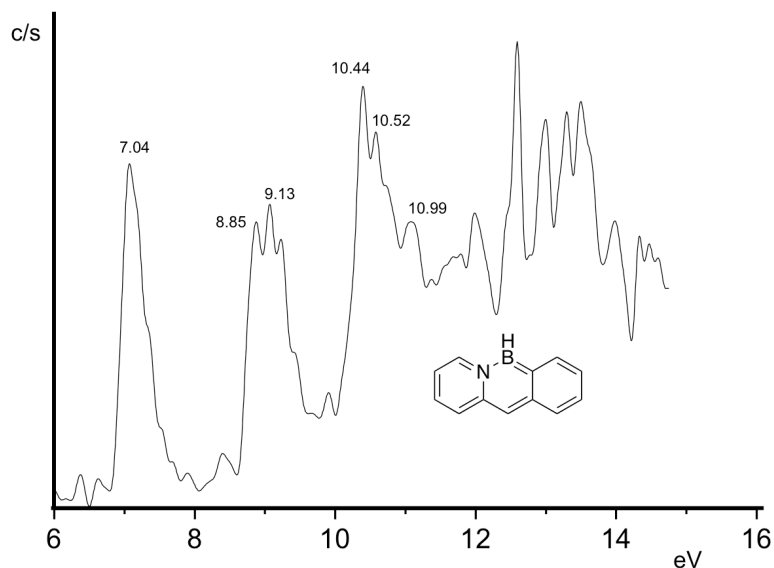


Figure 1.32. UV-Photoelectron spectrum of **2**

We also performed optical absorption and emission studies. In contrast to the previously reported BN-1,2-anthracene **1.5**, the absorption trace of **1.37** (Figure 1.33) appears in the visible range, indicating a HOMO-LUMO gap for **1.37** (optical gap = 2.78 eV) more similar to all-carbon tetracene (2.57 eV) than anthracene (3.26 eV).¹²² Compound **1.37** also has a lower HOMO-LUMO gap than its previously reported isomer BN-1,2-anthracene (3.22 eV). The absorption spectrum for mesitylated **1.38** is bathochromically shifted slightly from that of the parent **1.37**.

¹²² See Experimental Section for TD-DFT calculations predicting the first excited state corresponds to the HOMO-LUMO transition.

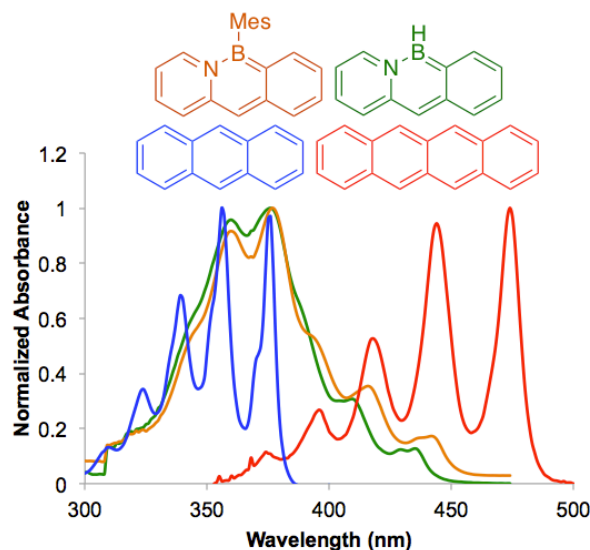


Figure 1.33. Normalized absorption spectra for **3**, **4**, collected from cyclohexane solution together with absorption spectra of anthracene and tetracene for comparison.

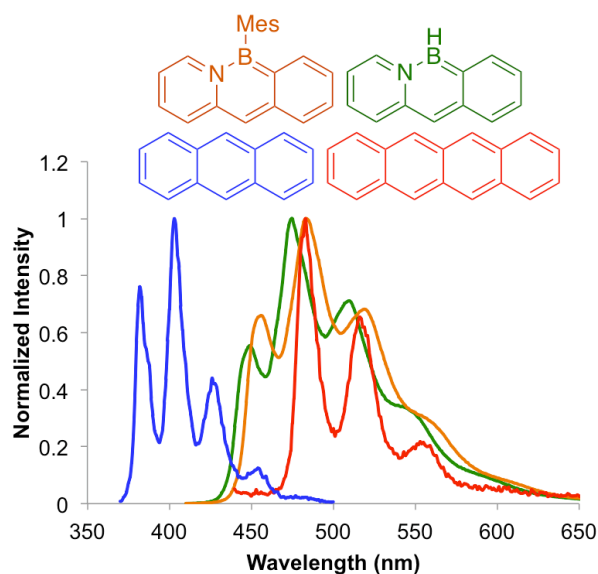


Figure 1.34. Normalized emission spectra collected from cyclohexane solution

The emission spectrum of **1.37** (Figure 1.34) appears similar in shape to that of anthracene and of BN-1,2-anthracene **1.5**. Unlike **1.5** and the all-carbon analogue, photoluminescence of **1.37** is *blue* ($\Phi_{\text{pl}} = 0.32$). The emission trace for mesitylated **1.38** is bathochromically shifted slightly with respect to those of **1.37**. The Stokes shift remains

small, and the solution-phase photoluminescence quantum yield of **1.38** is identical to that of the parent **1.37**.

We prepared a thin film of **1.38** by drop-casting a dichloromethane solution onto a glass slide, and we collected its emission spectrum by mounting it inside an integrating sphere (Figure 1.35). Its solid-state emission spectrum remains true to that of the cyclohexane solution; the general shape of the spectrum is maintained with loss in the definition of the fine structure, and the $\lambda_{\text{max(em)}}$ has bathochromically shifted by only 85 cm^{-1} . Notably, the fluorescence quantum yield of solid **1.38** ($\Phi_{\text{pl(film)}} = 0.85$) is much higher than that of its cyclohexane solution.¹²³

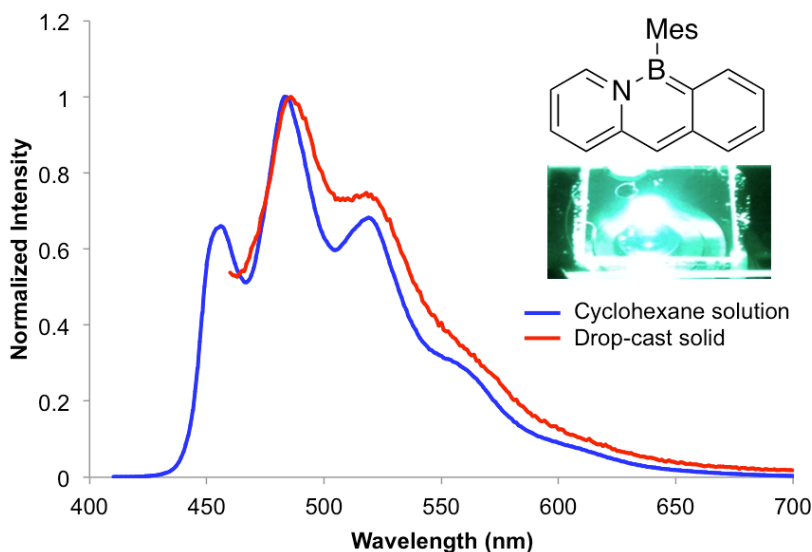


Figure 1.35. Solution-phase fluorescence spectrum and solid-phase fluorescence spectrum of **4** with a photograph of the sample under UV light.

¹²³ Φ_{p} is inversely proportional to the non-radiative decay rate constant k_{nr} . The value of k_{nr} can be increased by collision with quenchers or when vibrational modes become more available. Both collisions with quenchers and the number of available vibrational modes are necessarily increased when a fluorophore is placed in solution versus the solid state. See: Lakowicz, J. R. *Principles of Fluorescence Spectroscopy* *Principles of Fluorescence Spectroscopy*, 3rd ed. Springer, New York, 2006.

1.6.5 Periphery Modification Guided by Theory

The HOMO and LUMO maps (CAM-B3LYP/6-311G(d,p)) of **1.37** show that substitution at many sites may influence the frontier orbital energies (Figure 1.36). Nearly every peripheral position has significant HOMO and LUMO coefficient present. Additionally, the electrostatic potential map shows that **1.37** has some donor-acceptor character. Further electronic perturbation by electron donors and acceptors could yield a significant shift in the HOMO-LUMO gap, resulting in longer wavelength emission.

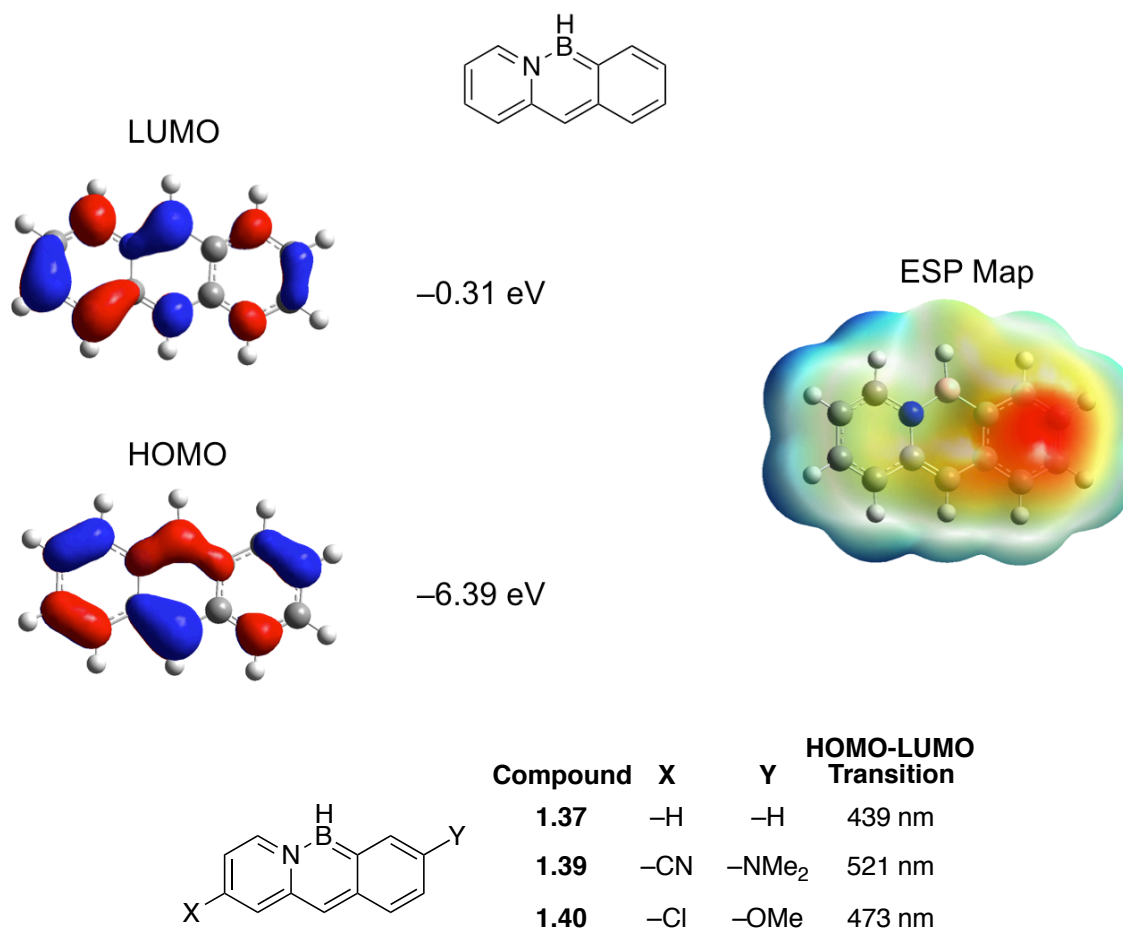


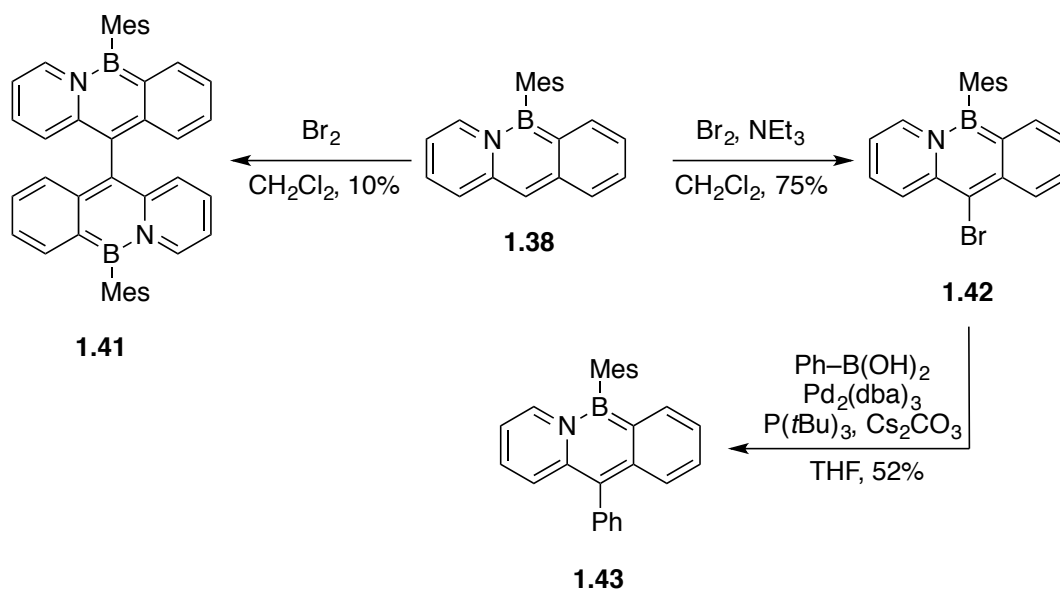
Figure 1.36. Calculated Kohn-Sham HOMO and LUMO for parent **1.37** and first transition (TD CAM-B3LYP/6-311G(d,p)) of some model donor-acceptor BN-9a,9-anthracenes.

Indeed, TD-DFT investigation of a prototypical donor-acceptor system **1.39** substituted by a cyano group and a dimethylamino group (Figure 1.36) shows that the first excited state energy is bathochromically shifted from that of the parent by 3585 cm^{-1} (from 439 nm for the parent and 521 nm for the donor-acceptor system). A more synthetically accessible target **1.40** gives a bathochromic shift of 1637 cm^{-1} (from 439 nm for the parent and 473 nm for the donor-acceptor system).

We wanted to explore two substitution paradigms: bottom-up and late-stage substitution. With respect to late-stage substitution, we attempted to brominate **1.38** using elemental bromine; surprisingly, the only isolable product was oxidatively coupled dimer **1.41** (Scheme 1.22). Because this interesting reaction product was obtained in such low yield, we attempted electrochemical oxidation instead.¹²⁴ However, we only observed decomposition of the starting material into an intractable mixture. This result suggests that the mechanism of oxidative coupling is not radical in nature, but rather follows a two-electron pathway, perhaps similar in nature electrophilic aromatic substitution reaction. The desired bromination proceeded smoothly when bromine was added to a solution of **1.38** and excess triethylamine in CH_2Cl_2 . The brominated product **1.42** could be further functionalized using Suzuki-Miyaura coupling conditions, forming 10-phenyl substituted **1.43** in 52% yield.

¹²⁴ Reviews on electrochemical oxidation in preparative organic synthesis: (a) Moeller, K. D. *Tetrahedron* **2000**, 56, 9527–9554. (b) Horn, E. J.; Rosen, B. R.; Baran, P. S. *ACS Cent. Sci.* **2016**, 2, 302–308.

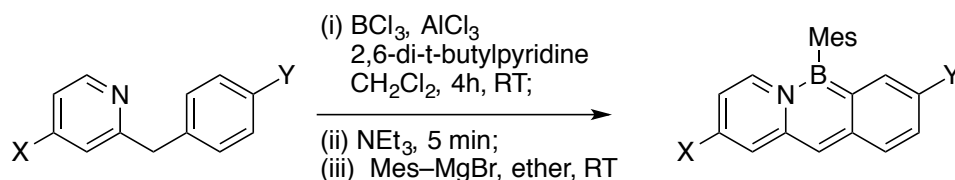
Scheme 1.22. Treatment of 1.38 with elemental bromine and further reaction



For substitution at other positions, we utilized a bottom-up approach, since electrophilic aromatic substitution was selective for the central ring. Substituted benzylpyridines were synthesized using the palladium-catalyzed coupling of aryl halides with 2-picoline-based synthons described by Oshima.¹²⁵ Using the borenium-mediated chemistry, we were able to construct the expected BN anthracenes. Methoxy-containing substrates gave poor yields, given that Lewis- and Bronsted-acidic conditions are widely used to cleave aryl methyl ethers.¹²⁶ Chlorides were also tolerated (Table 1.11).

¹²⁵ Niwa, T.; Yorimitsu, H.; Oshima, K. *Angew. Chem. Int. Chem. Int. Ed.* **2007**, *46*, 2643–2645.

¹²⁶ Wuts, P. G. M.; Greene, T. W. *Greene's Protective Groups in Organic Synthesis*, 4th ed. John Wiley & Sons, Hoboken, 2007.

Table 1.11. Synthesis of substituted BN-9a,9-anthracenes and optical properties

	X =	Y =	Yield	$\lambda_{\text{max(abs)}}^b$	$\lambda_{\text{max(em)}}^c$	Φ_{pl}^d
1.38	H	H	63% ^a	442 nm	483 nm	0.32
1.44	H	Cl	44%	444 nm	482 nm	0.27
1.45	H	OMe	9%	447 nm	496 nm	0.60
1.46	Cl	H	40%	458 nm	496 nm	0.17
1.47	Cl	OMe	33%	462 nm	514 nm	0.33

^a Mes-Li used. ^b Peak of lowest-energy absorption band. ^c Peak at highest intensity emission ^d Absolute quantum yield was determined using an integrating sphere.

Figure 1.36 shows the absorption spectra of the substituted BN-9a,9-anthracenes, and Figure 1.37 shows their fluorescence spectra. While the chloro-substituent on the carbonaceous ring (compound **1.44**) did not significantly affect the lowest-energy absorption and emission relative to the *B*-Mes unsubstituted species **1.38**, placing a methoxy group at the same position created a stronger donor-acceptor situation through the BN anthracene, bathochromically shifting both the absorption and emission spectra (compound **1.45**). Similarly, placing the acceptor chloro-group on the pyridyl ring also bathochromically shifted the spectra (compound **1.46**). Utilizing both donor and acceptor further shifted absorption and emission to even lower energy (Compound **1.47**). Cyclization was not observed for cyano- or dimethylamino-substituted substrates, possibly because of interference from the nitrogen lone pairs. Fluorinated substrates also were not cyclized under the reaction conditions.

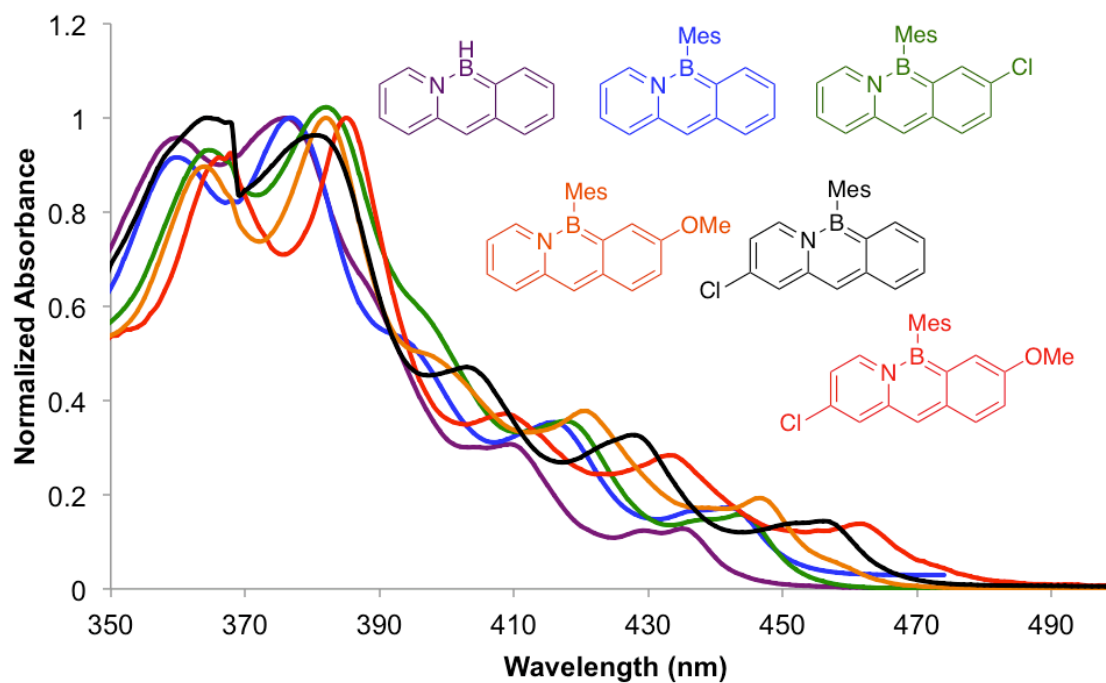


Figure 1.37. Normalized absorption spectra of substituted 9a,9-BN-anthracenes

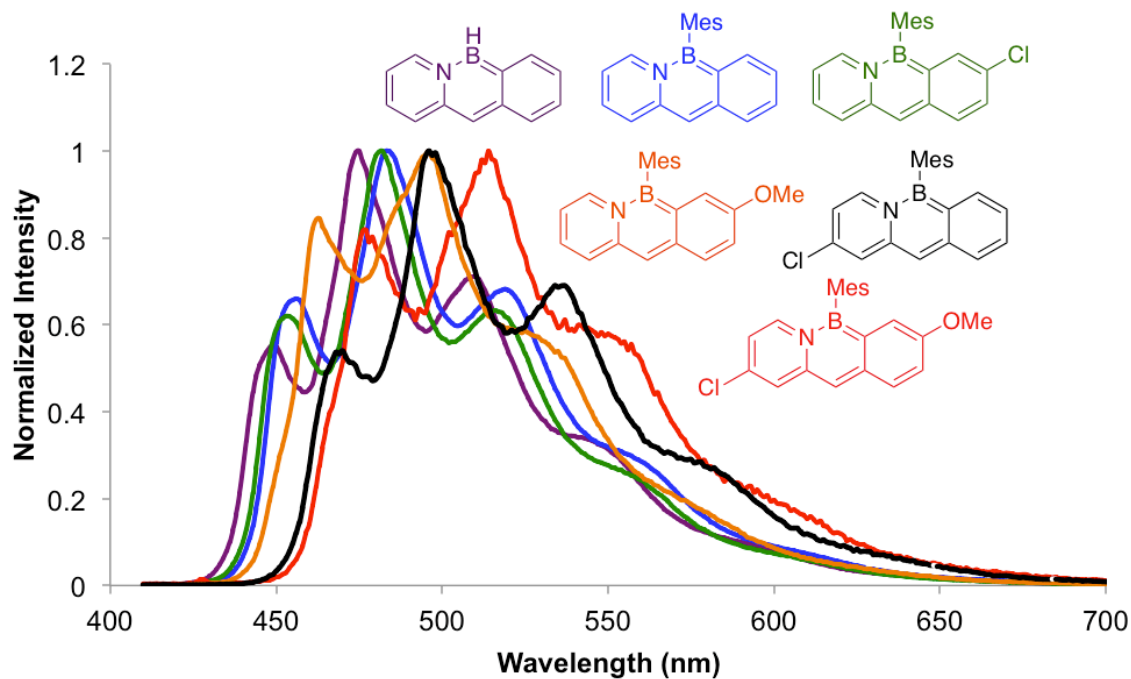


Figure 1.38. Normalized emission spectra of substituted 9a,9-BN-anthracenes

1.6.6 Conclusion

We have successfully demonstrated the application of the general principles of BN acene design by synthesizing BN-9a,9-anthracenes using borenium-intermediated cyclization and aromatization. These various BN-9a,9-anthracenes are electronically distinct from our previously synthesized BN-1,2-anthracenes; BN-9a,9-anthracene **1.37** has a higher-lying HOMO as measured by UV-photoelectron spectroscopy, and it has a smaller HOMO-LUMO gap which results in visible emission. These optical properties are tunable through substitution. We observe a 1597 cm^{-1} (39 nm) bathochromic shift in the emission maximum peak from the parent BN-9a,9-anthracene to a methoxy- and chloro-substituted donor-acceptor system. Visually, this spectral shift also shifts the emission color from blue to green. This work also represents an avenue to cost-effective synthesis of smaller acene topologies with device-relevant HOMO-LUMO gaps.

1.6.7 Experimental Section

All oxygen- and moisture-sensitive manipulations were carried out under an inert atmosphere using either standard Schlenk technique or a nitrogen-filled glovebox.

For air- and moisture-sensitive techniques, tetrahydrofuran, diethyl ether, methylene chloride, pentane, and toluene were purified by passing through a neutral alumina column under argon. All other solvents for air- and moisture-sensitive work were distilled after drying over calcium hydride.

For all chromatography involving air- and moisture-sensitive compounds, silica gel (240-300 mesh) was heated under vacuum in a $150\text{ }^{\circ}\text{C}$ oil bath for 12 hours. Chromatography for those compounds was performed in a glovebox using the dry, degassed solvents previously mentioned.

^{11}B NMR spectra were recorded on a Varian 500 spectrometer and externally referenced to neat $\text{BF}_3\cdot\text{Et}_2\text{O}$. (δ 0). ^1H and ^{13}C NMR spectra were recorded on a Varian 500 spectrometer, or a Varian 600 spectrometer.

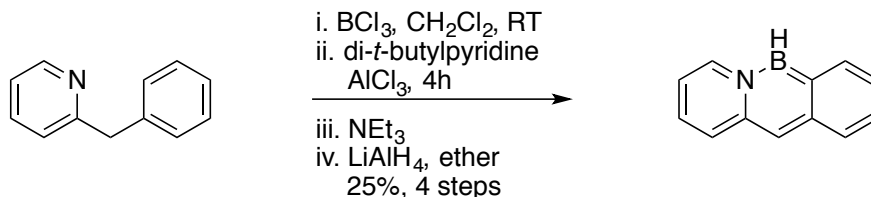
High-resolution mass spectrometry (HRMS) data were collected by Mr. Marek Domin at the Boston College Center for Mass Spectrometry using the Direct Analysis in Real Time (DART) technique.

UV-visible absorption spectra were acquired on a Cary 100 spectrometer. Emission spectra were acquired on a Quanta Master 40 spectrofluorimeter (Photon Technology International) in dry, degassed cyclohexane as solvent. Solution-phase quantum yields were determined using the comparative method using anthracene and 9-phenylanthracene as cross-referenced standards or using a PTI K-Sphere “petite” integrating sphere. Solid-state fluorescence spectra and quantum yield measurements were collected using the integrating sphere, and the solid was drop-cast on a glass slide. The slide was oriented 72° from normal with respect to the detector, and excitation beam went through the slide before reaching the sample.

Calculations were carried out using the Gaussian 09 program and the Linux cluster at Boston College.

Synthetic Details

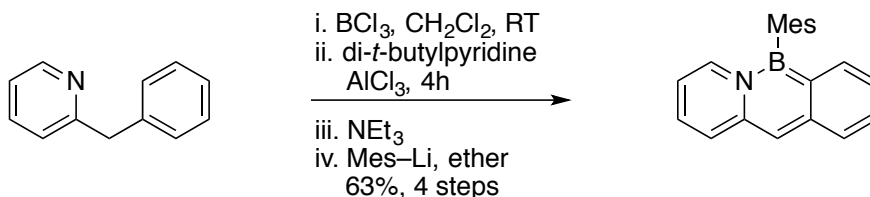
B-chloro-9a,9-*BN*-anthracene (1.37)



2-benzylpyridine (158 mg, 0.937 mmol, 1 equiv) and boron trichloride (0.94 mL 1M solution in hexanes, 0.94 mmol, 1 equiv) was stirred at room temperature in 10 mL CH_2Cl_2 for 10 minutes. Aluminum chloride (250. mg, 1.87 mmol 2 equiv) and 2,6-di-*tert*-butylpyridine (179 mg, 0.937 mmol, 1 equiv) were added and the reaction was stirred under inert gas for 6 hours. The solvent was removed and the residue was rinsed with pentane (Borenium ^{11}B NMR δ 45 (s)). The remaining solid was re-dissolved in 50 mL CH_2Cl_2 (some solid did not dissolve) and triethylamine (0.36 mL, 2.8 mmol, 3 equiv). Pentane (20 mL) was added to the mixture, which became turbid and separated into two phases. The mixture was allowed to sit at room temperature until the layers became clear. The upper, yellow phase contains the product, while the bottom, red phase contains triethylammonium salts. The top phase was decanted off the bottom, and volatiles were removed to reveal a yellow powder, which is compound **1.36**. ^{11}B NMR (160 MHz, CH_2Cl_2) δ 34.7 (s). HRMS (DART+) $[\text{M}+\text{H}]^+$ calcd for $\text{C}_{12}\text{H}_{10}\text{BNCl}$ 214.05948, found 214.05953. Ether (50 mL) was added to the mixture, and The crude *B*-Cl anthracene was suspended in ether, and cooled to $-30\text{ }^\circ\text{C}$ in the glovebox freezer. Lithium aluminum hydride (14 mg, 0.38 mmol, 0.4 equiv) was carefully added, and the reaction mixture was allowed to warm to room temperature over 4.5 hours. The mixture was passed through an acrodisc and concentrated *in vacuo*. The residue was recrystallized from ether at $-30\text{ }^\circ\text{C}$ to yield a yellow solid (42 mg, 25% over 2 steps). ^1H NMR (500 MHz, CD_2Cl_2) δ 8.25 (d, $J = 7.7$ Hz, 1H), 8.03 (d, $J = 7.2$ Hz, 1H), 7.77 (d, $J = 8.1$ Hz, 1H), 7.69 (ddd, $J = 8.2$, 6.8, 1.4 Hz, 1H), 7.37 (ddd, $J = 7.8$, 6.8, 1.1 Hz, 1H), 7.29 (d, $J = 9.3$ Hz, 1H), 6.86 (ddd, $J = 9.4$, 6.2, 1.2 Hz, 1H), 6.38 (ddd, $J = 7.4$, 6.2, 1.3 Hz, 1H). *B*-H can be observed as a broad signal from 6.5–5.5 ppm. ^{13}C NMR (151 MHz, CD_2Cl_2) δ 144.5 141.1, 138.1, 136.80, 131.3, 126.1, 125.93, 125.0, 122.6, 110.4, 107.4. Carbon adjacent to boron not observed. ^{11}B NMR (160 MHz, CD_2Cl_2) δ 37.5 (d, $J = 133.5$ Hz). FTIR (ATR thin film):

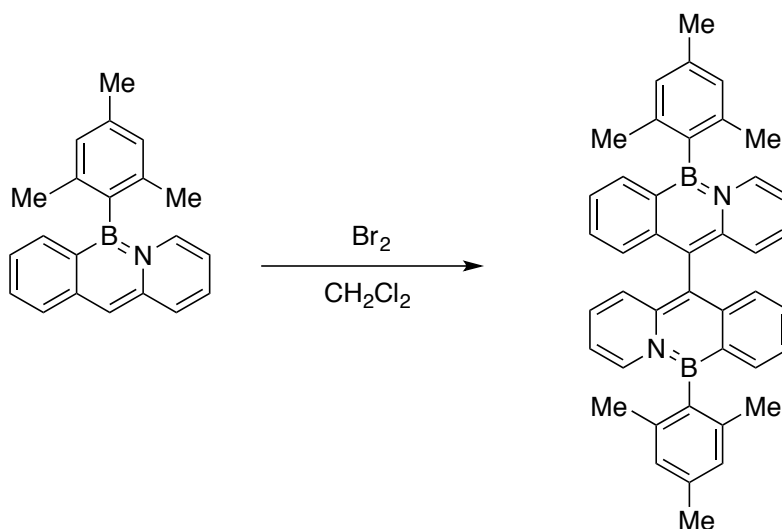
3049, 2546, 1622, 1515, 1361, 1262, 807. HRMS (DART+) $[M+H]^+$ calcd for $C_{12}H_{11}NB$ 180.09845, found 180.09886. X-ray quality crystals were obtained by crystallization from a saturated ether solution at $-30\text{ }^{\circ}\text{C}$.

***B*-Mesityl-9,9a-BN-anthracene (1.38)**



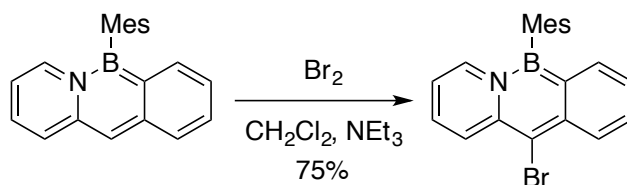
This procedure assumes a 100% yield of the *B*-Cl BN anthracene from an 11.8 mmol reaction of 2-benzylpyridine. Solid mesityllithium was used as the nucleophile, and it was added at room temperature until reaction was judged complete by ^{11}B NMR (1.42 g, 11.3 mmol, 0.96 equiv). Silica gel was added to the crude mixture, and the volatiles were removed under reduced pressure. The residue was filtered through a plug of silica gel using methylene chloride as the eluent, and the filtrate was concentrated under reduced pressure. The residue was rinsed with small amounts of pentane, yielding a bright yellow powder (yield: 2.20 g, 63%). ^1H NMR (500 MHz, CD_2Cl_2) δ 7.85 (s, 1H), 7.79 (d, $J = 7.9$ Hz, 1H), 7.74 – 7.67 (m, 1H), 7.64 (d, $J = 7.1$ Hz, 1H), 7.35 (d, $J = 9.7$ Hz, 1H), 7.29 (td, $J = 7.4, 6.8, 1.1$ Hz, 1H), 7.13 (s, 1H), 7.04 (s, 1H), 6.85 (td, $J = 6.2, 3.1$ Hz, 1H), 6.25 (t, $J = 7.5$ Hz, 1H), 2.44 (s, 3H), 2.03 (s, 6H). ^{13}C NMR (151 MHz, CD_2Cl_2) δ 141.3, 140.7, 139.5, 138.2, 136.3, 134.8, 131.5, 127.8, 127.2, 126.4, 125.0, 123.1, 110.9, 107.6, 22.6, 21.6. Carbons adjacent to boron not observed. ^{11}B NMR (160 MHz, CD_2Cl_2) δ 40.7. FTIR (ATR thin film): 2913, 1640, 1606, 1514, 907, 807. HRMS (DART+) $[\text{M}+\text{H}]^+$ calcd. for $\text{C}_{21}\text{H}_{21}\text{NB}$ 298.17766, found 298.17670. X-ray quality crystals were obtained from cooling a saturated ether solution to -30°C .

BN Bianthryl (1.41)



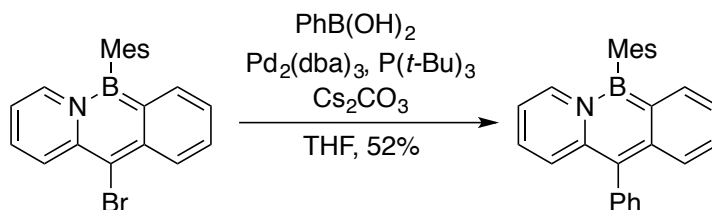
B-mesityl-BN-anthracene (90. mg, 0.30 mmol, 1 equiv) was dissolved in 5 mL methylene chloride. Bromine (8 μ L, 0.151 mmol, 0.5 equiv) was separately dissolved in 3 mL methylene chloride. The bromine solution was added dropwise over 5 minutes at room temperature, and the reaction was allowed to stir 15 minutes. The reaction mixture was then passed through a short plug of silica gel, and the solution, which fluoresced bright green, was pumped down to afford a yellow powder (16 mg, 18% yield). The chiral axis formed by the connection of the BN heterocyclic rings at the 10-position of the anthracene renders diastereotopicity, and some signals are distinct from one another. ^1H NMR (500 MHz, CD_2Cl_2) δ 7.87 (dd, $J = 7.9, 1.5$ Hz, 1H), 7.81 (dd, $J = 7.4, 1.3$ Hz, 1H), 7.44 (ddd, $J = 8.4, 6.8, 1.5$ Hz, 1H), 7.25 (ddd, $J = 7.9, 6.7, 1.1$ Hz, 1H), 7.16 (d, $J = 8.4$ Hz, 1H), 7.07 (s, 2H), 6.84 (dd, $J = 9.5, 1.3$ Hz, 1H), 6.67 (ddd, $J = 9.5, 6.1, 1.3$ Hz, 1H), 6.28 (ddd, $J = 7.4, 6.0, 1.4$ Hz, 1H), 2.44 (s, 3H), 2.16 (app d, 6H). ^{13}C NMR (151 MHz, CD_2Cl_2) δ 144.1, 142.9, 142.8, 140.7, 140.4, 138.9, 137.8, 133.9, 130.01, 129.97, 128.0, 127.4, 127.4, 125.4, 115.4, 113.0, 24.9, 23.7. Carbons adjacent to boron were not observed. ^{11}B NMR (160 MHz, CD_2Cl_2) δ 41.93 (brs). FTIR (ATR thin film): 2914, 1601, 1450, 1293, 908, 783, 658 HRMS (DART+) $[\text{M}+\text{H}]^+$ calcd for $\text{C}_{42}\text{H}_{39}\text{N}_2\text{B}_2$ 593.32993, found 593.33216.

10-bromo-9-mesityl-9,9a-BN-anthracene (1.42)



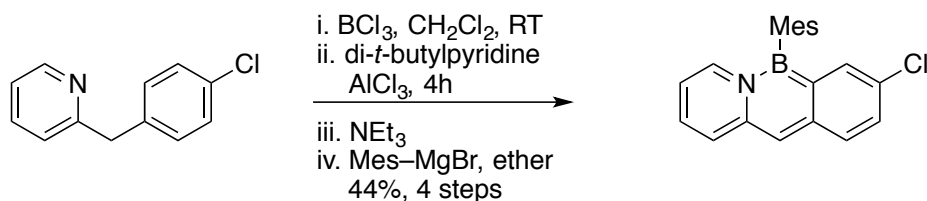
In a glovebox, the BN anthracene (301 mg, 1.01 mmol, 1 equiv) was dissolved in 50 mL dichloromethane, and triethylamine (0.7 mL, 5.05 mmol, 5 equiv) was added. Bromine (52 μL , 1.01 mmol, 1 equiv) was separately dissolved in 10 mL dichloromethane, and this solution was carefully added to the starting material. The reaction was monitored by ^1H NMR, and completion took approximately 20 minutes. The crude reaction mixture was passed through a short plug of silica gel with dichloromethane as the eluent. The solvent was removed under reduced pressure to yield a yellow solid (283 mg, 75%). ^1H NMR (500 MHz, CD_2Cl_2) δ 8.36 (d, $J = 8.4$ Hz, 1H), 8.10 (d, $J = 9.6$ Hz, 1H), 7.82 (ddd, $J = 8.4, 6.9, 1.5$ Hz, 1H), 7.76 – 7.73 (m, 1H), 7.71 (dt, $J = 7.3, 1.2$ Hz, 1H), 7.35 – 7.29 (m, 1H), 7.11 – 7.05 (m, 1H), 6.99 (s, 2H), 6.34 (ddd, $J = 7.5, 6.2, 1.3$ Hz, 1H), 2.39 (s, 3H), 1.95 (s, 6H). ^{13}C NMR (151 MHz, CD_2Cl_2) δ 140.6, 138.6, 136.7, 135.8, 132.9, 128.2, 128.0, 127.36, 127.35, 126.5, 126.1, 123.9, 111.0, 102.5, 22.6, 21.6. Carbons adjacent to boron were not observed. FTIR (ATR thin film): 2917, 1604, 1555, 1475, 1047, 750, 593. ^{11}B NMR (160 MHz, CD_2Cl_2) δ 41.6 (s). HRMS (DART+) $[\text{M}+\text{H}]^+$ calcd. for $\text{C}_{21}\text{H}_{20}\text{NBBBr}$ 376.08722, found 376.08552.

10-phenyl-9-mesityl-9,9a-BN-anthracene (1.43)



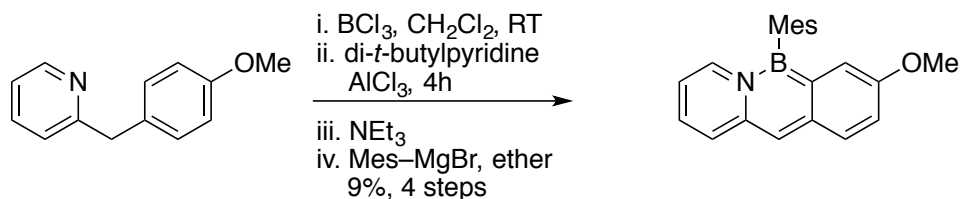
In a glovebox, the brominated anthracene (134 mg, 0.356 mmol, 1 equiv) was combined in 6 mL THF with phenylboronic acid (65 mg, 0.53 mmol, 1.5 equiv), and cesium carbonate (232 mg, 0.712 mmol, 2 equiv). Separately in 2 mL THF, tris(dibenzylideneacetone)dipalladium(0) (8 mg, 0.009 mmol, 3 mol%) and tri-tert-butylphosphine (4 mg, 0.02 mmol, 6 mol%) were combined and stirred for 5 minutes. The palladium catalyst solution was added by pipet to the rest of the reaction mixture. The mixture was stirred at room temperature for 24 hours, and the mixture was subsequently filtered. The volatiles were removed under reduced pressure, and the residue was passed through a plug of silica gel using CH_2Cl_2 as the eluent. The filtrate was concentrated to a yellow-orange powder under reduced pressure. The powder was rinsed with small amounts of pentane (The pentane was red in color.), and the final product was a bright yellow powder Yield: 69 mg, 52%. ^1H NMR (500 MHz, CD_2Cl_2) δ 7.79 (d, $J = 7.1$ Hz, 1H), 7.69 (d, $J = 7.4$ Hz, 1H), 7.61 – 7.47 (m, 4H), 7.42 (app. d 2H), 7.36 (d, $J = 8.4$ Hz, 1H), 7.24 (ddd, $J = 7.8, 6.8, 1.1$ Hz, 1H), 7.07 – 7.03 (m, 1H), 7.02 (s, 2H), 6.71 (ddd, $J = 9.5, 6.1, 1.3$ Hz, 1H), 6.24 (ddd, $J = 7.4, 6.0, 1.4$ Hz, 1H), 2.41 (s, 3H), 2.05 (s, 6H). ^{13}C NMR (151 MHz, CD_2Cl_2) δ 141.1, 140.8, 140.0, 138.2, 136.9, 136.4, 135.1, 132.7, 131.4, 129.5, 127.9, 127.7, 125.7, 125.5, 124.9, 123.0, 118.69, 110.7, 22.7, 21.6. Carbons adjacent to boron were not observed. FTIR (ATR thin film): 2912, 1563, 1491, 1386, 852, 783. ^{11}B NMR (160 MHz, CD_2Cl_2) δ 41.2 (s). HRMS (DART+) $[\text{M}+\text{H}]^+$ calcd. for $\text{C}_{27}\text{H}_{25}\text{NB}$ 374.20880, found 374.20899.

2-Chloro-BN-9a,9-anthracene (1.44)



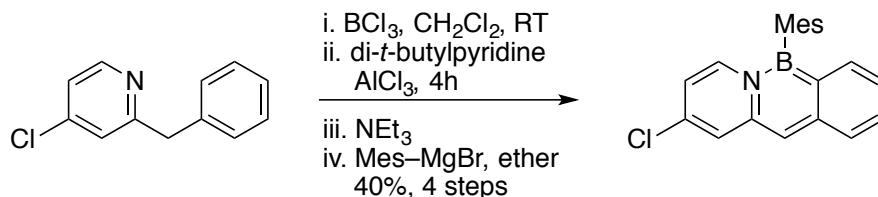
This procedure mirrors that of the unsubstituted species and was performed at a 2.45 mmol scale using mesitylmagnesium bromide as the nucleophile. Yield: 359 mg, 44%. ^1H NMR (500 MHz, CD_2Cl_2) δ 7.76 (d, $J = 8.7$ Hz, 1H), 7.63 (s, 1H), 7.61 – 7.57 (m, 2H), 7.34 (dd, $J = 9.3, 1.4$ Hz, 1H), 7.09 (s, 1H), 6.98 (s, 2H), 6.88 (ddd, $J = 9.3, 6.2, 1.3$ Hz, 1H), 6.28 (ddd, $J = 7.5, 6.2, 1.4$ Hz, 1H), 2.39 (s, 3H), 1.96 (s, 6H). ^{13}C NMR (151 MHz, CD_2Cl_2) δ 140.7, 139.9, 139.5, 138.5, 134.77, 134.75, 132.0, 129.6, 128.4, 128.0, 127.2, 125.5, 111.5, 107.2, 22.6, 21.6. ^{11}B NMR (160 MHz, CD_2Cl_2) δ 40.7 (s). FTIR (ATR thin film) 2915, 1641, 1455, 1169, 846. HRMS (DART+) $[\text{M}+\text{H}]^+$ calcd. for $\text{C}_{21}\text{H}_{20}\text{BNCl}$ 332.13773, found 332.13760.

2-methoxy-*B*-mesityl-9a,9-*BN*-anthracene (1.45)



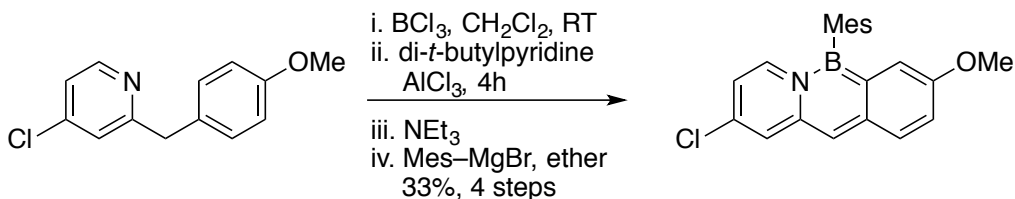
The procedure mirrors that of the unsubstituted compound, completed on a 2.76 mmol scale using mesitylmagnesium bromide as the nucleophile. Yield: 82 mg, 9%. ¹H NMR (500 MHz, CD₂Cl₂) δ 7.75 (d, *J* = 8.7 Hz, 1H), 7.50 (d, *J* = 7.3 Hz, 1H), 7.33 (dd, *J* = 8.8, 2.7 Hz, 1H), 7.30 – 7.27 (m, 1H), 7.08 (d, *J* = 2.8 Hz, 1H), 7.05 (s, 1H), 6.97 (s, 2H), 6.75 (dd, *J* = 9.3, 6.3 Hz, 1H), 6.19 (ddd, *J* = 7.5, 6.1, 1.6 Hz, 1H), 3.72 (s, 3H), 2.38 (s, 3H), 1.97 (s, 6H). ¹³C NMR (126 MHz, CD₂Cl₂) δ 156.1, 140.7, 138.1, 137.9, 136.0, 134.4, 128.4, 127.9, 127.3, 123.8, 122.6, 115.2, 111.0, 107.5, 55.8, 22.5, 21.6. Carbons adjacent to boron were not observed. ¹¹B NMR (160 MHz, CD₂Cl₂) δ 39.9 (s). FTIR (ATR thin film): 2914, 1584, 1554, 1030, 798. HRMS (DART+) [M+H]⁺ calcd. for C₂₂H₂₃BNO 328.18727, found 328.18616.

3-Chloro-BN-9a-9-anthracene (1.46)



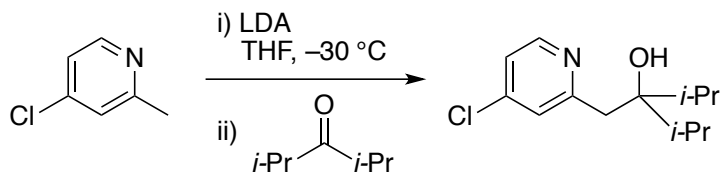
The procedure mirrors that of the unsubstituted compound, completed on a 3.91 mmol scale. Yield: 515 mg, 40%. ¹H NMR (500 MHz, CD₂Cl₂) δ 7.82 (d, *J* = 8.1 Hz, 1H), 7.74 (d, *J* = 7.5 Hz, 1H), 7.72 – 7.70 (m, 1H), 7.57 (d, 1H), 7.35 (d, *J* = 2.3 Hz, 1H), 7.31 (ddd, *J* = 7.9, 6.8, 1.1 Hz, 1H), 7.05 (s, 1H), 7.01 (s, 2H), 6.21 (dd, *J* = 7.7, 2.2 Hz, 1H), 2.42 (s, 3H), 2.00 (s, 6H). ¹³C NMR (151 MHz, CD₂Cl₂) δ 141.3, 140.7, 138.8, 138.5, 137.8, 136.4, 132.0, 131.1, 127.9, 126.5, 124.7, 123.7, 112.5, 107.5, 22.6, 21.6. Carbons adjacent to boron were not observed. ¹¹B NMR (160 MHz, CD₂Cl₂) δ 41.4 (s). FTIR (ATR thin film): 2913, 1631, 1607, 1519, 1334, 937, 751, 638. HRMS (DART+) [M+H]⁺ calcd. for C₂₁H₂₀BNCl 332.13773, found 332.13628.

3-Chloro-8-methoxy-*B*-mesityl-9a,9-*BN*-anthracene (1.47)



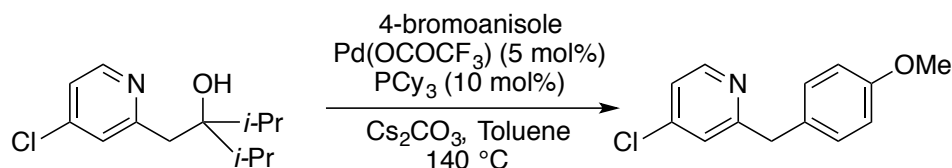
This procedure mirrors that for the unsubstituted compound and was performed on a 2.14 mmol scale using mesitylmagnesium bromide as the nucleophile. Yield: 255 mg, 33% ¹H NMR (500 MHz, CD₂Cl₂) δ 7.74 (d, *J* = 8.8 Hz, 1H), 7.45 (d, *J* = 7.8 Hz, 1H), 7.34 (dd, *J* = 8.8, 2.7 Hz, 1H), 7.27 (d, *J* = 2.3 Hz, 1H), 7.08 (d, *J* = 2.7 Hz, 1H), 6.97 (s, 2H), 6.12 (dd, *J* = 7.8, 2.2 Hz, 1H), 3.72 (s, 3H), 2.37 (s, 3H), 1.97 (s, 6H). ¹³C NMR (126 MHz, CD₂Cl₂) δ 140.6, 138.4, 137.2, 136.1, 135.9, 129.7, 128.4, 128.0, 124.8, 122.9, 115.5, 112.5, 110.6, 107.4, 55.8, 22.5, 21.6. ¹¹B NMR (160 MHz, CD₂Cl₂) δ 40.6 (s). FTIR (ATR thin film) 2961, 1630, 1557, 1285, 1068, 798. HRMS (DART+) [M+H]⁺ calcd. for C₂₂H₂₂ONBCl 362.14871, found 362.14846.

3-((4-chloropyridin-2-yl)methyl)-2,4-dimethylpentan-3-ol



Diisopropylamine (6.35 mL, 45.1 mmol, 1.15 equiv) was cooled to $-30\text{ }^{\circ}\text{C}$, and *n*-butyllithium (2.5 M in hexanes) (17.2 mL, 43.1 mmol, 1.1 equiv) was added dropwise at $-30\text{ }^{\circ}\text{C}$. The mixture was stirred 10 minutes at this temperature, then 4-chloro-2-picoline (5.00 g, 39.2 mmol, 1 equiv) was added dropwise at $-30\text{ }^{\circ}\text{C}$. After stirring 30 minutes at this temperature, diisopropyl ketone (5.37 g, 47.0 mmol, 1.2 equiv) was added dropwise, and then the bath was removed. The mixture was stirred for 2 hours more, whereupon it was poured into 30 mL water. The organics were extracted into ethyl acetate and washed with brine. The volatiles were removed using a rotary evaporator. The residue was purified using silica gel chromatography (3:1 hexane:ethyl acetate as the mobile phase). Yielded a pale yellow liquid which solidified upon further evacuation (9.37 g, 98%). ^1H NMR (500 MHz, CDCl_3) δ 8.36 (d, $J = 5.4$ Hz, 1H), 7.22 (s, 1H), 7.16 (dd, $J = 5.4, 1.9$ Hz, 1H), 5.86 (s, 1H), 2.89 (s, 2H), 1.91 (hept, $J = 6.9$ Hz, 2H), 0.90 (d, $J = 6.6$ Hz, 6H) 0.89 (d, $J = 6.6$ Hz, 6H). ^{13}C NMR (151 MHz, CDCl_3) δ 163.5, 149.0, 144.9, 124.9, 121.7, 78.3, 38.5, 35.3, 18.3, 18.1. FTIR (ATR thin film): 3362, 2961, 1678, 1469, 1029, 710. HRMS (DART+) $[\text{M}+\text{H}]^+$ calcd for $\text{C}_{13}\text{H}_{21}\text{NOCl}$ 242.13117, found 242.13162.

4-((4-chloropyridin-2-yl)methyl)phenol

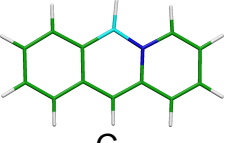
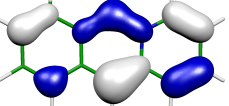
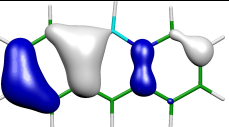
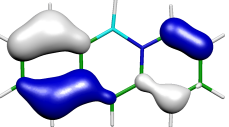
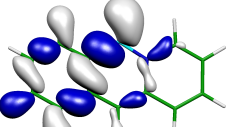
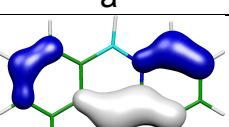
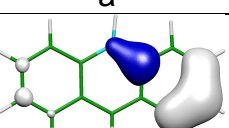


The pyridine (3.21 g, 13.2 mmol, 1 equiv) was combined in a pressure vessel with 4-bromoanisole (2.72 g, 14.6 mmol, 1.1 equiv), cesium carbonate (5.19 g, 15.9 mmol, 1.2 equiv) Pd(TFA)₂ (221 mg, 0.664 mmol, 5 mol%) and tricyclohexylphosphine (372 mg, 1.33 mmol, 10 mol%) and 10 mL toluene. The pressure vessel was sealed and heated to 140 °C for 16 hours. The mixture was cooled to room temperature, diluted with ethyl acetate, and the mixture was passed through a short plug of silica gel using ethyl acetate as the eluent. The filtrate was concentrated using a rotary evaporator. The residue was subjected to silica gel chromatography (10:1 hexane:ethyl acetate gradient to 3:1) to yield a yellow oil. Yield: 1.25 g, 40%. ¹H NMR (500 MHz, CDCl₃) δ 8.44 (d, *J* = 5.4 Hz, 1H), 7.17 (d, *J* = 8.3 Hz, 2H), 7.12 (d, *J* = 5.5 Hz, 1H), 7.09 (s, 1H), 6.86 (d, *J* = 8.3 Hz, 2H), 4.08 (s, 2H), 3.79 (s, 3H). ¹³C NMR (126 MHz, CDCl₃) δ 163.3, 158.6, 150.3, 144.6, 130.8, 130.3, 123.4, 121.8, 114.3, 55.4, 43.7. FTIR (ATR thin film): 2931, 2835, 1612, 1573, 1247, 1035, 885. HRMS (DART+) [M+H]⁺ calcd for C₁₃H₁₃NOCl 234.06857, found 234.06765.

UV-Photoelectron Spectroscopy

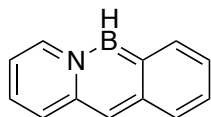
This spectrum was collected in the same manner as for the BN-1,2-anthracenes.

Table 1.12. UV-PES and calculated ionization energies.

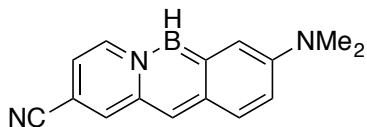
Nature of MO  C _s	$-\epsilon^{\text{K-S}}$	$\Delta\text{SCF+TD-DFT}$	OVGF	P3	SAC-CI	Corrected $x_{\text{exp}} = 0.655$	Exp.
 HOMO a''	6.385	6.893	6.768	6.931	6.180	7.04	7.04
 a''	8.371	8.937	8.600	8.856	8.284	9.026	8.85
 a''	8.613	9.119	8.907	9.080	8.600	9.268	9.13
 a'	10.194	10.505	10.444	10.503	10.150	10.849	10.44
 a''	10.210	10.734	10.730	10.869	10.275	10.865	10.52
 a''	10.365	10.691	10.652	10.738	10.427	11.020	10.99

Computational Details

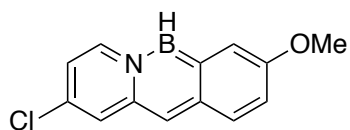
All calculations were performed using the Gaussian 09 program. TD-DFT optimizations were carried out at the CAM-B3LYP/6-311G(d,p) level using the PCM solvent model for cyclohexane.



C	2.478195	-1.391867	-0.000001
C	3.693863	-0.719198	0.000000
C	1.271306	-0.671974	-0.000001
C	1.303837	0.751100	0.000000
C	2.534302	1.394147	0.000001
C	3.730234	0.667759	0.000002
N	-1.267325	0.711132	-0.000003
B	-0.034002	1.481765	-0.000001
H	2.455183	-2.475703	-0.000004
H	4.618691	-1.283829	0.000003
H	2.567429	2.477991	0.000001
H	4.680814	1.186903	0.000004
C	0.018303	-1.321416	0.000003
C	-1.241066	-0.681916	0.000000
C	-2.485151	1.356053	-0.000007
C	-3.692412	0.654331	0.000005
C	-3.687174	-0.718773	0.000004
C	-2.438316	-1.393187	-0.000005
H	-0.001958	-2.404805	0.000006
H	-4.610727	-1.281939	0.000017
H	-2.389652	-2.472798	-0.000016
H	-2.434334	2.433292	-0.000016
H	-4.615380	1.218697	0.000014
H	-0.144319	2.665086	0.000009

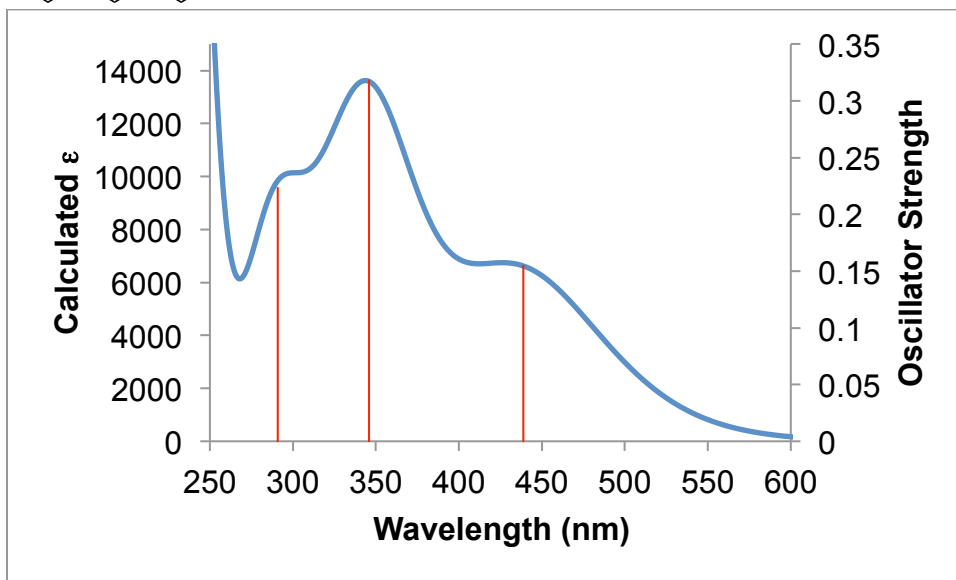
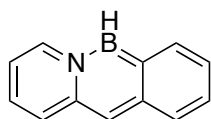


C	1.627599	-1.900555	-0.000450
C	2.939641	-1.501179	-0.000424
C	0.568583	-0.962246	-0.000295
C	0.903408	0.422079	-0.000079
C	2.228157	0.814760	-0.000080
C	3.287949	-0.127295	-0.000303
N	-1.604988	0.911889	0.000079
B	-0.251278	1.419599	0.000151
H	1.396081	-2.959845	-0.000610
H	3.714132	-2.254251	-0.000659
H	2.451166	1.872599	0.000277
C	-0.775829	-1.345808	-0.000325
C	-1.868883	-0.456859	-0.000084
C	-2.669189	1.806184	0.000219
C	-3.975616	1.389475	0.000222
C	-4.275717	0.025465	0.000120
C	-3.196884	-0.901969	0.000018
H	-1.019533	-2.401672	-0.000511
H	-3.385795	-1.964763	-0.000052
H	-4.763131	2.130316	0.000293
H	-0.111947	2.599547	0.000378
H	-2.389533	2.847708	0.000283
C	-5.618008	-0.415766	0.000120
N	-6.712066	-0.786013	0.000126
N	4.588631	0.273714	-0.000467
C	5.656897	-0.708113	0.001679
H	5.616351	-1.348196	-0.885191
H	6.613764	-0.193283	0.003295
H	5.613089	-1.347717	0.888719
C	4.925356	1.686048	-0.000734
H	4.536048	2.193549	0.887034
H	6.006755	1.791954	-0.002658
H	4.533118	2.193599	-0.887130



C	-2.227359	1.762635	-0.000001
C	-3.402650	1.021004	-0.000012
C	-0.974167	1.133855	-0.000002
C	-0.907180	-0.288175	-0.000014
C	-2.080833	-1.013986	-0.000025
C	-3.334033	-0.370402	-0.000023
N	1.668180	-0.112435	-0.000003
B	0.469072	-0.949222	-0.000015
H	-2.282396	2.845334	0.000006
H	-4.354938	1.531572	-0.000018
H	-2.070357	-2.097265	-0.000034
C	0.235821	1.847136	0.000005
C	1.526928	1.286725	0.000001
C	2.952774	-0.615612	0.000003
C	4.095157	0.192162	0.000004
C	3.954438	1.556267	0.000002
C	2.659495	2.105411	0.000002
H	0.201177	2.930206	0.000013
H	4.823786	2.200185	0.000003
H	2.508576	3.175125	0.000002
H	5.062159	-0.287961	0.000006
H	0.592024	-2.121820	-0.000023
Cl	3.179825	-2.330943	0.000012
O	-4.402449	-1.189787	-0.000046
C	-5.701166	-0.619938	0.000064
H	-5.864710	-0.011584	-0.893629
H	-6.394176	-1.457229	0.000123
H	-5.864557	-0.011583	0.893783

TD-DFT Results

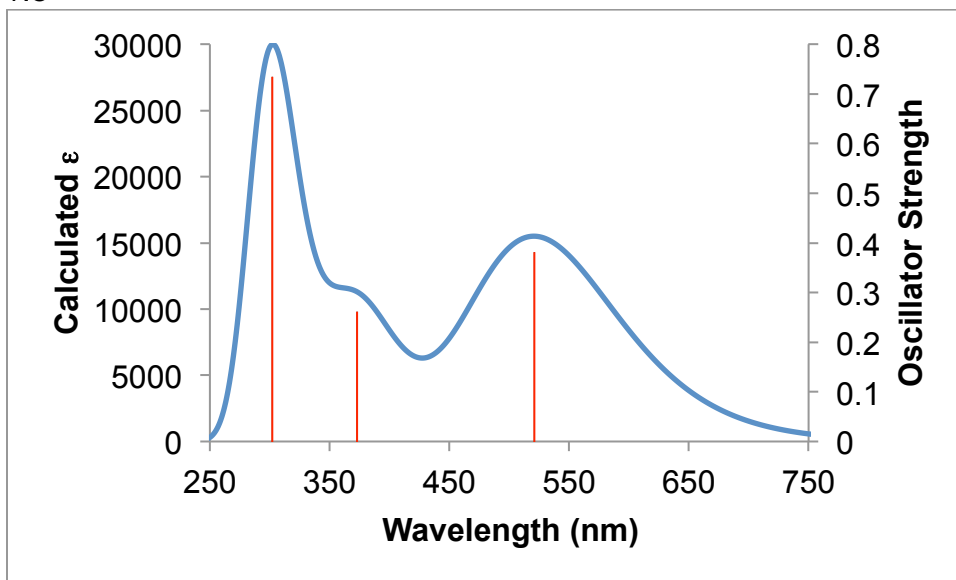
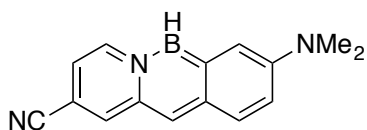


Excitation energies and oscillator strengths:

Excited State 1: Singlet-A 2.8251 eV 438.87 nm f=0.1548 $\langle S^2 \rangle$ =0.000
47 -> 48 -0.69996

Excited State 2: Singlet-A 3.58 eV 345.88 nm f=0.3187 $\langle S^2 \rangle$ =0.000
46 -> 48 0.15213
47 -> 49 0.67809

Excited State 3: Singlet-A 4.26 eV 290.85 nm f=0.2239 $\langle S^2 \rangle$ =0.000
47 -> 50 0.69036



Excitation energies and oscillator strengths:

Excited State 1: Singlet-A 2.38 eV 521.11 nm $f=0.3818$ $\langle S^2 \rangle=0.000$

64 -> 66 -0.10361

65 -> 66 0.68563

Excited State 2: Singlet-A 3.32 eV 373.12 nm $f=0.2612$ $\langle S^2 \rangle=0.000$

64 -> 66 -0.17885

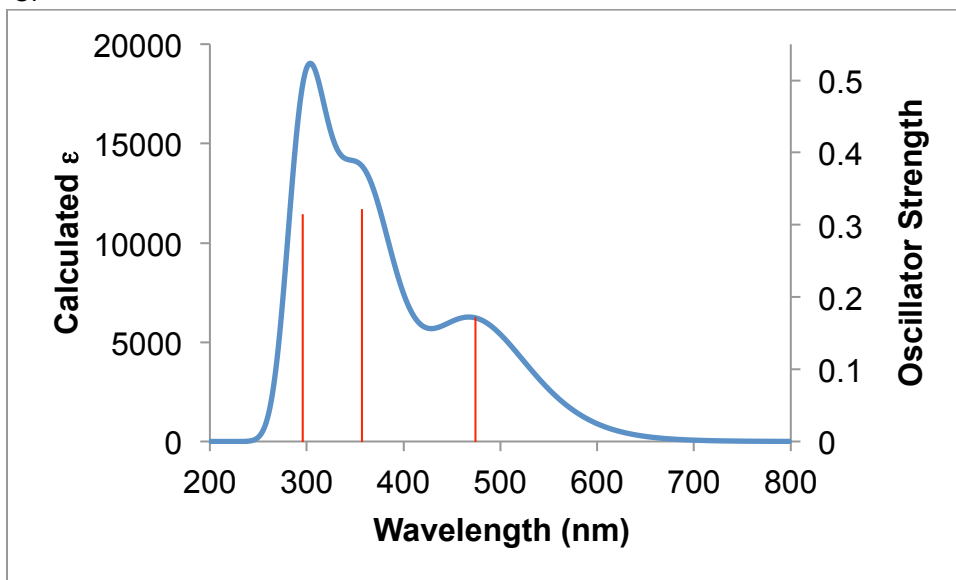
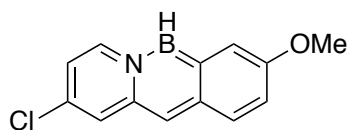
65 -> 67 0.66818

Excited State 3: Singlet-A 4.10 eV 302.11 nm $f=0.7348$ $\langle S^2 \rangle=0.000$

64 -> 66 0.24662

65 -> 66 0.11426

65 -> 68 0.62839



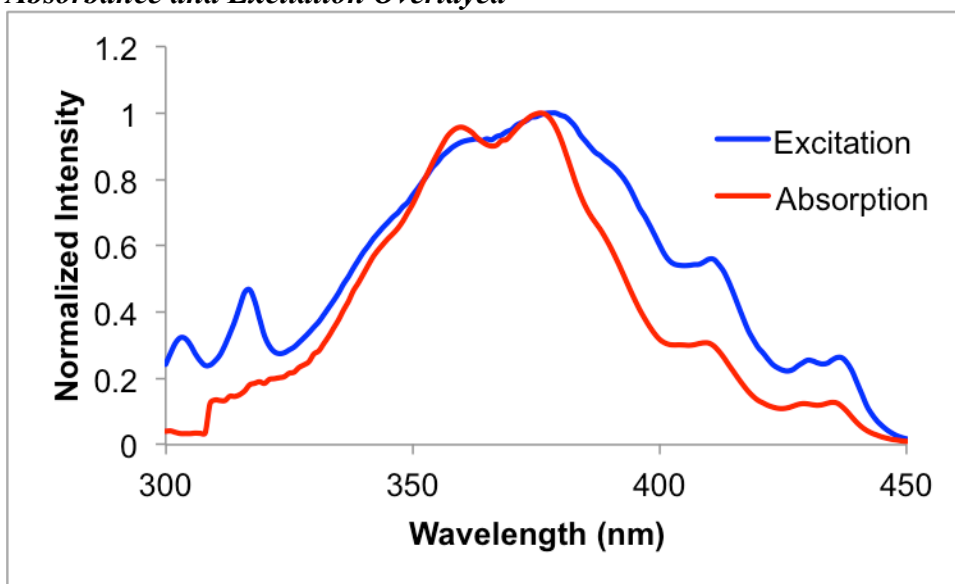
Excitation energies and oscillator strengths:

Excited State 1: Singlet-A 2.61 eV 474.52 nm $f=0.1719$ $\langle S^2 \rangle=0.000$
 63 -> 64 0.69929

Excited State 2: Singlet-A 3.47 eV 357.03 nm $f=0.3214$ $\langle S^2 \rangle=0.000$
 62 -> 64 -0.18028
 63 -> 65 -0.67059

Excited State 3: Singlet-A 4.19 eV 296.12 nm $f=0.3145$ $\langle S^2 \rangle=0.000$
 63 -> 66 0.68706

Absorbance and Excitation Overlayed



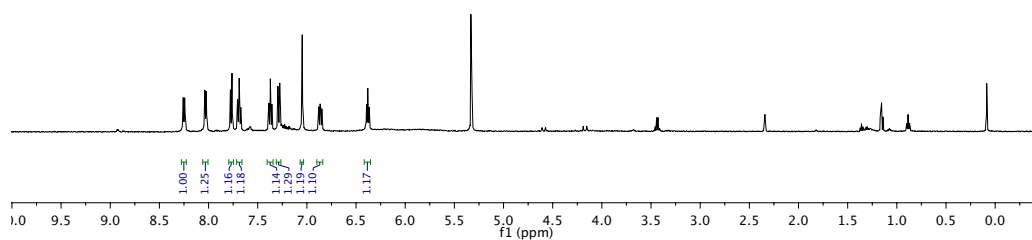
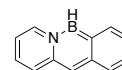
Crystal data and structure refinement for 1.37.

Identification code	C12H10BN	
Empirical formula	C ₁₂ H ₁₀ B N	
Formula weight	179.02	
Temperature	100(2) K	
Wavelength	1.54178 \approx	
Crystal system	Monoclinic	
Space group	P2 ₁ /c	
Unit cell dimensions	a = 9.2912(5) \approx b = 6.0861(3) \approx c = 8.3411(5) \approx	$\alpha = 90^\circ$. $\beta = 102.492(3)^\circ$. $\gamma = 90^\circ$.
Volume	460.50(4) \approx^3	
Z	2	
Density (calculated)	1.291 Mg/m ³	
Absorption coefficient	0.565 mm ⁻¹	
F(000)	188	
Crystal size	0.180 x 0.080 x 0.060 mm ³	
Theta range for data collection	4.875 to 67.325 $^\circ$.	
Index ranges	-11 \leq h \leq 10, -7 \leq k \leq 7, -9 \leq l \leq 9	
Reflections collected	3742	
Independent reflections	822 [R(int) = 0.0216]	
Completeness to theta = 67.325 $^\circ$	99.6 %	
Absorption correction	Semi-empirical from equivalents	
Max. and min. transmission	0.7529 and 0.6754	
Refinement method	Full-matrix least-squares on F ²	
Data / restraints / parameters	822 / 0 / 67	
Goodness-of-fit on F ²	1.089	
Final R indices [I > 2sigma(I)]	R ₁ = 0.0379, wR ₂ = 0.1028	
R indices (all data)	R ₁ = 0.0398, wR ₂ = 0.1048	
Extinction coefficient	n/a	
Largest diff. peak and hole	0.220 and -0.201 e. \approx^3	

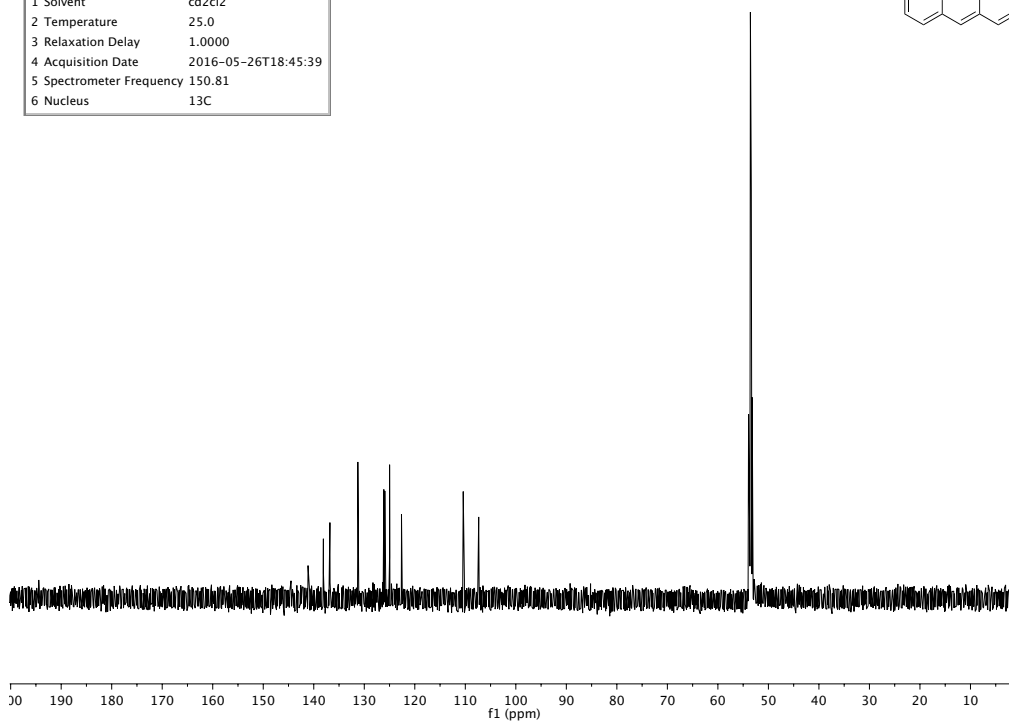
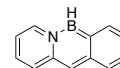
Crystal data and structure refinement for 1.38.

Identification code	C21H20BN	
Empirical formula	C ₂₁ H ₂₀ B N	
Formula weight	297.19	
Temperature	100(2) K	
Wavelength	0.71073 \approx	
Crystal system	Triclinic	
Space group	P1	
Unit cell dimensions	a = 8.8660(6) \approx b = 9.3604(7) \approx c = 11.0495(8) \approx	α = 82.031(2) $^\circ$. β = 82.674(2) $^\circ$. γ = 66.299(2) $^\circ$.
Volume	828.93(10) \approx^3	
Z	2	
Density (calculated)	1.191 Mg/m ³	
Absorption coefficient	0.068 mm ⁻¹	
F(000)	316	
Crystal size	0.600 x 0.370 x 0.240 mm ³	
Theta range for data collection	1.867 to 33.316 $^\circ$.	
Index ranges	-13 \leq h \leq 13, -14 \leq k \leq 14, -17 \leq l \leq 17	
Reflections collected	31412	
Independent reflections	11905 [R(int) = 0.0206]	
Completeness to theta = 25.242 $^\circ$	100.0 %	
Absorption correction	Semi-empirical from equivalents	
Max. and min. transmission	0.7465 and 0.7101	
Refinement method	Full-matrix least-squares on F ²	
Data / restraints / parameters	11905 / 3 / 421	
Goodness-of-fit on F ²	1.032	
Final R indices [I \geq 2 σ (I)]	R1 = 0.0431, wR2 = 0.1179	
R indices (all data)	R1 = 0.0492, wR2 = 0.1231	
Extinction coefficient	n/a	
Largest diff. peak and hole	0.424 and -0.260 e. \approx^3	

Parameter	Value
1 Solvent	cd2cl2
2 Temperature	25.0
3 Relaxation Delay	1.0000
4 Acquisition Date	2016-05-26T17:32:03
5 Spectrometer Frequency	499.78
6 Nucleus	¹ H

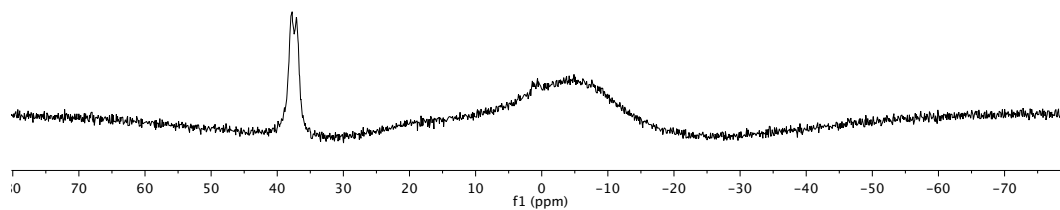
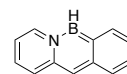


Parameter	Value
1 Solvent	cd2cl2
2 Temperature	25.0
3 Relaxation Delay	1.0000
4 Acquisition Date	2016-05-26T18:45:39
5 Spectrometer Frequency	150.81
6 Nucleus	¹³ C

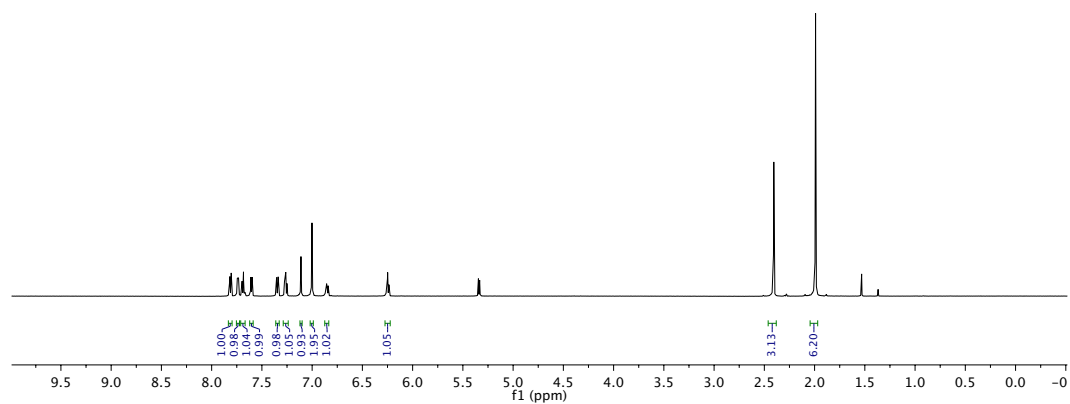
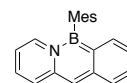


ji-VI-B227 D

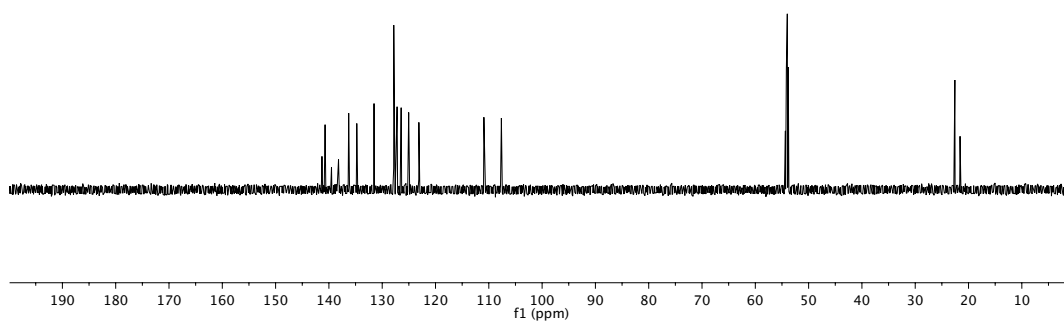
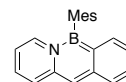
Parameter	Value
1 Solvent	cd2cl2
2 Temperature	25.0
3 Relaxation Delay	0.0100
4 Acquisition Date	2016-05-26T17:33:10
5 Spectrometer Frequency	160.35
6 Nucleus	11B



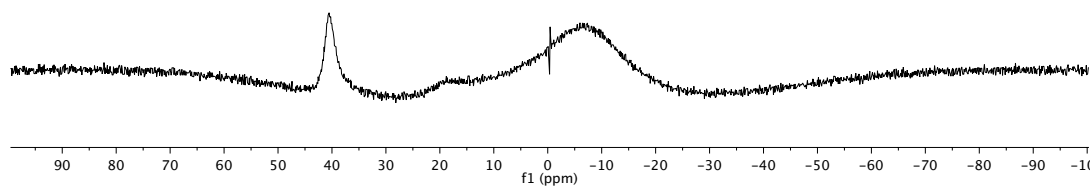
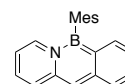
Parameter	Value
1 Solvent	cd2cl2
2 Temperature	25.0
3 Relaxation Delay	1.0000
4 Acquisition Date	2017-06-04T15:46:47
5 Spectrometer Frequency	599.69
6 Nucleus	1H



Parameter	Value
1 Solvent	cd2cl2
2 Temperature	25.0
3 Relaxation Delay	1.0000
4 Acquisition Date	2017-06-04T15:46:53
5 Spectrometer Frequency	150.81
6 Nucleus	13C

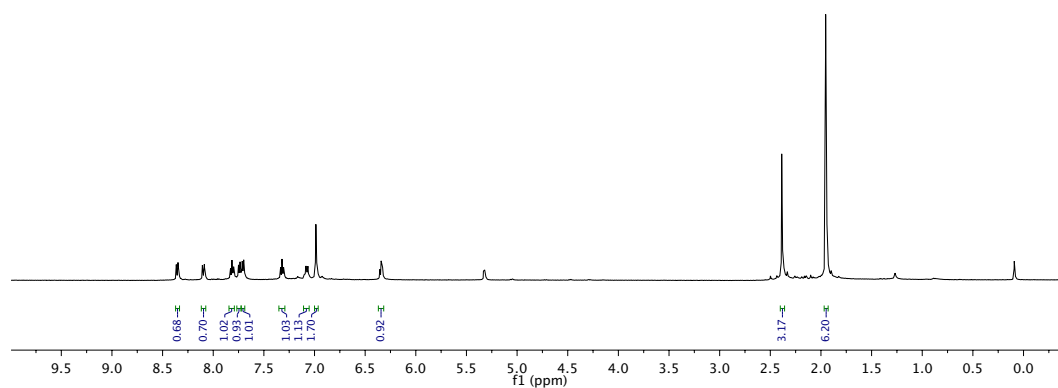
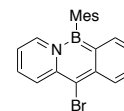


Parameter	Value
1 Solvent	cd2cl2
2 Temperature	25.0
3 Relaxation Delay	0.0100
4 Acquisition Date	2016-08-05T12:34:46
5 Spectrometer Frequency	160.35
6 Nucleus	11B

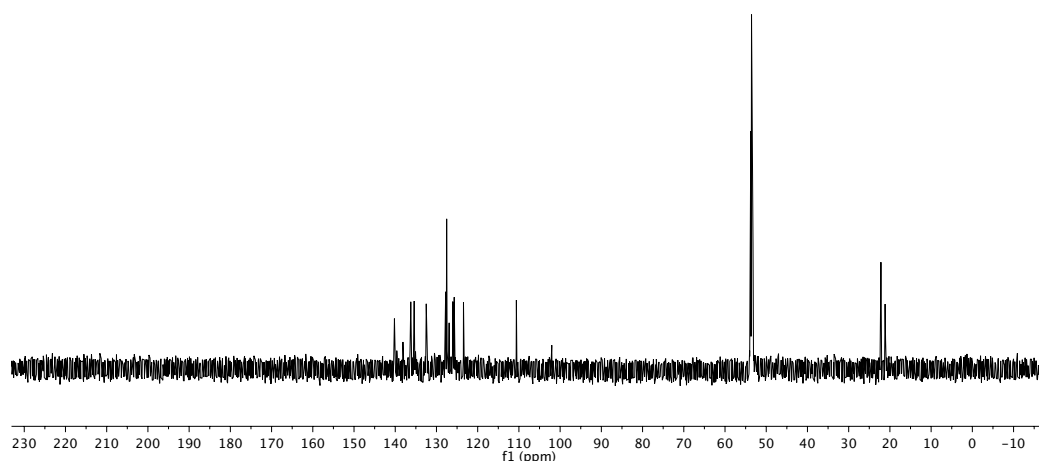
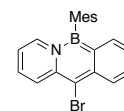


ji-1-015 1H C

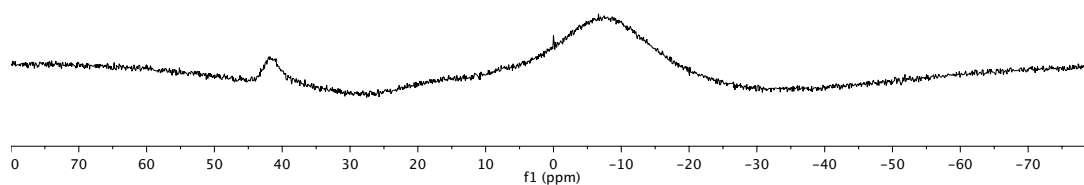
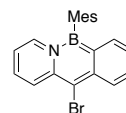
Parameter	Value
1 Solvent	cd2cl2
2 Temperature	25.0
3 Relaxation Delay	1.0000
4 Acquisition Date	2016-09-07T17:40:53
5 Spectrometer Frequency	499.78
6 Nucleus	1H



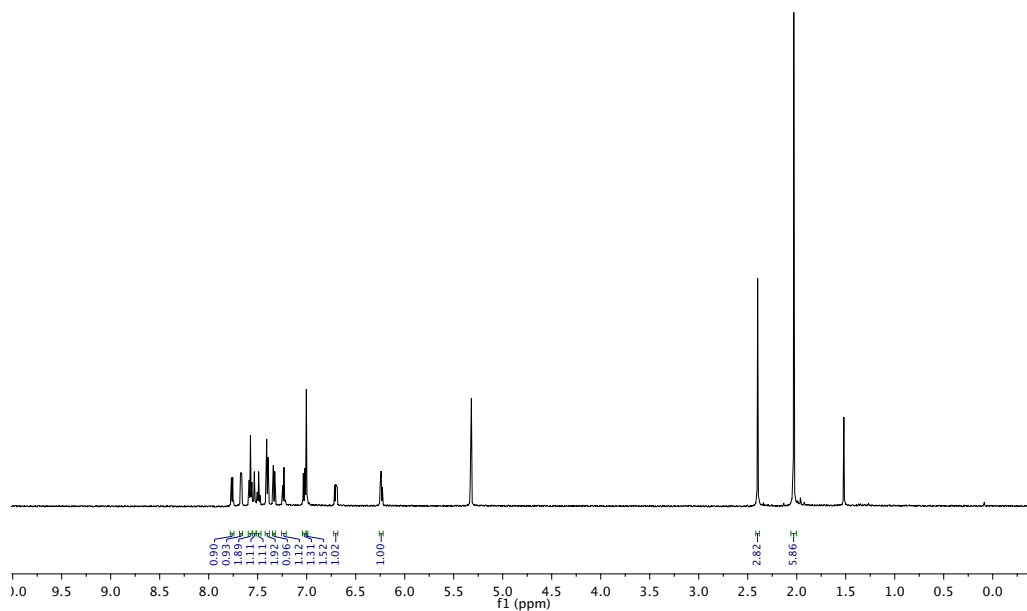
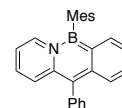
Parameter	Value
1 Solvent	cd2cl2
2 Temperature	25.0
3 Relaxation Delay	1.0000
4 Acquisition Date	2016-09-08T17:31:08
5 Spectrometer Frequency	150.81
6 Nucleus	13C



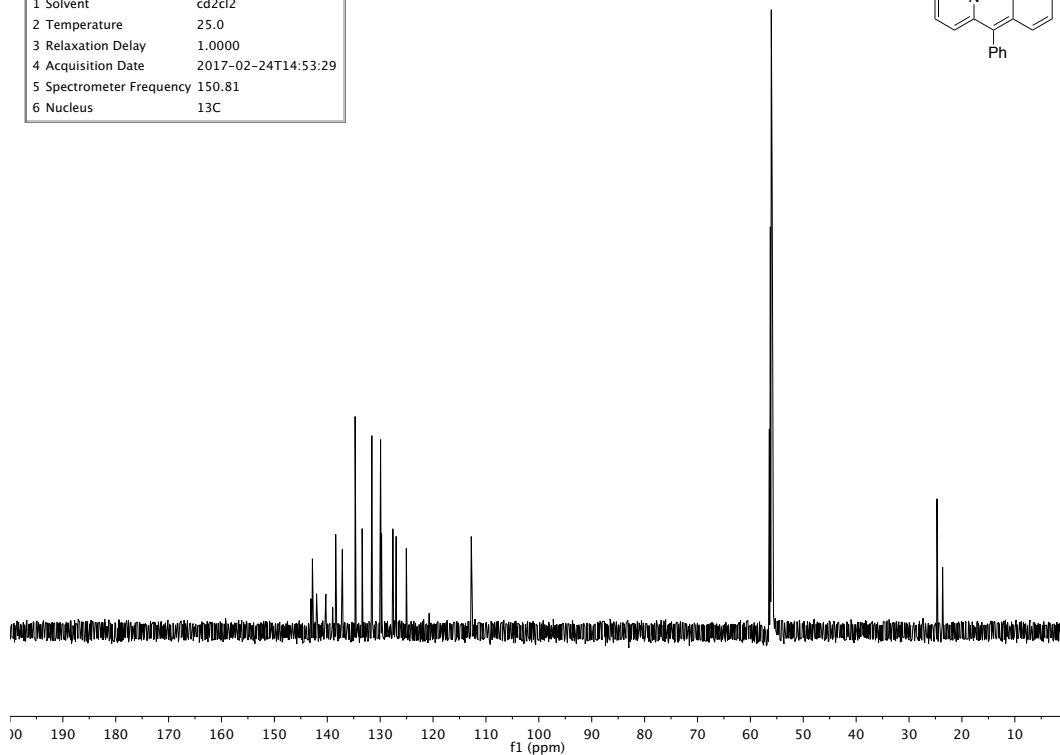
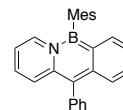
Parameter	Value
1 Solvent	cd2cl2
2 Temperature	25.0
3 Relaxation Delay	0.0100
4 Acquisition Date	2016-09-07T13:42:40
5 Spectrometer Frequency	160.35
6 Nucleus	11B



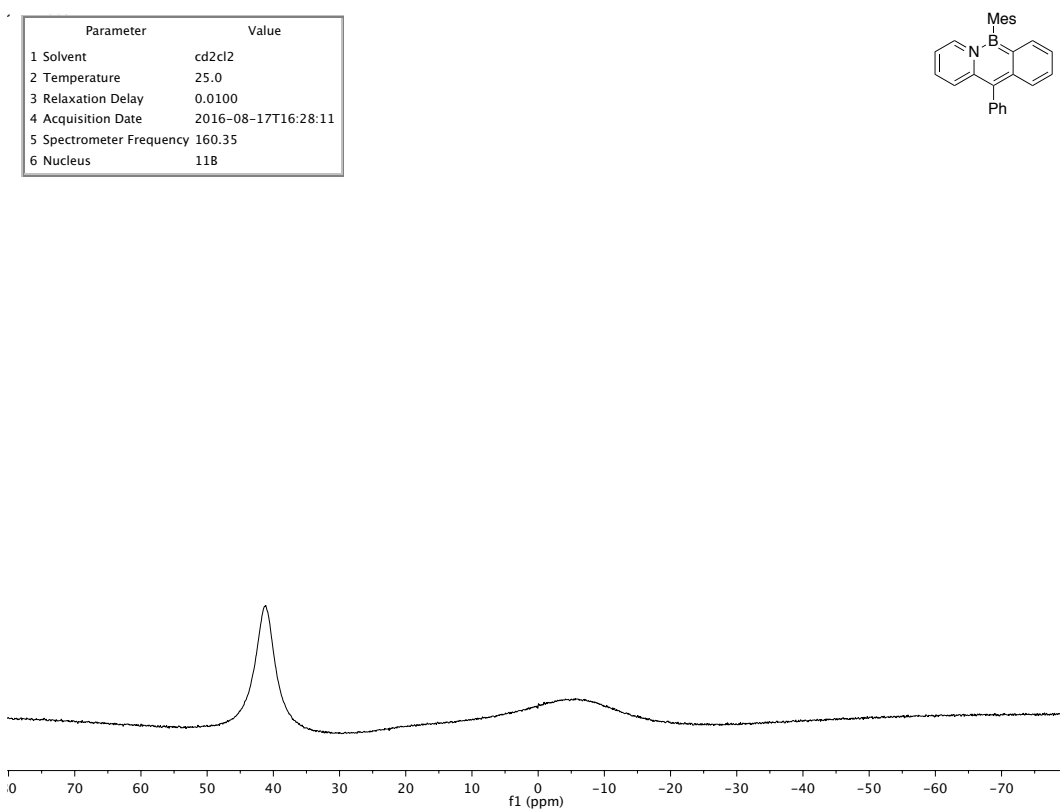
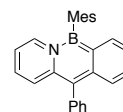
Parameter	Value
1 Solvent	cd2cl2
2 Temperature	25.0
3 Relaxation Delay	1.0000
4 Acquisition Date	2017-02-24T14:53:16
5 Spectrometer Frequency	599.69
6 Nucleus	1H



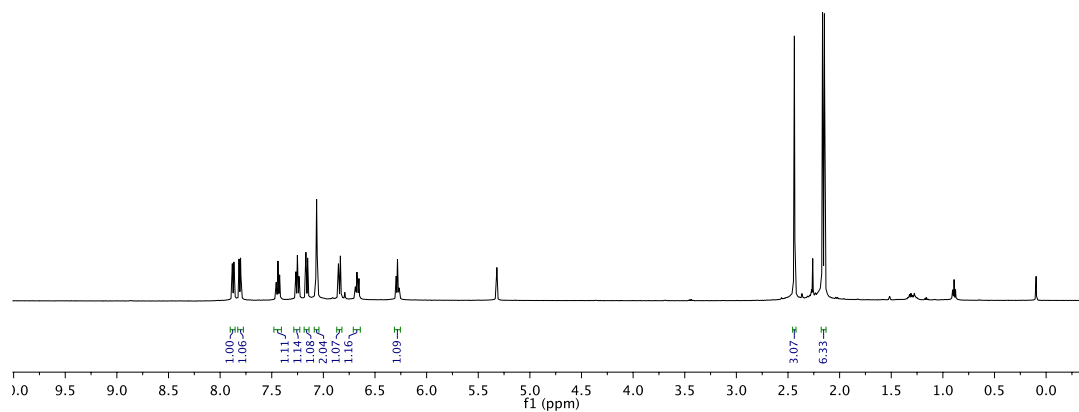
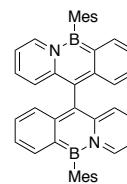
Parameter	Value
1 Solvent	cd2cl2
2 Temperature	25.0
3 Relaxation Delay	1.0000
4 Acquisition Date	2017-02-24T14:53:29
5 Spectrometer Frequency	150.81
6 Nucleus	¹³ C



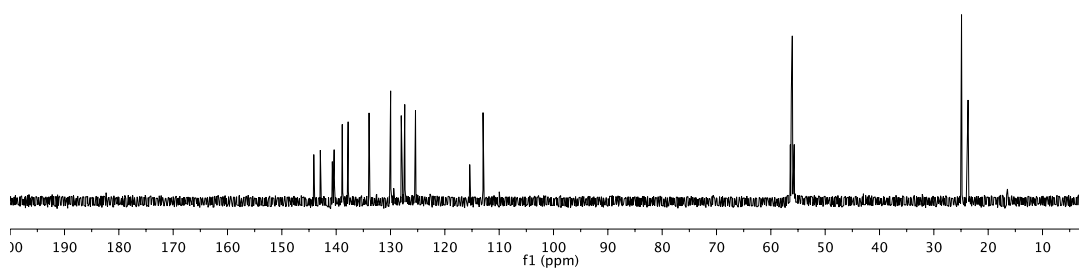
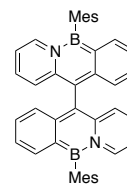
Parameter	Value
1 Solvent	cd2cl2
2 Temperature	25.0
3 Relaxation Delay	0.0100
4 Acquisition Date	2016-08-17T16:28:11
5 Spectrometer Frequency	160.35
6 Nucleus	¹¹ B



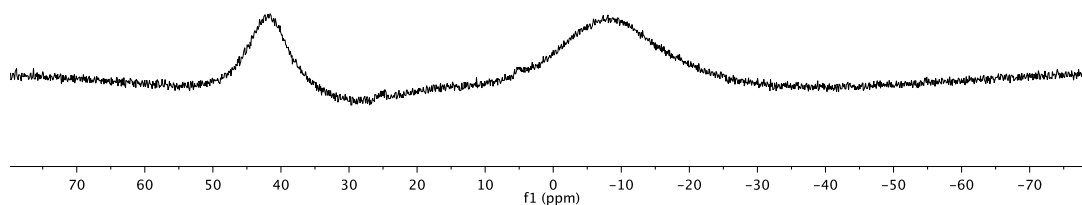
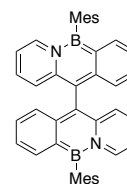
Parameter	Value
1 Solvent	cd2cl2
2 Temperature	25.0
3 Relaxation Delay	1.0000
4 Acquisition Date	2016-07-07T19:37:20
5 Spectrometer Frequency	499.78
6 Nucleus	¹ H



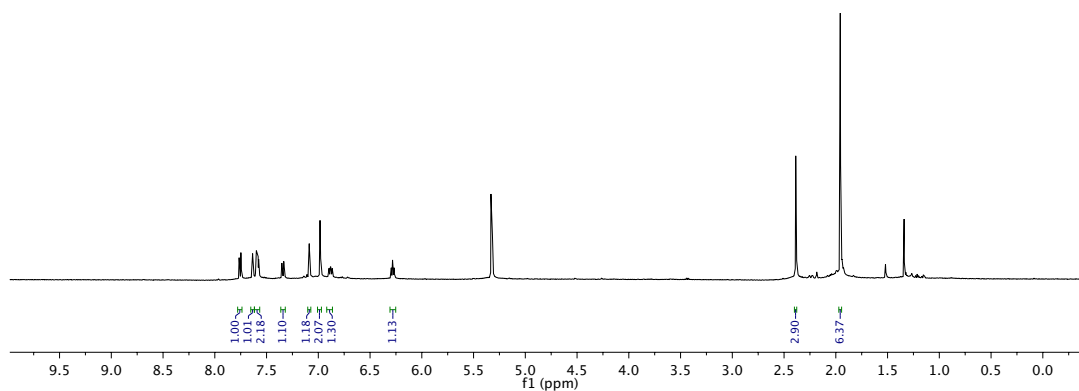
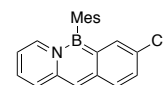
Parameter	Value
1 Solvent	cd2cl2
2 Temperature	25.0
3 Relaxation Delay	1.0000
4 Acquisition Date	2016-07-08T10:33:25
5 Spectrometer Frequency	150.81
6 Nucleus	¹³ C



Parameter	Value
1 Solvent	cd2cl2
2 Temperature	25.0
3 Relaxation Delay	0.0100
4 Acquisition Date	2016-07-07T19:34:45
5 Spectrometer Frequency	160.35
6 Nucleus	11B

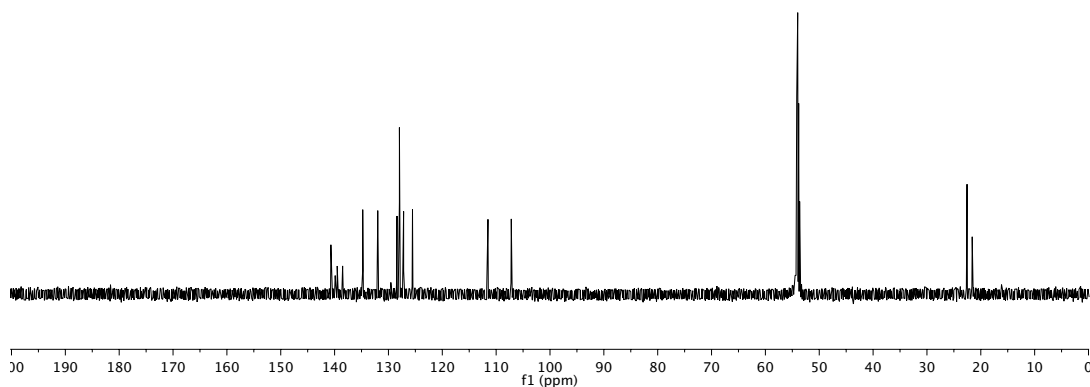
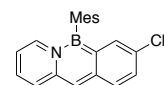


Parameter	Value
1 Solvent	cd2cl2
2 Temperature	25.0
3 Relaxation Delay	1.0000
4 Acquisition Date	2017-03-21T15:02:32
5 Spectrometer Frequency	499.78
6 Nucleus	1H

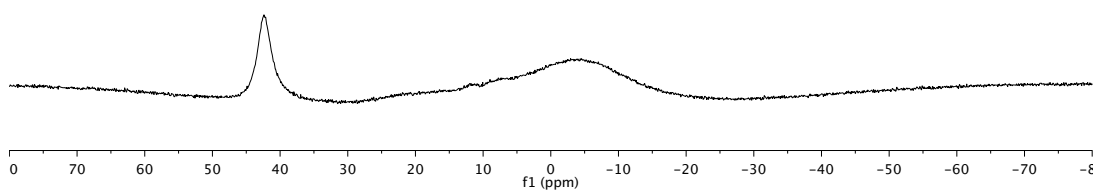
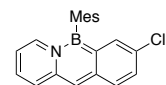


ji-2-067 13C J2

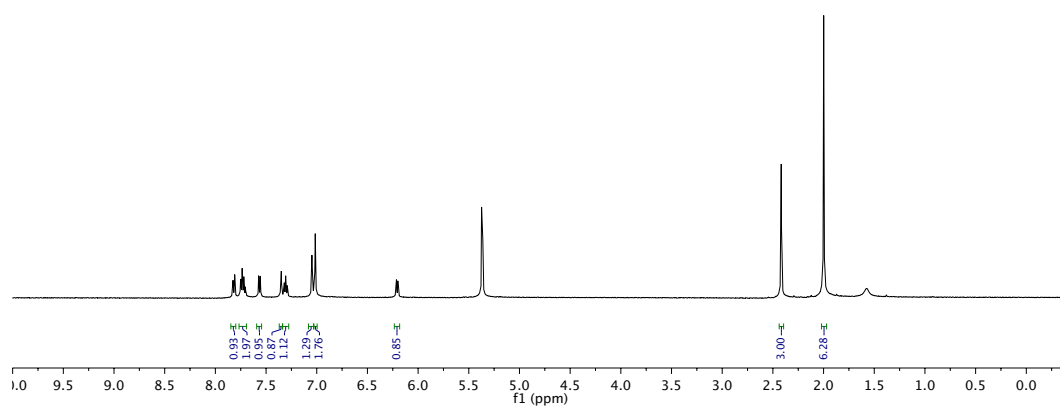
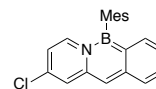
Parameter	Value
1 Solvent	cd2cl2
2 Temperature	25.0
3 Relaxation Delay	1.0000
4 Acquisition Date	2017-04-12T12:12:39
5 Spectrometer Frequency	150.81
6 Nucleus	13C



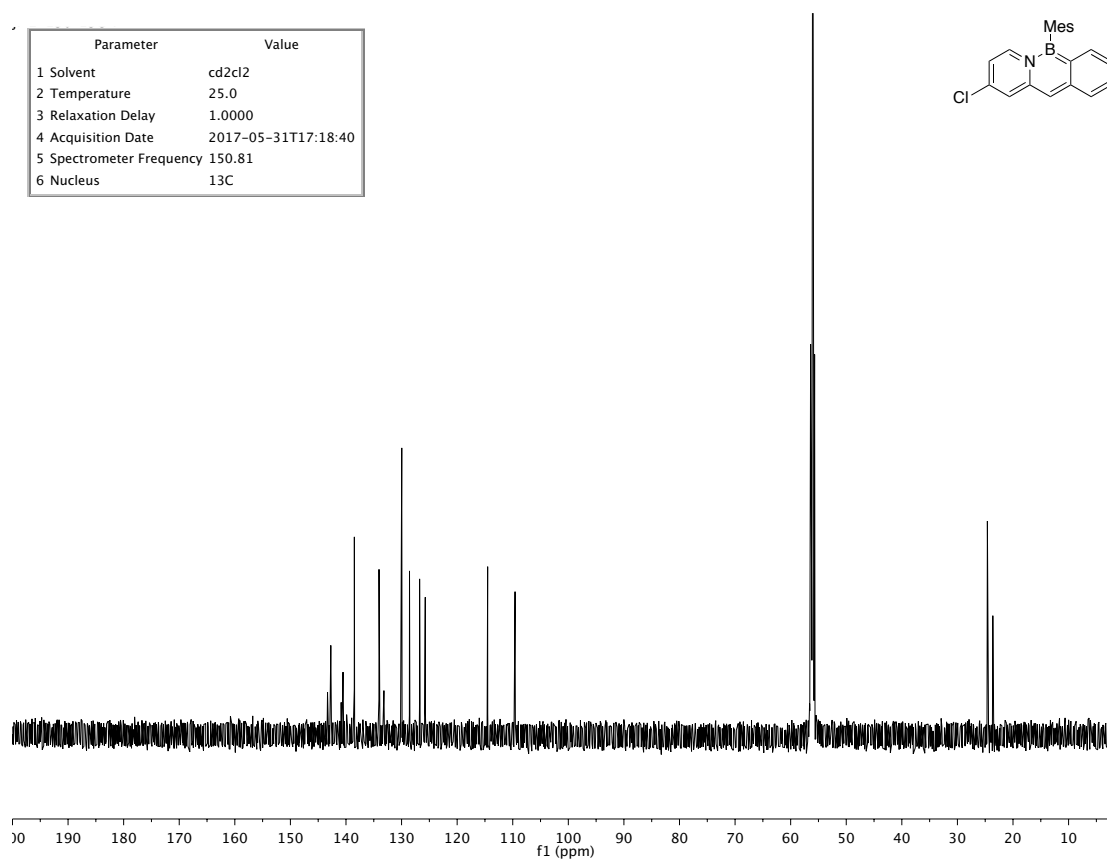
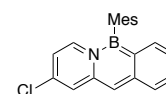
Parameter	Value
1 Solvent	cd2cl2
2 Temperature	25.0
3 Relaxation Delay	0.0100
4 Acquisition Date	2017-03-20T16:01:06
5 Spectrometer Frequency	160.35
6 Nucleus	11B



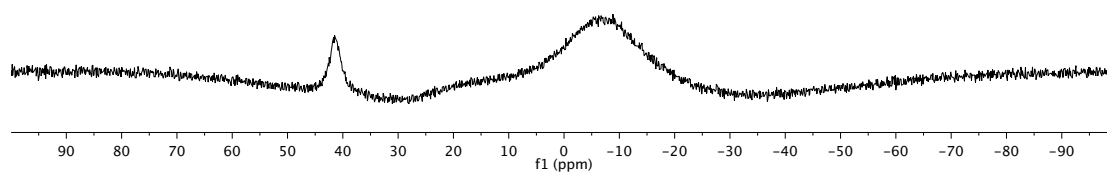
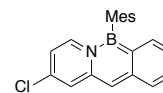
Parameter	Value
1 Solvent	cd2cl2
2 Temperature	25.0
3 Relaxation Delay	1.0000
4 Acquisition Date	2017-05-31T17:12:13
5 Spectrometer Frequency	499.78
6 Nucleus	¹ H



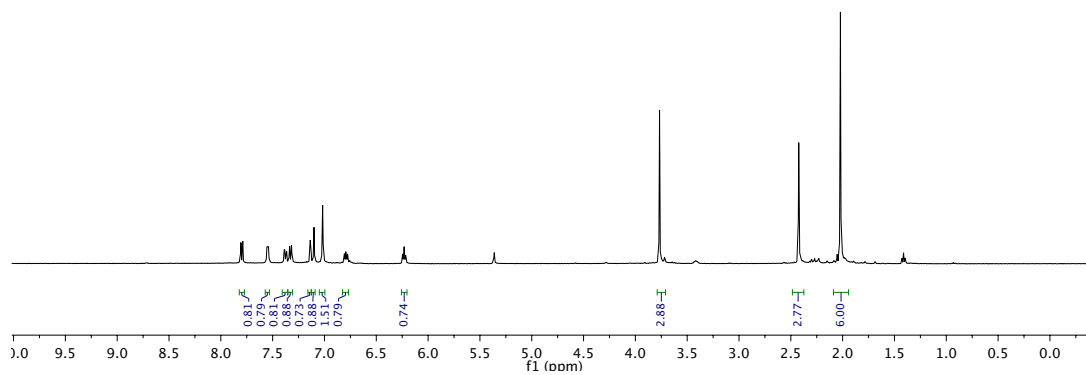
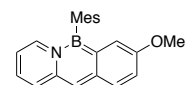
Parameter	Value
1 Solvent	cd2cl2
2 Temperature	25.0
3 Relaxation Delay	1.0000
4 Acquisition Date	2017-05-31T17:18:40
5 Spectrometer Frequency	150.81
6 Nucleus	¹³ C



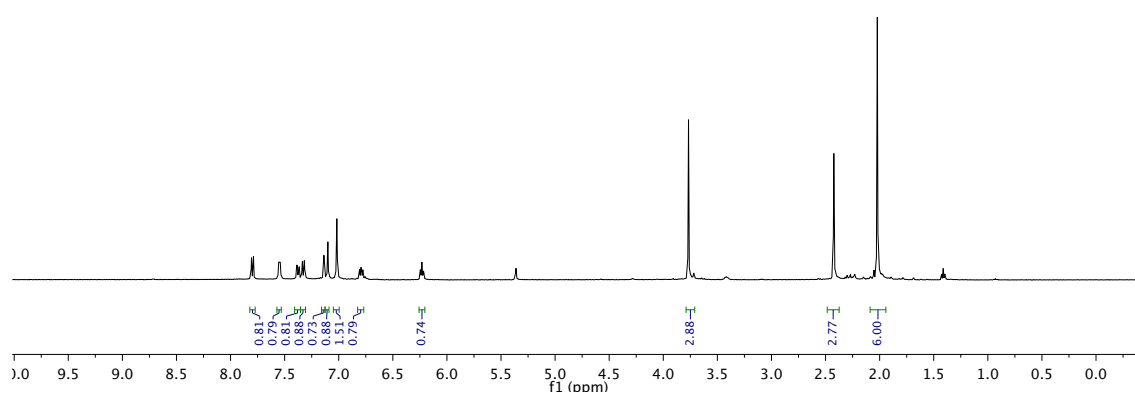
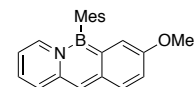
Parameter	Value
1 Solvent	cd2cl2
2 Temperature	25.0
3 Relaxation Delay	0.0100
4 Acquisition Date	2017-05-31T17:10:47
5 Spectrometer Frequency	160.35
6 Nucleus	11B



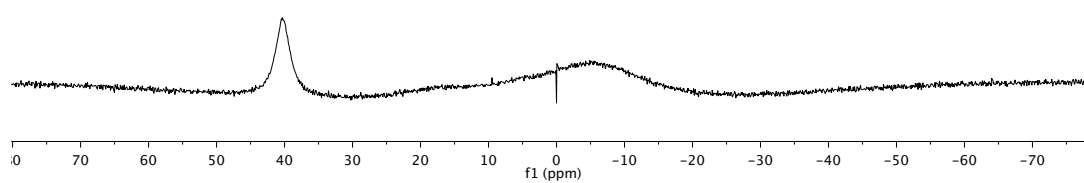
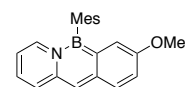
Parameter	Value
1 Solvent	cd2cl2
2 Temperature	25.0
3 Relaxation Delay	1.0000
4 Acquisition Date	2017-06-04T18:42:09
5 Spectrometer Frequency	499.78
6 Nucleus	1H



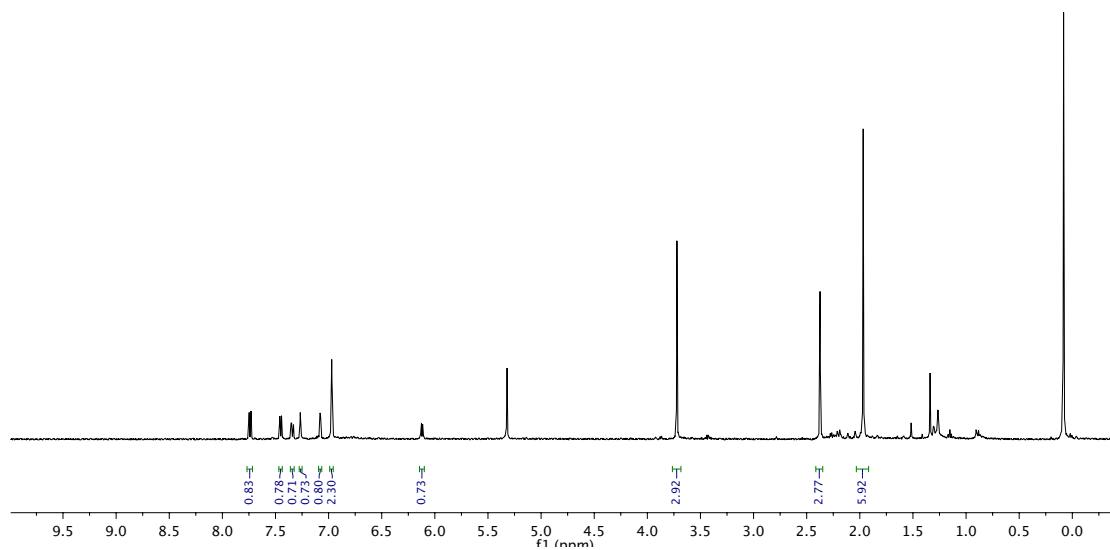
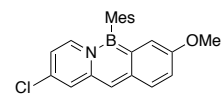
Parameter	Value
1 Solvent	cd2cl2
2 Temperature	25.0
3 Relaxation Delay	1.0000
4 Acquisition Date	2017-06-04T18:42:09
5 Spectrometer Frequency	499.78
6 Nucleus	¹ H



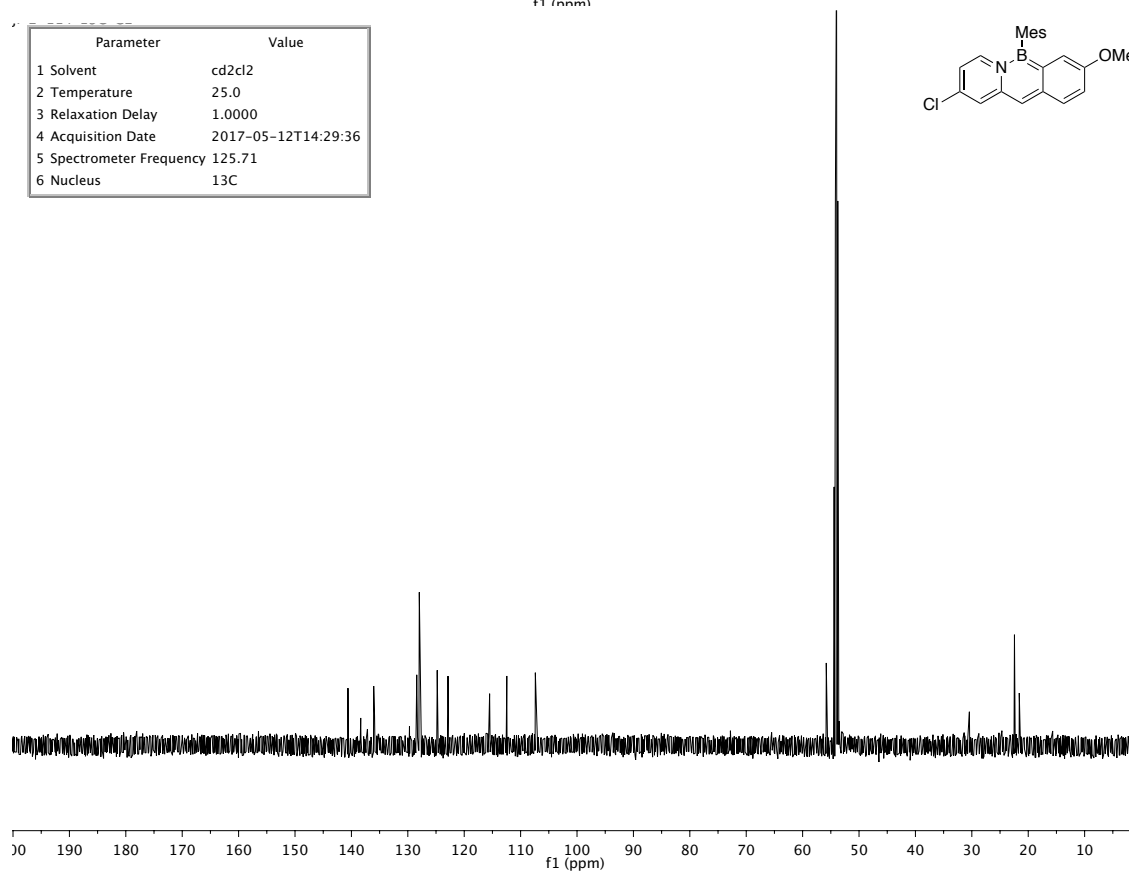
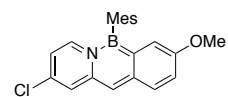
Parameter	Value
1 Solvent	cd2cl2
2 Temperature	25.0
3 Relaxation Delay	0.0100
4 Acquisition Date	2017-06-04T18:40:13
5 Spectrometer Frequency	160.35
6 Nucleus	¹³ C



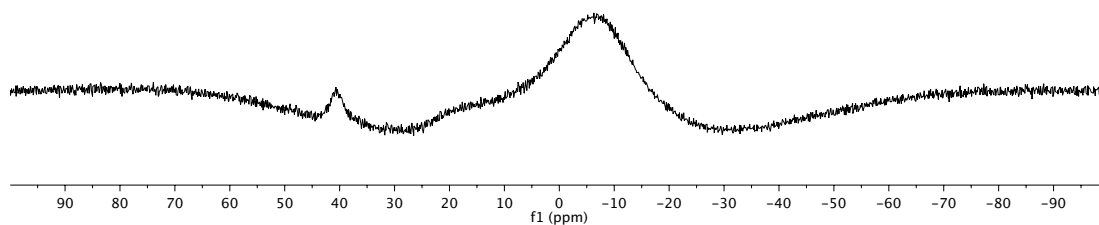
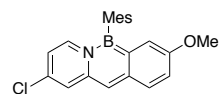
Parameter	Value
1 Solvent	cd2cl2
2 Temperature	25.0
3 Relaxation Delay	1.0000
4 Acquisition Date	2017-05-12T10:02:20
5 Spectrometer Frequency	499.78
6 Nucleus	¹ H



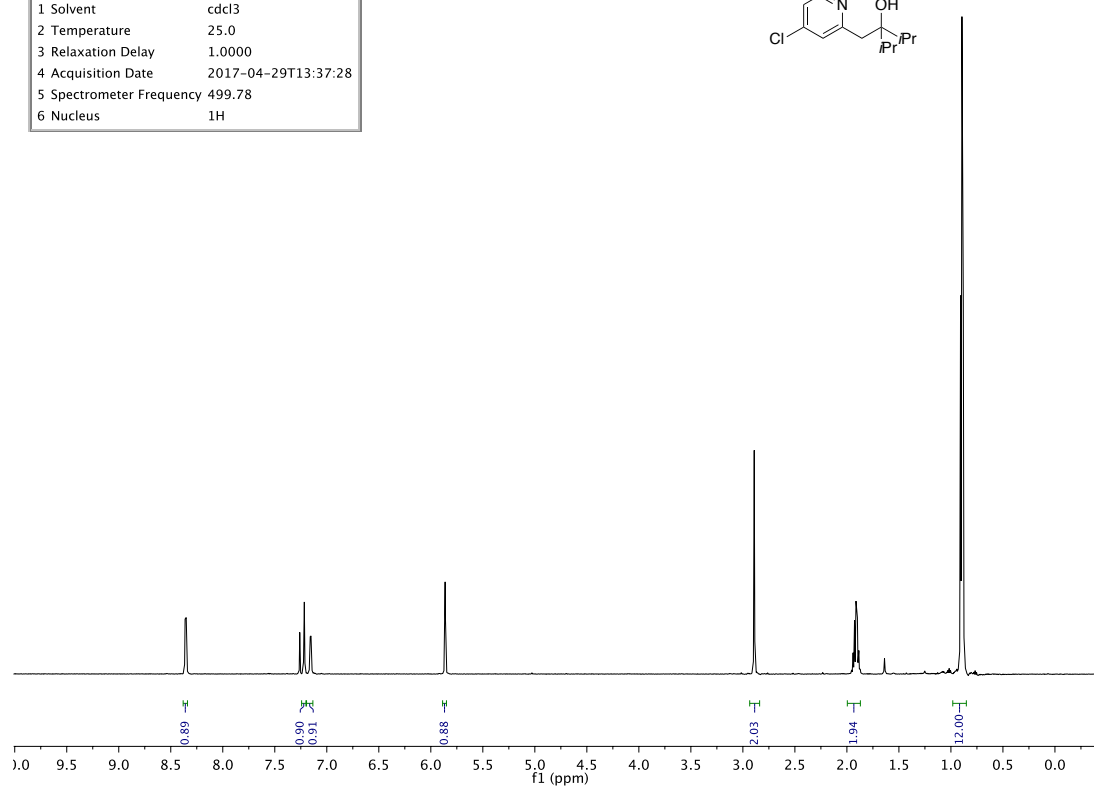
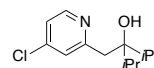
Parameter	Value
1 Solvent	cd2cl2
2 Temperature	25.0
3 Relaxation Delay	1.0000
4 Acquisition Date	2017-05-12T14:29:36
5 Spectrometer Frequency	125.71
6 Nucleus	¹³ C



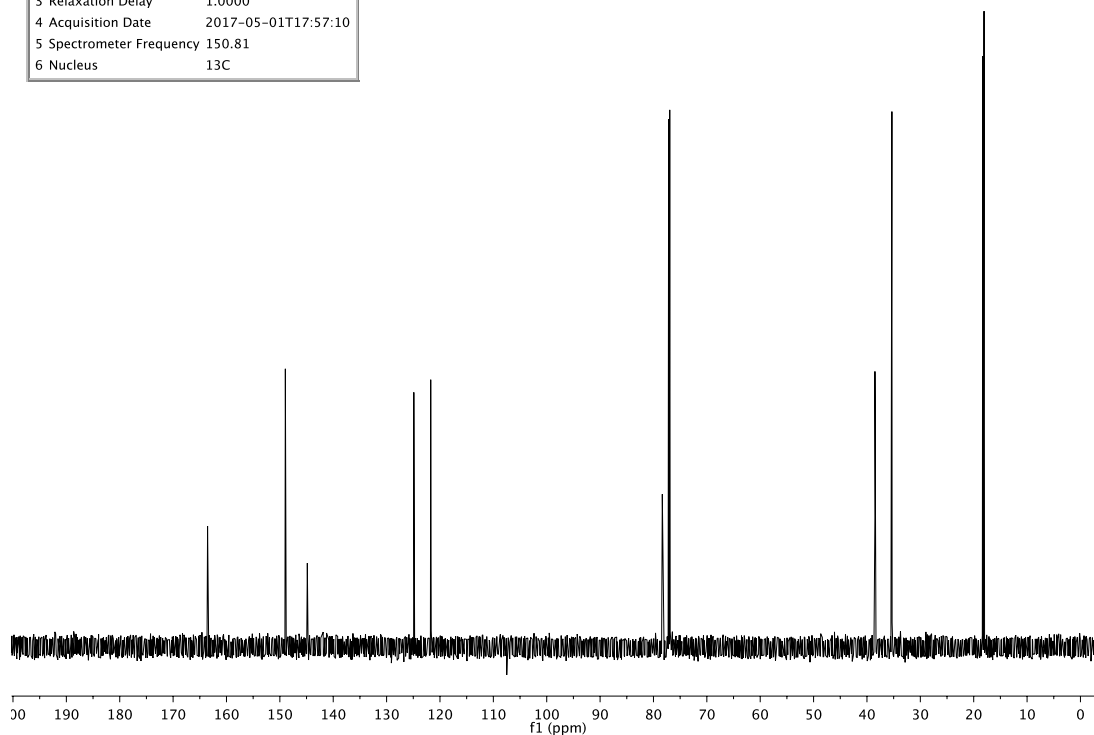
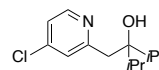
Parameter	Value
1 Solvent	cd2cl2
2 Temperature	25.0
3 Relaxation Delay	0.0100
4 Acquisition Date	2017-05-10T11:58:14
5 Spectrometer Frequency	160.35
6 Nucleus	11B



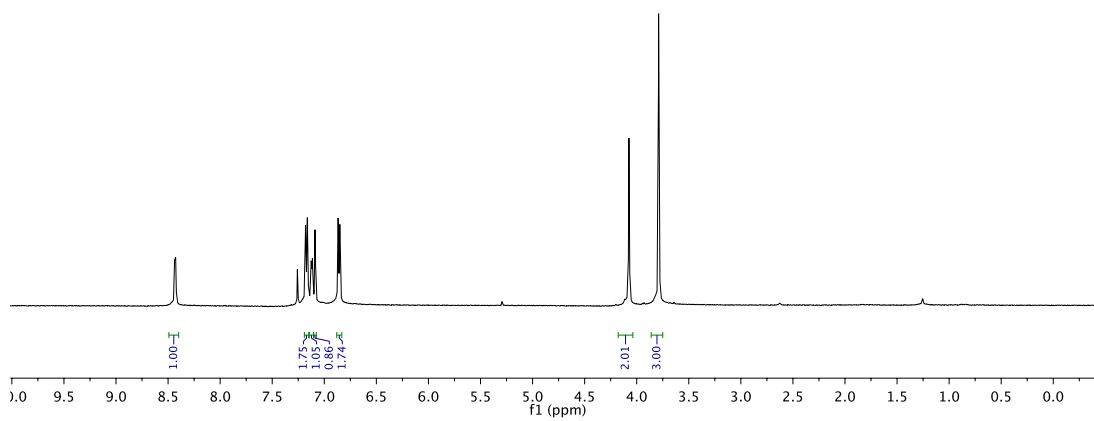
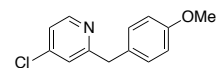
Parameter	Value
1 Solvent	cdcl3
2 Temperature	25.0
3 Relaxation Delay	1.0000
4 Acquisition Date	2017-04-29T13:37:28
5 Spectrometer Frequency	499.78
6 Nucleus	1H



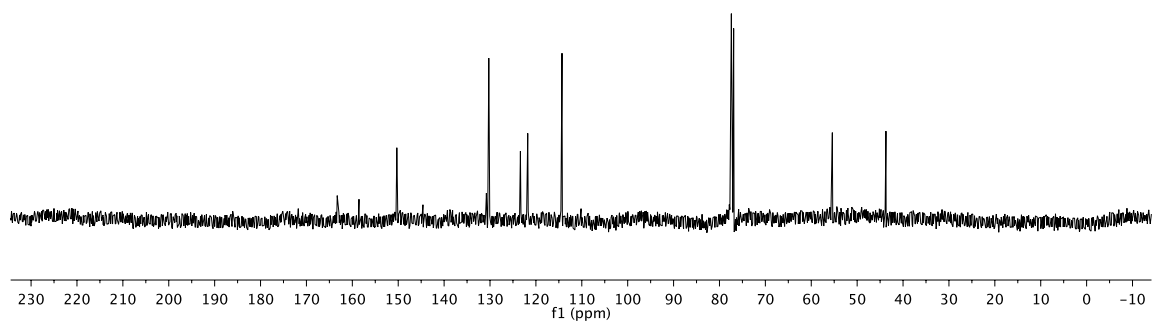
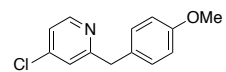
Parameter	Value
1 Solvent	cdcl3
2 Temperature	25.0
3 Relaxation Delay	1.0000
4 Acquisition Date	2017-05-01T17:57:10
5 Spectrometer Frequency	150.81
6 Nucleus	¹³ C



Parameter	Value
1 Solvent	cdcl3
2 Temperature	25.0
3 Relaxation Delay	1.0000
4 Acquisition Date	2017-05-05T19:14:29
5 Spectrometer Frequency	499.88
6 Nucleus	¹ H



Parameter	Value
1 Solvent	cdcl3
2 Temperature	25.0
3 Relaxation Delay	1.0000
4 Acquisition Date	2017-05-05T19:15:51
5 Spectrometer Frequency	125.71
6 Nucleus	13C



Chapter 2

The Aromatic Claisen Rearrangement of Azaborines

2.1 Introduction

The previous chapter demonstrated BN/CC isosterism as a tool to change electronic structure of a given aromatic system without changing the steric profile. BN/CC isosterism therefore also has consequences in terms of aromaticity and reactivity, and it has many potential applications. For example, isosteric azaborines and benzenes can bind to protein cavities in a similar structural way¹ but may convey different function² perhaps as a result of hydrogen bonding³ or the dipole moment introduced by the heteroatoms.⁴ Uncovering the basic properties and reactivity of monocyclic azaborines should therefore inform future applications.

Our group, as well as the group of Ashe, has investigated the energetic⁵, magnetic⁴, structural⁶, and reactivity-related⁷ consequences of BN/CC isosterism with respect to the aromaticity of the monocyclic 1,2-azaborine core.⁸ One important energetic parameter, resonance stabilization energy (RSE), measures the additional thermodynamic stability associated with conjugated unsaturation, (e.g., in aromatic molecules) relative to

¹ Liu, L.; Marwitz, A. J. V.; Matthews, B. W.; Liu, S.-Y. *Angew. Chem. Int. Ed.* **2009**, *48*, 6817–6819.

² (a) Knack, D. H.; Marshall, J. L.; Harlow, G. P.; Dudzik, A.; Szaleniec, M.; Liu, S.-Y.; Heider, J. *Angew.*

² (a) Knack, D. H.; Marshall, J. L.; Harlow, G. P.; Dudzik, A.; Szaleniec, M.; Liu, S.-Y.; Heider, J. *Angew. Chem. Int. Ed.* **2013**, *52*, 2599–2601. (b) Zhao, P.; Nettleton, D. O.; Karki, R. G.; Zécari, F. J.; Liu, S.-Y. *ChemMedChem* **2017**, *12*, 358–361.

³ Lee, H.; Fischer, M.; Shoichet, B. K.; Liu, S.-Y. *J. Am. Chem. Soc.* **2016**, *138*, 12021–12024.

⁴ Marwitz, A. J. V.; Matus, M. H.; Zakharov, L. N.; Dixon, D. A.; Liu, S.-Y. *Angew. Chem. Int. Ed.* **2009**, *48*, 973–977.

⁵ (a) Campbell, P. G.; Abbey, E. R.; Neiner, D.; Grant, D. J.; Dixon, D. A.; Liu, S.-Y. *J. Am. Chem. Soc.* **2010**, *132*, 18048–18050. (b) Chrostowska, A.; Xu, S.; Lamm, A. N.; Mazière, A.; Weber, C. D.; Dargelos, A.; Baylère, P.; Graciaa, A.; Liu, S.-Y. *J. Am. Chem. Soc.* **2012**, *134*, 10279–10285.

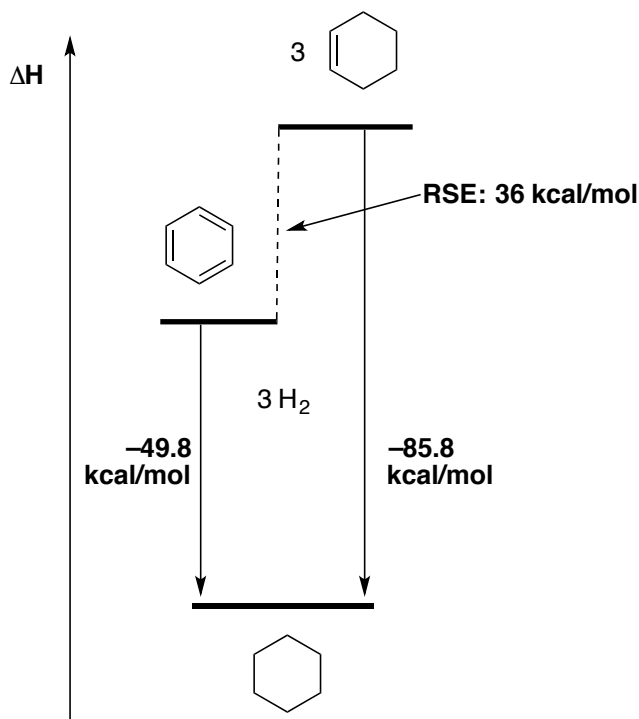
⁶ Abbey, E. R.; Zakharov, L. N.; Liu, S.-Y. *J. Am. Chem. Soc.* **2008**, *130*, 7250–7252.

⁷ (a) Lamm, A. N.; Garner, E. B.; Dixon, D. A.; Liu, S.-Y. *Angew. Chem. Int. Ed.* **2011**, *50*, 8157–8160. (b) Ashe III, A. J.; Fang, X.; Kampf, J. *Organometallics* **2001**, *20*, 5413–5418. (c) Pan, J.; Kampf, J. W.; Ashe III, A. J. *Org. Lett.* **2007**, *9*, 679–681.

⁸ Campbell, P. G.; Marwitz, A. J. V.; Liu, S.-Y. *Angew. Chem. Int. Ed.* **2012**, *51*, 6074–6092.

isolated double bonds. When compared to the heats of hydrogenation for isolated olefins, ΔH for conjugated molecules are less than ΔH for the equivalent number of isolated olefins; this difference is defined as the RSE. It is important to note here that though this chapter will invoke RSE in the context of aromaticity, RSE can be measured in any instance of resonance. For example, in an early calorimetric study, Kistiakowsky measured the heat of hydrogenation for various polyunsaturated hydrocarbons including conjugated and skipped dienes. Importantly, benzene was included as one of the substances investigated.⁹ The RSEs are: essentially zero for non-conjugated 1,4-cyclohexadiene, 1.8 kcal/mol for 1,3-cyclohexadiene, 3.4 kcal/mol for 1,3-butadiene, and 36 kcal/mol for benzene (See Scheme 2.1 for the benzene example).

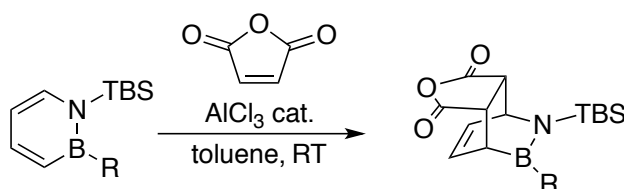
Scheme 2.1. Kistiakowsky's Determination of Benzene's RSE



⁹ Kistiakowsky, G. B.; Ruhoff, J. R.; Smith, H. A.; Vaughan, W. E. *J. Am. Chem. Soc.* **1936**, 58, 146–153.

Using a calorimetric method in analogy to that of Kistiakowsky, our group found that azaborines have RSE of 16.6 kcal/mol versus 32.4 kcal/mol¹⁰ for benzene.^{5a} Exploiting the greatly reduced RSE of azaborines with respect to benzenes, we showed that the Diels-Alder is possible between azaborines and a number of activated dienophiles; this result contrasts with the lack of Diels-Alder reactivity for benzenes (Scheme 2.2).¹¹

Scheme 2.2. Diels-Alder Reaction of 1,2-Azaborines



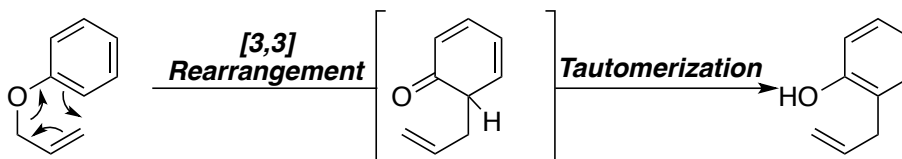
The Diels-Alder reaction of azaborines ($\Delta G_{\text{rxn}} = +17.4$ kcal/mol for benzene versus -2.3 kcal/mol for the azaborine used in our group's previous study), provided some insight into the differences in *thermodynamics* between azaborines and benzenes. Lacking in our understanding are the effects of BN/CC isosterism on the *kinetics* of an aromaticity-breaking reaction that is thermodynamically favorable in both the azaborine and all-carbon substrates. The aromatic Claisen rearrangement is one such reaction. This classic [3,3] sigmatropic rearrangement is generally followed by a tautomerization to yield the more stable phenol (Scheme 2.3). The aromatic Claisen rearrangement has been

¹⁰ The 32.4 kcal/mol value results from the difference between the $\Delta H_{\text{hydrogenation}}$ of benzene to cyclohexene and $2 \times \Delta H_{\text{hydrogenation}}$ of 1,3-cyclohexadiene to cyclohexene. In this manner, a direct comparison of azaborine to BN cyclohexene may be made.

¹¹ Burford, R. J.; Li, B.; Vasiliu, M.; Dixon, D. A.; Liu, S.-Y. *Angew. Chem. Int. Ed.* **2015**, *54*, 7823–7827.

part of the organic chemistry canon for over 100 years¹², and it has been exploited in numerous complex molecule syntheses.¹³

Scheme 2.3. The Aromatic Claisen Rearrangement



In order to uncover mechanistic details, early researchers such as White¹⁴, Goering, and Jacobson¹⁵ performed kinetic studies of the aromatic Claisen rearrangement, finding that Eyring activation parameters are generally large and positive in enthalpy but moderate and negative with regard to entropy ($\Delta H^\ddagger = +29.8$ to $+33.6$ kcal/mol; $\Delta S^\ddagger = -7.3$ to -14.8 e.u.). The reaction rate is increased by the presence of electron-donating substituents on the aromatic ring, and rates are increased in polar, protic media, and an unusual acceleration is observed when water is used as solvent.¹⁶ These data, taken together with the fact that crossover products are generally not observed¹⁷, are consistent with an asynchronous concerted, intramolecular reaction mechanism.

Later researchers worked to further parse the mechanistic details of the general Claisen rearrangement. The Claisen rearrangement of substituted, geometrically pure vinyl allylic ethers gave single diastereomers for rearrangement products, establishing the

¹² Claisen, L. *Ber. Deut. Chem. Ges.* **1912**, 45, 3157–3166.

¹³ (a) Majumdar, K. C.; Nandi, R. K. *Tetrahedron* **2013**, 69, 6921–6957. (b) Nicolaou, K. C.; Li, J. *Angew. Chem. Int. Ed.* **2001**, 40, 4264–4268. (c) Tisdale, E. J.; Slobodov, I.; Theodorakis, E. A. *Proc. Natl. Acad. Sci. U. S. A.* **2004**, 101, 12030–12035. (d) Pettus, T. R. R.; Chen, X.-T.; Danishefsky, S. J. *J. Am. Chem. Soc.* **1998**, 120, 12684–12685. (e) Zhang, X.; Li, X.; Sun, H.; Wang, X.; Zhao, L.; Gao, Y.; Liu, X.; Zhang, S.; Wang, Y.; Yang, Y.; Zeng, S.; Guo, Q.; You, Q. *J. Med. Chem.* **2013**, 56, 276–292.

¹⁴ White, W. N.; Gwynn, D.; Schlitt, R.; Girard, C.; Fife, W. *J. Am. Chem. Soc.* **1958**, 80, 3271–3277.

¹⁵ Goering, H. L.; Jacobson, R. R. *J. Am. Chem. Soc.* **1958**, 80, 3277–3285.

¹⁶ This is described as a hydrophobic effect: Gajewski, J. J. *Acc. Chem. Res.* **1997**, 30, 219–225.

¹⁷ Hurd, C. D.; Schmerling, L. *J. Am. Chem. Soc.* **1937**, 59, 107–109.

preference for a chair-like, six-membered transition state (Figure 2.1).¹⁸ Indeed, Houk and co-workers computed transition state geometries that predict lower activation energies for the chair in comparison to the boat-like transition state.¹⁹ Yamabe calculated that this chair-versus-boat preference is also present in the aromatic version as well.²⁰

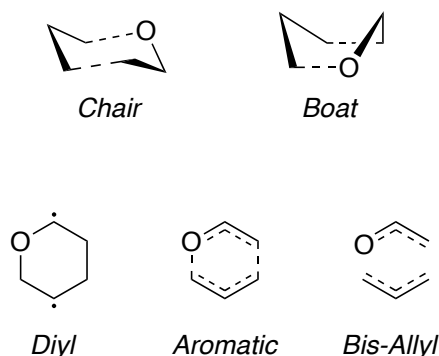


Figure 2.1. Possible transition structures for the Claisen rearrangement

The transition state might be roughly described as “diyl,” “aromatic,” or “bis-allyl” (Figure 2.1 above). A “diyl” transition state is one where bond formation has occurred prior to the of the transition state. “Bis-allyl,” on the other hand, is where bond cleavage has occurred to a greater extent prior to the transition state. “Aromatic” is a halfway measure between the two extremes, where bond formation and cleavage are balanced. “Bis-allyl” or “diyl” transition states have the potential to be polarized, which is consistent with the observed^{14,15} solvent and electronic substituent effects on rate.²¹ On the other hand, Houk’s calculations support the existence of an “aromatic” transition state

¹⁸ Vittorelli, P.; Winkler, T.; Hansen, H.-J.; Schmid, H. *Helv. Chim. Acta* **1968**, *51*, 1457–1461.

¹⁹ Vance, R. L.; Rondan, N. G.; Houk, K. N.; Jensen, F.; Borden, W. T.; Komornicki, A.; Wimmer, E. *J. Am. Chem. Soc.* **1988**, *110*, 2314–2315.

²⁰ Yamabe, S.; Okumoto, S.; Hayashi, T. *J. Org. Chem.* **1996**, *61*, 6218–6226.

²¹ In spite of the conventional outlook toward radical-based reactions, they can indeed exhibit kinetic solvent effects. For a brief review, see: (a) Litwinienko, G.; Beckwith, A. L. J.; Ingold, K. U. *Chem. Soc. Rev.* **2011**, *40*, 2157–2163. For a recent example of Minisci-type additions implying kinetic selectivity, see: (b) O’Hara, F.; Blackmond, D. G.; Baran, P. S. *J. Am. Chem. Soc.* **2013**, *135*, 12122–12134. For solvent effect kinetic data in benzene and THF of triethylborane/oxygen- and AIBN-initiated hydrostannylation see: (c) Oderinde, M. S.; Organ, M. G. *Chem. Eur. J.* **2013**, *19*, 2615–2618.

based on comparisons between experimental and computed activation energy and some secondary deuterium kinetic isotope effect (KIE) values (Figure 2.2).²² “Aromatic” transition states have been expounded upon by Zimmerman²³ and have even been investigated computationally using the NICS method by the group of Schleyer (NICS value at the central point for the six atoms: -21.2 which indicates extreme electronic delocalization).²⁴

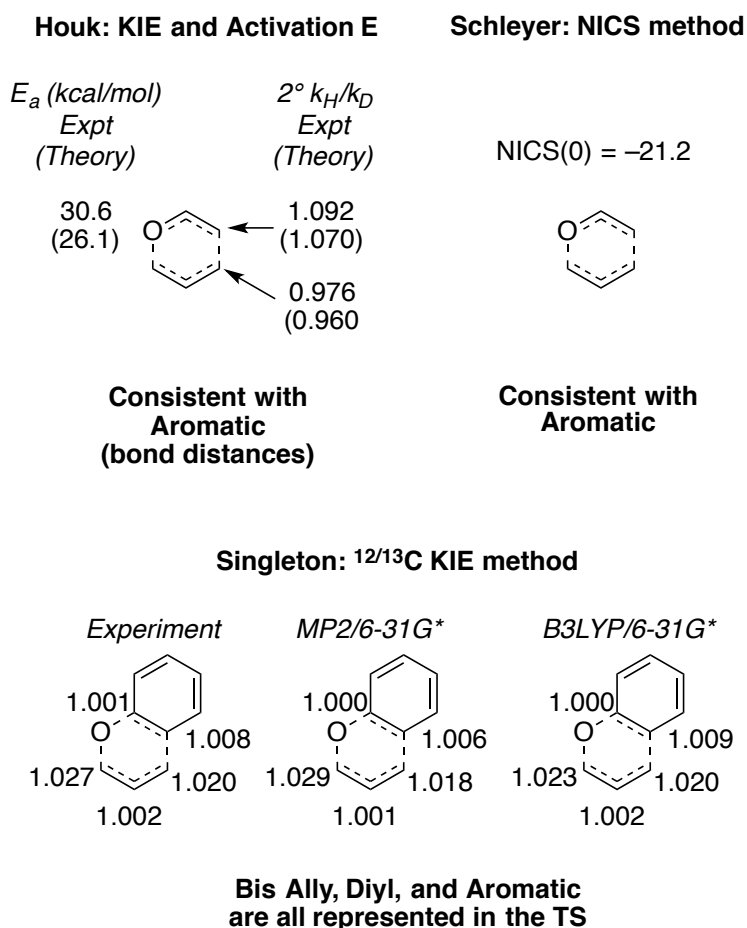


Figure 2.2. Various computational methods for investigating the Claisen rearrangement

²² Wiest, O.; Black, K. A.; Houk, K. N. *J. Am. Chem. Soc.* **1994**, *116*, 10336–10337.

²³ Zimmerman, H. E. *Pure Appl. Chem.* **2006**, *78*, 2193–2203.

²⁴ Chen, Z.; Wannere, C. S.; Corminboeuf, C.; Puchta, R.; Schleyer, P. v. R. *Chem. Rev.* **2005**, *105*, 3842–3888.

Singleton generated new KIE values for the Claisen rearrangement using his natural abundance heavy atom KIE method,²⁵ and these were explored computationally.²⁶ Singleton notes that the transition state perhaps ought not to be discussed using a “diyl” vs. “aromatic” vs. “bis-allyl” comparison. Because multiple bonds are modified, this approximation cannot really take into consideration further intermediate cases; for example, partial C–O cleavage might follow C–C formation or the opposite. The transition state structures that give theoretical KIEs close to experiment resemble the “Bis-allyl” transition state in which bond breakage is dominant. However, the experimental KIEs are also close to those obtained from other levels of theory (which give other resulting transition geometries). Furthermore, it is noted that the calculated $\Delta\Delta H_f$ between phenyl allyl ether either a diyl or bis allyl extreme is much higher (>48 kcal/mol) than the calculated transition state.

Claisen rearrangements of heteroaryl allyl ethers have been explored thoroughly, reviewed notably by Rhoads and Raulins in addition to Moody.²⁷ These heteroaromatic Claisen rearrangements tend to be regioselective²⁸ in contrast with aromatic Claisen rearrangements of benzenes containing elements of asymmetry (Scheme 2.4).²⁹ Kruse and Cha showed that the Claisen rearrangement of 2-allyloxynaphthalenes is regioselective for the 1-position. Since the C(1)–C(2) bond in naphthalenes is generally compressed (and therefore more π -like) with respect to the C(2)–C(3) bond.³⁰ It was

²⁵ Singleton, D. A.; Thomas, A. A. *J. Am. Chem. Soc.* **1995**, *117*, 9357–9358.

²⁶ Meyer, M. P.; DelMonte, A. J.; Singleton, D. A. *J. Am. Chem. Soc.* **1999**, *121*, 10865–10874.

²⁷ (a) Rhoads, S. J.; Raulins, N. R. *Org. React.* **1975**, *22*, 1–252. (b) Moody, C. J. *Adv. Heterocycl. Chem.* **1987**, *42*, 203–244.

²⁸ (a) O’Brien, D. F.; Gates, J. W. *J. Org. Chem.* **1966**, *31*, 1538–1542. (b) Moody, C. J. *J. Chem. Soc. Chem. Commun.* **1983**, 1129–1131. (c) Moody, C. J. *J. Chem. Soc. Perkin Trans. I* **1984**, 1333–1337.

²⁹ (a) White, W. N.; Slater, C. D. *J. Org. Chem.* **1961**, *26*, 3631–3638. (b) Gozzo, F. C.; Fernandes, S. A.; Rodrigues, D. C.; Eberlin, M. N.; Marsaioli, A. J. *J. Org. Chem.* **2003**, *68*, 5493–5499.

³⁰ Kruse, L. I.; Cha, J. K. *J. Chem. Soc. Chem. Commun.* **1982**, 1333–1336.

hypothesized that this bond order alternation may lead to regioselectivity for the aromatic Claisen rearrangement. Being a pericyclic reaction, the Claisen rearrangement proceeds through the interaction of π -like orbitals.³¹

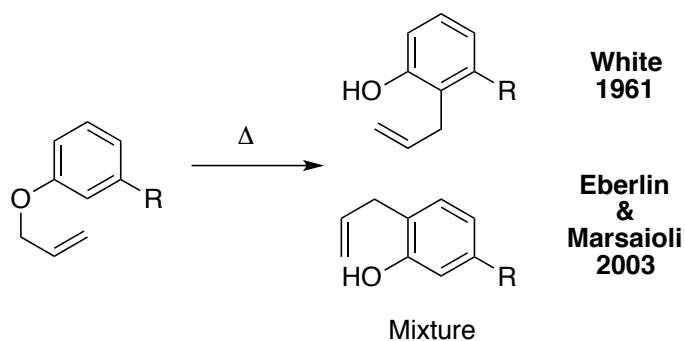
To the best of our knowledge, only Johnstone has studied the reaction kinetics for the Claisen rearrangement of any heteroaromatic allyl ether.³² However, Johnstone's studies of the aromatic Claisen rearrangement of tetrazoles cannot, strictly speaking, compare directly to a classic aromatic Claisen rearrangement because a C–N bond is formed instead of a C–C bond. Additionally, Johnstone found that a crossover experiment produced crossed products, so the Claisen rearrangement of tetrazoles is thought to proceed through ionic dissociation rather than through the traditional concerted, asynchronous mechanism.

³¹ Woodward, R. B.; Hoffmann, R. *J. Am. Chem. Soc.* **1965**, 87, 2511–2513.

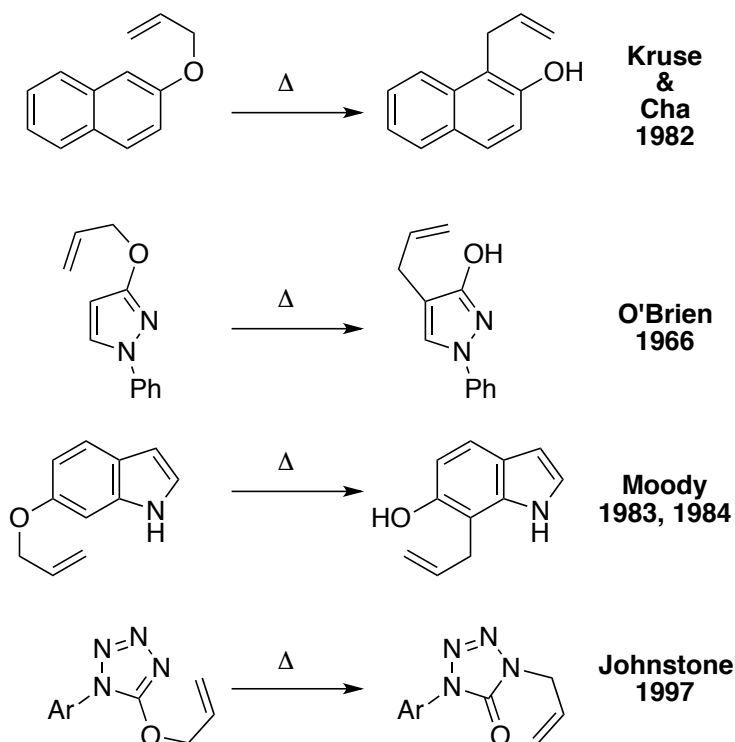
³² Cristiano, M. L. S.; Johnstone, R. A. W. *J. Chem. Soc. Trans. 2* **1997**, 489–494.

Scheme 2.4. Aromatic Claisen Rearrangement Regioselectivity

Non-Regioselective: Asymmetric Benzenes



Regioselective: Bond Length Alternating Systems



Because azaborines exhibit much lower RSE versus their all-carbon analogues, it is reasonable to expect the aromatic Claisen rearrangement might be faster with BN substrates relative to their direct all-carbon analogues. This chapter will describe our efforts toward synthesis of suitable substrates for the comparative study of the effects of BN/CC isosterism on the kinetics of the aromatic Claisen rearrangement.

2.2 Results: Synthesis of Substrates

It is important to stress here that only a *direct* comparison between an azaborine and its all-carbon analogue should be made. That is to say, there should be no topological difference between the two molecules, leaving the presence of the BN unit in one and a CC unit in the other as the only differentiating feature. Extra substitution that is present in one species and not the other may invalidate the comparison. Unfortunately, synthetic constraints, as will be made clear in the next few pages, do not allow a parental comparison or even a comparison of *p*-tolyl allyl ether and a BN isostere. We designed the substrates with the following points in mind:

- 1) The boron atom on the BN substrate **A** must be protected from nucleophilic attack using a mesityl group. This will become clearer as the synthesis is described.
- 2) For the purpose of clean kinetic measurements, the all-carbon substrate **B** must be symmetric to avoid product mixtures.

The synthesis of **A** began with borylated compound **2.1** (Scheme 2.5), which underwent Suzuki-Miyaura cross-coupling to give mesityl-substituted **2.2**.³³ This compound was borylated once more at the 4-position to yield **2.3**. This reaction is sterically controlled in contrast to the borylation reaction giving rise to compound **2.1**.³⁴ Furthermore, while the borylation reaction to form **2.1** was quite facile and proceeded at room temperature, the second borylation required to form **2.3** was much more difficult and required considerable heating for an extended period of time. Oxidation of the newly-

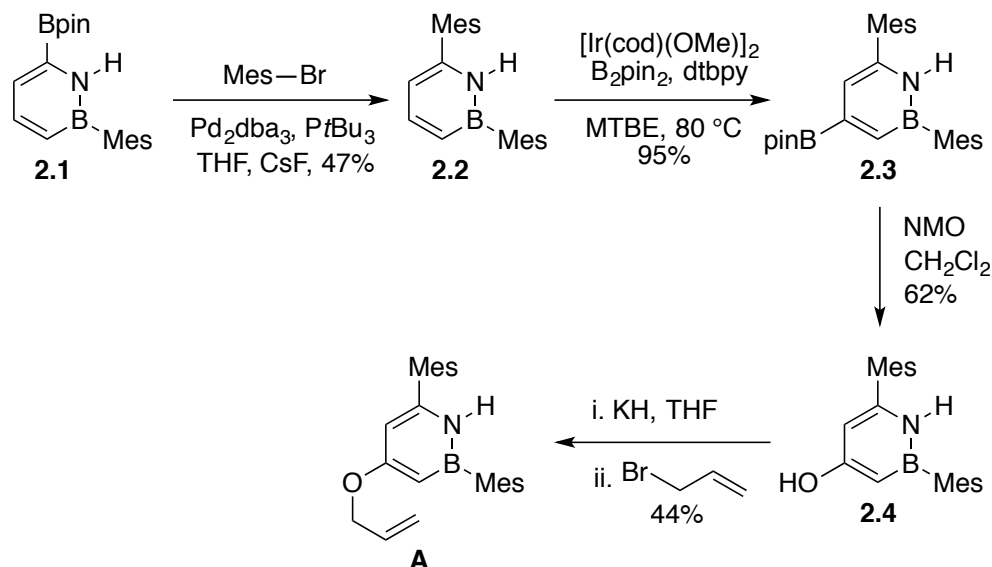
³³ Baggett, A. W.; Vasiliu, M.; Li, B.; Dixon, D. A.; Liu, S.-Y. *J. Am. Chem. Soc.* **2015**, *137*, 5536–5541.

³⁴ (a) Ishiyama, T.; Takagi, J.; Ishida, K.; Miyaura, N.; Anastasi, N. R.; Hartwig, J. F. *J. Am. Chem. Soc.* **2002**, *124*, 390–391. (b) Ishiyama, T.; Takagi, J.; Hartwig, J. F.; Miyaura, N. *Angew. Chem. Int. Ed.* **2002**, *41*, 3056–3058. (c) Boller, T. M.; Murphy, J. M.; Hapke, M.; Ishiyama, T.; Miyaura, N.; Hartwig, J. F. *J. Am. Chem. Soc.* **2005**, *127*, 14263–14278.

installed Bpin with *N*-methylmorpholine-*N*-oxide (NMO)³⁵ yielded phenolic compound

2.4. Azaborophenol **2.4** was allylated after treatment with potassium hydride and allyl bromide to give **A**.

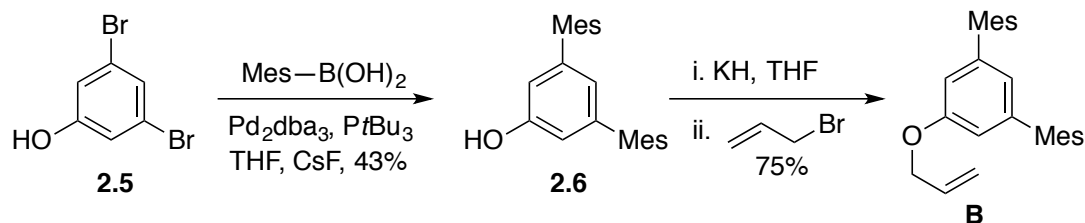
Scheme 2.5. Synthesis of Azaborine Substrate A



The direct, all-carbon analogue **B** was also synthesized (Scheme 2.6). Commercially available phenol **2.5** can be coupled with mesityl boronic acid under standard Suzuki conditions to yield 3,5-dimesitylphenol **2.6**. Standard etherification conditions can again give the substrate of interest **B**.

³⁵ Zhu, C.; Wang, R.; Falck, J. R. *Org. Lett.* **2012**, *14*, 3494–3497. I am indebted to Andrew Baggett, who first used NMO to synthesize phenolic azaborines, and Lifeng Chen, who under my guidance, provided preliminary results for this work.

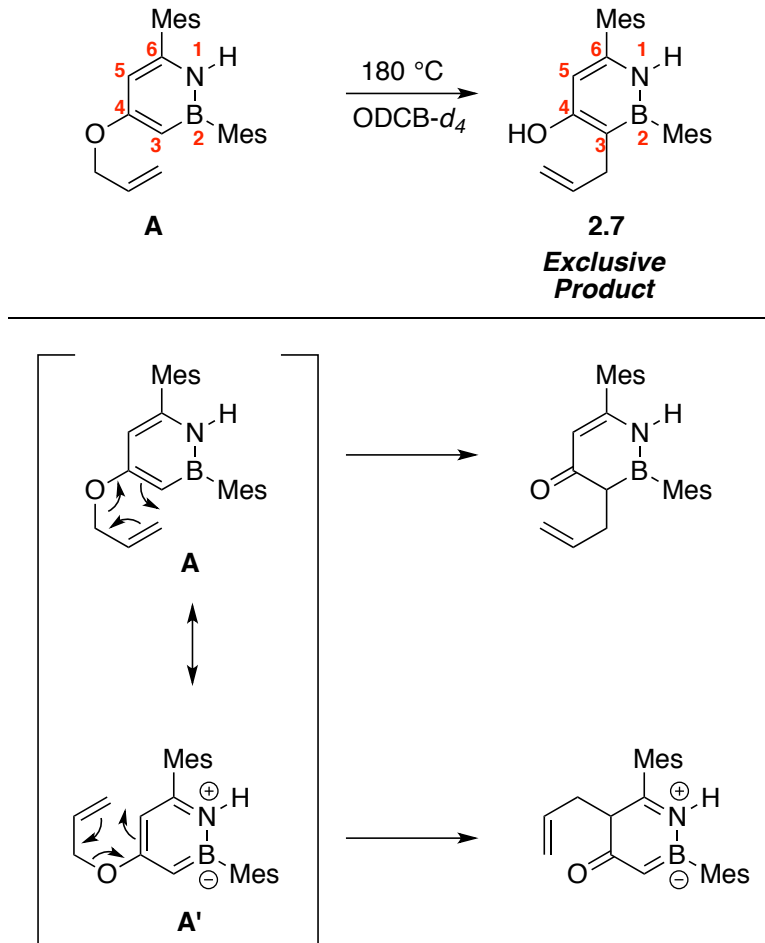
Scheme 2.6. Synthesis of All-Carbon Substrate B



2.3 Results: Regioselectivity of the Azaboryl Claisen Rearrangement

We observed full conversion of **A** regioselectively to **2.7** after heating **A** to 180 °C for 18 hours in ortho-dichlorobenzene- d_4 (ODCB- d_4) (Scheme 2.7), and we determined the regiochemistry of the product using HSQC and HMBC NMR techniques. While meta-substituted phenyl allyl ethers do not undergo the aromatic Claisen rearrangement regioselectively,²⁹ aromatic systems with greater bond localization proceed in a regioselective fashion, since these shorter distances imply greater π -character, and the Claisen rearrangement proceeds through olefinic bonds rather than through more σ -like bonds.³⁰

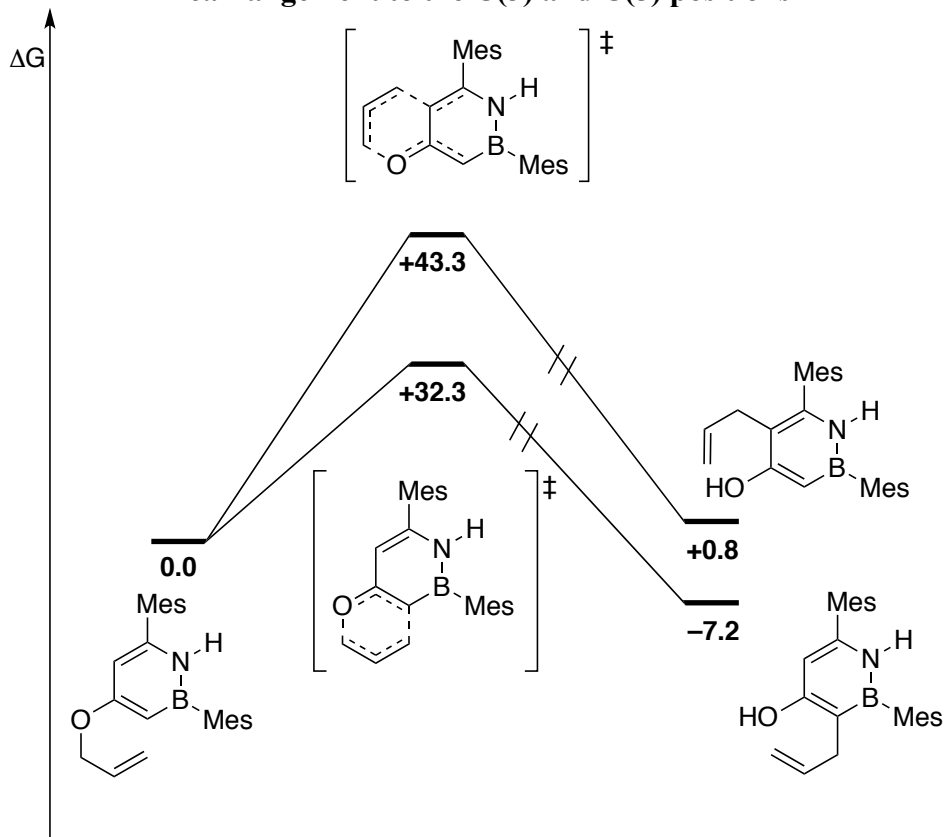
Scheme 2.7. Regioselectivity of the Aromatic Claisen Rearrangement of Azaborines



In our case, the observed product **2.7** may result from the reaction of the dominant resonance contributor, more accurately described using the neutral valence bond depiction **A** rather than the zwitterionic one **A'** (Scheme 2.4). In particular, the C(3)–C(4) and C(5)–C(6) bonds in a 1,2-azaborine are compressed relative to the C(4)–C(5) bond, which is consistent with the observed regiochemistry.⁶ We also performed calculations (B3LYP/DZVP2 with PCM solvent model for ODCB) to shed light on energetic reasons for the observed regioselectivity, and we found that rearrangement to the 3-position is predicted to be 11.0 kcal/mol more favored than rearrangement to the 5-position (Scheme

2.8). Additionally, the aromatic Claisen rearrangement to the 5-position is predicted to be endergonic by 0.8 kcal/mol.

Scheme 2.8. Calculated Reaction Coordinate Diagram for the Claisen Rearrangement to the C(3) and C(5) positions



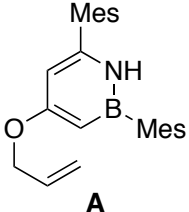
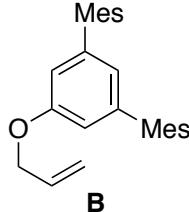
B3LYP/DZVP2 (o-dichlorobenzene solvent). Energies in kcal/mol (298 K)

2.4 Results: Kinetic Comparison

We performed a kinetic comparison of the aromatic Claisen rearrangements of **A** and **B** using ^1H NMR ($\text{ODCB-}d_4$, 140–180 °C, 10 °C increments). The first-order rate constants for the aromatic Claisen rearrangements of **A** and **B** are reported in Table 2.1 as the average of three runs at each temperature (error reported is the standard deviation). The aromatic Claisen rearrangement of **A** is faster than the analogous reaction of **B** at all temperatures investigated. The reaction for **A** is nearly twofold faster than **B** at 140 °C

and almost fivefold faster at 180 °C. Indeed, it appears that BN/CC isosterism accelerates the aromatic Claisen rearrangement as we hypothesized.

Table 2.1. First-order rate constants for the aromatic Claisen rearrangements of **A** and **B** as measured by NMR; Eyring activation parameters extracted from analysis of the rate constants

	<div style="display: flex; justify-content: space-around; align-items: center;"> <div style="text-align: center;">  <p>A</p> </div> <div style="text-align: center;">  <p>B</p> </div> </div>	
T (°C)	<i>k</i> x 10 ⁵ (s ⁻¹)	
180	16.0±1.5	3.32±0.22
170	5.87±1.2	1.95±0.14
160	3.42±0.03	1.40±0.23
150	2.10±0.52	0.73±0.03
140	0.85±0.08	0.43±0.10
ΔG [‡] (160 °C) (kcal/mol)	+34.5	+35.4
ΔH [‡] (kcal/mol)	+24.8	+18.3
ΔS [‡] (e.u.)	-22.3	-39.5

2.5 Discussion

Using an Eyring plot (Figure 2.3), we determined that ΔG[‡] for **A** is less than that of **B** by 0.9 kcal/mol at 160 °C (433 K, the average temperature), representing a nearly three-fold rate enhancement as a result of BN/CC isosterism. ΔH[‡] is smaller for **B** than it is for **A** (+18.3 vs. +24.8 kcal/mol, respectively). Conversely, ΔS[‡] is higher in magnitude for **B** than it is for **A** (-39.5 vs. -22.3 e.u., respectively). These parameters indicate a highly ordered transition state for both reactions, but especially for the Claisen

rearrangement of the all-carbon **B**. Though we expected a much larger difference between ΔG^\ddagger for **A** and **B** given the difference in RSE between azaborines and benzenes (15.8 kcal/mol), the result is unsurprising *a posteriori*, since the Arrhenius activation energy difference between the generic aromatic Claisen rearrangement and its aliphatic counterpart (which does not have to break aromaticity) is only 1.0 kcal/mol (31.6 kcal/mol for the aromatic¹⁵ vs. 30.6 kcal/mol for vinyl allyl ether³⁶).

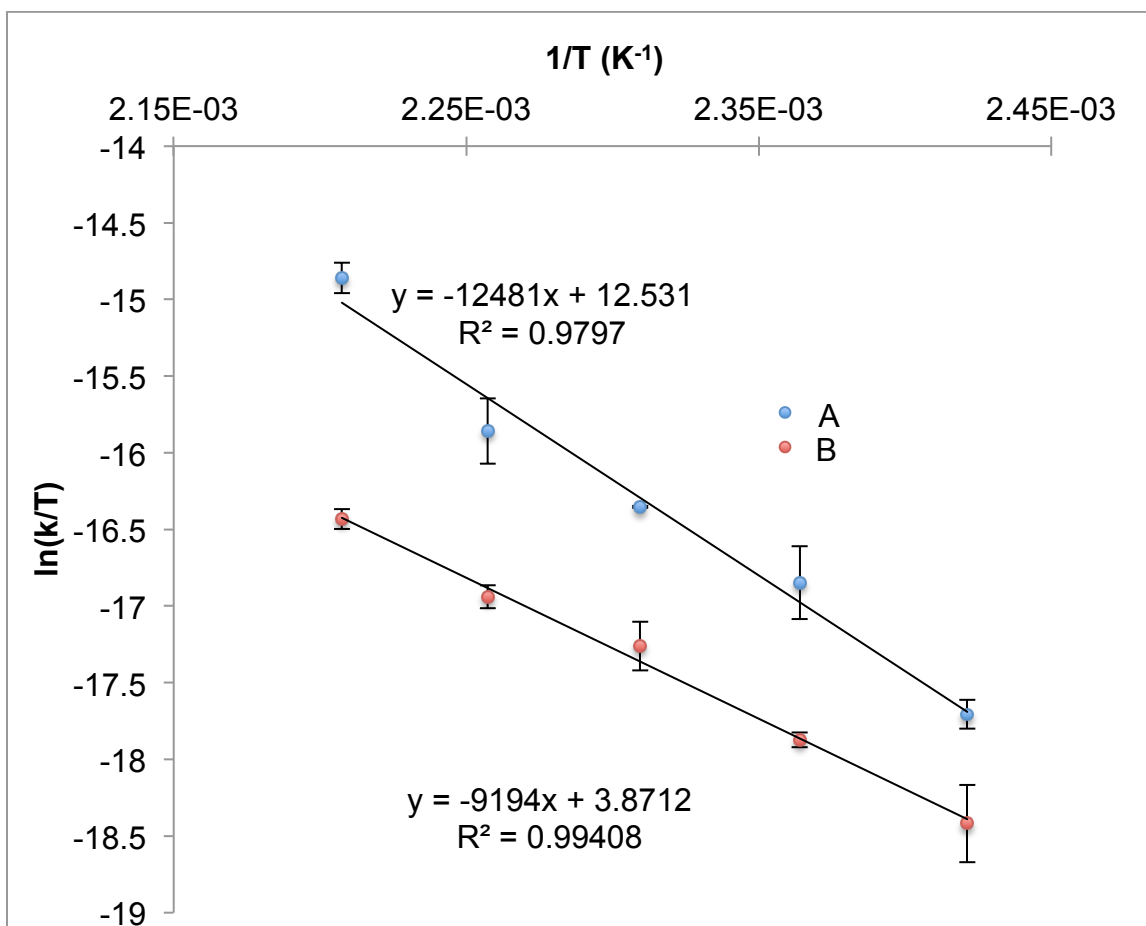


Figure 2.3. Eyring Plots for **A** and **B**. Error bars are the standard deviation of three separate measurements.

While these activation parameters appear to be at odds with those reported by White for the aromatic Claisen rearrangement of para-substituted aryl allyl ethers ($\Delta H^\ddagger =$

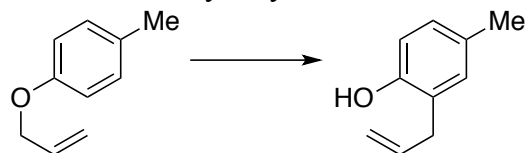
³⁶ Schuler, F. W.; Murphy, G. W. *J. Am. Chem. Soc.* **1950**, 72, 3155–3159.

+29.8 to +33.6 kcal/mol; $\Delta S^\ddagger = -7.3$ to -14.8 e.u.),¹⁴ meta-substitution has been reported by Goering and Jacobson to increase the magnitude of ΔS^\ddagger (from -6 to -13 e.u. for para vs. meta methoxy substituent) while decreasing the magnitude of ΔH^\ddagger (from 33.6 to 30.4 kcal/mol).¹⁵ To the best of our knowledge, there are no kinetic data for meta-diaryl-substituted aryl allyl ethers such as **B**, and the present work clarifies the effects of meta-substitution on Eyring activation parameters versus meta-unsubstituted substrates. We find experimentally that the Claisen rearrangement of the sterically unhindered *p*-tolyl allyl ether in ODCB-*d*₄ proceeds with greater enthalpic contribution, and lesser entropic contribution to free energy of activation (Table 2.2, $\Delta G_{433K}^\ddagger = +36.2$ kcal/mol; $\Delta H^\ddagger = +33.3$ kcal/mol; $\Delta S^\ddagger = -6.8$ e.u., 160–180 °C. See Experimental Section for Eyring plot.). Thus, meta-dimesityl substitution on aromatic Claisen rearrangement substrates decreases the enthalpic contribution to ΔG^\ddagger and increases the entropic contribution.

While we have confirmed the Claisen rearrangements of both **A** and **B** to be first order, the possibility of aryloxy-allyl partner separation (either ionic or diradical in nature) has not been explored through crossover experiments.³⁷ The possible ordering of solvent molecules in the transition state could account for the unusually high magnitude *negative* ΔS^\ddagger . On the other hand, this charge- or diradical-separation would likely result in a less ordered and *positive* ΔS^\ddagger if solvent molecules are not involved.

³⁷ A crossover experiment might also help to determine the reversibility of the Claisen rearrangement in **A** and **B**.

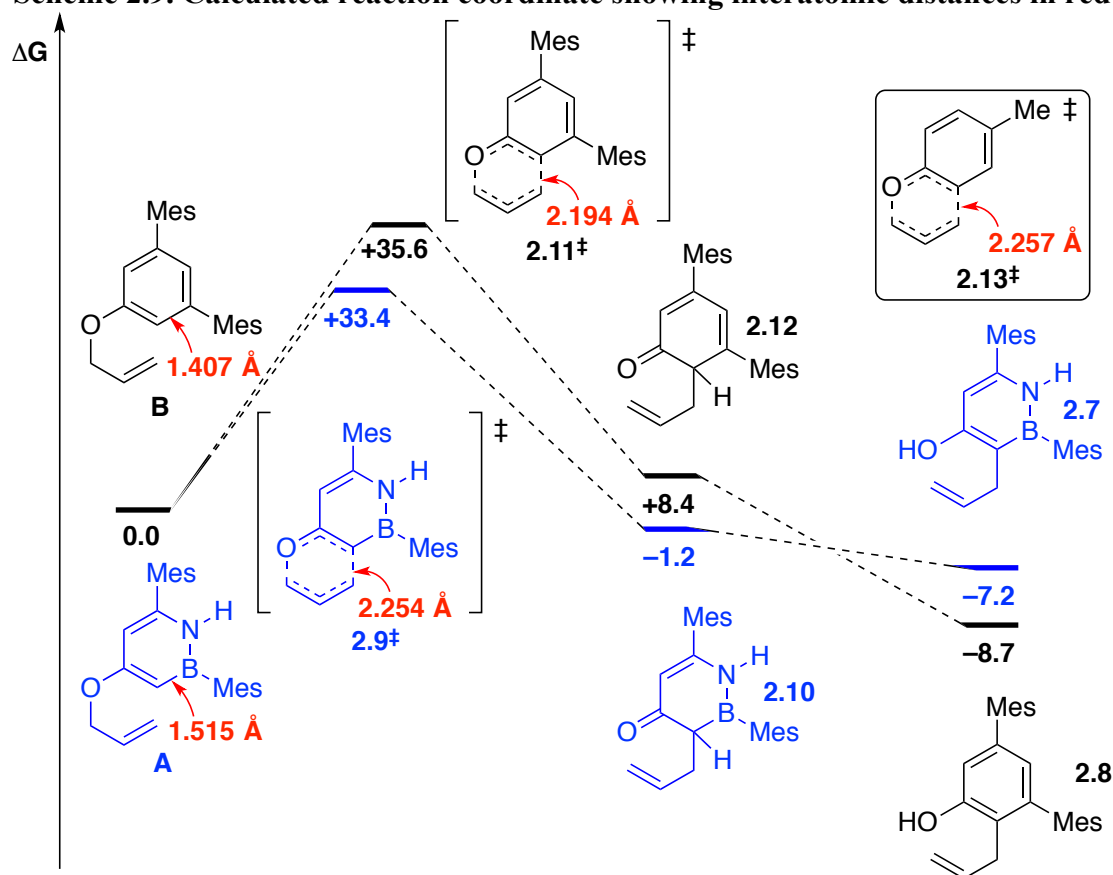
Table 2.2. Rate constants and activation parameters for the Claisen rearrangement of *p*-tolyl allyl ether



Temperature (°C)	k ($\times 10^5 \text{ s}^{-1}$)
180	2.46 ± 0.26
170	1.32 ± 0.21
160	0.43 ± 0.04
$\Delta G_{433\text{K}}^\ddagger = +36.2 \text{ kcal/mol}$	
$\Delta H^\ddagger = +33.3 \text{ kcal/mol}$	
$\Delta S^\ddagger = -6.8 \text{ e.u.}$	

We propose a relatively early transition state for the rearrangement of azaborine **A** to **2.7**, and a later transition state for the rearrangement of all-carbon **B** to **2.8** (Scheme 2.9). Theoretical calculations support this interpretation; the reaction leading from **A** to the keto intermediate species **2.10** is slightly exergonic, while the analogous reaction leading from **B** to its keto intermediate **2.12** is endergonic (Scheme 2.9). Invoking Hammond's postulate, a relatively early transition state **2.9[‡]** is expected for the azaborine, while a relatively late transition state **2.11[‡]** is expected for the all-carbon analogue. Finally, we predict a lower overall barrier in the BN case (transition state **2.9[‡]** versus **2.11[‡]**) even though the all-carbon Claisen rearrangement of all-carbon **B** to **2.8** is more thermodynamically favored than the analogous reaction of **A** to **2.7**.

Scheme 2.9. Calculated reaction coordinate showing interatomic distances in red



B3LYP/DZVP2 (o-dichlorobenzene solvent). Energies in kcal/mol (298 K)

What are the factors governing whether transition states **2.9[‡]** and **2.11[‡]** are “early” or “late?” The calculated (B3LYP/DZVP2) C(2)–C(3) bond in **B** is significantly shorter (0.1 Å, see Scheme 2.9) than the corresponding B–C(3) bond in **A**, bringing the bulky mesityl substituent into closer contact with the site of C–C bond formation in **2.11[‡]**; this more congested site may incur more entropic penalty (i.e., higher magnitude ΔS^\ddagger) in **2.11[‡]** than in **2.9[‡]**.

We therefore expect the transition state for an unhindered substrate such as *p*-tolyl allyl ether to be more similar to the azaborine transition state **2.9[‡]** than to the carbon analogue **2.11[‡]**. Indeed, the distance of the forming C–C bond in the transition state **2.13[‡]** for *p*-tolyl allyl ether (2.257 Å) is more similar to the analogous distance in azaborine

transition state **2.9**[‡] (2.254 Å) than to that same distance in carbonaceous **2.11**[‡] (2.194 Å). The trend of increasing magnitude for experimental ΔS^\ddagger from *p*-tolyl allyl ether (−6.8 e.u.) to **A** (−22.3 e.u.) and on to **B** (−39.5 e.u.) is also consistent with the idea that sterics at the meta-position exert an influence on the activation entropy. In the azaborine substrate **A**, the mesityl group is further away from the reaction site, thus incurring less of an entropic penalty in the transition state. Another effect of order in the transition state **2.11**[‡] might be idealizing reaction partner trajectory, resulting in a transition state where bond formation is very favorable and has occurred to an extent greater in **2.11**[‡] than in **2.9**[‡] or **2.13**[‡] and a transition state that is therefore lower in ΔH^\ddagger .

2.6 Summary

In summary, we used iterative C–H borylation and Suzuki cross-coupling to synthesize an azaboryl allyl ether to compare with a direct all-carbon analogue for the purpose of determining the effects of BN/CC isosterism on the reaction kinetics of the aromatic Claisen rearrangement. We found that the azaboryl allyl ether **A** reacted faster than its all-carbon analogue **B** at all temperatures investigated (140–180 °C). Eyring parameters showed a 0.9 kcal/mol difference in $\Delta G^\ddagger_{433\text{K}}$ between **A** and **B**, corresponding to a nearly 3-fold rate difference at the average temperature of analysis (160 °C, 433 K). The activation free energy for **A** has a much higher enthalpic component ($\Delta H^\ddagger = +24.8$ kcal/mol) than that of **B** ($\Delta H^\ddagger = +18.3$ kcal/mol). Consequently, the entropic component for **A** is much lower in magnitude ($\Delta S^\ddagger = -22.3$ e.u.) than that for **B** ($\Delta S^\ddagger = -39.5$ e.u.). These parameters indicate very ordered transition states for the Claisen rearrangement of both molecules, but especially for **B**. This difference may arise from enhanced steric clash with the meta-mesityl groups being held much closer to the reactive site in **B**.

relative to **A** as a result of the shorter C–C(Mes) bond in **B** relative to the analogous C–B bond in **A**.

2.7 Experimental Section

General Considerations

All oxygen- and moisture-sensitive manipulations were carried out under an inert atmosphere using either standard Schlenk technique or a nitrogen-filled glovebox. For air- and moisture-sensitive techniques, tetrahydrofuran, diethyl ether, methylene chloride, pentane, and toluene were purified by passing through a neutral alumina column under argon. All other solvents for air- and moisture-sensitive work were distilled after drying over calcium hydride. For all chromatography involving air- and moisture-sensitive compounds, silica gel (240-300 mesh) was heated under vacuum in a 150 °C oil bath for 12 hours. Chromatography for those compounds was performed in a glovebox using the dry, degassed solvents previously mentioned.

¹¹B NMR spectra were recorded on a Varian 500 spectrometer and externally referenced to neat BF₃·Et₂O. (δ 0). ¹H and ¹³C NMR spectra were recorded on a Varian 500 spectrometer, or a Varian 600 spectrometer. IR data were recorded using a Bruker Alpha instrument with the Platinum ATR attachment. High-resolution mass spectrometry (HRMS) data were collected by Mr. Marek Domin at the Boston College Center for Mass Spectrometry using the Direct Analysis in Real Time (DART) technique.

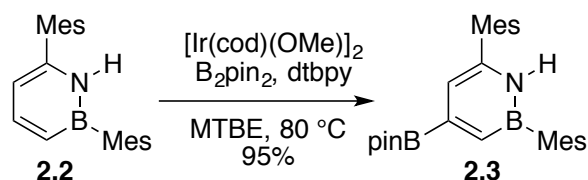
Synthetic Details

Compound 2.2



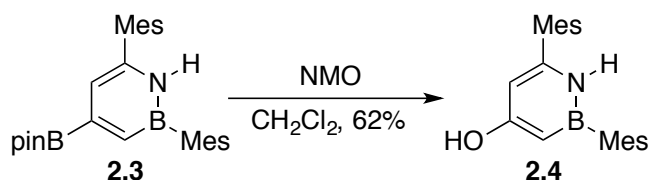
Under a nitrogen atmosphere, compound **2.1** (1.50 g, 4.64 mmol, 1 equiv) was combined in a 100 mL round-bottomed flask with 2-bromomesitylene (1.10 g 5.57 mmol, 1.2 equiv) cesium fluoride (2.12 g, 13.9 mmol, 3 equiv), $\text{Pd}_2(\text{dba})_3$ (120 mg, 0.116 mmol, 2.5 mol%), tri-*tert*-butylphosphine (470 mg, 0.232 mmol, 5 mol%), and 20 mL tetrahydrofuran. The mixture was stirred for 18 hours at room temperature then diluted with ethyl acetate and washed with brine. The product was obtained by recrystallization from methanol (687 mg, 47%). ^1H NMR (500 MHz, CD_2Cl_2) δ 7.79 (dd, $J = 11.1, 6.6$ Hz, 1H), 7.73 (brs, 1H), 6.92 (s, 2H), 6.82 (s, 2H), 6.77 (d, $J = 11.1$ Hz, 1H) 6.23 (d, $J = 6.7$ Hz, 1H), 2.30 (s, 3H), 2.25 (s, 3H), 2.17 (s, 6H), 2.12 (s, 6H). ^{13}C NMR (126 MHz, CD_2Cl_2) δ 144.9, 144.0, 139.7, 138.0, 136.8, 136.2, 135.93, 128.0, 126.9, 110.8, 22.9, 20.79, 20.75, 19.6. Carbons adjacent to boron not observed. ^{11}B NMR (160 MHz, CD_2Cl_2) δ 39.4 (s). FTIR (ATR thin film): 3368, 2915, 1609, 1542, 851, 771, 735. HRMS (DART+) $[\text{M}+\text{H}]^+$ calcd for $\text{C}_{22}\text{H}_{27}\text{BN}$ 316.22365, found 316.22247.

Compound 2.3



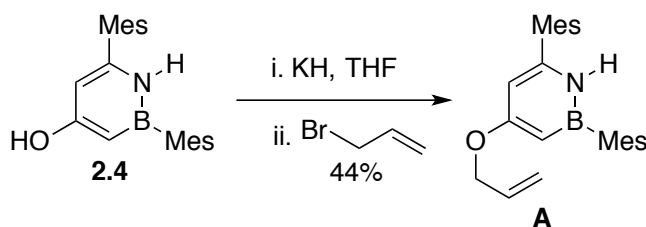
In a glovebox, compound **2.2** (637 mg, 2.02 mmol, 1 equiv) was combined in a 50 mL pressure vessel with B_2pin_2 (565 mg, 2.22 mmol, 1.1 equiv) $[\text{Ir}(\text{cod})(\text{OMe})]_2$ (40 mg, 0.061 mmol, 0.03 mol%) and di-*tert*-butylbipyridine (32 mg, 0.12 mmol, 0.06 mol%) with 10 mL methyl *tert*-butyl ether. The mixture was stirred at $80\text{ }^\circ\text{C}$ until it was judged to be complete by ^1H NMR (about 72 hours). After cooling to room temperature, the mixture was diluted with ethyl acetate and washed with saturated sodium bicarbonate solution. The organic layer was dried over sodium sulfate and concentrated using a rotary evaporator, and the residue was passed through a short plug of silica gel using methylene chloride as the eluent. Yield: 848 mg, 95%. ^1H NMR (500 MHz, CD_2Cl_2) δ 7.82 (brs, 1H), 7.39 (dd, $J = 2.1, 1.2$ Hz, 1H), 6.94 (s, 2H), 6.85 (s, 2H), 6.58 (dd, $J = 2.0, 1.2$ Hz, 1H), 2.33 (s, 3H), 2.29 (s, 3H), 2.20 (s, 6H), 2.15 (s, 6H), 1.36 (s, 12H). ^{13}C NMR (126 MHz, CD_2Cl_2) δ 144.0, 140.2, 138.8 (br), 138.3, 137.2, 136.7, 136.5, 128.5, 127.3, 114.7, 25.2, 23.4, 21.30, 21.26, 20.2. One of the carbons adjacent to boron was not observed. ^{11}B NMR (160 MHz, CD_2Cl_2) δ 35.66 (s), 30.8 (s). FTIR (ATR thin film): 3352, 2977, 2918, 2855, 1609, 1540, 1311, 1111, 850. HRMS (DART+) $[\text{M}+\text{H}]^+$ calcd for $\text{C}_{28}\text{H}_{38}\text{B}_2\text{NO}_2$ 442.3089, found 442.3102.

Compound 2.4



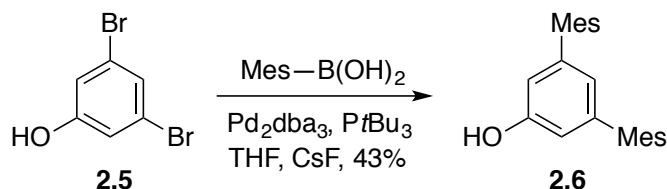
In a glovebox, compound **2.3** (848 mg, 1.92 mmol, 1 equiv) was combined in a 50 mL round-bottomed flask with *N*-methylmorpholine-*N*-oxide (NMO) (236 mg, 2.02 mmol, 1.05 equiv) and 15 mL methylene chloride. The reaction was monitored using TLC (100% CH₂Cl₂ eluent *R*_f = 0.5), and it was judged to be complete within 36 hours. The mixture was diluted with more methylene chloride and washed with saturated sodium bicarbonate solution. The organic layers were dried over sodium sulfate and concentrated using a rotary evaporator. The residue was purified in the glovebox using a short silica gel plug. The plug was flushed with two volumes of 5% methylene chloride in pentane, then and 100% methylene chloride. The latter fraction was collected and concentrated *in vacuo*. Yield: 391 mg, 62%. ¹H NMR (500 MHz, CD₂Cl₂) δ 7.28 (brs, 1H), 6.91 (s, 2H), 6.80 (s, 2H), 5.83 (dd, *J* = 2.8, 1.8 Hz, 1H), 5.65 (dd, *J* = 2.9, 1.6 Hz, 1H), 5.28 (s, 1H), 2.29 (s, 3H), 2.24 (s, 3H), 2.18 (s, 6H), 2.15 (s, 6H). ¹³C NMR (126 MHz, CD₂Cl₂) δ 167.2, 148.9, 140.2, 138.8, 137.2, 136.5, 135.8, 128.5, 127.3, 103.7, 23.2, 21.21, 21.20, 19.9. Carbons adjacent to boron not observed. FTIR (ATR thin film): 3500, 3359, 2917, 2856, 1618, 1556, 1453, 1133, 890, 760. ¹¹B NMR (160 MHz, CD₂Cl₂) δ 37.4 (s). HRMS (DART+) [M+H]⁺ calcd for C₂₂H₂₇BNO 332.21857, found 332.21792.

Compound A



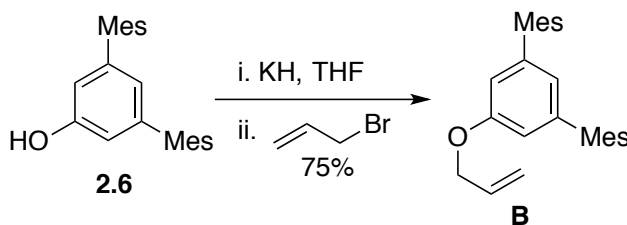
In a glovebox, compound **4** was dissolved in 3 mL tetrahydrofuran in a 20 mL vial. The solution was cooled to $-30\text{ }^{\circ}\text{C}$ and potassium hydride (66 mg 1.7 mmol, 1.4 equiv) was carefully added. The mixture was stirred for an hour in the absence of cooling. The mixture was passed through an acrodisc to remove any solid residue. Allyl bromide (571 mg, 4.72 mmol, 4 equiv) was added dropwise at room temperature, and the mixture was stirred for 18 hours. The mixture was then passed through an acrodisc, and volatiles were removed *in vacuo*. The product was purified using a short plug of silica gel and 25% methylene chloride in hexane as the eluent. Yield: 191 mg, 44%. ^1H NMR (500 MHz, CD_2Cl_2) δ 7.22 (s, 2H), 6.91 (s, 2H), 6.81 (s, 2H), 6.14 – 6.03 (m, 1H), 5.87 (dd, $J = 2.9$, 1.8 Hz, 1H), 5.73 (dd, $J = 2.9$, 1.5 Hz, 1H), 5.41 (dd, $J = 17.2$, 1.7 Hz, 1H), 5.26 (dd, $J = 10.5$, 1.5 Hz, 1H), 4.53 (dt, $J = 5.5$, 1.5 Hz, 2H), 2.29 (s, 3H), 2.25 (s, 3H), 2.19 (s, 6H), 2.15 (s, 6H). ^{13}C NMR (151 MHz, CD_2Cl_2) δ 169.6, 147.7, 140.2, 138.5, 137.2, 136.5, 136.0, 134.0, 128.5, 127.3, 117.5, 105.1, 68.1, 23.2, 21.23, 21.21, 20.0. Carbons adjacent to boron not observed. ^{11}B NMR (160 MHz, CD_2Cl_2) δ 37.3 (s). FTIR (ATR thin film): 3364, 2917, 2858, 1620, 1542, 1418, 1157, 761. HRMS (DART+) $[\text{M}+\text{H}]^+$ calcd for $\text{C}_{25}\text{H}_{31}\text{BN}$ 372.24987, found 372.25170. **Claisen Rearrangement Product:** The product was obtained in full conversion after heating at $180\text{ }^{\circ}\text{C}$ for 18 hours. ^1H NMR (600 MHz, $\text{ODCB-}d_4$) δ 6.79 (s, 1H), 6.74 (s, 1H), 6.64 (s, 1H), 5.87 (d, $J = 1.6$ Hz, 1H), 5.82 (dtd, $J = 16.2$, 6.3, 3.2 Hz, 1H), 5.75 (d, $J = 2.8$ Hz, 1H), 5.09 (dt, $J = 17.3$, 1.8 Hz, 1H), 4.97 (dt, $J = 10.1$, 1.8 Hz, 1H), 3.03 (d, $J = 4.2$ Hz, 2H), 2.27 (s, 3H), 2.22 (s, 3H), 2.15 (s, 6H), 2.04 (s, 6H). ^{13}C NMR (151 MHz, $\text{ODCB-}d_4$) δ 168.1, 149.0, 142.2, 141.4, 140.5, 139.2, 138.5, 138.0, 131.0, 117.6, 107.0, 35.0, 25.6, 24.0, 23.8, 22.4. Carbons adjacent to boron not observed. One carbon signal overlaps with solvent residual signals.

Compound 2.6



Under an inert atmosphere, 3,5-dibromophenol **2.5** (1.00 g, 3.97 mmol, 1 equiv) was combined with mesitylboronic acid (1.43 g, 8.73 mmol, 2.2 equiv), cesium fluoride (3.62 g, 23.8 mmol, 6 equiv), Pd₂(dba)₃ (102 mg, 0.089 mmol, 2.5 mol%), tri-*tert*-butylphosphine (400. mg, 0.0198 mmol, 5 mol%), and 20 mL tetrahydrofuran in a 100 mL round-bottomed flask. The flask was affixed with a reflux condenser, and the mixture was heated to 80 °C for 18 hours. After cooling to room temperature, the volatiles were removed using a rotary evaporator. The residue was extracted with ether, and the ether was washed with brine. The organic layers were dried with magnesium sulfate and concentrated using a rotary evaporator. The residue was passed through a short silica gel plug using methylene chloride as the eluent. The pure product was obtained by recrystallization from hexane: 564 mg, 43%. ¹H NMR (600 MHz, CD₂Cl₂) δ 6.91 (s, 4H), 6.56 (d, *J* = 1.4 Hz, 2H), 6.43 (t, *J* = 1.4 Hz, 1H), 2.29 (s, 6H), 2.05 (s, 12H). ¹³C NMR (151 MHz, CD₂Cl₂) δ 155.8, 142.8, 138.6, 136.4, 135.6, 127.8, 122.9, 114.3, 20.7, 20.3. FTIR (ATR thin film): 3446, 2969, 2918, 1733, 1717, 1190, 766. HRMS (DART+) [M+H]⁺ calcd for C₂₄H₂₇O 331.20619, found 331.20650.

Compound B



Compound **2.6** (564 mg, 1.71 mmol, 1 equiv) was dissolved in 5 mL tetrahydrofuran and cooled to $-30\text{ }^{\circ}\text{C}$. Potassium hydride (96 mg, 2.39 mmol, 1.4 equiv) was added, and the mixture was stirred for 3 hours, warming to room temperature. Allyl bromide (826 mg, 6.83 mmol, 4 equiv) was added neat, dropwise, and the mixture was stirred an additional 18 hours at room temperature. The volatiles were removed using a rotary evaporator, and the residue was extracted with ether. After removing the volatiles again using a rotary evaporator, the product was obtained by crystallization from hexane at $-20\text{ }^{\circ}\text{C}$. Yield: 478 mg, 75%. ^1H NMR (600 MHz, CD_2Cl_2) δ 6.92 (s, 4H), 6.65 (s, 2H), 6.46 (s, 1H), 6.07 (ddt, $J = 17.0, 10.5, 5.2\text{ Hz}$, 1H), 5.40 (dd, $J = 17.3, 1.5\text{ Hz}$, 1H), 5.27 (dd, $J = 10.6, 1.5\text{ Hz}$, 1H), 4.55 (d, $J = 5.3\text{ Hz}$, 2H), 2.30 (s, 6H), 2.05 (s, 12H). ^{13}C NMR (151 MHz, CD_2Cl_2) δ 161.4, 145.2, 141.5, 139.1, 138.3, 136.2, 130.5, 125.5, 119.7, 116.4, 71.3, 23.3, 23.0. FTIR (ATR thin film): 2917, 2857, 1725, 1227, 849. HRMS (DART+) $[\text{M}+\text{H}]^+$ calcd for $\text{C}_{27}\text{H}_{31}\text{O}$ 371.23749, found 371.23880.

Claisen Rearrangement Product: The product was obtained with full conversion after heating at $180\text{ }^{\circ}\text{C}$ for 72 hours. ^1H NMR (600 MHz, $\text{ODCB-}d_4$) δ 6.70 (s, 2H), 6.68 (s, 2H), 6.47 (s, 1H), 6.10 (s, 1H), 5.72 – 5.59 (m, 1H), 5.00 (brs, 1H), 4.82 (s, 1H), 2.99 (d, $J = 5.8\text{ Hz}$, 1H), 2.12 (s, 4H), 2.11 (s, 3H), 1.92 (s, 6H), 1.85 (s, 6H). ^{13}C NMR (151 MHz, $\text{ODCB-}d_4$) δ 157.8, 144.6, 143.6, 141.0, 140.1, 138.7, 138.5, 138.0, 137.8, 137.7, 130.7, 130.6, 125.5, 123.9, 118.5, 117.9, 34.6, 23.6, 23.2, 23.0.

A Sample Procedure for Kinetic Analysis

A stock solution of **A** or **B** (20 mM) and 1,3,5-trimethoxybenzene internal standard (20 mM) in 1,2-dichlorobenzene- d_4 (ODCB- d_4) was divided into four aliquots in J-Young NMR tubes. An NMR measurement was taken to establish the initial ratio of internal standard to analyte in the stock solution. The tubes were then submerged simultaneously in a temperature-controlled oil bath pre-heated to the given temperature. At given timepoints, the J-Young tubes were removed from the bath in succession, and NMR measurements of the allylic protons established the decay of **A** or **B** relative to the constant concentration of the internal standard. The data were fit to first-order decay according to the equation:

$$\text{Conv}_t = e^{-kt}$$

Where

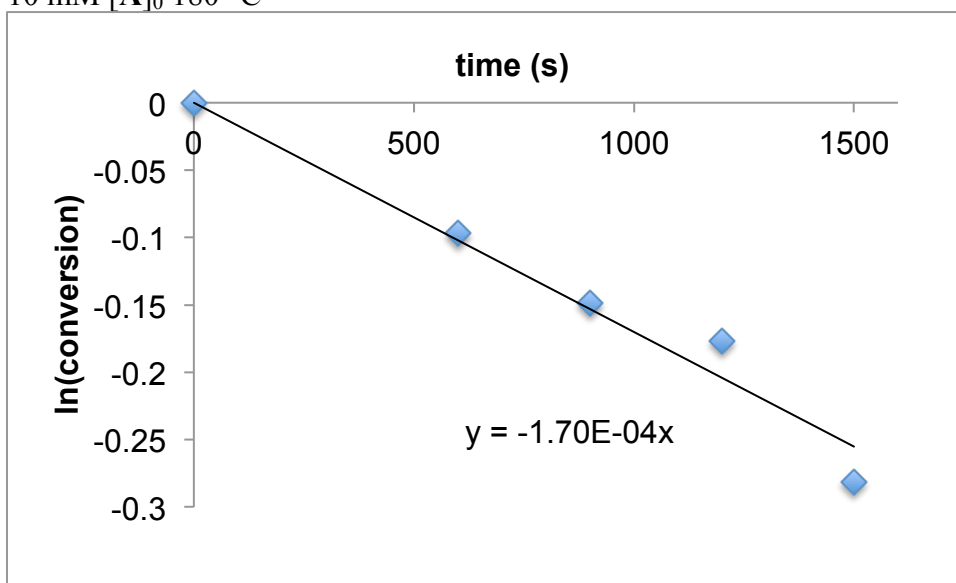
“**Conv**” = the ratio of the allylic peak integration at time = t to the integration at time = 0 s. The values of “**Conv**” begin at 1 at time = 0 s and decrease as the reaction progresses.

The equation can be linearized:

$$\ln(\text{Conv}_t) = -kt$$

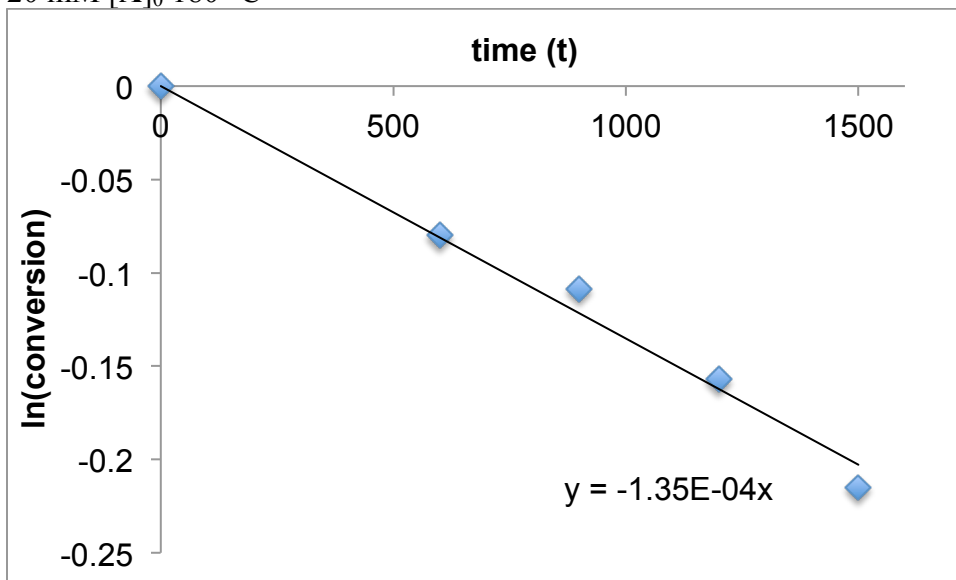
Reaction Order Analysis for Compound A

10 mM [A]₀ 180 °C



$R^2 = 0.97$

20 mM [A]₀ 180 °C

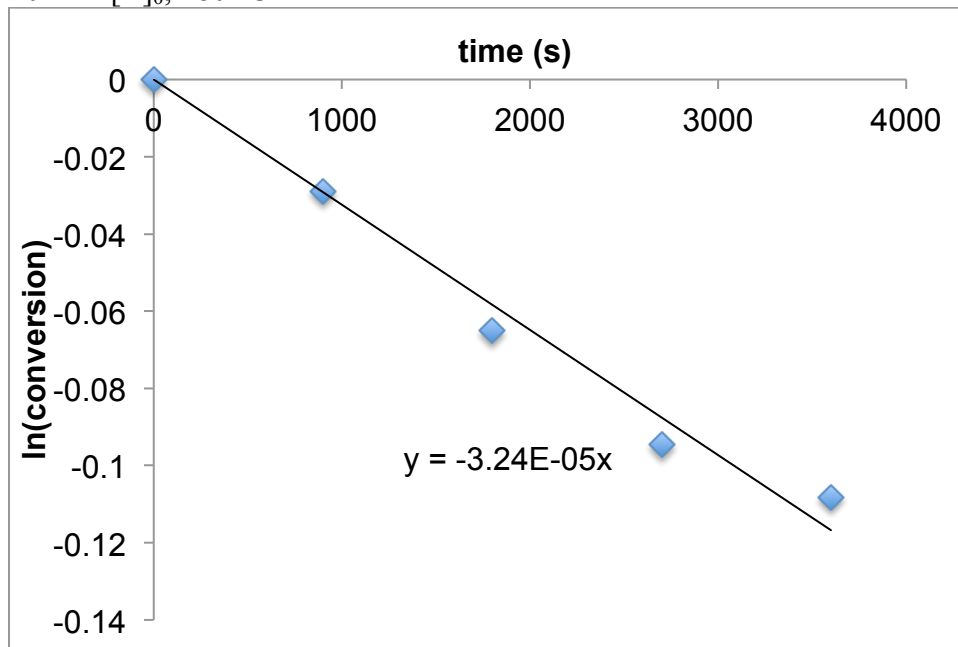


$R^2 = 0.99$

Rate constants k_{obs} indicate first-order behavior.

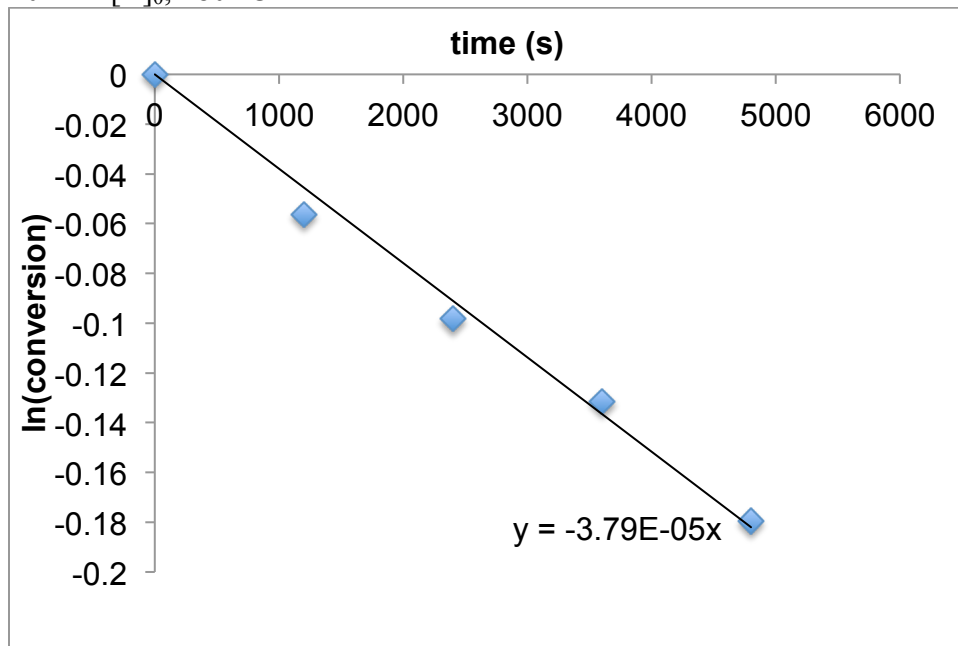
Reaction Order Analysis for Compound B

20 mM [B]₀, 180 °C



$R^2 = 0.97$

40 mM [B]₀, 180 °C



$R^2 = 0.98$

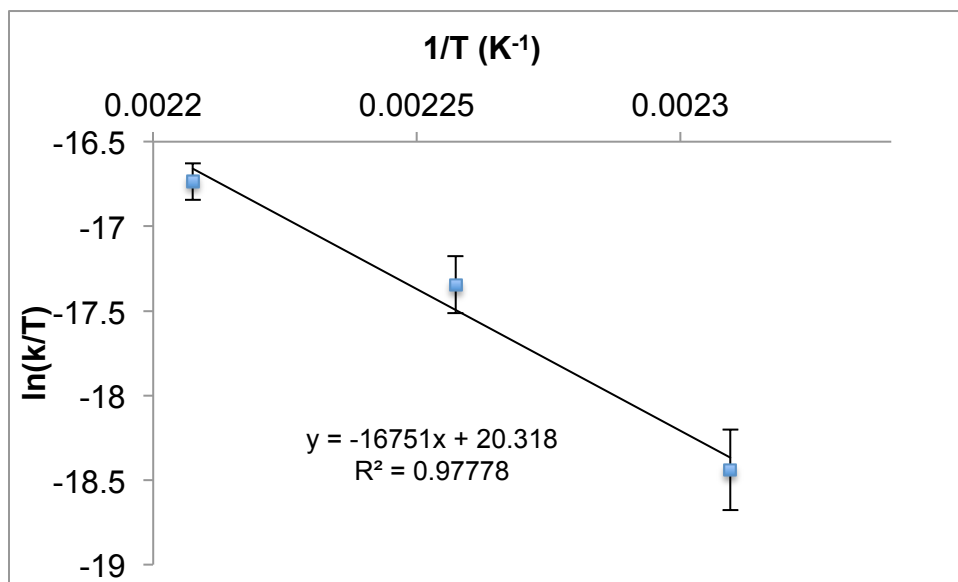
Rate constants k_{obs} indicate first-order behavior.

Rate Constants and Eyring Plot for p-Tolyl Allyl Ether

Each rate constant k is the average of three separate trials, and the error is the standard deviation.

Temperature (°C)	k ($\times 10^5 \text{ s}^{-1}$)
160	0.43 ± 0.04
170	1.32 ± 0.21
180	2.46 ± 0.26

The reaction below 160 °C is does not yield significant conversion for kinetic analysis.



$$\Delta G_{433\text{K}}^\ddagger = +36.2 \text{ kcal/mol}$$

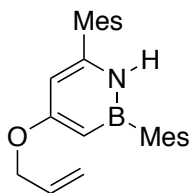
$$\Delta H^\ddagger = +33.3 \text{ kcal/mol}$$

$$\Delta S^\ddagger = -6.8 \text{ e.u.}$$

Calculation Details

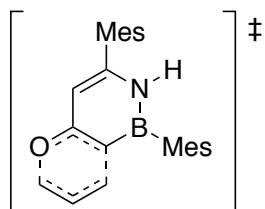
Calculations were carried out using the Gaussian 09 program using the B3LYP method, the DZVP2 basis set and the PCM solvent model for ortho-dichlorobenzene.

Optimized Coordinates



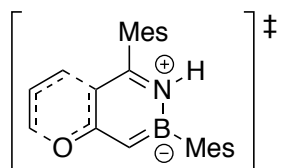
C	-1.229311	0.789795	0.288309
C	-2.214875	0.136709	0.984504
N	-0.080955	0.116180	-0.059139
B	0.174246	-1.270580	0.262339
C	-0.932378	-1.963486	1.031042
C	-2.066946	-1.240361	1.355993
C	1.538450	-1.935187	-0.196286
C	-1.345803	2.225486	-0.120045
C	-0.826660	3.240385	0.716408
C	-0.938685	4.576766	0.312569
C	-1.548681	4.935062	-0.900006
C	-2.054118	3.912304	-1.712129
C	-1.964795	2.560771	-1.342569
C	-0.157543	2.906741	2.034159
C	-2.537183	1.494970	-2.254747
C	-1.646527	6.387707	-1.313515
C	1.649675	-2.575404	-1.456486
C	2.670210	-1.927632	0.652470
C	3.866389	-2.541200	0.244090
C	3.980397	-3.175208	-0.999413
C	2.855026	-3.180858	-1.838366
C	0.468936	-2.612487	-2.409447
C	2.611424	-1.259223	2.014022
C	5.271736	-3.836437	-1.432115
H	2.918597	-3.669109	-2.808912
H	0.189919	-1.604598	-2.737178
H	-0.415455	-3.046445	-1.930830
H	0.698385	-3.202842	-3.300512
H	4.724617	-2.524907	0.912403
H	6.034595	-3.763262	-0.652528
H	5.670271	-3.370239	-2.340216
H	5.116608	-4.897563	-1.656343
H	1.812992	-1.684261	2.631826
H	2.405019	-0.186835	1.923914
H	3.555735	-1.375265	2.552514

H	0.598824	0.663862	-0.574948
H	-3.121223	0.661570	1.261280
O	-3.152395	-1.720779	2.044972
H	-0.541156	5.355929	0.958822
H	-2.530253	4.168152	-2.655359
H	-0.828487	2.343258	2.690081
H	0.144754	3.818160	2.554733
H	0.735162	2.290048	1.885372
H	-2.859296	1.931138	-3.203089
H	-3.401796	1.003606	-1.796310
H	-1.803344	0.712331	-2.470344
H	-2.144722	6.984086	-0.541928
H	-2.207756	6.497875	-2.244614
H	-0.651427	6.820723	-1.464473
H	-0.855959	-3.004244	1.328812
C	-3.123899	-3.084567	2.471389
C	-4.391598	-3.428703	3.202621
H	-2.260027	-3.255178	3.129200
H	-3.006873	-3.748313	1.603132
C	-5.420238	-2.604246	3.437574
H	-4.428869	-4.458955	3.554695
H	-5.411559	-1.573423	3.099434
H	-6.295403	-2.953062	3.978236



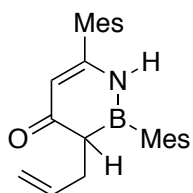
C	2.080963	-0.902133	-0.617360
C	0.932535	-1.526983	-0.217759
H	-0.677185	0.778744	-1.447655
H	0.749797	-2.552020	-0.520663
C	-1.222022	1.188143	-0.602719
H	-2.037782	-1.349394	-1.114003
H	-1.109097	2.256147	-0.443832
C	-0.038324	-0.886419	0.655650
C	0.153417	0.509606	0.966541
C	-2.581298	-0.808828	-0.348375
C	-2.412216	0.549248	-0.177618
O	-1.104732	-1.509358	1.011238
H	-0.483865	0.901916	1.752652
H	-3.047750	1.069391	0.535265
C	1.910766	2.665212	1.008175
C	2.151508	2.965072	2.373436
C	2.068430	3.706552	0.057621

C	2.531303	4.260111	2.757458
C	2.433217	4.995160	0.474944
C	2.673881	5.294465	1.823185
H	2.716404	4.466312	3.809370
H	2.532069	5.782936	-0.269212
C	1.863142	3.468757	-1.428981
H	2.758890	3.035461	-1.889889
H	1.035879	2.783763	-1.629189
H	1.656165	4.409134	-1.946883
C	2.015357	1.902207	3.449191
H	0.964718	1.657787	3.639995
H	2.514315	0.970555	3.164793
H	2.451526	2.244239	4.391421
C	3.093763	6.685380	2.247484
H	4.140170	6.877653	1.982366
H	2.488517	7.450591	1.751270
H	2.994804	6.817018	3.328218
C	3.112991	-1.578011	-1.466288
C	3.059524	-1.456478	-2.873814
C	4.144211	-2.323462	-0.856343
C	4.041473	-2.087968	-3.647757
C	5.109165	-2.940100	-1.668188
C	5.075482	-2.836995	-3.064512
H	3.998897	-1.993332	-4.730297
H	5.903751	-3.512217	-1.195905
C	1.960367	-0.665947	-3.553997
H	0.979047	-1.117128	-3.373992
H	1.913398	0.362025	-3.180951
H	2.123632	-0.628287	-4.633402
C	4.226318	-2.469946	0.649325
H	4.243883	-1.495579	1.148052
H	3.361605	-3.014134	1.042551
H	5.129323	-3.014030	0.935175
C	6.116336	-3.517172	-3.927382
H	5.667064	-4.318800	-4.524330
H	6.572531	-2.809498	-4.627347
H	6.910800	-3.955824	-3.318619
B	1.476594	1.204864	0.583361
N	2.347760	0.404652	-0.230412
H	3.245771	0.760888	-0.536701
H	-3.435108	-1.319180	0.085210



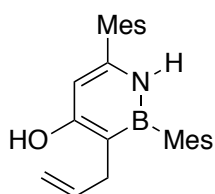
B	2.063265	-0.925224	-0.628400
C	0.806245	-1.546776	-0.115430
H	-0.688450	0.826656	-1.368989
H	0.529410	-2.581564	-0.309811
C	-1.179984	1.339821	-0.548610
H	-2.193237	-1.142515	-0.878561
H	-0.962352	2.397798	-0.443446
C	-0.068072	-0.818082	0.720749
C	0.215320	0.607577	0.955807
C	-2.659887	-0.525834	-0.119686
C	-2.385795	0.831954	-0.037467
O	-1.174479	-1.292212	1.215432
H	-0.336445	1.100016	1.744580
H	-2.951065	1.439035	0.665120
C	1.842803	2.561935	0.993488
C	2.013686	2.853207	2.372095
C	2.061847	3.572311	0.027374
C	2.389249	4.146747	2.750264
C	2.420459	4.859555	0.457283
C	2.589507	5.170145	1.810689
H	2.534990	4.360391	3.806482
H	2.569516	5.635815	-0.289033
C	1.929638	3.330505	-1.465089
H	2.881416	3.002986	-1.899772
H	1.185619	2.570050	-1.705633
H	1.647435	4.255894	-1.972858
C	1.839066	1.804615	3.454030
H	0.787133	1.685798	3.735012
H	2.203011	0.823597	3.139110
H	2.384923	2.099443	4.353424
C	2.979492	6.561740	2.256992
H	3.894073	6.538337	2.858822
H	3.150247	7.219668	1.401646
H	2.195299	7.007924	2.878350
C	3.180686	-1.597171	-1.531528
C	3.054286	-1.637720	-2.943404
C	4.325448	-2.190267	-0.947074
C	4.043037	-2.250473	-3.726104
C	5.299736	-2.800130	-1.755085
C	5.178924	-2.839840	-3.149671
H	3.924530	-2.272388	-4.807657
H	6.168352	-3.255290	-1.284170
C	1.849301	-1.021609	-3.630854
H	0.917198	-1.477736	-3.281440
H	1.775111	0.051760	-3.422179
H	1.905895	-1.149305	-4.715200
C	4.519425	-2.182445	0.558300

H	4.657682	-1.163811	0.939012
H	3.647254	-2.597897	1.073667
H	5.397410	-2.766968	0.845890
C	6.239520	-3.487025	-4.014859
H	6.790239	-2.735398	-4.592580
H	6.962948	-4.038781	-3.408780
H	5.794045	-4.183136	-4.733203
C	1.448579	1.185544	0.575436
N	2.280201	0.471060	-0.208030
H	3.136789	0.947529	-0.472414
H	-3.528402	-0.945050	0.377539



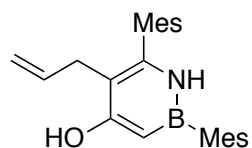
C	-0.224359	1.281219	-0.021955
C	-1.438647	0.749974	-0.318745
N	0.892213	0.463013	0.219406
B	0.891820	-0.956522	0.098272
C	-0.445551	-1.595022	-0.473029
C	-1.673657	-0.702356	-0.339673
C	0.002564	2.753772	0.114512
C	2.185239	-1.779872	0.466873
C	2.178375	-2.626713	1.605479
C	3.368635	-1.703758	-0.305810
C	4.490479	-2.469640	0.047459
C	4.488362	-3.306698	1.167880
C	3.319867	-3.362715	1.941595
C	0.948434	-2.749085	2.487492
C	3.474385	-0.793041	-1.517156
C	5.700514	-4.133920	1.535815
O	-2.813474	-1.171236	-0.261928
H	1.717611	0.961402	0.529554
H	-2.298462	1.398897	-0.439518
H	5.386469	-2.406857	-0.566053
H	3.298303	-3.995765	2.826398
H	2.547640	-0.762817	-2.095648
H	4.273893	-1.125767	-2.184695
H	3.708201	0.237503	-1.222634
H	6.563922	-3.869411	0.919757
H	5.503898	-5.203228	1.396242
H	5.974921	-3.988788	2.586016
H	0.451142	-1.785765	2.637998
H	1.213892	-3.141759	3.472616
H	0.209340	-3.431294	2.052267

C	0.432363	3.503753	-1.000297
C	0.653991	4.879790	-0.847881
C	0.457884	5.528131	0.377649
C	0.032918	4.760376	1.471250
C	-0.199824	3.383663	1.362786
C	0.676518	7.018767	0.518254
C	0.646629	2.851972	-2.350891
C	-0.663862	2.600197	2.573660
H	-0.723833	3.247355	3.451726
H	0.018910	1.776569	2.808038
H	-1.650890	2.157723	2.407093
H	0.985217	5.456286	-1.708114
H	-0.122374	5.244295	2.432621
H	-0.286869	2.432511	-2.739463
H	1.367724	2.029936	-2.292889
H	1.021215	3.578393	-3.075752
H	1.277627	7.411806	-0.305825
H	1.185468	7.258147	1.456952
H	-0.279495	7.555545	0.518536
C	-0.190979	-1.895458	-1.998169
C	-1.337114	-2.592967	-2.685588
C	-1.881746	-2.198907	-3.843688
H	-2.693566	-2.755833	-4.302696
H	-1.540800	-1.304486	-4.359994
H	-1.724779	-3.483034	-2.191693
H	0.697262	-2.537794	-2.054521
H	0.043179	-0.969644	-2.536034
H	-0.685258	-2.555343	-0.005959



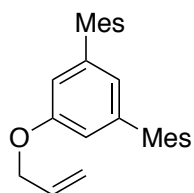
C	-0.221337	1.530314	-0.081186
C	-1.424536	1.065979	-0.554711
N	0.801763	0.639005	0.122020
B	0.712523	-0.784016	-0.131138
C	-0.622745	-1.275043	-0.659409
C	-1.615652	-0.323582	-0.835537
C	0.024675	2.972740	0.233712
C	1.983409	-1.681055	0.179091
C	2.097274	-2.374003	1.411078
C	3.031263	-1.814810	-0.761880
C	4.148855	-2.614513	-0.469445
C	4.266200	-3.298390	0.746869
C	3.224176	-3.163732	1.677869
C	1.004153	-2.269888	2.458701

C	2.966173	-1.100400	-2.099210
C	5.474274	-4.156929	1.056049
O	-2.850339	-0.732941	-1.300189
H	1.660435	1.044571	0.477894
H	-2.236196	1.769052	-0.714027
H	4.941874	-2.705503	-1.208525
H	3.291956	-3.685396	2.630555
H	2.046436	-1.352018	-2.637886
H	3.815966	-1.369726	-2.732211
H	2.975287	-0.012116	-1.972041
H	6.184107	-4.156036	0.224670
H	5.182580	-5.194853	1.251279
H	5.997578	-3.796035	1.948521
H	0.049086	-2.646675	2.076489
H	0.836390	-1.230057	2.759852
H	1.259365	-2.843214	3.353896
C	0.448581	3.854607	-0.782680
C	0.682495	5.201317	-0.461415
C	0.505296	5.692386	0.837979
C	0.083106	4.795850	1.832355
C	-0.159389	3.444809	1.554021
C	0.760282	7.146704	1.170391
C	0.654818	3.377324	-2.205657
C	-0.614037	2.518721	2.663616
H	-0.737881	3.068872	3.599027
H	0.109506	1.715430	2.837481
H	-1.567946	2.041350	2.418183
H	1.010904	5.878330	-1.246024
H	-0.060654	5.157481	2.847875
H	-0.288509	3.054690	-2.658156
H	1.337050	2.522519	-2.247880
H	1.071594	4.176036	-2.823378
H	1.093659	7.702342	0.290488
H	1.528158	7.244042	1.945421
H	-0.146895	7.627497	1.552248
C	-0.913116	-2.733699	-0.987565
C	-0.940714	-3.006257	-2.476863
C	-0.183840	-3.916760	-3.106602
H	-0.255115	-4.063499	-4.181547
H	0.528706	-4.537203	-2.567302
H	-1.637951	-2.401256	-3.055362
H	-1.889234	-3.015485	-0.569477
H	-0.159278	-3.374326	-0.521697
H	-3.449067	0.027872	-1.341388



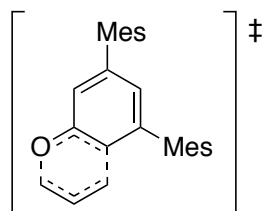
C	-1.014764	0.315598	-0.200346
C	-1.288440	1.650050	-0.433337
N	0.284509	-0.122039	-0.082384
B	1.455110	0.717300	-0.188416
C	1.139915	2.169736	-0.452066
C	-0.180890	2.561407	-0.561710
C	2.895934	0.074963	-0.035664
C	-2.075281	-0.734287	-0.059654
C	-2.640807	-1.323460	-1.215647
C	-3.610777	-2.320786	-1.065284
C	-4.040135	-2.752208	0.200909
C	-3.458072	-2.164191	1.329293
C	-2.474960	-1.166285	1.221735
C	-2.210946	-0.897438	-2.604393
C	-1.848607	-0.606366	2.482848
C	-5.100730	-3.823924	0.330158
C	3.553540	0.055095	1.220408
C	3.569979	-0.472731	-1.152426
C	4.857402	-1.016746	-1.006363
C	5.509980	-1.039061	0.232285
C	4.837234	-0.495736	1.338120
C	2.879232	0.627550	2.453825
C	2.916400	-0.484791	-2.522333
C	6.899478	-1.621683	0.381388
H	5.324700	-0.500988	2.311102
H	1.954112	0.089534	2.689649
H	2.605363	1.677638	2.305905
H	3.535063	0.566574	3.326344
H	5.359813	-1.429423	-1.878581
H	7.255391	-2.043761	-0.562137
H	6.917065	-2.415146	1.136525
H	7.616619	-0.857081	0.700939
H	2.572358	0.514666	-2.808728
H	2.037758	-1.139842	-2.539142
H	3.611481	-0.838815	-3.288268
H	0.379493	-1.117482	0.084966
O	-0.539906	3.866821	-0.816486
H	-4.043139	-2.772440	-1.955112
H	-3.771602	-2.486563	2.319162
H	-2.513987	0.132766	-2.819085
H	-2.659404	-1.544594	-3.361611
H	-1.123232	-0.939527	-2.718433
H	-2.529085	-0.708768	3.331871

H	-1.583215	0.447823	2.375549
H	-0.927224	-1.145639	2.732744
H	-6.046996	-3.494992	-0.113188
H	-5.286271	-4.074049	1.377555
H	-4.800654	-4.739142	-0.191220
H	1.909655	2.932784	-0.568462
H	0.269292	4.395560	-0.893088
C	-2.713441	2.170655	-0.555058
C	-3.263474	2.735920	0.738472
H	-3.361813	1.346648	-0.869075
H	-2.761230	2.939321	-1.330373
C	-3.754548	3.973303	0.892385
H	-3.267208	2.057111	1.590928
H	-3.767219	4.686821	0.071625
H	-4.153075	4.306698	1.847036



C	-1.125862	0.853301	0.216814
C	-2.122236	0.183514	0.932741
C	0.046229	0.160763	-0.140013
C	0.221078	-1.182555	0.213746
C	-0.787106	-1.849621	0.933688
C	-1.955779	-1.164499	1.291111
C	1.471166	-1.919530	-0.166063
C	-1.309404	2.291142	-0.167470
C	-0.827782	3.318923	0.675833
C	-1.012259	4.656425	0.300797
C	-1.661520	5.008325	-0.892729
C	-2.129877	3.975771	-1.714363
C	-1.965605	2.623590	-1.371794
C	-0.119539	2.998048	1.976311
C	-2.496167	1.548751	-2.298561
C	-1.843480	6.462255	-1.273692
C	1.564761	-2.558040	-1.424605
C	2.556642	-1.984070	0.733394
C	3.716426	-2.684056	0.362285
C	3.828186	-3.324831	-0.877741
C	2.737383	-3.249325	-1.757705
C	0.419621	-2.507164	-2.415352
C	2.493414	-1.311792	2.089818
C	5.084228	-4.075529	-1.266018
H	2.800631	-3.740201	-2.726398
H	0.219376	-1.480542	-2.739557

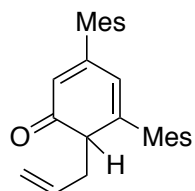
H	-0.507725	-2.886108	-1.974157
H	0.647534	-3.104951	-3.301077
H	4.549020	-2.727467	1.060288
H	5.815492	-4.070362	-0.453766
H	5.554973	-3.627395	-2.148111
H	4.859644	-5.118329	-1.514853
H	1.702326	-1.742344	2.712637
H	2.275140	-0.243349	1.995217
H	3.441646	-1.422276	2.621249
H	0.823666	0.675056	-0.697135
H	-3.036381	0.692305	1.221642
O	-2.999212	-1.721445	1.992689
H	-0.641317	5.441656	0.955894
H	-2.636474	4.224029	-2.643898
H	-0.748122	2.388668	2.633554
H	0.144722	3.914867	2.508608
H	0.799326	2.429094	1.799987
H	-2.936786	1.992806	-3.194329
H	-3.262721	0.941015	-1.806644
H	-1.701512	0.863560	-2.610853
H	-2.386236	7.009256	-0.495211
H	-2.401376	6.559773	-2.208436
H	-0.876070	6.960025	-1.403367
H	-0.641803	-2.889292	1.200203
C	-2.893096	-3.091381	2.382072
C	-4.125805	-3.515540	3.131283
H	-2.008834	-3.237560	3.019415
H	-2.765668	-3.729301	1.495384
C	-5.184287	-2.745239	3.412406
H	-4.107432	-4.555615	3.454435
H	-5.229466	-1.706401	3.103093
H	-6.029924	-3.148047	3.962377



C	2.137624	-0.828128	-0.678418
C	0.910442	-1.386376	-0.371111
H	-0.503545	0.976178	-1.698753
H	0.668468	-2.400501	-0.675297
C	-1.079450	1.456579	-0.914998
H	-2.050998	-1.012911	-1.444966
H	-0.862959	2.503887	-0.731594
C	-0.054177	-0.673204	0.417361

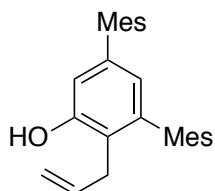
C	0.238236	0.701585	0.741236
C	-2.576393	-0.433607	-0.695133
C	-2.310326	0.918868	-0.522243
O	-1.190355	-1.201812	0.742470
H	-0.400625	1.189190	1.466185
H	-2.935290	1.489678	0.160198
C	1.880557	2.616854	0.993058
C	1.944045	2.845086	2.389150
C	2.149900	3.686758	0.103435
C	2.258009	4.127044	2.865800
C	2.445562	4.955046	0.622699
C	2.501213	5.201284	2.001630
H	2.318812	4.285094	3.939946
H	2.639526	5.771228	-0.069680
C	2.144323	3.514451	-1.403798
H	3.092729	3.096196	-1.758942
H	1.353958	2.842369	-1.742600
H	2.009124	4.480945	-1.896101
C	1.720947	1.735038	3.398729
H	0.655227	1.559925	3.582517
H	2.150024	0.788163	3.061159
H	2.177464	1.997260	4.356553
C	2.806219	6.585608	2.532049
H	3.657805	7.031909	2.008947
H	1.950808	7.256416	2.390209
H	3.035453	6.558965	3.600401
C	3.165820	-1.607099	-1.442803
C	3.288516	-1.439813	-2.841700
C	4.020780	-2.502959	-0.766267
C	4.258323	-2.173941	-3.537258
C	4.982326	-3.218591	-1.498282
C	5.117487	-3.071141	-2.884147
H	4.345395	-2.042076	-4.613441
H	5.640294	-3.904418	-0.970061
C	2.384091	-0.489637	-3.600055
H	1.330004	-0.757656	-3.472914
H	2.495449	0.539981	-3.244826
H	2.614010	-0.506985	-4.667974
C	3.924459	-2.702895	0.732650
H	3.997426	-1.750889	1.268147
H	2.967091	-3.152869	1.015358
H	4.724442	-3.357228	1.086918
C	6.152454	-3.855831	-3.662057
H	5.675048	-4.555260	-4.357574
H	6.787321	-3.190887	-4.257125
H	6.796398	-4.432727	-2.993458
C	1.536760	1.253114	0.479615

C	2.445090	0.497158	-0.239615
H	3.430763	0.898489	-0.454530
H	-3.480023	-0.876140	-0.289127



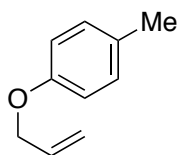
C	-0.146097	1.365801	-0.020313
C	-1.351539	0.836986	-0.377274
C	0.994342	0.497698	0.273358
C	0.943804	-0.845870	0.116810
C	-0.308293	-1.493063	-0.440859
C	-1.548266	-0.607570	-0.431900
C	0.035092	2.844609	0.127844
C	2.111214	-1.723273	0.433978
C	2.031685	-2.639068	1.513386
C	3.303896	-1.647529	-0.327063
C	4.373277	-2.499828	-0.012032
C	4.308962	-3.416578	1.044313
C	3.130068	-3.459081	1.801736
C	0.807889	-2.735345	2.405307
C	3.478041	-0.670397	-1.474099
C	5.467693	-4.337609	1.358378
O	-2.681706	-1.113752	-0.492229
H	1.899657	0.969347	0.642944
H	-2.221824	1.466219	-0.535494
H	5.280481	-2.441279	-0.608280
H	3.065157	-4.141690	2.646108
H	2.597855	-0.629580	-2.119728
H	4.337513	-0.954479	-2.086101
H	3.654561	0.347003	-1.109608
H	6.380029	-4.015054	0.850336
H	5.250281	-5.362836	1.036793
H	5.665805	-4.370836	2.434211
H	0.305143	-1.771634	2.518277
H	1.092956	-3.086520	3.400199
H	0.074651	-3.448486	2.011048
C	0.399272	3.624828	-0.990238
C	0.578275	5.006729	-0.826604
C	0.403695	5.634031	0.414422
C	0.049261	4.836061	1.512169
C	-0.136702	3.451940	1.391619
C	0.571485	7.130780	0.564706
C	0.601536	2.997612	-2.354529
C	-0.524224	2.635894	2.607757
H	-0.580353	3.269442	3.495742

H	0.200484	1.838831	2.804542
H	-1.498124	2.154730	2.469808
H	0.863227	5.604016	-1.689403
H	-0.084597	5.299895	2.486552
H	-0.333562	2.582530	-2.744705
H	1.324518	2.176223	-2.315128
H	0.967510	3.738181	-3.069276
H	1.208143	7.539736	-0.224336
H	1.014537	7.384897	1.532052
H	-0.397644	7.640397	0.505490
C	-0.027602	-1.950731	-1.920363
C	-1.087338	-2.848255	-2.500373
C	-1.688875	-2.652209	-3.682219
H	-2.416942	-3.361394	-4.066696
H	-1.474142	-1.779667	-4.294858
H	-1.341777	-3.732148	-1.915969
H	0.920346	-2.500177	-1.895070
H	0.116632	-1.073908	-2.558791
H	-0.547886	-2.399070	0.121550



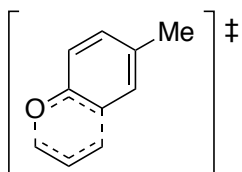
C	-0.111111	1.529240	-0.043914
C	-1.335729	1.056584	-0.536504
C	0.924603	0.609322	0.162837
C	0.761004	-0.759041	-0.115691
C	-0.466359	-1.237133	-0.616788
C	-1.502622	-0.303113	-0.814234
C	0.074504	2.985898	0.257518
C	1.914362	-1.683032	0.153189
C	1.995045	-2.374799	1.384457
C	2.942417	-1.835317	-0.801365
C	4.027170	-2.680019	-0.514737
C	4.123565	-3.376309	0.696141
C	3.094134	-3.206751	1.635002
C	0.916249	-2.226773	2.437707
C	2.897636	-1.104159	-2.126943
C	5.299532	-4.282428	0.992597
O	-2.705411	-0.792287	-1.290565
H	1.877733	0.957783	0.549660
H	-2.160072	1.746769	-0.700469
H	4.813501	-2.793712	-1.257078
H	3.149245	-3.732660	2.585620
H	1.982262	-1.339860	-2.678501

H	3.752850	-1.379233	-2.749068
H	2.915581	-0.018842	-1.984267
H	6.015307	-4.284977	0.166637
H	4.970817	-5.314153	1.159341
H	5.826665	-3.961247	1.897580
H	-0.045361	-2.615434	2.085291
H	0.756211	-1.176095	2.699428
H	1.186223	-2.769698	3.346651
C	0.460929	3.878387	-0.765134
C	0.630147	5.239606	-0.462596
C	0.422918	5.741007	0.828160
C	0.037055	4.837652	1.830650
C	-0.139312	3.472475	1.568283
C	0.607806	7.210528	1.141846
C	0.699036	3.394200	-2.180920
C	-0.558447	2.544564	2.690336
H	-0.712424	3.103305	3.616529
H	0.199038	1.776549	2.877210
H	-1.488323	2.019814	2.448170
H	0.931523	5.919934	-1.255505
H	-0.129944	5.204718	2.840942
H	-0.218163	2.995077	-2.626725
H	1.439642	2.588698	-2.207341
H	1.056395	4.210064	-2.813673
H	0.915561	7.769464	0.254463
H	1.369813	7.356019	1.915346
H	-0.321201	7.654156	1.516538
C	-0.711121	-2.702451	-0.941609
C	-0.755024	-2.978624	-2.430434
C	-0.009082	-3.899162	-3.056640
H	-0.095987	-4.058872	-4.128409
H	0.708259	-4.515811	-2.519733
H	-1.459611	-2.379351	-3.004382
H	-1.675588	-2.996169	-0.508146
H	0.060804	-3.321422	-0.481165
H	-3.339129	-0.062455	-1.358355



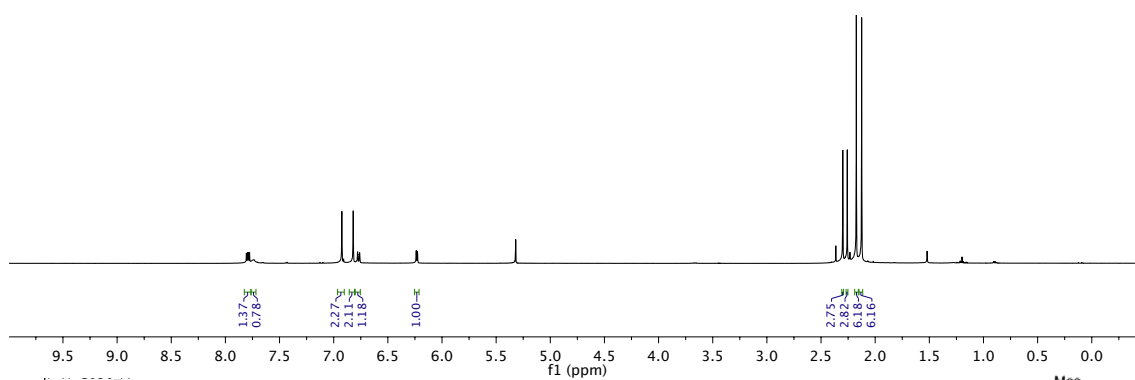
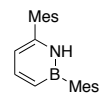
C	-0.804970	2.613042	-0.787079
C	-1.935650	1.806014	-0.911344
C	0.173711	2.362928	0.196788
C	-0.030578	1.269820	1.047010
C	-1.162829	0.443194	0.938701
C	-2.122905	0.712357	-0.045400

C	1.395154	3.250019	0.319592
O	-3.266757	-0.025336	-0.249701
C	-3.521630	-1.129232	0.639776
H	-0.680227	3.453298	-1.465650
H	-2.684001	2.007574	-1.671701
H	0.703894	1.045802	1.816254
H	-1.273464	-0.393408	1.617987
H	1.112065	4.288891	0.522193
H	1.981037	3.249254	-0.606242
H	2.046583	2.914514	1.130679
C	-4.862422	-1.707393	0.283619
C	-5.064801	-3.001592	0.003476
H	-5.698545	-1.009826	0.286925
H	-4.246096	-3.716880	-0.010988
H	-6.059946	-3.380228	-0.213302
H	-3.531188	-0.762440	1.675690
H	-2.734566	-1.886432	0.543265

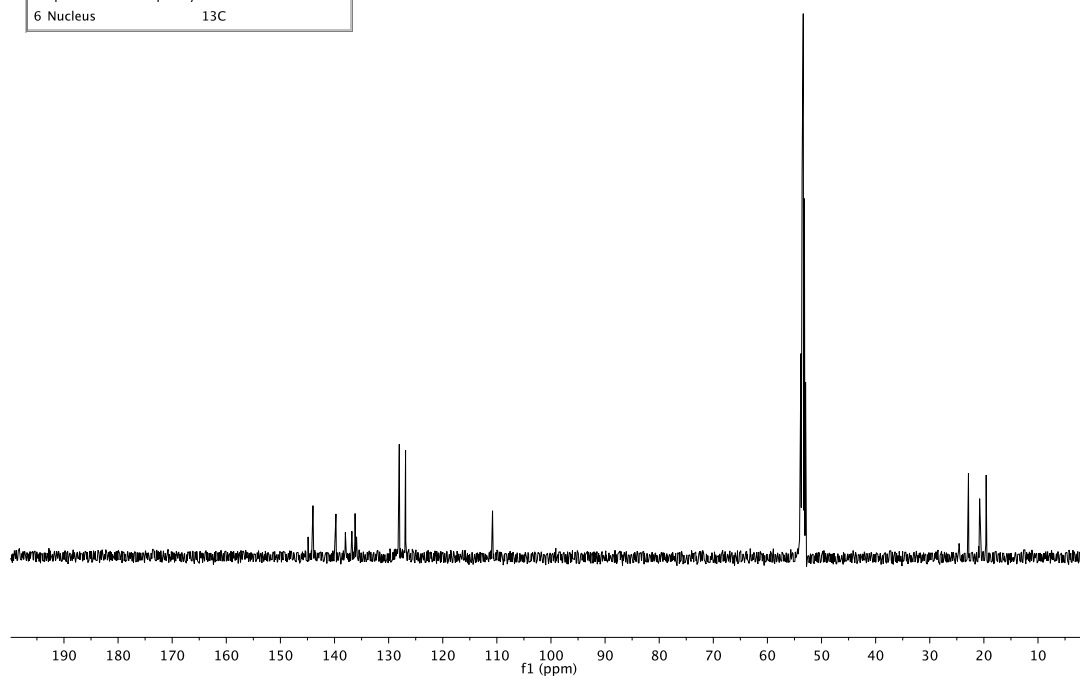


C	2.124509	-0.817450	-0.629449
C	0.905563	-1.385197	-0.325136
H	-0.473679	0.945577	-1.694650
H	0.670914	-2.401694	-0.628639
C	-1.069173	1.438623	-0.933782
H	-2.041088	-1.039184	-1.437020
H	-0.850650	2.487477	-0.762309
C	-0.071827	-0.671091	0.455637
C	0.229307	0.706511	0.760423
C	-2.580314	-0.443295	-0.710463
C	-2.308317	0.909534	-0.553477
O	-1.209989	-1.197043	0.772264
H	-0.407042	1.213422	1.476766
H	-2.945881	1.496061	0.103721
C	1.525658	1.240564	0.482342
C	2.466814	0.513345	-0.222082
H	-3.493992	-0.873906	-0.314058
H	2.858487	-1.395955	-1.186424
H	1.757466	2.249244	0.814410
C	3.832622	1.070728	-0.554514
H	4.627167	0.441932	-0.137291
H	3.988948	1.108264	-1.638712
H	3.954868	2.081961	-0.158686

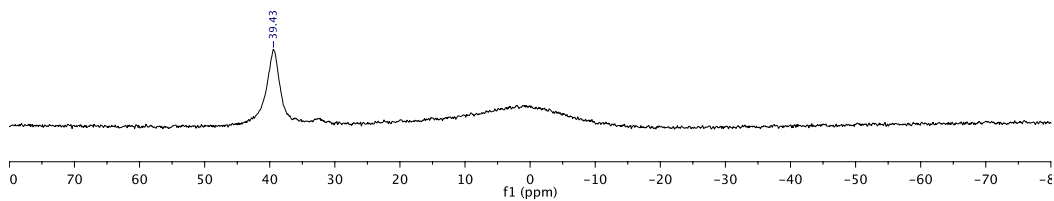
Parameter	Value
1 Solvent	cd2cl2
2 Temperature	25.0
3 Relaxation Delay	1.0000
4 Acquisition Date	2015-09-01T13:32:10
5 Spectrometer Frequency	599.69
6 Nucleus	¹ H



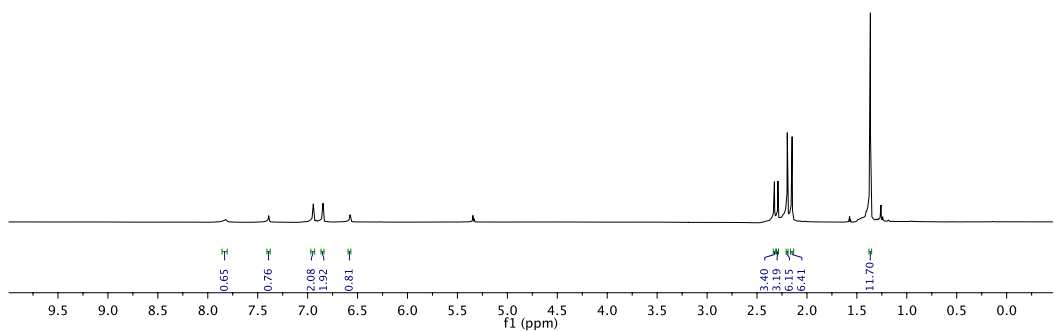
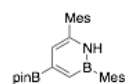
Parameter	Value
1 Solvent	cd2cl2
2 Temperature	25.0
3 Relaxation Delay	5.0000
4 Acquisition Date	2015-11-10T17:59:22
5 Spectrometer Frequency	125.71
6 Nucleus	¹³ C



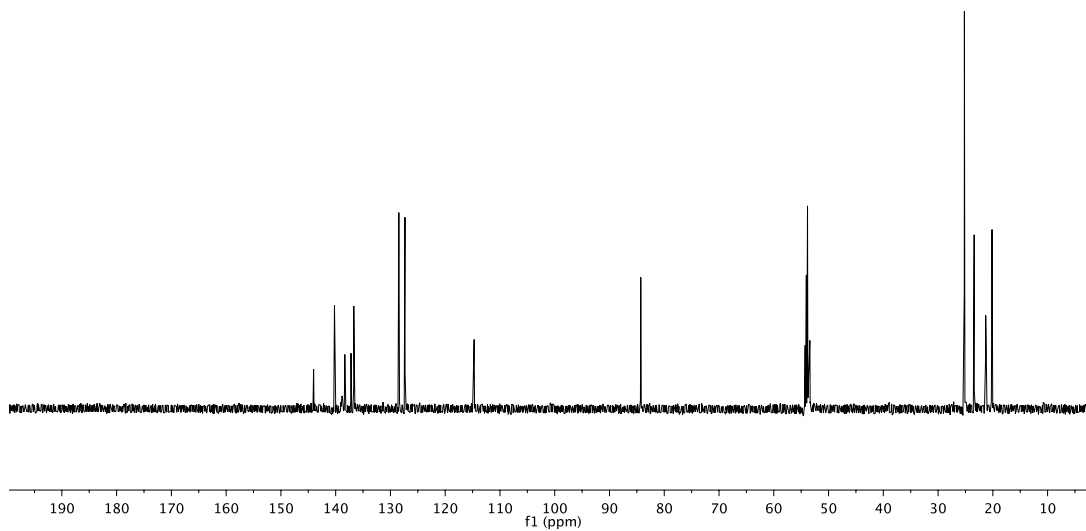
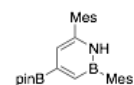
Parameter	Value
1 Solvent	cd2cl2
2 Temperature	25.0
3 Relaxation Delay	0.0100
4 Acquisition Date	2015-11-10T17:54:24
5 Spectrometer Frequency	160.38
6 Nucleus	11B



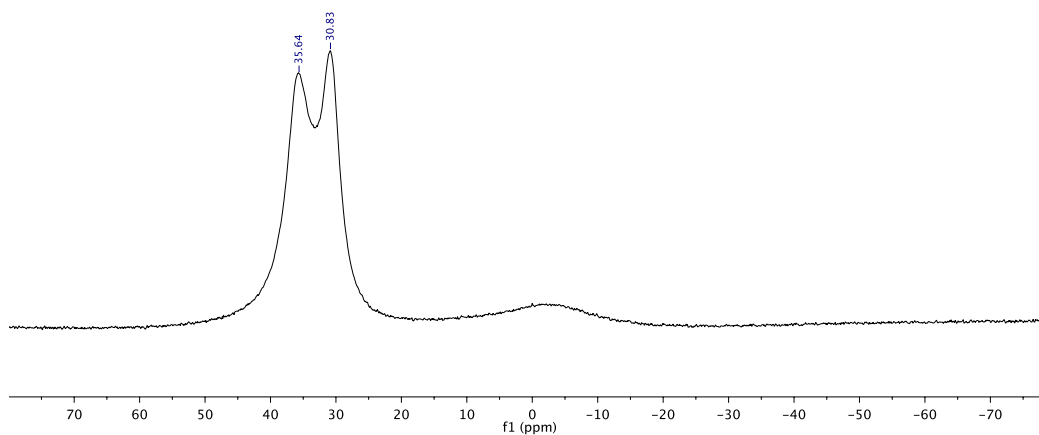
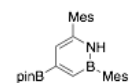
Parameter	Value
1 Solvent	cd2cl2
2 Temperature	25.0
3 Relaxation Delay	1.0000
4 Acquisition Date	2015-09-08T16:32:03
5 Spectrometer Frequency	499.88
6 Nucleus	1H



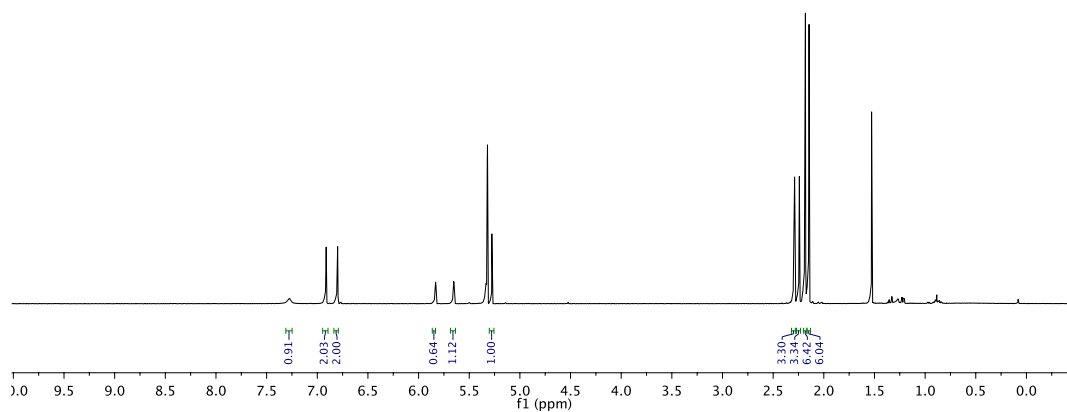
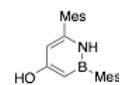
Parameter	Value
1 Solvent	cd2cl2
2 Temperature	25.0
3 Relaxation Delay	5.0000
4 Acquisition Date	2015-09-08T16:34:48
5 Spectrometer Frequency	125.71
6 Nucleus	¹³ C



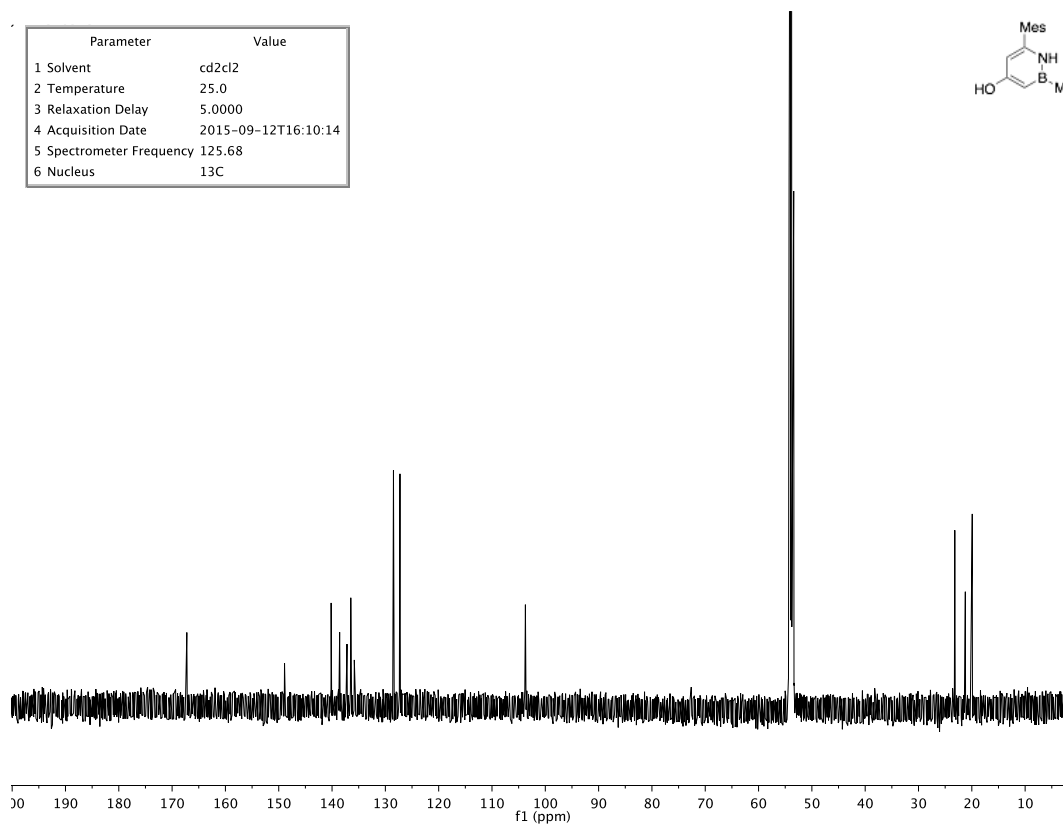
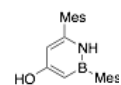
Parameter	Value
1 Solvent	cd2cl2
2 Temperature	25.0
3 Relaxation Delay	0.0100
4 Acquisition Date	2015-09-08T16:27:21
5 Spectrometer Frequency	160.38
6 Nucleus	¹¹ B



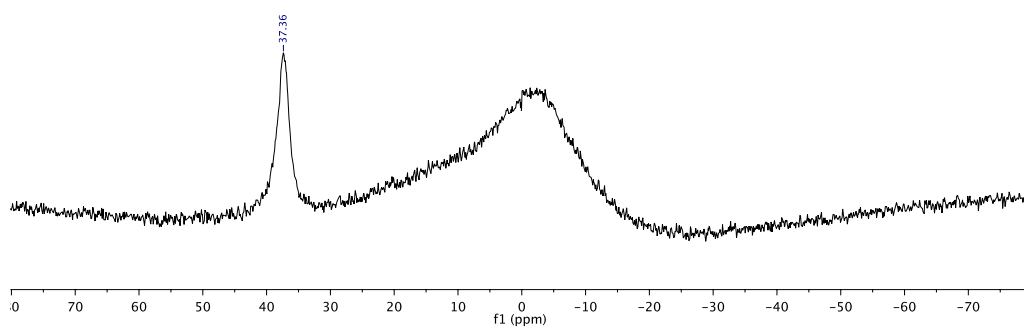
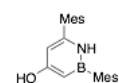
Parameter	Value
1 Solvent	cd2cl2
2 Temperature	25.0
3 Relaxation Delay	1.0000
4 Acquisition Date	2015-09-12T15:57:20
5 Spectrometer Frequency	499.88
6 Nucleus	¹ H



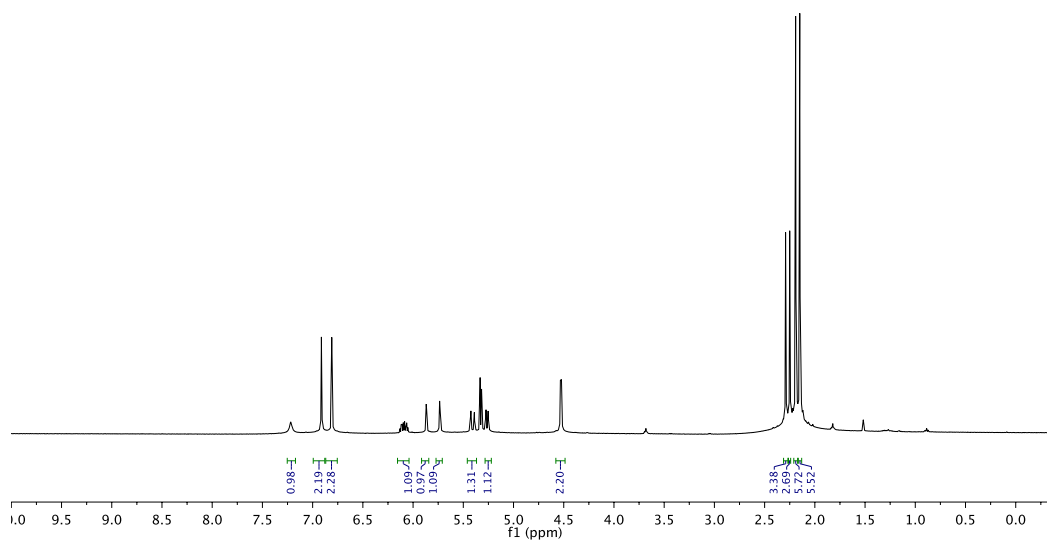
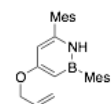
Parameter	Value
1 Solvent	cd2cl2
2 Temperature	25.0
3 Relaxation Delay	5.0000
4 Acquisition Date	2015-09-12T16:10:14
5 Spectrometer Frequency	125.68
6 Nucleus	¹³ C

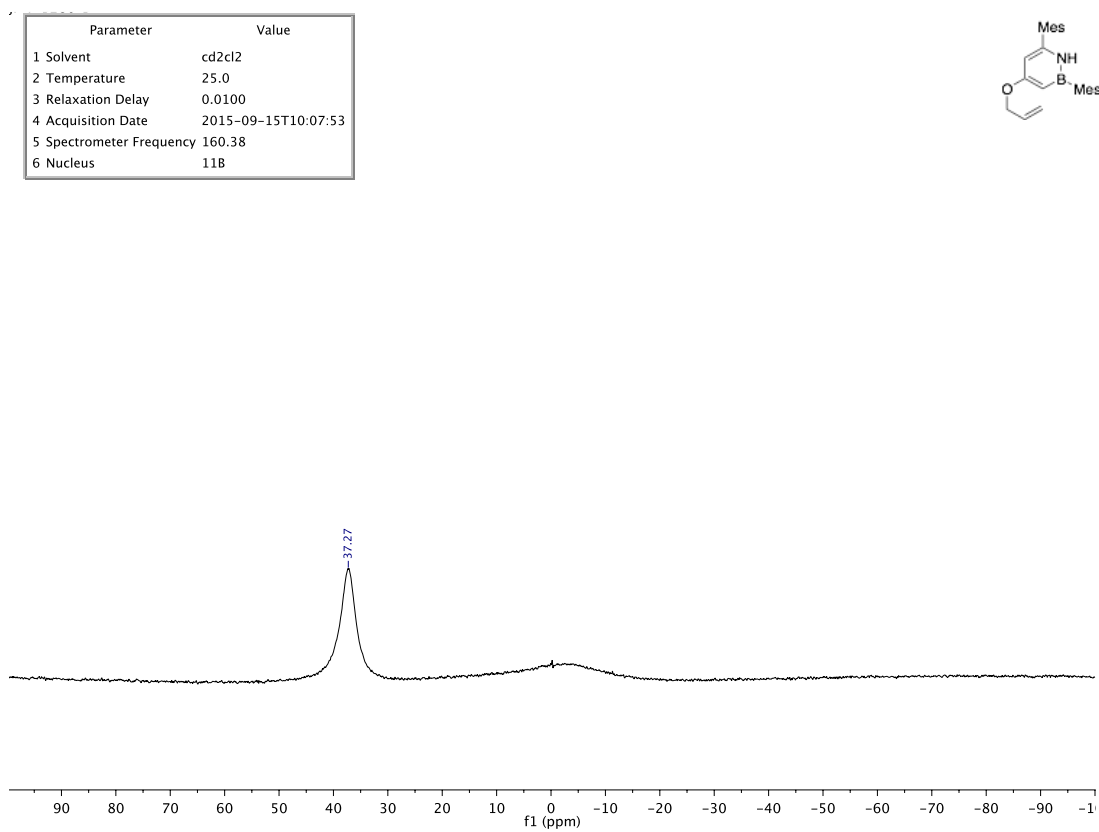
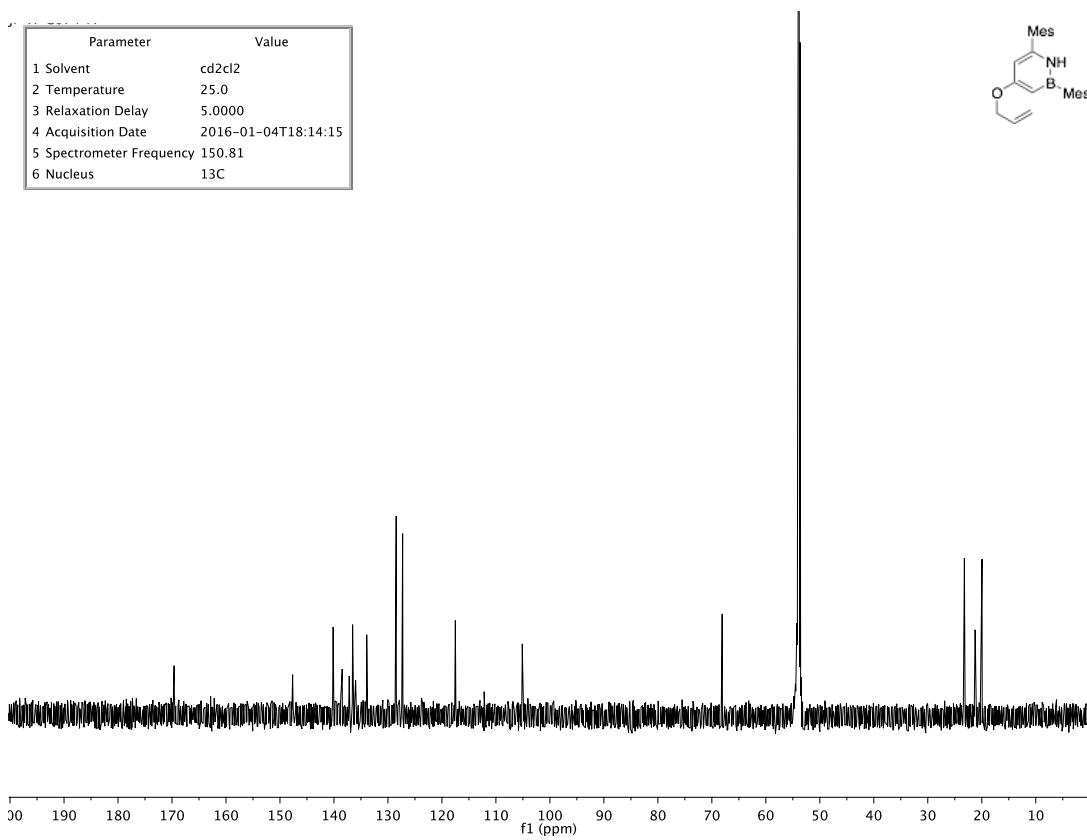


Parameter	Value
1 Solvent	cd2cl2
2 Temperature	25.0
3 Relaxation Delay	0.0100
4 Acquisition Date	2015-09-12T15:54:28
5 Spectrometer Frequency	160.38
6 Nucleus	11B

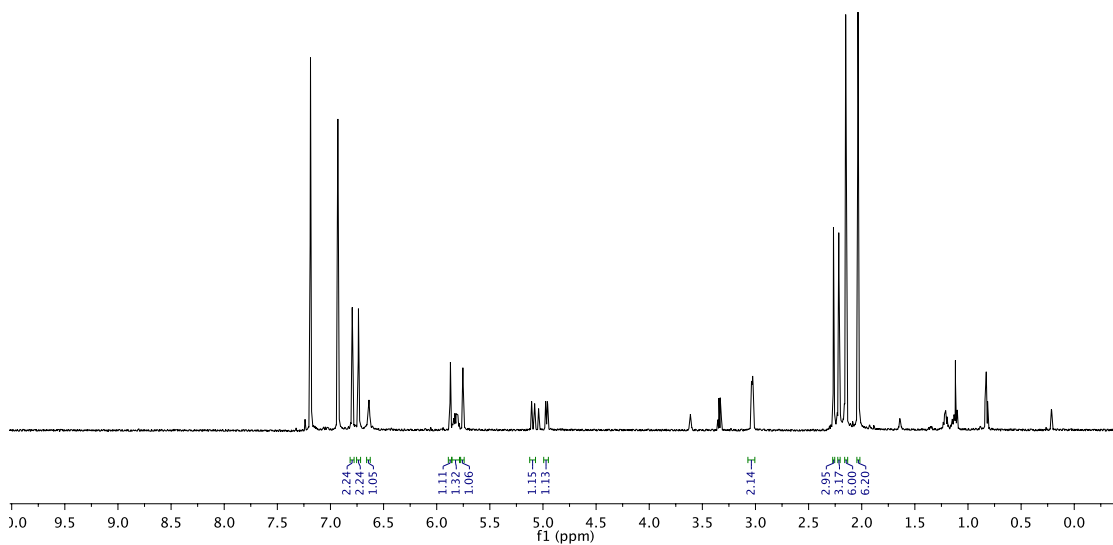
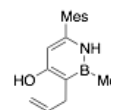


Parameter	Value
1 Solvent	cd2cl2
2 Temperature	25.0
3 Relaxation Delay	1.0000
4 Acquisition Date	2016-01-04T17:04:24
5 Spectrometer Frequency	499.88
6 Nucleus	1H

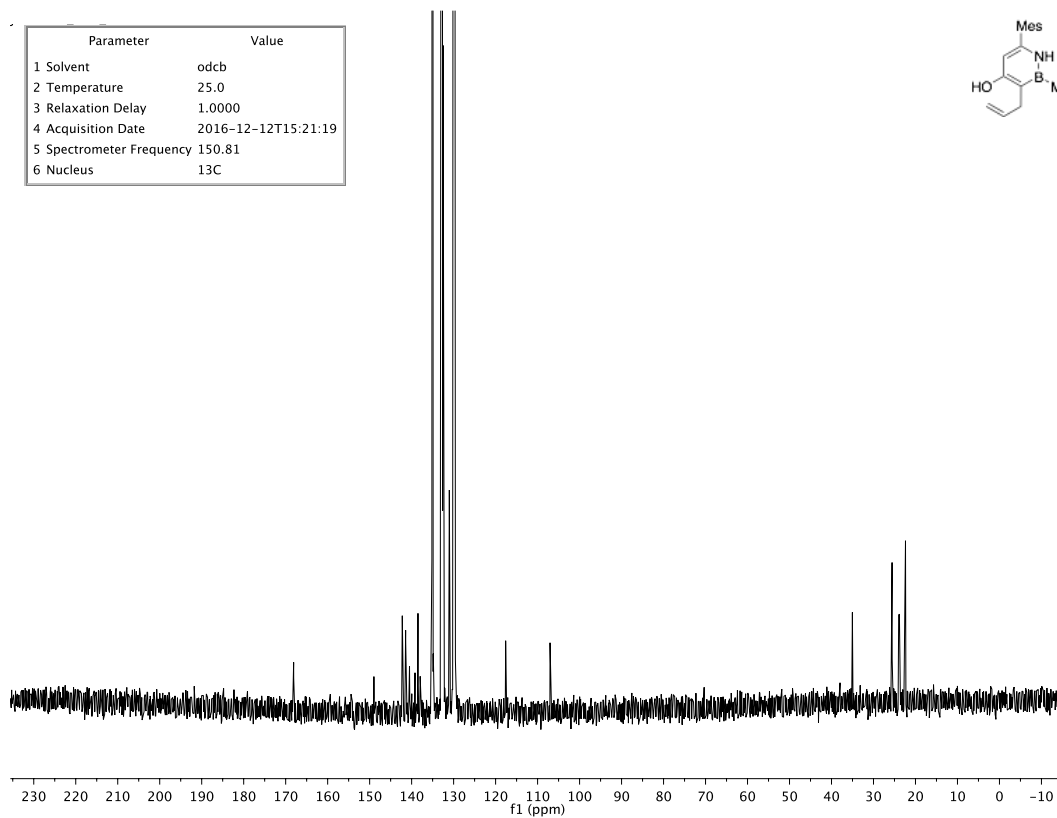
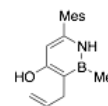


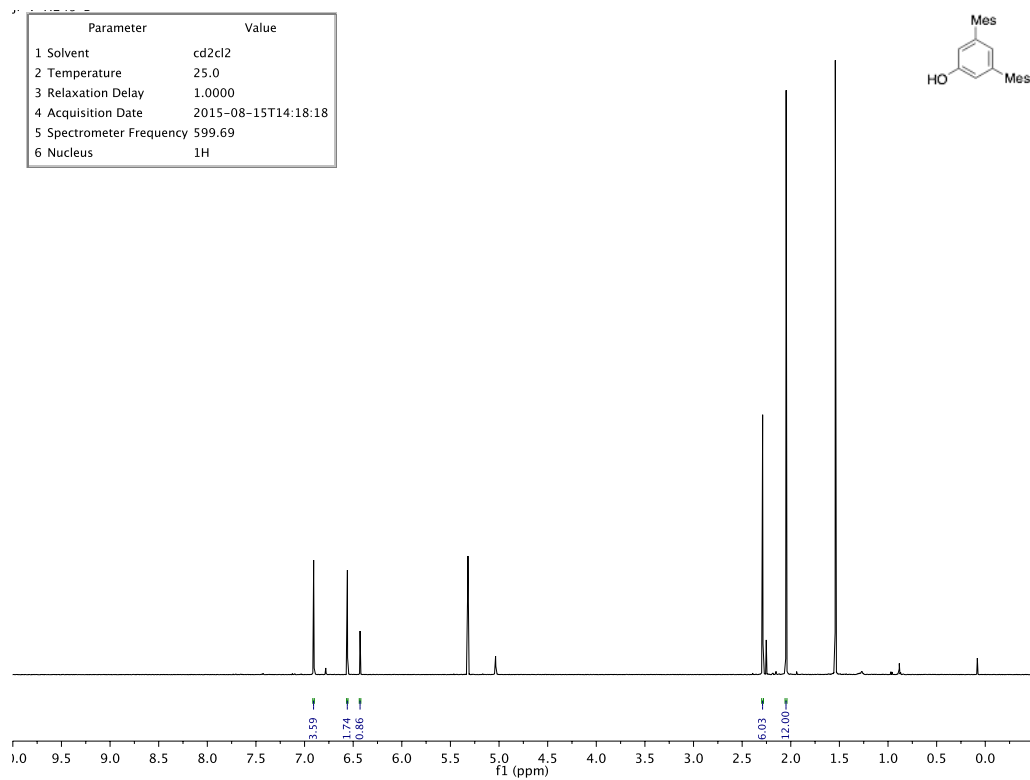
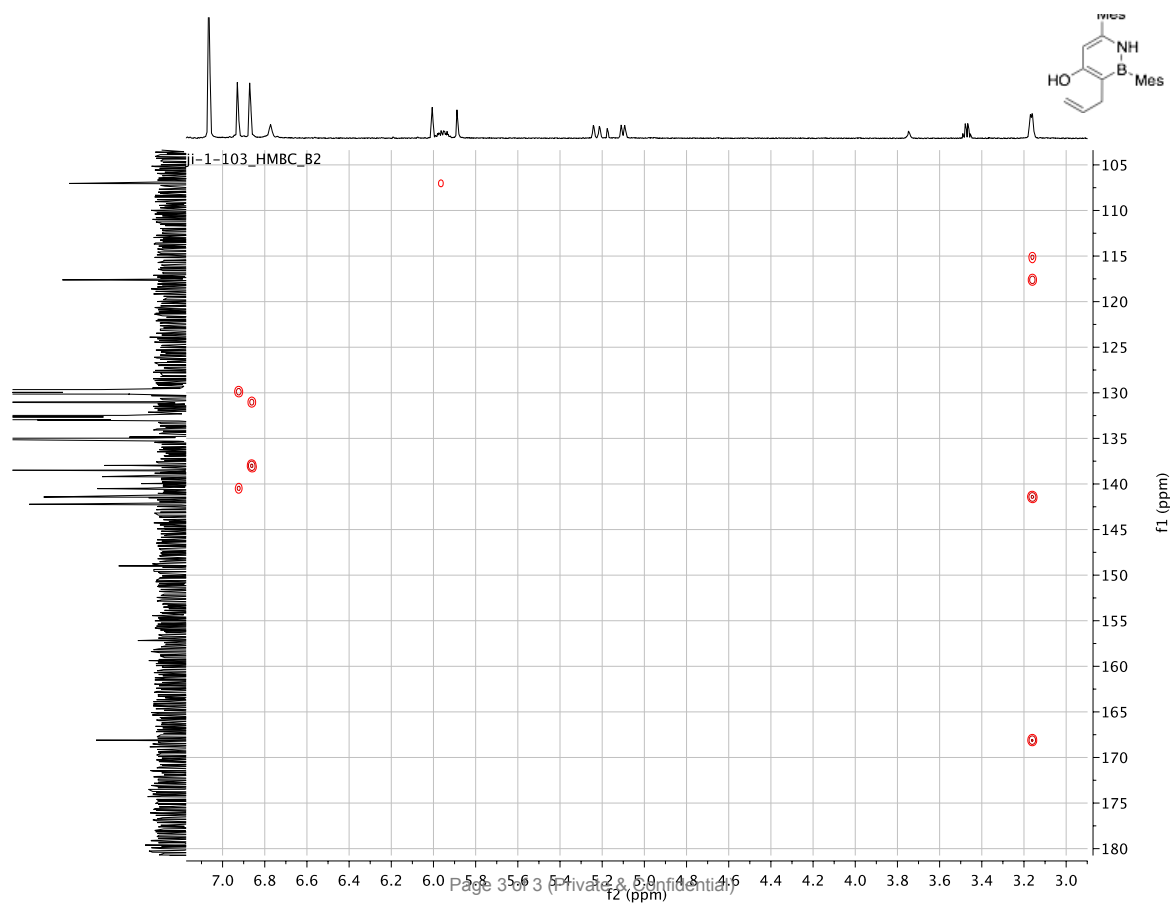


Parameter	Value
1 Solvent	odcb
2 Temperature	25.0
3 Relaxation Delay	1.0000
4 Acquisition Date	2016-01-15T14:39:38
5 Spectrometer Frequency	599.69
6 Nucleus	¹ H

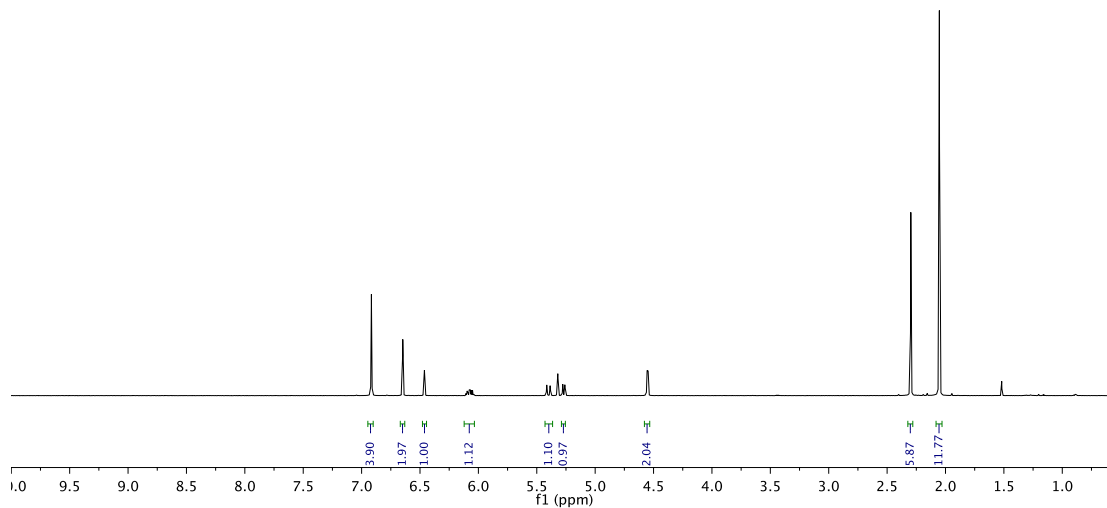
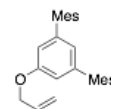


Parameter	Value
1 Solvent	odcb
2 Temperature	25.0
3 Relaxation Delay	1.0000
4 Acquisition Date	2016-12-12T15:21:19
5 Spectrometer Frequency	150.81
6 Nucleus	¹³ C

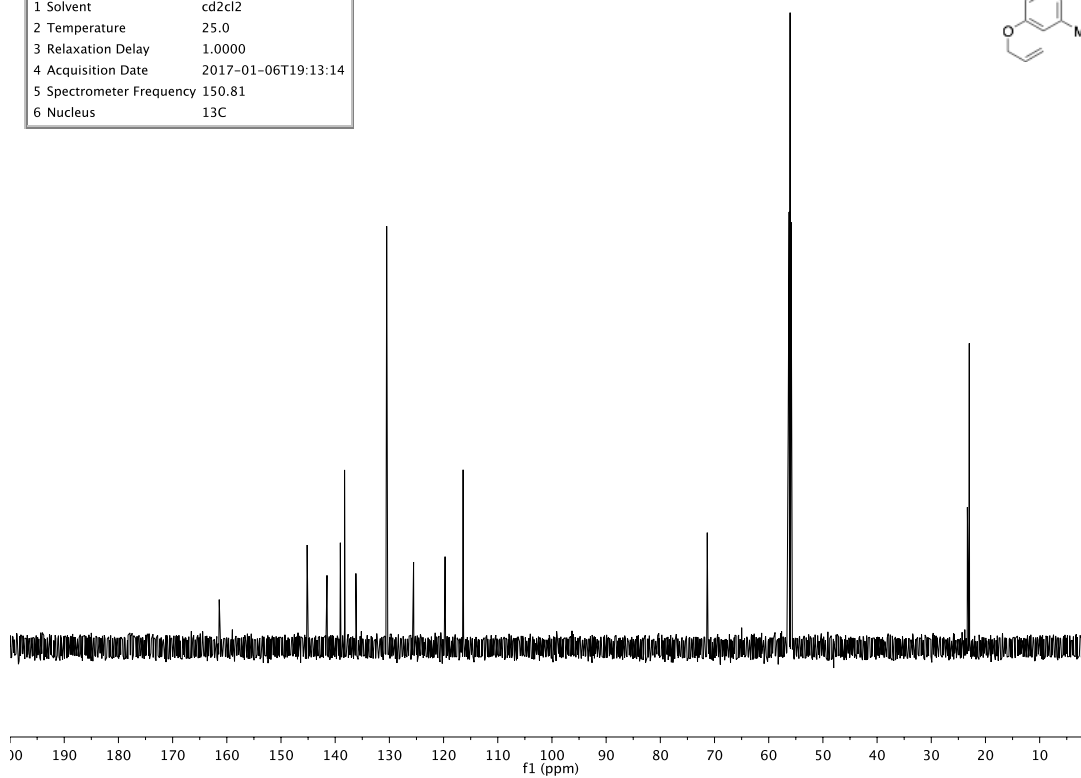
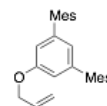




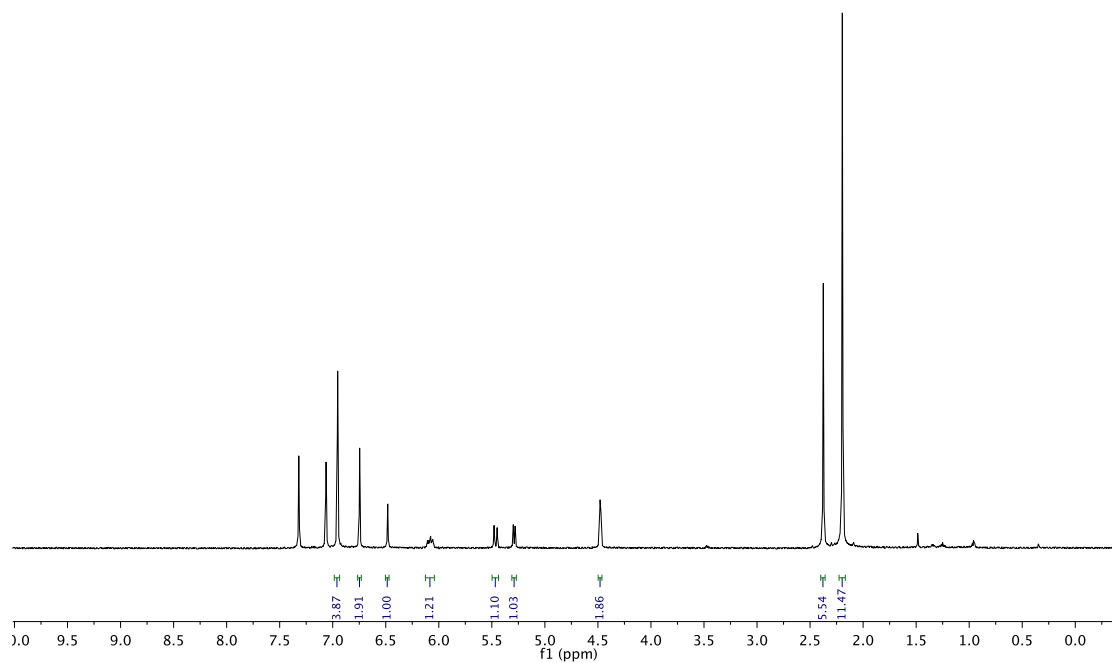
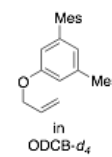
Parameter	Value
1 Solvent	cd2cl2
2 Temperature	25.0
3 Relaxation Delay	5.0000
4 Acquisition Date	2017-01-06T19:12:25
5 Spectrometer Frequency	599.69
6 Nucleus	¹ H



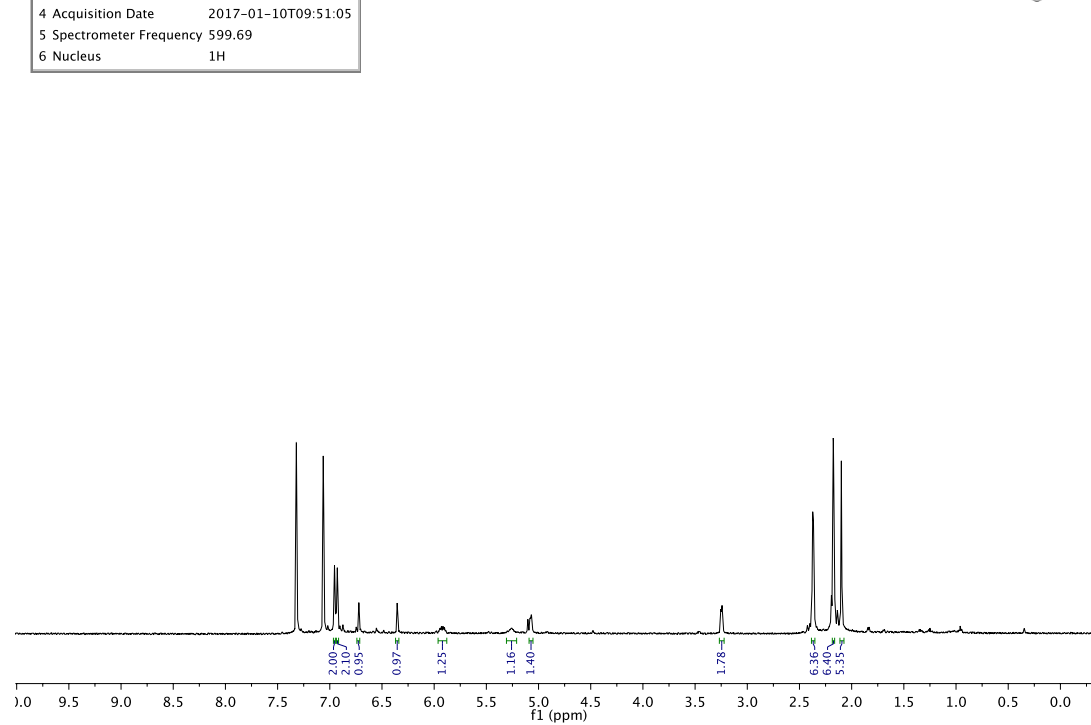
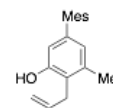
Parameter	Value
1 Solvent	cd2cl2
2 Temperature	25.0
3 Relaxation Delay	1.0000
4 Acquisition Date	2017-01-06T19:13:14
5 Spectrometer Frequency	150.81
6 Nucleus	¹³ C

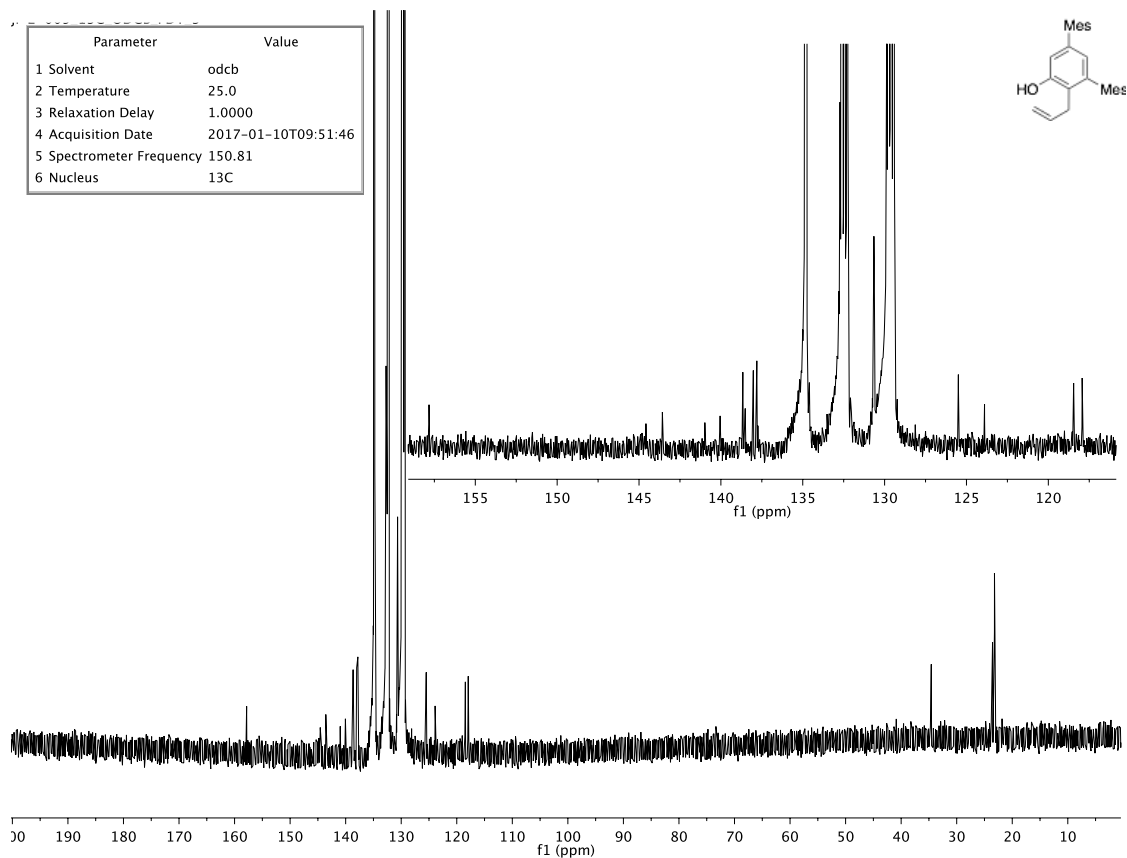


Parameter	Value
1 Solvent	odcb
2 Temperature	25.0
3 Relaxation Delay	5.0000
4 Acquisition Date	2017-01-06T19:00:19
5 Spectrometer Frequency	599.69
6 Nucleus	¹ H



Parameter	Value
1 Solvent	odcb
2 Temperature	25.0
3 Relaxation Delay	1.0000
4 Acquisition Date	2017-01-10T09:51:05
5 Spectrometer Frequency	599.69
6 Nucleus	¹ H





Appendix

Chemistry of Saturated BN Heterocycles

A.1 Purpose

This section describes smaller projects that do not warrant their own chapters but nonetheless deserve to be included in the dissertation. The two projects discussed are: 1) the Iridium-POCOP-catalyzed transfer dehydrogenation of [6,6]-BN-fused saturated heterocycles to give fused azaborines and 2) syntheses of saturated BN heterocycles for application in hydrogen storage. The work described here was completed largely while the author was a doctoral student supervised by Professor Shih-Yuan Liu at the University of Oregon.

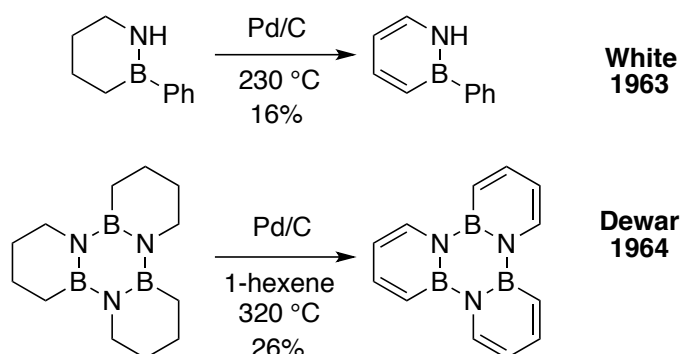
A.2.1 Introduction: Azaborine Synthesis by Dehydrogenation

One of the original methods used by White to synthesize azaborines was the dehydrogenation of a BN cyclohexene derivative under palladium catalysis, high temperatures (230 °C), and a dynamic flow of nitrogen (Scheme A.1).¹ Dewar was able to improve the yield of fully dehydrogenated product by using 1-hexene as a hydrogen acceptor.² Both of these methods were low-yielding, likely due in part the harsh conditions involved; these conditions might be improved upon by modern chemical methods.

¹ White, D. G. *J. Am. Chem. Soc.* **1963**, 85, 3634–3636.

² Culling, G. C.; Dewar, M. J. S.; Marr, P. A. *J. Am. Chem. Soc.* **1964**, 86, 1125–1127.

Scheme A.1. Dehydrogenation of Fully Saturated Carbon Backbones to Form Fully Aromatic Azaborines



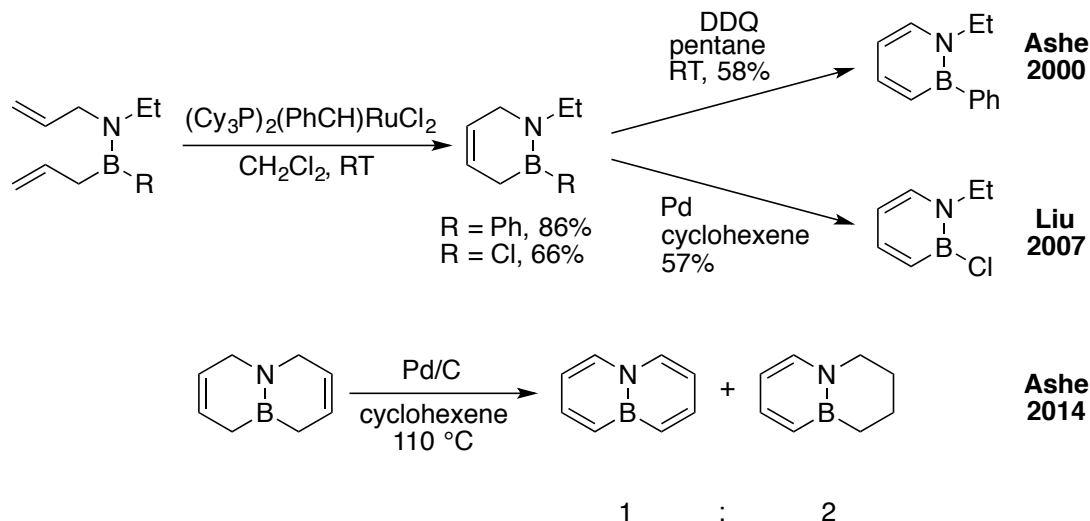
Ashe's more recent olefin metathesis-centered synthesis of azaborines was much milder³, and our group's modification, which aromatized the azaborine using Pd/C instead of DDQ, meant that late-stage modification at boron was possible. Palladium-mediated oxidation can leave a labile B–Cl bond in place, while treatment of the dehydrogenation precursor with DDQ results in decomposition (Scheme A.2).⁴ When Ashe attempted to apply the ring-closing metathesis (RCM)/oxidation protocol to a [6,6]-BN-fused system, a mixture of fully and partially oxidized products was obtained because of the thermodynamic favorability of “passing” hydrogen from one ring to the other.⁵

³ Ashe, A. J., III; Fang, X. *Org. Lett.* **2000**, *14*, 2089–2091.

⁴ Marwitz, A. J. V; Abbey, E. R.; Jenkins, J. T.; Zakharov, L. N.; Liu, S.-Y. *Org. Lett.* **2007**, *9*, 4905–4908.

⁵ Rohr, A. D.; Kampf, J. W.; Ashe, A. J. III *Organometallics* **2014**, *33*, 1318–1321.

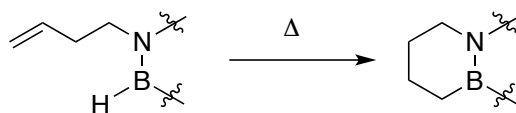
Scheme A.2. Modern Azaborine Synthesis



A.2.2 Introduction: Iridium-Catalyzed Transfer Dehydrogenation

We chose to re-investigate dehydrogenation of saturated BN heterocyclic substrates to obtain the desired, fully aromatic BN-fused products. One advantage this synthetic strategy has over the RCM/oxidation pathway is that saturated substrates can be exceedingly simple to prepare through intramolecular hydroboration (Scheme A.3).⁶ One possible solution-phase method is iridium-pincer catalyzed transfer dehydrogenation. Jensen, Brookhart, and Goldman have dehydrogenated cyclic and acyclic precursors using iridium pincer (so-called-PCP for the atomic connectivity to the iridium center) catalysts to form aromatic products.⁷

Scheme A.3. Hydroboration Method for Synthesis of Saturated BN Heterocycles

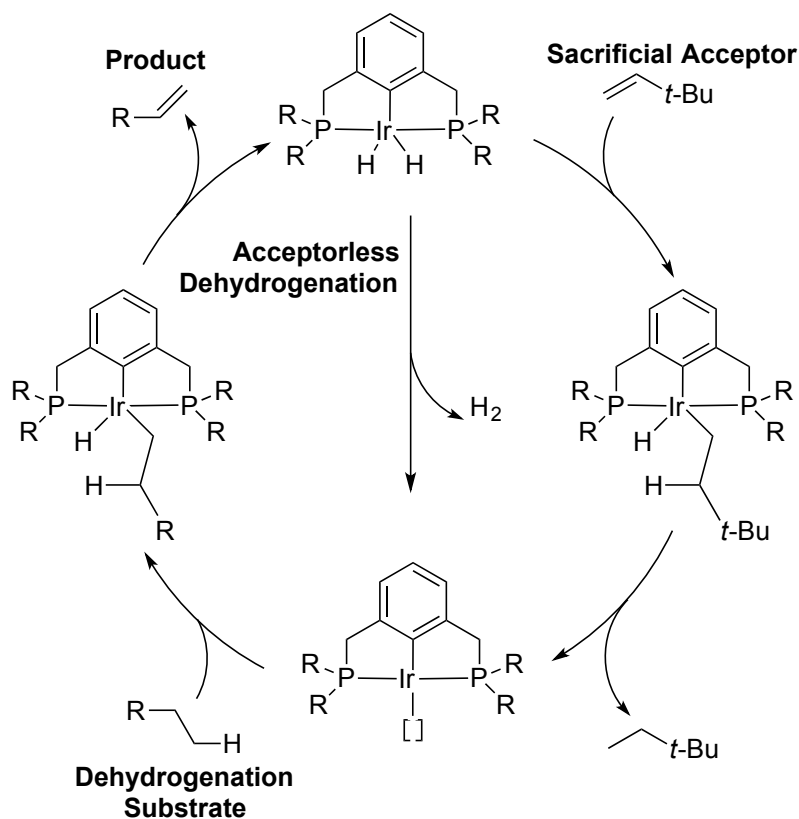


⁶ (a) Luo, W.; Zakharov, L. N.; Liu, S.-Y. *J. Am. Chem. Soc.* **2011**, *133*, 13006–13009. (b) Kumar, A.; Ishibashi, J. S. A.; Hooper, T. N.; Mikulas, T. C.; Dixon, D. A.; Liu, S.-Y.; Weller, A. S. *Chem. Eur. J.* **2016**, *22*, 310–322.

⁷ (a) Gupta, M.; Kaska, C.; Jensen, C. M. *Chem. Commun.* **1997**, 461–462. Acyclic precursors can be oxidized and cyclized. See: (b) Ahuja, R.; Punji, B.; Findlater, M.; Supplee, C.; Schinski, W.; Brookhart, M.; Goldman, A. S. *Nat. Chem.* **2011**, *3*, 167–171.

These pincer-ligated iridium complexes operate according to the following accepted mechanism (Scheme A.4).⁸ Traditionally, the starting catalyst is a dihydrido-iridium(III) complex. The olefinic acceptor, usually *tert*-butylethylene undergoes β -migratory insertion to give an iridium(III) alkyl species. Reductive elimination gives an iridium(I) 14-electron intermediate and the reduced acceptor as a byproduct. The iridium(I) intermediate oxidatively adds into the substrate's C(sp³)-H bond, where it then performs a β -hydride elimination to form the dehydrogenated product and re-form the iridium(III) dihydride.

Scheme A.4 Accepted Mechanism of Iridium-catalyzed Transfer Dehydrogenation



⁸ For an overview see: (a) Jensen, C. M. *Chem. Commun.* **1999**, 3, 2443–2449. (b) Choi, J.; MacArthur, A. H. R.; Brookhart, M.; Goldman, A. S. *Chem. Rev.* **2011**, 111, 1761–1779. (c) Giustra, Z. X.; Ishibashi, J. S. A.; Liu, S.-Y. *Coord. Chem. Rev.* **2016**, 314, 134–181.

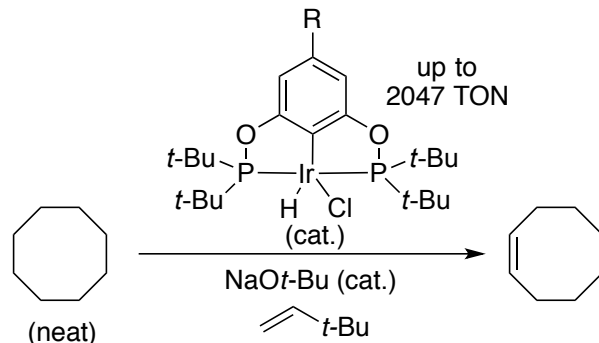
It is important to note that each step of this catalytic cycle is reversible. In the case of aromatization, reversibility, i.e., insertion of the Ir–H bond into the unsaturation formed in the azaborine product, should not be a problem due to the thermodynamic and kinetic stability afforded by aromaticity. Secondly, it should be noted that though direct reductive elimination of hydrogen from the iridium(III) dihydride is possible, this process is extremely slow, even at the elevated temperatures typically employed for these reactions.^{8a}

Brookhart⁹ and Jensen¹⁰ synthesized a modified PCP ligand scaffold bridged with oxygen atoms instead of methylene groups. This so-called POCOP scaffold gave enhanced turnover with respect to the previous PCP scaffold in the benchmark cyclooctane-to-cyclooctene transfer dehydrogenation reaction (Scheme A.5). Brookhart hypothesized that the POCOP scaffold, having less electron-rich phosphines than the PCP scaffold, better stabilized the iridium(I) oxidation state so that inhibiting pathways such as metallacyclopropane formation with an olefin (the sacrificial acceptor or the olefin-containing product) were suppressed.^{9b} Moreover, Brookhart showed that the sensitive iridium(III) dihydride need not be isolated, and that catalytically competent species could be generated from the much more accessible iridium(III) hydrido-chloride, simply by treating the latter complex with base.^{9a}

⁹ (a) Göttker-Schnetmann, I.; White, P.; Brookhart, M. *J. Am. Chem. Soc.* **2004**, *126*, 1804–1811. (b) Göttker-Schnetmann, I.; Brookhart, M. *J. Am. Chem. Soc.* **2004**, *126*, 9330–9338. (c) Göttker-Schnetmann, I.; White, P. S.; Brookhart, M. *Organometallics* **2004**, *23*, 1766–1776.

¹⁰ Morales-Morales, D.; Redón, R.; Yung, C.; Jensen, C. M. *Inorg. Chim. Acta* **2004**, *357*, 2953–2956.

Scheme A.5 Ir-POCOP-Catalyzed Transfer Dehydrogenation of Cyclooctane



Jensen previously highlighted the utility of iridium-pincer catalyzed transfer dehydrogenation in heteroarene synthesis¹¹, though no examples are boron-containing.¹² We envisioned, however, that POCOP-Ir complexes could catalyze transfer dehydrogenation and yield our desired [6,6] fused azaborines.

A.2.3 Results: Screening

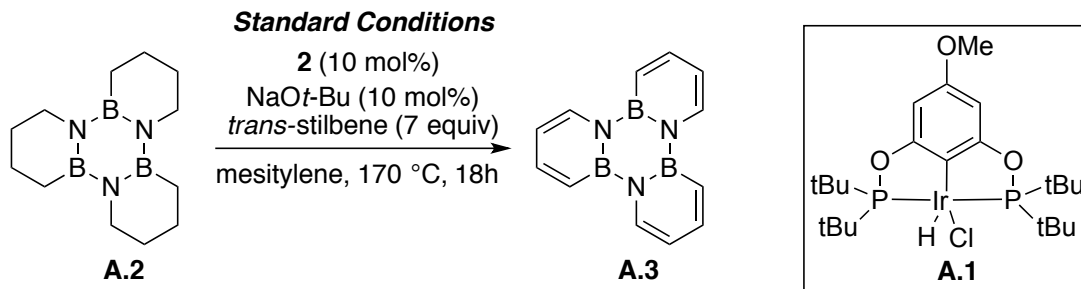
Where the initial studies by Jensen, Goldman, and Brookhart were concerned with efficiency benchmarks such as turnover frequency (TOF) and turnover number (TON) with respect to cheap hydrocarbons, we are interested in a higher-value substrate. We cannot be certain that irregularities such as the introduction of boron^{8a} will not interfere with the desired reaction. We also will not be able to perform the reactions neat, introducing the need for solvents that could interfere with the catalytic cycle detailed above.^{9c}

We performed Brookhart's *in situ* generation of active iridium(I) species using *p*-MeO(POCOP)IrHCl **A.1** as the precatalyst and decided to dehydrogenate BN-

¹¹ (a) Wang, Z.; Tonks, I.; Belli, J.; Jensen, C. M. *J. Organomet. Chem.* **2009**, 694, 2854–2857. (b) Brayton, D. F.; Beaumont, P. R.; Fukushima, E. Y.; Sartain, H. T.; Morales-Morales, D.; Jensen, C. M. *Organometallics* **2014**, 33, 5198–5202. (c) Brayton, D. F.; Jensen, C. M. *Chem. Commun.* **2014**, 50, 5987–5989.

¹² Brookhart and Jensen both cite “boron-containing impurities” as deleterious to the transfer dehydrogenation process. See refs 8a and 9a.

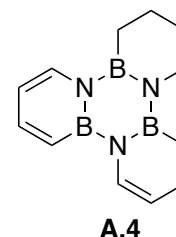
cyclohexane trimer **A.2**^{6a} to BN-triphenylene **A.3**² as our model for optimization studies. Screening studies identified the optimal conditions as 10 mol% catalyst, an equimolar amount of activating sodium *tert*-butoxide, *trans*-stilbene as the hydrogen acceptor, and mesitylene as the solvent. Using the customary *tert*-butylethylene (TBE) or norbornene (NBE) as the hydrogen acceptor, we observed a decrease in yield (57% from >95%) (Table A.1, entry 2). Similarly, substituted stilbenes and styrenes decreased yields; 4-fluorostilbene, however, gave good results. A screen of solvents showed that solvents with many sterically accessible Ar–H bonds (toluene and *m*-xylene) gave poor results (entries 7 and 8); using chlorobenzene, a solvent with an activatable C–Cl bond, stifled reactivity altogether (entry 9).

Table A.1. Conditions for Ir-POCOP Transfer Dehydrogenation

Entry	Deviation from Standard Conditions	Yield (%) ^a
1	No Deviation	>95 (92%)
2	TBE H ₂ Acceptor	57
3	Styrene H ₂ Acceptor	13
4	4-F(stilbene) H ₂ Acceptor	91
5	4-MeO(stilbene) H ₂ Acceptor	0
6	4-CN(stilbene) H ₂ Acceptor	0
7	Toluene Solvent	41
8	<i>m</i> -Xylene Solvent	36
9	Chlorobenzene Solvent	0

^a Yields determined by GC, the average of two runs. NMR Yield (in parentheses) determined using hexamethylbenzene as internal standard

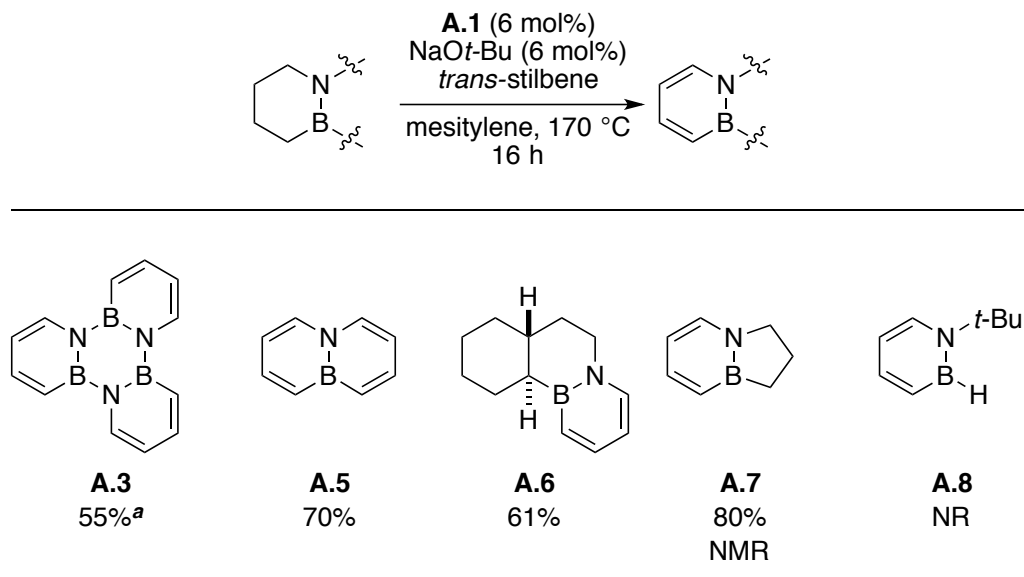
We isolated an intermediate **A.4**, which has two aromatic rings and one saturated ring, from unoptimized dehydrogenation reactions of **A.2**. We observed no isolated olefins in any reaction mixture. This “all-or-nothing” dehydrogenation is consistent with the findings of Jensen, who similarly observed only aromatic or saturated ring systems in the (POCOP)Ir-catalyzed dehydrogenation of another poly-ring-fused heterocyclic compound, perhydro-*N*-ethylcarbazole.^{11a}



A.2.4 Results: Scope

We quickly discovered that the scope of the dehydrogenation reaction of saturated BN-heterocycles was limited to molecules featuring BN-fusion (Table A.2). We also found we could decrease the catalyst loading to 6 mol%.

Table A.2: Scope of transfer dehydrogenation of BN-fused heterocycles



Isolated yield. Relative stereochemistry shown. $[n + 1]$ equiv H_2 acceptor used where $n = \#$ double bonds formed. ^a Isolated by sublimation of spent acceptor

We could isolate compound **A.3** (55% yield) only by subliming away the bibenzyl side-product and excess stilbene hydrogen acceptor. Known BN naphthalene **A.5** was isolated in good yield using preparative size-exclusion HPLC, while novel heterocyclic species **A.6** was isolated using standard column chromatography. Compound **A.7** was observed by NMR, but it was not stable to silica gel chromatography, and its sensitivity to ambient conditions prohibited its isolation using size-exclusion chromatography. Finally, the saturated analogue of **A.8** did not react under the standard conditions. Thus, the catalyst does not tolerate boron-hydrides embedded in amino-boranes. This result agrees with observations by Kaska and Jensen for the PCP-Ir system^{8a} and by Brookhart

in the POCOP-Ir system^{9a} which showed borane-derived impurities inhibited catalysis, presumably by coordinating to the metal through bridging hydrides.¹³ This result also underscores that the presence of boron itself does not intrinsically inhibit catalysis, though Brookhart and Jensen both cited “boron containing impurities” for catalyst inhibition.

Using iridium-catalyzed transfer dehydrogenation of saturated precursors, we overcame the limitation of the RCM/oxidation strategy discussed by Ashe⁵ and Fang¹⁴; using our optimized conditions, we observed full conversion to the desired product without any BN-tetralin.

BN-heterocycle **A.7** was the only product observed by NMR, even when we used 7 equivalents stilbene acceptor. The *anti* orientation of the hydrogen atoms at the C–C ring fusion, a result of the preceding hydroboration reaction (Scheme A.3 *vide supra*), likely prohibits the dehydrogenation of the middle ring in **A.7**; elimination of H₂ equivalents in the dehydrogenation substrate must occur in a syn fashion due to the mechanism of reaction.

A.2.5 Conclusion

We have utilized the *p*-MeO(POCOP)IrHCl/NaOt-Bu catalyst system to dehydrogenate boron-containing heterocycles for the first time, synthesizing BN-fused 1,2-azaborines from saturated precursors. We found the reaction to be selective in its targeted organic products. We have also defined the scope of solvents and hydrogen acceptors that may be employed in the transfer dehydrogenation of saturated BN-heterocycles to 1,2-azaborines.

¹³ Denney, M. C.; Pons, V.; Hebden, T. J.; Heinekey, D. M.; Goldberg, K. I. *J. Am. Chem. Soc.* **2006**, *128*, 12048–12049.

¹⁴ Sun, F.; Lv, L.; Huang, M.; Zhou, Z.; Fang, X. *Org. Lett.* **2014**, *16*, 5024–5027.

A.2.6 Experimental Section

General Considerations

All preparative manipulations were carried out under inert nitrogen atmosphere using standard Schlenk or glovebox techniques unless specifically stated otherwise. Reagents purchased from Sigma-Aldrich, TCI America, and Strem Chemicals were used without further purification. Toluene, methylene chloride, pentane, THF, and ethyl ether were taken from a solvent purification system and used without further purification; the remaining solvents were dried over calcium hydride, distilled, and freeze-pump-thaw degassed before use. Additionally, all materials used under argon were either purged with argon (in the case of solids) or stirred over calcium hydride, distilled, then freeze-pump-thaw degassed (in the case of liquids). BN-cyclohexane trimer,^{6a} 9,10-azaboradecalin,¹⁵ and iridium catalysts⁹ were prepared *via* literature methods. ¹¹B NMR spectra were recorded on a Varian Unity/Inova 300 at ambient temperature and were externally referenced to BF₃•Et₂O (δ = 0). ¹H NMR spectra were recorded on a Varian Unity/Inova 300 or 500 spectrometer. ¹³C NMR spectra were recorded on a Varian Inova 500 spectrometer. ³¹P NMR spectra were recorded on a Varian Inova 300 spectrometer and externally referenced to a H₃PO₄ in D₂O standard (δ = 0). High Resolution Mass Spectrometry was performed using the electron impact method at the Mass Spectrometry Core at Oregon State University.

Description of Entries from Table A.1

In an argon-filled glovebox, the *p*-X(POCOP)IrHCl precatalyst (0.021 mmol, 10 mol%) was combined dry with an equimolar amount of sodium *tert*-butoxide (2 mg) and the full amount of hydrogen acceptor (1.43 mmol, 7 eq. relative to the BN-cyclohexane trimer added). This mixture was combined with 0.6 mL solvent and aged for two hours in a sealed pressure vessel before the BN-cyclohexane trimer substrate (50 mg, 0.21 mmol) was added. The pressure vessels were then taken out of the glovebox and heated to 170 °C for 18 hours. GC yields were obtained using an Agilent 6850 Series II GC-FID instrument. Hexadecane was used as the internal standard, and reported yields are the average of two runs. Control experiments showed no reaction of BN-cyclohexane trimer

¹⁵ Dewar, M. J. S.; Dietz, R. J. *Chem. Soc.* **1959**, 2728–2730.

A.2 with any of the reagents alone. A second control experiment showed no reaction of BN-cyclohexane trimer without the use of a sacrificial acceptor. Yields reported are the average of two runs. **Optimized conditions for Table A.2 use 6 mol% precatalyst and mesitylene as the solvent.**

Entry 1: The general procedure was used with mesitylene as the solvent, *p*-MeO(POCOP)IrHCl (13.5 mg), and *trans*-stilbene as the acceptor (260 mg). Yield: >95%.

Entry 2: The general procedure was used with mesitylene as the solvent, *p*-MeO(POCOP)IrHCl (13.5 mg), and *tert*-butylethylene as the acceptor (0.18 mL). Yield: 57%.

Entry 3: The general procedure was used with mesitylene as the solvent, *p*-MeO(POCOP)IrHCl (13.5 mg), and styrene as the acceptor (150 mg). Yield: 13%.

Entry 4: The general procedure was used with mesitylene as the solvent, *p*-MeO(POCOP)IrHCl (13.5 mg), and 4-fluorostilbene as the acceptor (327 mg). Yield: 91%.

Entry 5: The general procedure was used with mesitylene as the solvent, *p*-MeO(POCOP)IrHCl (13.5 mg), and 4-methoxystilbene as the acceptor (300 mg). Yield: 0%.

Entry 6: The general procedure was used with mesitylene as the solvent, *p*-MeO(POCOP)IrHCl (13.5 mg), and 4-cyanostilbene as the acceptor (293 mg). Yield: 0%.

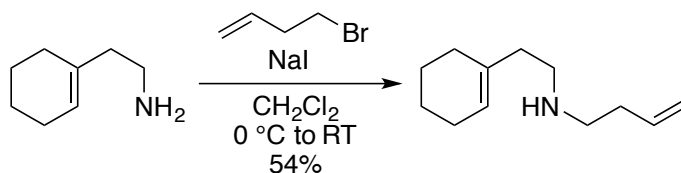
Entry 7: The general procedure was used with toluene as the solvent, *p*-MeO(POCOP)IrHCl (13.5 mg), and *trans*-stilbene as the acceptor (260 mg). Yield: 41%.

Entry 8: The general procedure was used with *m*-xylene as the solvent, *p*-MeO(POCOP)IrHCl (13.5 mg), and *trans*-stilbene as the acceptor (260 mg). Yield: 36%.

Entry 9: The general procedure was used with chlorobenzene as the solvent, *p*-MeO(POCOP)IrHCl (13.5 mg), and *trans*-stilbene as the acceptor (260 mg). Yield: 0%.

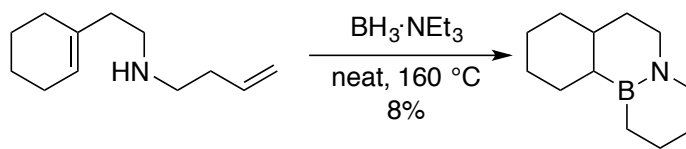
Synthetic Details for Dehydrogenation Precursors

N-Homoallyl-2-(1-cyclohexenyl)ethylamine (A.10)



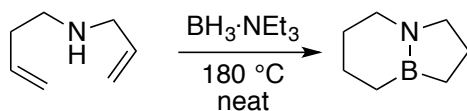
Freshly distilled 2-(1-cyclohexenyl)ethylamine (23.1 g, 163 mmol, 2.2 equiv) was dissolved in dry methylene chloride (50 mL) with sodium iodide (0.5 g) under nitrogen and cooled with an ice bath. 4-Bromo-1-butene (10.0 g, 74 mmol, 1 equiv) was added dropwise, and the reaction mixture was allowed to warm up to room temperature and was stirred 18 hours. The solvent was then removed by rotary evaporator. Saturated sodium bicarbonate was added to freebase products, and the organics were extracted into ether. The ether was washed with brine and dried with sodium sulfate. The ether was removed by rotary evaporator, and the yellow liquid was dried over calcium hydride and fractionally distilled. Starting material 2-(1-cyclohexenyl)ethylamine distills at 34 °C, 150 millitorr. The product distills at 61 °C, 150 millitorr as a clear, colorless liquid (7.68 g, 54%). ¹H NMR (300 MHz, C₆D₆) δ 5.79 (m, 1H), 5.48 (brs, 1H), 5.01 (m, 2H), 2.59 (dt, *J* = 6.91 Hz, 23.86 Hz, 4H), 2.15 (m, 4H), 1.91 (d, *J* = 46.39 Hz, 4H), 1.50 (m, 4H), 0.64 (s, 1H). ¹³C NMR (151 MHz, C₆D₆) δ 137.4, 136.2, 122.5, 115.6, 49.4, 48.3, 39.2, 35.1, 28.6, 25.7, 23.4, 23.0. HRMS (EI⁺) [*M*]⁺ calcd. for C₁₂H₂₁N 179.16740, found 179.16698.

Compound A.11



The starting amine **A.10** (3.00 g, 15.7 mmol) was combined with borane-triethylamine complex (2.84 g, 24.7 mmol) in a pressure vessel. The vessel was sealed and heated to 160°C for 18 hours. The resulting solution fractionally distilled to separate excess borane-triethylamine (35°C , 150 millitorr) from the product (60°C , 150 millitorr). The product fraction then passed through a plug of dry alumina with pentane as the eluent. Yield: 227 mg (8%). ^1H NMR (500 MHz, C_6D_6) δ 2.88 (td, $J = 12.4, 4.5$ Hz, 1H), 2.65 (m, 1H), 2.57 (dd, $J = 12.0, 5.7$ Hz, 1H), 1.91 (d, $J = 12.7$ Hz, 1H), 1.82 (t, $J = 11.1$ Hz, 2H), 1.61 (m, 4H), 1.46 (m, 3H), 1.32 (m, 3H), 1.04 (m, 3H), 0.91 (brs, 2H), 0.35 (t, $J = 12.0$ Hz, 1H). ^{13}C NMR (126 MHz, C_6D_6) δ 51.4, 50.8, 38.9, 35.8, 35.5 (br), 34.5, 29.0, 28.7, 27.9, 27.5, 21.5, 14.4 (br). ^{11}B NMR (97 MHz, C_6D_6) δ 42.9 (brs). HRMS (EI+) $[\text{M}]^+$ calcd. for $\text{C}_{12}\text{H}_{22}\text{NB}$ 191.18453, found 191.18514.

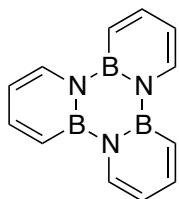
Compound A.12



Allyl homoallylamine (CAS No. 80662-96-0) (14.68 g, 132.0 mmol, 1 equiv) was combined in a pressure vessel with neat triethylamine borane complex (15.19 g, 132.0 mmol, 1 equiv) and heated to 160 °C for 18 hours. The mixture was cooled and the mixture was fractionally distilled (71 °C, 55 torr). The distillate was filtered through a plug of alumina using pentane as the eluent. Yielded a clear, colorless liquid (1.93 g, 12%). ¹H NMR (300 MHz, C₆D₆) δ 2.95 (t, *J* = 7.1 Hz, 2H), 2.73 (brs, 2H), 1.75 (p, *J* = 7.5 Hz, 2H), 1.54 (brs, 4H), 1.09 (t, *J* = 7.8 Hz, 2H), 0.97 (s, 2H). ¹³C NMR (126 MHz, C₆D₆) δ 55.3, 46.0, 27.7, 22.9, 21.6, 19.1 (br), 13.5 (br). ¹¹B NMR (96 MHz, C₆D₆) δ 45.5 (s). HRMS (DART+) [M+H]⁺ calcd. for C₇H₁₅BN 124.12975, found 124.12929.

Characterization of Dehydrogenation Products

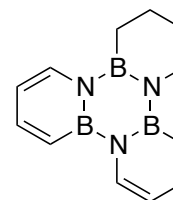
BN-Triphenylene (A.3) [CAS# 316-20-1]



BN-cyclohexane trimer **A.2** (48 mg, 0.206 mmol) was subjected to the optimized conditions with *p*-MeO(POCOP)IrHCl precatalyst (6 mol%). The reaction mixture was passed through a short plug of silica using pentane as the mobile phase. The resulting white powder was a mixture of BN-triphenylene, remaining stilbene, and bibenzyl, which are inseparable via silica gel chromatography. Bibenzyl and stilbene were sublimed away from BN triphenylene at 150 mtorr and 70 °C. The remaining solid was pure BN-Triphenylene. Significant amounts of BN-triphenylene were found in the sublimate. Yield: 25.2 mg, 52% (92% yield by NMR). NMR spectra are consistent with a previous report.¹⁶ ¹H NMR (300 MHz, C₆D₆) δ 7.95 (d, *J* = 6.9 Hz, 2H), 7.64 (dd, *J* = 11.7, 6.2 Hz, 2H), 6.94 (d, *J* = 11.7 Hz, 2H), 6.26 (t, *J* = 6.4 Hz, 2H). ¹¹B NMR (96 MHz, C₆D₆) δ 30.0 (brs).

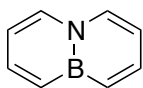
Isolation of Intermediate A.4

BN-triphenylene and the intermediate **A.4** were both isolated from an unoptimized reaction via preparatory silica TLC using pentane as the eluent. Compound collected from two bands were then re-run using the same GC method used to obtain yields. Each band thus contained a different, single peak, identical to peaks found in the original GC-FID



trace. ¹H NMR (500 MHz, C₆D₆) δ 7.99 (d, *J* = 6.4 Hz, 1H), 7.66 (m, 2H), 7.30 (d, *J* = 6.3 Hz, 1H), 7.03 (d, *J* = 11.8 Hz, 1H), 6.78 (d, *J* = 11.5 Hz, 1H), 6.25 (t, *J* = 6.5 Hz, 1H), 6.19 (t, *J* = 6.5 Hz, 1H), 3.43 (t, *J* = 5.5 Hz, 2H); 1.48 (m, 2H); 1.31 (m, 2H); 1.08 (app. t, 2H). ¹¹B NMR (97 MHz, C₆D₆) δ 35.27 (brs), 29.85 (brs). ¹³C NMR (151 MHz, C₆D₆) δ 145.9, 145.1, 135.7, 135.4, 121.9 (br), 111.1, 110.3, 46.2, 28.1, 21.8, 12.9 (br). One of the aromatic carbons adjacent to boron was not observed. HRMS (EI+) [*M*]⁺ calcd. for C₁₂H₁₆N₃B₃ 235.16234, found 235.16186.

BN-9,10-naphthalene (A.5) (CAS No. 1425-58-7)

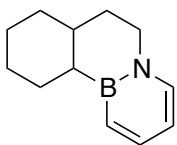


9,10-Azaboradecalin (98 mg, 0.715 mmol) was subjected to the optimized dehydrogenation conditions with *p*-MeO(POCOP)IrHCl precatalyst (6

¹⁶ Lamm, A. N. Dissertation, University of Oregon, 2012.

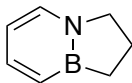
mol%). It was isolated by first running the crude starting material through a plug of silica and then by passing the mixture through a size-exclusion column on a recycling preparatory HPLC under ambient conditions with chloroform as the eluent. This is a known compound.¹⁷ ¹H NMR (300 MHz, CD₂Cl₂) δ 7.86 (d, *J* = 7.0 Hz, 2H), 7.73 (dd, *J* = 11.2, 6.4 Hz, 2H), 7.44 (d, *J* = 11.2 Hz, 2H), 6.77 (t, *J* = 6.7 Hz, 2H). Yield: 64 mg, 70% (80% NMR).

Compound A.6



The precursor (115 mg, 0.602 mmol) was subjected to the optimized dehydrogenation conditions with *p*-MeO(POCOPiHCl) precatalyst (6 mol%). It was isolated by silica gel chromatography with pentane as the mobile phase. Yield: 69 mg (61%). ¹H NMR (500 MHz, C₆D₆) δ 7.57 (dd, *J* = 11.1, 6.4 Hz, 1H), 6.99 (d, *J* = 11.0 Hz, 1H), 6.63 (d, *J* = 6.8 Hz, 1H), 6.17 – 6.08 (m, 1H), 3.40 (td, *J* = 12.6, 4.9 Hz, 1H), 3.14 (dd, *J* = 12.8, 5.2 Hz, 1H), 2.38 – 2.31 (m, 1H), 1.92 – 1.84 (m, 1H), 1.82 (dd, *J* = 8.0, 3.1 Hz, 1H), 1.60 (dd, *J* = 12.9, 2.7 Hz, 1H), 1.43 – 1.19 (m, 5H), 1.14 – 1.05 (m, 1H), 1.04 – 0.95 (m, 1H), 0.89 (dt, *J* = 13.4, 5.5 Hz, 1H). ¹³C NMR (126 MHz, C₆D₆) δ 142.3, 138.5, 110.3, 52.7, 39.2, 35.6, 34.0 (br), 33.2, 29.6, 28.8, 27.5. Aromatic carbon adjacent to boron was not observed. ¹¹B NMR (97 MHz, C₆D₆) δ 36.5 (brs). HRMS (EI+) [*M*]⁺ calcd. for C₁₂H₈NB 187.5323, found 187.15373.

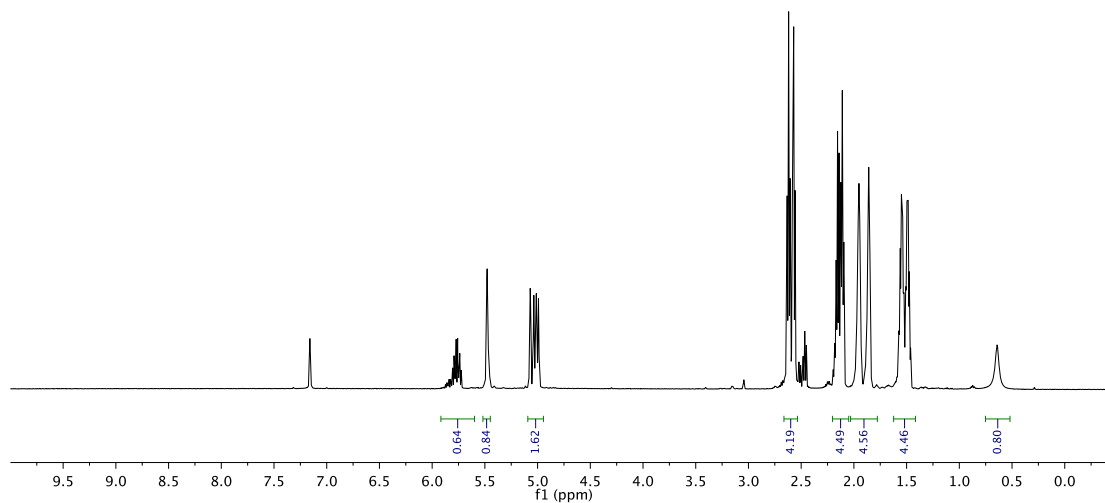
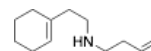
Compound A.7



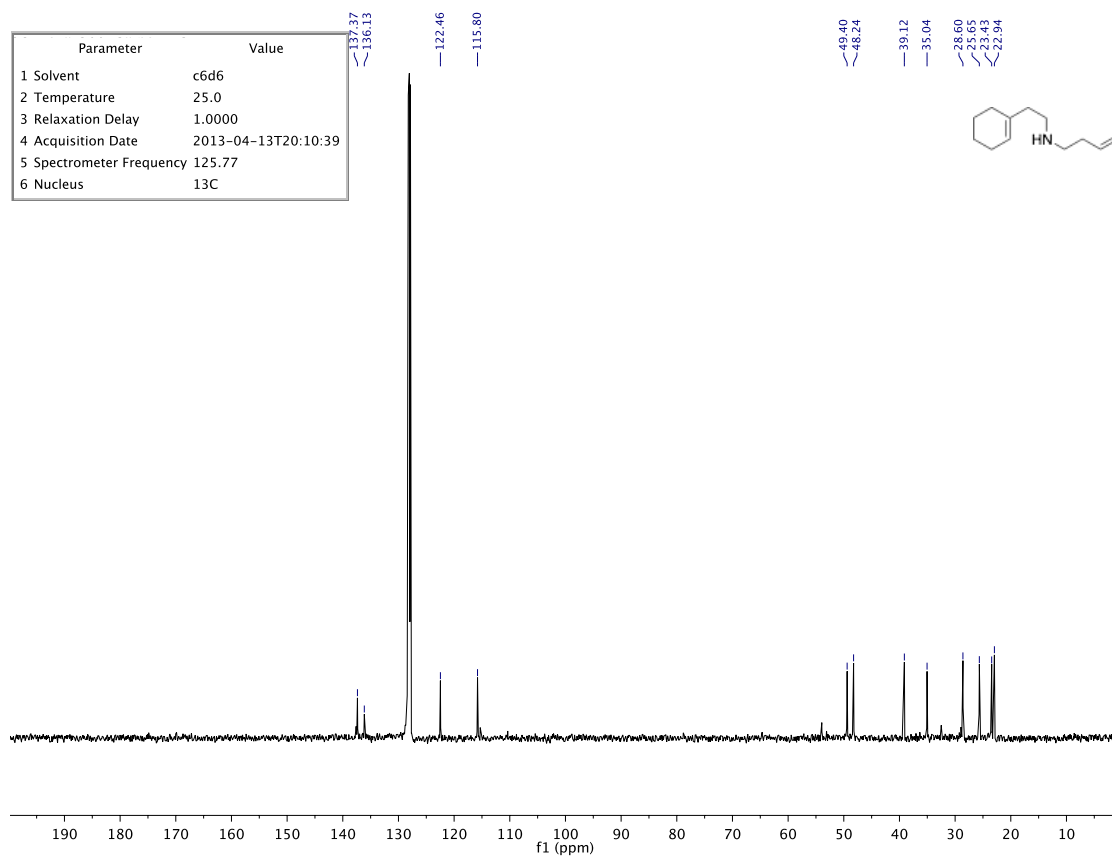
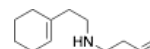
The precursor (70. mg, 0.569 mmol, 1 equiv) was subjected to the optimized dehydrogenation conditions with *p*-MeO(POCOPiHCl) precatalyst (6 mol%). The mixture was passed through an acrodisc. The product was not stable to silica gel chromatography, so hexamethylbenzene was added to assess yield by NMR (71%). The peaks associated with the product are partially obscured by the remaining bibenzyl and the stilbene acceptor. Partial list of peaks: ¹H NMR (500 MHz, CD₂Cl₂) δ 6.82 (d, *J* = 11.2 Hz, 1H), 6.36 (t, *J* = 6.7 Hz, 1H), 3.99 (td, *J* = 7.2, 2.2 Hz, 2H), 2.12 (td, *J* = 7.3, 2.2 Hz, 2H), 1.57 (td, *J* = 7.6, 2.2 Hz, 2H). ¹¹B NMR (97 MHz, CD₂Cl₂) δ 38.6 (brs).

¹⁷ Fang, X.; Yang, H.; Kampf, J. W.; Banaszak Holl, M. M.; Ashe III, A. J. *Organometallics* **2006**, 25, 513–518.

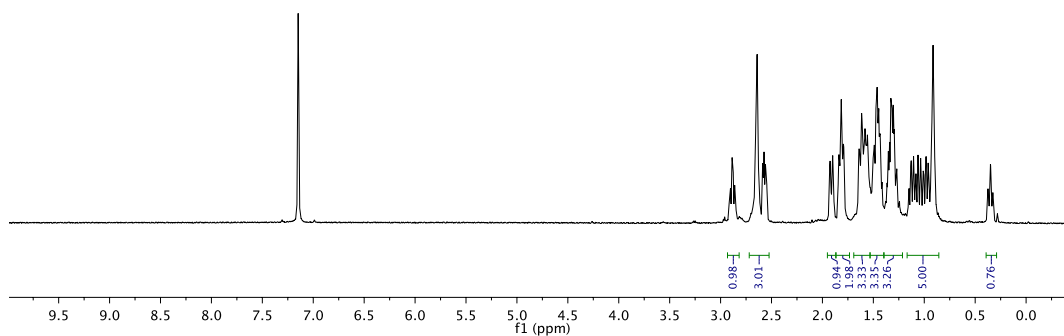
Parameter	Value
1 Solvent	c6d6
2 Temperature	25.0
3 Relaxation Delay	1.0000
4 Acquisition Date	2013-04-13T20:08:56
5 Spectrometer Frequency	500.11
6 Nucleus	¹ H



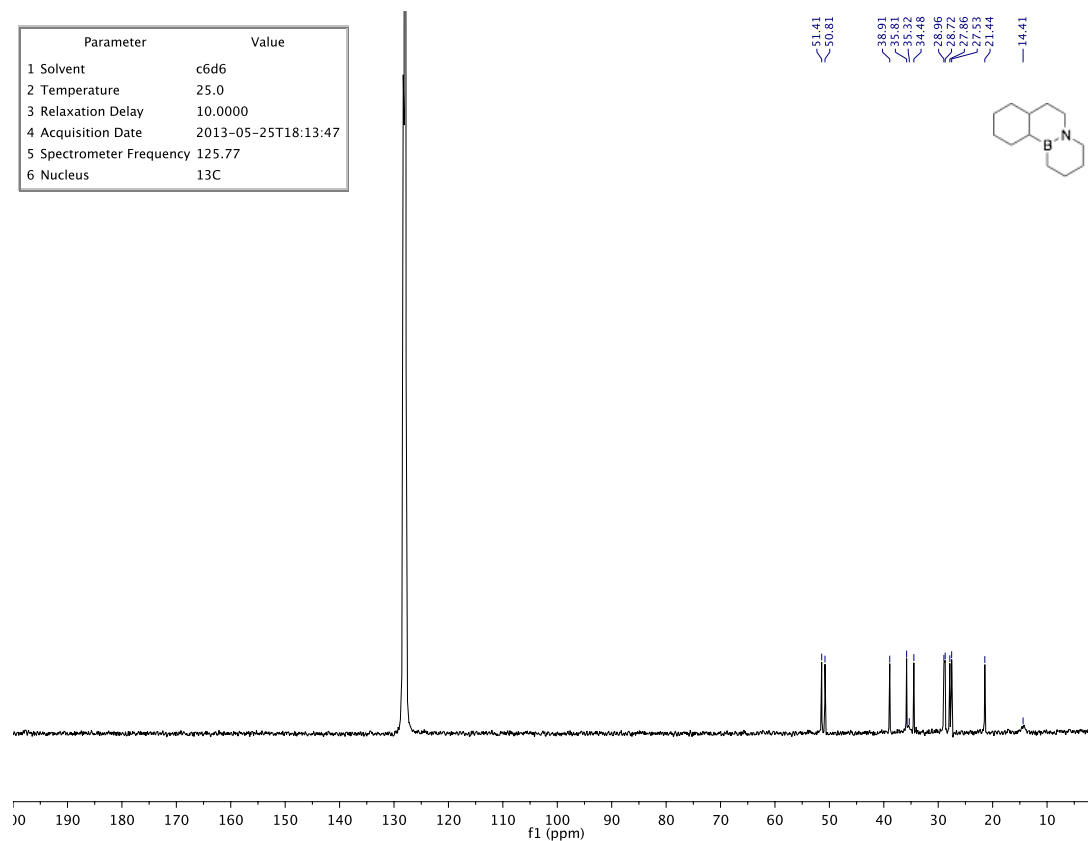
Parameter	Value
1 Solvent	c6d6
2 Temperature	25.0
3 Relaxation Delay	1.0000
4 Acquisition Date	2013-04-13T20:10:39
5 Spectrometer Frequency	125.77
6 Nucleus	¹³ C



Parameter	Value
1 Solvent	c6d6
2 Temperature	25.0
3 Relaxation Delay	5.0000
4 Acquisition Date	2013-05-25T18:13:14
5 Spectrometer Frequency	500.11
6 Nucleus	¹ H



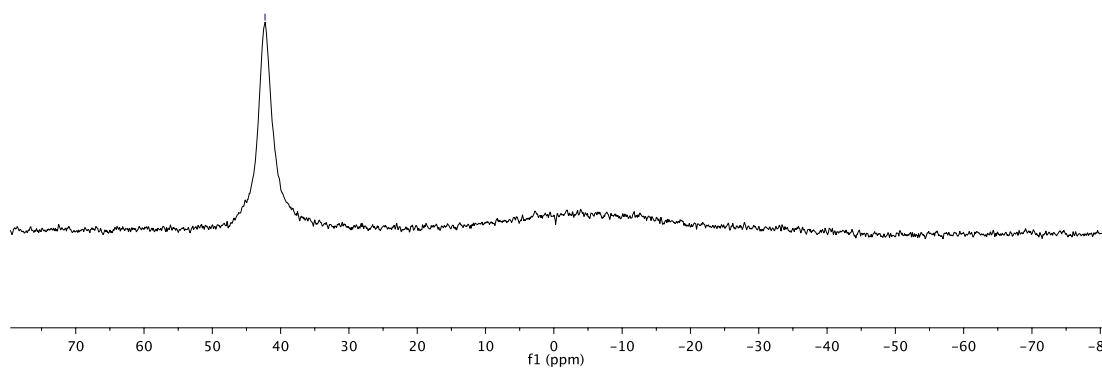
Parameter	Value
1 Solvent	c6d6
2 Temperature	25.0
3 Relaxation Delay	10.0000
4 Acquisition Date	2013-05-25T18:13:47
5 Spectrometer Frequency	125.77
6 Nucleus	¹³ C



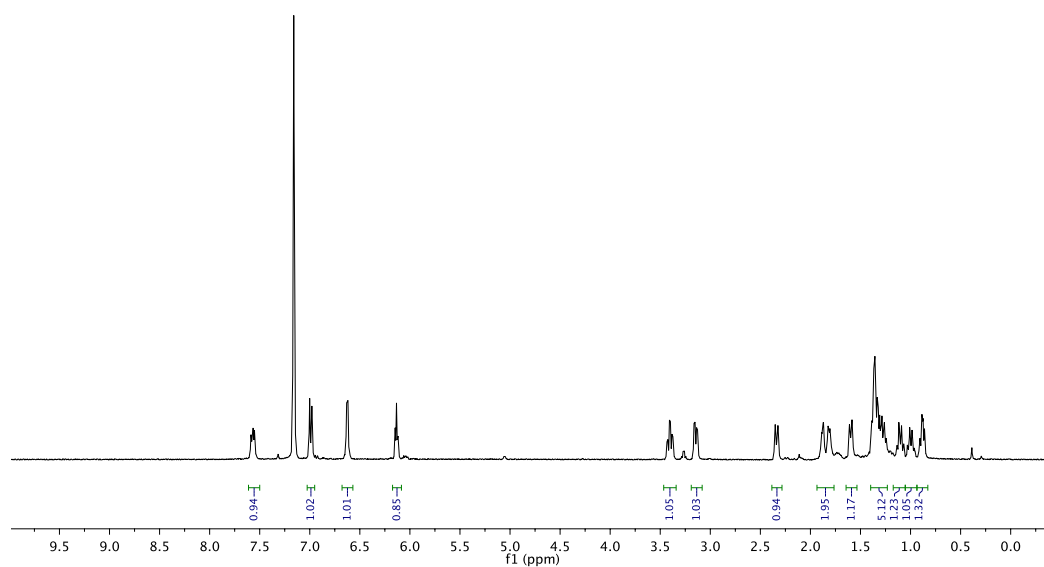


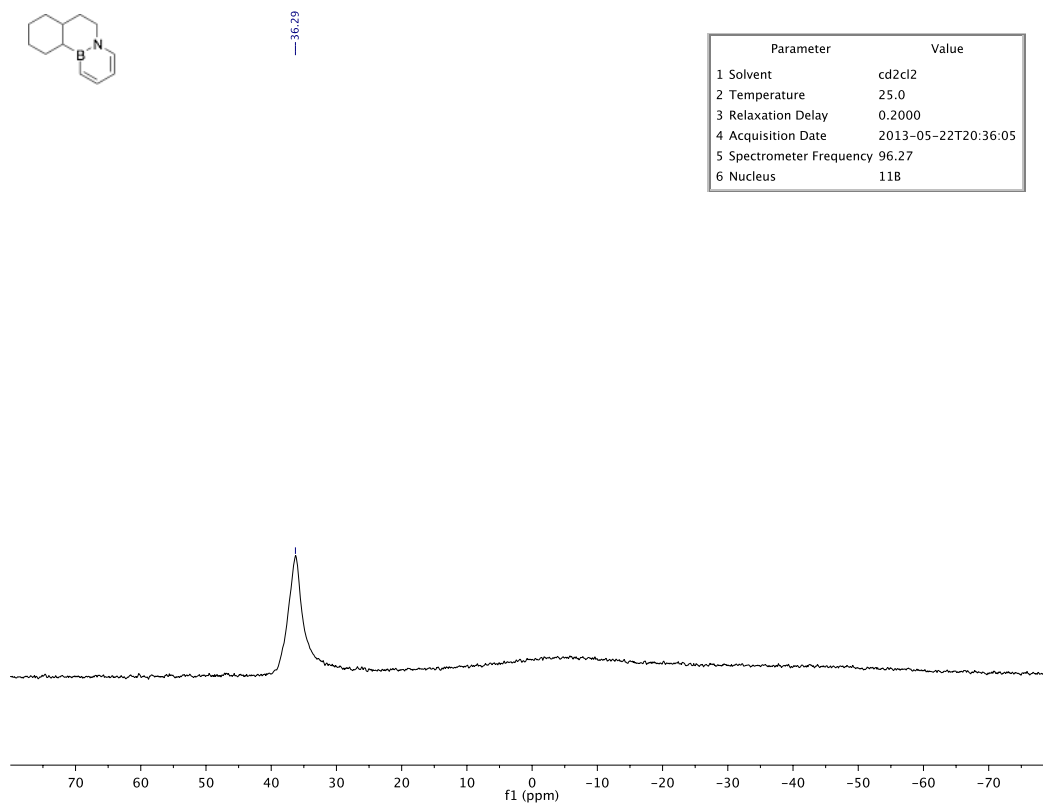
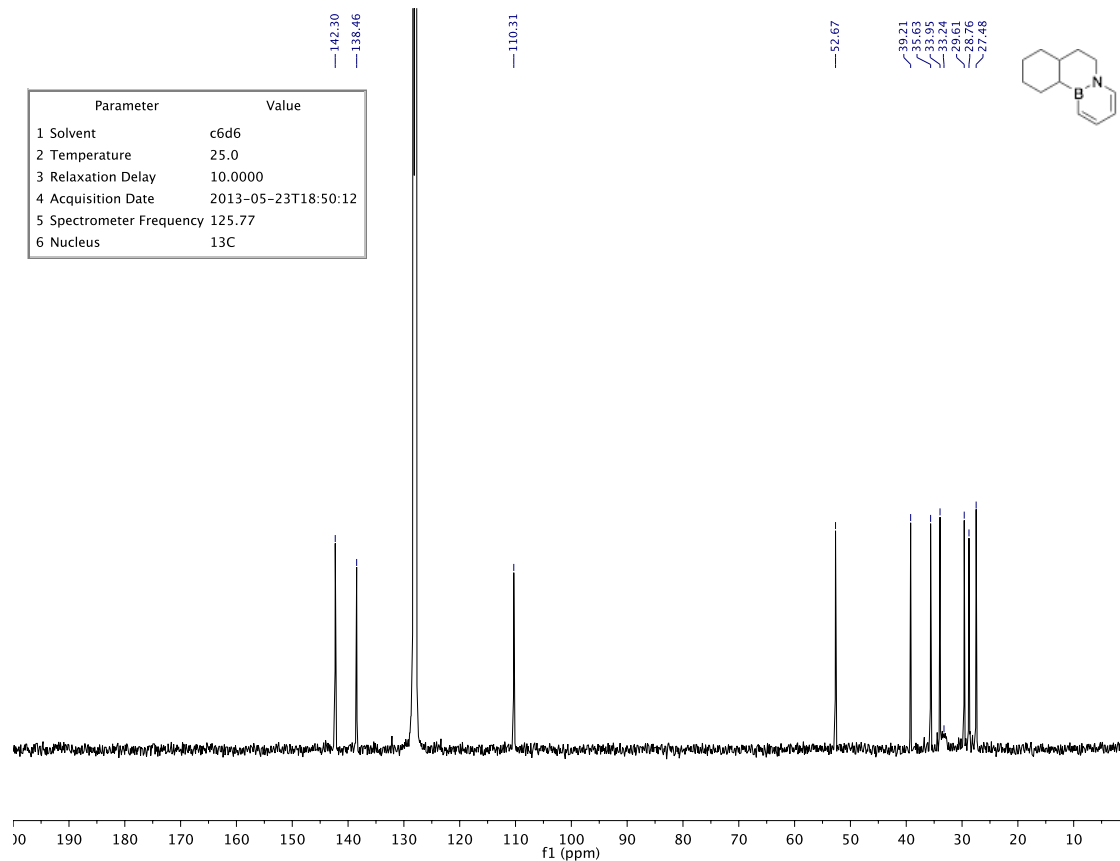
42.28

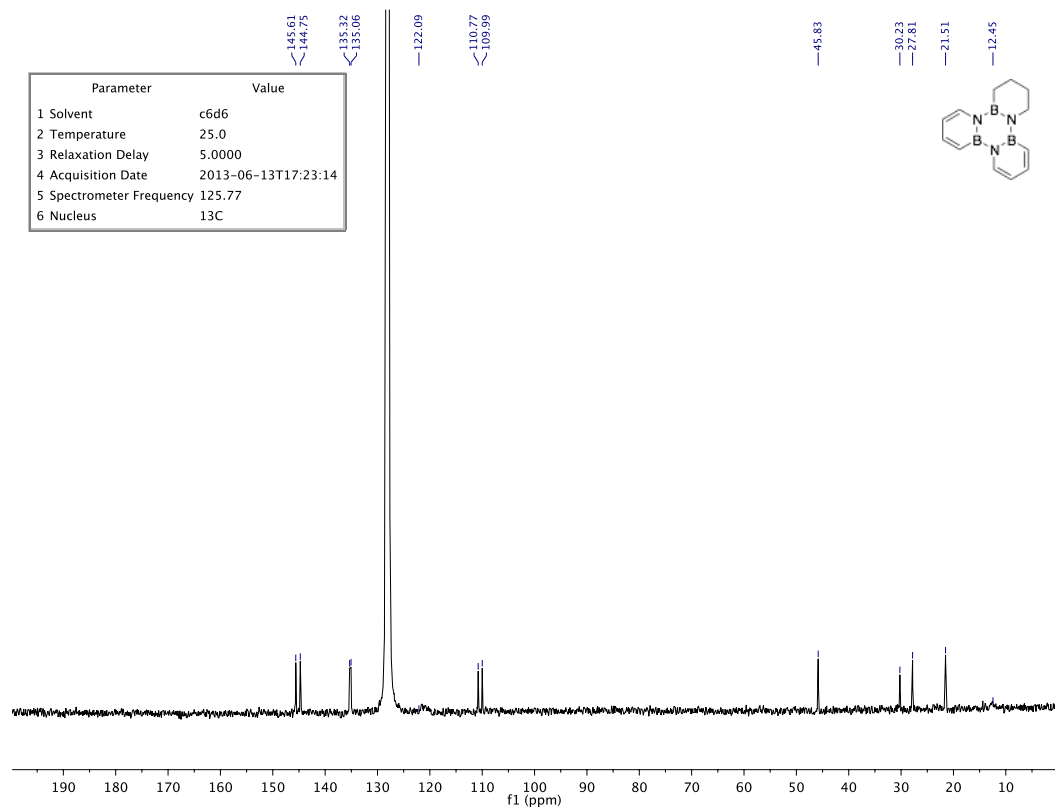
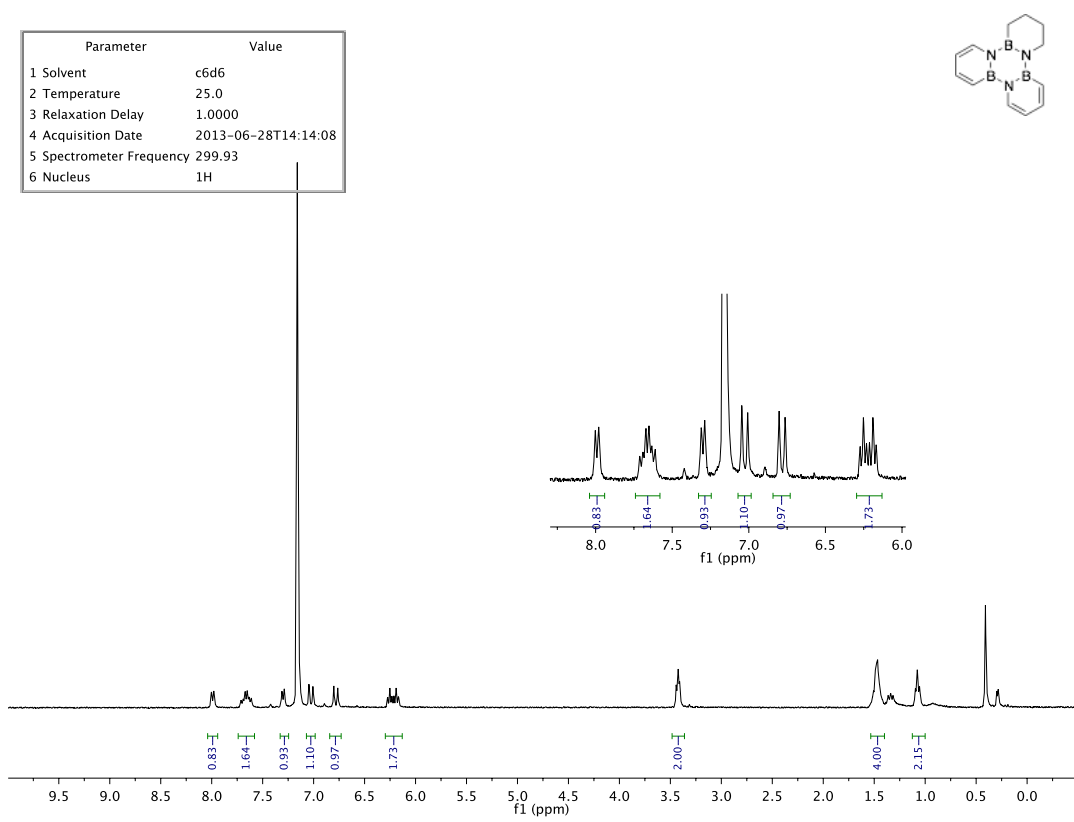
Parameter	Value
1 Solvent	c6d6
2 Temperature	25.0
3 Relaxation Delay	0.2000
4 Acquisition Date	2013-05-25T17:54:59
5 Spectrometer Frequency	96.27
6 Nucleus	11B

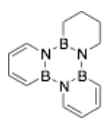


Parameter	Value
1 Solvent	c6d6
2 Temperature	25.0
3 Relaxation Delay	10.0000
4 Acquisition Date	2013-05-23T15:18:53
5 Spectrometer Frequency	500.11
6 Nucleus	1H



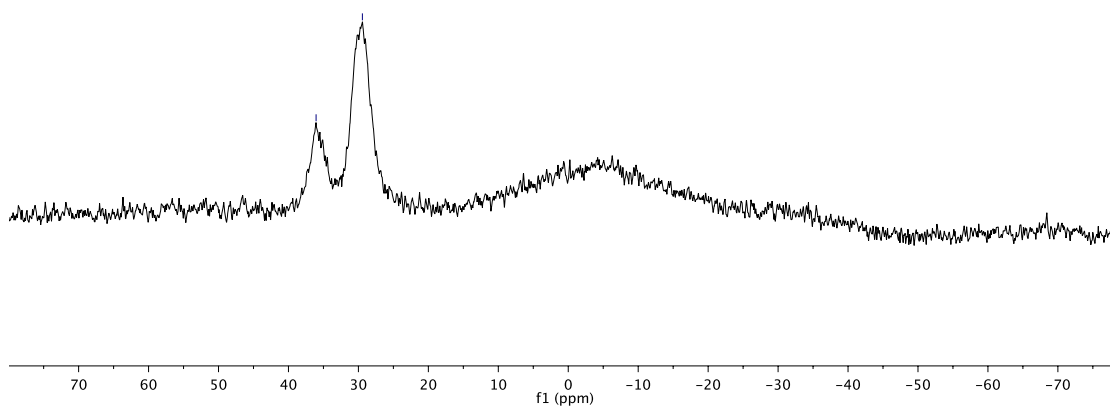




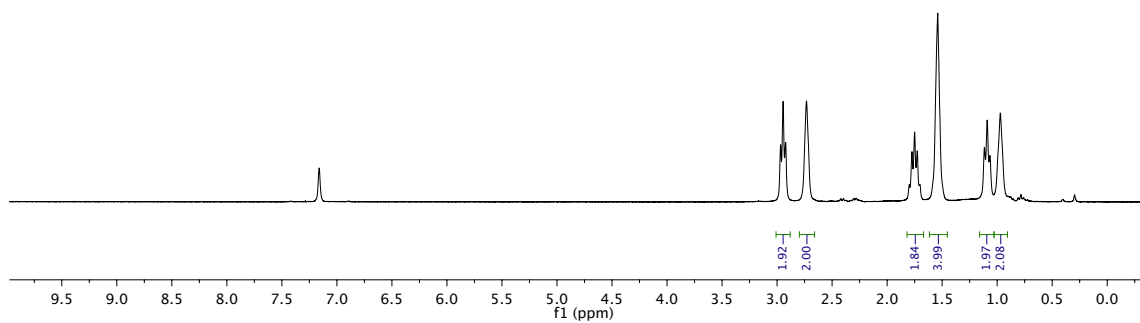


— 36.05
— 29.43

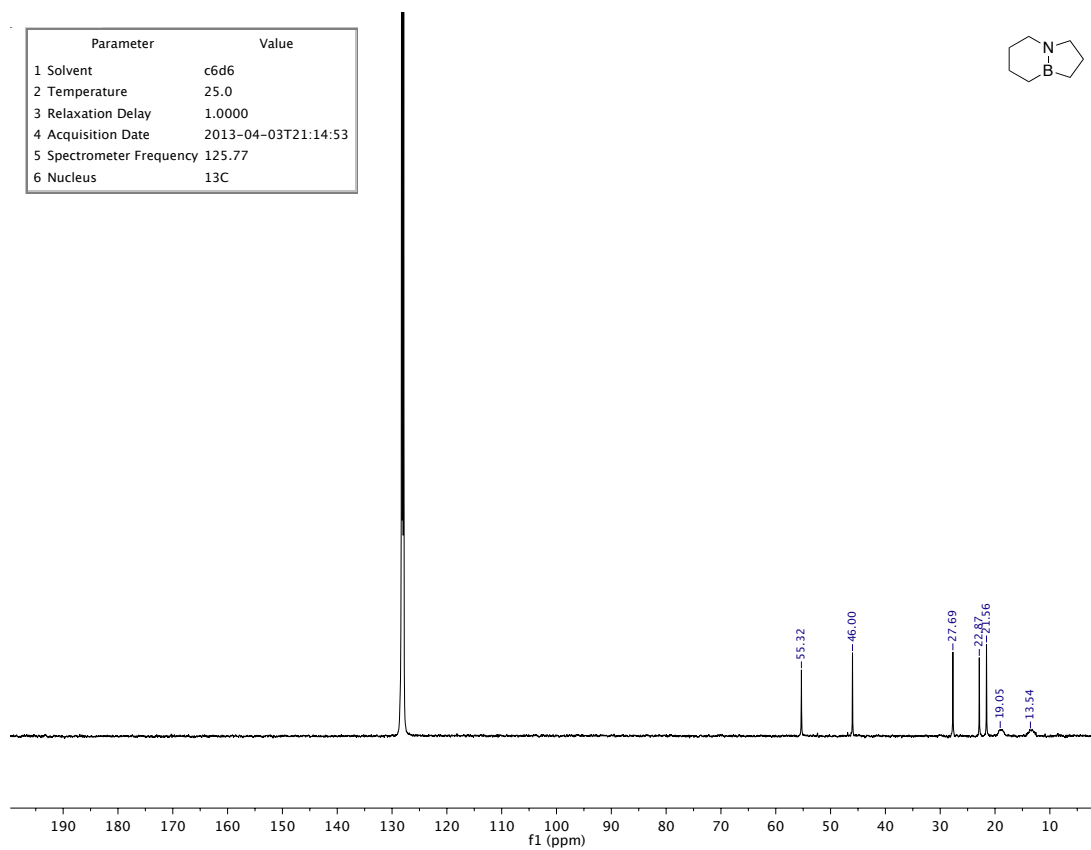
Parameter	Value
1 Solvent	c6d6
2 Temperature	25.0
3 Relaxation Delay	0.2000
4 Acquisition Date	2013-06-13T12:18:45
5 Spectrometer Frequency	96.27
6 Nucleus	11B



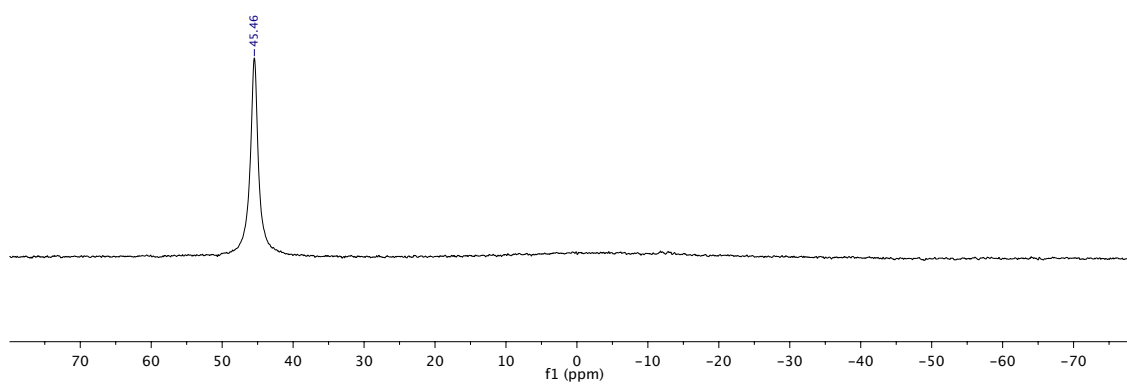
Parameter	Value
1 Solvent	c6d6
2 Temperature	25.0
3 Relaxation Delay	1.0000
4 Acquisition Date	2013-04-03T17:49:37
5 Spectrometer Frequency	300.05
6 Nucleus	1H



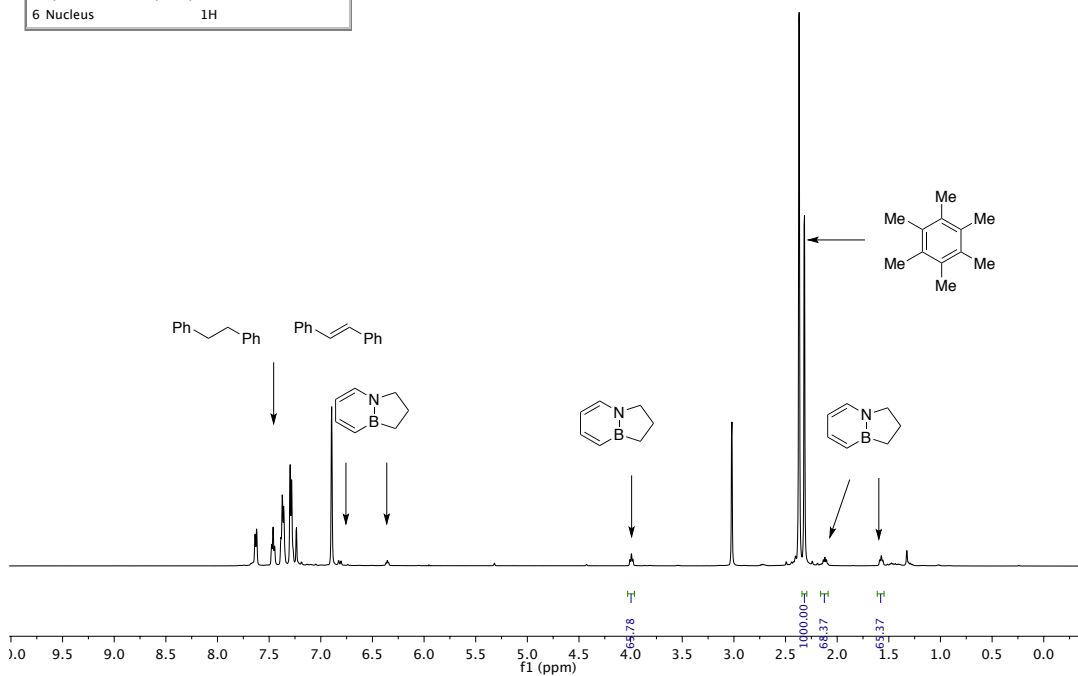
Parameter	Value
1 Solvent	c6d6
2 Temperature	25.0
3 Relaxation Delay	1.0000
4 Acquisition Date	2013-04-03T21:14:53
5 Spectrometer Frequency	125.77
6 Nucleus	¹³ C



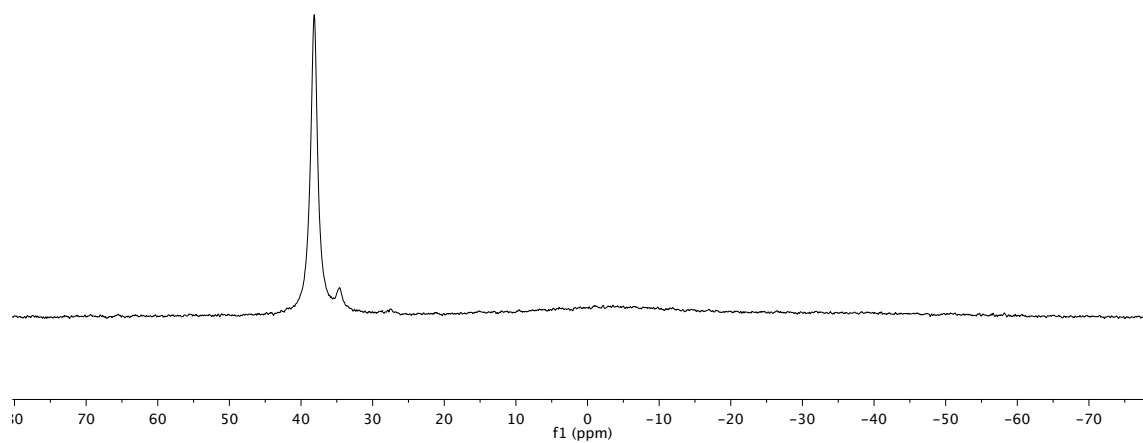
Parameter	Value
1 Solvent	c6d6
2 Temperature	25.0
3 Relaxation Delay	0.2000
4 Acquisition Date	2013-04-03T17:47:54
5 Spectrometer Frequency	96.27
6 Nucleus	11B



Parameter	Value
1 Solvent	cd2cl2
2 Temperature	25.0
3 Relaxation Delay	10.0000
4 Acquisition Date	2013-04-05T16:30:22
5 Spectrometer Frequency	500.11
6 Nucleus	1H



Parameter	Value
1 Solvent	cd2cl2
2 Temperature	25.0
3 Relaxation Delay	0.2000
4 Acquisition Date	2013-04-05T09:41:25
5 Spectrometer Frequency	96.27
6 Nucleus	11B



A.3 Introduction: Saturated BN Heterocycles for Hydrogen Storage

Hydrogen storage is among the chief challenges in adopting a hydrogen energy economy. One of the principle molecules of interest with respect to chemical hydrogen storage is ammonia borane (AB).¹⁸ Some of AB's major advantages include its thermodynamically favorable dehydrogenation ($\Delta G = -14$ kcal/mol for the first equivalent of H₂), ready availability¹⁹ and its high gravimetric hydrogen capacity (19.4 wt%).²⁰ Its major disadvantages are:

- 1) As a high-melting solid (104 °C) which decomposes upon melting, AB cannot be transported or used as a liquid without diluting with solvents; this dilution ultimately decrease its gravimetric hydrogen capacity and negates one of its advantages.
- 2) Products of AB dehydrogenation are often poorly defined and often polymeric species, making the study of AB regeneration difficult.
- 3) The hydrogen gas evolved from AB decomposition often contains volatile impurities such as ammonia or borazine that are potent proton exchange membrane (PEM) fuel cell poisons.

Synthesizing Carbon-Boron-Nitrogen (CBN) containing hydrogen carriers, we attempted to address these three points. When one C–C bond in cyclohexane is replaced by a B–N bond we obtain BN cyclohexane **J**, the melting point is of which is 62 °C.^{6a} A constitutional isomer of BN cyclohexane, 3-methyl-BN-cyclopentane **B** is actually a

¹⁸ For an overview of AB and amine borane-based hydrogen storage technologies see: (a) Staubitz, A.; Robertson, A. P. M.; Manners, I. *Chem. Rev.* **2010**, *110*, 4079–4124. (b) Hamilton, C. W.; Baker, R. T.; Staubitz, A.; Manners, I. *Chem. Soc. Rev.* **2009**, *38*, 279–293. (c) Bowden, M.; Autrey, T. *Curr. Opin. Solid State Mater. Sci.* **2011**, *15*, 73–79. (d) Huang, Z.; Autrey, T. *Energy Environ. Sci.* **2012**, *5*, 9257–9286.

¹⁹ Heldebrant, D. J.; Karkamkar, A.; Linehan, J. C.; Autrey, T. *Energy Environ. Sci.* **2008**, *1*, 156–160.

²⁰ Keaton, R. J.; Blacquiere, J. M.; Baker, R. T. *J. Am. Chem. Soc.* **2007**, *129*, 1844–1845.

liquid at room temperature.²¹ Dehydrogenation of these species always yields molecular dehydrotrimers featuring a borazine core. Furthermore, hydrogen gas evolved from these mixtures does not contain any parent borazine.²² Another advantage of CBN H₂ storage materials that we and others have observed is notable dehydrogenation rate enhancement relative to AB.²³ These promising results warrant further synthesis of cyclic amine boranes for hydrogen storage applications.

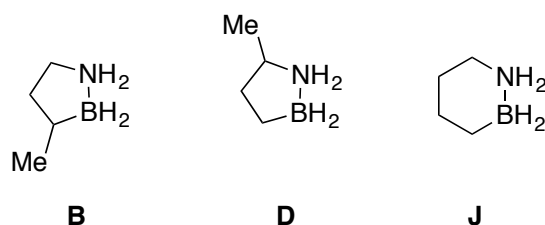


Figure A.1. Examples of Cyclic Amine Boranes

A.3.1 Synthesis of Compound D

The same overall strategy to synthesize compound **B** is applied in this case. The secondary amine is masked using a chelating *bis*-silyl protecting group, and the remaining one-pot sequence (hydroboration, hydride addition, and deprotection) furnished the desired compound after column chromatography (Scheme A.6). Compound **D** was then used by Dr. Tom Autrey's group (Pacific Northwest National Laboratory) to investigate CBN blends.²⁴

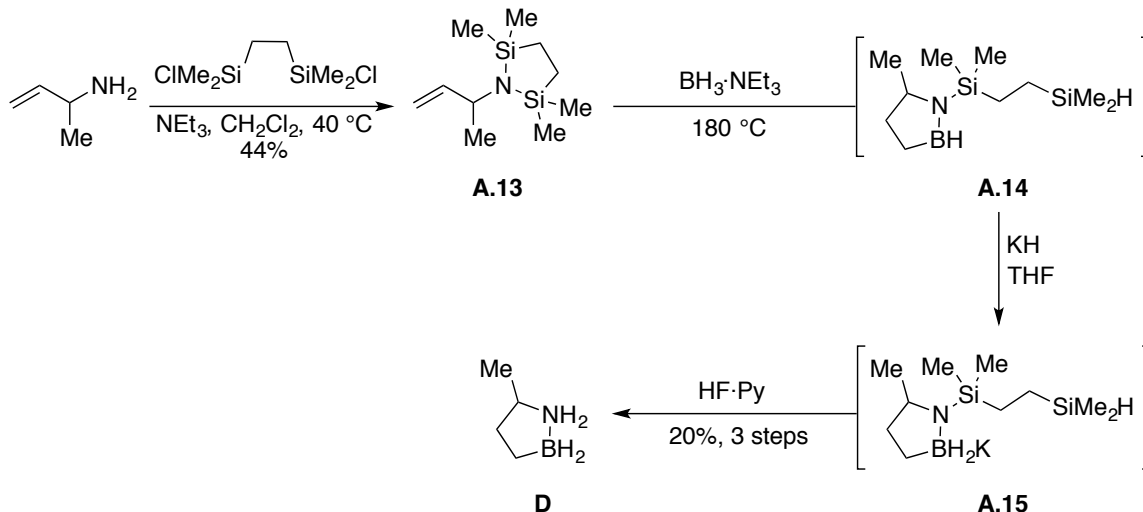
²¹ Luo, W.; Campbell, P. G.; Zakharov, L. N.; Liu, S.-Y. *J. Am. Chem. Soc.* **2011**, *133*, 19326–19329.

²² Luo, W.; Neiner, D.; Karkamkar, A.; Parab, K.; Garner, E. B., III; Dixon, D. A.; Matson, D.; Autrey, T.; Liu, S.-Y. *Dalton Trans.* **2012**, *42*, 611–614.

²³(a) Campbell, P. G.; Ishibashi, J. S. A.; Zakharov, L. N.; Liu, S.-Y. *Aust. J. Chem.* **2014**, *67*, 521–524. (b) Stubbs, N. E.; Schäfer, A.; Robertson, A. P. M.; Leitao, E. M.; Jurca, T.; Sparkes, H. A.; Woodall, C. H.; Haddow, M. F.; Manners, I. *Inorg. Chem.* **2015**, *54*, 10878–10889.

²⁴Whittemore, S. M.; Bowden, M.; Karkamkar, A.; Parab, K.; Neiner, D.; Autrey, T.; Ishibashi, J. S. A.; Chen, G.; Liu, S.-Y.; Dixon, D. A. *Dalton Trans.* **2016**, *45*, 6196–6203.

Scheme A.6 Synthesis of Compound D



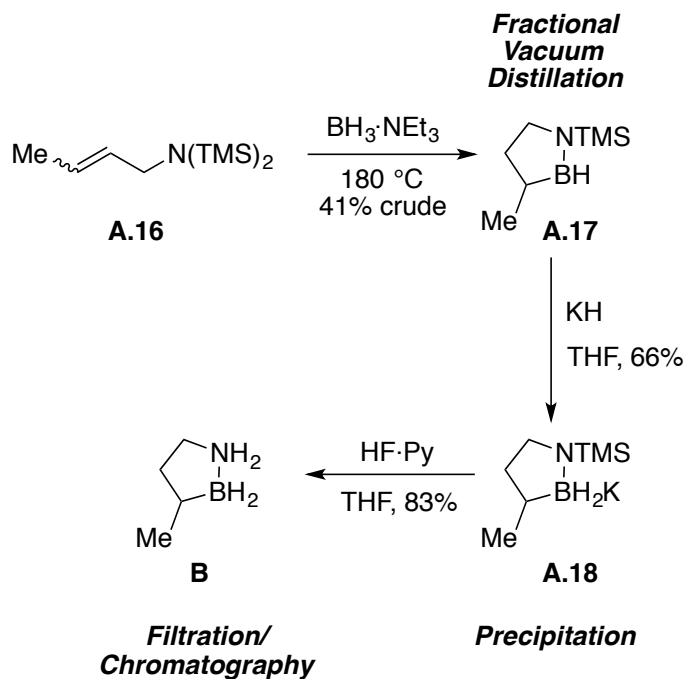
A.3.2 Synthetic Process Optimization of Compound B and Fuel Cell Testing

The next step in the development of liquid chemical hydrogen carrier **B** was the scaling of the synthesis to quantities where its hydrogen could be used in PEM fuel cell operation. This work was done in collaboration with Dr. James Sisco and Dr. Paul Osenar of Protonex Technology Corporation (Southborough, MA). When synthesizing compound **D** and small amounts of **B**, we found that the one-pot procedure from hydroboration through to the final product produced mixtures that had to be separated multiple times using column chromatography. Additionally, we found that while the allylic amine fully converted in the hydroboration reaction, the borane triethylamine did not. This was the leading factor in the need for multiple chromatographic separations. As the quantities of **B** required for testing would be large ($>40\text{ g}$ final product) and the largest amount of **B** produced in a single run was quite small ($< 1\text{ g}$), these large-scale chromatographic separations would be impractical. One-pot operations and the assumption of 100% conversion of triethylamine-borane also led to overuse of the dangerous reagents potassium hydride and hydrogen fluoride. By purifying the product

after every step, we were able to obtain the required amount of liquid carrier **B** (Scheme A.7).

The cyclization was achieved by intramolecular hydroboration of allylic amine **A.16** with triethylamine-borane complex at 180 °C. The product **A.17** was distilled away from byproduct triethylamine and residual $\text{BH}_3\cdot\text{NEt}_3$, yielding >90 g crude material (41%) at a time. Addition of potassium hydride afforded potassium salt **A.18** in 65% yield after precipitation with pentane. Finally, the liquid hydrogen carrier **B** was produced by treatment of **A.18** with hydrogen fluoride pyridine. We achieved additional purification by silica gel chromatography under ambient conditions and could obtain over 8 g of compound **B** through a single silica gel column pass.

Scheme A.7 Synthesis of Compound B at Large Scale



We used all plastic or PTFE when handling HF-pyridine. When first attempting the scale-up, we found that the use of plastic facilitated filtration of the solid byproducts than in the one-pot protocol and its use of glass vessels. Because the reaction of HF and

glass forms a gel-like substance, it became very difficult to separate the gel from the desired product at larger scale.

Large Scale Dehydrogenation of Compound B

The experimental setup for fuel cell testing is sketched in cartoon form in Figure A.2. The reaction was initiated by heating **B** with 5 mol% FeCl₂ at 80 °C. Hydrogen flow out of the reaction vessel was monitored using an airflow controller, and the gas was collected in a bag. Once the reaction was complete, the bag was sealed from the back end, and hydrogen was pushed out of the bag at a controlled rate through a cold trap and into the fuel cell stack, where the stack's performance was evaluated by monitoring its voltage throughout the run; constant voltage indicates that the stack is running normally, while a decrease in voltage indicates inhibition of the fuel cell catalyst sites, usually by Lewis basic impurities. The fuel cell stack was operated using pure hydrogen obtained by electrolysis when it was not being supplied by hydrogen generated from **B**.

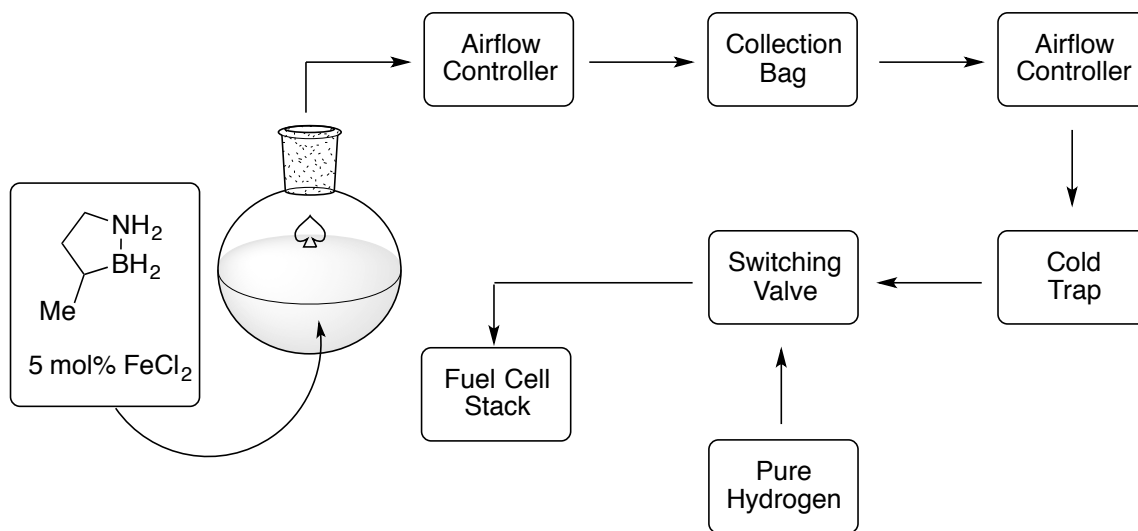


Figure A.2. Cartoon schematic of the Protonex fuel cell testing apparatus

Neat liquid **B** can release two molar equivalents of hydrogen at 80 °C with FeCl₂ as the precatalyst. The largest reaction we reported previously was a 10 mmol (850 mg)

reaction that released 20 mmol hydrogen (< 0.5 L at standard temperature and pressure). We wanted to confirm reaction completion at a larger volume, so we continuously measured the flow rate out of the reactor and into the bag and integrated for total output of hydrogen. For a 5 g reaction, we could reproducibly obtain close to the ideal (2.11 L for 5.00 g) amount of hydrogen (Figure A.3).

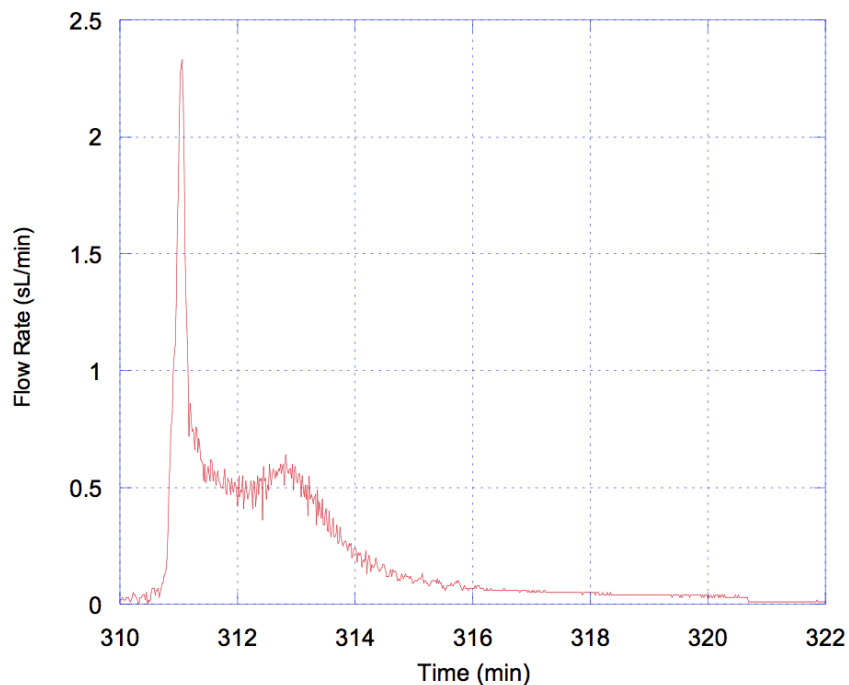
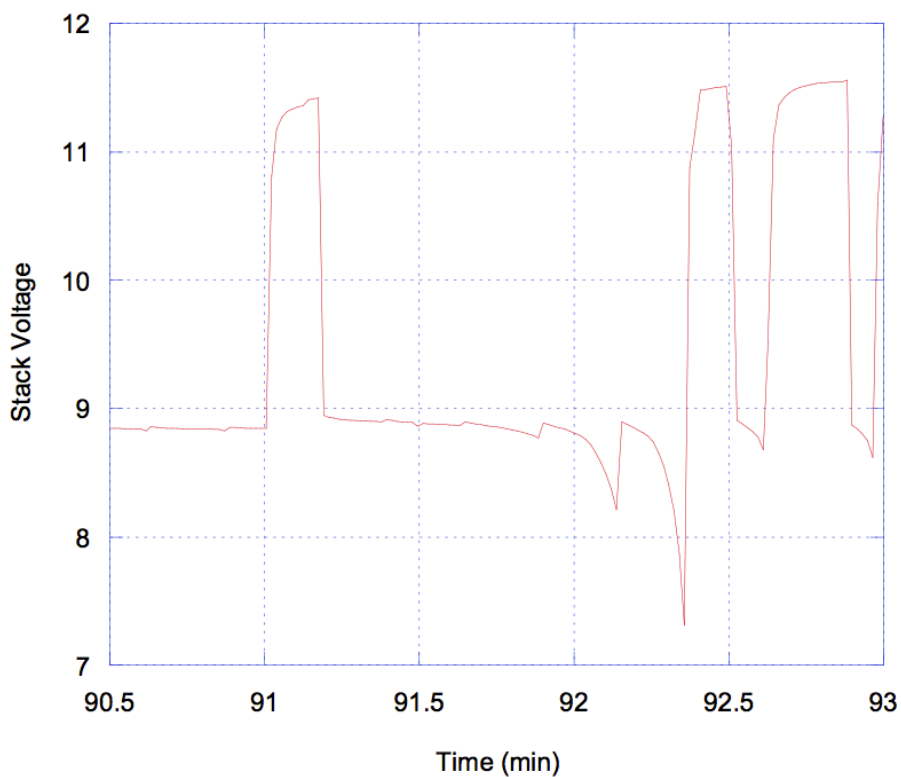


Figure A.3: Hydrogen release flow rate vs. time for a 5 g run. Time was recorded on a running scale.

Compound **B** released the majority of its hydrogen within 2–3 minutes, and the peak release rate also occurred in this time period. These results are consistent with our previous, small-scale results as measured by automated gas burette.²¹ Depending on the run and the variability in measuring exactly 5 grams, we measured 2.1–2.5 L hydrogen evolved in each of three runs.

Fuel Cell Operation

With minimal impurities in the gas stream generated from **1** detected by previous residual gas analysis studies,²² we set out to run a hydrogen fuel cell stack without the filters that are often necessary for fuel cell operation; common impurities generated by AB dehydrogenation, including ammonia and borazine, are potent fuel cell poisons.²⁵ Unfortunately, an unfettered stream of hydrogen produced from **B** rapidly eroded the performance of the fuel cell stack as evidenced by the precipitous drop in stack voltage at constant current (Figure A.4); this indicated that some coordinating impurities were contained within the stream. Jumps in stack voltage (i.e., ~11.5 V at the 91 minute mark in Figure A.4) are the open-circuit voltage of the load bank and are caused by switching the stack load off while changing the hydrogen source.



²⁵ Hügle, T.; Hartl, M.; Lentz, D. *Chem. Eur. J.* **2011**, *17*, 10184–10207.

Figure A.4. Fuel cell stack performance using an unfettered stream of hydrogen produced from the dehydrogenation of **B**.

We then employed the use of an activated carbon trap and a dry-ice/methanol trap to condense any volatiles that might have interfered with stack operation. To our delight, we were able to achieve stable operation of the stack for as long as hydrogen was supplied. Our longest continuous operation has been 7 minutes, the result of 7.6 L hydrogen produced (Figure A.5). To date, a total of approximately 23 minutes of successful fuel cell operation has been achieved on the fuel cell stack at varying power levels using the test configuration described above.

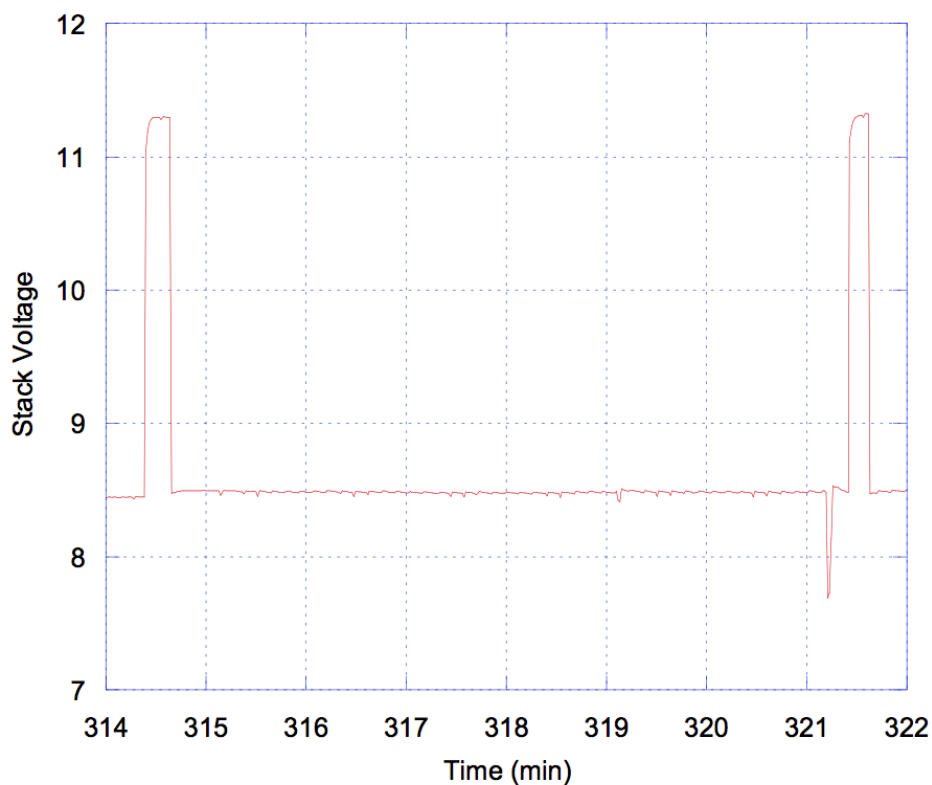


Figure A.5. Stack voltage vs. time using hydrogen from **B** protected by a carbon filter and a dry ice/methanol trap. Note the drop in stack voltage after 321 minutes is due to the depletion of the hydrogen generated from **B**

Identifying Impurities in the Hydrogen Stream

By using the cold trap, we were able to concurrently purify the hydrogen stream to give much better stack performance when using hydrogen generated from **B** and also investigate the identity of the impurity. We determined by ^1H NMR spectroscopy that the only species present in the trap was tetrahydrofuran, a coordinating solvent used in the synthesis of **1**. We observed no boron-containing species by ^{11}B NMR. We attribute the decrease in stack performance with an unfettered hydrogen stream to be caused mostly by the THF.

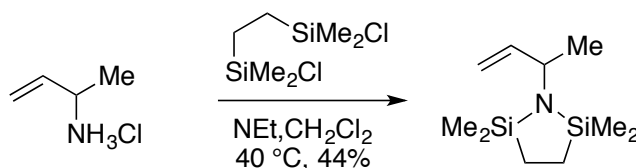
A.2.3 Experimental Section

General Considerations

All oxygen- and moisture-sensitive manipulations were carried out under an inert atmosphere using either standard Schlenk techniques or a glove box unless stated otherwise. THF, Et_2O , CH_2Cl_2 and pentane were purified by passing through a neutral alumina column under argon. Potassium hydride was washed with pentane three times and pumped dry under vacuum prior to use. All other chemicals were purchased (Aldrich, Strem or TCI) and used as received. The synthesis of compound **B** is known,²¹ and these experimental details report an optimized, large-scale synthesis using the same route. ^{11}B NMR spectra were recorded on a Varian Unity/Inova 300 or 600 spectrometer at ambient temperature. ^1H NMR spectra were recorded at the University of Oregon on a Varian Unity/Inova 300 spectrometer. ^{13}C NMR spectra were recorded on a Varian Unity/Inova 500 spectrometer. ^{11}B NMR spectra were externally referenced to $\text{BF}_3\cdot\text{Et}_2\text{O}$ ($\delta=0$). High Resolution Mass Spectrometry was performed using the electron impact method at the Mass Spectrometry Core at Oregon State University. Fuel cell testing was carried out at Protonex Technology Corporation, Southborough, MA, USA.

Synthetic Details

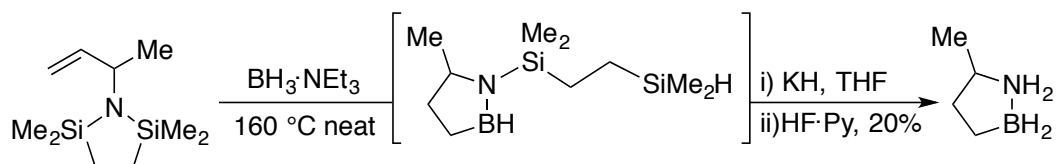
Bis-Silylamine (A.13)



In a glovebox, 3-amino-1-butene hydrochloride²⁶ (8.00 g, 74.3 mmol, 1.05 equiv) was suspended in methylene chloride and cooled to −30 °C. Triethylamine (22.57 g, 223 mmol, 3.15 equiv) was added slowly along with 1,2-bis(dimethylchlorosilyl)ethane (15.24 g, 70.8 mmol, 1 equiv). The reaction was warmed to room temperature over 1 hour then refluxed at 40 °C for 18 hours. The reaction was cooled to room temperature, and the solvent was removed using a rotary evaporator. Dry ether was added to extract the product. The solids were filtered off, and the solvent was removed using a rotary evaporator. Crude ¹H NMR showed a 5:1 ratio of product to unreacted silyl chloride. Fractionally distilled under vacuum (35 °C, 250 mTorr) to yield 6.89 g (44%) of a clear, colorless liquid. ¹H NMR (300 MHz, C₆D₆) δ 5.88 (ddd, *J* = 17.2, 10.2, 5.9 Hz, 1H), 4.94 (dt, *J* = 26.4, 1.6 Hz, 1H), 4.89 (dt, *J* = 19.4, 1.6 Hz, 1H), 3.60 (ddt, *J* = 7.3, 6.1, 1.5 Hz, 1H), 1.19 (d, *J* = 6.8 Hz, 3H), 0.84 – 0.67 (m, 4H), 0.14 (d, *J* = 2.8 Hz, 12H). ¹³C NMR (75 MHz, C₆D₆) δ 145.7, 110.0, 51.6, 24.1, 8.8, 1.8, 1.5. HRMS (EI+) [*M*]⁺ calcd. for C₁₀H₂₃NSi₂ 214.13648, found 214.13697.

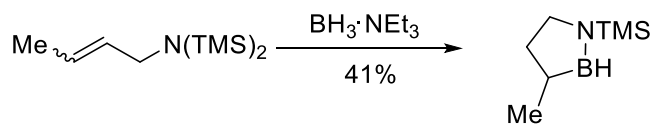
²⁶ The secondary amine was synthesized by the Gabriel synthesis (3-chloro-1-butene and potassium phthalimide). The exact freebased amine has been synthesized before: King, R. B.; Borodinsky, L. *Tetrahedron* **1985**, *41*, 3235–3240. A more detailed procedure: Roberts, J. D.; Mazur, R. H. *J. Am. Chem. Soc.* **1951**, *73*, 2509–2520. The amine was isolated as the hydrochloride salt by bubbling anhydrous HCl through an ethanol solution of the freebased amine, then removing the ethanol. This was to ensure an anhydrous environment for future reactions.

Compound D



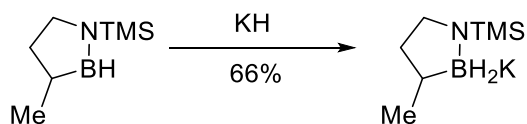
In a glovebox, bis-silylamine **A.13** (4.887 g, 22.9 mmol, 1 equiv) was mixed with neat borane-triethylamine (5.802 g, 50.4 mmol, 2.2 equiv) in a pressure vessel. The vessel was sealed and heated to $180\text{ }^\circ\text{C}$ for 18 hours. Upon cooling, the reaction mixture was brought into the glovebox, and THF (100 mL) was added followed by careful addition of potassium hydride. This was stirred for 18 hours, and the mixture was filtered through a fritted funnel. The filtrate was treated with HF-pyridine (2M HF in THF, 22.9 mL 48.8 mmol, 2 equiv) *via* dropwise addition and stirred for two hours, keeping the temperature at or below room temperature through the course of the reaction to avoid thermally-induced dehydrogenation of the product. The solvent was removed using a rotary evaporator, and the residue extracted with ether. This mixture was filtered through a Whatman #5 filter paper to remove the potassium fluoride byproduct. Pure product was obtained by silica gel flash chromatography (35% v/v ether in pentane) in the air. Yield: 403 mg, 20% of an off-white solid mp $35\text{--}37\text{ }^\circ\text{C}$. ^1H NMR (300 MHz, C_6D_6) δ 3.12–2.48 (m, 2H), 2.37 (h, $J = 7.2\text{ Hz}$, 2H), 2.02 (brs, 1H), 1.72 (brs, 1H), 1.25–0.98 (m, 3H), 0.51 (d, $J = 6.4\text{ Hz}$, 3H). ^{13}C NMR (126 MHz, C_6D_6) δ 55.1, 34.7, 19.7, 12.8 (br). ^{11}B NMR (96 MHz, C_6D_6) δ -11.7 (t, $J = 97.6\text{ Hz}$). HRMS (EI+) $[\text{M}-\text{H}]^+$ calcd. for $\text{C}_4\text{H}_{11}\text{NB}$ 84.098455, found 84.098367.

Cyclized Product (A.17)



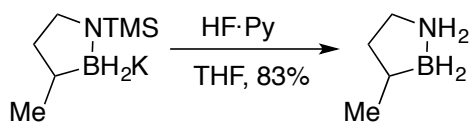
Six batches of 209 mmol crotyl hexamethyldisilazane were executed at the same time. Crotyl hexamethyldisilazane (45 g, 209 mmol) and borane-triethylamine complex (27 g, 230 mmol, 1.1 equiv.) were added neat into a 300 mL pressure vessel. The pressure vessels were sealed with Viton o-rings and heated to 160 °C for 14 hours. CAUTION: reaction evolves volatiles triethylamine and trimethylsilane. Pressure vessel seals may break later on in the reaction, but this is of little consequence to the outcome of the reaction. Using PTFE seals may mitigate the loss of pressure. Do not attempt at normal pressure (with a reflux condenser), as the hot NEt₃ and TMS-H may dissolve vacuum grease. The batches were combined, and the product was fractionally distilled using attenuated vacuum (53 torr). Three fractions may be collected. The first was largely triethylamine (30–35 °C). The second fraction was largely the product (65 °C), yielding 80.6 g (520 mmol, 41% crude). The second fraction, though it contains very small amounts of triethylamine and borane-triethylamine complex, may be carried on to the next step because the purification there will eliminate those impurities. ¹H NMR (300 MHz, C₆D₆) 3.08 (m, 2H), 1.96 (m, 1H), 1.36 (m, 2H), 0.15 (s, 9H). B–H proton not observed. ¹¹B NMR (96 MHz, C₆D₆) δ 48.25 (d, *J* = 128.5 Hz).

Potassium salt (A.18)



Potassium hydride (17.7 g, 441 mmol., 1.1 equiv.) was added in ~5 g portions to the distillate from the last step (62.2 g, 400 mmol.) in THF in the drybox at room temperature. CAUTION: while adding KH slowly, stir the reaction, as it evolves heat. The reaction was stirred for 14 hours under inert atmosphere. The solids were filtered off in the drybox, and the solvent was removed *via* high-vacuum with slight heat (30 °C). Remaining volatiles, which may include residual THF, triethylamine, and borane-triethylamine, can be removed with the high-vacuum and more applied heat (70 °C). The tacky white residue was rinsed with a minimal amount of pentane in the drybox, and the remaining white solid, now a powder, was collected. The filtrate was evaporated, and the residue was washed with even less pentane to collect more product. Combining the collected solids yielded 51.2 g (262 mmol, 66%) of the white powder. ¹H NMR (300 MHz, C₆D₆) δ 2.92 (m, 2H), 1.95 (m, 1H), 1.43 (m, 2H), 1.21 (app. d 4H), 0.21 (s, 9H) BH₂ protons not observed. ¹³C NMR (151 MHz, C₆D₆) δ 43.7, 40.0, 25.2 (br.), 22.1, 0.4. ¹¹B NMR (96 MHz, C₆D₆) δ -8.1 (t, *J* = 79.6 Hz). CAUTION: Quench excess KH carefully with cold isopropanol and ice-water and keep liquid N₂ on hand to quell any flames.

3-Methyl-BN-cyclopentane (B)



The potassium salt (24.0 g, 123 mmol) was taken into 200 mL THF and cooled to $-78\text{ }^{\circ}\text{C}$ in a plastic vessel. Hydrogen fluoride pyridine (7.03 g, 245 mmol of ca. 70 wt.% HF, 2 equiv.) diluted with 100 mL THF was added slowly *via* Teflon tubing cannula from another plastic vessel. WARNING: Hydrogen fluoride is corrosive and toxic. Take extra care with addition, since it has been dissolved in polar aprotic solvent. Keep calcium gluconate HF treatment on hand. Care must be taken to make sure the mixing is constant throughout the course of the addition. The reaction was left to warm slowly to room temperature. Once at room temperature, the reaction was stirred for 2 hours. The solids were removed in the air by passing the reaction mixture through a plug of celite, and the solvent was removed *via* rotary evaporator. Care must be taken to apply as little heat as possible. The bath may be maintained at $\sim 35\text{ }^{\circ}\text{C}$ for the duration of the solvent removal. Residual solvent was removed with a high-vacuum at room temperature. The residue was purified using silica gel chromatography (gradient from 10% v/v THF in hexane as the mobile phase) in the air. Products may be visualized on TLC using a phosphomolybdic acid stain and slight heat. Yield: 8.70 g, 83%. ^1H NMR (300 MHz, C_6D_6) 1.75, (br m, 2H), 1.60 (br m, 1H), 1.38 (br s, 3H), 1.04 (br m, 1H). ^{11}B NMR (96 MHz, C_6D_6) δ -9 (t, $J = 99.8\text{ Hz}$).

Fuel Cell and Test Setup Details

A Protonex 12 cell, 9.5 cm² active area PEM fuel cell stack (“Tweety”) was selected for the test setup; the stack provided a capability to produce approximately 30 W of power (8.5 V at 4 A) at a 0.3 sLpm hydrogen consumption rate under steady state conditions.

The hydrogen evolved through the dehydrogenation reaction was collected in the hydrogen storage subsystem that consisted of the hydrogen storage assembly, a regulated nitrogen supply system, and a flow meter to continuously measure the hydrogen generation rate. The hydrogen storage assembly consisted of a custom formed plastic bag contained within a clear PVC pressure vessel. Hydrogen generated through the dehydrogenation reaction was collected within the bag providing 10 sL of total collection capacity. Upon completion of the reaction the bag was pressurized externally with nitrogen to about 8 psig to enable delivery to the fuel cell. The hydrogen storage system was also connected to the facility hydrogen supply to enable filling of the hydrogen storage assembly for functionality checks and back-filling of the hydrogen generation subsystem during test operations (more detail in following subsection).

The reactant flow control and conditioning system consisted of air and hydrogen supply systems. The air supply system was tied into the facility compressed air supply and included an air flow controller to regulate air flow rate to the cathode. A Nafion-based moisture exchange humidifier was used to provide a passive means to humidify the dry air supply. A refrigerated bath was employed to pump deionized water through one side of the humidifier at 60 °C, while room temperature, dry air was passed through the opposing side. As a result of the water vapor partial pressure gradient created within the humidifier, the air left the humidifier for the fuel cell at approximately 60 °C and 100% relative humidity.

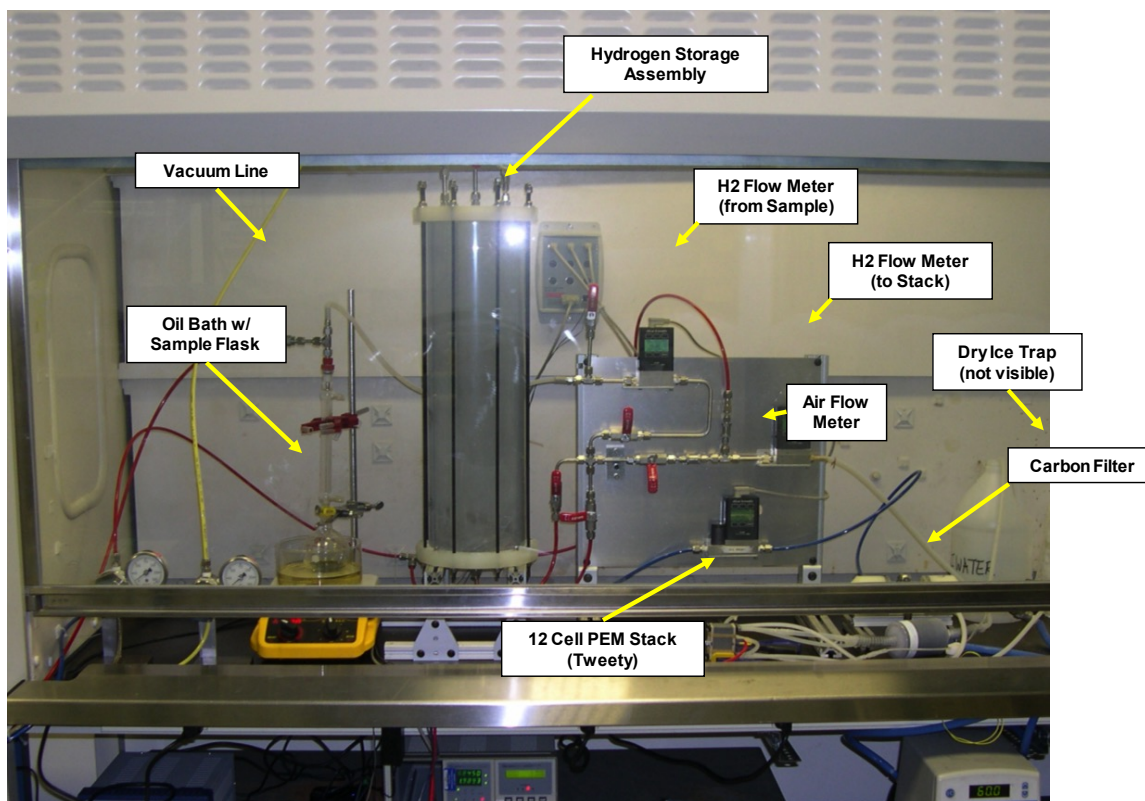
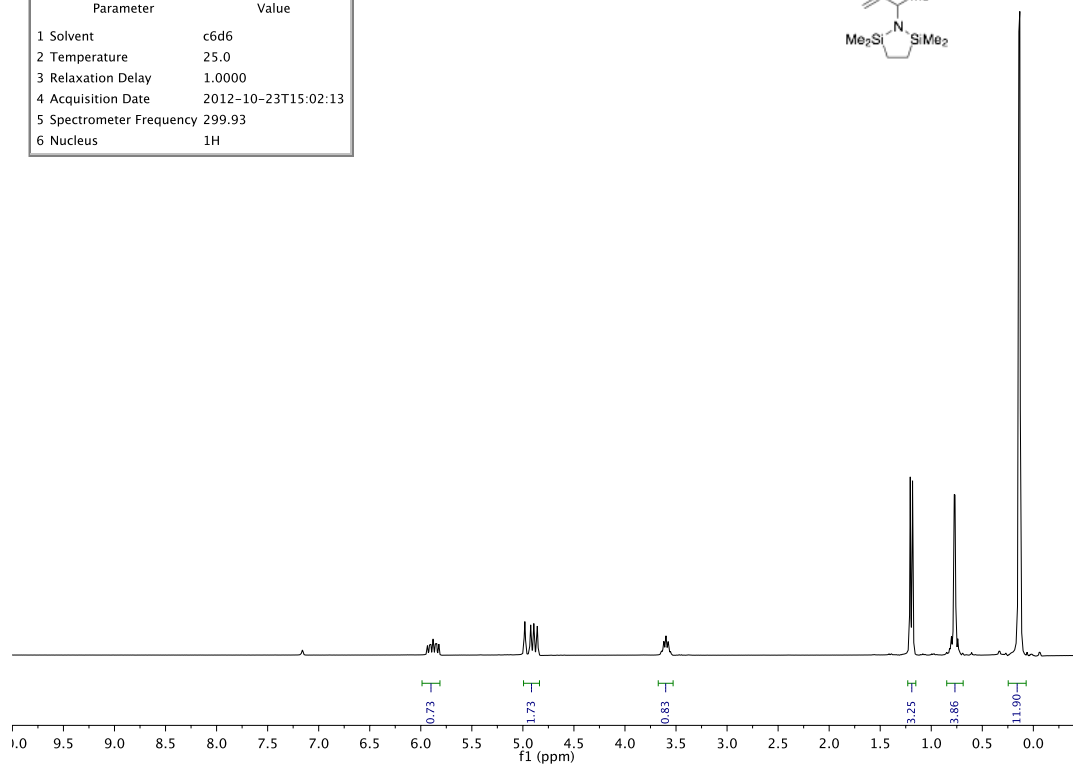
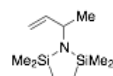


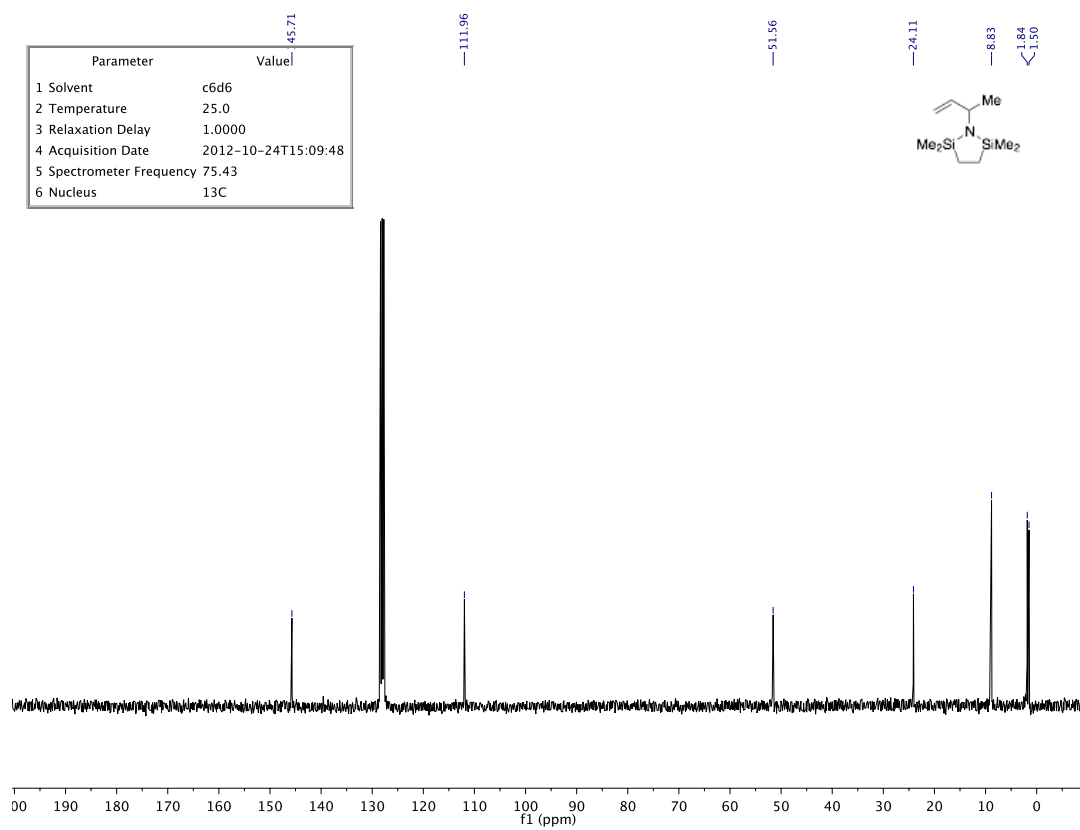
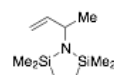
Figure A.5: Photo of fuel cell feed assembly

The air and hydrogen streams were fed to the cathode and anode sides respectively of the fuel cell stack. The airflow stream was configured to flow continuously through the stack and its outlet side was fed to a small, open-topped plastic container. The container enabled the collection of water that was produced through electrochemical reactions within the stack and then carried out in the air stream. The hydrogen flow through the stack was controlled via a small solenoid actuated pinch valve positioned downstream of the stack. The valve was opened only for a brief period of time (about 250 ms) at regular intervals (about 10 s) to allow a burst of hydrogen flow through the stack. This so-called dead-headed operational scheme provided a means to clear water produced through electrochemical reactions from the anode side of the fuel cell.

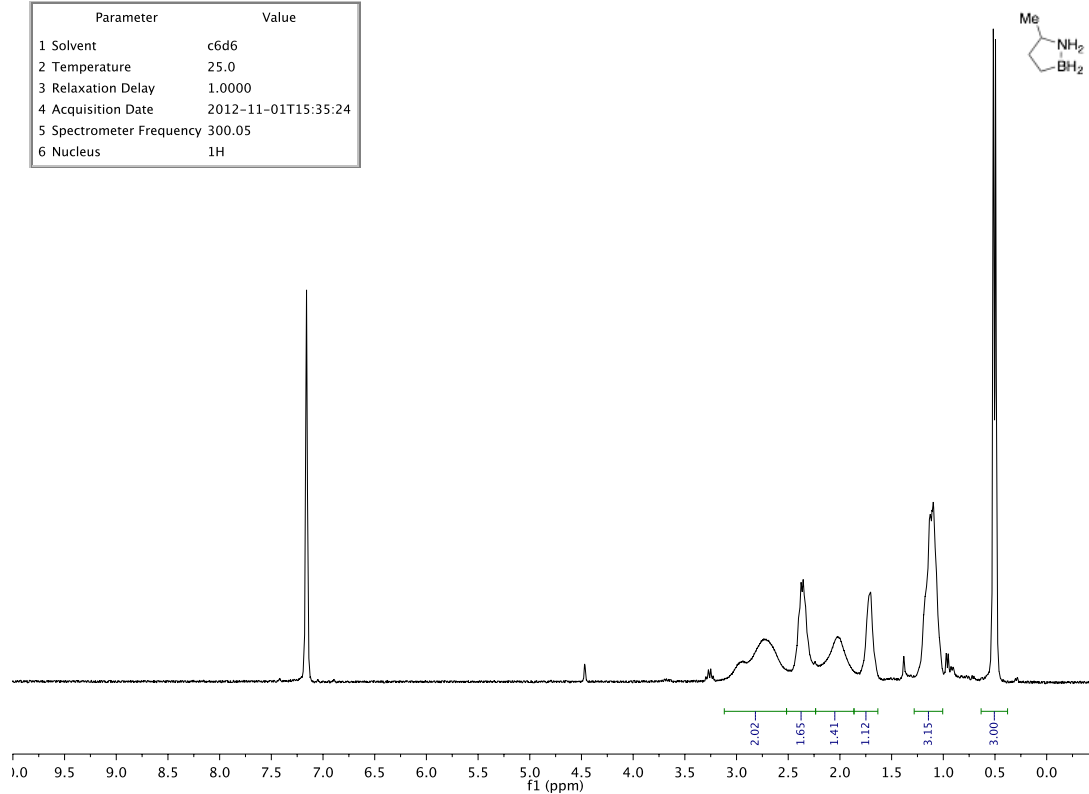
Parameter	Value
1 Solvent	c6d6
2 Temperature	25.0
3 Relaxation Delay	1.0000
4 Acquisition Date	2012-10-23T15:02:13
5 Spectrometer Frequency	299.93
6 Nucleus	¹ H



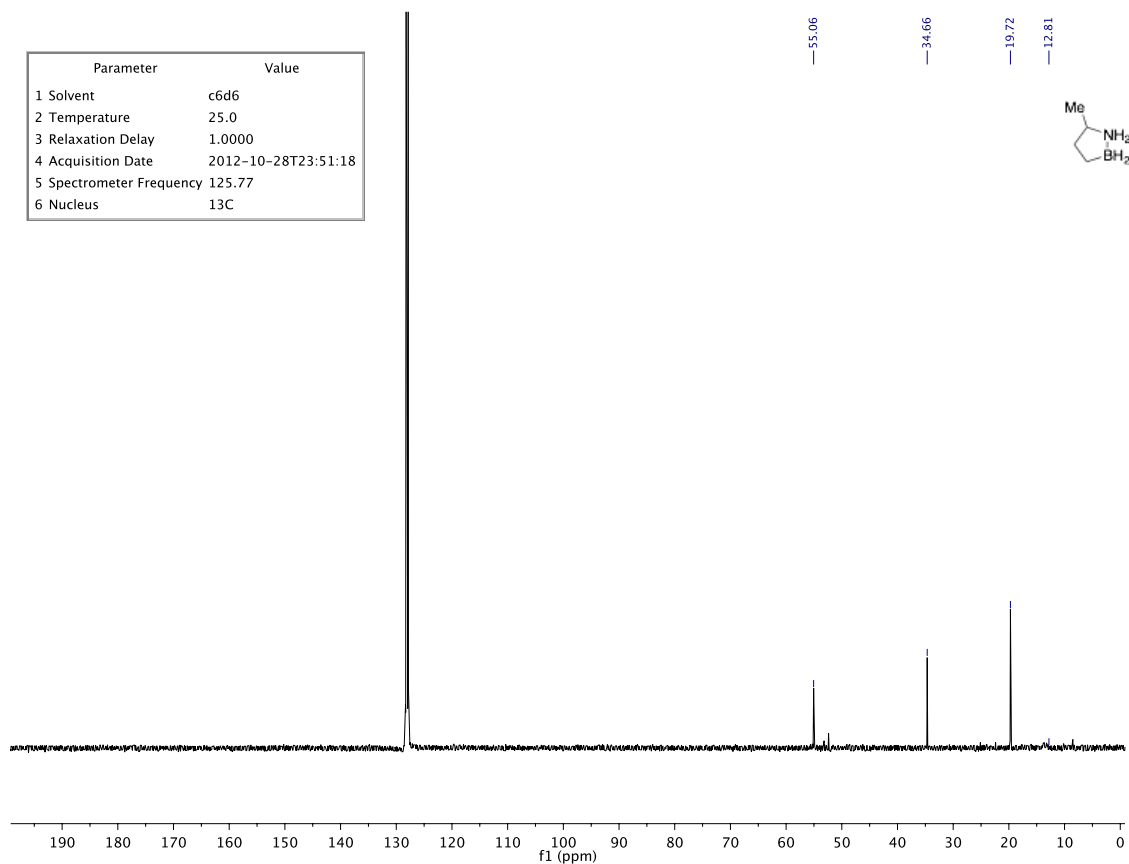
Parameter	Value
1 Solvent	c6d6
2 Temperature	25.0
3 Relaxation Delay	1.0000
4 Acquisition Date	2012-10-24T15:09:48
5 Spectrometer Frequency	75.43
6 Nucleus	¹³ C



Parameter	Value
1 Solvent	c6d6
2 Temperature	25.0
3 Relaxation Delay	1.0000
4 Acquisition Date	2012-11-01T15:35:24
5 Spectrometer Frequency	300.05
6 Nucleus	¹ H



Parameter	Value
1 Solvent	c6d6
2 Temperature	25.0
3 Relaxation Delay	1.0000
4 Acquisition Date	2012-10-28T23:51:18
5 Spectrometer Frequency	125.77
6 Nucleus	¹³ C



Parameter	Value
1 Solvent	c6d6
2 Temperature	25.0
3 Relaxation Delay	0.2000
4 Acquisition Date	2012-10-29T17:54:46
5 Spectrometer Frequency	96.27
6 Nucleus	11B

-10.73
-11.74
-12.76

